Oceano Dunes State Vehicular Recreation Area

Dust Control Program

DRAFT 2022 Annual Report and Work Plan

August 1, 2022

ATTACHMENTS

Attachment 01: 2011 to 2021 Dust Control Measures

Attachment 02: PMRP Evaluation Metrics

Attachment 03: 2021/2022 ODSVRA Dust Control Program Vegetation Restoration Projects (State Parks ARWP Work Product)

Attachment 04: Oceano Dunes: Status 2022 (DRI Presentation)

Attachment 05: Computation Fluid Dynamic Modeling of ODSVRA Foredunes (DRI, UCSB, and ASU Report)

Attachment 06: Summary of Vegetation Monitoring of Restoration Sites at ODSVRA (2021)

Attachment 07: Compilation of Studies Reviewed and Comments Provided by the Scientific Advisory Group from 08/01/21 to 07/31/22:

- *07-01: Dust Emissions and OHV Activity at the ODSVRA*
- *07-02: Scripps/UCSD Interim Report 2021: Preliminary Results from May 2021 Aerosol Measurements*
- *07-03: Quantifying the value of a coastal foredune for wind erosion and dust emissions through numerical simulation*
- *07-04: UCSB Historical Vegetation Cover Change Analysis*

Attachment 08: ODSVRA Dust Control Program Scientific Review Process (State Parks and SAG Work Product)

Attachment 09: 2022/2023 ODSVRA Dust Control Program Vegetation Restoration Projects (State Parks ARWP Work Product)

THIS PAGE INTENTIONALLY LEFT BLANK.

Oceano Dunes State Vehicular Recreation Area Dust Control Program

DRAFT 2022 Annual Report and Work Plan

ATTACHMENT 01

2011 to 2021 Dust Control Measures

THIS PAGE INTENTIONALLY LEFT BLANK.

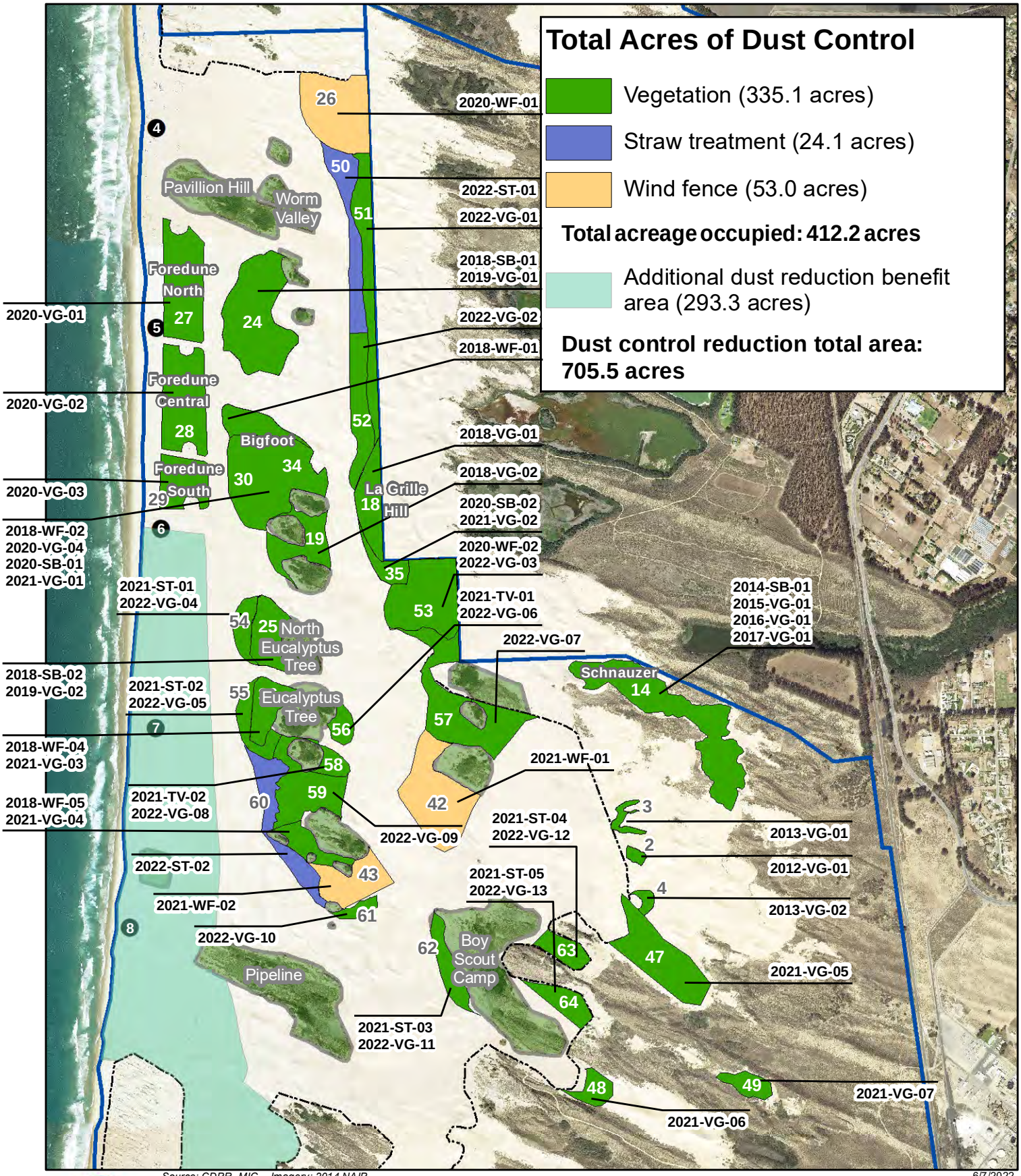

Source: CDPR, MIG Imagery: 2014 NAIP

6/7/2022

Feet
0 500 1,000 2,000

N

A01-01: Cumulative Dust Control as of 7/31/22

2022 ARWP

Marker post
Existing fenced vegetated islands
Park boundary
Open riding and camping area boundary fence

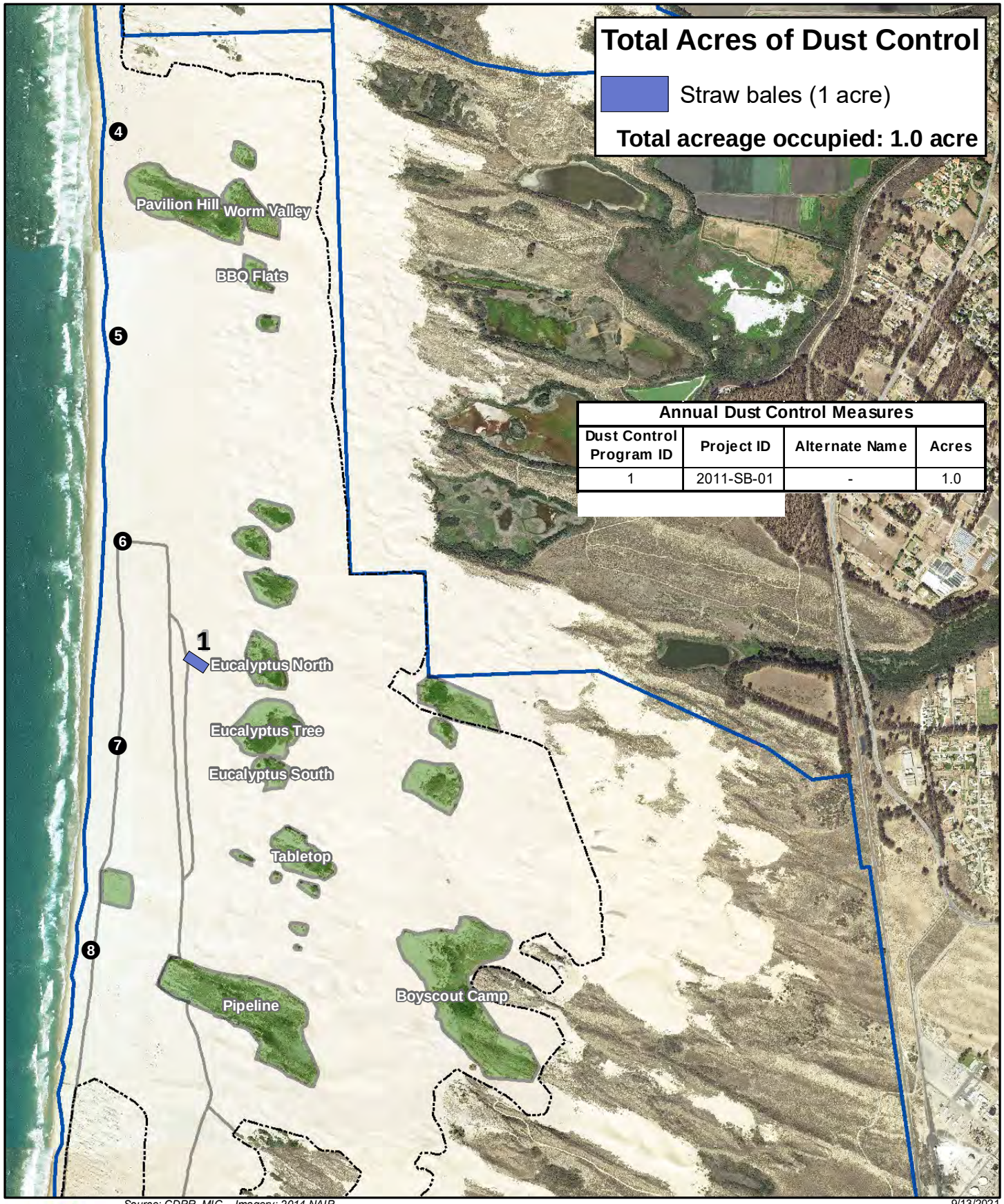

Source: CDPR, MIG Imagery: 2014 NAIP

9/13/2021

Feet
0 500 1,000 2,000

N

A01-02: 2011 Dust Control Treatment Areas

2022 ARWP

Marker post

Existing fenced vegetated islands

Park boundary

Nesting exclosure from 2020

Open riding and camping area boundary fence

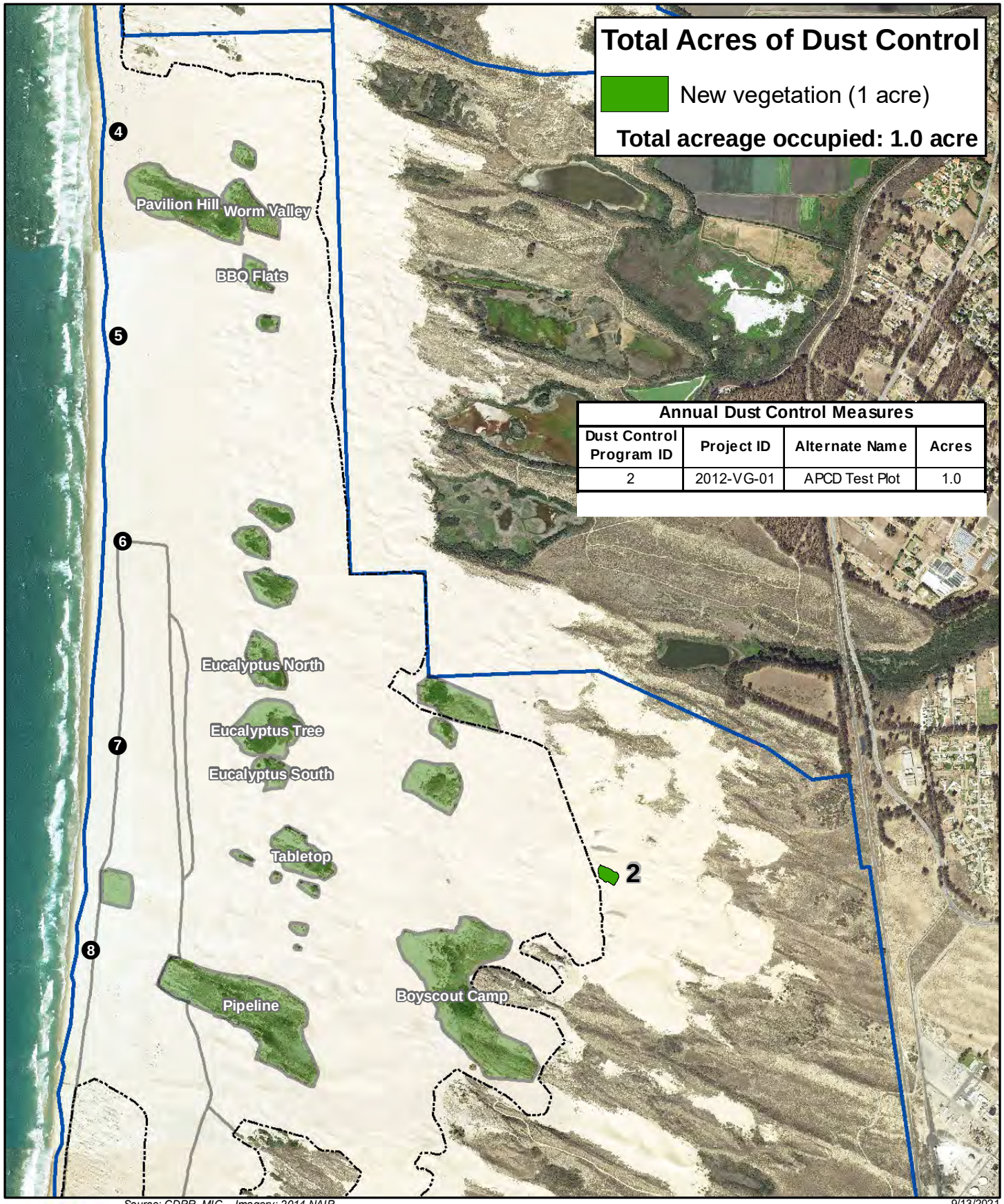

Source: CDPR, MIG Imagery: 2014 NAIP

9/13/2021

Feet
0 500 1,000 2,000

N

A01-03: 2012 Dust Control Treatment Areas

2022 ARWP

Marker post

Existing fenced vegetated islands

Park boundary

Nesting exclosure from 2020

Open riding and camping area boundary fence

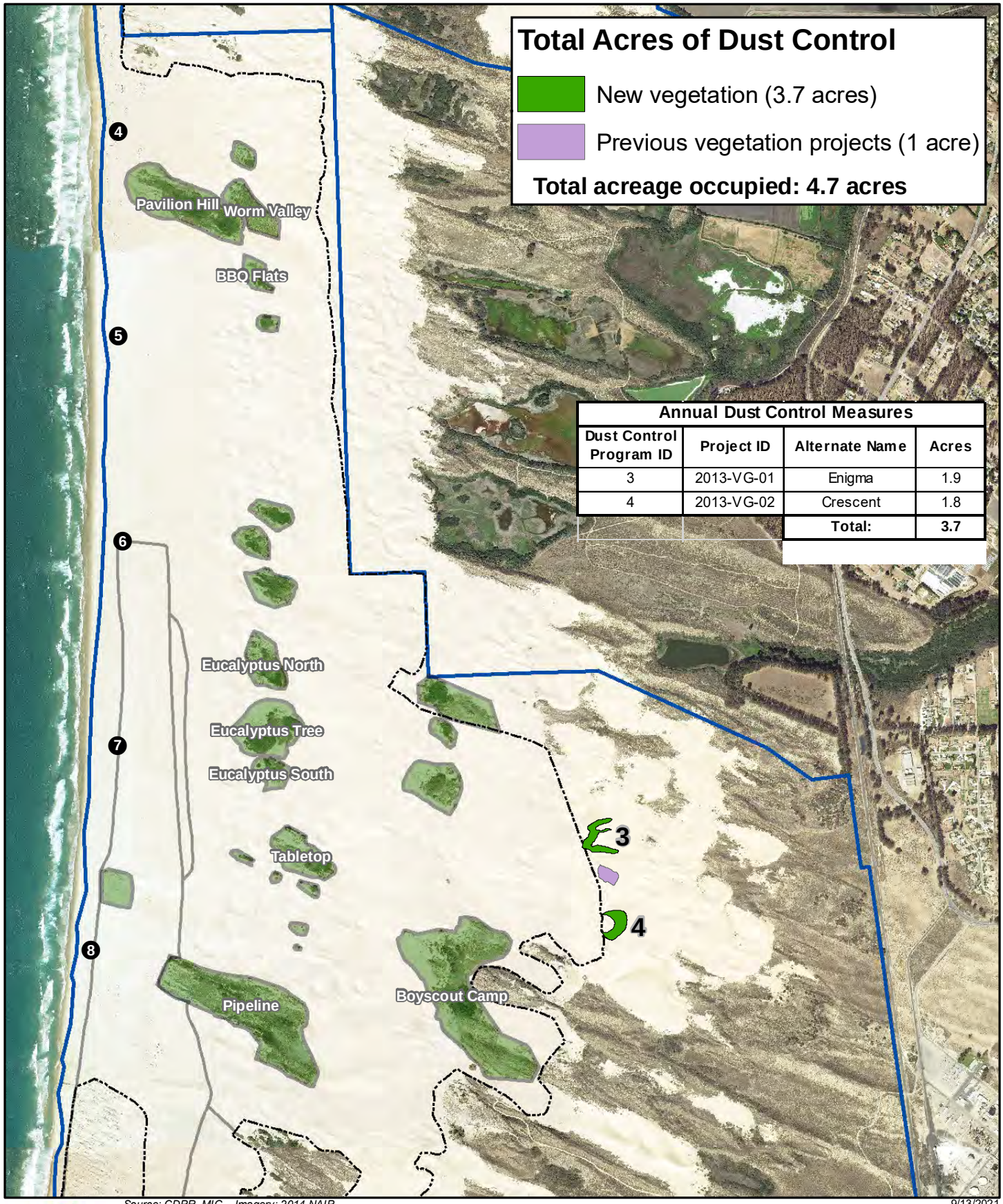

Source: CDPR, MIG Imagery: 2014 NAIP

9/13/2021

Feet
0 500 1,000 2,000

N

A01-04: 2013 Dust Control Treatment Areas

2022 ARWP

Marker post

Existing fenced vegetated islands

Park boundary

Nesting exclosure from 2020

Open riding and camping area boundary fence

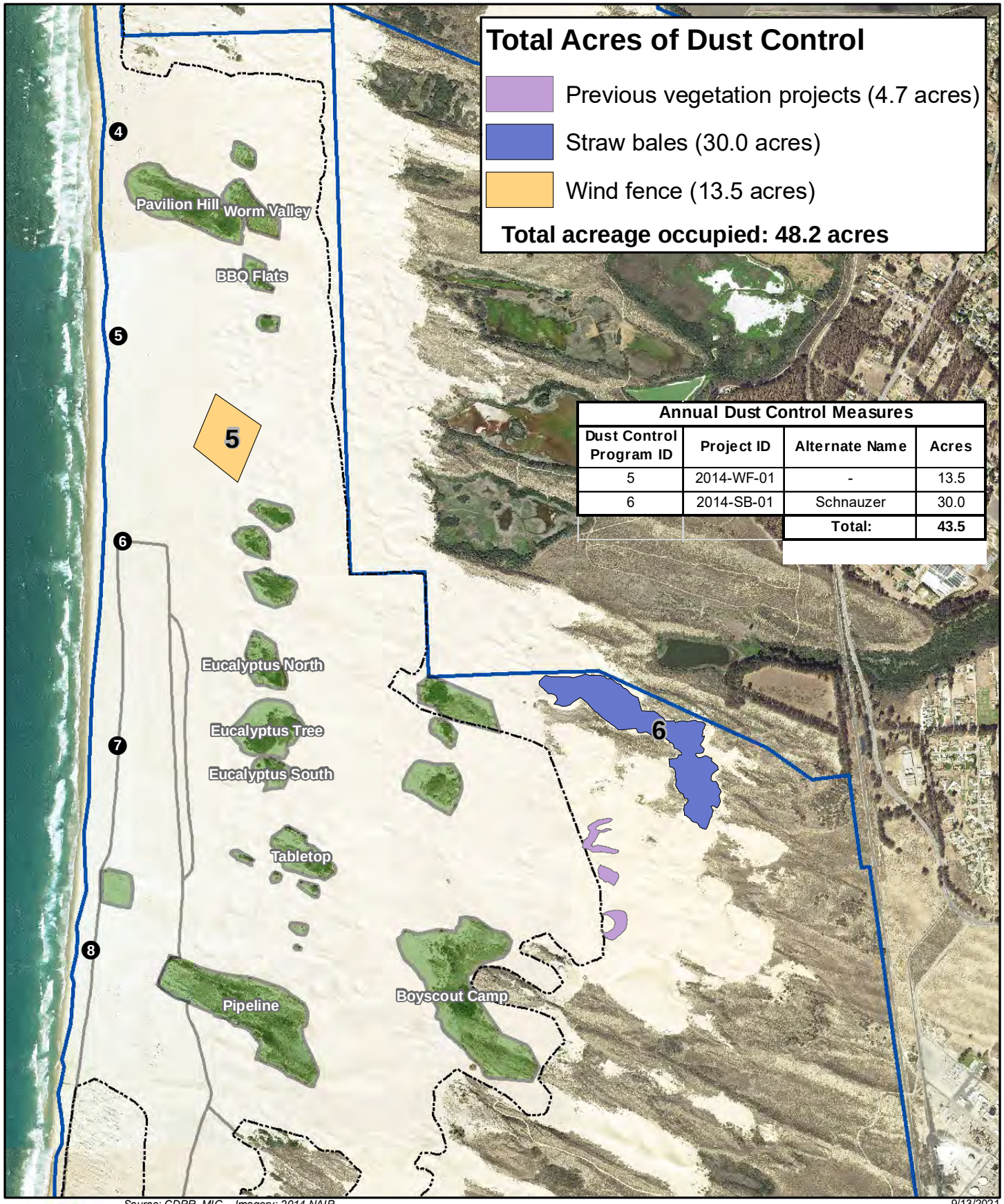

Source: CDPR, MIG Imagery: 2014 NAIP

9/13/2021

Feet
0 500 1,000 2,000

N

A01-05: 2014 Dust Control Treatment Areas

2022 ARWP

Marker post

Existing fenced vegetated islands

Park boundary

Nesting exclosure from 2020

Open riding and camping area boundary fence

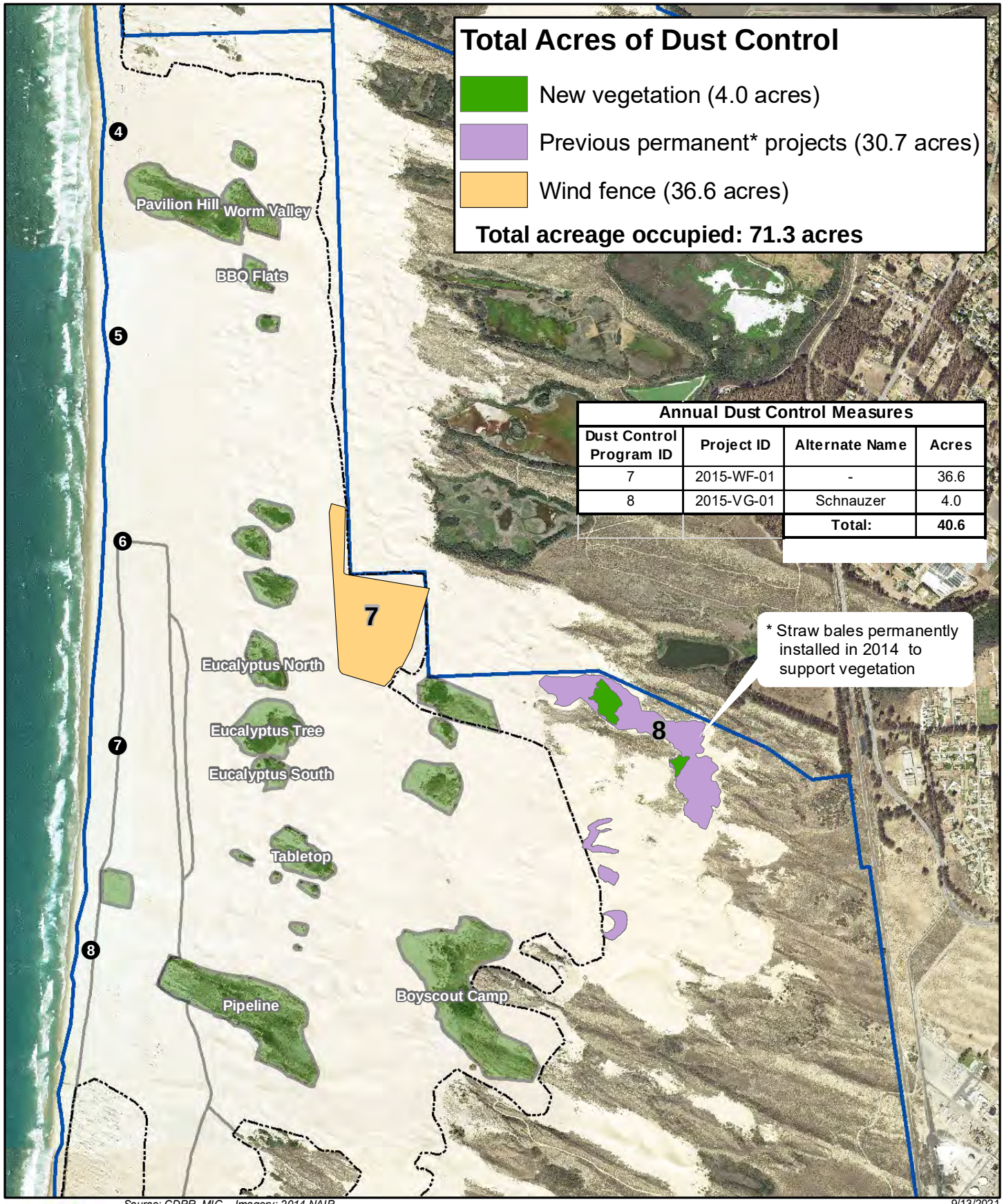

Source: CDPR, MIG Imagery: 2014 NAIP

9/13/2021

Feet
0 500 1,000 2,000

N

A01-06: 2015 Dust Control Treatment Areas

2022 ARWP

Marker post

Existing fenced vegetated islands

Park boundary

Nesting exclosure from 2020

Open riding and camping area boundary fence

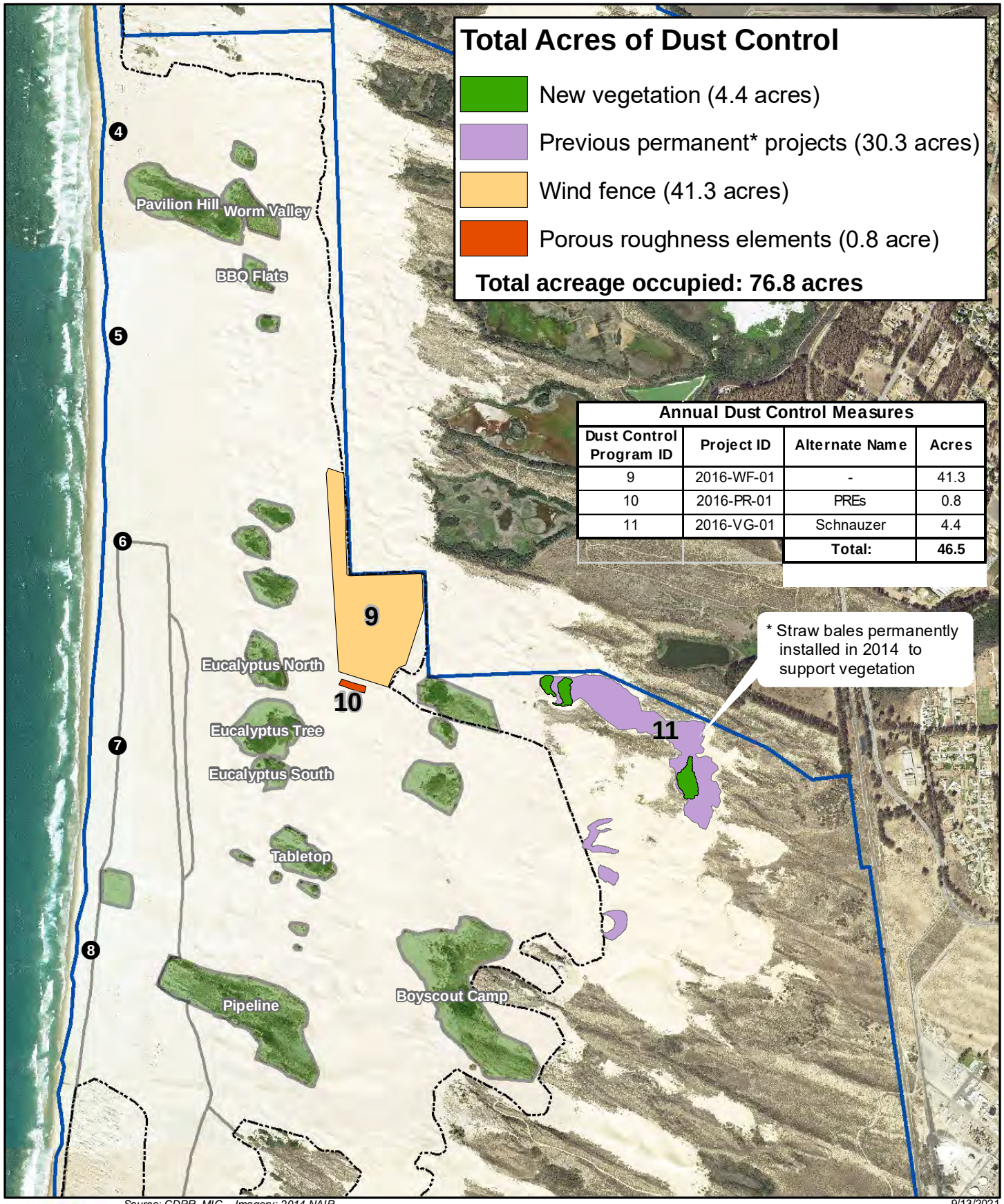

Source: CDPR, MIG Imagery: 2014 NAIP

9/13/2021

Feet
0 500 1,000 2,000

N

A01-07: 2016 Dust Control Treatment Areas

2022 ARWP

Marker post

Existing fenced vegetated islands

Park boundary

Nesting exclosure from 2020

Open riding and camping area boundary fence

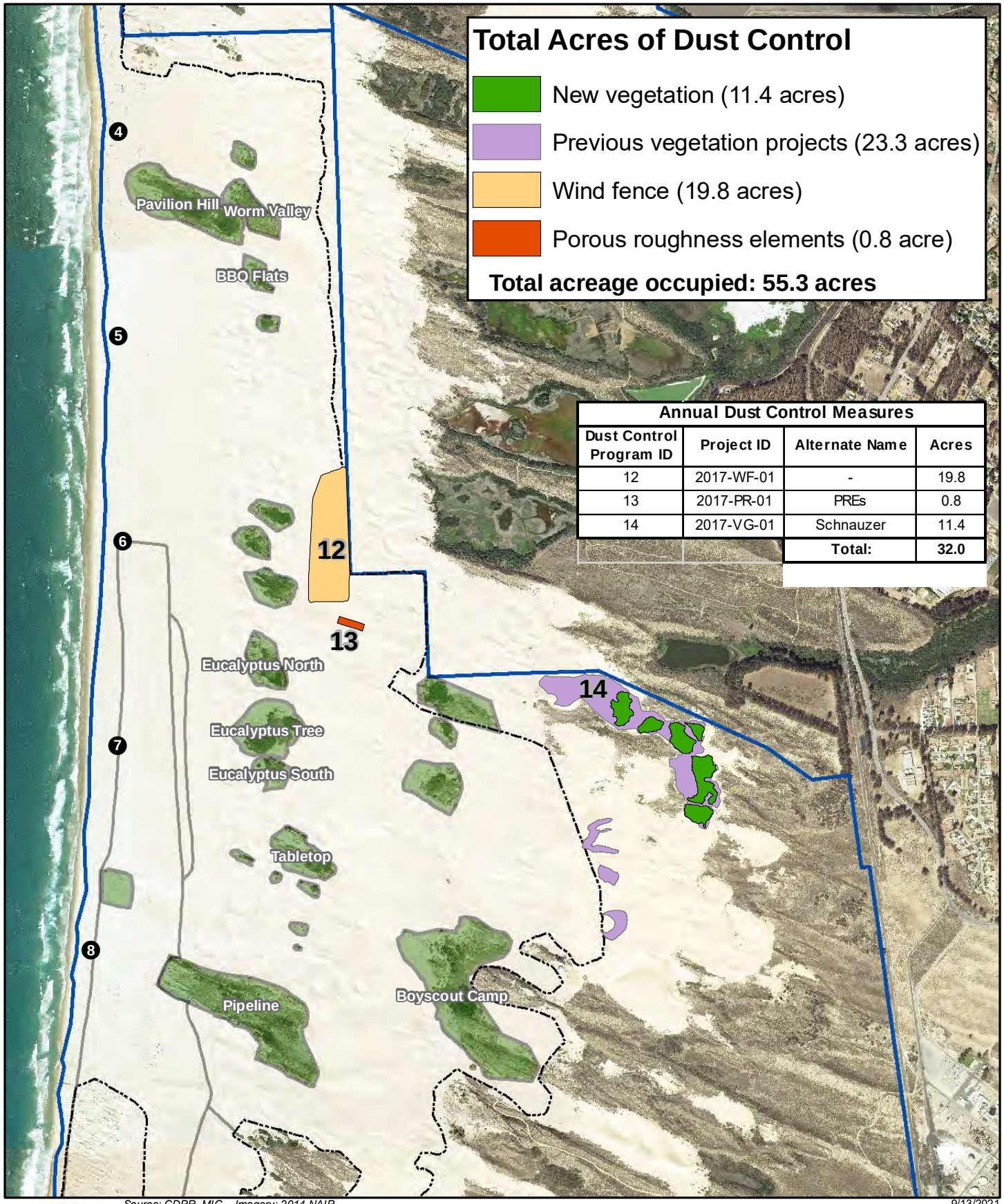

Source: CDPR, MIG Imagery: 2014 NAIP

9/13/2021

Feet
0 500 1,000 2,000

N

A01-08: 2017 Dust Control Treatment Areas

2022 ARWP

Marker post

Existing fenced vegetated islands

Park boundary

Nesting exclosure from 2020

Open riding and camping area boundary fence

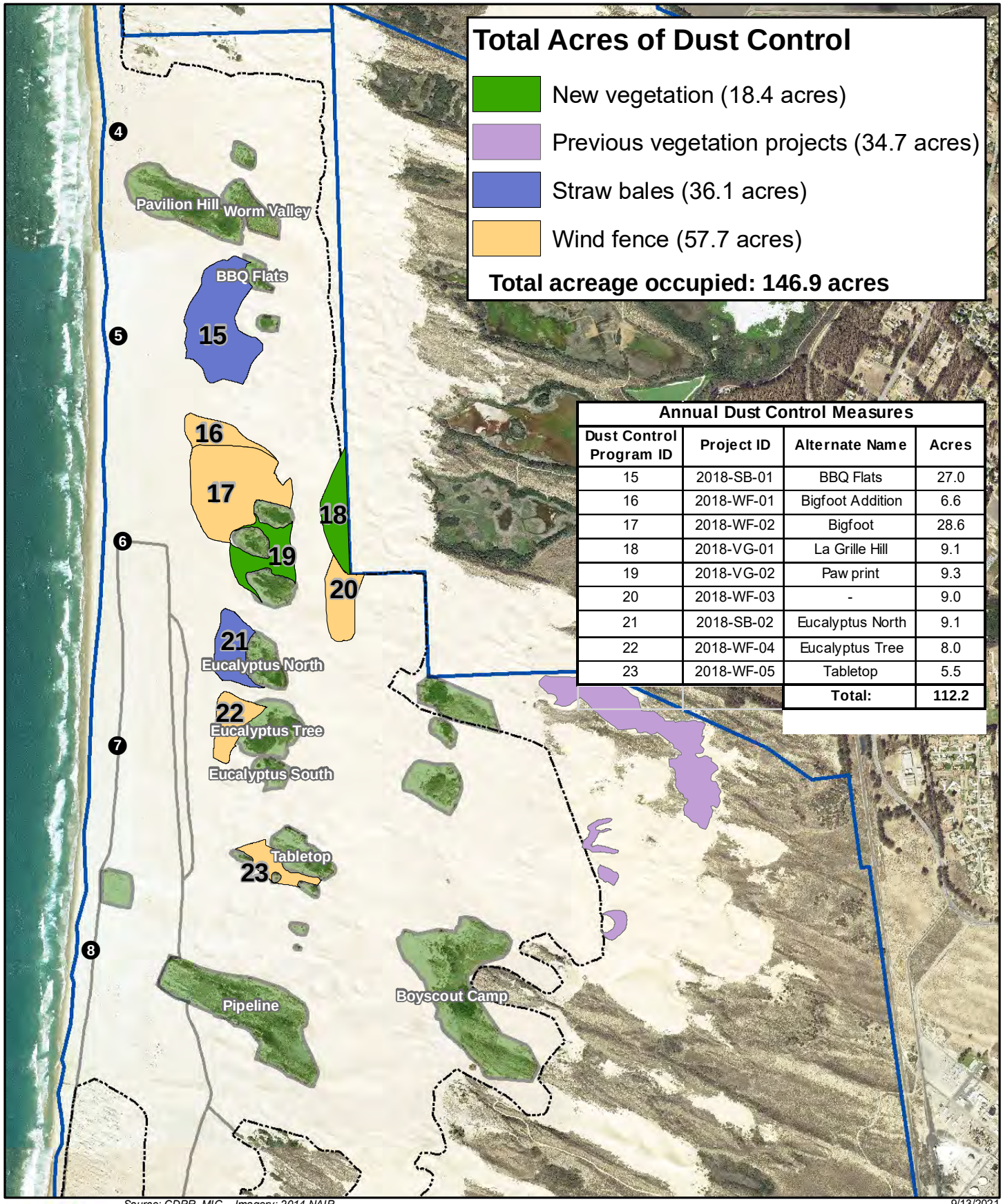

Annual Dust Control Measures			
Dust Control Program ID	Project ID	Alternate Name	Acres
15	2018-SB-01	BBQ Flats	27.0
16	2018-WF-01	Bigfoot Addition	6.6
17	2018-WF-02	Bigfoot	28.6
18	2018-VG-01	La Grille Hill	9.1
19	2018-VG-02	Paw print	9.3
20	2018-WF-03	-	9.0
21	2018-SB-02	Eucalyptus North	9.1
22	2018-WF-04	Eucalyptus Tree	8.0
23	2018-WF-05	Tabletop	5.5
		Total:	**112.2**

Source: CDPR, MIG Imagery: 2014 NAIP

9/13/2021

Feet
0 500 1,000 2,000

N

A01-09: 2018 Dust Control Treatment Areas

2022 ARWP

Marker post

Existing fenced vegetated islands

Park boundary

Nesting exclosure from 2020

Open riding and camping area boundary fence

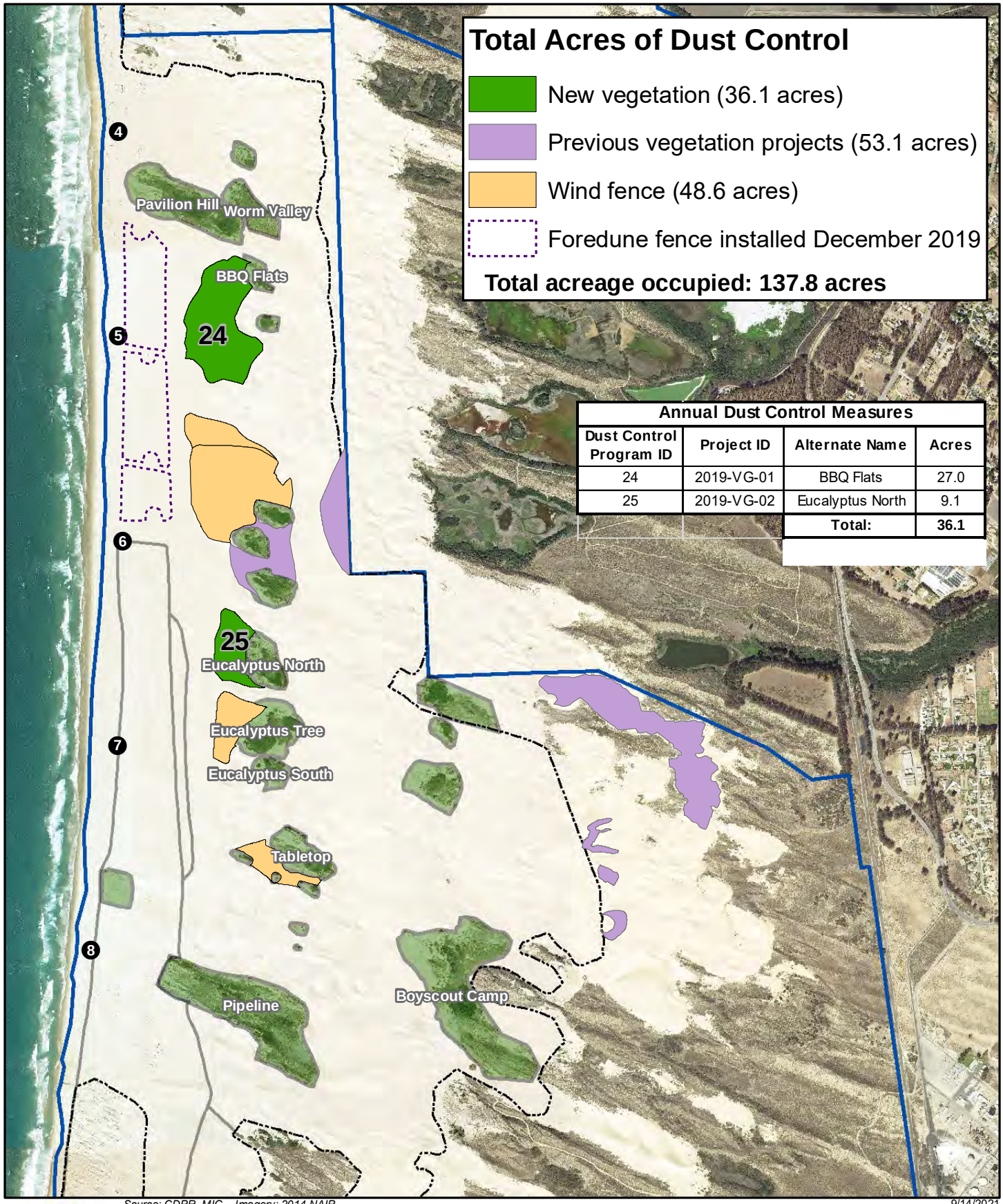

Source: CDPR, MIG Imagery: 2014 NAIP

9/14/2021

Feet
0 500 1,000 2,000

N

A01-10: 2019 Dust Control Treatment Areas

2022 ARWP

Marker post

Existing fenced vegetated islands

Park boundary

Nesting exclosure from 2020

Open riding and camping area boundary fence

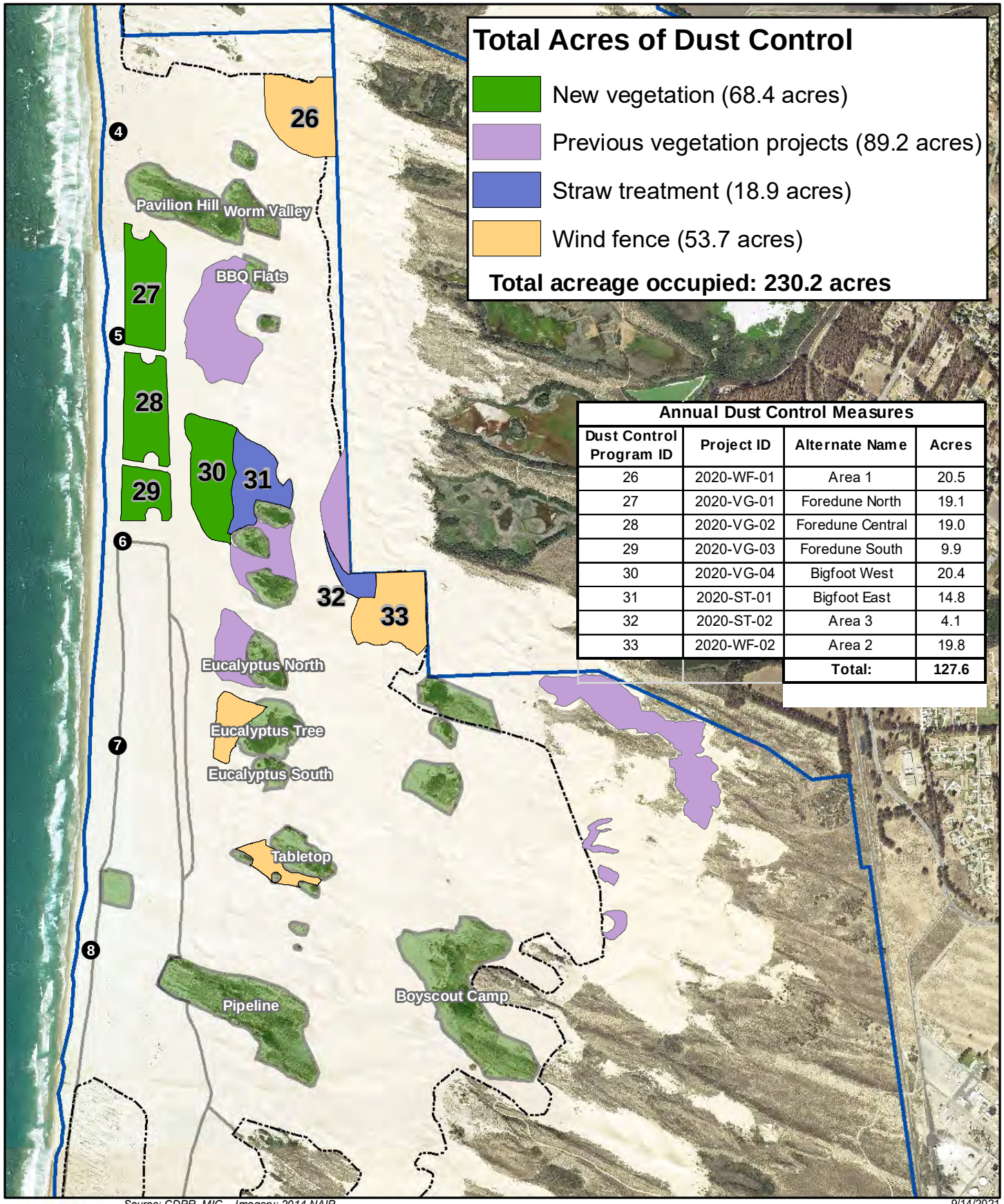

Annual Dust Control Measures			
Dust Control Program ID	Project ID	Alternate Name	Acres
26	2020-WF-01	Area 1	20.5
27	2020-VG-01	Foredune North	19.1
28	2020-VG-02	Foredune Central	19.0
29	2020-VG-03	Foredune South	9.9
30	2020-VG-04	Bigfoot West	20.4
31	2020-ST-01	Bigfoot East	14.8
32	2020-ST-02	Area 3	4.1
33	2020-WF-02	Area 2	19.8
		Total:	**127.6**

Source: CDPR, MIG Imagery: 2014 NAIP

9/14/2021

Feet
0 500 1,000 2,000

N

A01-11: 2020 Dust Control Treatment Areas

2022 ARWP

Marker post

Existing fenced vegetated islands

Park boundary

Nesting exclosure from 2020

Open riding and camping area boundary fence

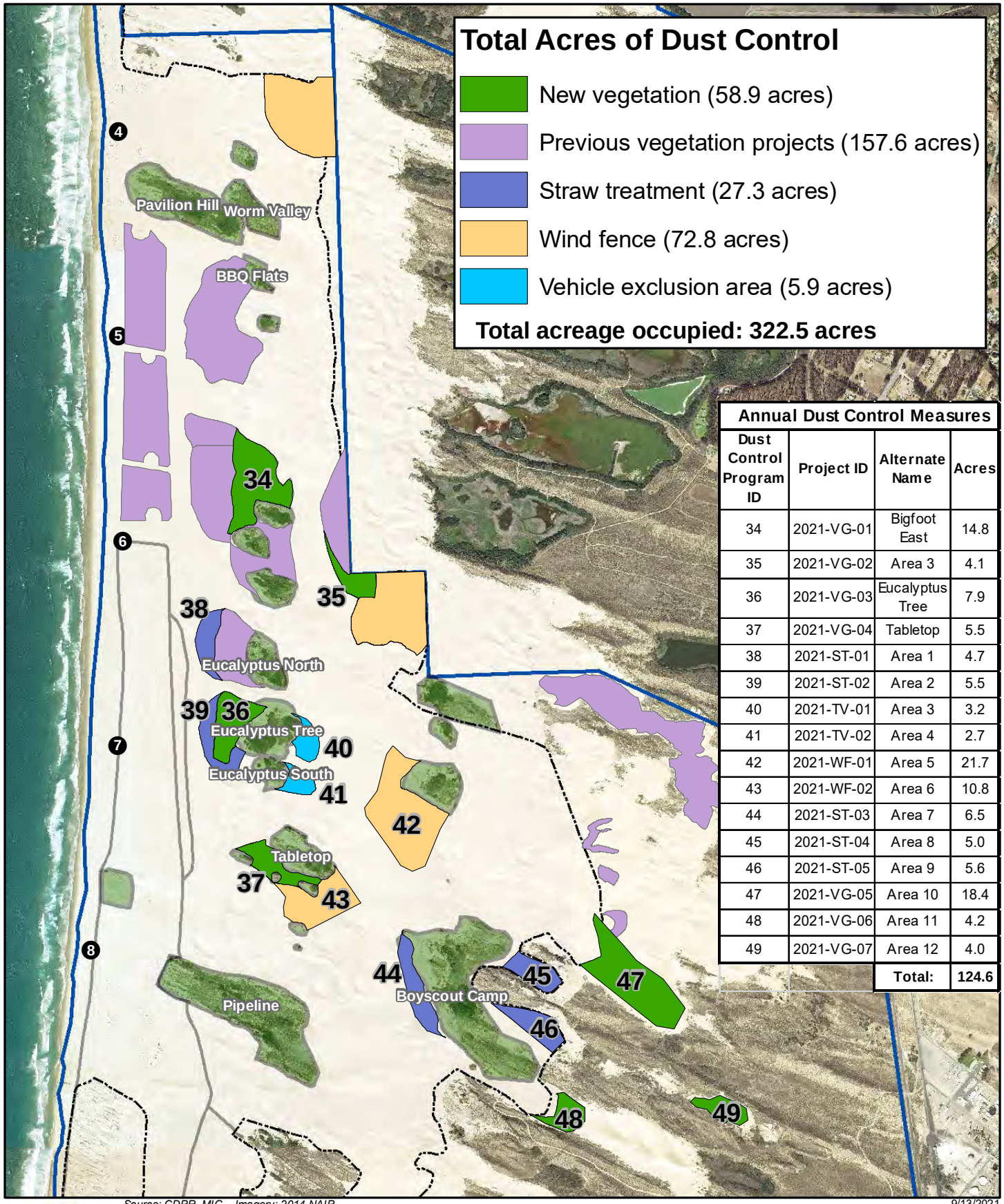

Annual Dust Control Measures			
Dust Control Program ID	Project ID	Alternate Name	Acres
34	2021-VG-01	Bigfoot East	14.8
35	2021-VG-02	Area 3	4.1
36	2021-VG-03	Eucalyptus Tree	7.9
37	2021-VG-04	Tabletop	5.5
38	2021-ST-01	Area 1	4.7
39	2021-ST-02	Area 2	5.5
40	2021-TV-01	Area 3	3.2
41	2021-TV-02	Area 4	2.7
42	2021-WF-01	Area 5	21.7
43	2021-WF-02	Area 6	10.8
44	2021-ST-03	Area 7	6.5
45	2021-ST-04	Area 8	5.0
46	2021-ST-05	Area 9	5.6
47	2021-VG-05	Area 10	18.4
48	2021-VG-06	Area 11	4.2
49	2021-VG-07	Area 12	4.0
		Total:	124.6

Source: CDPR, MIG Imagery: 2014 NAIP

9/13/2021

Feet
0 500 1,000 2,000

N

A01-12: 2021 Dust Control Treatment Areas

2022 ARWP

Marker post

Existing fenced vegetated islands

Park boundary

Nesting exclosure from 2020

Open riding and camping area boundary fence

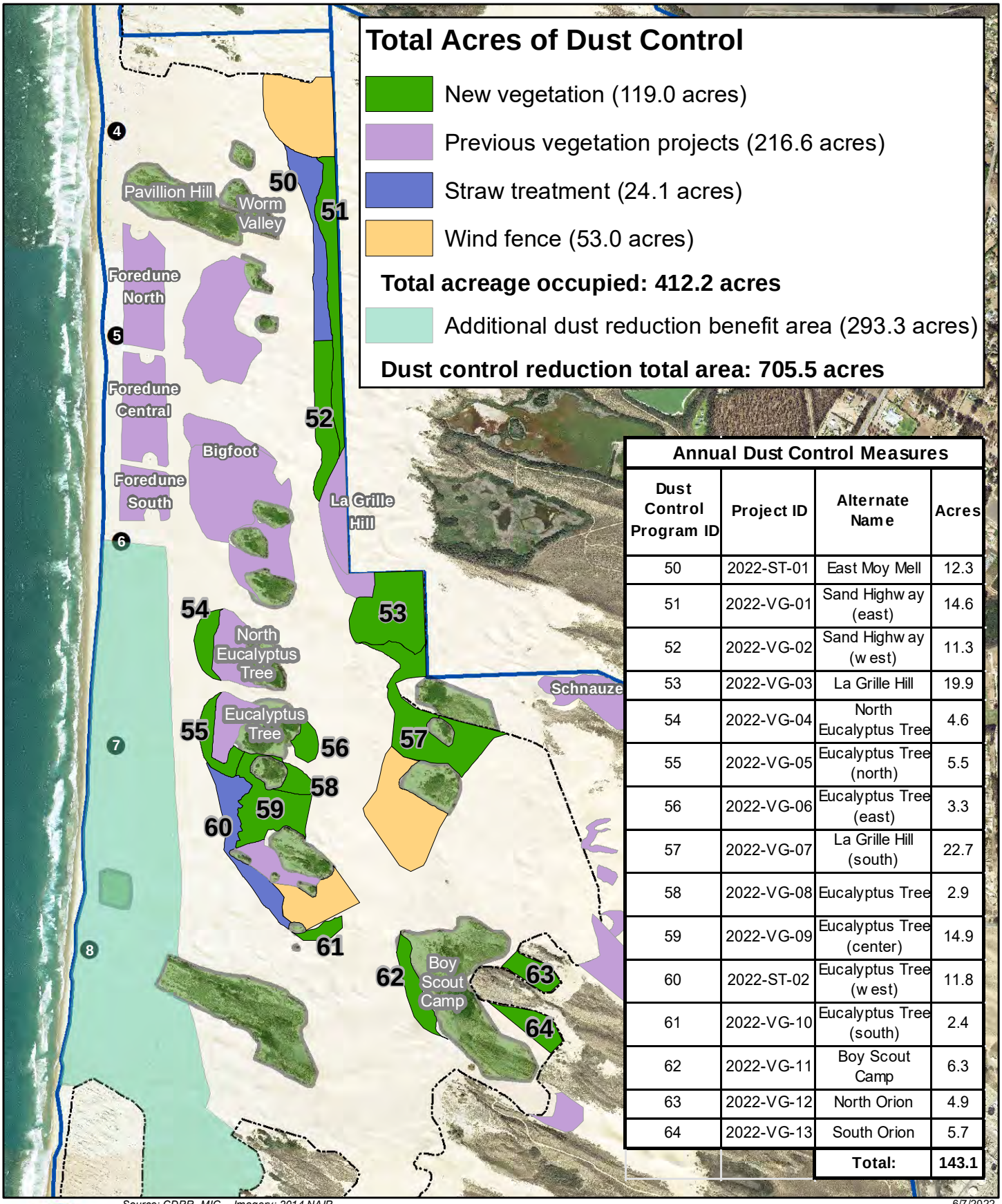

Annual Dust Control Measures			
Dust Control Program ID	Project ID	Alternate Name	Acres
50	2022-ST-01	East Moy Mell	12.3
51	2022-VG-01	Sand Highway (east)	14.6
52	2022-VG-02	Sand Highway (west)	11.3
53	2022-VG-03	La Grille Hill	19.9
54	2022-VG-04	North Eucalyptus Tree	4.6
55	2022-VG-05	Eucalyptus Tree (north)	5.5
56	2022-VG-06	Eucalyptus Tree (east)	3.3
57	2022-VG-07	La Grille Hill (south)	22.7
58	2022-VG-08	Eucalyptus Tree	2.9
59	2022-VG-09	Eucalyptus Tree (center)	14.9
60	2022-ST-02	Eucalyptus Tree (west)	11.8
61	2022-VG-10	Eucalyptus Tree (south)	2.4
62	2022-VG-11	Boy Scout Camp	6.3
63	2022-VG-12	North Orion	4.9
64	2022-VG-13	South Orion	5.7
		Total:	**143.1**

Source: CDPR, MIG Imagery: 2014 NAIP

6/7/2022

Feet
0 500 1,000 2,000

N

A01-13: 2022 Dust Control Treatment Areas

2022 ARWP

Marker post
Existing fenced vegetated islands
Park boundary
Open riding and camping area boundary fence

THIS PAGE INTENTIONALLY LEFT BLANK.

Oceano Dunes State Vehicular Recreation Area Dust Control Program

DRAFT 2022 Annual Report and Work Plan

ATTACHMENT 02

PMRP Evaluation Metrics

THIS PAGE INTENTIONALLY LEFT BLANK.

PMRP Evaluation Metrics – Annual Record 2021-22

In 2021, the SAG, in consultation with State Parks, updated the PMRP evaluation metrics used to track dust control progress. The updated metrics provide a more streamlined dashboard that make it easier to track progress and to inform adaptative management. "Dust Mitigation Targets" refer to evaluation metrics with specific measurable endpoints. "Dust Mitigation Indicators" refer to values indicating progress but for which specific targets are not defined.

In 2022, the SAG recommended specific changes to the current DRI Model to more accurately account for the effectiveness of dust mitigation treatments (see State Parks' 2022 ARWP Section 2.2.1.3). The SAG's recommendations were incorporated into a "revised" DRI model that results in different estimates of PM_{10} mass emissions and concentration reductions compared to the current DRI model. The revised DRI model does not change the modeled 2013 baseline information against which evaluation metrics and Dust Control Program progress has historically been measured.

Where applicable, this attachment presents metrics using both the revised DRI model and the current DRI model. The revise DRI model results are presented first and the current DRI model results are presented second and formatted to be in italicized text placed in parentheses. For example, as shown in State Parks' 2022 ARWP, Table 2-10, the revised DRI model estimates that State Parks' Dust Control Program has reduced mass emissions from the ODSVRA open riding and camping area to 104.9 metric tons per day as of July 31, 2022. This value is reported first in the Dust Mitigation Targets metrics. The corresponding current DRI model estimate of mass emissions from the ODSVRA as of July 31, 2022 is 108.2 metric tons per day (see State Parks 2022 ARWP, Table 2-9). This value is reported second in the Dust Mitigation Targets table provided below. The example below identifies the way in which evaluation metrics are reported in this attachment.

EXAMPLE 2022 ARWP EVALUATION METRIC REPORTING			
PM_{10} mass emissions		**2013 Baseline**	**2022**
B. Riding Area mean PM_{10} emissions for 10 baseline days - modeled	B1. Mass emissions (metric tons / day)	182.8	104.9 *(108.2)*

Revised DRI Model estimate in regular font

(*Current DRI Model estimate in italicized font)*

Evaluation Metric table notes are provided at the end of this document.

EVALUATION METRICS TABLE 1: DUST MITIGATION TARGETS								
Dust mitigation treatments		**2013 baseline**	**2019**	**2020**	**2021**	**2022**	**2023**	**Current target[1]**
A. Cumulative area under treatment within ODSVRA, as of July 31 of current year, relative to 2013 baseline (acres)	A1. Total	0	137.8	230.2	322.5	705.5	N/A	N/A
	A2. Back dunes inside Riding Area	0	103.1	195.5	213.2	336.3	N/A	
	A3. Back dunes outside Riding Area	4.7	34.7	34.7	61.3	75.9	N/A	
	A4. Foredunes	0	0.0	48.0	48.0	48.0	N/A	
	A5. Plover Exclosure	0	0.0	0.0	0.0	293.3	N/A	
PM_{10} mass emissions		**2013 baseline**	**2019**	**2020**	**2021**	**2022**	**2023**	**Current target[2]**
B. Riding Area mean PM_{10} emissions for 10 baseline days - modeled	B1. Mass emissions (metric tons / day)	182.8	135.0 *(160.8)[3]*	131.6 *(153.1)*	123.9 *(142.0)*	104.0 *(108.2)*	N/A	91.4
	B2. Relative to 2013	100%	73.9% *(88.0%)*	72.0 *(83.8%)*	67.8 *(77.7%)*	56.9% *(59.2%)*	N/A	50%
PM_{10} concentrations		**2013 baseline**	**2019**	**2020**	**2021**	**2022**	**2023**	**Current target[4]**
C. CDF mean PM_{10} concentration for 10 baseline days ($\mu g/m^3$) - modeled		124.7	N/A *(99.7)*	N/A *(72.4)*	N/A *(72.2)*	63.8 *(65.7)*	N/A	N/A
D. Mesa2 mean PM_{10} concentration for 10 baseline days ($\mu g/m^3$) - modeled		97.5	N/A *(N/A)[4]*	N/A *(91.2)*	N/A *(73.8)*	63.7 *(59.9)*	(N/A	

DUST MITIGATION INDICATORS						
Air quality indicators		**2013 baseline**	**2019**	**2020**	**2021**	**2022**
1. Actual number of high wind event days[5]		59	30	55	51	64
2. Actual number of exceedances of California air quality standard[6]	2a. at CDF	58	16	30	28	54
	2b. at Mesa2	43	14	28	30	38
3. Actual number of exceedances of Federal air quality standard[7]	3a. at CDF	1	0	0	0	0
	3b. at Mesa2	0	0	0	0	0
Foredune restoration		**2013 baseline**	**2019**	**2020**	**2021**	**2022**
4. Foredune plant fractional cover, at time of spring survey (%)	4a. Treatment 1	N/A	N/A	N/A	0	0
	4b. Treatment 2				0.1	1.91
	4c. Treatment 3				4.02	12.31
	4d. Treatment 4				0.76	5.69
	4e. Treatment 5				0.4	2.14
	4f. Treatment 6				3.57	12.66
5. Foredune species richness index relative to Oso Flaco site[8]	5a. Treatment 1	N/A	N/A	N/A	0	0
	5b. Treatment 2				33	40
	5c. Treatment 3				50	50
	5d. Treatment 4				100	60
	5e. Treatment 5				110	100
	5f. Treatment 6				110	80
6. Foredune sand volume, current spring survey relative to previous fall survey (m^3 m^{-2} $month^{-1}$)	6a. Treatment 1	N/A	N/A	N/A	0.0011	TBD[9]
	6b. Treatment 2				0.0006	TBD
	6c. Treatment 3				0.0022	TBD
	6d. Treatment 4				0.0009	TBD
	6e. Treatment 5				0.0020	TBD
	6f. Treatment 6				0.0031	TBD
Back dune stabilization		**2013 baseline**	**2019**	**2020**	**2021**	**2022**
7. Cumulative area of back dune stabilization within ODSVRA, as of July 31 of current year (acres)	7a. Planting area	TBD[10]	89.2	109.6	168.5	287.1
	7b. Fencing area	0	48.6	53.7	72.8	53.0
	7c. Straw bales area	0	0	18.9	27.3	24.1
	7d. Temporary vehicle exclusion areas	0	0	0	5.9	0.0
	7e. Stabilized vegetation surface area	TBD[11]	137.8	182.2	274.5	364.2
8. Native seed harvest for all plants during current ARWP reporting period (kg/year)		N/A	203.2	307.3	193.0	252.6
9. Plant species cultivation for all plants during current ARWP reporting period (#/year)			106,350	89,433	127,464	125,380

EVALUATION METRIC TABLE NOTES

[1] State Parks' June 2019 PMRP included a preliminary compliance analysis, or sensitivity analysis, prepared by DRI, that evaluated the approximate size, scale, and level of effort necessary to comply with the SOA's air quality objectives, namely the 50% reduction in maximum modeled baseline PM_{10} mass emissions identified in SOA condition 2.c. The preliminary PMRP modeling conducted by DRI indicated that approximately 500 acres of dust control measures could be needed to achieve SOA air quality objectives. State Parks' 2021 ARWP included an updated estimate of the amount of dust control measures that may be required to achieve SOA air quality objectives. The 2021 ARWP's updated sensitivity analysis increased the estimate of the amount of dust control measures necessary to comply with SOA Condition 2.C from 500 acres (as preliminary estimated in the 2019 PMRP) to 602 acres, assuming 100% effectiveness for all dust control measures. This target may be revised in the future based on further modeling of dust mitigation effectiveness and monitoring of actual air quality improvements.

[2] The current PM_{10} mass emissions target is defined according to Stipulated Order of Abatement (SOA) provision 2c, which "…establish[es] an initial target of reducing the maximum 24-hour PM_{10} baseline emissions by fifty percent (50%), based on air quality modeling based on a modeling scenario for the period May 1 through August 31, 2013." The air quality modeling approach is described in the PMRP. The 10 baseline days for this scenario are defined in the 2020 Annual Report and Work Plan (ARWP), Attachment 6. As described in the 2022 ARWP (Section 2.2.1.1), the SAG has recommended potential scientifically-informed refinements to the initial SOA target that are based on a comprehensive determination of the difference in PM_{10} emissions between the SOA's 2013 baseline scenario and a "pre-disturbance" historical scenario identified to simulate conditions prior to significant OHV disturbance. Ongoing efforts to revisit the SOA target may result in changes to these values.

[3] For the current DRI model, the estimate of mass emission reductions come from State Parks 2020 ARWP, Attachment 3 (Oceano Dunes Emission, Dispersion, and Attribution Model Results and Treatment Assessment. The estimate of the CDF concentration reduction comes from State Parks' 2019 ARWP, p. 2-6 (dated December 31, 2019). The 2019 ARWP did not provide a modeled concentration reduction for Mesa2.

[4] SOA provision 2b states that "…the [Particulate Matter Reduction] Plan shall be designed to achieve state and federal ambient PM_{10} air quality standards." However, it does not designate a specific PM_{10} airborne concentration target for the baseline modeling scenario. Refer to State Parks' 2022 ARWP (Table 2-3) for the current California and National Ambient Air Quality Standards for PM_{10}. As described in the 2022 ARWP (Section 2.2.1.1), the SAG has recommended potential scientifically-informed refinements to the SOA's targets that are based on a comprehensive determination of the difference in PM_{10} emissions between the SOA's 2013 baseline scenario and a "pre-disturbance" historical scenario identified to simulate conditions prior to significant OHV disturbance. Ongoing efforts to revisit the SOA target may result in establishing new targets based on modeled PM_{10} concentrations for the baseline scenario.

[5] Values are determined using the SLO Air Pollution Control District (APCD) definition of "high wind event day" as any day when the 3 p.m. PST hourly wind speed at CDF exceeds 8 mph and the 1 p.m. PST hourly wind direction is between 290 and 360°. The period of consideration is January 1 - June 28. Data may be preliminary and subject to change.

[6] The California Ambient Air Quality Standard is a mean value of 50 µg/m^3 over a 24-hour period. The period of consideration is January 1 - June 28. Data may be preliminary and subject to change.

[7] The National Ambient Air Quality Standard is a mean value of 150 µg/m^3 over a 24-hour period. The period of consideration is January 1 - June 28. Data may be preliminary and subject to change.

[8] The number of native plant species recorded for each treatment area as compared to reference site at Oso Flaco. Long term goal is to have a stable or increasing richness value versus reference site.

[9] Foredune sand volumes will be determined from the latest uncrewed aerial system (UAS) survey conducted by UCSB. The latest survey results are under review by State Parks. Foredune sand volumes will be updated following the State Parks' review of the UCSB UAS survey data.

[10] The baseline 2013 back dune stabilization "planting area" metric may be estimated from UCSB's historic vegetation report; however, the SAG has not established the methodology for establishing baseline vegetation conditions. State Parks will coordinate with the SAG to finalize the methodology for determining baseline 2013 back dune stabilization planting areas. Currently, the yearly estimates of planting area for the Dust Control Program (e.g., 89.2 acres in 2019) are based on the amount of back dune vegetation planted under the Dust Control Program (i.e., excludes foredune vegetation and non-vegetation projects such as wind fencing).

[11] The baseline 2013 back dune "stabilized vegetation surface area" metric may be estimated from vegetation coverage estimates determined from aerial imagery; however, the SAG has not established the methodology for establishing baseline vegetation conditions. State Parks will coordinate with the SAG to finalize the methodology for determining baseline 2013 back dune stabilization planting areas. Currently, the yearly estimates of stabilized vegetation surface area for the Dust Control Program (e.g., 137.8 acres in 2019) reflect the sum of the stabilization approaches in metrics 7a to 7d.

THIS PAGE INTENTIONALLY LEFT BLANK.

Oceano Dunes State Vehicular Recreation Area Dust Control Program

DRAFT 2022 Annual Report and Work Plan

ATTACHMENT 03

2021/2022 ODSVRA Dust Control Program Vegetation Restoration Projects

(State Parks ARWP Work Product)

THIS PAGE INTENTIONALLY LEFT BLANK.

2021/2022 ODSVRA Dust Control Program - New Vegetation Restoration Projects															
Scientific Name Common Name	Plant Counts Native Seed (lbs)	Season Totals	Sand Highway (east) 2022-VG-01	Sand Highway (west) 2022-VG-02	La Grille Hill 2022-VG-03	North Euc. Tree 2022-VG-04	Euc. Tree (north) 2022-VG-05	Euc. Tree (east) 2022-VG-06	La Grille Hill (south) 2022-VG-07	Euc. Tree 2022-VG-08	Euc. Tree (center) 2022-VG-09	Euc. Tree (south) 2022-VG-10	Boy Scout Camp 2022-VG-11	North Orion 2022-VG-12	South Orion 2022-VG-12
Acreage		119	14.6	11.3	19.9	4.6	5.5	3.3	22.7	2.9	14.9	2.4	6.3	4.9	5.7
Straw - (large bales)		430	-	-	280	66	45	-	-	-	-	-	39		
Fertilizer (lbs) - 15-15-15		2675	-	-	1000	235	290	160	-	140	-	-	320	250	280
Triticale Seed (lbs) - sterile		3550	175	125	1000	235	290	160	325	140	200	50	320	250	280
Jute Netting (acres)		1.9	-	-	-	-	-	-	-	1.9	-	-	-	-	-
Total plants		117,709	-	-	58,141	11,881	11,858	3,547	-	3,668	-	-	14,427	7,105	7,082
Total Native Seed (lbs)		540.1	-	-	219.1	45.2	53.9	24.0	-	19.6	-	-	61.1	59.8	57.5
Abronia latifolia		-	-	-	-	-	-	-	-	-	-	-	-	-	-
Yellow sand verbena		0.7	-	-	-	0.4	0.3	-	-	-	-	-	-	-	-
Abronia maritima		-	-	-	-	-	-	-	-	-	-	-	-	-	-
Sticky sand verbena		21.5	-	-	-	9.6	11.9	-	-	-	-	-	-	-	-
Abronia umbellata		-	-	-	-	-	-	-	-	-	-	-	-	-	-
Beach sand verbena		0.5	-	-	0.2	-	-	-	-	-	-	-	0.1	0.1	0.1
Acmispon glaber		2,874	-	-	1,329	245	245	-	-	-	-	-	539	245	271
Deerweed		21.3	-	-	10.9	1.4	1.5	1.0	-	0.8	-	-	2.7	2.2	0.8
Acmispon heermannii		-	-	-	-	-	-	-	-	-	-	-	-	-	-
Heermann's lotus		0.5	-	-	0.2	-	-	0.1	-	0.1	-	-	-	0.1	0.1
Achillea millefolium		8,863	-	-	4,413	980	833	294	-	294	-	-	530	980	539
Common yarrow		32.8	-	-	15.9	2.4	2.9	1.6	-	0.8	-	-	2.8	3.5	3.0
Ambrosia chamissonis		-	-	-	-	-	-	-	-	-	-	-	-	-	-
Beach bur		25.6	-	-	-	11.8	13.9	-	-	-	-	-	-	-	-
Astragalus nuttallii		461	-	-	45	-	-	147	-	269	-	-	-	-	-
Nuttall's milkvetch		2.7	-	-	-	-	-	1.4	-	1.2	-	-	-	-	-
Baccharis pilularis		368	-	-	-	-	-	294	-	74	-	-	-	-	-
Coyote brush		0.1	-	-	-	-	-	-	-	0.1	-	-	-	-	-
Camissoniopsis cheiranthifolia		2,764	-	-	706	735	735	-	-	-	-	-	588	-	-
Beach evening-primrose		0.0	-	-	-	-	-	-	-	0.0	-	-	-	-	-
Carex praegracilis		294	-	-	-	-	-	147	-	147	-	-	-	-	-

Scientific Name / Common Name	Plant Counts / Native Seed (lbs)	Season Totals	Sand Highway (east) 2022-VG-01	Sand Highway (west) 2022-VG-02	La Grille Hill 2022-VG-03	North Euc. Tree 2022-VG-04	Euc. Tree (north) 2022-VG-05	Euc. Tree (east) 2022-VG-06	La Grille Hill (south) 2022-VG-07	Euc. Tree 2022-VG-08	Euc. Tree (center) 2022-VG-09	Euc. Tree (south) 2022-VG-10	Boy Scout Camp 2022-VG-11	North Orion 2022-VG-12	South Orion 2022-VG-12
Field sedge		-	-	-	-	-	-	-	-	-	-	-	-	-	-
Chenopodium californicum		-	-	-	-	-	-	-	-	-	-	-	-	-	-
California goosefoot		0.8	-	-	0.4	-	-	-	-	-	-	-	0.1	0.1	0.2
Cirsium occidentale		-	-	-	-	-	-	-	-	-	-	-	-	-	-
Cobweb thistle		4.0	-	-	2.2	-	-	0.3	-	0.2	-	-	0.5	0.4	0.4
Corethrogyne filaginifolia		2,690	-	-	400	134	245	441	-	441	-	-	245	245	539
Common sandaster		21.9	-	-	10.1	1.4	1.4	0.9	-	0.8	-	-	2.4	2.5	2.4
Dudleya lanceolata		967	-	-	967	-	-	-	-	-	-	-	-	-	-
Southern California dudleya		0.4	-	-	0.2	-	-	0.0	-	0.0	-	-	0.1	0.1	0.1
Erigeron blochmaniae		4,201	-	-	2,058	232	245	147	-	147	-	-	588	245	539
Blochman's leafy daisy		14.0	-	-	6.2	0.5	0.6	0.3	-	0.3	-	-	2.3	1.9	2.0
Eriastrum densifolium		1,484	-	-	969	-	-	-	-	-	-	-	-	245	270
Giant eriastrum		0.1	-	-	-	-	-	0.0	-	0.0	-	-	-	-	-
Ericameria ericoides		8,437	-	-	4,934	245	490	294	-	294	-	-	637	735	808
Mock heather		135.6	-	-	57.4	5.9	7.3	4.0	-	3.4	-	-	16.4	19.5	21.8
Eriogonum parvifolium		7,693	-	-	3,969	490	490	294	-	294	-	-	637	980	539
Coastal buckwheat		51.4	-	-	26.0	2.4	2.9	0.8	-	0.7	-	-	7.3	6.5	4.9
Eriophyllum staechadifolium		8,095	-	-	4,665	735	490	147	-	147	-	-	637	735	539
Seaside golden yarrow		50.5	-	-	28.7	1.2	1.5	0.8	-	0.7	-	-	5.8	6.7	5.2
Erysimum suffrutescens		7,053	-	-	2,986	490	490	441	-	441	-	-	686	980	539
Suffrutescent wallflower		0.4	-	-	0.2	-	-	-	-	-	-	-	0.0	0.1	0.1
Horkelia cuneata		1,738	-	-	881	-	-	147	-	122	-	-	-	245	343
Wedge leaved horkelia		1.2	-	-	0.6	-	-	0.1	-	0.1	-	-	0.2	0.2	0.1
Juncus lescurii/breweri		539	-	-	-	-	-	294	-	245	-	-	-	-	-
Dune rush		8.3	-	-	-	-	-	4.5	-	3.8	-	-	-	-	-
Lupinus chamissonis		35,966	-	-	17,738	4,410	4,900	294	-	588	-	-	5,978	980	1,078
Dune bush lupine		32.8	-	-	12.9	2.4	2.9	1.6	-	1.2	-	-	4.5	3.2	4.1
Monardella undulata crispa		5,929	-	-	3,087	980	980	-	-	-	-	-	882	-	-
Crisp monardella		18.8	-	-	8.4	1.4	1.2	0.6	-	0.5	-	-	2.5	2.1	2.0

Scientific Name Common Name	Plant Counts Native Seed (lbs)	Season Totals	Sand Highway (east) 2022-VG-01	Sand Highway (west) 2022-VG-02	La Grille Hill 2022-VG-03	North Euc. Tree 2022-VG-04	Euc. Tree (north) 2022-VG-05	Euc. Tree (east) 2022-VG-06	La Grille Hill (south) 2022-VG-07	Euc. Tree 2022-VG-08	Euc. Tree (center) 2022-VG-09	Euc. Tree (south) 2022-VG-10	Boy Scout Camp 2022-VG-11	North Orion 2022-VG-12	South Orion 2022-VG-12
Morella californica		6	-	-	-	-	-	3	-	3	-	-	-	-	-
Wax myrtle		3.5	-	-	-	-	-	1.9	-	1.6	-	-	-	-	-
Phacelia ramosissima		8,155	-	-	4,431	980	735	-	-	-	-	-	1,225	245	539
Branching phacelia		70.6	-	-	29.7	3.5	4.4	3.2	-	2.7	-	-	10.6	8.7	7.9
Salix lasiolepis		315	-	-	254	-	-	16	-	15	-	-	30	-	-
Arroyo willow		-	-	-	-	-	-	-	-	-	-	-	-	-	-
Senecio blochmaniae		8,817	-	-	4,309	1,225	980	147	-	147	-	-	1,225	245	539
Dune ragwort		20.0	-	-	8.7	1.2	1.5	0.8	-	0.7	-	-	2.6	2.2	2.4
Total plants		117,709	-	-	58,141	11,881	11,858	3,547	-	3,668	-	-	14,427	7,105	7,082
Total Seed		540.1	-	-	219.1	45.2	53.9	24.0	-	19.6	-	-	61.1	59.8	57.5

2021/2022 ODSVRA Dust Control Program - Supplemental Vegetation Restoration Projects					
Scientific Name Common Name	Plant Counts Seed (lbs)	Season Totals	North Eucalyptus Tree 2019-VG-02	Eucalyptus Tree 2021-VG-03	Boy Scout Camp (Not Dust Control)
Acreage		3.43	0.74	1.57	1.12
Straw - (large bales)		45	-	9	36
Fertilizer (lbs) - 15-15-15		685	235	290	160
Triticale Seed (lbs) - sterile		685	235	290	160
Jute Netting (acres)		-	-	-	-
Total plants		7,671	1,546	3,479	2,646
Total Native Seed (lbs)		16.73	3.50	7.39	5.84
Acmispon glaber		294	98	147	49
Deerweed		0.8	0.2	0.3	0.3
Acmispon heermannii		-	-	-	-
Heermann's lotus		0.1	0.0	0.0	-
Achillea millefolium		588	98	294	196
Common yarrow		1.6	0.4	0.8	0.4
Camissoniopsis cheiranthifolia		359	65	196	98
Beach evening-primrose		-	-	-	-
Chenopodium californicum		-	-	-	-
California goosefoot		0.0	-	-	0.0
Cirsium occidentale		-	-	-	-
Cobweb thistle		0.2	0.1	0.1	0.1
Corethrogyne filaginifolia		11	11	-	-
Common sandaster		1.7	0.4	0.8	0.5
Dudleya lanceolata		-	-	-	-
Southern California dudleya		0.0	0.0	0.0	0.0
Erigeron blochmaniae		147	49	49	49
Blochman's leafy daisy		0.5	0.1	0.2	0.3
Ericameria ericoides		343	98	147	98
Mock heather		3.4	0.8	1.6	1.0
Eriogonum parvifolium		392	98	147	147
Coastal buckwheat		1.3	0.2	0.4	0.8
Eriophyllum staechadifolium		392	98	147	147
Seaside golden yarrow		1.3	0.2	0.4	0.8
Erysimum suffrutescens		343	98	147	98
Suffrutescent wallflower		-	-	-	-
Horkelia cuneata		-	-	-	-
Wedge leaved horkelia		0.1	0.0	0.0	0.0
Lupinus chamissonis		3,038	490	1,470	1,078
Dune bush lupine		1.7	0.4	0.8	0.5
Monardella undulata crispa		588	98	294	196
Crisp monardella		0.7	0.2	0.3	0.2
Phacelia ramosissima		686	147	294	245
Branching phacelia		3.4	0.8	1.6	1.0
Senecio blochmaniae		490	98	147	245
Dune ragwort		-	-	-	-
Total plants		7,671	1,546	3,479	2,646
Total Seed (lbs)		16.73	3.50	7.39	5.84

Oceano Dunes State Vehicular Recreation Area Dust Control Program

DRAFT 2022 Annual Report and Work Plan

ATTACHMENT 04

Oceano Dunes: Status 2022 (DRI Presentation)

THIS PAGE INTENTIONALLY LEFT BLANK.

ODSVRA Dust Control Program – 2022 ARWP Status Report

Dr. Jack Gillies, Dr. John Mejia

Desert Research Institute

PM_{10} Mass Emissions and Concentration Comparisons: Modeled 2013 Baseline and Modeled Pre-OHV Disturbance Conditions (1939 and 1966) based on SAG-suggested Assumptions (2022 ARWP Section 2.2.1.1)

Assumed Emissivity Conditions

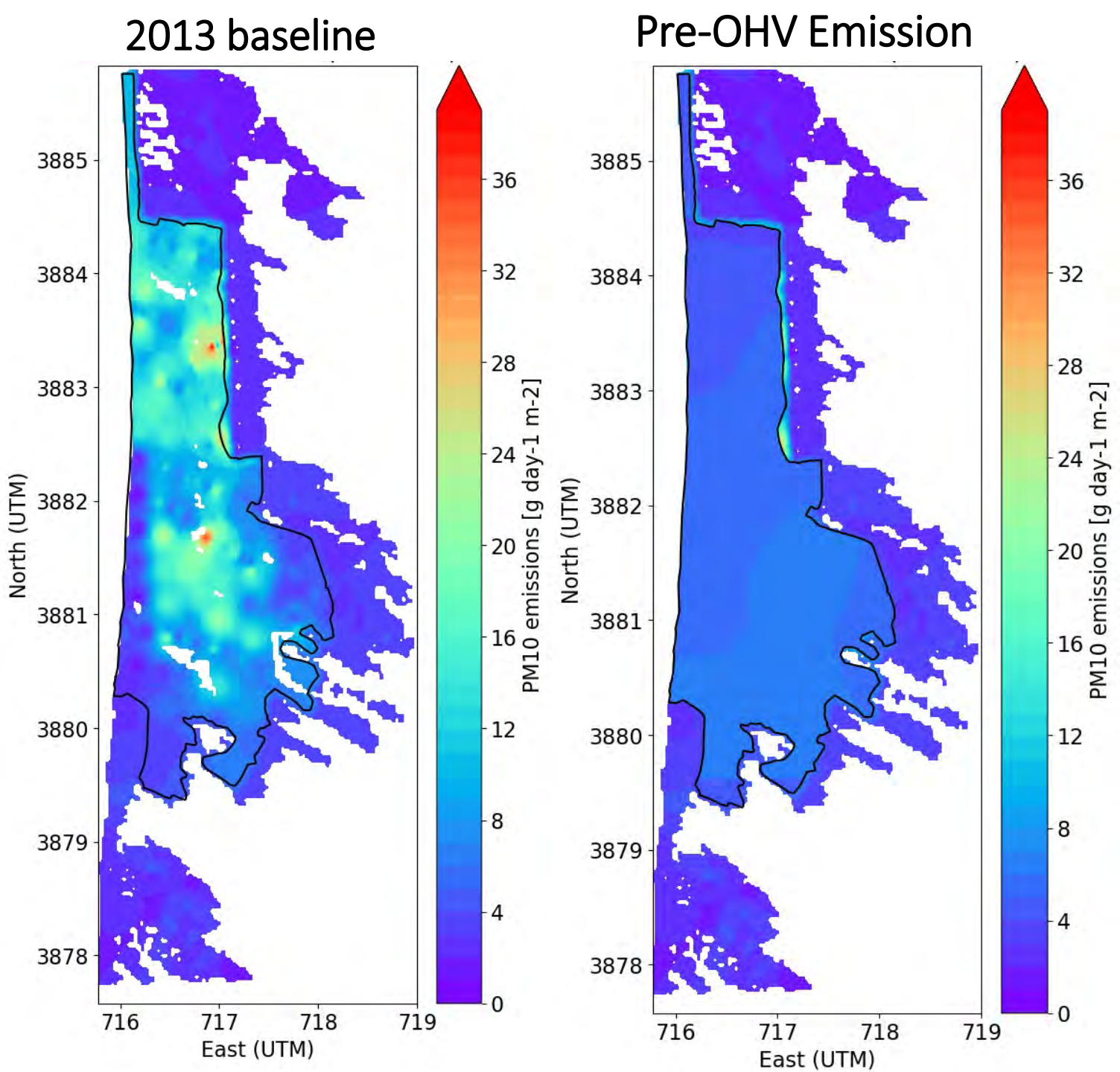

Mean Pre-OHV Emissions & Natural Vegetation Coverage (white empty cells)

1939 Vegetation

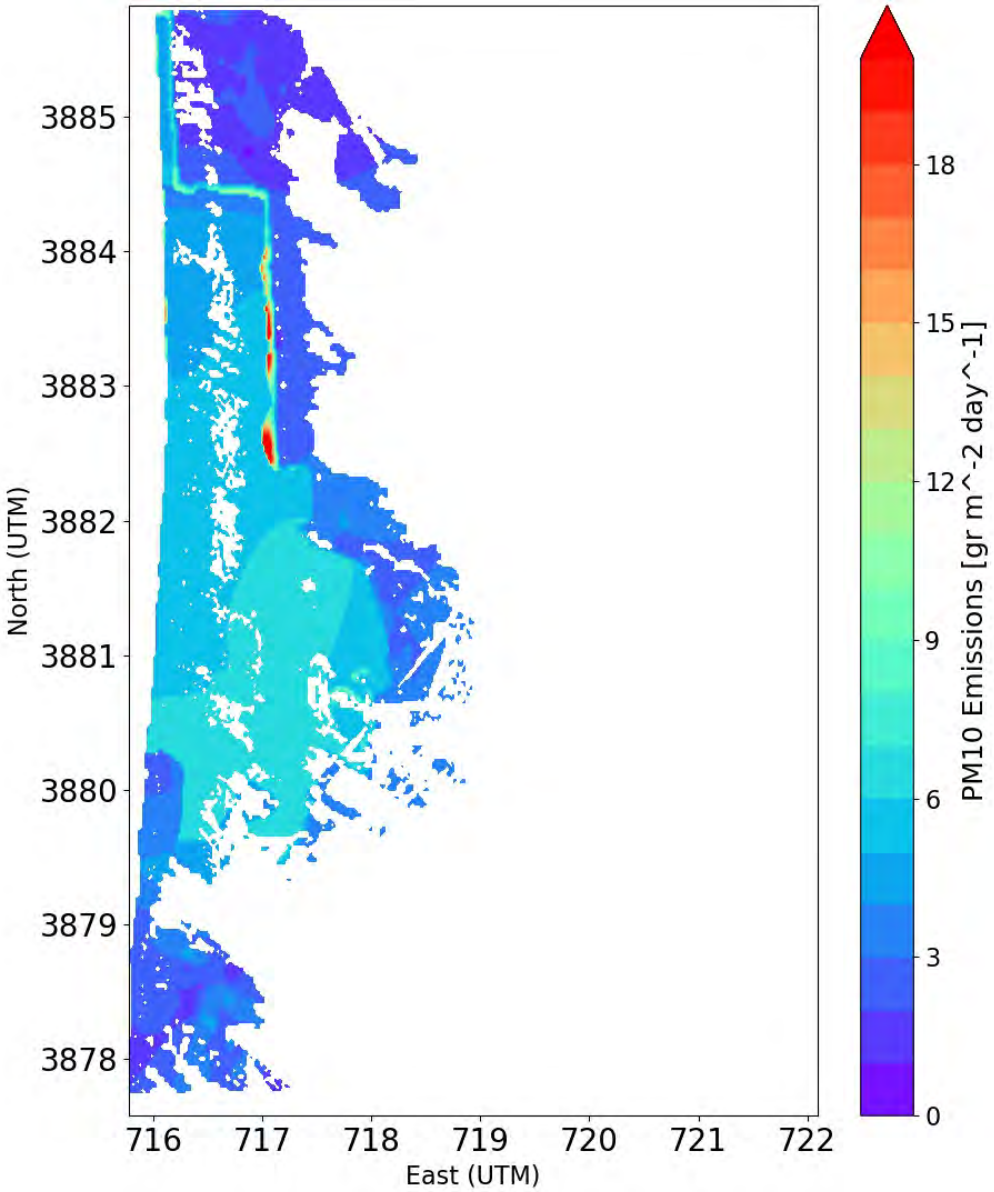

1966 Vegetation

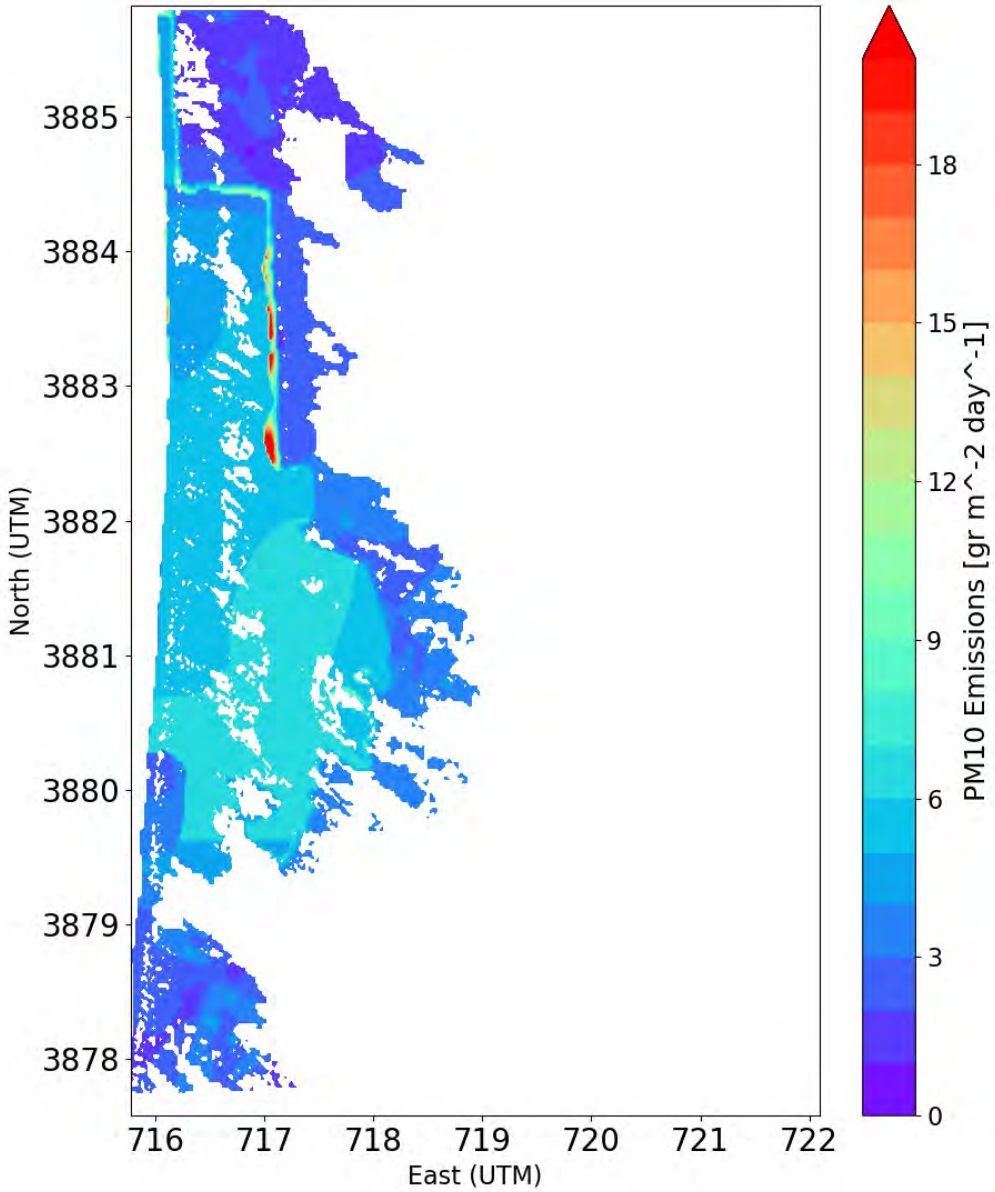

Baseline PM_{10} Mass Emission Estimates: 2013 Baseline*, Pre-OHV Emission Grid with 1939, 1966 Vegetation Maps, Open Riding Area (ORA) only

10 highest emission days	Mass Emissions [Metric Tons/day] and % Change from 2013 Baseline
2013 Baseline	182.8
Pre-OHV Emission Grid and 1939 Vegetation	108.4 (40.7%)
Pre-OHV Emission Grid and 1966 Vegetation	108.9 (40.4%)

Modeled Baseline PM_{10} Concentrations at CDF (10 highest emissions days; 24-hour mean): 2013 SOA Baseline Scenario, 1939 Pre-OHV Disturbance Scenario, and 1966 Pre-OHV Disturbance Scenario

CDF	
10 Highest Emission Days	PM_{10} [µg m^{-3}]
Observations	128.2
Modeled Baseline 2013	124.7
Modeled Pre-disturbance Baseline & 1939 vegetation removal	88.0
Modeled Pre-disturbance Baseline & 1966 vegetation removal	87.0

Modeled Baseline PM_{10} Concentrations at Mesa 2 (10 highest emissions days; 24-hour mean): 2013 SOA Baseline Scenario, 1939 Pre-OHV Disturbance Scenario, and 1966 Pre-OHV Disturbance Scenario

Mesa2	
10 Highest Emission Days	PM_{10} [µg m^{-3}]
Observations	95.4
Modeled Baseline 2013	97.5
Modeled Pre-disturbance Baseline & 1939 vegetation removal	71.2
Modeled Pre-disturbance Baseline & 1966 vegetation removal	75.7

Current DRI Model Estimates of PM_{10} Mass Emission and Concentration Reductions (2022 ARWP Sections 2.2.3.1, 2.2.4.1, and 2.2.4.3)

2021 and 2022 Dust Control Program Measures

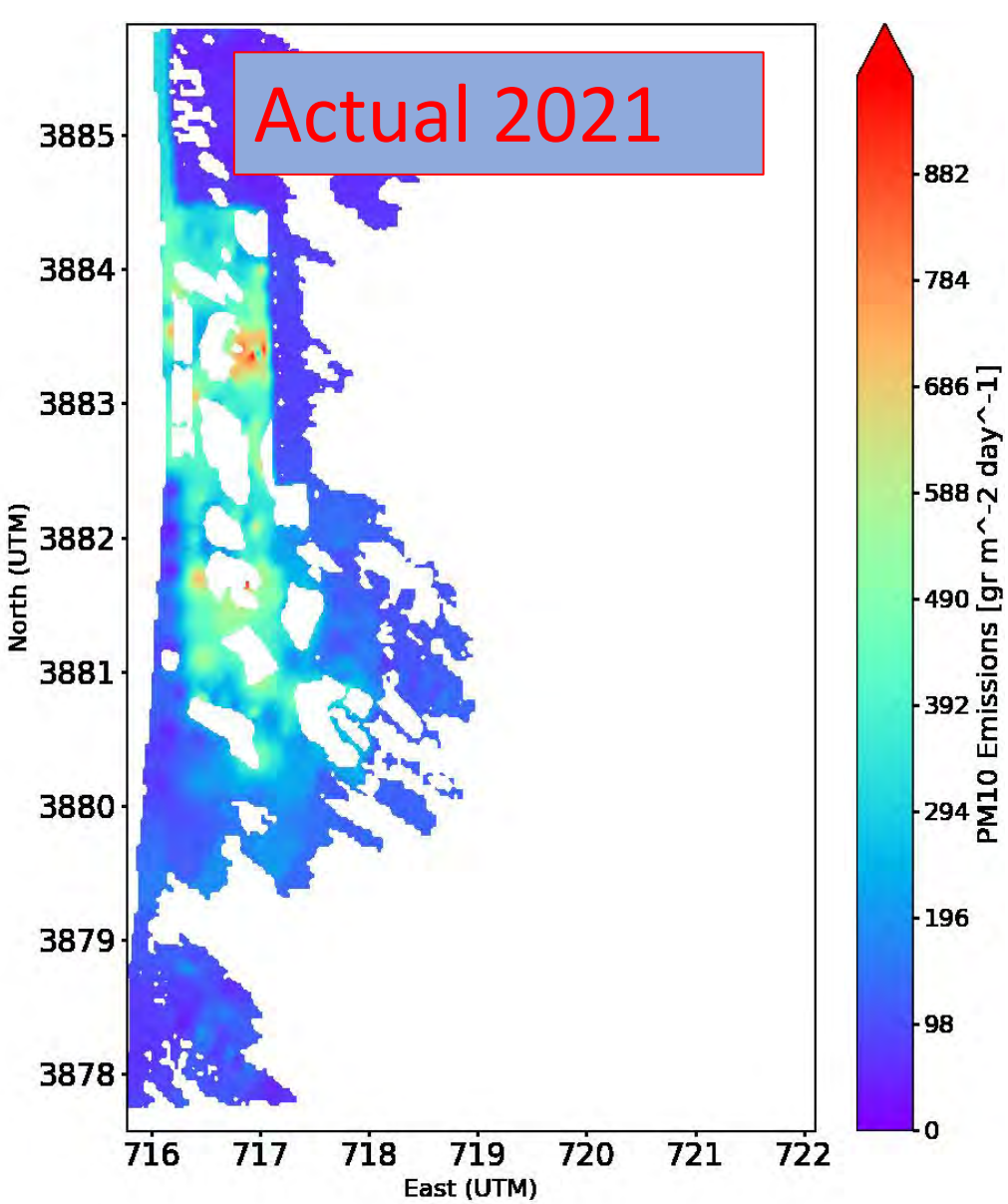

New 2022 treatments

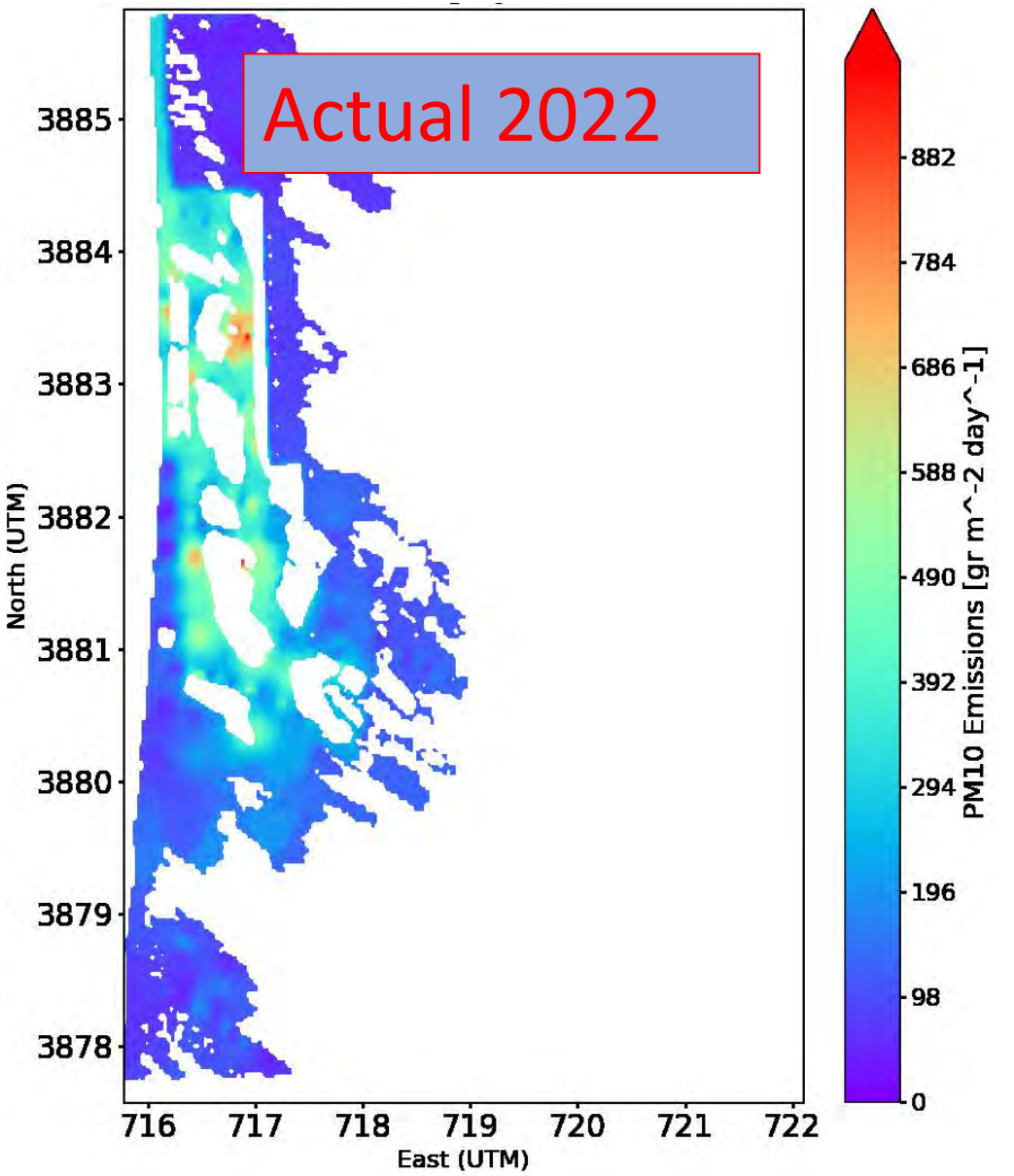

Current DRI Model: 2022 Dust Control Program Mass Emissions Reductions Estimates

							Riding and non-riding areas				Riding areas only			
Polygon ID	Description	Year Implemented	Status	Area Polygon [Acres]	Area Model [Acres]	Area treated [Acres]	Emissions [Metric Tons/day]	Abatement [Metric Tons/day]	Cumulative Abatement [Metric Tons/day]	Cumulative Abatement [%]	Emissions [Metric Tons/day]	Abatement [Metric Tons/day]	Cumulative Abatement [Metric Tons/day]	Cumulative Abatement [%]
55	straw bales near S1 tower	2011	Removed	1.05	1.09	1.09	182.80	0.00	0.00	100.00	182.80	0.00	0.00	100.00
53	APCD Test Plot	2012	Vegetation	1.07	1.09	0.00	182.80	0.00	0.00	100.00	182.80	0.00	0.00	100.00
54	Enigma	2013	Vegetation	1.96	1.96	0.33	182.78	0.02	0.02	99.99	182.80	0.00	0.00	100.00
52	Crescent	2013	Vegetation	1.77	1.85	0.11	182.78	0.01	0.02	99.99	182.80	0.00	0.00	100.00
3	'14	2014	Removed	13.50	13.51	13.51	182.78	0.00	0.02	99.99	182.80	0.00	0.00	100.00
47	Trial area 2014	2014	Vegetation	30.05	29.86	28.01	181.51	1.27	1.29	99.30	182.80	0.00	0.00	100.00
2	'15	2015	Removed	36.64	37.16	37.16	181.51	0.00	1.29	99.30	182.80	0.00	0.00	100.00
4	'16	2016	Removed	41.35	42.17	42.17	181.51	0.00	1.29	99.30	182.80	0.00	0.00	100.00
5		2016	Removed	0.75	0.76	0.76	181.51	0.00	1.29	99.30	182.80	0.00	0.00	100.00
73	Wind fence 2017	2017	Removed	19.83	19.51	19.51	181.51	0.00	1.29	99.30	182.80	0.00	0.00	100.00
44	Dust reduction project Spring 2018	2017	Vegetation	9.27	9.37	9.37	180.16	1.35	2.63	98.56	181.45	1.35	1.35	99.26
45	Dust reduction project Spring 2018	2017	Vegetation	9.08	8.83	8.83	178.69	1.48	4.11	97.75	181.45	0.00	1.35	99.26
8		2017	Removed	0.75	0.76	0.76	178.69	0.00	4.11	97.75	181.45	0.00	1.35	99.26
39	Stipulated Abatement Order 2018	2018	Vegetation	26.99	26.81	26.81	174.73	3.96	8.07	95.59	177.49	3.96	5.30	97.10
40	Stipulated Abatement Order 2018	2018	Vegetation	6.55	6.97	6.97	173.70	1.03	9.10	95.02	176.46	1.03	6.34	96.53
41	Stipulated Abatement Order 2018	2018	Vegetation	9.14	8.83	8.83	172.74	0.96	10.06	94.50	175.50	0.96	7.29	96.01
42	Stipulated Abatement Order 2018	2018	Vegetation	7.94	7.96	7.96	171.79	0.95	11.01	93.98	174.55	0.95	8.24	95.49
43	Stipulated Abatement Order 2018	2018	Vegetation	5.50	5.45	5.45	170.78	1.01	12.02	93.43	173.54	1.01	9.25	94.94
46	Dust reduction project Spring 2018	2018	Vegetation	28.64	28.01	27.79	166.23	4.55	16.56	90.94	169.00	4.55	13.80	92.45
48	SAO installed and removed 2018	2018	Removed	9.01	9.37	9.37	166.23	0.00	16.56	90.94	169.00	0.00	13.80	92.45
49	Foredune December 2019	2019	Vegetation	9.94	9.92	9.92	164.40	1.83	18.39	89.94	167.17	1.83	15.63	91.45
50	Foredune December 2019	2019	Vegetation	18.98	19.40	19.40	161.24	3.16	21.56	88.21	164.00	3.16	18.79	89.72
51	Foredune December 2019	2019	Vegetation	19.07	19.29	19.29	157.98	3.26	24.82	86.42	160.74	3.26	22.06	87.93
9	Vegetation	2020	Vegetation	4.09	4.03	4.03	157.39	0.58	25.40	86.10	160.16	0.58	22.64	87.62
10	Wind Fence	2020	Vegetation	19.81	19.94	19.94	155.41	1.99	27.39	85.02	158.17	1.99	24.63	86.53
11	Wind Fence	2020	Wind Fence	20.47	21.03	21.03	153.12	2.28	29.67	83.77	156.18	1.99	26.62	85.44
83	New vegetation	2021	Vegetation	5.74	5.88	5.88	152.51	0.61	30.28	83.43	155.57	0.61	27.23	85.11
80	New vegetation	2021	Vegetation	4.61	4.58	4.58	152.06	0.45	30.73	83.19	155.12	0.45	27.68	84.86
82	New vegetation	2021	Vegetation	4.87	5.01	5.01	151.48	0.58	31.31	82.87	154.54	0.58	28.26	84.54
81	New vegetation	2021	Vegetation	6.30	6.43	5.88	150.67	0.81	32.12	82.43	153.73	0.81	29.07	84.10
56	Proposed shape - in ground but this is not	2021	Wind Fence	10.81	10.79	10.68	148.57	2.11	34.23	81.27	151.62	2.11	31.17	82.95
67	Proposed	2021	Vegetation	18.38	18.31	17.87	147.69	0.88	35.11	80.79	151.62	0.00	31.17	82.95
66	Proposed	2021	Vegetation	4.02	4.03	4.03	147.49	0.21	35.31	80.68	151.62	0.00	31.17	82.95
65	Proposed	2021	Vegetation	4.17	4.36	4.36	147.26	0.23	35.54	80.56	151.62	0.00	31.17	82.95
57	Proposed shape - in ground but this is not	2021	Wind Fence	21.71	21.79	21.47	144.46	2.80	38.34	79.03	148.83	2.80	33.97	81.42
91	New vegetation	2021	Vegetation	2.90	3.16	2.94	143.78	0.68	39.01	78.66	148.15	0.68	34.65	81.05
70	Actual GPSd 3/31/21	2021	Vegetation	3.22	3.27	3.16	143.00	0.78	39.80	78.23	147.37	0.78	35.43	80.62
92	New vegetation	2021	Vegetation	5.48	5.45	5.45	142.04	0.96	40.76	77.70	146.40	0.96	36.39	80.09
84	New vegetation	2022	Vegetation	2.40	2.40	2.40	141.52	0.51	41.27	77.42	145.89	0.51	36.91	79.81
85	New vegetation	2022	Vegetation	14.86	14.71	14.71	138.35	3.17	44.44	75.69	142.72	3.17	40.08	78.08
86	Straw treatment	2022	Straw	11.84	12.10	12.10	136.02	2.33	46.78	74.41	140.39	2.33	42.41	76.80
87	New vegetation	2022	Vegetation	42.24	22.67	22.67	134.21	1.81	48.59	73.42	138.70	1.69	44.10	75.88
88	New vegetation	2022	Vegetation	14.63	14.38	14.38	132.02	2.19	50.78	72.22	138.58	0.12	44.22	75.81
89	Straw treatment	2022	Straw	12.33	12.10	12.10	129.62	2.40	53.18	70.91	136.23	2.35	46.57	74.52
90	New vegetation	2022	Vegetation	11.31	11.66	11.66	127.45	2.17	55.35	69.72	134.11	2.12	48.69	73.36
32	PloverExclosure	2022	None	293.25	292.92	292.92	108.20	19.24	74.59	59.19	114.92	19.18	67.87	62.87

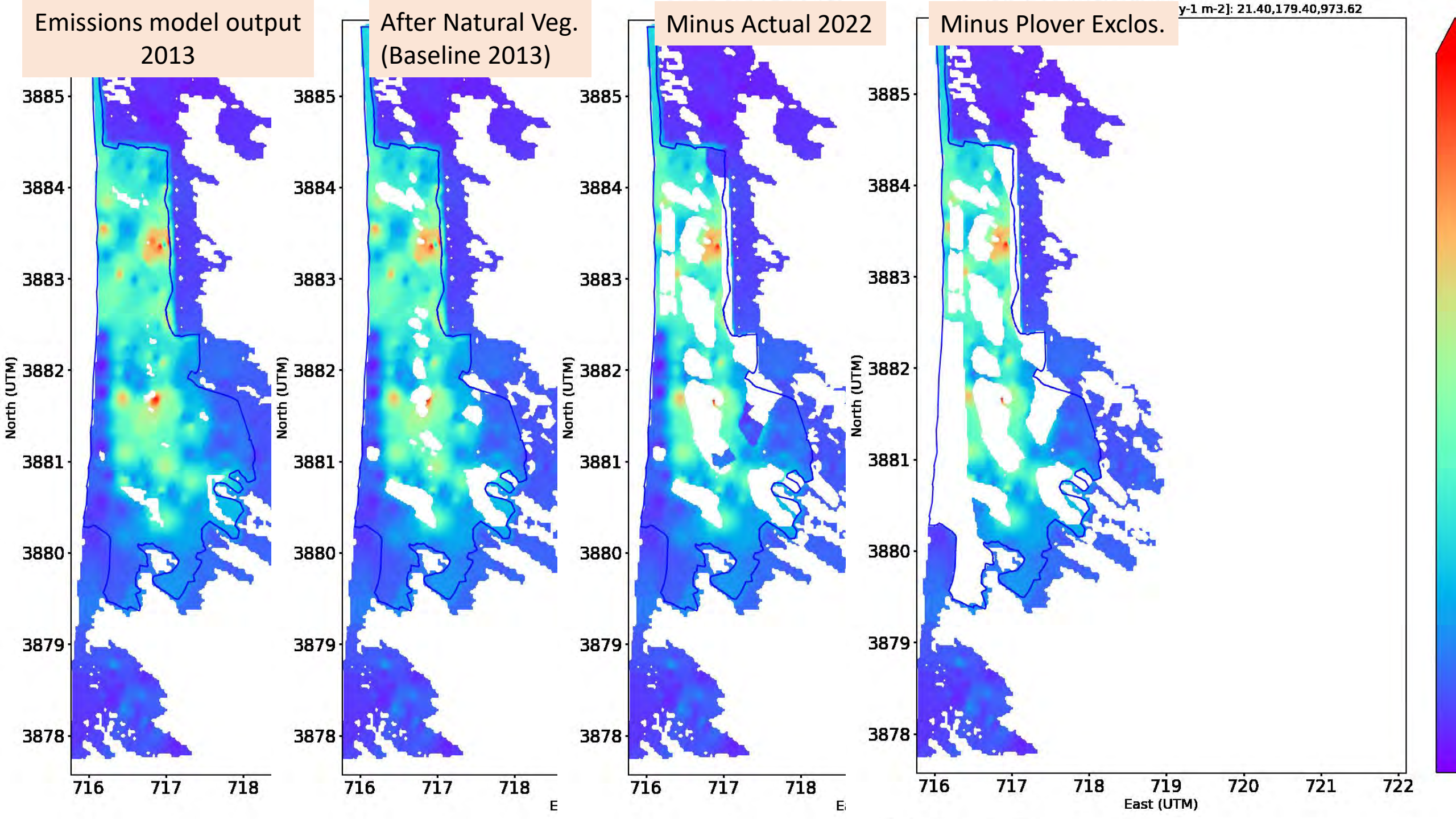
Emissions model output 2013
After Natural Veg. (Baseline 2013)
Minus Actual 2022
Minus Plover Exclos.
y-1 m-2]: 21.40,179.40,973.62
North (UTM)
East (UTM)
3885
3884
3883
3882
3881
3880
3879
3878
716
717
718
719
720
721
722

Current DRI Model: 2022 Dust Control Program Mass Emissions Reductions Estimates

	2013
Emissions baseline ORA Only [Metric Tons/day]	182.8
Emissions 2022 ORA Only [Metric Tons/day]	108.2
Mass reduction relative to 2013 (182.8 Metric Tons/day) [Metric Tons/day]	74.6
% Reduction relative to 2013 (182.8 Metric Tons/day)	59.2

Current DRI model: 2022 dust control program concentration reductions estimates

CDF

Concentration at CDF (24-hour means)	PM10 [microg/m^3]	% left after Removing
Mean 15 May-15 July		
Observations	52.4	
Modeled Baseline	51.1	100.0
Modeled Removing 2011-2020	33.8	65.5
Modeled Removing 2011-2021	33.5	62.5
2022 Actual	31.0	60.6
2022 Actual + Plover Exclosure	30.5	59.7
10 Highest Emission Days	PM10 [microg/m^3]	% left after Removing
Observations	128.2	
Modeled Baseline	124.7	100.0
Modeled Removing 2011-2020	72.4	58.1
Modeled Removing 2011-2021	72.2	57.9
2022 Actual	66.4	53.3
2022 Actual + Plover Exclosure	65.7	52.7
Modeled Pre-disturbance Baseline & 1939 vegetation removal	88.0	
Modeled Pre-disturbance Baseline & 1966 vegetation removal	87.0	

Mesa 2

Concentration at Mesa 2 (24-hour means)	PM10 [microg/m^3]	% left after Removing
Mean 15 May-15 July		
Observations	39.7	
Modeled Baseline	34.4	100.0
Modeled Removing 2011-2020	32.2	93.6
Modeled Removing 2011-2021	27.1	78.8
2022 Actual	24.8	72.1
2022 Actual + Plover Exclosure	22.4	65.0
10 Highest Emission Days	PM10 [microg/m^3]	% left after Removing
Observations	95.4	
Modeled Baseline	97.5	100.0
Modeled Removing 2011-2020	91.2	93.6
Modeled Removing 2011-2021	73.8	75.8
2022 Actual	66.9	68.6
2022 Actual + Plover Exclosure	59.9	61.3
Modeled Pre-disturbance Baseline & 1939 vegetation removal	71.2	
Modeled Pre-disturbance Baseline & 1966 vegetation removal	75.7	

Revised DRI Model Estimates of PM_{10} Mass Emission and Concentration Reductions (2022 ARWP Sections 2.2.3.2, 2.2.4.2, and 2.2.4.4)

SAG-Recommended Changes to the Current DRI Model

- Future projects area based on 2019 data.
- Wind Fence abatement efficiency 72%
- Foredune (mean non-riding area): E (mg m-2 s-1)=21.51 u*^6.85
- Plover Exclosure based on observations and take 50% credit.
- CFD recovery curve (wake effect) downstream Foredune and Oso Flaco.

Revised DRI Model: 2022 Dust Control Program Mass Emissions Reductions Estimates

	2013	2019 SAG Improvements
Emissions baseline ORA only [Metric Tons/day]	182.8	182.8
Emissions 2022 ORA only [Metric Tons/day]	108.2	104.0
Mass reduction relative to 2013 (182.8 Metric Tons/day) [Metric Tons/day]	74.6	78.8
% Reduction relative to 2013 (182.8 Metric Tons/day)	59.2	56.9
Area project left to reach 40.7 % [acres]	0	0
SAG improvements include: Foredune non-riding area; Plover Exclosure using emissions data but 50% credited (SAG approved); Foredune and Oso Flaco wake effect (CFD study); wind fence only removes 72%.		
Foredure Obs and non-riding	8.26	3.37
Computational Fluid Dynamics (Foredure and Oso flaco wake effect)	0.00	1.86
Plover Exclosure Credit	19.40	9.25

Revised DRI Model: 2022 Dust Control Program Concentration Reductions Estimates at CDF

CDF		
10 Highest Emission Days	PM_{10} [µg m^{-3}]	% Change from 2013 Baseline, Pre-OHV Baseline 1939 & 1966 Vegetation
Observations	128.2	
Modeled Baseline 2013	124.7	
Modeled Pre-disturbance Baseline & 1939 vegetation removal	88.0	
Modeled Pre-disturbance Baseline & 1966 vegetation removal	87.0	
2021 Controls in Place (322.5 acres) Current	72.2	-42.1 (2013), -17.9 (1939), -17.0 (1966)
2022 Controls in Place (412.5 acres) Current	**66.4**	**-46.7 (2013), -24.5 (1939), -23.7 (1966)**
2022 Controls in Place (412.5 acres) + revised model (SAG Revisions)	**63.8**	**-48.8 (2013), -27.5 (1939), -26.6 (1966)**

Revised DRI Model: 2022 Dust Control Program Concentration Reductions Estimates at Mesa 2

Mesa 2		
10 Highest Emission Days	PM_{10} [µg m^{-3}]	% Change from 2013 Baseline, Pre-OHV Baseline 1939 & 1966 Vegetation
Observations	95.4	
Modeled Baseline 2013	97.5	
Modeled Pre-disturbance Baseline & 1939 vegetation removal	71.2	
Modeled Pre-disturbance Baseline & 1966 vegetation removal	75.7	
2021 Controls in Place (322.5 acres) Current	73.8	-24.3 (2013), +3.7 (1939), -2.6 (1966)
2022 Controls in Place (412.5 acres) Current	**66.9**	**-31.3 (2013), -6.0 (1939), -11.6 (1966)**
2022 Controls in Place (412.5 acres) + revised model (SAG Revisions)	**63.7**	**-34.6 (2013), -10.5 (1939), -15.8 (1966)**

Oceano Dunes State Vehicular Recreation Area Dust Control Program

DRAFT 2022 Annual Report and Work Plan

ATTACHMENT 05

Summary of Vegetation Monitoring of Restoration Sites at ODSVRA (2021)

(State Parks ARWP Work Product)

THIS PAGE INTENTIONALLY LEFT BLANK.

Summary of Vegetation Monitoring of Restoration Sites at ODSVRA (2021)

Line Intercept Transect Sampling

Methods

Line Intercept method (Line intercept: % cover = distance a+b+c+d+e+f / total transect length, where a, b, c, etc. are the intercept lengths of vegetation canopy) was used to estimate percent cover of species within each project area.

For this assessment both foredune and back dune project areas and reference sites were sampled. Reference sites were selected in areas that had been closed to vehicular activity for at least 20 years and had not been subject to restoration plantings in the past. Within back dune habitats, early succession communities (early seral) and climax communities (late seral) can vary considerably in species composition and percent cover. For this reason, both early seral and late seral reference sites were sampled for comparison.

Within each foredune project area and reference site, a total of four transects of 30 meters each were sampled. Within each back dune project area and reference site, a total of three transects of 30 meters each were sampled. In 2021, the project areas that were surveyed included the 48-Acre Foredune (planted February 2020), North Eucalyptus Tree (planted February 2019) and La Grille Hill (planted February 2019). In 2020, the 48-Acre Foredune and BBQ Flats (planted February 2019) were sampled.

Starting points for the transect lines were randomly selected within each project area using GIS software. Three transect lines in each project area were randomly selected from the eight cardinal and intermediate directions (i.e. N, NE, E, SE, S, SW, W, and NW). For the 2021 survey within the 48-Acre Foredune Project Area, a fourth transect line was included in each treatment area and was run parallel to the direction of the prevailing wind.

A measuring tape was run along the transect and secured with wooden stakes. As the vegetation canopy intersected the line, the species was noted on the datasheet along with the beginning and ending measurements of the canopy under “Start” and “Stop”. When the canopies of two different species overlapped, each species was documented separately as two different canopies. A closed canopy for a given species was assumed until gaps in vegetation exceed the width of 5 centimeters. All dead woody vegetation was included separately and noted as “Dead” unless it was clearly the result of seasonal dieback of a perennial plant that was still viable.

Once each 30-meter transect was surveyed, a walk around assessment within an area of 10 meters from the transect line was conducted and all addition observed species were noted.

Results

48-acre Foredune Project

In 2021, after the second growing season for the project area, none of the treatment areas met the vegetative cover of the reference site at 23.03% vegetative cover and only one of the six treatment areas met the species diversity of the reference site with at least 10 species represented. However, an increase in vegetation cover was observed in each of the treatment areas except for the control, which showed no change. The treatment area that saw the highest percent cover was Area 3 with 12.66%

cover followed closely by Area 3 with 12.31% cover. Both Area 5 and Area 6 showed the highest level of species diversity with 10 and 8 species represented respectively in each area. The plant cover was highly variable between transects in all treatment areas due to the clustered pattern of the vegetation. Area 6 had the lowest level of variability with a percent cover of 12.66% and a 95% confidence interval of ±9.52% (Refer to Table 1 and Figure 1).

Comparison of Line Intercept Transect Sampling Method and Results from Independent Studies

State Parks methods were designed to monitor the establishment of vegetation cover and species richness within specific project areas. Two recent and independent reports also evaluated vegetation cover within the ODSVRA using aerial imagery to analyze total vegetation cover, each using different imagery sources. Both studies were used to cross reference the State Parks results. These reports include:

UCSB Historical Vegetation Cover Change Analysis (1930-2020) within the Oceano Dunes SVRA" (N. Swet, Z. Hilgendorf, I. Walker, December 28, 2021). Published as Attachment 07-04 in the 2022 ARWP

Hilgendorf, Z., Turner, C, Walker, I.J. UCSB-ASU 2020-2021 ODSVRA Foredune Restoration UAS Survey Report. 37p. Produced for CDPR-ODSVRA and published as Attachment 8 in the 2021 ARWP.

The aerial imagery analysis of the North Oso Flaco foredune presented in (Swet et al., 2021) covered the same area as the State Parks transect monitoring reference site in North Oso Flaco and found that vegetation cover ranged from between 24.41% in 2012 and 19.05% in 2020. State Parks vegetation monitoring of the area corroborates these findings with a vegetation cover mean of 23.0% in the fall of 2021. It should be noted that State Parks sampled only four (4) randomly selected 30-meter transects within the area with a high degree of variation between samples (± 39.66% for 95% confidence interval) and that the aerial imagery analysis looked at the entire area so some variation in the results between the two studies is expected. For the remainder of the study, (Swet et al., 2021) did not analyze project specific areas that are comparable with the State Parks transects so further analysis of their source imagery would need to be conducted to cross-reference their study with State Parks transect monitoring.

In (Hilgendorf et al., 2021) the authors did analyze vegetation cover within specific project areas but limited their analysis to the 48 Acre Foredune Project. A comparison of the two studies can be seen in Table 2 below. In general, State Parks results follow a similar pattern as (Hilgendorf et al., 2021) with vegetation cover increasing over time across all treatment areas except the control (Area 1). When comparing results from the fall of 2020, the only monitoring season that was the same for both studies, the treatment areas rank in a similar order with only Areas 4 and 5 ranking differently. This difference in ranking between Area 4 and 5 is also seen in subsequent seasons. It would be expected that Area 5 would have a higher percent cover than Area 4 given that it was planted at a higher density, which is consistent with the assessment in (Hilgendorf et al., 2021) but not with State Parks transect monitoring. This inconsistency is likely a result of the State Parks transects having high degree of variability in cover between transects and a small sample size. This is apparent in the large 95% confidence interval in comparison to the mean. For example, in 2021 Area 5 had a mean of 2.14% and a 95% confidence interval of ±4.29% and Area 4 had a mean of 5.69% with a 95% confidence interval of ±8.70%. Furthermore, when comparing the results from the State Parks transect monitoring with the results from (Hilgendorf et al., 2021) it needs to be clarified that the two studies had differing ways of defining

vegetation and therefore variation in the results is expected between the two studies. State Parks transect monitoring measured canopy cover, ignoring small gaps between leaves or stems (<5 cm), and included all parts of the vegetation canopy, not only the leaf cover, but also the woody stems and seasonally dormant plants. (Hilgendorf et al., 2021) used 5-band multispectral imagery acquired from uncrewed aerial system (UAS) surveys and Normalized Difference Vegetation Index (NDVI) method to determine vegetation cover. NDVI looks at the differences in reflected near infrared light and red light which in turn is used to determine leaf cover. This is noteworthy because with NDVI method seasonal variations in cover are expected as seasonal changes in the leaf cover occurs. Also, NDVI does not tend to consider live woody stems or dormant vegetation that does not have photosynthesizing leaves. For these reasons, it is expected that the results of the two studies would vary, specifically when data was collected in different seasons. Furthermore, because (Hilgendorf et al., 2021) used a more limiting method in how vegetation cover was classified, it is expected that their results would show lower percent cover for data collected within the same season.

Back Dune Projects

All back dune project areas that were surveyed showed healthy levels of vegetation cover and showed similar vegetation composition compared to the early seral reference site. Of the 20 native species present within the early seral reference site, the project areas had between 12 and 14 of them and a total native species richness of between 16 and 23 species. The dominant species within the early seral reference site, *Lupinus chamissonis*, showed similar percent cover in the project areas with a mean cover of 27.84% in the project areas and 29.27% in the reference site. All project areas had lower percent cover than both reference sites. However, growth is anticipated to continue and percent cover is anticipated to approach the cover of the reference sites within the upcoming growing seasons. Refer to Table 3 and Figure 2.

Photo Point Monitoring

On-the-ground photo point monitoring was conducted at the 48-Acre Foredune project prior to project installation in February 2020 and following project installation in May 2020, October 2020 and October 2021. Photo point monitoring is scheduled to continue in October in future years. Photo points are located on all four corners of each treatment area. For each photo point, two photos are taken, each with one of the treatment area boundary lines on the outer edge of the photo with the interior of the treatment area centered in the photo. There is also one photo point overlooking the entire 48-Acre Foredune project from a distance. Refer to figures 3 and 4. On-the-ground photo point monitoring was also conducted throughout the back dune project areas during the Summer and Fall of 2021 and has been conducted annually since 2018. Back dune photo points are positioned to capture changes within the general areas where back dune projects are located. The number of photos for each photo point and the number of photo points varies at each location to sufficiently capture each area. In total, 53 photo points were monitored in the back dunes in 2021. Refer to figures 5-8. In addition to on-the-ground monitoring, drone aerial imagery photo point monitoring was conducted in May 2020, December 2020 and December 2021. Within the 48-Acre Foredune, two photo points were taken of each treatment area, one from the east and one from the west for each area. In addition, drone photo points were conducted within the back dune project areas in December 2020 and 2021. The number of photos for each photo point and the number of photo points varied at each location to sufficiently capture each area. Refer to figure 9-12. Both on-the-ground and drone photo point monitoring are scheduled to continue annually.

Table 1. Table of results from the 48 Acre Foredune Restoration Project line intercept transect sampling.

Foredune Restoration Project Vegetation Assessment							
*Non-native species P=Present within 10m of transect	**Area 1 Control**	**Area 2 Native Seed**	**Area 3 Native Seed & Grain Seed**	**Area 4 Low Density Nodes**	**Area 5 High Density Nodes**	**Area 6 Parks Classic**	**Reference North Oso Flaco Foredune**
Age of Planting (years)	**1.5**	**1.5**	**1.5**	**1.5**	**1.5**	**1.5**	**-**
Species Richness	**0**	**4**	**5**	**6**	**10**	**8**	**10**
Total Percent Cover	**0.00%**	**1.91%**	**12.31%**	**5.69%**	**2.14%**	**12.66%**	**23.03%**
95% Confidence Interval	**±0.00%**	**± 6.07%**	**± 20.86%**	**± 8.70%**	**± 4.29%**	**± 9.52%**	**± 39.66%**
Species	**Percent Cover**						
Abronia maritima	-	0.95%	11.59%	4.09%	p	4.90%	15.48%
Ambrosia chamissonis	-	0.60%	1.41%	1.73%	0.79%	3.05%	5.73%
**Cakile maritima*	-	0.58%	p	p	p	0.03%	3.15%
**Carpobrotus sp.*	-	-	-	-	-	-	1.38%
Malicothrix incana	-	-	-	p	p	0.38%	0.34%
Calestegia soldanella	-	-	-	-	-	-	0.13%
Camissoniopsis cheiranthifolia	-	-	p	0.03%	1.03%	4.30%	0.02%
Abronia latifolia	-	p	p	-	p	p	p
Erigeron blochmaniae	-	-	-	-	-	-	p
Senecio blochmaniae	-	-	-	-	-	-	p
Atriplex leucopylla	-	-	-	0.95%	0.57%	p	-
Eriophyllum staechadifolium	-	-	-	-	p	0.08%	-
Achillea millefolium	-	-	-	-	p	-	-
Monardella undulata crispa	-	-	-	-	p	-	-

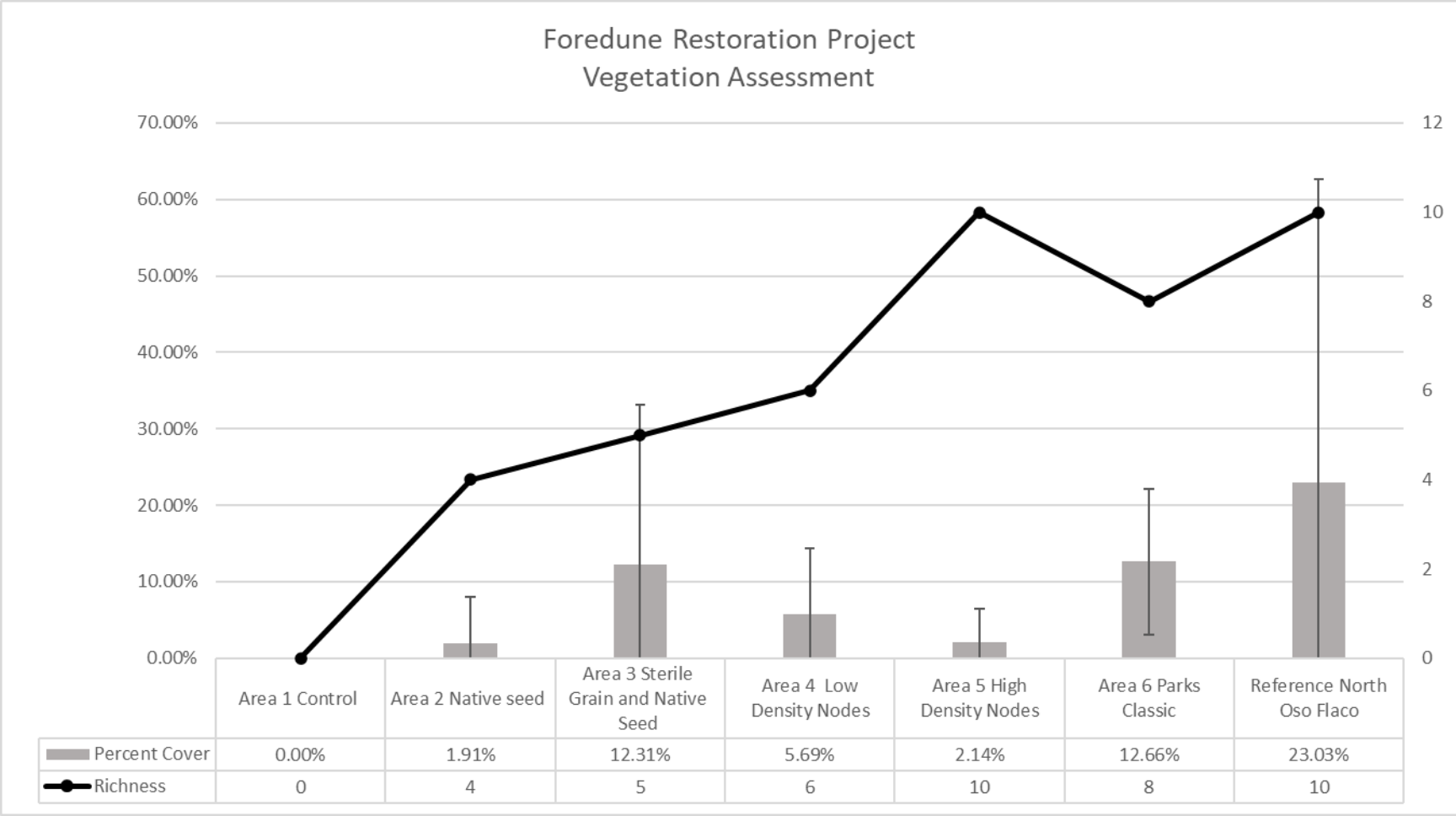

Figure 1. Vegetation composition in 48 Acre Foredune project areas compared to reference site. Error bars are 95% confidence intervals. Four 30-meter transects were sampled in each of the Foredune areas and Reference Site.

Table 2. Comparison of Vegetation Cover between State Parks Transect Monitoring and the (Hilgendorf et al., 2021) Survey Report.

48 Acre Foredune	Area 1	Area 2	Area 3	Area 4	Area 5	Area 6
Parks-Fall 2020 (mean of three 30-meter transects)	0.0%	0.1%	4.02%	0.76%	0.4%	3.57%
UCSB/ASU -Oct 2020 (total area)	0.02%	0.37%	2.36%	0.79%	1.51%	2.16%
UCSB/ASU-Feb 2020 (total area)	0.04%	0.58%	3.21%	1.29%	2.4%	4.91%
Parks-Fall 2021 (mean of four 30-meter transects)	0.0%	1.9%	12.3%	5.7%	2.1%	12.7%

Table 3. Table of results from the back dune restoration project line intercept transect sampling

Back Dune Restoration Project Vegetation Assessment					
*Non-native species P=Present within 10m of transect	**BBQ Flats**	**La Grille Hill**	**North Eucalyptus**	**Reference - Early Seral**	**Reference - Late Seral**
Age of Planting (years)	**1.5**	**3.5**	**2.5**	**-**	**-**
Species Richness	**23**	**17**	**16**	**22**	**14**
Total Percent Cover	**31.36%**	**34.97%**	**51.40%**	**68.76%**	**77.06%**
Total Percent Cover 95% Confidence Interval	**± 17.05%**	**± 44.12%**	**± 55.61%**	**± 17.48%**	**± 3.47%**
Species	**Percent Cover**				
Lupinus chamissonis	24.57%	23.88%	35.08%	29.27%	-
Ericameria ericoides	0.18%	0.21%	0.51%	22.62%	57.86%
Dead woody vegetation	-	0.99%	2.73%	12.80%	13.43%
Achillea millefolium	1.09%	0.49%	1.18%	4.63%	p
Senecio blochmaniae	0.43%	p	0.18%	2.54%	p
Erigeron blochmaniae	0.88%	0.07%	p	1.32%	-
**Conicosia pugioniformis*	-	-	-	0.89%	0.08%
Cirsium occidentale	-	-	-	0.42%	-
Pseudognaphalium biolettii	-	-	-	0.06%	-
Pseudognaphalium sp.	p	-	-	p	p
Ambrosia chamissonis	-	1.60%	11.98%	p	-
Acmispon glaber	-	2.16%	p	p	3.51%
Phacelia ramosissima	1.88%	0.79%	p	p	-
Camissoniopsis cheiranthifolia	0.77%	p	p	p	-
Monardella undulata crispa	0.28%	0.36%	0.53%	p	-
Erysimum suffrutescens	0.31%	-	p	p	-
Baccharis pilularis	p	-	-	p	0.17%
Salix lasiolepis	p	p	p	p	-
Castilleja affinis	p	-	-	p	-
**Ehrharta calycina*	-	-	-	p	p
Pseudognaphalium californicum	-	-	-	p	-
Cryptantha clevelandii	-	-	-	p	-
Pseudognaphalium ramosissimum	-	-	-	p	-
Chorizanthe eastwoodiae	-	-	-	p	-
Chorizanthe sp.	p	-	-	p	-
Eriophyllum staechadifolium	0.39%	5.34%	0.88%	-	-
Eriogonum parvifolium	3.07%	p	0.60%	-	0.03%
Oenothera elata	0.47%	-	-	-	-
Corethrogyne filaginifolia	0.10%	p	p	-	6.12%
Dudleya lanceolata	-	-	-	-	0.36%
Fragaria chiloensis	p	p	-	-	-
Malicothrix incana	p	-	-	-	-
Abronia umbellata	p	-	-	-	-
Erigeron canadensis	p	-	-	-	-
Nemacaulis denudata	p	-	-	-	-
Eriastrum densifolium	-	-	p	-	-
Chenopodium californicum	-	-	-	-	p
Silene laciniata	-	-	-	-	p

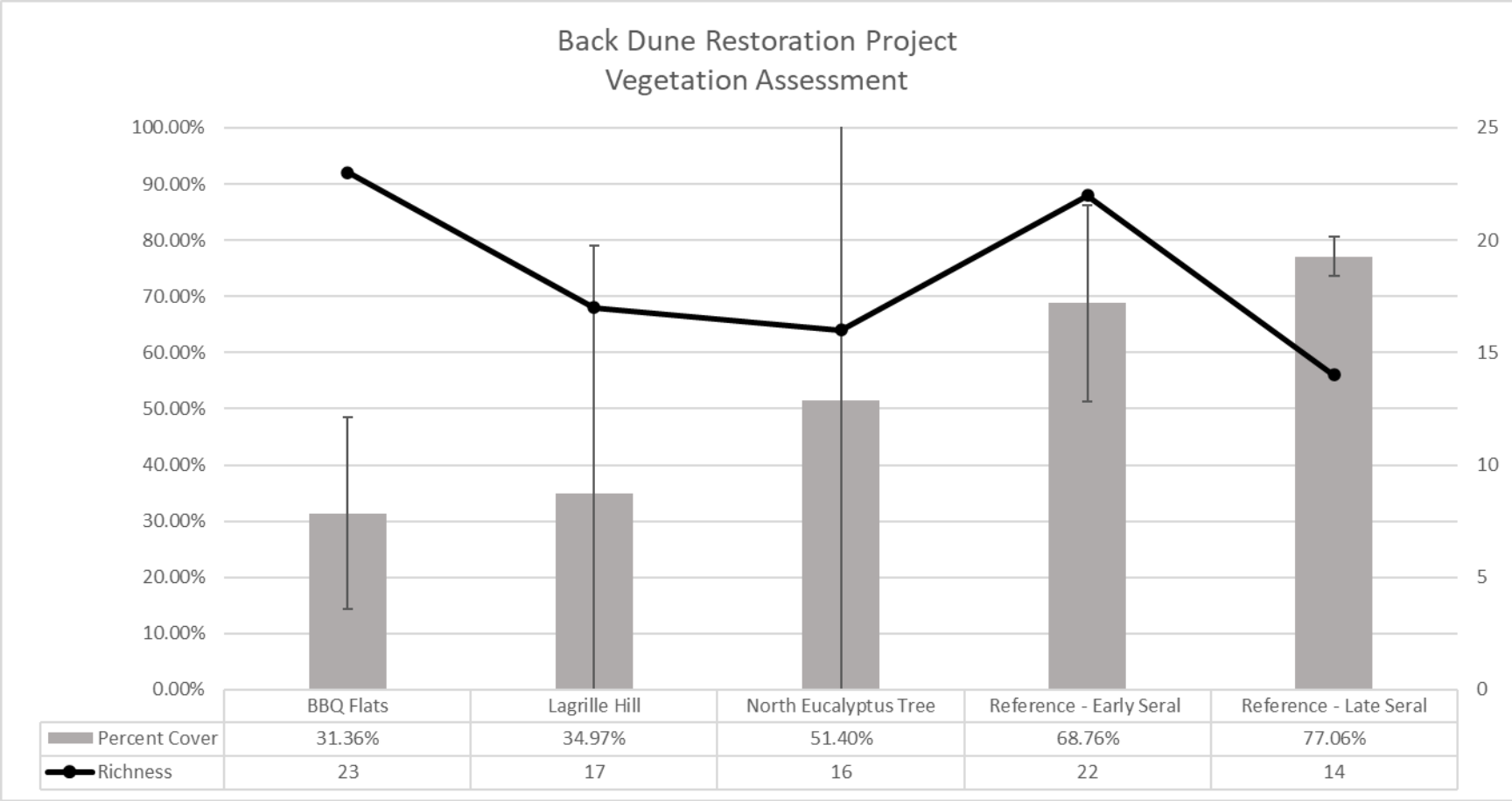

Figure 2. Vegetation composition in back dune project areas compared to reference site. Error bars are 95% confidence intervals. Three 30-meter transects were sampled in each of the back dune areas and reference site.

Figure 3. Photo point of 48 Acre Foredune Area 3 facing west prior to treatment. Photo taken on February 4, 2020.

Figure 4. Photo point of 48 Acre Foredune Area 3 facing west 1.5 years after treatment. Photo taken on October 19, 2021.

Figure 5. Photo point of 48 Acre Foredune Area 3 facing north prior to treatment. Photo taken on February 4, 2020.

Figure 6. Photo point of 48 Acre Foredune Area 3 facing north 1.5 years after treatment. Photo taken on October 19, 2021.

Figure 7. Photo point of North Eucalyptus Tree project area facing northeast prior to planting. Photo taken on October 17, 2018.

Figure 8. Photo point of North Eucalyptus Tree project area facing northeast. Photo taken on November 8, 2021.

Figure 9. Drone photo point of 48 Acre Foredune High Density Node Area 5 facing east. Image taken on May 2020.

Figure 10. Drone photo point of 48 Acre Foredune High Density Node Area 5 facing east. Image taken on February 2022.

Figure 11. Drone photo point of Bigfoot restoration project area facing south. Image taken on May 8, 2020.

Figure 12. Drone photo point of Bigfoot restoration project area facing south. Image taken on February 17, 2022

THIS PAGE INTENTIONALLY LEFT BLANK.

Oceano Dunes State Vehicular Recreation Area Dust Control Program

DRAFT 2022 Annual Report and Work Plan

ATTACHMENT 06

Compilation of Studies Reviewed and Comments Provided by the Scientific Advisory Group from 08/01/21 to 07/31/22

THIS PAGE INTENTIONALLY LEFT BLANK.

Oceano Dunes State Vehicular Recreation Area Dust Control Program

DRAFT 2022 Annual Report and Work Plan

ATTACHMENT 06-01

Dust Emissions and OHV Activity at the ODSVRA

THIS PAGE INTENTIONALLY LEFT BLANK.

DRAFT- Dust Emissions and OHV Activity at the ODSVRA

Oceano Dunes State Vehicular Recreation Area (ODSVRA) is located on the central coast of California south of the town of San Luis Obispo in the 'five cities' area. It is the only coastal State Vehicular Recreation Area (SVRA), and one of the most popular Park Units in the state with over 2 million visitors annually. ODSVRA is 3,600 acres and is part of the greater Nipomo-Guadalupe Dunes Complex that encompasses approximately 18,000 acres. The riding area within ODSVRA is approximately 1,000 acres. The Nipomo-Guadalupe Dune Complex is characterized by high winds and dusty conditions. Dust, or particulate matter (PM10), is created through a natural process called saltation where the wind causes sand grains to bounce across the dune surface thereby emitting PM10 into the air.

California State Parks (Parks) has been working with the San Luis Obispo County Air Pollution Control District (APCD) on managing PM10 emissions from the riding area since 2011. Concerning air quality at ODSVRA, the APCD imposed Air District Rule 1001 in 2011, requiring Parks to reduce particulate matter. Later Rule 1001 was superseded by a Consent Decree between Parks and the APCD in 2014. Parks then entered into a Stipulated Order of Abatement (SOA) with the APCD in 2018. The Order was amended in 2019. The SOA has three air quality targets:

1. To meet the State ambient air quality standard
2. To meet the Federal ambient air quality standard
3. To reduce the maximum 24-hour PM10 baseline mass emissions by 50% (initial target; based on 2013 mass emission estimate)

Air quality modeling is required, as per the SOA, to determine the change in PM10 mass emissions through time from the baseline year of 2013 for 10 specified days. Mass emissions quantifies the metric tons of PM10 emissions per day. This quantity is derived from a computer model that also predicts PM10 concentrations ($\mu g\ m^{-3}$) at downwind locations and is used as an indicator of regional air quality. As of 2021, Parks had installed over 300 acres of dust mitigation projects at ODSVRA.

Parks has commissioned substantial research at ODSVRA aimed at better understanding the science of dust and emissivity in the area. As part of this effort, the Desert Research Institute (DRI), has been collecting dust emissivity data at ODSVRA since 2011. In addition, a network of air quality and meteorological monitoring stations have been in place within and downwind, of the park since 2014. Parks also works with a Scientific Advisory Group (SAG) on scientific issues at the park. The SAG was established by the SOA and is comprised of scientists with expertise in atmospheric science, dune geomorphology, botany, and horticulture.

Part of this research has been to answer two fundamental questions:

1. What effects, if any, does OHV activity have on dust emissivity at, and downwind, of ODSVRA?
2. Are the dust mitigation projects in place improving regional air quality downwind of ODSVRA?

***Does OHV have an impact on dust emissions at ODSVRA (see reference 1 below)*?**

The first question of how OHV may impact dust emissions at ODSVRA has been a point of discussion raised by the OHV Commission, the OHV community, the San Luis Obispo County Air Pollution Control District, and other stakeholders for several years. In addition to analyzing the impacts off-highway vehicles may have on dust emissivity at ODSVRA, DRI also explored how any impacts on emissivity are related to observed changes in PM10 concentrations in the ODSVRA as well as downwind of the Park from 2017 to 2020. For clarity,

DRAFT

emissivity is defined as how much particulate matter is released from the sand surface per unit area and time under the action of the wind. PM10 concentration is the mass of PM_{10} in a volume of air being moved by the wind and is typically measured at a downwind receptor site.

To address any impacts on emissivity, measurements of emissivity from dune sands were made using a specialized instrument (PI-SWERL®) from 2013 through to 2020 in the area with OHV activity and in areas where OHV access is not permitted**.** These measurements indicated that the mean emissivity of the sand inside of the riding area was two to three time higher than the mean of the non-riding areas, for wind conditions well-above the threshold where saltation begins on the dunes. Note that these data above quantify the PM10 emissivity of the sand, as opposed to downwind PM10 concentrations.

In addition to analyzing the sand emissivity data, measurements of Wind Power Density (WPD), a measure of the ability of the wind to cause sand to saltate and emit dust and suspended particulate matter (concentrations of PM10) were made at 15 monitoring stations in the riding areas (11 stations) and downwind of the riding areas (4 stations). These measurements have been made annually between May and September 2017 to 2020. In 2017, 2018, and 2019 these data indicate that PM_{10} concentrations in the air at ODSVRA, increased from April through August per month for similar wind conditions. In 2019, that increase was approximately 12% per month for similar wind conditions. The increase was also observed at the four monitoring stations downwind of the riding area mentioned above.

Public vehicle activity was prohibited beginning in late March 2020 due to the SARS-CoV-2 pandemic. Measurements of PM_{10} and WPD, April to August, 2020 in the ODSVRA indicated an approximate 11% decrease per month for similar wind conditions.

The cessation of OHV activity resulted in the dunes producing lower concentrations of PM_{10} for similar wind conditions during sand transport (saltation) in the ODSVRA. The decrease was also observed at the four monitoring stations downwind of the riding area.

Are the dust mitigation projects improving regional air quality downwind of ODSVRA (see reference 2 below)?

Dust controls—temporary wind fences and vegetation projects—have been used within the Oceano Dunes State Vehicular Recreation Area to reduce PM10 emissions originating from within the park. These controls are also expected to lower the regional PM10 concentrations helping to meet the SOA requirements. Beginning in 2014, 28 acres of dust control was implemented, and the acreage had increased to 223 acres in 2020. That is approximately 15% of the available riding area. According to emission and dispersion modeling undertaken by DRI, the 223 acres reduced PM10 measured at the Calfire monitoring station (CDF) by ≈42% with respect to the values modeled for the 2013 baseline days.

Using the PM10 measurements at CDF and wind speed data from the S1 tower in the ODSVRA, DRI demonstrated that dust emission in locations where controls have been placed produces less PM10 now than prior to these controls and that this reduction is consistent with the increase in acres of dust control. Specifically, these data indicate that emplacement of dust controls upwind of the CDF station reduced PM10 production by 48% for similar wind conditions with the controls in place in 2020 compared with the no-control conditions of 2011–2013. DRI's analysis of the data also agrees with model results that indicate PM10 reduction at the CDF receptor site is due to the dust controls.

DRAFT

Air quality modeling and analyses of the wind and PM10 data presented in the DRI report indicate that the actions taken by Parks to reduce dust-generated impacts within the ODSVRA through the dust control program are demonstrable with decreased emissions of PM10 as the size of the control areas have increased through time, and these impacts amount to a reduction of ≈45% near the CDF measurement site since 2011. This has been documented by sophisticated computer modeling of concentrations at sensitive receptor sites and has been verified by measurements at EPA monitoring sites downwind of ODSVRA. This analysis shows that the ongoing dust control efforts have eliminated exceedances of the federal ambient air quality standard and are making strong progress to meet the state ambient standard as well.

Conclusion:

The analyses by DRI indicates that OHV activity increases emissivity and dust levels in the active dune field, in addition to PM10 concentrations downwind of ODSVRA. However, the dust mitigation measures in place have significantly improved air quality downwind of ODSVRA. Parks continues to implement projects to mitigate dust emissions, monitor changes in emissivity and PM10 due to the dust control projects, and refine the DRI dust emission-dispersion model to better understand the relationships between OHV activity and sensitive receptors on the Nipomo Mesa.

In compliance with the SOA, more dust mitigation projects will be installed, which are expected to further reduce PM10 emissions from ODSVRA thereby improving regional air quality downwind of the Park. Both the SAG and the APCD have stated that they believe that it is possible to meet the requirements of the SOA while maintaining off-highway vehicle recreation at ODSVRA. In a letter to the California Coastal Commission on March 12th, 2021 (see reference 3 below), the SAG wrote, "…from an air quality perspective the work of the SAG thus far indicates that there is a workable approach to achieving the targets set by the SOA while retaining some level of off-highway vehicular activity at the ODSVRA."

Improved air quality and continued OHV activities are compatible at ODSVRA. The ongoing research and analyses continue to help Parks refine dust control efforts and activities. Parks will continue to work with the APCD and the SAG towards meeting the goals of the SOA and improving regional air quality, while maintaining high quality recreational opportunities.

References:

1. Examining Dust Emissions and OHV Activity at ODSVRA. Desert Research Institute. February 2021
2. Gillies, J.A, E. Furtak-Cole, V. Etyemezian. Increments of Progress Towards Air Quality Objectives-ODSVRA Dust Controls. Desert Research Institute. December 2020
3. Letter from the SAG to the CA Coastal Commission. March 12th, 2021

DRAFT

August 9, 2021

Memo: SAG review of draft CDPR report, "Dust Emissions and OHV Activity at the ODSVRA"

From: The Scientific Advisory Group (SAG)

To: Jon O'Brien, California Department of Parks and Recreation

Cc: Sarah Miggins, California Department of Parks and Recreation
Liz McGuirk, California Department of Parks and Recreation

Intent of SAG review
On July 26, 2021, the California Department of Parks and Recreation (CDPR) asked the Scientific Advisory Group (SAG) to prepare an independent scientific review of the draft CDPR report, "Dust Emissions and OHV Activity at the ODSVRA." As per the terms of the amended Stipulated Order of Abatement (SOA), the SAG is granted at least 10 business days to prepare such a scientific review. Based on the draft nature of the CDPR report, the SAG submits this current review only to the CDPR with the expectation that the final CDPR report will be released in a timely manner. In the spirit of trust and cooperation, the SAG also strongly encourages CDPR to share its draft report with the San Luis Obispo Air Pollution Control District (SLOAPCD) in advance of final publication. When the final CDPR report is released, the SAG reserves the right to publish a further independent scientific review of the final report.

Scope of SAG review
This SAG review addresses the scientific merits of the draft CDPR report and the accuracy of its representations of the referenced reports from the Desert Research Institute (DRI), "Examining Dust Emissions and OHV Activity at the ODSVRA" (by J.A. Gillies, E. Furtak-Cole, G. Nikolich, and V. Etyemezian) and "Increments of Progress Towards Air Quality Objectives - ODSVRA Dust Controls" (by J.A. Gillies, E. Furtak-Cole, V. Etyemezian). However, this SAG review does **not** address the scientific merits of the referenced DRI reports. The SAG previously provided some comments to CDPR on preliminary versions of these DRI reports, though it has not yet reviewed the current versions.

SAG review of draft CDPR report
Overall, the SAG finds that the draft CDPR report accurately describes several key findings of the referenced DRI reports. Regarding the DRI report on "Examining Dust Emissions...", the draft CDPR report correctly references the fact that Riding Areas within the ODSVRA display significantly higher PM10 emissivity than Non-Riding Areas. Furthermore, the CDPR report correctly references the DRI report finding that PM10 concentrations relative to wind power density (WPD) declined through the spring/summer 2020 closure of the ODSVRA due to the state-imposed COVID-19 pandemic restrictions, in contrast to the typical increase in PM10 emissivity (relative to WPD) that occured in previous windy seasons, such as spring/summer 2019. Regarding the DRI report on "Increments of Progress...", the draft CDPR report correctly references the finding of a long-term decline in the ratio of PM10 concentration relative to WPD at the CDF monitoring station, which indicates the effectiveness of dust controls implemented within the ODSVRA to reduce airborne PM10 concentrations.

The SAG notes, however, that the draft CDPR report provides interpretations that go well beyond the material in the referenced DRI reports, and the SAG is concerned that the draft CDPR report does not tell the full story of key findings from these referenced DRI reports. Instead, as currently written, the CDPR report appears to provide a distinctive statement of CDPR findings and priorities, based only in part on the referenced DRI reports. Therefore, the SAG recommends that the CDPR report clearly acknowledge that it is **not** simply an executive summary of the referenced DRI reports, as it contains interpretations and statements derived by CDPR. The SAG also requests that the CDPR report tell a more complete story of what is contained in the referenced DRI reports.

In support of the above mentioned concerns, the SAG provides the following comments and recommendations to improve the draft CDPR report:

(1) Though not explicitly stated, this draft CDPR report has informally been referred to as an "executive summary" of the referenced DRI reports. Though CDPR staff have assured the SAG to the contrary, the SAG remains concerned that members of the public may nonetheless incorrectly perceive this CDPR report to be an executive summary of the DRI reports, when in fact it is not. **Therefore, the SAG recommends that the CDPR report include a statement clearly describing its intent in relation to the underlying DRI reports.**

(2) The draft CDPR report section "Does OHV have an impact on dust emissions at ODSVRA?" omits a key finding of the referenced DRI "Examining Dust Emissions..." report, namely, that a significant reduction in PM10 emissivity was observed within the Lagrande tract between 2019 and 2020, as measured by the PI-SWERL (i.e., Figs. 9-10 in this DRI report). This is an important line of evidence that cessation of OHV activity in spring 2020 is directly associated with a significant decline in PM10 emissions. The draft CDPR report does reference the separate DRI finding of a **reduction in PM10 concentrations** relative to WPD between 2019 and 2020, but the distinctive finding of a **reduction in PM10 emissivity** should also be noted. The SAG acknowledges that the draft CDPR report is a summary that necessarily must omit certain minor details. Nonetheless, this reduction in PM10 emissivity from 2019 to 2020 is an important finding of the DRI report which should not be omitted from any summary. **Therefore, the SAG recommends that the CDPR report directly describe this DRI finding regarding the change in PM10 emissivity from surfaces within the ODSVRA between 2019 and 2020.**

(3) Related to the above point, the draft CDPR report omits a central argument of the DRI "Examining Dust Emissions..." report, namely, that "…the cessation of OHV activity has likely allowed the dust emission system to evolve towards a new state representing a less impacted dune system." Two independent findings from the DRI report – reduction in PM10 concentrations relative to wind power density **and** reduction in PM10 emissivity – provide very strong evidence to support this statement in the DRI report about the effect of the cessation of OHV activity on dust emissions. **Therefore, the SAG recommends that the CDPR report include a clear statement regarding the effect of cessation of OHV activity on changes in emissivity in the ODSVRA dune system.**

(4) Also related to the previous points, the SAG is concerned that presentation of information in the draft CDPR report, especially in the section on "Does OHV have an impact on dust

emissions at ODSVRA?", is organized in a way that obscures key findings of the referenced DRI reports. For example, the draft CDPR report references the expected seasonal trends of increasing PM10 concentrations (relative to WPD) in 2017-2019, and the decreasing PM10 concentrations (relative to WPD) in 2020 during the closure, but it never acknowledges the contrast between these two trends that provides strong evidence for the likely response of dust emissions to the cessation of OHV activity. **Therefore, the SAG recommends that the CDPR report provide descriptions of observed trends in PM10 emissions directly in tandem with resulting inferences about the effects of OHV on these PM10 emissions.**

(5) The draft CDPR report section "Are the dust mitigation projects improving regional air quality downwind of ODSVRA" correctly describes encouraging findings from the referenced DRI "Increments of Progress..." report regarding declining PM10 concentrations (relative to WPD) at the CDF receptor site, but it fails to mention the fact that such declines in PM10 concentrations (relative to WPD) are not observed at the Mesa2 receptor site (i.e., Fig. 8 in this DRI report). This is an important finding that reflects the fact that ODSVRA dust controls thus far have primarily been installed upwind of the CDF receptor site. **Therefore, the SAG recommends that the CDPR report describe the finding of this DRI report regarding the difference in long-term PM10 concentration trends at CDF versus Mesa2.**

(6) The SAG is concerned that the statement from our March 12, 2021, letter to the California Coastal Commission has been referenced out of context in the draft CDPR report. Though the SAG stands by its opinion that the SOA target is achievable within the context of continuing OHV activity, the referencing of this statement within the draft CDPR report appears to be a distraction from the two key questions of the report regarding the effect of OHVs on PM10 emissions and the progress of dust mitigation projects toward reducing PM10 emissions. **Therefore, the SAG recommends removal of the reference to the SAG letter to the California Coastal Commission from the CDPR report.**

The SAG also offers some additional comments on the draft CDPR report in Appendix 1 below.

Yours Sincerely,
The Scientific Advisory Group

Dr. Raleigh Martin (Acting Chair of SAG); Dr. William Nickling; Dr. Ian Walker; Ms. Carla Scheidlinger; Mr. Earl Withycombe; Mr. Mike Bush
(Because he is co-author of the DRI studies referenced in the draft CDPR report, SAG member Dr. Jack Gillies is not a signatory of this SAG letter.)

Appendix 1: Additional comments on the draft CDPR report from the SAG

p. 2, 1st full paragraph: The following statement in the draft CDPR report appears to be at odds with the DRI "Examining Dust Emissions" report, "These measurements indicated that the mean emissivity of the sand inside of the riding area was two to three time higher than the mean of the non-riding areas, for wind conditions well-above the threshold where saltation begins on the dunes." The value quoted in the DRI report is "between 3.6 and 1.9 times greater." Please report the correct values from the DRI report. If rounding, then please report "two to four times higher."

p. 2, 2nd full paragraph: The following statement in the draft CDPR report appears to omit numerical values associated with the per month increase, "These measurements have been made annually between May and September 2017 to 2020. In 2017, 2018, and 2019 these data indicate that PM10 concentrations in the air at ODSVRA, increased from April through August per month for similar wind conditions." Please provide these values.

p. 2, 5th full paragraph: For consistency with the 2021 draft ARWP (Table 2-5), the acreage value for dust controls implemented thus far should be 231 acres (not 233 acres). In addition, for consistency with the ARWP reporting of findings relative to the 2013 SOA baseline, the SAG suggests that acreage values be reported relative to 2013 (not 2014).

State of California • The Natural Resources Agency
Gavin Newsom, *Governor*

DEPARTMENT OF PARKS AND RECREATION
Armando Quintero, *Director*
Off-Highway Motor Vehicle Recreation Division
1725 23rd Street, Suite 200
Sacramento, California 95816
Telephone: (916) 324-5801 • Fax: (916) 324-0271

OHMVR COMMISSION MEETING
Sacramento, CA

August 26, 2021

STAFF REPORT: **Dust Emissions and OHV Activity at ODSVRA**

STAFF: Jon O'Brien, Environmental Program Manager, OHMVR Division

SUBJECT: Update on the Oceano Dust Program and Recent Research

---

Summary

- State Parks has been working with the San Luis Obispo County Air Pollution Control District since 2011 on dust issues downwind of Oceano Dunes SVRA (ODSVRA)
- State Parks entered into a Stipulated Order of Abatement with the APCD in 2018, with an aim of reducing particulate matter (PM10) in the Oceano Dunes area
- There have been substantial dust mitigation efforts at ODSVRA, in addition to research aimed at better understanding the science around dust at Oceano. Two recent Desert Research Institute reports used seven years of data to explore the questions:
    - What effects, if any, does OHV activity have on dust emissivity at the ODSVRA and PM10 concentrations downwind?
    - Are the dust mitigation projects improving air quality downwind of ODSVRA?
- Dust emissivity measurements at ODSVRA indicate that the dunes within the riding area are two to three times more emissive than the dunes in the non-riding area
- In addition, PM10 concentrations within, and downwind, of ODSVRA decreased through the spring and summer during the COVID closure of ODSVRA in 2020. In 2019, the PM10 concentrations increased through the spring and summer
- However, due to the substantial dust mitigation efforts at ODSVRA since 2014, there have been significant reductions over time in PM10 concentrations downwind of ODSVRA
- These reductions in PM10 concentrations indicate that, even though the riding area is more emissive than the non-riding area, the dust mitigation efforts at ODSVRA are improving air quality in south San Luis Obispo County
- These results show that improved air quality and OHV activity can coexist at ODSVRA, and more dust mitigation projects will be needed to meet the targets of the Stipulated Order of Abatement

Discussion

Oceano Dunes State Vehicular Recreation Area (ODSVRA) is located on the central coast of California south of the town of San Luis Obispo in the 'five cities' area. It is the only coastal State Vehicular Recreation Area (SVRA), and one of the most popular Park Units in the state with over 2 million visitors annually. ODSVRA is 3,600 acres and is part of the greater Nipomo-Guadalupe Dunes Complex that encompasses approximately 18,000 acres. The riding area within ODSVRA is approximately 1,000 acres. The Nipomo-Guadalupe Dune Complex is characterized by high winds and dusty conditions. Dust, or particulate matter (PM10), is created through a natural process called saltation where the wind causes sand grains to bounce across the dune surface thereby emitting PM10 into the air.

California State Parks (Parks) has been working with the San Luis Obispo County Air Pollution Control District (APCD) on managing PM10 emissions from the riding area since 2011. Concerning air quality at ODSVRA, the APCD imposed Air District Rule 1001 in 2011, requiring Parks to reduce particulate matter; a Consent Decree was signed between Parks and the APCD in 2014. Parks then entered into a Stipulated Order of Abatement (SOA) with the APCD in 2018. The Order was amended in 2019. The SOA has three air quality targets:

1. To meet the State ambient air quality standard for PM10
2. To meet the Federal ambient air quality standard for PM10
3. To reduce the maximum 24-hour PM10 baseline mass emissions by 50% (initial target; based on 2013 mass emission estimate)

Air quality modeling is required, as per the SOA, to determine the change in PM10 mass emissions through time from the baseline year of 2013 for 10 specified days. Mass emissions quantifies the metric tons of PM10 emissions per day. This quantity is derived from a computer model that also predicts PM10 concentrations ($\mu g\ m^{-3}$) at downwind locations. As of 2021, Parks had installed over 300 acres of dust mitigation projects at ODSVRA.

Parks has commissioned substantial research at ODSVRA aimed at better understanding the science of dust and emissivity in the area. As part of this effort, the Desert Research Institute (DRI), has been collecting dust emissivity data at ODSVRA since 2013. In addition, a network of air quality and meteorological monitoring stations have been in place within, and downwind, of the park since 2017. Parks also works with a Scientific Advisory Group (SAG) on scientific issues at the park. The SAG was established by the SOA and is comprised of scientists with expertise in atmospheric science, dune geomorphology, botany, and horticulture.

Part of this research has been to answer two fundamental questions:

1. What effects, if any, does OHV activity have on dust emissivity at, and downwind, of ODSVRA?
2. Are the dust mitigation projects in place improving air quality downwind of ODSVRA?

Does OHV have an impact on dust emissions at ODSVRA (see attachment 1)?

The first question of how OHV may impact dust emissions at ODSVRA has been a point of discussion raised by the OHV Commission, the OHV community, the San Luis Obispo County Air Pollution Control District, and other stakeholders for several years. In addition to analyzing

the impacts off-highway vehicles may have on dust emissivity at ODSVRA, DRI also explored how any impacts on emissivity are related to observed changes in PM10 concentrations in the ODSVRA as well as downwind of the park from 2017 to 2020. For clarity, emissivity is defined as how much particulate matter is released from the sand surface per unit area and time under the action of the wind. PM10 concentration is the mass of PM_{10} in a volume of air being moved by the wind and is typically measured at a downwind receptor site.

To address any impacts on emissivity, measurements of emissivity from dune sands were made using a specialized instrument (PI-SWERL®) from 2013 through to 2020 in the area with OHV activity and in areas where OHV access is not permitted**.** These measurements indicated that the mean emissivity of the sand inside of the riding area was two the three times higher than the mean of the non-riding areas, for wind conditions well-above the threshold where saltation begins on the dunes. In addition, emissivity data specific to the La Grande Tract from 2020 was lower than in 2019. Note that these data quantify the PM10 emissivity of the sand, as opposed to downwind PM10 concentrations.

In addition to analyzing the sand emissivity data, measurements of Wind Power Density (WPD), a measure of the ability of the wind to cause sand to saltate and emit dust and suspended particulate matter (concentrations of PM10) were made at 15 monitoring stations in the riding areas (11 stations) and downwind of the riding areas (4 stations). These measurements have been made annually between May and September 2017 to 2020. In 2017, 2018, and 2019, these data indicate that PM_{10} concentrations in the air at ODSVRA, increased from May through July per month for similar wind conditions. The increase was observed from May through September for 2019 (Figures 17 and 18). In 2019, that increase was approximately 12% per month for similar wind conditions (Figure 17). The increase was also observed at the four monitoring stations downwind of the riding area mentioned above (see slide 19 from DRI 'Examining Dust Emissions and OHV Activity at ODSVRA' presentation).

Public vehicle activity was prohibited beginning in late March 2020 due to the SARS-CoV-2 pandemic. In contrast with the 2019 data, measurements of PM_{10} and WPD, April to August 2020 in the ODSVRA indicated an approximate 11% decrease per month for similar wind conditions (Figure 20).

The cessation of OHV activity resulted in the dunes producing lower concentrations of PM_{10} for similar wind conditions during sand transport (saltation) in the ODSVRA. The decrease was also observed at the four monitoring stations downwind of the riding area (see slide 19 from DRI 'Examining Dust Emissions and OHV Activity at ODSVRA' presentation).

Are the dust mitigation projects improving air quality downwind of ODSVRA (see attachment 2)?

Dust controls—temporary wind fences and vegetation projects—have been used within the Oceano Dunes State Vehicular Recreation Area to reduce PM10 emissions originating from within the park. These controls are also expected to lower the PM10 concentrations helping to meet the SOA requirements. Beginning in 2014, 28 acres of dust control was implemented, and the acreage had increased to 223 acres in 2020. That is approximately 15% of the available riding area. According to emission and dispersion modeling undertaken by DRI, the

223 acres reduced PM10 measured at the Cal Fire monitoring station (CDF) by ≈42% with respect to the values modeled for the 2013 baseline days.

Using the PM10 measurements at CDF and wind speed data from the S1 tower in the ODSVRA, DRI demonstrated that dust emission in locations where controls have been placed produces less PM10 now than prior to these controls and that this reduction is consistent with the increase in acres of dust control. Specifically, these data indicate that emplacement of dust controls upwind of the CDF station reduced PM10 production by 48% for similar wind conditions with the controls in place in 2020 compared with the no-control conditions of 2011–2013. DRI's analysis of the data also agrees with model results that indicate PM10 reduction at the CDF receptor site is due to the dust controls.

Air quality modeling and analyses of the wind and PM10 data presented in the DRI report indicate that the actions taken by Parks to reduce dust-generated impacts within the ODSVRA through the dust control program are demonstrable with decreased emissions of PM10 as the size of the control areas have increased through time, and these impacts amount to a reduction of ≈45% near the CDF measurement site since 2011. This has been documented by sophisticated computer modeling of concentrations at sensitive receptor sites and has been verified by measurements at EPA monitoring sites downwind of ODSVRA. This analysis shows that the ongoing dust control efforts have eliminated exceedances of the Federal ambient air quality PM10 standard and are making strong progress to meet the State standard as well.

Conclusion:

The analyses by DRI indicates that OHV activity increases emissivity and dust levels in the active dune field, in addition to PM10 concentrations, downwind of ODSVRA. However, the dust mitigation measures in place have significantly improved air quality downwind of ODSVRA. Parks continues to implement projects to mitigate dust emissions, monitor changes in emissivity and PM10 due to the dust control projects, and refine the DRI dust emission-dispersion model to better understand the relationships between OHV activity and sensitive receptors on the Nipomo Mesa.

In compliance with the SOA, more dust mitigation projects will be installed, which are expected to further reduce PM10 emissions from ODSVRA thereby improving air quality downwind of the park. Both the SAG and the APCD have stated that they believe that it is possible to meet the requirements of the SOA while maintaining off-highway vehicle recreation at ODSVRA. In a letter to the California Coastal Commission on March 12th, 2021 (see attachment 3), the SAG wrote, "…from an air quality perspective the work of the SAG thus far indicates that there is a workable approach to achieving the targets set by the SOA while retaining some level of off-highway vehicular activity at the ODSVRA."

Improved air quality and continued OHV activities are compatible at ODSVRA. The ongoing research and analyses continue to help Parks refine dust control efforts and activities. Parks will continue to work with the APCD and the SAG towards meeting the goals of the SOA and improving air quality, while maintaining high quality off-highway vehicle recreational opportunities at ODSVRA.

Commission Action

For information only.

Attachments

1. Examining Dust Emissions and OHV Activity at ODSVRA. Desert Research Institute. February 2021
2. Gillies, J.A, E. Furtak-Cole, V. Etyemezian. Increments of Progress Towards Air Quality Objectives-ODSVRA Dust Controls. Desert Research Institute. December 2020
3. Letter from the SAG to the CA Coastal Commission. March 12th, 2021

Oceano Dunes State Vehicular Recreation Area Dust Control Program

DRAFT 2022 Annual Report and Work Plan

ATTACHMENT 06-02

Scripps/UCSD Interim Report 2021: Preliminary Results from May 2021 Aerosol Measurements

THIS PAGE INTENTIONALLY LEFT BLANK.

UNIVERSITY OF CALIFORNIA, SAN DIEGO UCSD

BERKELEY • DAVIS • IRVINE • LOS ANGELES • MERCED • RIVERSIDE • SAN DIEGO • SAN FRANCISCO

SANTA BARBARA • SANTA CRUZ

SCRIPPS INSTITUTION OF OCEANOGRAPHY

9500 GILMAN DRIVE
LA JOLLA, CALIFORNIA 92093-0221

30 September 2021

Sarah Miggins, Deputy Director
Off-Highway Motor Vehicle Recreation Division
California Department of Parks and Recreation
1725 23rd Street, Suite 200
Sacramento, CA 95816

Dear Deputy Director Miggins,

Please find attached my report of findings regarding our spring 2021 sampling and analyses of airborne particulate matter (PM) collected at the location known as the CDF site on the Nipomo Mesa (Mesa) in south San Luis Obispo County, California. The CDF site is approximately two miles downwind of the Oceano Dunes State Vehicular Recreation Area (SVRA). The primary purpose of this investigation, which is part of a larger three-year study, is to quantify that portion of measured PM that consists of mineral dust. Mineral dust is generated from the windblown sand dune building process called saltation, and so quantifying the mineral dust portion of PM at the CDF site provides a conservative measure of that portion of PM on the Mesa that could possibly be from the Oceano Dunes SVRA. The mineral dust measure is conservative because saltation occurs in the dunes inside and outside the SVRA, and mineral dust is also derived from agricultural operations and vehicles driving on dirt roads—activities that occur in the region that lies between the SVRA and the Mesa.

Samples of PM10 and PM2.5 (PM that is aerodynamically $\leq$10 microns and $\leq$2.5 microns in diameter, respectively) were collected for 30 consecutive days, from late April to late May. May was targeted because May is typically the windiest month in the region. Each day, the air was sampled continuously for seven hours, from noon to 7:00PM (local time) because this is the timeframe when the seasonal westerly winds rise and fall, when saltation in the dunes is at its most active, and when some of the highest hourly PM10 and PM2.5 concentrations at the CDF site are recorded by the SLO County Air Pollution Control District (APCD).

Mineral dust content was determined using gravimetric and elemental analyses as detailed in the report. Key findings from the analyses show that on average, 14% of the PM10 measured at the CDF site consists of mineral dust and 4% consists of sea salt. The remaining 82% of the PM10 is likely from atmospheric water, organic components, ammonium, nitrate, non-sea-salt sulfate, and other semi-volatile chemical species.

I would like to extend our appreciation to the California Geological Survey and to the California Department of Parks and Recreation for their assistance and access that has made our investigation possible.

Best regards,

Lynn M. Russell
Distinguished Professor of Atmospheric Chemistry
Scripps Institution of Oceanography
University of California, San Diego
lmrussell@ucsd.edu; Tel. 858-534-4852.

Scripps/UCSD Interim Report 2021:

Preliminary Results from May 2021 Aerosol Measurements

30 September 2021

Introduction

Building upon the results of the Scripps Institution of Oceanography (UCSD) Reports of 5 February 2020 and 20 September 2020, the Scripps team has undertaken additional quantitative chemical sampling to improve the understanding of the sources of airborne particles in the Oceano Dunes area. This interim report covers the gravimetric and elemental analyses of the teflon filters collected during the most recent sampling period from 27 April 2021 to 26 May 2021 (hereafter “Scripps May 2021” study). The objectives of this part of the research were to

1) Quantify the gravimetric mass and elemental component mass of PM10 aerosol particles at CDF.
2) Quantify the gravimetric mass and elemental component mass of PM2.5 aerosol particles at CDF;

It is important to note that some COVID-19 restrictions continued during this sampling period.

While prior work has focused on identifying sea spray components of PM2.5 at CDF (with a focus on PM with potential health effects) and of PM10 at a Beach site, the May 2021 sampling was designed to provide a quantitative assessment of the mineral dust fraction of the reported beta attenuation monitor (BAM) PM10 and PM2.5 concentrations during the conditions with the highest PM10 concentrations -- namely afternoons (the time of day with highest wind) in May (the month of the year with highest wind). For PM10 size cutoffs, we have used a standard method, and for PM2.5 we have used both a standard method (Very Sharp Cut Cyclone or VSCC) and an alternative method that was used previously to reduce costs (Sharp Cut Cyclone or SCC). In order to quantify the mineral dust contribution during the time with the highest PM10 concentrations, samples were collected for the afternoon hours of 1200 to 1900 local time (1100 to 1800 standard time). During spring in this area, westerly winds typically

have the highest speeds from late morning to early evening (see Appendix, Figure A3). These high wind speeds increase saltation of the dunes and coincide with elevated PM concentrations measured at CDF (Figure A3). Accordingly, it is during the afternoon hours that PM at CDF is expected to contain the largest concentration and the highest percentage of mineral dust. In this sense, the chemical identification of mineral dust in the afternoon provides an upper bound on the contribution of dust from Oceano Dunes, although a more extensive study could separate out the contributions of other sandy regions, agricultural zones, and road dust.

Background

The particle concentration in the Oceano Dunes region is expected to be a mixture of organic and inorganic components from natural and man-made sources. Its seaside location means that sea spray from breaking waves in the ocean will contribute particles with salt (NaCl as well as some trace additional salts) and organic components (from nutrients and exudates that are produced and consumed by marine biota) [Russell et al., 2010]. Another proximate natural source is mineral dust from sand-covered areas, which is generally associated with wind erosion [Li et al., 2013]. Contributions to dust emission by human activities has been estimated to be 10% or less in agricultural areas and as much as 50% for land use changes that remove vegetation [Shepherd et al., 2016; Tegen et al., 2004; Tegen and Fung, 1995]. However, the lack of difference between weekday and weekend coarse particle emissions supports natural rather than anthropogenic sources [Li et al., 2013]. Both sea spray and mineral dust emissions are increased by wind speed [Malm et al., 1994] as well as by source areas, both have substantial supermicron mass contributions with short atmospheric lifetimes, and neither is associated with evidence of chronic respiratory effects (since they are removed by impaction in the nasal passages and upper airways and since the salt and mineral components have not been associated with toxicity). In addition to these natural sources, local emissions associated with motor vehicles [Russell et al., 2011], residential and commercial activities (including use of personal care products [McDonald et al., 2018], food preparation [Chen et al., 2018], and heating), seasonal agricultural harvesting and fertilizing, wildfires, and long-range transport from high-population areas also contribute both organic and inorganic particle mass to PM2.5 and PM10, with the contribution from each varying with wind direction as well as other conditions.

PM2.5 and PM10 are regulated by U.S. and California clean air standards because of their known association with degraded visibility and detrimental health effects [US Clean Air Act (https://www.epa.gov/laws-regulations/summary-clean-air-act); Dockery et al., 1993; Pope et al., 2009; Apte et al., 2018]. PM10 exceedances of the 24-hr NAAQS (150 μg m^{-3}) are infrequent, but the California 24-hr PM10 standard of 50 μg m^{-3} is exceeded 25% of the time [Motallebi et al., 2003]. These standards were developed based on measurements completed by federal reference methods (FRM) that relied on gravimetric measurements of filters that were equilibrated for 24 hr at 35% relative humidity (https://www.ecfr.gov/current/title-40/chapter-I/subchapter-C/part-50). Since then, BAM has been approved as a federal equivalent method (FEM) based on the similarity of hourly BAM, when averaged over 24 hr, to FRM methods for a set of test locations [Chow and Watson, 2008]. Those test locations typically included concentrations below 100 μg m^{-3} and frequently below 30 μg m^{-3} [Chung et al., 2001; Gobeli et al., 2008; Hafkenscheid and Vonk, 2014; Hart, 2009], as these conditions were more typical of areas of concern for PM2.5.

Apte et al. [2018], calculated the U.S. average life expectancy decrement to be 0.38 yr for PM2.5, which is 3 times lower than that of countries with higher PM2.5 (e.g. China, India). While the widespread availability of PM2.5 measurements often makes it the best proxy for epidemiological studies of populations, physiological studies of health effects have shown that the causes of cell degradation are most likely from specific toxic compounds, which are also regulated and include such compounds as polycyclic aromatic hydrocarbons that are associated with fossil fuel combustion and black carbon. Consequently PM1 has been recommended as a better cutoff for targeting health-related aerosol sizes [Lundgren and Burton, 2008]. Recent evidence also suggests that nanoparticles (less than 100 nm diameter) and transition metals, which are also associated with fossil fuel combustion, may also play an important role [Knol et al., 2009; Oberdorster et al., 2007; Gwinn and Vallyathan, 2006; Janssen et al., 2003; Hoek et al., 2002]. Since the association of PM2.5 with toxics is likely responsible for the association of PM2.5 with health effects, the use of PM2.5 as a health indicator assumes it co-occurs with toxics.

There is no evidence that toxic compounds (such as heavy metals or polycyclic aromatic hydrocarbons) are associated with the two major PM2.5 sources (dune dust and sea spray) during windy conditions at Oceano Dunes, so association of PM2.5 with detrimental health effects may be without foundation. In urban locations that serve as the basis for epidemiological health studies, the large population density means that PM2.5 is largely associated with emissions from motor vehicles that include high amounts of toxics, nanoparticles, and transition metals. In areas where PM2.5 is

dominated by natural emission sources rather than man-made combustion activities, the causal link between toxics and health effects is unlikely to hold; exceptions could include severe dust storms [Krasnov et al., 2014], with concentrations exceeding 1000 μg m^{-3} [Aghababaeian et al., 2021] or associated with Valley fever [Tong et al., 2017], which have not been identified in coastal California [Crooks et al., 2016]. For this reason, assessing whether health effects are associated with PM2.5 requires identifying what fraction of PM2.5 is from natural (non-toxic) sources and what fraction is from combustion emissions.

The chemical composition provides the first critical step to identifying how much of total particle mass is associated with different sources, each of which is associated with different health effects. In the 5 February 2020 UCSD/SIO Report, we used Fourier Transform Infrared (FTIR) spectroscopy and X-ray Fluorescence (XRF) to provide a first cut at the PM2.5 sources, using elemental composition to provide tracers for sea spray, mineral dust, and combustion emissions. This report builds on those results to quantify explicitly the substantial difference between the chemical measurements of dust components and the BAM PM2.5 and PM10 measurements regularly reported by the San Luis Obispo County Air Pollution Control District (APCD) at its CDF air monitoring station on the Nipomo Mesa, approximately 3.2 kilometers (2 miles) inland from Oceano Dunes. First, gravimetric measurements (at partially dried conditions of 35% relative humidity) are used to provide the analogous FRM method for particle mass for comparison to the FEM method hourly BAM. Then mineral dust components from XRF measurements are used to assess the fraction of the measured mass that is associated specifically with wind-blown mineral dust that likely originated from the Oceano Dunes region.

Methods

Aerosol particle sampling at CDF used two louvered PM10 sampling heads [Tolocka et al., 2001] on two separate lines at 16.67 L min^{-1}, followed by a PM10 filter (and bypass flow) on one line and a very sharp-cut cyclone with a calibrated cut at 2.5 μm (VSCC operated at 16.67 L min^{-1}, BGI Inc., Waltham, MA) on the other line. The bypass flow on the first line included a sharp-cut cyclone operated with a calibrated cut at 2.5 μm (SCC 2.229 operated at 7.5 L min^{-1}, BGI Inc., Waltham, MA). All flow rates were calibrated and recorded every ~10 s to verify cyclone performance. The VSCC has been EPA approved [Kenny et al., 2004], which allows for mass concentrations to perform at between -5% and +5% of the actual mass under testing conditions. Deviations from the expected cyclone performance have been shown to result for different reasons (see

Appendix): (1) differences between the actual measurement conditions and the testing conditions used for approval [Li et al., 2019], (2) degraded performance by dust accumulation [Lin et al., 2018], and (3) evaporation of liquid water and other semivolatile components by either the VSCC or SCC [Babila et al., 2020].

Teflon filters were used as substrates and have shown negligible adsorption of volatile organic compounds (VOCs) on duplicate back filters collected simultaneously with each sample [Maria et al., 2003; Gilardoni et al., 2007]. Filters for PM10 and PM2.5 were 1 µm pore size. Blank filters provided a measure of adsorption during sampling and contamination during handling (loading and unloading) and storage. Samples were quality-controlled with the following criteria: all filter and cyclone flow rates were within 5% for the duration of sampling, filter pressure increased by >0.01 psi per m^3 air collected, and no anomalous readings in pressure, temperature, and relative humidity (as defined by the instrument specifications). These quality-control criteria were met for all 30 PM10 samples, 25 of 30 PM2.5 VSCC samples, and 28 of 30 PM2.5 SCC samples. Correlation coefficients are Pearson's R values for linear fits forced to 0, and percentages are based on the fitted lines of quality-controlled, above-detection samples.

The gravimetric masses of reference filters were compared to the 7-hr average of co-located hourly BAM measurements. The hourly BAM concentrations (retrieved 7/1/21 from https://www.arb.ca.gov/aqmis2/aqdselect.php, where data after 2019 are noted as "preliminary") reported were averaged from the start time (1200 local, PDT) until the last measurement recorded at 1 hr before the stop time (1900 local, PDT), namely seven one-hr measurements reported for PST start times of 1100 through 1800 to provide comparison points (in accordance with the website information). At high relative humidity (>70%, such as those at CDF in May 2021, see Appendix, Figure A3), hourly measurements will report higher mass concentrations than multi-hour filter measurements [Schweizer et al., 2016]. Comparisons at other sites between gravimetric and BAM PM2.5 mass concentrations have shown correlation coefficients (R^2) that varied between 0.65 and 0.99 and slopes that differed by as much as 30% depending on season and chemical composition [Hauck et al. 2004].

BAM uses a glass fiber filter for particle collection because of its high efficiency, but the glass fibers are known to have a positive sampling artifact (relative to Teflon) because they can adsorb gaseous SO_2 and HNO_3 into particulate sulfate and nitrate, respectively [Lipfert, 1994]. The amount of artificial nitrate taken up onto glass-fiber filters varies with both relative humidity and temperature changes [Appel et al., 1979].

All filters were weighed prior to sampling to provide filter-specific tare weights. After sampling, filters were weighed again, and the difference between the sampled weight and the tare was the reported gravimetric mass. The weighing procedure (Chester LabNet) for all samples used the PM2.5 reference method at 35±5% relative humidity for the 24 hr period (logged every 5 min), making the samples potentially drier or wetter than the ambient conditions in which they were collected. BAM measurements may also be drier than ambient humidity due to heating of the air when it is drawn into the instrument to an unknown temperature, but values of internal relative humidity are logged with the BAM measurements. Other differences may result from the hour-to-hour differences in the online BAM measurements compared to the offline filter storage at constant conditions.

All samples (and associated blank filters) were non-destructively analyzed by X-ray Fluorescence (XRF) measurements conducted by Chester LabNet (Tigard, OR) on the same filters used for gravimetric measurements. XRF analysis provided trace metal concentrations for elements heavier than Na [Maria et al., 2003].

Sea salt was measured above detection when Na and Cl were above detection (defined as twice uncertainty), which was true for more than 92% of quality-controlled samples. Atmospheric ambient sea-salt concentrations were calculated using measured Cl^- and 1.47*Na^+ concentrations to account for the possible depletion of Cl^- in the atmosphere, where 1.47 is the ratio of $(Na^+ + Mg^{2+} + Ca^{2+} + K^+ + SO_4^{2-} + HCO_3^-)/Na^+$ in seawater [Holland, 1978; Frossard et al., 2014]. This sea-salt calculation represents an upper limit for sea-salt mass because the HCO_3^- would have been titrated before Cl^- was depleted significantly via acid displacement reactions. HCO_3^- is 0.3% of the total mass of sea salt. Excluding HCO_3^- from the ratio, as a lower limit, the ratio of $(Na^+ + Mg^{2+} + Ca^{2+} + K^+ + SO_4^{2-})/Na^+$ is 1.45, instead of 1.47, making the salt mass calculated <2% lower than calculated here.

Mineral dust was measured above detection if Al and Si were above detection (defined as twice uncertainty), which was true for more than 86% of quality-controlled samples. The mass of dust was calculated from XRF metal concentrations, assuming dust consists of $MgCO_3$, Al_2O_3 and SiO_2 (in the form of Al_2SiO_5), K_2O, $CaCO_3$, TiO_2, Fe_2O_3, MnO, and BaO [Liu et al., 2018; Gilardoni et al., 2007; Usher et al., 2003]. This calculation increases the mass by an average factor of 2.14 to account for the O and C associated with the measured elements for the PM10 samples. Because some elements are in both sea salt and mineral dust (K, Ca, Mg), the amount of those elements associated with the Na present was subtracted to avoid double-counting, resulting in ~2% less mass. Alternative approximations of the mineral dust contribution

based on other molecular forms of the same elements were also considered and are compared in the Appendix [Hains et al., 2007; Frank 2006; Malm et al. 1994].

Results

Samples were collected at CDF for the period of 27 April to 26 May 2021. The CDF site was co-located with the ongoing APCD sampling by BAM (beta attenuation monitor), which provides an hourly measurement of PM2.5 and PM10 concentration at near ambient conditions, which means that water and other semivolatile organic and inorganic components (notably ammonium nitrate) are included. The number of sampling days was maximized to document the day-to-day variability in the aerosol and to capture multiple days with high PM2.5 and PM10 concentration. Notably, the days with high PM at CDF were often predicted successfully from short-term forecasts of high-wind conditions, consistent with prior studies.

In order to optimize the sampling range for PM10 and PM2.5, flow rates were designed to not exceed the thin film assumption used for XRF. This condition was met for most samples as designed. However, the lower flow rate meant that some samples on low PM days were below detection limit for gravimetric mass (and some XRF elements). This limitation was by design, since the target of this study was high-PM10 days(defined to be those with 1-hr PM10 exceeding 140 μg m^{-3}), none of which exceeded the XRF thin film assumption and most of which were above detection limit (ADL).

The results addressing the objectives of the research are summarized below. We note that all of the results may differ by season, and their variability may be larger than could be captured in this short study.

1. Quantify the gravimetric mass and elemental component mass of PM10 aerosol particles at CDF.
    a. The time series of SIO gravimetric mass and APCD BAM PM10 concentration measurements tracked reasonably well (Figure 1). The offline gravimetric method is lower on average than the online BAM instrument for most samples at CDF for both VSCC and SCC cyclones (Figure 1). The difference is slightly larger on days with high PM10 (defined to be those with 1-hr PM10 exceeding 140 μg m^{-3}). These observations hold when the below-detection samples are removed (see Appendix).
    b. For the afternoons when hourly PM10 exceeded 140 μg m^{-3} for at least one hour, the gravimetric method PM10 concentration is on average 35%

lower than BAM PM10 concentration. For all samples above detection limit, the gravimetric method PM10 concentration is on average 29% lower than BAM PM10 concentration.

c. The mineral dust component of BAM PM10 ranged from 1% to 32% for ADL samples and from 2% to 32% for high-PM10 day samples. This amount represents an upper bound on the amount of PM10 that could be attributed to mineral dust from sand dune saltation. The average mineral dust amount of BAM PM10 was 14% with variability (standard deviation) of 17% for ADL samples and 14% with variability (standard deviation) of 14% for high-PM10 samples.

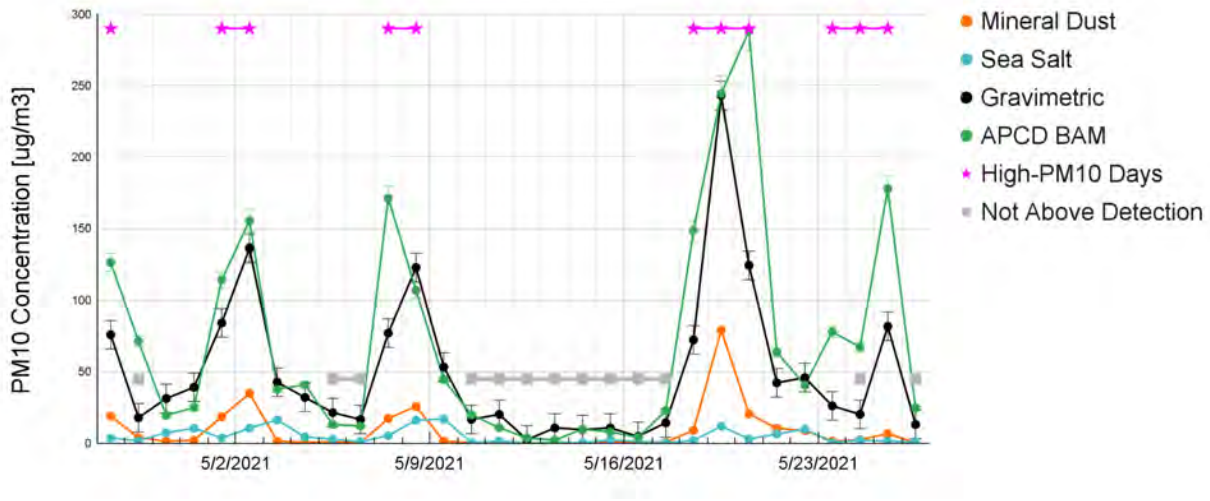

Figure 1. Time series of PM10 mass concentrations [µg m^{-3}] by Gravimetric and BAM methods at CDF from 27 April to 26 May 2021, with XRF Mineral Dust and Sea Salt concentrations (all samples). Error bars represent twice the method uncertainty.

2. Quantify the gravimetric mass and elemental component mass of PM2.5 aerosol particles at CDF.
   a. The time series of SIO gravimetric mass and APCD BAM PM2.5 concentration measurements tracked reasonably well (Figure 2). The offline gravimetric method is lower on average than the online BAM instrument for most samples at CDF for both VSCC and SCC cyclones (Figure 2). The difference is slightly larger on days with high PM10. These observations hold when the below-detection samples are removed (see Appendix).
   b. For the afternoons when hourly PM10 exceeded 140 µg m^{-3} for at least one hour, the gravimetric method PM2.5 is on average 18% for VSCC and

39% for SCC lower than BAM PM2.5. For all samples above detection limit, the gravimetric method PM2.5 is on average 13% for VSCC and 32% for SCC lower than BAM PM2.5.

c. The mineral dust component of BAM PM2.5 by VSCC ranged from 1% to 42% for ADL samples and from 11% to 42% for high-PM10 day samples. The mineral dust component of BAM PM2.5 by SCC ranged from 1% to 34% for ADL samples and from 2% to 31% for high-PM10 day samples. The average mineral dust amount by VSCC of BAM PM2.5 was 20±20% for ADL samples and 27±10% for high-PM10 day samples. The average mineral dust amount by SCC of BAM PM2.5 was 15±14% for ADL samples and 19±19% for high-PM10 day samples.
d. Organic mass concentration was quantified by FTIR for 13 PM2.5 SCC filters at mass concentrations of 0.8-3.7 μg m^{-3} for ADL samples, accounting for 1-18% of BAM PM2.5 concentrations.

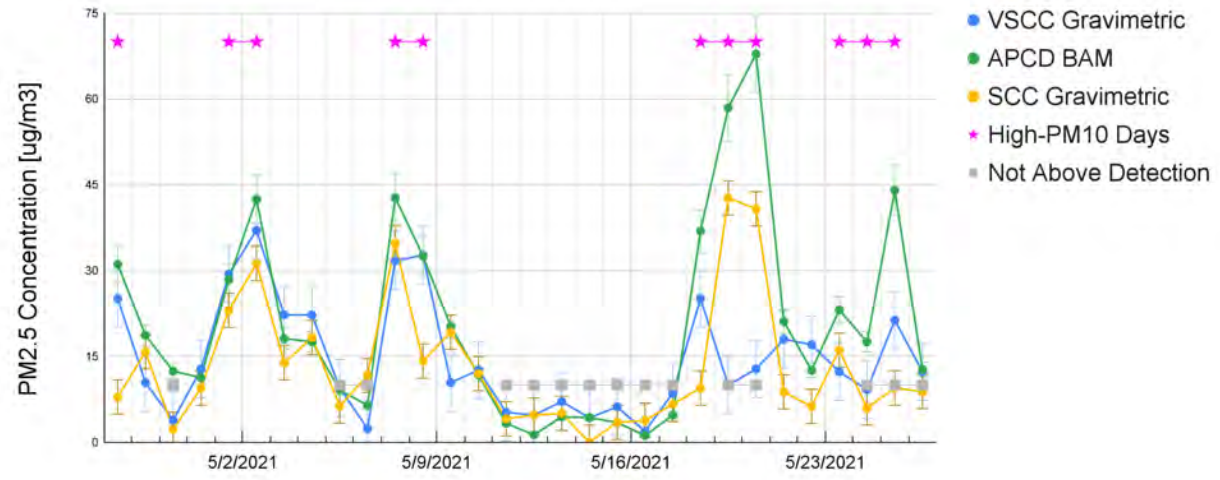

Figure 2. Time series of PM2.5 mass concentrations [μg m^{-3}] by Gravimetric (blue, yellow) and BAM (green) methods at CDF from 27 April to 26 May 2021 (all samples). Error bars represent twice the method uncertainty.

Discussion

BAM has been employed to provide hourly PM10 and PM2.5 concentrations across much of California since the approval of 24-hr average BAM as a federal equivalent method (FEM) in 2008 [USEPA, 2013]. Comparisons of BAM and filter-based reference

methods have shown that BAM values are often higher than filter-based methods because of the loss of the more volatile, or semivolatile, components during collection and equilibration on Teflon filters [Tao and Harley, 2015; Takahashi et al., 2008; Chow et al., 2006]. This has been especially true in regions like California, in which a substantial amount of PM2.5 is contributed by ammonium nitrate, causing the South Coast Air Quality Management District to apply to exclude BAM PM2.5 measurements from determination of attainment [Tao and Harley, 2015], since the standards are based on equilibrated filters by the federal reference method (FRM) rather than BAM. Corrections for BAM to gravimetric have been developed for some regions in order to use BAM to determine if air quality standards are exceeded [Le et al., 2020]

One reason for higher BAM concentrations in coastal areas with high ambient relative humidity is that the BAM may not have sufficient residence time to allow for full equilibration of particles to ~35% relative humidity, making the effective relative humidity of the measurement higher than the 35% required by the FRM. The role of sea salts and other minerals in delaying the loss of water from particles because of hydrate formation is well known [Frossard et al., 2012; Cziczo and Abbatt, 2000; Harvie et al., 1980]. One coastal study in Greece has shown that the amount that BAM exceeds gravimetric is correlated to the normalized water vapor pressure in the air and that the positive bias is highest for relative humidity 40-80% and temperature 11-22°C [Triantafyllou et al., 2016]. Another study showed a 30% positive bias of BAM to gravimetric for temperatures above 16°C and above 80% relative humidity at concentrations of 30-60 μg m^{-3} [Takahashi et al. 2008]. The PM2.5 sampling reference method (https://www3.epa.gov/ttn/amtic/files/ambient/pm25/qa/m212.pdf) requires that samples be stored at 35% relative humidity for a minimum of 24 hr in order to dry the particles to what is assumed to be equilibrium. In contrast, BAM and EBAM measurements are collected at ambient relative humidity and then heated during flowing through the instrument to bring the relative humidity to 35%, allowing only minutes for equilibration on the glass-fiber filter. At CDF ambient relative humidity exceeded 35% for 27 April through 26 May 2021 (Figure A3), meaning that the BAM measurements needed to be dried in order to remove particle-bound water that was present at ambient conditions. Even at relative humidity as low as 50%, the amount of particle-bound water in PM10 has been shown to be as high as 33% by mass compared to filters below 30% relative humidity [Imre et al., 2014]. Some water can even remain after 24 hr equilibration, contributing to reference filter mass concentrations [Rees et al., 2004]. These results make it likely that the difference in mass on high-PM10 days is due to adsorbed water and other semivolatile components (ammonium nitrate and organic mass) evaporating less in the BAM method and more in the gravimetric method [Le et al., 2020; Tao and Harley, 2015]. The lower gravimetric than BAM mass concentrations

are consistent with the expectation that the BAM method includes more water and other semivolatiles that can evaporate during the gravimetric reference method. The increase in the difference between BAM and gravimetric mass concentration on days with high PM10 (35% compared to 29%) is consistent with higher particle loadings giving less complete evaporation in BAM. The water contribution could be assessed by repeating the gravimetric method at higher relative humidities.

Another possibility is that the BAM calibration does not apply well to the composition and concentration conditions that are relevant to this site. EPA approval of BAM relied on testing conditions that were typically limited to concentrations lower than 100 μg m^{-3} and that were 24-hr average measurements [Chung et al., 2001; Gobeli et al., 2008; Hafkenscheid and Vonk, 2014; Hart, 2009]. At PM10 concentrations exceeding 30 μg m^{-3}, BAM and gravimetric methods were not found to be equivalent using consistency criteria [Gebicki and Szymanska, 2012]. BAM PM2.5 performance relative to reference methods has been shown to vary seasonally and to include an uncertainty of 16% [Hafkenscheid and Vonk, 2014]. A large fraction of PM2.5 can be volatile, and comparisons to reference filters typically show a high bias for the BAM [Hart, 2009], especially for PM2.5 concentrations exceeding 40 μg m^{-3} [Le et al., 2020]. This difference varies with relative humidity, often reducing the correlation between BAM and filters [Chow et al., 2005; Hains et al., 2007]. Since relative humidity often varies with a daily cycle (as it does at CDF in May 2021, Figure A3), comparisons of BAM and gravimetric may tend to have a larger bias for comparing partial days (e.g. afternoon only) than for a 24-hr measurement.

Central California studies have shown that 80% of nitrate in PM2.5 can volatilize in spring and summer conditions [Chow et al., 2005]. Particulate nitrate is higher when ambient relative humidity is high [Dassios and Pandis, 1999]. There is also evidence that the positive bias of BAM relative to gravimetric increases for ambient temperatures below 25°C, when the amount of particulate nitrate may be high [Le et al., 2020]. These errors often vary with time of day, with water adsorption in the BAM affecting afternoon readings and desorption affecting readings after midnight, so that hourly BAM concentrations may have biases of ~20 μg m^{-3} even when 24 hr averages include cancelling errors [Kiss et al., 2017].

In summary, there are two types of reasons for the differences between BAM and gravimetric filter measurements here. The first and very well-known reason is the contribution of semivolatile components. These are components that evaporate from particles when temperature increases, including water, ammonium nitrate, and other semivolatiles. Sampling for 24 hr means that some particles on an FRM filter will lose

mass when these components evaporate. Sampling periods shorter than 24 hr can reduce this evaporation if they reduce the amount of temperature change during sample collection [Mader et al., 2001]. This effect means that the online BAM measurement may be closer to ambient particle mass concentrations (i.e. more similar to the atmosphere) but the longer filter measurement is closer to federal and state standard methods (i.e. more similar to the regulated quantity). For this reason, the gravimetric mass concentrations should be used to assess PM10 and PM2.5 exceedances. Since BAM is used to provide more frequent and routine measurements, here we report the fractions of components relative to BAM.

The second reason is different performance of the samplers because of size cut design or flow rate issues. For PM10, both BAM and gravimetric samplers used nominally the same size cut design at the same flow rate [Tolocka et al., 2001]. The performance of the samplers may be affected by the accumulation of particles on the walls of the sampling head (which may entrain large solid particles above the size cut, as has been observed in testing in agricultural regions [Faulkner et al., 2014; Le et al., 2019]). However, the difference between BAM and gravimetric concentrations persisted from the beginning (with a clean sampling head for gravimetric filters) to end (after 30 days without cleaning) of the sampling with similar magnitude (Figure 1), making it difficult to show any effect from either recent cleaning or accumulated particles. This makes it likely that the 35% (56.8 μg m^{-3}) difference on high-PM10 days is attributable to the first reason (semivolatile components) rather than to size cut performance issues [Triantafyllou et al., 2016]. For PM2.5, the same reasoning applies for the 18% (6.3 μg m^{-3}) difference between the VSCC filters and the BAM. The correlation coefficients (see Appendix) are lower than the range found in other studies (R2 .72-.90) [Triantafyllou et al., 2016], which is not surprising given the less than 24-hr averaging times (7 hr), the variable conditions of the short (30-day) study, and the limited number of high-PM10 days (10).

The PM2.5 and PM10 apportionments by component of the BAM concentrations measured at CDF are summarized in Figure 3, where we have labeled the difference between BAM and gravimetric mass as the “Semivolatile” fraction. This fraction is likely from atmospheric water associated with the high ambient relative humidity. Ammonium nitrate and semivolatile organic components may also contribute. Figure 3 also illustrates the measured mass component contributions: mineral dust accounts for 14% of BAM PM10 at CDF on high-PM10 afternoons, ranging from 2% to a single-day high of 32%. This means that on average less than one fifth of the BAM-based PM10 at CDF can be attributed to mineral dust during the 10 high-PM10 days sampled in April-May 2021. The average PM10 concentration on high-PM10 afternoons was 161.2 μg m^{-3}, of

which only 23.2 µg m^{-3} was dust. PM2.5 on high-PM10 days had an average afternoon BAM concentration of 33.9 µg m^{-3}, of which mineral dust accounted for 27% of BAM PM2.5 at CDF (ranging from a low of 11% to a high of 42%).

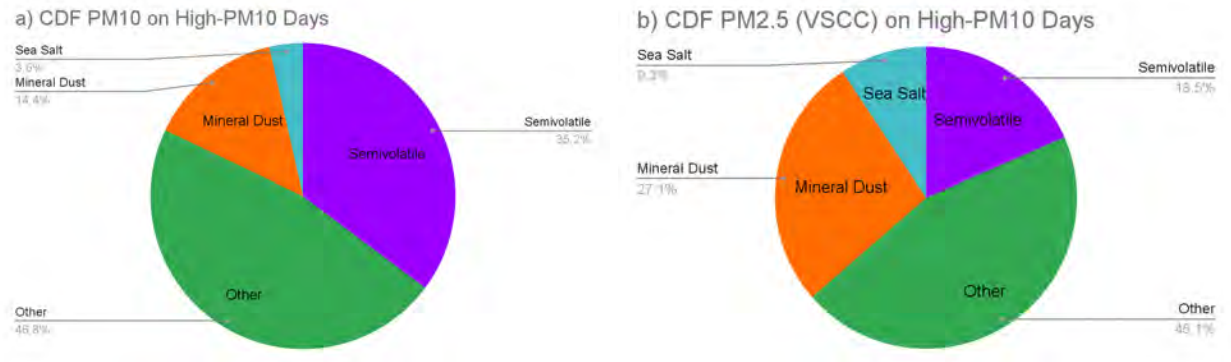

Figure 3. Summary of apportionment of BAM mass concentrations by component for High-PM10 days for (a) PM10 and (b) PM2.5 by VSCC. High-PM10 day samples are those with 1-hr PM10 exceeding 140 µg m^{-3}. "Mineral Dust" provides the upper bound on the amount of PM that could be associated with the sand dune source. The "Semivolatile" is the difference between BAM and gravimetric mass concentration, which may be a combination of incomplete drying of water in BAM and loss of semivolatile components by the filter reference method. The category labeled "Other" (green) includes water and other semivolatile components (ammonium, nitrate, sulfate and organic components), and small amounts of trace metals.

Conclusions

Filter-based chemical mass concentration measurements show that on average 14% of PM10 and 27% (VSCC) of PM2.5 can be attributed to mineral dust on high-PM10 days. Sea salt contributed roughly 4% for PM10 and 9% (VSCC) for PM2.5 on high-PM10 days. The remaining 64% of BAM PM2.5 and 82% of BAM PM10 is likely from water, organic components, ammonium, nitrate, non-sea salt-sulfate, and other semivolatile chemical species. While prior results did not report the mineral dust fraction of BAM or gravimetric PM10 [SLOAPCD, 2007], the reported mineral dust (crustal) fraction of gravimetric PM2.5 reported by the San Luis Obispo Air Pollution Control District for its Nipomo Mesa Particulate Study (Phase 1) for the Mesa2 annual 24-hr average was 20% [SLOAPCD, 2007]. This value is similar to the 7-hr afternoon average in May 2021 for above detection samples reported here (23% of gravimetric), with the higher value

for the afternoons in May being consistent with the timing and season providing a conservative upper bound.

These results show that on average less than one-fifth of the BAM PM10 at CDF can be attributed to dust during the high-PM10 days sampled in April-May 2021. Rarely (one in 10 high-PM10 days sampled) mineral dust accounted for almost one-third of the BAM PM10. There is no evidence of mineral dust contributing all or even the majority of BAM PM10, as has apparently been assumed in past reporting [SLOAPCD, 2007].

The association of high PM10 and PM2.5 with high wind conditions, even when recreational vehicles were limited at Oceano Dunes compared to prior years, indicates that dune-derived mineral dust is more likely to be primarily caused by natural forces (*i.e.* wind) rather than human activities. The attribution of mineral dust to natural wind is a common feature of air quality in the western U.S. [Malm et al., 1994; Noll et al. 1985]. While the short duration of this study provides only limited statistics in support of this result, the longer records provided by APCD provide additional confirmation [Li et al., 2013]. For this reason, the contribution of mineral dust to high PM10 concentrations measured on high wind days in and downwind of Oceano Dunes are likely dominated by natural saltation processes associated with the indigenous geomorphological dune structure rather than by recreational activities, as negligible differences were observed between weekday and weekend concentrations [Li et al., 2013].

PM2.5 and PM10 mass concentrations at CDF show contributions of sea spray and mineral dust during high wind episodes. This result means that a substantial fraction of PM2.5 was not associated with fossil-fuel combustion emissions, so that PM2.5 is not a good predictor of toxic emissions or health effects for this location in high wind conditions. For this reason, direct measurements of toxics would be needed in order to associate PM2.5 (or PM10) with health effects at this location.

Acknowledgments

The Scripps/UCSD team is grateful for the insight, advice, and assistance of Will Harris with the California Geological Survey, California Department of Parks and Recreation Oceano Dunes District personnel, CalFire Arroyo Grande Station staff, and APCD personnel.

References

Aghababaeian, H., Ostadtaghizadeh, A., Ardalan, A., Asgary, A., Akbary, M., Yekaninejad, M. S., & Stephens, C. (2021). Global Health Impacts of Dust Storms: A Systematic Review. *Environmental health insights*. https://doi.org/10.1177/11786302211018390

Appel, B. R., Wall, S. M., Tokiwa, Y., & Haik, M. (1979). INTERFERENCE EFFECTS IN SAMPLING PARTICULATE NITRATE IN AMBIENT AIR. *Atmospheric Environment*, *13*(2), 319-325. https://doi.org/10.1016/0004-6981(79)90175-6

Apte, J. S., Brauer, M., Cohen, A. J., Ezzati, M., & Pope, C. A. (2018). Ambient PM2.5 Reduces Global and Regional Life Expectancy. *Environmental Science & Technology Letters*, *5*(9), 546-551. https://doi.org/10.1021/acs.estlett.8b00360

Babila, J. E., Carlton, A. G., Hennigan, C. J., & Ghate, V. P. (2020). On Aerosol Liquid Water and Sulfate Associations: The Potential for Fine Particulate Matter Biases. *Atmosphere*, *11*(2), Article 194. https://doi.org/10.3390/atmos11020194

Chen, C.-L., Chen, S., Russell, L. M., Liu, J., Price, D. J., Betha, R., . . . Cappa, C. D. (2018). Organic Aerosol Particle Chemical Properties Associated With Residential Burning and Fog in Wintertime San Joaquin Valley (Fresno) and With Vehicle and Firework Emissions in Summertime South Coast Air Basin (Fontana). *Journal of Geophysical Research: Atmospheres*, *123*(18), 10,707-710,731. https://doi.org/doi:10.1029/2018JD028374

Chen, C. C., & Huang, S. H. (1999). Shift of aerosol penetration in respirable cyclone samplers. *American Industrial Hygiene Association Journal*, *60*(6), 720-729. https://doi.org/10.1080/00028899908984494

Chow, J. C., & Watson, J. G. (2008). New directions: Beyond compliance air quality measurements. *Atmospheric Environment*, *42*(20), 5166-5168. https://doi.org/10.1016/j.atmosenv.2008.05.004

Chow, J. C., Watson, J. G., Lowenthal, D. H., & Magliano, K. L. (2005). Loss of PM2.5 nitrate from filter samples in central California. *Journal of the Air & Waste Management Association*, *55*(8), 1158-1168. https://doi.org/10.1080/10473289.2005.10464704

Chung, A., Chang, D. P. Y., Kleeman, M. J., Perry, K. D., Cahill, T. A., Dutcher, D., . . . Stroud, K. (2001). Comparison of real-time instruments used to monitor airborne particulate matter. *Journal of the Air & Waste Management Association*, *51*(1), 109-120. https://doi.org/10.1080/10473289.2001.10464254

Craig, J. (2011). *Memo on Mesa2 PM2.5/10 Ratio Data Analysis from Joel Craig (SLOAPCD) to Larry Allen, Richard Countess on 11 March 2011*.

Crooks, J. L., Cascio, W. E., Percy, M. S., Reyes, J., Neas, L. M., & Hilborn, E. D. (2016). The Association between Dust Storms and Daily Non-Accidental Mortality in the United States, 1993-2005. *Environmental Health Perspectives*, *124*(11), 1735-1743. https://doi.org/10.1289/ehp216

Cziczo, D. J., & Abbatt, J. P. D. (2000). Infrared observations of the response of NaCl, MgCl2, NH4HSO4, and NH4NO3 aerosols to changes in relative humidity from 298 to 238 K. *Journal of Physical Chemistry A*, *104*(10), 2038-2047. https://doi.org/10.1021/jp9931408

Dassios, K. G., & Pandis, S. N. (1999). The mass accommodation coefficient of ammonium nitrate aerosol. *Atmospheric Environment*, *33*(18), 2993-3003. https://doi.org/10.1016/s1352-2310(99)00079-5

Dockery, D. W., Pope, C. A., 3rd, Xu, X., Spengler, J. D., Ware, J. H., Fay, M. E., . . . Speizer, F. E. (1993). An association between air pollution and mortality in six U.S. cities. *The New England journal of medicine*, *329*(24), 1753-1759. https://doi.org/10.1056/nejm199312093292401

Faulkner, W. B., Smith, R., & Haglund, J. (2014). Large Particle Penetration During PM10 Sampling. *Aerosol Science and Technology*, *48*(6), 676-687. https://doi.org/10.1080/02786826.2014.915005

Frank, N. H. (2006). Retained nitrate, hydrated sulfates, and carbonaceous mass in Federal Reference Method fine particulate matter for six eastern US cities. *Journal of the Air & Waste Management Association*, *56*(4), 500-511. https://doi.org/10.1080/10473289.2006.10464517

Frossard, A. A., & Russell, L. M. (2012). Removal of Sea Salt Hydrate Water from Seawater-Derived Samples by Dehydration. *Environmental Science & Technology*, *46*(24), 13326-13333. https://doi.org/10.1021/es3032083

Frossard, A. A., Russell, L. M., Burrows, S. M., Elliott, S. M., Bates, T. S., & Quinn, P. K. (2014). Sources and composition of submicron organic mass in marine aerosol particles. *Journal of Geophysical Research: Atmospheres*, *119*(22), 12,977-913,003. https://doi.org/10.1002/2014JD021913

Gebicki, J., & Szymanska, K. (2012). Comparative field test for measurement of PM10 dust in atmospheric air using gravimetric (reference) method and beta-absorption method (Eberline FH 62-1). *Atmospheric Environment*, *54*, 18-24. https://doi.org/10.1016/j.atmosenv.2012.02.068

Gilardoni, S., Russell, L. M., Sorooshian, A., Flagan, R. C., Seinfeld, J. H., Bates, T. S., . . . Worsnop, D. R. (2007). Regional variation of organic functional groups in aerosol particles on four US east coast platforms during the International Consortium for Atmospheric Research on Transport and Transformation 2004 campaign. *Journal of Geophysical Research-Atmospheres*, *112*(D10), Article D10s27. https://doi.org/10.1029/2006jd007737

Gobeli, D., Schloesser, H., & Pottberg, T. (2008). *Met One Instruments BAM-1020 Beta Attenuation Monitor US-EPA PM2.5 Federal Equivalent Method Field Test Results*. Air and Waste Management Association. https://citeseerx.ist.psu.edu/viewdoc/download?doi=10.1.1.584.2489&rep=rep1&type=pdf

Gwinn, M. R., & Vallyathan, V. (2006). Nanoparticles: Health effects - Pros and cons. *Environmental Health Perspectives*, *114*(12), 1818-1825. https://doi.org/10.1289/ehp.8871

Hafkenscheid, T. L., & Vonk, J. (2014). *Evaluation of equivalence of the MetOne BAM-1020 for the measurement of PM2.5 in ambient air*. National Institute for Public Health and the Environment, Bilthoven, the Netherlands. https://www.rivm.nl/bibliotheek/rapporten/2014-0078.pdf

Hains, J. C., Chen, L. W. A., Taubman, B. F., Doddridge, B. G., & Dickerson, R. R. (2007). A, side-by-side comparison of filter-based PM2.5 measurements at a suburban site: A closure study. *Atmospheric Environment*, *41*(29), 6167-6184. https://doi.org/10.1016/j.atmosenv.2007.04.008

Hart, D. (2009). *What is the Difference Between the New BAM-1020 PM2.5 FEM and Older BAM-1020 Monitors?* . Met One Technical Bulletin. https://metone.com/wp-content/uploads/2019/04/bam_pm2.5_fem_compared_to_older_bam-1020.pdf

Harvie, C. E., Weare, J. H., Hardie, L. A., & Eugster, H. P. (1980). EVAPORATION OF SEAWATER - CALCULATED MINERAL SEQUENCES. *Science*, *208*(4443), 498-500.

Hauck, H., Berner, A., Gomiscek, B., Stopper, S., Puxbaum, H., Kundi, M., & Preining, O. (2004). On the equivalence of gravimetric PM data with TEOM and beta-attenuation measurements. *Journal of Aerosol Science*, *35*(9), 1135-1149. https://doi.org/10.1016/j.jaerosci.2004.04.004

Hoek, G., Brunekreef, B., Goldbohm, S., Fischer, P., & van den Brandt, P. A. (2002). Association between mortality and indicators of traffic-related air pollution in the Netherlands: a cohort study. *Lancet*, *360*(9341), 1203-1209. https://doi.org/10.1016/s0140-6736(02)11280-3

Holland, H. D. (1978). *The Chemistry of the Atmosphere and Oceans*. John Wiley.

Huang, C. H., & Tai, C. Y. (2008). Relative humidity effect on PM2.5 readings recorded by collocated beta attenuation monitors. *Environmental Engineering Science*, *25*(7), 1079-1089. https://doi.org/10.1089/ees.2007.0142

Imre, K., Molnar, A., Dezsi, V., & Geleneser, A. (2014). Positive bias caused by residual water in reference PM10 measurements. *Idojaras*, *118*(3), 207-216.

Janssen, N. A. H., Brunekreef, B., van Vliet, P., Aarts, F., Meliefste, K., Harssema, H., & Fischer, P. (2003). The relationship between air pollution from heavy traffic and allergic sensitization, bronchial hyperresponsiveness, and respiratory symptoms in Dutch schoolchildren. *Environmental Health Perspectives*, *111*(12), 1512-1518. https://doi.org/10.1289/ehp.6243

Kenny, L. C., Merrifield, T., Mark, D., Gussman, R., & Thorpe, A. (2004). The development and designation testing of a new USEPA-approved fine particle inlet: A study of the USEPA designation process. *Aerosol Science and Technology*, *38*, 15-22. https://doi.org/10.1080/027868290502290

Kenny, L. C., & Thorpe, A. (2000). *Evaluation of VSCC Cyclones for BGI Incorporated*. Mesa Labs. https://bgi.mesalabs.com/wp-content/uploads/sites/35/2015/02/vsccref6-2.946.pdf

Kenny, L. C., Thorpe, A., & Stacey, P. (2017). A collection of experimental data for aerosol monitoring cyclones. *Aerosol Science and Technology*, *51*(10), 1190-1200. https://doi.org/10.1080/02786826.2017.1341620

Kiss, G., Imre, K., Molnar, A., & Gelencser, A. (2017). Bias caused by water adsorption in hourly PM measurements. *Atmospheric Measurement Techniques*, *10*(7). https://doi.org/10.5194/amt-10-2477-2017

Knol, A. B., de Hartog, J. J., Boogaard, H., Slottje, P., van der Sluijs, J. P., Lebret, E., . . . Hoek, G. (2009). Expert elicitation on ultrafine particles: likelihood of health effects and causal pathways. *Particle and Fibre Toxicology*, *6*, Article 19. https://doi.org/10.1186/1743-8977-6-19

Krasnov, H., Katra, I., Koutrakis, P., & Friger, M. D. (2014). Contribution of dust storms to PM10 levels in an urban arid environment. *Journal of the Air & Waste Management Association*, *64*(1), 89-94. https://doi.org/10.1080/10962247.2013.841599

Le, T. C., Shukla, K. K., Chen, Y. T., Chang, S. C., Lin, T. Y., Li, Z., . . . Tsai, C. J. (2020). On the concentration differences between PM2.5 FEM monitors and FRM samplers. *Atmospheric Environment*, *222*, Article 117138. https://doi.org/10.1016/j.atmosenv.2019.117138

Le, T. C., Shukla, K. K., Sung, J. C., Li, Z. Y., Yeh, H. J., Huang, W., & Tsai, C. J. (2019). Sampling efficiency of low-volume PM10 inlets with different impaction

substrates. *Aerosol Science and Technology*, *53*(3), 295-308. https://doi.org/10.1080/02786826.2018.1559919

Li, R., Wiedinmyer, C., & Hannigan, M. P. (2013). Contrast and correlations between coarse and fine particulate matter in the United States. *Science of the Total Environment*, *456*, 346-358. https://doi.org/10.1016/j.scitotenv.2013.03.041

Li, X. H., Ruan, B., Hopke, P. K., & Mehmood, T. (2019). On the Performance Parameters of PM2.5 and PM1 Size Separators for Ambient Aerosol Monitoring. *Aerosol and Air Quality Research*, *19*(10), 2173-2184. https://doi.org/10.4209/aaqr.2019.03.0103

Lin, C. W., Chen, T. J., Huang, S. H., Kuo, Y. M., Gui, H. Q., & Chen, C. C. (2018). Effect of Aerosol Loading on Separation Performance of PM2.5 Cyclone Separators. *Aerosol and Air Quality Research*, *18*(6), 1366-1374. https://doi.org/10.4209/aaqr.2017.11.0458

Lipfert, F. W. (1994). FILTER ARTIFACTS ASSOCIATED WITH PARTICULATE MEASUREMENTS - RECENT-EVIDENCE AND EFFECTS ON STATISTICAL RELATIONSHIPS. *Atmospheric Environment*, *28*(20), 3233-3249. https://doi.org/10.1016/1352-2310(94)00167-j

Liu, J., Dedrick, J., Russell, L. M., Senum, G. I., Uin, J., Kuang, C. G., . . . Lubin, D. (2018). High summertime aerosol organic functional group concentrations from marine and seabird sources at Ross Island, Antarctica, during AWARE. *Atmospheric Chemistry and Physics*, *18*(12), 8571-8587. https://doi.org/10.5194/acp-18-8571-2018

Lundgren, D. A., & Burton, R. M. (1995). EFFECT OF PARTICLE-SIZE DISTRIBUTION ON THE CUT POINT BETWEEN FINE AND COARSE AMBIENT MASS FRACTIONS. *Inhalation Toxicology*, *7*(1), 131-148.

Mader, B. T., & Pankow, J. F. (2001). Gas/solid partitioning of semivolatile organic compounds (SOCs) to air filters. 3. An analysis of gas adsorption artifacts in measurements of atmospheric SOCs and organic carbon (OC) when using Teflon membrane filters and quartz fiber filters [Article]. *Environmental Science & Technology*, *35*(17), 3422-3432. https://doi.org/10.1021/es0015951

Malm, W. C., Sisler, J. F., Huffman, D., Eldred, R. A., & Cahill, T. A. (1994). SPATIAL AND SEASONAL TRENDS IN PARTICLE CONCENTRATION AND OPTICAL EXTINCTION IN THE UNITED-STATES. *Journal of Geophysical Research-Atmospheres*, *99*(D1), 1347-1370. https://doi.org/10.1029/93jd02916

Maria, S. F., Russell, L. M., Turpin, B. J., Porcja, R. J., Campos, T. L., Weber, R. J., & Huebert, B. J. (2003). Source signatures of carbon monoxide and organic functional groups in Asian Pacific Regional Aerosol Characterization Experiment (ACE-Asia)

submicron aerosol types. *Journal of Geophysical Research-Atmospheres*, *108*(D23), Article 8637. https://doi.org/10.1029/2003jd003703

McDonald, B. C., de Gouw, J. A., Gilman, J. B., Jathar, S. H., Akherati, A., Cappa, C. D., . . . Trainer, M. (2018). Volatile chemical products emerging as largest petrochemical source of urban organic emissions [Article]. *Science*, *359*(6377), 760-764, Article aaq0524. https://doi.org/10.1126/science.aaq0524

Motallebi, N., Taylor, C. A., & Croes, B. E. (2003). Particulate matter in California: Part 2 - Spatial, temporal, and compositional patterns of PM2.5, PM10-2.5, and PM10. *Journal of the Air & Waste Management Association*, *53*(12), 1517-1530. https://doi.org/10.1080/10473289.2003.10466323

Noll, K. E., Pontius, A., Frey, R., & Gould, M. (1985). COMPARISON OF ATMOSPHERIC COARSE PARTICLES AT AN URBAN AND NON-URBAN SITE. *Atmospheric Environment*, *19*(11), 1931-1943. https://doi.org/10.1016/0004-6981(85)90019-8

Oberdorster, G., Stone, V., & Donaldson, K. (2007). Toxicology of nanoparticles: A historical perspective. *Nanotoxicology*, *1*(1), 2-25. https://doi.org/10.1080/17435390701314761

Peters, T. M., Gussman, R. A., Kenny, L. C., & Vanderpool, R. W. (2001). Evaluation of PM2.5 size selectors used in speciation samplers. *Aerosol Science and Technology*, *34*(5), 422-429.

Pope, C. A., Ezzati, M., & Dockery, D. W. (2009). Fine-Particulate Air Pollution and Life Expectancy in the United States. *New England Journal of Medicine*, *360*(4), 376-386. https://doi.org/10.1056/NEJMsa0805646

Rees, S. L., Robinson, A. L., Khlystov, A., Stanier, C. O., & Pandis, S. N. (2004). Mass balance closure and the federal reference method for PM2.5 in Pittsburgh, Pennsylvania. *Atmospheric Environment*, *38*(20), 3305-3318. https://doi.org/10.1016/j.atmosenv.2004.03.016

Russell, L. M. (2003). Aerosol organic-mass-to-organic-carbon ratio measurements. *Environmental Science & Technology*, *37*(13), 2982-2987. https://doi.org/10.1021/es026123w

Russell, L. M., Bahadur, R., & Ziemann, P. J. (2011). Identifying organic aerosol sources by comparing functional group composition in chamber and atmospheric particles [Article]. *Proceedings of the National Academy of Sciences of the United States of America*, *108*(9), 3516-3521. https://doi.org/10.1073/pnas.1006461108

Russell, L. M., Hawkins, L. N., Frossard, A. A., Quinn, P. K., & Bates, T. S. (2010). Carbohydrate-like composition of submicron atmospheric particles and their production from ocean bubble bursting. *Proceedings of the National Academy of*

Sciences of the United States of America, *107*(15), 6652-6657. https://doi.org/10.1073/pnas.0908905107

Schweizer, D., Cisneros, R., & Shaw, G. (2016). A comparative analysis of temporary and permanent beta attenuation monitors: The importance of understanding data and equipment limitations when creating PM2.5 air quality health advisories. *Atmospheric Pollution Research*, *7*(5), 865-875. https://doi.org/10.1016/j.apr.2016.02.003

Shepherd, G., Terradellas , E., Baklanov, A., Kang, U., Sprigg, W. A., & Nickovic, S. B., A.D. Al-Dousari , A. Basart , S. Benedetti, A. Sealy, A. Tong, D. Zhang, X. Shumake-Guillemot , J. Kebin, Z. Knippertz, P. Mohammed, A. A. A. Al-Dabbas, M. Cheng, L. Otani , S. Wang, F. Zhang, C. Ryoo, S. B. Cha, J. (2016). *Global Assessment of Sand and Dust Storms*. United Nations Environment Program. https://uneplive.unep.org/redesign/media/docs/assessments/global_assessment_of_sand_and_dust_storms.pdf

SLOAPCD. (2007). *Nipomo Mesa Particulate Study (Phase 1)*. San Luis Obispo Air Pollution Control District. https://storage.googleapis.com/slocleanair-org/images/cms/upload/files/Phase1PMStudyReport2.pdf

Takahashi, K., Minoura, H., & Sakamoto, K. (2008). Examination of discrepancies between beta-attenuation and gravimetric methods for the monitoring of particulate matter. *Atmospheric Environment*, *42*(21), 5232-5240. https://doi.org/10.1016/j.atmosenv.2008.02.057

Tao, L., & Harley, R. A. (2014). Changes in fine particulate matter measurement methods and ambient concentrations in California. *Atmospheric Environment*, *98*, 676-684. https://doi.org/10.1016/j.atmosenv.2014.09.044

Tegen, I., & Fung, I. (1995). CONTRIBUTION TO THE ATMOSPHERIC MINERAL AEROSOL LOAD FROM LAND-SURFACE MODIFICATION. *Journal of Geophysical Research-Atmospheres*, *100*(D9), 18707-18726. https://doi.org/10.1029/95jd02051

Tegen, I., Werner, M., Harrison, S. P., & Kohfeld, K. E. (2004). Relative importance of climate and land use in determining present and future global soil dust emission. *Geophysical Research Letters*, *31*(5), Article L05105. https://doi.org/10.1029/2003gl019216

Tolocka, M. P., Peters, T. M., Vanderpool, R. W., Chen, F. L., & Wiener, R. W. (2001). On the modification of the low flow-rate PM10 dichotomous sampler inlet. *Aerosol Science and Technology*, *34*(5), 407-415. https://doi.org/10.1080/02786820119350

Tong, D. Q., Wang, J. X. L., Gill, T. E., Lei, H., & Wang, B. Y. (2017). Intensified dust storm activity and Valley fever infection in the southwestern United States.

Geophysical Research Letters, *44*(9), 4304-4312. https://doi.org/10.1002/2017gl073524

Triantafyllou, E., Diapouli, E., Tsilibari, E. M., Adamopoulos, A. D., Biskos, G., & Eleftheriadis, K. (2016). Assessment of factors influencing PM mass concentration measured by gravimetric & beta attenuation techniques at a suburban site. *Atmospheric Environment*, *131*, 409-417. https://doi.org/10.1016/j.atmosenv.2016.02.010

USEPA. (2013). *Revised Requirements for Designation of Reference and Equivalent Methods for PMINF2.5/INF and Ambient Air Quality Surveillance for Particulate Matter*. United States Environmental Protection Agency. https://www.govinfo.gov/app/details/FR-1997-07-18/97-18579

Appendix

For completeness, the measured composition of all CDF PM10 and PM2.5 measurements are shown in Figure A1. These include PM10 and VSCC and SCC PM2.5 for High-PM10 days and for all days that were above detection. The mineral dust contribution is 14% for PM10 on both High-PM10 days and all days above detection. For PM2.5, the High-PM10 days have a higher contribution of 27% for VSCC (19% for SCC) compared to 20% for VSCC (15% for SCC) on all days above detection.

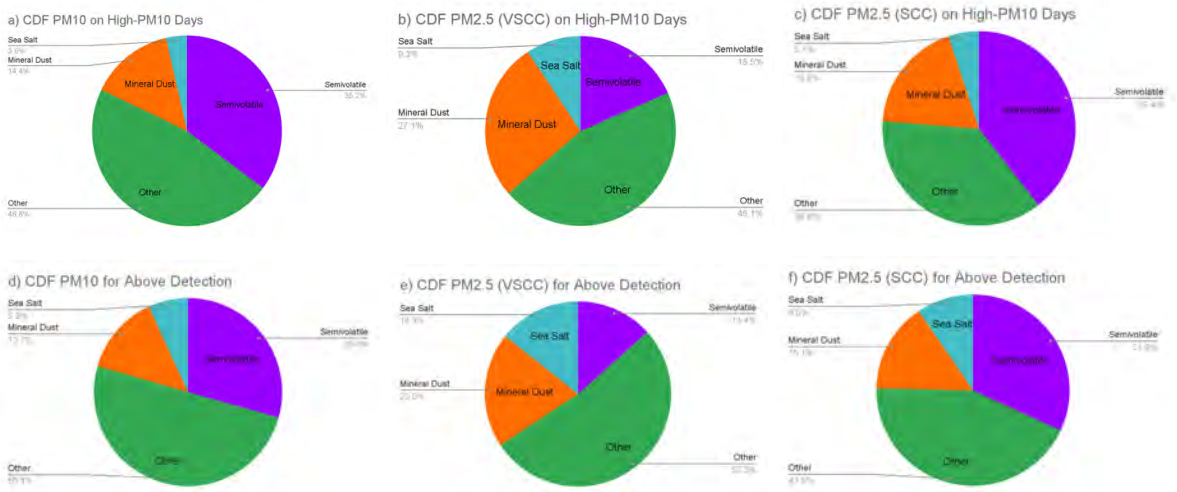

Figure A1. Summary of apportionment of BAM mass concentrations by Component for (a,b,c) Hi-PM10 days and (d,e,f) all samples that were above the detection limits. High PM10 day samples are those with 1-hr PM10 exceeding 140 µg m^{-3}. "Mineral Dust" provides the upper bound on the amount of PM that could be associated with the sand dune source. The "Semivolatile" is the difference between BAM and gravimetric mass concentration based on incomplete drying in BAM, and it is likely to include water, ammonium nitrate, and other semivolatile components. The category labeled "Other" (green) may include water and other semivolatile components (ammonium, nitrate, sulfate and organic components) as well as non-volatile components that remain at 35% relative humidity and were not measured by this project.

There were 14 measurements that were above detection limits for VSCC and SCC; 11 of these were at mass concentrations below 20 µg m^{-3} which meant an uncertainty of 25-50% for a gravimetric measurement error of 10 µg, resulting in only a moderate correlation (R=0.51). This lack of sufficient data for a comparison is the result of targeting higher concentrations and a short time period in order to quantify the maximum mineral dust contribution. Nevertheless, on average, the SCC measurements were consistently lower than the VSCC 27%. As noted above, the less-sharp SCC

cutoff can only explain this if ~30% of PM2.5 mass concentration lies directly below the PM2.5 cutoff with very little mass above the PM2.5 cutoff. While this is possible, it is an unusual particle size distribution for mineral dust and should be confirmed with size-resolved composition measurements.

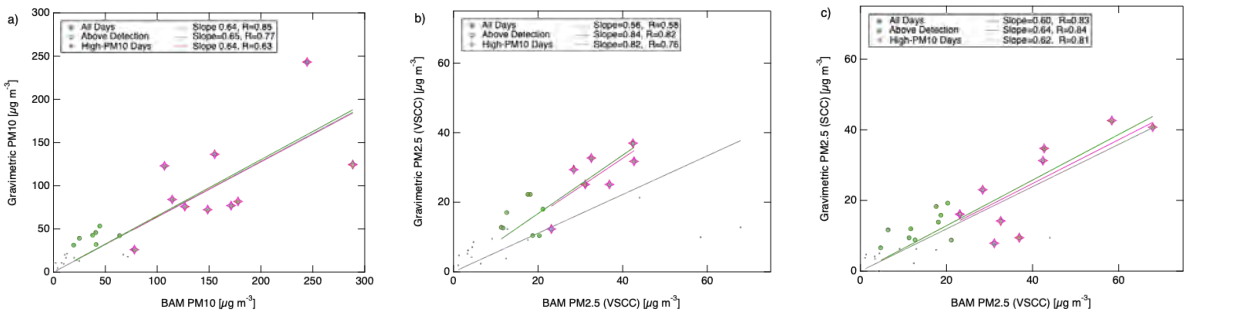

Figure A2. Comparison of gravimetric and BAM PM10 and PM2.5 (VSCC and SCC) at CDF. Legends include slopes and correlation coefficients for linear fits forced to zero.

The SCC method has demonstrated size cut sharpness of 1.25 [Cauda et al., 2014].The VSCC method has a reported sharpness of 1.16 under clean conditions [Kenny and Thorpe, 2000], although that sharpness is expected to increase (i.e. become less sharp) as particles accumulate in the cyclone between cleaning [Kenny et al., 2004]. There is also evidence that performance of similar cyclones degrades at increasing relative humidity due to wall effects [Chen and Huang, 1999]. Desorption or adsorption of semivolatile components can occur during sampling and during storage, tending to increase with higher flow rates, longer sampling times, changing temperatures, and changing ambient conditions [Lipfert, 1994; Appel et al., 1979; Mader et al., 2001].

We can further investigate the PM2.5 differences by comparing the VSCC and the SCC mass concentrations. On the 7 high-PM10 days when both VSCC and SCC sampled, the average gravimetric mass concentration was 27.6 μg m^{-3} for VSCC and 19.5 μg m^{-3} for SCC. Of the difference of 8.1 μg m^{-3}, the concentration that is attributable to salt is 1.2 μg m^{-3} and to mineral dust is 3.6 μg m^{-3} leaving 3.2 μg m^{-3} attributable to differences in semivolatile or unmeasured components. This result indicates that 60% of the difference was due to size cut performance with the VSCC collecting more mass than the SCC, and that up to 40% of the difference may have been due to differences in adsorption and desorption associated with the different flow rates. As expected, this difference is small compared to the 6.3 μg m^{-3} difference between VSCC filters and BAM PM2.5 on high-PM10 days, since both filter methods will have more net desorption of semivolatiles than BAM. The difference in size cut performance of 4.8 μg m^{-3} (18%) between VSCC and SCC is higher than has been reported for other intercomparisons in

the literature [Kenny et al., 2017; Peters et al., 2001]. The low bias of SCC relative to VSCC could only be explained by the larger sharpness value of 1.25 compared to 1.16 if there are higher mass concentrations just below 2.5 µm than above the 2.5 µm, as that would be the condition under which the higher sharpness of VSCC collection exceeds SCC collection [Li et al., 2019]. Further size-resolved chemical measurements could be used to confirm this assertion. This explanation seems unlikely given that SCC penetration curves often show a bias toward larger sizes [Peters et al., 2001]. This result is consistent with previous reports of high PM2.5 relative to PM10 near CDF [Craig, 2011; SLOAPCD, 2007].

There are a number of other reasons that VSCC and SCC differ, including performance degradation caused by changes in loading and humidity that can change VSCC or SCC cutoff performance or sharpness [Chen and Huang, 1999; Lin et al., 2018; Kenny et al., 2004]. For example, changes in VSCC sharpness from 1.16 to 1.19 have been observed after multiple days of high concentrations (150 µg m^{-3}), which resulted in a small positive bias by the VSCC when tested on coarse aerosol [Kenny et al., 2004]. The high bias of VSCC was also present in field tests with high ratios of coarse to fine aerosols, as in Phoenix, Arizona, although observations at high concentrations were not available [Kenny et al., 2004]. SCC differences from the EPA method of record (Well Impactor Ninety-Six, WINS, described in the US Federal Register 40 CFR Part 50, Appendix L, https://www.ecfr.gov/current/title-40/chapter-I/subchapter-C/part-50) for PM2.5 have typically been reported <5% [Lin et al., 2018], with a lower decrease in efficiency from high loading and higher differences for coarse aerosol [Kenny et al. 2000]. It is also possible that the lower flow rate used for the SCC could enhance particle losses in the cyclone [Mader et al., 2001; Appel et al. 1979]. While lower SCC sharpness could account for some of the mass difference between SCC and BAM PM2.5, the remaining difference of 18% for VSCC would still only be explained by evaporation of some components or BAM calibration issues. Moreover, it does not explain the 35% difference between gravimetric and BAM PM10. Records of the BAM internal temperature and relative humidity could show the water content in the BAM, which could have a strong effect on the comparison [Huang and Tai, 2007]. For consistency with the BAM (with VSCC size cut), the VSCC filter results are used for PM2.5 apportionment.

Ambient relative humidity varies during the course of a typical day at CDF, with a minimum of 60-80% at approximately noon (Figure A3). This means the relative humidity in the afternoon is typically increasing to the night time value of 60-80%. When ambient relative humidity is increasing, BAM measurements may tend to be higher than gravimetric even though the 24 hr average may be similar.

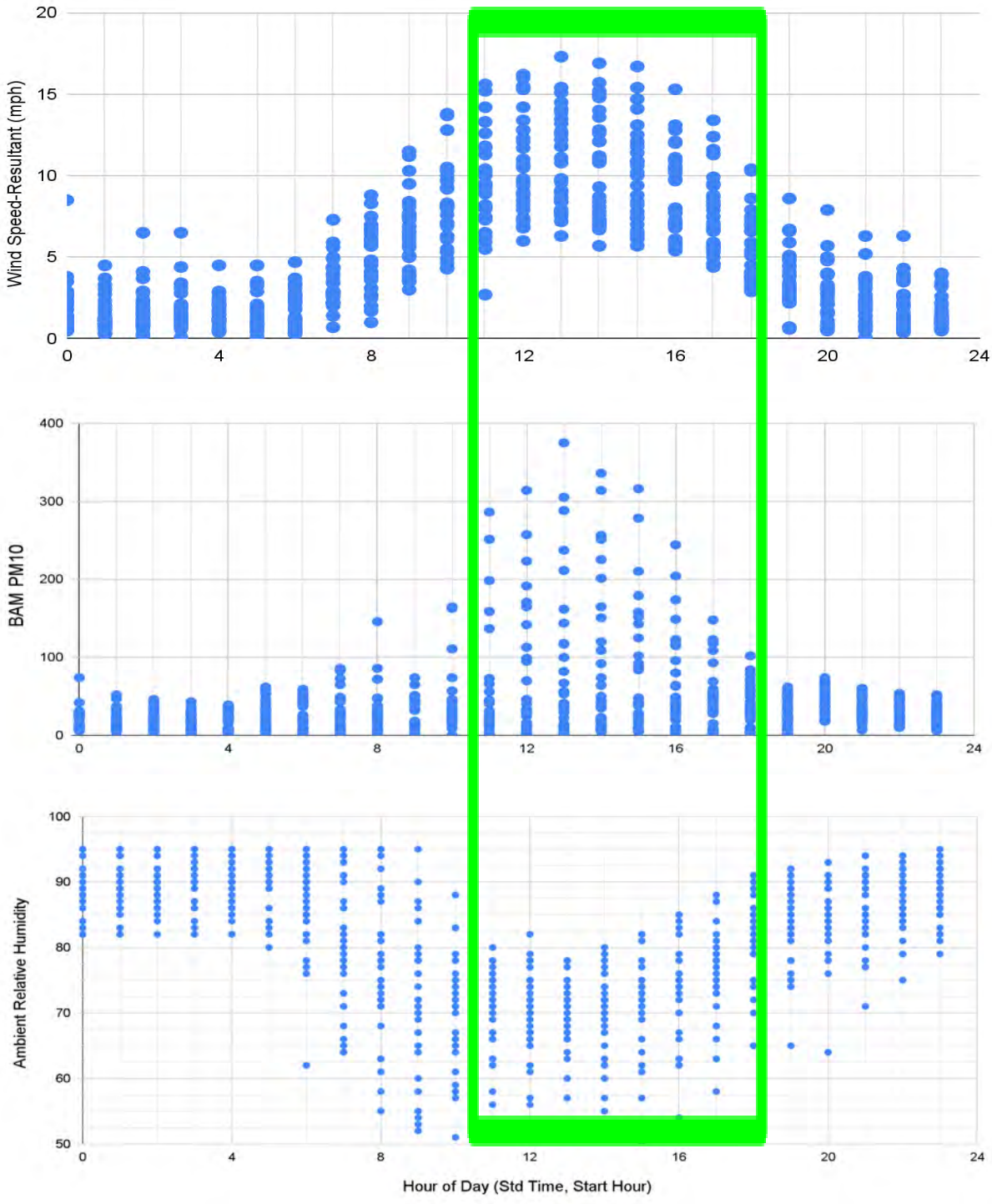

Figure A3. Daily time series of wind speed (top), BAM PM10 (middle), and ambient relative humidity (bottom) from 27 April to 26 May 2021 at CDF. The green box shows the filter sampling time to capture the highest wind speeds with the highest mineral dust contributions. This time period includes increasing ambient relative humidity.

There are several estimates for crustal material from elemental composition that have been introduced. A classic estimate for the western U.S. [Malm et al., 1994; Motallebi et al., 2003] is based on five of the most prevalent elements (Al, Si, Ca, Fe, Ti) and was also used by San Luis Obispo Air Pollution Control District for its Nipomo Mesa Particulate Study (Phase 1) [SLOAPCD, 2007]. A more comprehensive estimate was proposed to account for additional minerals from nine elements (Mg, Al, Si, K, Ca, Ti, Fe, Mn, Ba) [Usher et al., 2003], but needed to be corrected to avoid double counting of sea salt components (Mg, Ca, K) [Gilardoni et al, 2007]. Figure A4 shows that these three estimates are within ±3% of each other.

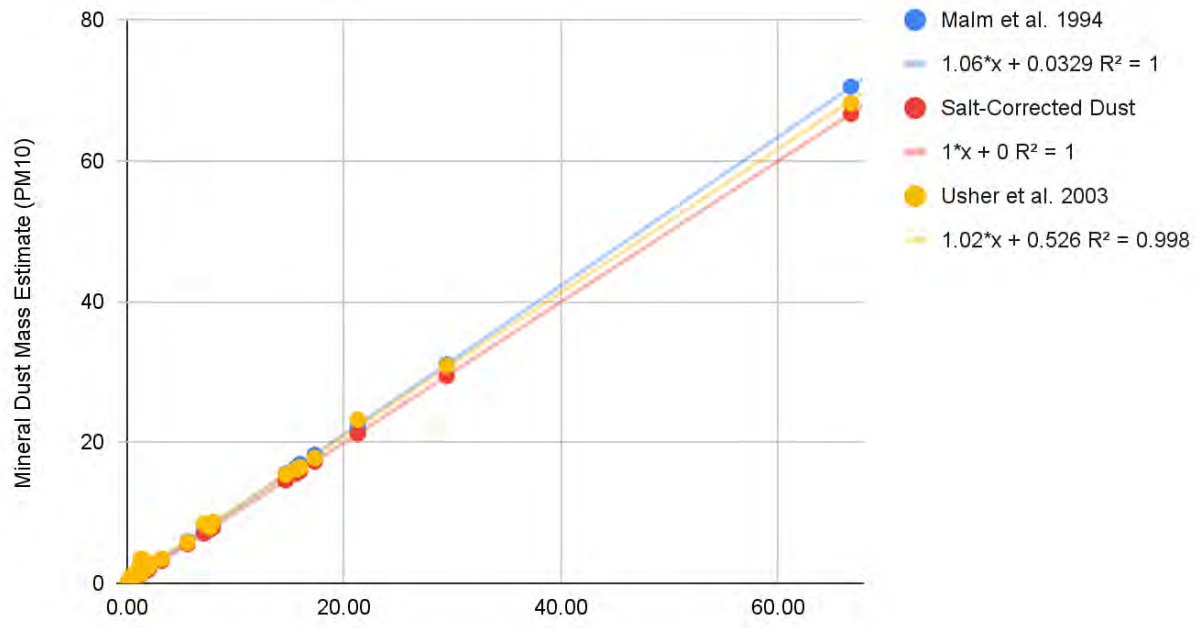

Figure A4. Mineral dust calculation comparison of Usher et al. (2003), after correction to exclude sea salt, and Malm et al. (1994), both without sea salt correction.

To compare these estimates of mineral dust to the specific composition of Oceano Dunes, we also collected samples of sand from Oceano Dunes to be resuspended and measured gravimetrically for PM10 concentration. The resuspension was completed at 35% relative humidity. It shows that at this low relative humidity there is still approximately 27% water present.

October 20, 2021

Memo: SAG Review of Scripps/UCSD "Interim Report 2021: Preliminary Results from May 2021 Aerosol Measurements"

From: Scientific Advisory Group (SAG)

To: Jon O'Brien, California Department of Parks and Recreation (CDPR)

Cc: Sarah Miggins, California Department of Parks and Recreation (CDPR)
Liz McGuirk, California Department of Parks and Recreation (CDPR)

Summary Statement

The Scientific Advisory Group (SAG) welcomes monitoring campaigns and scientific studies that seek to understand the sources of particulate matter (PM) emissions at and around the Oceano Dunes State Vehicular Recreation Area (ODSVRA) and to inform efforts to reduce ambient PM10 concentrations toward achieving the air quality goals of the Stipulated Order of Abatement (SOA). Here, the SAG reviews the most recent Scripps Institution of Oceanography at the University of California, San Diego (UCSD) study, "Interim Report 2021: Preliminary Results from May 2021 Aerosol Measurements," which reports new data and findings that build on previous studies conducted by the Scripps/UCSD team.

Scientists of the Scripps/UCSD team have conducted multiple monitoring campaigns and prepared multiple scientific reports with the goal of constraining the importance of PM emitted from the ODSVRA relative to other sources originating outside the ODSVRA. Unfortunately, the SAG finds serious deficiencies within the current Scripps/UCSD report and therefore urges caution in using its reported findings and interpretations to guide management decisions regarding PM mitigation at the ODSVRA.

In particular, the SAG disputes three major aspects of this report: (1) its treatment of health and legal imperatives, (2) its assessment of the effects of off-highway vehicles (OHV) on PM emissions, and (3) the inadequate justification provided for key analyses and interpretations. These three major concerns are described in further detail below. In addition, reviews from individual SAG members (see Appendix 1) address specific aspects of this report that lead to the overall SAG concerns.

SAG Major Concerns regarding Scripps/UCSD Interim Report 2021

1. Health and legal imperatives. The SAG disagrees with assertions within this report that minimize the health and legal importance of PM2.5 and PM10 associated with mineral dust. From a health perspective, PM2.5 and PM10 are known to cause deleterious health impacts regardless of their chemical composition. From a legal perspective (and related to the known health impacts), federal and state PM concentration standards do not distinguish between constituents, nor does the SOA. For these reasons, the SAG argues for the urgent need to

continue to reduce ambient PM2.5 and PM10 concentrations at Oceano Dunes regardless of the specific breakdown of PM constituents.

2. Effects of OHV on PM emissions. The SAG disagrees with assertions within this report that minimize the effect of OHV on PM10 emissions at the ODSVRA and PM10 concentrations at receptor sites downwind. By citing a lack of significant difference between weekday and weekend airborne PM10 concentrations as evidence for a lack of OHV impact on PM10, the report perpetuates the misconception that OHVs produce PM emissions primarily through mechanical action at their time of operation. Instead, the primary effect of OHVs is to degrade dune surfaces and to increase the long-term PM emissivity of the dunes. Eventually, removal of OHVs should reduce PM10 emissions and concentrations, but this adjustment would occur over a matter of months, not days. The recent Desert Research Institute (DRI) report, "Examining Dust Emissions and OHV Activity at the ODSVRA," presents strong evidence, based on years of data collection, for this understanding of effect of OHVs.

3. Analyses and interpretations. The SAG is not convinced by analyses within this report that lead to the conclusion that only a small percentage of overall ambient PM is composed of mineral dust. The SAG does not dispute the raw values reported regarding filter sample gravimetric masses, nor does the SAG question the quality of the X-ray Fluorescence (XRF) analyses used to determine raw elemental compositions. However, the SAG is concerned that the determination of mineral dust contribution rests on a series of untested assumptions regarding the interpretation of XRF analytical results. In addition, there appears to be a wide discrepancy between the dust speciation findings reported in this study as compared to speciation findings from the San Luis Obispo County Air Pollution Control District (APCD). The SAG encourages the authors of this report to coordinate with APCD to share and compare data across studies to identify differences in analyses and interpretations that may be leading to these discrepancies.

Conclusion

The SAG expresses major concerns with the current Scripps/UCSD study and cautions against its use to inform air quality management decisions at the ODSVRA. Despite these concerns, the SAG acknowledges the potential value of data from the May 2021 aerosol measurements along with data from previous Scripps/UCSD studies. The SAG encourages the authors of this study to coordinate with APCD staff to share and compare data across studies toward developing a robust and scientifically-justified understanding of PM10 sources that is consistent across studies.

Respectfully,
The Scientific Advisory Group

Dr. Raleigh Martin (Acting chair of SAG); Dr. William Nickling; Dr. Ian Walker; Ms. Carla Scheidlinger; Mr. Earl Withycombe; Mr. Mike Bush, Dr. John A. Gillies

Appendix 1: Reviews from Individual SAG Members

Reviewer 1

(p. 2, Background, 1st paragraph, 5th sentence) The fact that there is a lack of difference between weekday and weekend coarse particle emissions does not support the hypothesis that "natural" sources predominate over "anthropogenic" sources. Instead, it suggests that windblown sources predominate over mechanically-generated sources of dust emissions. Windblown sources include those that are entirely natural, such as undisturbed sand dunes outside the riding area at ODSVRA, and those that are anthropogenic, such as sand dunes disturbed by riding activities. DRI emissivity testing demonstrates that riding-disturbed dunes produce twice as much windblown dust as undisturbed dunes.

(p. 2, Background, 1st paragraph, 6th sentence) Supermicron particulate matter between 2.5 and 10 microns in size has been identified by U.S. EPA in assessments of health effects studies to contribute to increases in thoracic flow resistance and heart rate variability, among other impacts, regardless of elemental or chemical composition. It is on the basis of such studies that U.S. EPA maintains the PM_{10} ambient air quality standard to protect public health. Statements to the affect that windblown sand particles in the coarse particulate size range do not contribute to chronic respiratory effects are erroneous.

(p. 3, last paragraph, 1st sentence) U.S. EPA has designated $PM_{2.5}$ to be an air pollutant harmful to public health, regardless of elemental or chemical composition. To suggest that that the association of $PM_{2.5}$ with detrimental health effects may be without foundation is erroneous.

(p. 4, first partial paragraph, last sentence) Assessing the portions of $PM_{2.5}$ deriving from windblown dust or combustion emissions is irrelevant as to whether $PM_{2.5}$ is responsible for adverse health effects. U.S. EPA's several assessments of health effects resulting from $PM_{2.5}$ exposure – regardless of elemental or chemical composition – are comprehensive and consistent.

(p. 8, first paragraph) The mineral dust component of filter samples collected on high-PM_{10} days is reported to range from 2% to 32%, and average 14% with a standard deviation of 14%. In 2020, the SLOAPCD collected eight filter PM_{10} samples at the CDF monitoring site on windy days between April 23 and September 24, which were analyzed by XRF by the Desert Research Institute. Using the IMPROVE protocol for isolating the geological component of mass (2.2xAl + 2.49*Si +1.63xCa + 2.42*Fe + 1.94xTi), the average geological component was found to be 43.5% with a standard deviation of 10.2%. Because of these significantly different results, it would be useful for Scripps and SLOAPCD to exchange raw data in an attempt to resolve these differences in analytical results.

(p. 9, first paragraph) The mineral dust component of $PM_{2.5}$ filters collected on high-PM_{10} days is reported to average 27% by VSCC inlet and 19% by SCC inlet. Typically, the geologic component is predominately higher in PM_{10} samples than in $PM_{2.5}$ samples as the mean particle size of windblown dust is about 4 microns. These results suggesting that the geologic component is higher in the $PM_{2.5}$ fraction than in the PM_{10} fraction at the CDF monitoring station are unusual and warrant an explanation.

(p. 13, Figure 3) The labeling of the difference between BAM and PM_{10} filter measurements as "Semivolatile" is speculative in the absence of further testing. The positive identification of only 18% of PM_{10} mass results in very limited information with respect to the composition of PM_{10} measured at the CDF monitoring station.

(p. 13, Conclusions, first paragraph, last sentence) The statement that results of this study were consistent with the chemical composition reported by the SLOCAPCD in its Nipomo Mesa Particulate Study (Phase 1) is misleading in that the Phase 1 study analyzed only total mass, sulfate, nitrate, and chloride values in PM_{10} samples collected at the CDF monitoring site. As the Scripps study did not analyze sulfate, nitrate, and chloride contributions at CDF, there is almost no overlap in the constituents measured in the two studies with respect to samples collected at CDF.

(p. 14, first paragraph, first sentence) The statement that dune-derived mineral dust is more likely to be primarily caused by natural forces (i.e., wind) rather than human activities ignores the results of dune emissivity testing conducted almost annually since 2013 by the Desert Research Institute which shows riding-disturbed dunes are twice emissive as non-disturbed dunes at ODSVRA. These results demonstrate that human activity on the dunes is responsible for roughly 50% of windblown emissions of PM_{10} from the riding area.

(p. 14, second sentence, second paragraph) The statement that a substantial fraction of $PM_{2.5}$ was not associated with fossil-fuel combustion emissions ignores the failure in the paper to identify the composition and sources of 63.6% of total mass on $PM_{2.5}$ samples collected on high PM_{10} days.

Reviewer 2

(p. 2, Background, first paragraph, 6^{th} sentence, "as well as by source areas") Not clear what this means. How the source area increase emission?

(p. 2, Background, first paragraph, 7^{th} sentence) But they have been associated with negative impacts on human health. See literature cited by SAG in review of last report.

(p. 3, first partial paragraph, first full sentence) Where is this in reference to?

(p. 3, last partial paragraph, first sentence) What about research that links mineral particle inhalation with an asthmatic response?

(p. 4, first partial paragraph, last sentence) The opinion stated (still) does not mean that under current laws, that standards are not to be met. In addition, the focus on PM2.5 does not allow for the setting aside of the SOA's intent to control PM10.

(p. 7, bullet 1a) What does SIO stand for?

(p. 13, Figure 3 caption) No analytical measurements were carried out other than XRF. So doesn't that make the apportionment rather "cursory"?

(p. 13, Conclusions, first paragraph, last full sentence) On high PM days with winds from the west (292-ish degrees), what are the likely sources for the cited sources that cannot originate from the Ocean environment (ammonium nitrate, non-sea salt sulphate, other semi-volatile species)?

(p. 14, second full paragraph) There has been no recent debate on the source of the PM10 being generated by saltation processes driven by the wind. The recent analysis and reporting of DRI we suggest (the SAG) provide compelling data that demonstrates the OHV activity augments the emissivity of the dunes (PI-SWERL data). DRI and APCD data show that cessation of OHV activity in 2020 resulted in lower PM10 for the same wind conditions, suggesting that the dunes are becoming less emissive following the removal of OHV activity.

(p. 14, third full paragraph) This final paragraph again sets aside that the fact that the SOA is in place to lower PM10 and does not address the toxicity of the particles, regardless of the size.

Reviewer 3

I am not qualified to review the methods and some of the conclusions, but one of the conclusions stood out to me. Namely this:

> *"The association of high PM10 and PM2.5 with high wind conditions, even when recreational vehicles were limited at Oceano Dunes compared to prior years, indicates that dune-derived mineral dust is more likely to be primarily caused by natural forces (i.e. wind) rather than human activities."*

It seems to me that the results of the DRI study conducted on riding vs. non-riding areas would cast a lot of doubt on this conclusion. The DRI work demonstrated that the riding activity itself MODIFIED the sand surfaces in such a way as to make them more emissive, even when vehicles were not present. I don't think we dispute that it is wind that mobilizes dust. But it seems clear from the DRI work that the vehicles make surfaces more emissive of dust when those surfaces have been worked by vehicle activity.

Whatever other conclusions the paper promotes, this one should be flagged as not supported by the data.

UNIVERSITY OF CALIFORNIA, SAN DIEGO UCSD

BERKELEY • DAVIS • IRVINE • LOS ANGELES • MERCED • RIVERSIDE • SAN DIEGO • SAN FRANCISCO

SANTA BARBARA • SANTA CRUZ

SCRIPPS INSTITUTION OF OCEANOGRAPHY

9500 GILMAN DRIVE
LA JOLLA, CALIFORNIA 92093-0221

25 October 2021

Jon M. O'Brien, Environmental Program Manager
Off-Highway Motor Vehicle Recreation Division
California Department of Parks and Recreation
1725 23rd Street, Suite 200
Sacramento, CA 95816

Dear Mr. O'Brien,

Please find attached my specific responses to the comments provided by the SAG on 22 October 2021, as well as a supplemental report on the SLOAPCD 2020 measurements that Karl Tupper provided to me last week.

Their major points 1 and 2 are based on their neglect of my peer-reviewed literature references, many of which also appeared in my prior reports. They provided no contradictory peer-reviewed literature that could provide a basis for modifying this text. Major point 3 is the only one relevant to the analyses presented here and is somewhat contradictory. While first asserting the data's lack of value, it then concludes that it should be compared to data not yet available.

The failure of the SAG comments to note evidence in support of their major points 1 and 2 is worrisome and does not meet academic standards, with this lack of supporting detail providing the appearance of inattention or obfuscation. Despite this, I provide here attached constructive responses to each individual comment. Moreover, I suggest a path forward that lies at the intersection of our results, providing Parks with the information needed to move ahead considering the limited role of mineral dust from the ODSVRA (or any other source) in contributing to PM. For this intersection of results, I present the subset of the May 2021 results for which BAM and gravimetric methods agree similarly to that of the SLOAPCD 2020 measurements, showing that still only 15% of BAM PM10 is mineral dust (26% on high-PM10 days). While this does leave unanswered the scientific question of whether semivolatile components are sufficient to explain all of the difference between BAM and gravimetric methods on the remaining days, it provides a clear and consistent attribution of the dust from two independent groups.

The openness of the SAG to measurements to identify the ODSVRA contribution is welcome (SAG "welcomes monitoring campaigns and scientific studies…"), but it does beg the question of why such research was not conducted in the several preceding years of the SOA prior to the Scripps/UCSD contract. The methods I have introduced are standard and by no means unique to my laboratory, and yet the SAG did not call out the need for such measurements prior to my

work. It is concerning that they either lacked the expertise or the intent to provide Parks with such findings until my work pointed out this need in 2020. Their failure to note the implications of their own findings as well as mine provides further reason for concern.

Please do not hesitate to contact me if you have any questions; my cell is 858 405 8203.

Best regards,

Lynn M. Russell
Distinguished Professor of Atmospheric Chemistry
Scripps Institution of Oceanography
University of California, San Diego
lmrussell@ucsd.edu; Tel. 858-534-4852.

Supplemental Discussion of SLOAPCD 2020 Measurements

25 October 2021

The 2020 SLOAPCD confidential results were provided by Karl Tupper by email on 10/20/21 and 10/22/21. They collected 13 samples between April and September of 2020, with XRF, IC, and gravimetric measurements. Their results show that gravimetric measurements are consistently lower than BAM, with gravimetric averaging 88% of BAM for all 13 samples (Figure S1). Moreover, the mineral dust (or “geological”) part of BAM is 30%, which is well under half of the overall PM10 concentration, with a standard deviation of 14% and a minimum value of 5%. (Note that their results were reported per email on 10/22/21 as fractions of gravimetric, but here they are converted to fractions of BAM.) This result is consistent with the measurements of mineral dust reported for May 2021 by Scripps/UCSD for 11 high-PM10 days, which had an average of 14% with a standard deviation of 14% (and a maximum value of 32%). This means that the upper range (mean to maximum) of the Scripps/UCSD results (14%-32%) overlap the lower range of the SLOAPCD measurements (5%-30%). Given the small sample size of each (13 and 11), this overlap shows very similar results.

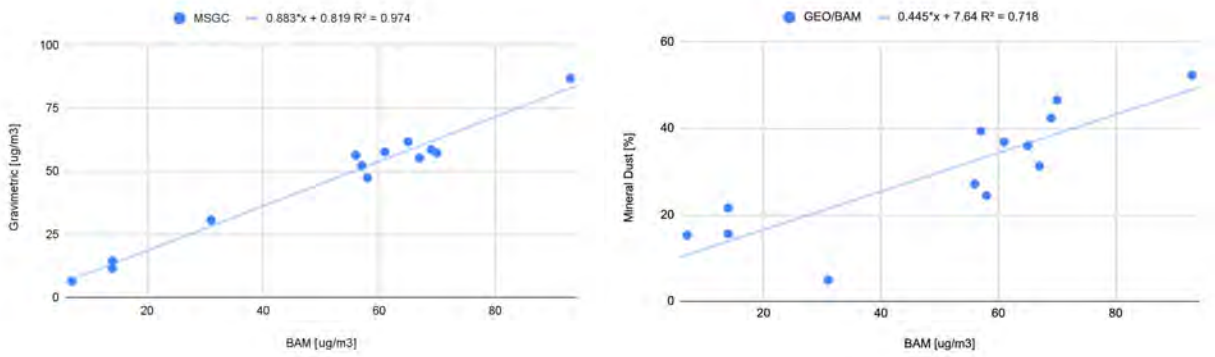

Figure S1. SLOAPCD 24-hr measurements between April and September of 2020, provided by Karl Tupper (10/20/21). Left panel shows the comparison of gravimetric and BAM concentrations, with a slope of 0.88 showing lower values of gravimetric relative to BAM concentration. Right panel shows the mineral dust percentage as a function of BAM concentration, with an average of 30% and standard deviation of 14%.

For a more specific comparison to the SLOAPCD results (Tupper, email 10/22/21), the Scripps May 2021 results can also be screened to match the criteria of their results (Figure S2). Specifically, if we include only the results for which the gravimetric method accounts for 82% or more of the BAM PM10 mass concentration, which includes 3 of the high-PM10 days and 5 of the other May 2021 days, then the agreement of the BAM and gravimetric is comparable to the

SLOAPCD as shown below. In addition, there is a correlation between the mineral dust fraction and the BAM concentration.

It is of course worth noting that this agreement is despite differences in the collection and analysis protocols, including the different collection times (24 vs. 7 hr) and the mineral dust approximation (Malm vs. Usher). Also, while the SLOAPCD measurements targeted windy days, it would be important to compare days of similar windiness.

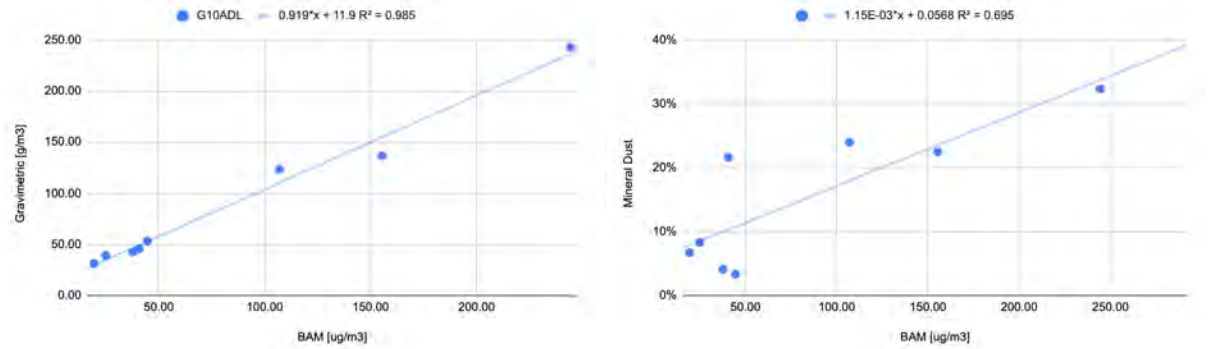

Figure S2. Scripps/UCSD 7-hr afternoon measurements in May of 2021 for the eight days that had agreement between gravimetric and BAM methods similar to that of the SLOAPCD study (namely gravimetric accounted for >82% of BAM concentration). Left panel shows the comparison of gravimetric and BAM concentrations for these 8 days, with a slope of 0.92 showing lower values of gravimetric relative to BAM concentration. Right panel shows the mineral dust percentage as a function of BAM concentration, with an average of 15% and standard deviation of 11% for these 8 days. If only the three high-PM10 days with matching gravimetric and BAM methods are included, the average is 26% and standard deviation of 5%.

Interestingly, when the Scripps/UCSD and SLOAPCD measurements are compared with similar screening, both the BAM and gravimetric comparisons are similar in terms of slope (0.88 and 0.92) and correlation (R^2 of 0.79 and 0.72) and mineral dust fraction (30±14% and 26±5%). This substantial agreement shows that the fraction of PM10 attributable to the ODSVRA consistently accounts for somewhat less than half of the PM10 concentration.

SAG Comments with Scripps Responses on Scripps/UCSD Interim Report 2021			
Reviewer	**SAG Description of Issue**	**SAG Comment**	**Scripps Response**
R1	(p. 2, Background, 1st paragraph, 5th sentence) The fact that there is a lack of difference between weekday and weekend coarse particle emissions does not support the hypothesis that "natural" sources predominate over "anthropogenic" sources. Instead, it suggests that windblown sources predominate over mechanically-generated sources of dust emissions. Windblown sources include those that are entirely natural, such as undisturbed sand dunes outside the riding area at ODSVRA, and those that are anthropogenic, such as sand dunes disturbed by riding activities.	DRI emissivity testing demonstrates that riding-disturbed dunes produce twice as much windblown dust as undisturbed dunes.	No citation is provided and the information discussed is not publicly available. The conclusion on weekend/weekday differences is a direct citation from a peer-reviewed publication that is not contradicted by the information provided. The DRI reports I have seen have not shown PM10 impacts at CDF and they provide informationon emissive potential not ambient PM10.
R1	(p. 2, Background, 1st paragraph, 6th sentence) Supermicron particulate matter between 2.5 and 10 microns in size has been identified by U.S. EPA in assessments of health effects studies to contribute to increases in thoracic flow resistance and heart rate variability, among other impacts, regardless of elemental or chemical composition. It is on the basis of such studies that U.S. EPA maintains the PM10 ambient air quality standard to protect public health. Statements to the affect that windblown sand particles in the coarse particulate size range do not contribute to chronic respiratory effects are erroneous.	Statements to the affect that windblown sand particles in the coarse particulate size range do not contribute to chronic respiratory effects are erroneous.	No citation is provided and the information discussed is not publicly available. The conclusion on the role of coarse dust for health effects is from a peer-reviewed publication that is not contradicted by the unreferenced information provided.
R1	(p. 3, last paragraph, 1st sentence) U.S. EPA has designated PM2.5 to be an air pollutant harmful to public health, regardless of elemental or chemical composition..	To suggest that that the association of PM2.5 with detrimental health effects may be without foundation is erroneous	The interpretation given is not consistent with the text. No contradictory peer-reviewed evidence is cited.
R1	(p. 4, first partial paragraph, last sentence) Assessing the portions of PM2.5 deriving from windblown dust or combustion emissions is irrelevant as to whether PM2.5 is responsible for adverse health effects.	U.S. EPA's several assessments of health effects resulting from PM2.5 exposure – regardless of elemental or chemical composition – are comprehensive and consistent.	No citation is provided and the information discussed is not publicly available. The conclusion on the role of compositiont for health effects is from a peer-reviewed publication that is not contradicted by the unreferenced information provided.
R1	(p. 8, first paragraph) The mineral dust component of filter samples collected on high-PM10 days is reported to range from 2% to 32%, and average 14% with a standard deviation of 14%. In 2020, the SLOAPCD collected eight filter PM10 samples at the CDF monitoring site on windy days between April 23 and September 24, which were analyzed by XRF by the Desert Research Institute. Using the IMPROVE protocol for isolating the geological component of mass (2.2xAl + 2.49*Si +1.63xCa + 2.42*Fe + 1.94xTi), the average geological component was found to be 43.5% with a standard deviation of 10.2%. Because of these significantly different results, it would be useful for Scripps and SLOAPCD to exchange raw data in an attempt to resolve these differences in analytical results.	Because of these significantly different results, it would be useful for Scripps and SLOAPCD to exchange raw data in an attempt to resolve these differences in analytical results.	I have now analyzed the APCD results for 24-hr measurements of dust fraction. While the information provided is not sufficient to review the accuracy of the results, and the results apply to different days, I have now applied a screening similar (but over different period for different sampling duration), and have obtained similar results, when compared on a consistent basis (i.e. BAM). When the APCD 2020 data are evaluated relative to BAM (rather than gravimetric) the average is 30% with standard deviation of 14% for 13 samples. Using a similar screening, the Scripps results give 26% on three high-PM10 days in May. These results are statistically indistinguishable.
R1	(p. 9, first paragraph) The mineral dust component of PM2.5 filters collected on high-PM10 days is reported to average 27% by VSCC inlet and 19% by SCC inlet. Typically, the geologic component is predominately higher in PM10 samples than in PM2.5 samples as the mean particle size of windblown dust is about 4 microns. These results suggesting that the geologic component is higher in the PM2.5 fraction than in the PM10 fraction at the CDF monitoring station are unusual and warrant an explanation.	These results suggesting that the geologic component is higher in the PM2.5 fraction than in the PM10 fraction at the CDF monitoring station are unusual and warrant an explanation.	The reviewer is partially correct that the results imply a mode peaking above the PM2.5 cutoff, but not that this implies a higher fraction of mass in PM10 than PM2.5. The explanation is provided that the size distribution is somewhat different than the canonical expectation, but entirely consistent with previous APCD findings about the size distribution of dust, as cited in the report (SLOAPCD memo).
R1	(p. 13, Figure 3) The labeling of the difference between BAM and PM10 filter measurements as "Semivolatile" is speculative in the absence of further testing.	The positive identification of only 18% of PM10 mass results in very limited information with respect to the composition of PM10 measured at the CDF monitoring	As noted above, while the Scripps study was not funded for complete speciation, the dust results are consistent with those reported by SLOAPCD (Tupper, email 10/22/21).
R1	(p. 13, Conclusions, first paragraph, last sentence) The statement that results of this study were consistent with the chemical composition reported by the SLOCAPCD in its Nipomo Mesa Particulate Study (Phase 1) is misleading in that the Phase 1 study analyzed only total mass, sulfate, nitrate, and chloride values in PM10 samples collected at the CDF monitoring site.	As the Scripps study did not analyze sulfate, nitrate, and chloride contributions at CDF, there is almost no overlap in the constituents measured in the two studies with respect to samples collected at CDF.	The report statement is still correct, in that the overlap of analyzed results for both PM10 and PM2.5 are consistent.
R1	(p. 14, first paragraph, first sentence) The statement that dune-derived mineral dust is more likely to be primarily caused by natural forces (i.e., wind) rather than human activities ignores the results of dune emissivity testing conducted almost annually since 2013 by the Desert Research Institute which shows riding-disturbed dunes are twice emissive as non-disturbed dunes at ODSVRA.	These results demonstrate that human activity on the dunes is responsible for roughly 50% of windblown emissions of PM10 from the riding area.	The interpretation given is not consistent with the text. No contradictory peer-reviewed evidence is cited.
R1	(p. 14, second sentence, second paragraph) The statement that a substantial fraction of PM2.5 was not associated with fossil-fuel combustion emissions ignores the failure in the paper to identify the composition and sources of 63.6% of total mass on PM2.5 samples collected on high PM10 days.		As discussed in the report in context, this statement about fossil fuel emissions is based on the amount of organic mass measured, and it will be supported by the organic composition presented in the final report. These details about minor components of PM do not affect the attribution of PM to mineral dust, which was the focus of the interim report due to its relevance to our study objectives.
R2	(p. 2, Background, first paragraph, 6th sentence, "as well as by source areas") Not clear what this means.	How the source area increase emission?	Emissions of dust increase with the size (area) of dunes, as discussed by references cited in the report. As an illustrative example, the amount of emissions from Oceano dunes is smaller than that of the Gobi desert because the area of the dust source at Oceano is smaller than the area of the Gobi desert.
R2	(p. 2, Background, first paragraph, 7th sentence) But they have been associated with negative impacts on human health. See literature cited by SAG in review of last report.	See literature cited by SAG in review of last report.	Comments in prior review did not cite peer-reviewed literature relevant to this issue, so it is not clear what is intended here.
R2	(p. 3, first partial paragraph, first full sentence)	Where is this in reference to?	The first paragraph on p.3 is a full paragraph, so it is unclear what this question is asking about.
R2	(p. 3, last partial paragraph, first sentence) What about research that links mineral particle inhalation with an asthmatic response?	What about research that links mineral particle inhalation with an asthmatic response?	The cited research does not link mineral dust particle inhalation with an asthmatic response, which is the point of the discussion.
R2	(p. 4, first partial paragraph, last sentence) The opinion stated (still) does not mean that under current laws, that standards are not to be met.	In addition, the focus on PM2.5 does not allow for the setting aside of the SOA's intent to control PM10.	The reviewer is partially correct in that the importance of PM2.5, and moreso of PM1 (and ultrafine particles), for health effects does not set aside the regulatory restrictions on PM10. However, it does imply that the value to society of regulating PM10 is less than believed at the time the regulations were set in force.
R2	(p. 7, bullet 1a)	What does SIO stand for?	Scripps/UCSD.
R2	(p. 13, Figure 3 caption) No analytical measurements were carried out other than XRF.	So doesn't that make the apportionment rather "cursory"?	The Reviewer is correct that the apportionment would be more complete with additional analyses that we had proposed. However, the dust source is effectively entirely mineral, so the dune-related fraction can be apportioned in the absence of characterizing the other remaining (and variable) sources. To summarize, the apportionment to all sources is certainly incomplete, but the apportionment to dust sources is very comprehensive (and not cursory).

	(p. 14, second full paragraph) There has been no recent debate on the source of the PM10 being generated by saltation processes driven by the wind. The recent analysis and reporting of DRI we suggest (the SAG) provide compelling data that demonstrates the OHV activity augments the emissivity of the dunes (PI-SWERL data).	DRI and APCD data show that cessation of OHV activity in 2020 resulted in lower PM10 for the same wind conditions, suggesting that the dunes are becoming less emissive following the removal of OHV activity.	The Scripps report is not an assessment of DRI results, although there appear to have been several confounding factors that may change the interpretation presented here by SAG of those results. However, as noted above, the SLOAPCD 2020 measurements show similar mineral dust contributions to those found in 2021.
	(p. 14, third full paragraph)	This final paragraph again sets aside that the fact that the SOA is in place to lower PM10 and does not address the toxicity of the particles, regardless of the	The reviewer is correct that in this paragraph the topic returns to the impact on the community (or lack thereof) rather than the PM10 regulation that is routinely violated statewide (Motallebi et al., 2003).
R3	I am not qualified to review the methods and some of the conclusions, but one of the conclusions stood out to me. Namely this: "The association of high PM10 and PM2.5 with high wind conditions, even when recreational vehicles were limited at Oceano Dunes compared to prior years, indicates that dune-derived mineral dust is more likely to be primarily caused by natural forces (i.e. wind) rather than human activities." It seems to me that the results of the DRI study conducted on riding vs. non-riding areas would cast a lot of doubt on this conclusion. The DRI work demonstrated that the riding activity itself MODIFIED the sand surfaces in such a way as to make them more emissive, even when vehicles were not present. I don't think we dispute that it is wind that mobilizes dust. But it seems clear from the DRI work that the vehicles make surfaces more emissive of dust when those surfaces have been worked by vehicle activity.	Whatever other conclusions the paper promotes, this one should be flagged as not supported by the data.	We thank the reviewer for noting his/her lack of expertise for the substantive content of the report. The DRI results presented to date, do not show a link between the emissivity differences and the CDF PM10 BAM concentrations, which is the quantity of interest for the SOA. While the DRI emissivity differences could result in differences at CDF (although their value relative to natural emissivity is not clear), they may not. For example, if the DRI emissivity differences are associated with higher emissivity of larger particles, the shorter lifetimes of those larger particles may preclude differences in ambient concentrations at CDF.

UNIVERSITY OF CALIFORNIA, SAN DIEGO UCSD

BERKELEY • DAVIS • IRVINE • LOS ANGELES • MERCED • RIVERSIDE • SAN DIEGO • SAN FRANCISCO

SANTA BARBARA • SANTA CRUZ

SCRIPPS INSTITUTION OF OCEANOGRAPHY

9500 GILMAN DRIVE
LA JOLLA, CALIFORNIA 92093-0221

8 November 2021

Sarah Miggins, Deputy Director
Off-Highway Motor Vehicle Recreation Division
California Department of Parks and Recreation
1725 23rd Street, Suite 200
Sacramento, CA 95816

Dear Deputy Director Miggins,

Please find attached my report of findings regarding our spring 2021 sampling and analyses of airborne particulate matter (PM) collected at the location known as the CDF site on the Nipomo Mesa (Mesa) in south San Luis Obispo County, California. The CDF site is approximately two miles downwind of the Oceano Dunes State Vehicular Recreation Area (SVRA). The primary purpose of this investigation, which is part of a larger three-year study, is to quantify that portion of measured PM that consists of mineral dust. Mineral dust is generated from the windblown sand dune building process called saltation, and so quantifying the mineral dust portion of PM at the CDF site provides a conservative measure of that portion of PM on the Mesa that could possibly be from the Oceano Dunes SVRA. The mineral dust measure is conservative because saltation occurs in the dunes inside and outside the SVRA, and mineral dust is also derived from agricultural operations and vehicles driving on dirt roads—activities that occur in the region that lies between the SVRA and the Mesa.

Samples of PM10 and PM2.5 (PM that is aerodynamically $\leq$10 microns and $\leq$2.5 microns in diameter, respectively) were collected for 30 consecutive days, from late April to late May. May was targeted because May is typically the windiest month in the region. Each day, the air was sampled continuously for seven hours, from 11:00AM to 6:00PM (local time) because this is the timeframe when the seasonal westerly winds rise and fall, when saltation in the dunes is at its most active, and when some of the highest hourly PM10 and PM2.5 concentrations at the CDF site are recorded by the SLO County Air Pollution Control District (APCD).

Mineral dust content was determined using gravimetric and elemental analyses as detailed in the report. Key findings from the analyses show that on average, 14% of the BAM PM10 measured at the CDF site consists of mineral dust and 4% consists of sea salt. Specifically, for May 2021, the mineral dust fraction ranged from 2% to 32% on high-PM10 days. The remaining 82% of the PM10 is likely from atmospheric water, organic components, ammonium, nitrate, non-sea-salt sulfate, and other semi-volatile chemical species.

I would like to extend our appreciation to the California Geological Survey and to the California Department of Parks and Recreation for their assistance and access that has made our investigation possible.

Best regards,

Lynn M. Russell
Distinguished Professor of Atmospheric Chemistry
Scripps Institution of Oceanography
University of California, San Diego
lmrussell@ucsd.edu; Tel. 858-534-4852.

Scripps/UCSD Interim Report 2021:

Preliminary Results from May 2021 Aerosol Measurements

8 November 2021

Introduction

Building upon the results of the Scripps Institution of Oceanography (UCSD) Reports of 5 February 2020 and 20 September 2020, the Scripps team has undertaken additional quantitative chemical sampling to improve the understanding of the sources of airborne particles in the Oceano Dunes area. This interim report covers the gravimetric and elemental analyses of the teflon filters collected during the most recent sampling period from 27 April 2021 to 26 May 2021 (hereafter “Scripps May 2021” study). The objectives of this part of the research were to

1) Quantify the gravimetric mass and elemental component mass of PM10 aerosol particles at CDF.
2) Quantify the gravimetric mass and elemental component mass of PM2.5 aerosol particles at CDF;

It is important to note that some COVID-19 restrictions continued during this sampling period.

While prior work has focused on identifying sea spray components of PM2.5 at CDF (with a focus on PM with potential health effects) and of PM10 at a Beach site, the May 2021 sampling was designed to provide a quantitative assessment of the mineral dust fraction of the reported beta attenuation monitor (BAM) PM10 and PM2.5 concentrations during the conditions with the highest PM10 concentrations -- namely afternoons (the time of day with highest wind) in May (the month of the year with highest wind). For PM10 size cutoffs, we have used a standard method, and for PM2.5 we have used both a standard method (Very Sharp Cut Cyclone or VSCC) and an alternative method that was used previously to reduce costs (Sharp Cut Cyclone or SCC). In order to quantify the mineral dust contribution during the time with the highest PM10 concentrations, samples were collected for the afternoon hours of 1200 to 1900 local time (1100 to 1800 standard time). During spring in this area, westerly winds typically

have the highest speeds from late morning to early evening (see Appendix, Figure A3). These high wind speeds increase saltation of the dunes and coincide with elevated PM concentrations measured at CDF (Figure A3). Accordingly, it is during the afternoon hours that PM at CDF is expected to contain the largest concentration and the highest percentage of mineral dust. In this sense, the chemical identification of mineral dust in the afternoon provides an upper bound on the contribution of dust from Oceano Dunes, although a more extensive study could separate out the contributions of other sandy regions, agricultural zones, and road dust.

Background

The particle concentration in the Oceano Dunes region is expected to be a mixture of organic and inorganic components from natural and man-made sources. Its seaside location means that sea spray from breaking waves in the ocean will contribute particles with salt (NaCl as well as some trace additional salts) and organic components (from nutrients and exudates that are produced and consumed by marine biota) [Russell et al., 2010]. Another proximate natural source is mineral dust from sand-covered areas, which is generally associated with wind erosion [Li et al., 2013]. Contributions to dust emission by human activities has been estimated to be 10% or less in agricultural areas and as much as 50% for land use changes that remove vegetation [Shepherd et al., 2016; Tegen et al., 2004; Tegen and Fung, 1995]. However, the lack of difference between weekday and weekend coarse particle emissions supports natural rather than anthropogenic sources [Li et al., 2013]. Both sea spray and mineral dust emissions are increased by wind speed [Malm et al., 1994] as well as by source areas, both have substantial supermicron mass contributions with short atmospheric lifetimes, and neither is associated with evidence of chronic respiratory effects (since they are removed by impaction in the nasal passages and upper airways and since the salt and mineral components have not been associated with toxicity). In addition to these natural sources, local emissions associated with motor vehicles [Russell et al., 2011], residential and commercial activities (including use of personal care products [McDonald et al., 2018], food preparation [Chen et al., 2018], and heating), seasonal agricultural harvesting and fertilizing, wildfires, and long-range transport from high-population areas also contribute both organic and inorganic particle mass to PM2.5 and PM10, with the contribution from each varying with wind direction as well as other conditions.

PM2.5 and PM10 are regulated by U.S. and California clean air standards because of their known association with degraded visibility and detrimental health effects [US Clean Air Act (https://www.epa.gov/laws-regulations/summary-clean-air-act); Dockery et al., 1993; Pope et al., 2009; Apte et al., 2018]. PM10 exceedances of the 24-hr NAAQS (150 μg m^{-3}) are infrequent, but the California 24-hr PM10 standard of 50 μg m^{-3} is exceeded 25% of the time [Motallebi et al., 2003]. These standards were developed based on measurements completed by federal reference methods (FRM) that relied on gravimetric measurements of filters that were equilibrated for 24 hr at 35% relative humidity (https://www.ecfr.gov/current/title-40/chapter-I/subchapter-C/part-50). Since then, BAM has been approved as a federal equivalent method (FEM) based on the similarity of hourly BAM, when averaged over 24 hr, to FRM methods for a set of test locations [Chow and Watson, 2008]. Those test locations typically included concentrations below 100 μg m^{-3} and frequently below 30 μg m^{-3} [Chung et al., 2001; Gobeli et al., 2008; Hafkenscheid and Vonk, 2014; Hart, 2009], as these conditions were more typical of areas of concern for PM2.5.

Apte et al. [2018], calculated the U.S. average life expectancy decrement to be 0.38 yr for PM2.5, which is 3 times lower than that of countries with higher PM2.5 (e.g. China, India). While the widespread availability of PM2.5 measurements often makes it the best proxy for epidemiological studies of populations, physiological studies of health effects have shown that the causes of cell degradation are most likely from specific toxic compounds, which are also regulated and include such compounds as polycyclic aromatic hydrocarbons that are associated with fossil fuel combustion and black carbon. Consequently PM1 has been recommended as a better cutoff for targeting health-related aerosol sizes [Lundgren and Burton, 2008]. Recent evidence also suggests that nanoparticles (less than 100 nm diameter) and transition metals, which are also associated with fossil fuel combustion, may also play an important role [Knol et al., 2009; Oberdorster et al., 2007; Gwinn and Vallyathan, 2006; Janssen et al., 2003; Hoek et al., 2002]. Since the association of PM2.5 with toxics is likely responsible for the association of PM2.5 with health effects, the use of PM2.5 as a health indicator assumes it co-occurs with toxics.

There is no evidence that toxic compounds (such as heavy metals or polycyclic aromatic hydrocarbons) are associated with the two major PM2.5 sources (dune dust and sea spray) during windy conditions at Oceano Dunes, so association of PM2.5 with detrimental health effects may be without foundation. In urban locations that serve as the basis for epidemiological health studies, the large population density means that PM2.5 is largely associated with emissions from motor vehicles that include high amounts of toxics, nanoparticles, and transition metals. In areas where PM2.5 is

dominated by natural emission sources rather than man-made combustion activities, the causal link between toxics and health effects is unlikely to hold; exceptions could include severe dust storms [Krasnov et al., 2014], with concentrations exceeding 1000 μg m^{-3} [Aghababaeian et al., 2021] or associated with Valley fever [Tong et al., 2017], which have not been identified in coastal California [Crooks et al., 2016]. For this reason, assessing whether health effects are associated with PM2.5 requires identifying what fraction of PM2.5 is from natural (non-toxic) sources and what fraction is from combustion emissions.

The chemical composition provides the first critical step to identifying how much of total particle mass is associated with different sources, each of which is associated with different health effects. In the 5 February 2020 UCSD/SIO Report, we used Fourier Transform Infrared (FTIR) spectroscopy and X-ray Fluorescence (XRF) to provide a first cut at the PM2.5 sources, using elemental composition to provide tracers for sea spray, mineral dust, and combustion emissions. This report builds on those results to quantify explicitly the substantial difference between the chemical measurements of dust components and the BAM PM2.5 and PM10 measurements regularly reported by the San Luis Obispo County Air Pollution Control District (APCD) at its CDF air monitoring station on the Nipomo Mesa, approximately 3.2 kilometers (2 miles) inland from Oceano Dunes. First, gravimetric measurements (at partially dried conditions of 35% relative humidity) are used to provide the analogous FRM method for particle mass for comparison to the FEM method hourly BAM. Then mineral dust components from XRF measurements are used to assess the fraction of the measured mass that is associated specifically with wind-blown mineral dust that likely originated from the Oceano Dunes region.

Methods

Aerosol particle sampling at CDF used two louvered PM10 sampling heads [Tolocka et al., 2001] on two separate lines at 16.67 L min^{-1}, followed by a PM10 filter (and bypass flow) on one line and a very sharp-cut cyclone with a calibrated cut at 2.5 μm (VSCC operated at 16.67 L min^{-1}, BGI Inc., Waltham, MA) on the other line. The bypass flow on the first line included a sharp-cut cyclone operated with a calibrated cut at 2.5 μm (SCC 2.229 operated at 7.5 L min^{-1}, BGI Inc., Waltham, MA). All flow rates were calibrated and recorded every ~10 s to verify cyclone performance. The VSCC has been EPA approved [Kenny et al., 2004], which allows for mass concentrations to perform at between -5% and +5% of the actual mass under testing conditions. Deviations from the expected cyclone performance have been shown to result for different reasons (see

Appendix): (1) differences between the actual measurement conditions and the testing conditions used for approval [Li et al., 2019], (2) degraded performance by dust accumulation [Lin et al., 2018], and (3) evaporation of liquid water and other semivolatile components by either the VSCC or SCC [Babila et al., 2020].

Teflon filters were used as substrates and have shown negligible adsorption of volatile organic compounds (VOCs) on duplicate back filters collected simultaneously with each sample [Maria et al., 2003; Gilardoni et al., 2007]. Filters for PM10 and PM2.5 were 1 µm pore size. Blank filters provided a measure of adsorption during sampling and contamination during handling (loading and unloading) and storage. Samples were quality-controlled with the following criteria: all filter and cyclone flow rates were within 5% for the duration of sampling, filter pressure increased by >0.01 psi per m^3 air collected, and no anomalous readings in pressure, temperature, and relative humidity (as defined by the instrument specifications). These quality-control criteria were met for all 30 PM10 samples, 25 of 30 PM2.5 VSCC samples, and 28 of 30 PM2.5 SCC samples. Correlation coefficients are Pearson's R values for linear fits forced to 0, and percentages are based on the fitted lines of quality-controlled, above-detection samples.

The gravimetric masses of reference filters were compared to the 7-hr average of co-located hourly BAM measurements. The hourly BAM concentrations (retrieved 7/1/21 from https://www.arb.ca.gov/aqmis2/aqdselect.php, where data after 2019 are noted as "preliminary") reported were averaged from the start time (1200 local, PDT) until the last measurement recorded at 1 hr before the stop time (1900 local, PDT), namely seven one-hr measurements reported for PST start times of 1100 through 1700 to provide comparison points (in accordance with the website information). At high relative humidity (>70%, such as those at CDF in May 2021, see Appendix, Figure A3), hourly measurements will report higher mass concentrations than multi-hour measurements [Schweizer et al., 2016]. Comparisons at other sites between gravimetric and BAM PM2.5 mass concentrations have shown correlation coefficients (R^2) that varied between 0.65 and 0.99 and slopes that differed by as much as 30% depending on season and chemical composition [Hauck et al. 2004].

BAM uses a glass fiber filter for particle collection because of its high efficiency, but the glass fibers are known to have a positive sampling artifact (relative to Teflon) because they can adsorb gaseous SO_2 and HNO_3 into particulate sulfate and nitrate, respectively [Lipfert, 1994]. The amount of artificial nitrate taken up onto glass-fiber filters varies with both relative humidity and temperature changes [Appel et al., 1979].

All filters were weighed prior to sampling to provide filter-specific tare weights. After sampling, filters were weighed again, and the difference between the sampled weight and the tare was the reported gravimetric mass. The weighing procedure (Chester LabNet) for all samples used the PM2.5 reference method at 35±5% relative humidity for the 24 hr period (logged every 5 min), making the samples potentially drier or wetter than the ambient conditions in which they were collected. BAM measurements may also be drier than ambient humidity due to heating of the air when it is drawn into the instrument to an unknown temperature, but values of internal relative humidity are logged with the BAM measurements. Other differences may result from the hour-to-hour differences in the online BAM measurements compared to the offline filter storage at constant conditions.

All samples (and associated blank filters) were non-destructively analyzed by X-ray Fluorescence (XRF) measurements conducted by Chester LabNet (Tigard, OR) on the same filters used for gravimetric measurements. XRF analysis provided trace metal concentrations for elements Na and heavier [Maria et al., 2003].

Sea salt was measured above detection when Na and Cl were above detection (defined as twice uncertainty), which was true for more than 92% of quality-controlled samples. Atmospheric ambient sea-salt concentrations were calculated using measured Cl and 1.47*Na concentrations to account for the possible depletion of Cl^- in the atmosphere, where 1.47 is the ratio of $(Na^+ + Mg^{2+} + Ca^{2+} + K^+ + SO_4^{2-} + HCO_3^-)/Na^+$ in seawater [Holland, 1978; Frossard et al., 2014]. This sea-salt calculation represents an upper limit for sea-salt mass because the HCO_3^- would have been titrated before Cl^- was depleted significantly via acid displacement reactions. HCO_3^- is 0.3% of the total mass of sea salt. Excluding HCO_3^- from the ratio, as a lower limit, the ratio of $(Na^+ + Mg^{2+} + Ca^{2+} + K^+ + SO_4^{2-})/Na^+$ is 1.45, instead of 1.47, making the salt mass calculated <2% lower than calculated here.

Mineral dust was measured above detection if Al and Si were above detection (defined as twice uncertainty), which was true for more than 86% of quality-controlled samples. The mass of dust was calculated from XRF metal concentrations, assuming dust consists of $MgCO_3$, Al_2O_3 and SiO_2 (in the form of Al_2SiO_5), K_2O, $CaCO_3$, TiO_2, Fe_2O_3, MnO, and BaO [Liu et al., 2018; Gilardoni et al., 2007; Usher et al., 2003]. This calculation increases the mass by an average factor of 2.14 to account for the O and C associated with the measured elements for the PM10 samples. Because some elements are in both sea salt and mineral dust (K, Ca, Mg), the amount of those elements associated with the Na present was subtracted to avoid double-counting, resulting in ~2% less mass. Alternative approximations of the mineral dust contribution

based on other molecular forms of the same elements were also considered and are compared in the Appendix [Hains et al., 2007; Frank 2006; Malm et al. 1994].

Results

Samples were collected at CDF for the period of 27 April to 26 May 2021. The CDF site was co-located with the ongoing APCD sampling by BAM (beta attenuation monitor), which provides an hourly measurement of PM2.5 and PM10 concentration at near ambient conditions, which means that water and other semivolatile organic and inorganic components (notably ammonium nitrate) are included. The number of sampling days was maximized to document the day-to-day variability in the aerosol and to capture multiple days with high PM2.5 and PM10 concentration. Notably, the days with high PM at CDF were often predicted successfully from short-term forecasts of high-wind conditions, consistent with prior studies.

In order to optimize the sampling range for PM10 and PM2.5, flow rates were designed to not exceed the thin film assumption used for XRF. This condition was met for most samples as designed. However, the lower flow rate meant that some samples on low PM days were below detection limit for gravimetric mass (and some XRF elements). This limitation was by design, since the target of this study was high-PM10 days(defined to be those with 1-hr PM10 exceeding 140 μg m^{-3}), none of which exceeded the XRF thin film assumption and most of which were above detection limit (ADL).

The results addressing the objectives of the research are summarized below. We note that all of the results may differ by season, and their variability may be larger than could be captured in this short study.

1. Quantify the gravimetric mass and elemental component mass of PM10 aerosol particles at CDF.
    a. The time series of SIO gravimetric mass and APCD BAM PM10 concentration measurements tracked reasonably well (Figure 1). The offline gravimetric method is lower on average than the online BAM instrument for most samples at CDF (Figure 1). The difference is slightly larger on days with high PM10 (defined to be those with 1-hr PM10 exceeding 140 μg m^{-3}). These observations hold when the below-detection samples are removed (see Appendix).
    b. For the afternoons when hourly PM10 exceeded 140 μg m^{-3} for at least one hour, the gravimetric method PM10 concentration is on average 35% lower than BAM PM10 concentration. For all samples above detection

limit, the gravimetric method PM10 concentration is on average 29% lower than BAM PM10 concentration.

c. The mineral dust component of BAM PM10 ranged from 1% to 32% for ADL samples and from 2% to 32% for high-PM10 day samples. This amount represents an upper bound on the amount of PM10 that could be attributed to mineral dust from sand dune saltation. The average mineral dust amount of BAM PM10 was 14% with variability (standard deviation) of 17% for ADL samples and 14% with variability (standard deviation) of 14% for high-PM10 samples.

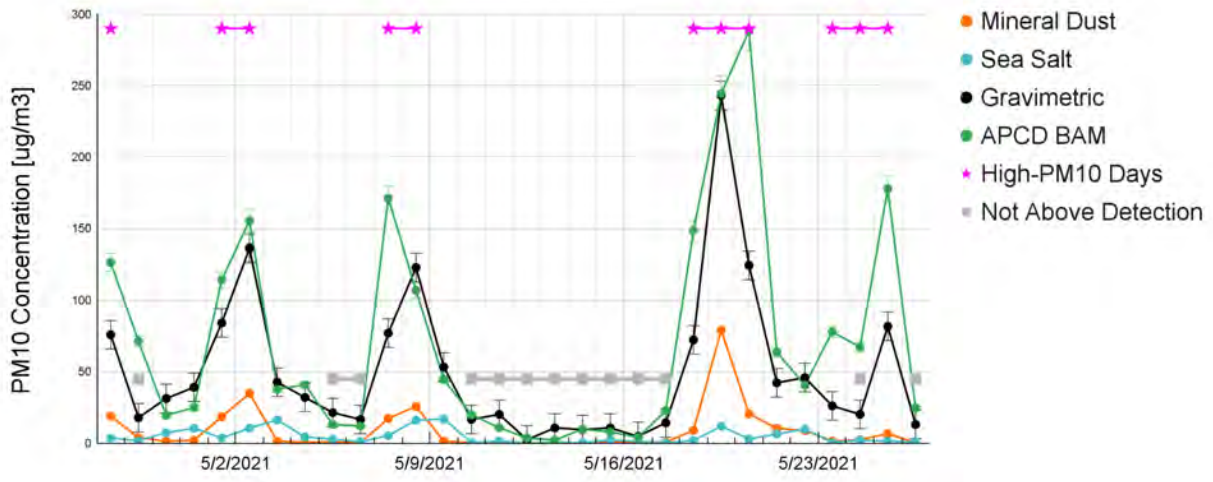

Figure 1. Time series of PM10 mass concentrations [µg m^{-3}] by Gravimetric and BAM methods at CDF from 27 April to 26 May 2021, with XRF Mineral Dust and Sea Salt concentrations (all samples). Error bars represent twice the method uncertainty.

2. Quantify the gravimetric mass and elemental component mass of PM2.5 aerosol particles at CDF.
    a. The time series of SIO gravimetric mass and APCD BAM PM2.5 concentration measurements tracked reasonably well (Figure 2). The offline gravimetric method is lower on average than the online BAM instrument for most samples at CDF for both VSCC and SCC cyclones (Figure 2). The difference is slightly larger on days with high PM10. These observations hold when the below-detection samples are removed (see Appendix).
    b. For the afternoons when hourly PM10 exceeded 140 µg m^{-3} for at least one hour, the gravimetric method PM2.5 is on average 18% for VSCC and 39% for SCC lower than BAM PM2.5. For all samples above detection

limit, the gravimetric method PM2.5 is on average 13% for VSCC and 32% for SCC lower than BAM PM2.5.

c. The mineral dust component of BAM PM2.5 by VSCC ranged from 1% to 42% for ADL samples and from 11% to 42% for high-PM10 day samples. The mineral dust component of BAM PM2.5 by SCC ranged from 1% to 34% for ADL samples and from 2% to 31% for high-PM10 day samples. The average mineral dust amount by VSCC of BAM PM2.5 was 20±20% for ADL samples and 27±10% for high-PM10 day samples. The average mineral dust amount by SCC of BAM PM2.5 was 15±14% for ADL samples and 19±19% for high-PM10 day samples.
d. Organic mass concentration was quantified by FTIR for 13 PM2.5 SCC filters at mass concentrations of 0.8-3.7 μg m^{-3} for ADL samples, accounting for 1-18% of BAM PM2.5 concentrations.

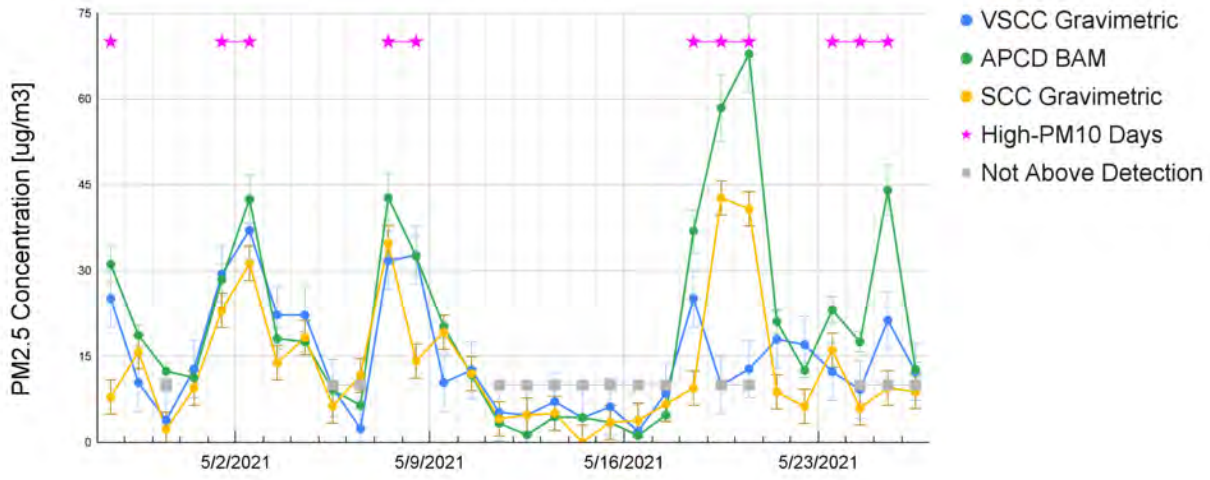

Figure 2. Time series of PM2.5 mass concentrations [μg m^{-3}] by Gravimetric (blue, yellow) and BAM (green) methods at CDF from 27 April to 26 May 2021 (all samples). Error bars represent twice the method uncertainty.

Discussion

BAM has been employed to provide hourly PM10 and PM2.5 concentrations across much of California since the approval of 24-hr average BAM as a federal equivalent method (FEM) in 2008 [USEPA, 2013]. Comparisons of BAM and filter-based reference methods have shown that BAM values are often higher than filter-based methods

because of the loss of the more volatile, or semivolatile, components during collection and equilibration on Teflon filters [Tao and Harley, 2015; Takahashi et al., 2008; Chow et al., 2006]. This has been especially true in regions like California, in which a substantial amount of PM2.5 is contributed by ammonium nitrate, causing the South Coast Air Quality Management District to apply to exclude BAM PM2.5 measurements from determination of attainment [Tao and Harley, 2015], since the standards are based on equilibrated filters by the federal reference method (FRM) rather than BAM. Corrections for BAM to gravimetric have been developed for some regions in order to use BAM to determine if air quality standards are exceeded [Le et al., 2020]

One reason for higher BAM concentrations in coastal areas with high ambient relative humidity is that the BAM may not have sufficient residence time to allow for full equilibration of particles to ~35% relative humidity, making the effective relative humidity of the measurement higher than the 35% required by the FRM. The role of sea salts and other minerals in delaying the loss of water from particles because of hydrate formation is well known [Frossard et al., 2012; Cziczo and Abbatt, 2000; Harvie et al., 1980]. One coastal study in Greece has shown that the amount that BAM exceeds gravimetric is correlated to the normalized water vapor pressure in the air and that the positive bias is highest for relative humidity 40-80% and temperature 11-22°C [Triantafyllou et al., 2016]. Another study showed a 30% positive bias of BAM to gravimetric for temperatures above 16°C and above 80% relative humidity at concentrations of 30-60 μg m^{-3} [Takahashi et al. 2008]. The PM2.5 sampling reference method (https://www3.epa.gov/ttn/amtic/files/ambient/pm25/qa/m212.pdf) requires that samples be stored at 35% relative humidity for a minimum of 24 hr in order to dry the particles to what is assumed to be equilibrium. In contrast, BAM and EBAM measurements are collected at ambient relative humidity and then heated during flowing through the instrument to bring the relative humidity to 35%, allowing only minutes for equilibration on the glass-fiber filter. At CDF ambient relative humidity exceeded 35% for 27 April through 26 May 2021 (Figure A3), meaning that the BAM measurements needed to be dried in order to remove particle-bound water that was present at ambient conditions. Even at relative humidity as low as 50%, the amount of particle-bound water in PM10 has been shown to be as high as 33% by mass compared to filters below 30% relative humidity [Imre et al., 2014]. Some water can even remain after 24 hr equilibration, contributing to reference filter mass concentrations [Rees et al., 2004]. These results make it likely that the difference in mass on high-PM10 days is due to adsorbed water and other semivolatile components (ammonium nitrate and organic mass) evaporating less in the BAM method and more in the gravimetric method [Le et al., 2020; Tao and Harley, 2015]. The lower gravimetric than BAM mass concentrations are consistent with the expectation that the BAM method includes more water and other

semivolatiles that can evaporate during the gravimetric reference method. The increase in the difference between BAM and gravimetric mass concentration on days with high PM10 (35% compared to 29%) is consistent with higher particle loadings giving less complete evaporation in BAM. The water contribution could be assessed by repeating the gravimetric method at higher relative humidities.

Another possibility is that the BAM calibration does not apply well to the composition and concentration conditions that are relevant to this site. EPA approval of BAM relied on testing conditions that were typically limited to concentrations lower than 100 μg m^{-3} and that were 24-hr average measurements [Chung et al., 2001; Gobeli et al., 2008; Hafkenscheid and Vonk, 2014; Hart, 2009]. At PM10 concentrations exceeding 30 μg m^{-3}, BAM and gravimetric methods were not found to be equivalent using consistency criteria [Gebicki and Szymanska, 2012]. BAM PM2.5 performance relative to reference methods has been shown to vary seasonally and to include an uncertainty of 16% [Hafkenscheid and Vonk, 2014]. A large fraction of PM2.5 can be volatile, and comparisons to reference filters typically show a high bias for the BAM [Hart, 2009], especially for PM2.5 concentrations exceeding 40 μg m^{-3} [Le et al., 2020]. This difference varies with relative humidity, often reducing the correlation between BAM and filters [Chow et al., 2005; Hains et al., 2007]. Since relative humidity often varies with a daily cycle (as it does at CDF in May 2021, Figure A3), comparisons of BAM and gravimetric may tend to have a larger bias for comparing partial days (e.g. afternoon only) than for a 24-hr measurement.

Central California studies have shown that 80% of nitrate in PM2.5 can volatilize in spring and summer conditions [Chow et al., 2005]. Particulate nitrate is higher when ambient relative humidity is high [Dassios and Pandis, 1999]. There is also evidence that the positive bias of BAM relative to gravimetric increases for ambient temperatures below 25°C, when the amount of particulate nitrate may be high [Le et al., 2020]. These errors often vary with time of day, with water adsorption in the BAM affecting afternoon readings and desorption affecting readings after midnight, so that hourly BAM concentrations may have biases of ~20 μg m^{-3} even when 24 hr averages include cancelling errors [Kiss et al., 2017].

In summary, there are two types of reasons for the differences between BAM and gravimetric filter measurements here. The first and very well-known reason is the contribution of semivolatile components. These are components that evaporate from particles when temperature increases, including water, ammonium nitrate, and other semivolatiles. Sampling for 24 hr means that some particles on an FRM filter will lose mass when these components evaporate. Sampling periods shorter than 24 hr can

reduce this evaporation if they reduce the amount of temperature change during sample collection [Mader et al., 2001]. This effect means that the online BAM measurement may be closer to ambient particle mass concentrations (i.e. more similar to the atmosphere) but the longer filter measurement is closer to federal and state standard methods (i.e. more similar to the regulated quantity). For this reason, the gravimetric mass concentrations should be used to assess PM10 and PM2.5 exceedances. Since BAM is used to provide more frequent and routine measurements, here we report the fractions of components relative to BAM.

The second reason is different performance of the samplers because of size cut design or flow rate issues. For PM10, both BAM and gravimetric samplers used nominally the same size cut design at the same flow rate [Tolocka et al., 2001]. The performance of the samplers may be affected by the accumulation of particles on the walls of the sampling head (which may entrain large solid particles above the size cut, as has been observed in testing in agricultural regions [Faulkner et al., 2014; Le et al., 2019]). However, the difference between BAM and gravimetric concentrations persisted from the beginning (with a clean sampling head for gravimetric filters) to end (after 30 days without cleaning) of the sampling with similar magnitude (Figure 1), making it difficult to show any effect from either recent cleaning or accumulated particles. This makes it likely that the 35% (56.8 μg m^{-3}) difference on high-PM10 days is attributable to the first reason (semivolatile components) rather than to size cut performance issues [Triantafyllou et al., 2016]. For PM2.5, the same reasoning applies for the 18% (6.3 μg m^{-3}) difference between the VSCC filters and the BAM. The correlation coefficients (see Appendix) are lower than the range found in other studies ($0.72 < R^2 < 0.90$) [Triantafyllou et al., 2016], which is not surprising given the less than 24-hr averaging times (7 hr), the variable conditions of the short (30-day) study, and the limited number of high-PM10 days (10).

The PM2.5 and PM10 apportionments by component of the BAM concentrations measured at CDF are summarized in Figure 3, where we have labeled the difference between BAM and gravimetric mass as the “Semivolatile” fraction. This fraction is likely from atmospheric water associated with the high ambient relative humidity. Ammonium nitrate and semivolatile organic components may also contribute. Figure 3 also illustrates the measured mass component contributions: mineral dust accounts for 14% of BAM PM10 at CDF on high-PM10 afternoons, ranging from 2% to a single-day high of 32%. This means that on average less than one fifth of the BAM-based PM10 at CDF can be attributed to mineral dust during the 10 high-PM10 days sampled in April-May 2021. The average PM10 concentration on high-PM10 afternoons was 161.2 μg m^{-3}, of which only 23.2 μg m^{-3} was dust. PM2.5 on high-PM10 days had an average afternoon

BAM concentration of 33.9 µg m^{-3}, of which mineral dust accounted for 27% of BAM PM2.5 at CDF (ranging from a low of 11% to a high of 42%).

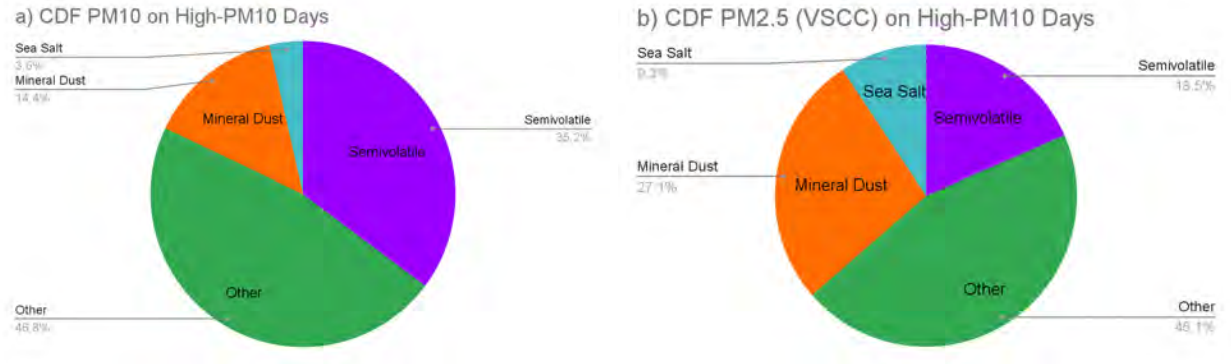

Figure 3. Summary of apportionment of BAM mass concentrations by component for High-PM10 days for (a) PM10 and (b) PM2.5 by VSCC. High-PM10 day samples are those with 1-hr PM10 exceeding 140 µg m^{-3}. "Mineral Dust" provides the upper bound on the amount of PM that could be associated with the sand dune source. The "Semivolatile" is the difference between BAM and gravimetric mass concentration, which may be a combination of incomplete drying of water in BAM and loss of semivolatile components by the filter reference method. The category labeled "Other" (green) includes water and other semivolatile components (ammonium, nitrate, sulfate and organic components), and small amounts of trace metals.

Conclusions

Filter-based chemical mass concentration measurements show that on average 14% of PM10 and 27% (VSCC) of PM2.5 can be attributed to mineral dust on high-PM10 days. Sea salt contributed roughly 4% for PM10 and 9% (VSCC) for PM2.5 on high-PM10 days. The remaining 64% of BAM PM2.5 and 82% of BAM PM10 is likely from water, organic components, ammonium, nitrate, non-sea salt-sulfate, and other semivolatile chemical species. While prior results did not report the mineral dust fraction of BAM or gravimetric PM10 [SLOAPCD, 2007], the reported mineral dust (crustal) fraction of gravimetric PM2.5 reported by the San Luis Obispo Air Pollution Control District for its Nipomo Mesa Particulate Study (Phase 1) for the Mesa2 annual 24-hr average was 20% [SLOAPCD, 2007]. This value is similar to the 7-hr afternoon average in May 2021 for above detection samples reported here (23% of gravimetric), with the higher value for the afternoons in May being consistent with the timing and season providing a conservative upper bound.

These results show that on average less than one-fifth of the BAM PM10 at CDF can be attributed to dust during the high-PM10 days sampled in April-May 2021. Rarely (one in 10 high-PM10 days sampled) mineral dust accounted for almost one-third of the BAM PM10. There is no evidence of mineral dust contributing all or even the majority of BAM PM10, as has apparently been assumed in past reporting [SLOAPCD, 2007].

The association of high PM10 and PM2.5 with high wind conditions, even when recreational vehicles were limited at Oceano Dunes compared to prior years, indicates that dune-derived mineral dust is more likely to be primarily caused by natural forces (*i.e.* wind) rather than human activities. The attribution of mineral dust to natural wind is a common feature of air quality in the western U.S. [Malm et al., 1994; Noll et al. 1985]. While the short duration of this study provides only limited statistics in support of this result, the longer records provided by APCD provide additional confirmation [Li et al., 2013]. For this reason, the contribution of mineral dust to high PM10 concentrations measured on high wind days in and downwind of Oceano Dunes are likely dominated by natural saltation processes associated with the indigenous geomorphological dune structure rather than by recreational activities, as negligible differences were observed between weekday and weekend concentrations [Li et al., 2013].

PM2.5 and PM10 mass concentrations at CDF show contributions of sea spray and mineral dust during high wind episodes. This result means that a substantial fraction of PM2.5 was not associated with fossil-fuel combustion emissions, so that PM2.5 is not a good predictor of toxic emissions or health effects for this location in high wind conditions. For this reason, direct measurements of toxics would be needed in order to associate PM2.5 (or PM10) with health effects at this location.

Acknowledgments

The Scripps/UCSD team is grateful for the insight, advice, and assistance of Will Harris with the California Geological Survey, California Department of Parks and Recreation Oceano Dunes District personnel, CalFire Arroyo Grande Station staff, and APCD personnel.

References

Aghababaeian, H., Ostadtaghizadeh, A., Ardalan, A., Asgary, A., Akbary, M., Yekaninejad, M. S., & Stephens, C. (2021). Global Health Impacts of Dust Storms: A Systematic Review. *Environmental health insights*. https://doi.org/10.1177/11786302211018390

Appel, B. R., Wall, S. M., Tokiwa, Y., & Haik, M. (1979). INTERFERENCE EFFECTS IN SAMPLING PARTICULATE NITRATE IN AMBIENT AIR. *Atmospheric Environment*, *13*(2), 319-325. https://doi.org/10.1016/0004-6981(79)90175-6

Apte, J. S., Brauer, M., Cohen, A. J., Ezzati, M., & Pope, C. A. (2018). Ambient PM2.5 Reduces Global and Regional Life Expectancy. *Environmental Science & Technology Letters*, *5*(9), 546-551. https://doi.org/10.1021/acs.estlett.8b00360

Babila, J. E., Carlton, A. G., Hennigan, C. J., & Ghate, V. P. (2020). On Aerosol Liquid Water and Sulfate Associations: The Potential for Fine Particulate Matter Biases. *Atmosphere*, *11*(2), Article 194. https://doi.org/10.3390/atmos11020194

Chen, C.-L., Chen, S., Russell, L. M., Liu, J., Price, D. J., Betha, R., . . . Cappa, C. D. (2018). Organic Aerosol Particle Chemical Properties Associated With Residential Burning and Fog in Wintertime San Joaquin Valley (Fresno) and With Vehicle and Firework Emissions in Summertime South Coast Air Basin (Fontana). *Journal of Geophysical Research: Atmospheres*, *123*(18), 10,707-710,731. https://doi.org/doi:10.1029/2018JD028374

Chen, C. C., & Huang, S. H. (1999). Shift of aerosol penetration in respirable cyclone samplers. *American Industrial Hygiene Association Journal*, *60*(6), 720-729. https://doi.org/10.1080/00028899908984494

Chow, J. C., & Watson, J. G. (2008). New directions: Beyond compliance air quality measurements. *Atmospheric Environment*, *42*(20), 5166-5168. https://doi.org/10.1016/j.atmosenv.2008.05.004

Chow, J. C., Watson, J. G., Lowenthal, D. H., & Magliano, K. L. (2005). Loss of PM2.5 nitrate from filter samples in central California. *Journal of the Air & Waste Management Association*, *55*(8), 1158-1168. https://doi.org/10.1080/10473289.2005.10464704

Chung, A., Chang, D. P. Y., Kleeman, M. J., Perry, K. D., Cahill, T. A., Dutcher, D., . . . Stroud, K. (2001). Comparison of real-time instruments used to monitor airborne particulate matter. *Journal of the Air & Waste Management Association*, *51*(1), 109-120. https://doi.org/10.1080/10473289.2001.10464254

Craig, J. (2011). *Memo on Mesa2 PM2.5/10 Ratio Data Analysis from Joel Craig (SLOAPCD) to Larry Allen, Richard Countess on 11 March 2011*.

Crooks, J. L., Cascio, W. E., Percy, M. S., Reyes, J., Neas, L. M., & Hilborn, E. D. (2016). The Association between Dust Storms and Daily Non-Accidental Mortality in the United States, 1993-2005. *Environmental Health Perspectives*, *124*(11), 1735-1743. https://doi.org/10.1289/ehp216

Cziczo, D. J., & Abbatt, J. P. D. (2000). Infrared observations of the response of NaCl, MgCl2, NH4HSO4, and NH4NO3 aerosols to changes in relative humidity from 298 to 238 K. *Journal of Physical Chemistry A*, *104*(10), 2038-2047. https://doi.org/10.1021/jp9931408

Dassios, K. G., & Pandis, S. N. (1999). The mass accommodation coefficient of ammonium nitrate aerosol. *Atmospheric Environment*, *33*(18), 2993-3003. https://doi.org/10.1016/s1352-2310(99)00079-5

Dockery, D. W., Pope, C. A., 3rd, Xu, X., Spengler, J. D., Ware, J. H., Fay, M. E., . . . Speizer, F. E. (1993). An association between air pollution and mortality in six U.S. cities. *The New England journal of medicine*, *329*(24), 1753-1759. https://doi.org/10.1056/nejm199312093292401

Faulkner, W. B., Smith, R., & Haglund, J. (2014). Large Particle Penetration During PM10 Sampling. *Aerosol Science and Technology*, *48*(6), 676-687. https://doi.org/10.1080/02786826.2014.915005

Frank, N. H. (2006). Retained nitrate, hydrated sulfates, and carbonaceous mass in Federal Reference Method fine particulate matter for six eastern US cities. *Journal of the Air & Waste Management Association*, *56*(4), 500-511. https://doi.org/10.1080/10473289.2006.10464517

Frossard, A. A., & Russell, L. M. (2012). Removal of Sea Salt Hydrate Water from Seawater-Derived Samples by Dehydration. *Environmental Science & Technology*, *46*(24), 13326-13333. https://doi.org/10.1021/es3032083

Frossard, A. A., Russell, L. M., Burrows, S. M., Elliott, S. M., Bates, T. S., & Quinn, P. K. (2014). Sources and composition of submicron organic mass in marine aerosol particles. *Journal of Geophysical Research: Atmospheres*, *119*(22), 12,977-913,003. https://doi.org/10.1002/2014JD021913

Gebicki, J., & Szymanska, K. (2012). Comparative field test for measurement of PM10 dust in atmospheric air using gravimetric (reference) method and beta-absorption method (Eberline FH 62-1). *Atmospheric Environment*, *54*, 18-24. https://doi.org/10.1016/j.atmosenv.2012.02.068

Gilardoni, S., Russell, L. M., Sorooshian, A., Flagan, R. C., Seinfeld, J. H., Bates, T. S., . . . Worsnop, D. R. (2007). Regional variation of organic functional groups in aerosol particles on four US east coast platforms during the International Consortium for Atmospheric Research on Transport and Transformation 2004 campaign. *Journal of*

Geophysical Research-Atmospheres, *112*(D10), Article D10s27. https://doi.org/10.1029/2006jd007737

Gobeli, D., Schloesser, H., & Pottberg, T. (2008). *Met One Instruments BAM-1020 Beta Attenuation Monitor US-EPA PM2.5 Federal Equivalent Method Field Test Results*. Air and Waste Management Association. https://citeseerx.ist.psu.edu/viewdoc/download?doi=10.1.1.584.2489&rep=rep1&type=pdf

Gwinn, M. R., & Vallyathan, V. (2006). Nanoparticles: Health effects - Pros and cons. *Environmental Health Perspectives*, *114*(12), 1818-1825. https://doi.org/10.1289/ehp.8871

Hafkenscheid, T. L., & Vonk, J. (2014). *Evaluation of equivalence of the MetOne BAM-1020 for the measurement of PM2.5 in ambient air*. National Institute for Public Health and the Environment, Bilthoven, the Netherlands. https://www.rivm.nl/bibliotheek/rapporten/2014-0078.pdf

Hains, J. C., Chen, L. W. A., Taubman, B. F., Doddridge, B. G., & Dickerson, R. R. (2007). A, side-by-side comparison of filter-based PM2.5 measurements at a suburban site: A closure study. *Atmospheric Environment*, *41*(29), 6167-6184. https://doi.org/10.1016/j.atmosenv.2007.04.008

Hart, D. (2009). *What is the Difference Between the New BAM-1020 PM2.5 FEM and Older BAM-1020 Monitors?* . Met One Technical Bulletin. https://metone.com/wp-content/uploads/2019/04/bam_pm2.5_fem_compared_to_older_bam-1020.pdf

Harvie, C. E., Weare, J. H., Hardie, L. A., & Eugster, H. P. (1980). EVAPORATION OF SEAWATER - CALCULATED MINERAL SEQUENCES. *Science*, *208*(4443), 498-500.

Hauck, H., Berner, A., Gomiscek, B., Stopper, S., Puxbaum, H., Kundi, M., & Preining, O. (2004). On the equivalence of gravimetric PM data with TEOM and beta-attenuation measurements. *Journal of Aerosol Science*, *35*(9), 1135-1149. https://doi.org/10.1016/j.jaerosci.2004.04.004

Hoek, G., Brunekreef, B., Goldbohm, S., Fischer, P., & van den Brandt, P. A. (2002). Association between mortality and indicators of traffic-related air pollution in the Netherlands: a cohort study. *Lancet*, *360*(9341), 1203-1209. https://doi.org/10.1016/s0140-6736(02)11280-3

Holland, H. D. (1978). *The Chemistry of the Atmosphere and Oceans*. John Wiley.

Huang, C. H., & Tai, C. Y. (2008). Relative humidity effect on PM2.5 readings recorded by collocated beta attenuation monitors. *Environmental Engineering Science*, *25*(7), 1079-1089. https://doi.org/10.1089/ees.2007.0142

Imre, K., Molnar, A., Dezsi, V., & Geleneser, A. (2014). Positive bias caused by residual water in reference PM10 measurements. *Idojaras*, *118*(3), 207-216.

Janssen, N. A. H., Brunekreef, B., van Vliet, P., Aarts, F., Meliefste, K., Harssema, H., & Fischer, P. (2003). The relationship between air pollution from heavy traffic and allergic sensitization, bronchial hyperresponsiveness, and respiratory symptoms in Dutch schoolchildren. *Environmental Health Perspectives*, *111*(12), 1512-1518. https://doi.org/10.1289/ehp.6243

Kenny, L. C., Merrifield, T., Mark, D., Gussman, R., & Thorpe, A. (2004). The development and designation testing of a new USEPA-approved fine particle inlet: A study of the USEPA designation process. *Aerosol Science and Technology*, *38*, 15-22. https://doi.org/10.1080/027868290502290

Kenny, L. C., & Thorpe, A. (2000). *Evaluation of VSCC Cyclones for BGI Incorporated*. Mesa Labs. https://bgi.mesalabs.com/wp-content/uploads/sites/35/2015/02/vsccref6-2.946.pdf

Kenny, L. C., Thorpe, A., & Stacey, P. (2017). A collection of experimental data for aerosol monitoring cyclones. *Aerosol Science and Technology*, *51*(10), 1190-1200. https://doi.org/10.1080/02786826.2017.1341620

Kiss, G., Imre, K., Molnar, A., & Gelencser, A. (2017). Bias caused by water adsorption in hourly PM measurements. *Atmospheric Measurement Techniques*, *10*(7). https://doi.org/10.5194/amt-10-2477-2017

Knol, A. B., de Hartog, J. J., Boogaard, H., Slottje, P., van der Sluijs, J. P., Lebret, E., . . . Hoek, G. (2009). Expert elicitation on ultrafine particles: likelihood of health effects and causal pathways. *Particle and Fibre Toxicology*, *6*, Article 19. https://doi.org/10.1186/1743-8977-6-19

Krasnov, H., Katra, I., Koutrakis, P., & Friger, M. D. (2014). Contribution of dust storms to PM10 levels in an urban arid environment. *Journal of the Air & Waste Management Association*, *64*(1), 89-94. https://doi.org/10.1080/10962247.2013.841599

Le, T. C., Shukla, K. K., Chen, Y. T., Chang, S. C., Lin, T. Y., Li, Z., . . . Tsai, C. J. (2020). On the concentration differences between PM2.5 FEM monitors and FRM samplers. *Atmospheric Environment*, *222*, Article 117138. https://doi.org/10.1016/j.atmosenv.2019.117138

Le, T. C., Shukla, K. K., Sung, J. C., Li, Z. Y., Yeh, H. J., Huang, W., & Tsai, C. J. (2019). Sampling efficiency of low-volume PM10 inlets with different impaction substrates. *Aerosol Science and Technology*, *53*(3), 295-308. https://doi.org/10.1080/02786826.2018.1559919

Li, R., Wiedinmyer, C., & Hannigan, M. P. (2013). Contrast and correlations between coarse and fine particulate matter in the United States. *Science of the Total Environment*, *456*, 346-358. https://doi.org/10.1016/j.scitotenv.2013.03.041

Li, X. H., Ruan, B., Hopke, P. K., & Mehmood, T. (2019). On the Performance Parameters of PM2.5 and PM1 Size Separators for Ambient Aerosol Monitoring. *Aerosol and Air Quality Research*, *19*(10), 2173-2184. https://doi.org/10.4209/aaqr.2019.03.0103

Lin, C. W., Chen, T. J., Huang, S. H., Kuo, Y. M., Gui, H. Q., & Chen, C. C. (2018). Effect of Aerosol Loading on Separation Performance of PM2.5 Cyclone Separators. *Aerosol and Air Quality Research*, *18*(6), 1366-1374. https://doi.org/10.4209/aaqr.2017.11.0458

Lipfert, F. W. (1994). FILTER ARTIFACTS ASSOCIATED WITH PARTICULATE MEASUREMENTS - RECENT-EVIDENCE AND EFFECTS ON STATISTICAL RELATIONSHIPS. *Atmospheric Environment*, *28*(20), 3233-3249. https://doi.org/10.1016/1352-2310(94)00167-j

Liu, J., Dedrick, J., Russell, L. M., Senum, G. I., Uin, J., Kuang, C. G., . . . Lubin, D. (2018). High summertime aerosol organic functional group concentrations from marine and seabird sources at Ross Island, Antarctica, during AWARE. *Atmospheric Chemistry and Physics*, *18*(12), 8571-8587. https://doi.org/10.5194/acp-18-8571-2018

Lundgren, D. A., & Burton, R. M. (1995). EFFECT OF PARTICLE-SIZE DISTRIBUTION ON THE CUT POINT BETWEEN FINE AND COARSE AMBIENT MASS FRACTIONS. *Inhalation Toxicology*, *7*(1), 131-148.

Mader, B. T., & Pankow, J. F. (2001). Gas/solid partitioning of semivolatile organic compounds (SOCs) to air filters. 3. An analysis of gas adsorption artifacts in measurements of atmospheric SOCs and organic carbon (OC) when using Teflon membrane filters and quartz fiber filters [Article]. *Environmental Science & Technology*, *35*(17), 3422-3432. https://doi.org/10.1021/es0015951

Malm, W. C., Sisler, J. F., Huffman, D., Eldred, R. A., & Cahill, T. A. (1994). SPATIAL AND SEASONAL TRENDS IN PARTICLE CONCENTRATION AND OPTICAL EXTINCTION IN THE UNITED-STATES. *Journal of Geophysical Research-Atmospheres*, *99*(D1), 1347-1370. https://doi.org/10.1029/93jd02916

Maria, S. F., Russell, L. M., Turpin, B. J., Porcja, R. J., Campos, T. L., Weber, R. J., & Huebert, B. J. (2003). Source signatures of carbon monoxide and organic functional groups in Asian Pacific Regional Aerosol Characterization Experiment (ACE-Asia) submicron aerosol types. *Journal of Geophysical Research-Atmospheres*, *108*(D23), Article 8637. https://doi.org/10.1029/2003jd003703

McDonald, B. C., de Gouw, J. A., Gilman, J. B., Jathar, S. H., Akherati, A., Cappa, C. D., . . . Trainer, M. (2018). Volatile chemical products emerging as largest petrochemical source of urban organic emissions [Article]. *Science*, *359*(6377), 760-764, Article aaq0524. https://doi.org/10.1126/science.aaq0524

Motallebi, N., Taylor, C. A., & Croes, B. E. (2003). Particulate matter in California: Part 2 - Spatial, temporal, and compositional patterns of PM2.5, PM10-2.5, and PM10. *Journal of the Air & Waste Management Association*, *53*(12), 1517-1530. https://doi.org/10.1080/10473289.2003.10466323

Noll, K. E., Pontius, A., Frey, R., & Gould, M. (1985). COMPARISON OF ATMOSPHERIC COARSE PARTICLES AT AN URBAN AND NON-URBAN SITE. *Atmospheric Environment*, *19*(11), 1931-1943. https://doi.org/10.1016/0004-6981(85)90019-8

Oberdorster, G., Stone, V., & Donaldson, K. (2007). Toxicology of nanoparticles: A historical perspective. *Nanotoxicology*, *1*(1), 2-25. https://doi.org/10.1080/17435390701314761

Peters, T. M., Gussman, R. A., Kenny, L. C., & Vanderpool, R. W. (2001). Evaluation of PM2.5 size selectors used in speciation samplers. *Aerosol Science and Technology*, *34*(5), 422-429.

Pope, C. A., Ezzati, M., & Dockery, D. W. (2009). Fine-Particulate Air Pollution and Life Expectancy in the United States. *New England Journal of Medicine*, *360*(4), 376-386. https://doi.org/10.1056/NEJMsa0805646

Rees, S. L., Robinson, A. L., Khlystov, A., Stanier, C. O., & Pandis, S. N. (2004). Mass balance closure and the federal reference method for PM2.5 in Pittsburgh, Pennsylvania. *Atmospheric Environment*, *38*(20), 3305-3318. https://doi.org/10.1016/j.atmosenv.2004.03.016

Russell, L. M. (2003). Aerosol organic-mass-to-organic-carbon ratio measurements. *Environmental Science & Technology*, *37*(13), 2982-2987. https://doi.org/10.1021/es026123w

Russell, L. M., Bahadur, R., & Ziemann, P. J. (2011). Identifying organic aerosol sources by comparing functional group composition in chamber and atmospheric particles [Article]. *Proceedings of the National Academy of Sciences of the United States of America*, *108*(9), 3516-3521. https://doi.org/10.1073/pnas.1006461108

Russell, L. M., Hawkins, L. N., Frossard, A. A., Quinn, P. K., & Bates, T. S. (2010). Carbohydrate-like composition of submicron atmospheric particles and their production from ocean bubble bursting. *Proceedings of the National Academy of Sciences of the United States of America*, *107*(15), 6652-6657. https://doi.org/10.1073/pnas.0908905107

Schweizer, D., Cisneros, R., & Shaw, G. (2016). A comparative analysis of temporary and permanent beta attenuation monitors: The importance of understanding data and equipment limitations when creating PM2.5 air quality health advisories. *Atmospheric Pollution Research*, *7*(5), 865-875. https://doi.org/10.1016/j.apr.2016.02.003

Shepherd, G., Terradellas , E., Baklanov, A., Kang, U., Sprigg, W. A., & Nickovic, S. B., A.D. Al-Dousari , A. Basart , S. Benedetti, A. Sealy, A. Tong, D. Zhang, X. Shumake-Guillemot , J. Kebin, Z. Knippertz, P. Mohammed, A. A. A. Al-Dabbas, M. Cheng, L. Otani , S. Wang, F. Zhang, C. Ryoo, S. B. Cha, J. (2016). *Global Assessment of Sand and Dust Storms*. United Nations Environment Program. https://uneplive.unep.org/redesign/media/docs/assessments/global_assessment_of_sand_and_dust_storms.pdf

SLOAPCD. (2007). *Nipomo Mesa Particulate Study (Phase 1)*. San Luis Obispo Air Pollution Control District. https://storage.googleapis.com/slocleanair-org/images/cms/upload/files/Phase1PMStudyReport2.pdf

Takahashi, K., Minoura, H., & Sakamoto, K. (2008). Examination of discrepancies between beta-attenuation and gravimetric methods for the monitoring of particulate matter. *Atmospheric Environment*, *42*(21), 5232-5240. https://doi.org/10.1016/j.atmosenv.2008.02.057

Tao, L., & Harley, R. A. (2014). Changes in fine particulate matter measurement methods and ambient concentrations in California. *Atmospheric Environment*, *98*, 676-684. https://doi.org/10.1016/j.atmosenv.2014.09.044

Tegen, I., & Fung, I. (1995). CONTRIBUTION TO THE ATMOSPHERIC MINERAL AEROSOL LOAD FROM LAND-SURFACE MODIFICATION. *Journal of Geophysical Research-Atmospheres*, *100*(D9), 18707-18726. https://doi.org/10.1029/95jd02051

Tegen, I., Werner, M., Harrison, S. P., & Kohfeld, K. E. (2004). Relative importance of climate and land use in determining present and future global soil dust emission. *Geophysical Research Letters*, *31*(5), Article L05105. https://doi.org/10.1029/2003gl019216

Tolocka, M. P., Peters, T. M., Vanderpool, R. W., Chen, F. L., & Wiener, R. W. (2001). On the modification of the low flow-rate PM10 dichotomous sampler inlet. *Aerosol Science and Technology*, *34*(5), 407-415. https://doi.org/10.1080/02786820119350

Tong, D. Q., Wang, J. X. L., Gill, T. E., Lei, H., & Wang, B. Y. (2017). Intensified dust storm activity and Valley fever infection in the southwestern United States. *Geophysical Research Letters*, *44*(9), 4304-4312. https://doi.org/10.1002/2017gl073524

Triantafyllou, E., Diapouli, E., Tsilibari, E. M., Adamopoulos, A. D., Biskos, G., & Eleftheriadis, K. (2016). Assessment of factors influencing PM mass concentration measured by gravimetric & beta attenuation techniques at a suburban site. *Atmospheric Environment*, *131*, 409-417. https://doi.org/10.1016/j.atmosenv.2016.02.010

USEPA. (2013). *Revised Requirements for Designation of Reference and Equivalent Methods for PMINF2.5/INF and Ambient Air Quality Surveillance for Particulate Matter*. United States Environmental Protection Agency. https://www.govinfo.gov/app/details/FR-1997-07-18/97-18579

Appendix A

For completeness, the measured composition of all CDF PM10 and PM2.5 measurements are shown in Figure A1. These include PM10 and VSCC and SCC PM2.5 for High-PM10 days and for all days that were above detection. The mineral dust contribution is 14% for PM10 on both High-PM10 days and all days above detection. For PM2.5, the High-PM10 days have a higher contribution of 27% for VSCC (19% for SCC) compared to 20% for VSCC (15% for SCC) on all days above detection.

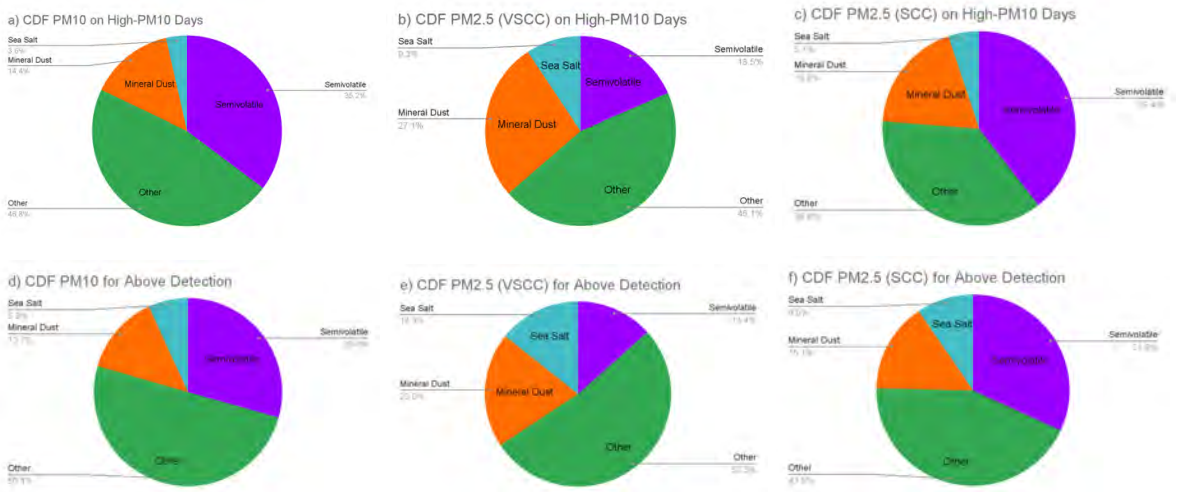

Figure A1. Summary of apportionment of BAM mass concentrations by Component for (a,b,c) Hi-PM10 days and (d,e,f) all samples that were above the detection limits. High PM10 day samples are those with 1-hr PM10 exceeding 140 µg m^{-3}. "Mineral Dust" provides the upper bound on the amount of PM that could be associated with the sand dune source. The "Semivolatile" is the difference between BAM and gravimetric mass concentration based on incomplete drying in BAM, and it is likely to include water, ammonium nitrate, and other semivolatile components. The category labeled "Other" (green) may include water and other semivolatile components (ammonium, nitrate, sulfate and organic components) as well as non-volatile components that remain at 35% relative humidity and were not measured by this project.

There were 14 measurements that were above detection limits for VSCC and SCC; 11 of these were at mass concentrations below 20 µg m^{-3} which meant an uncertainty of 25-50% for a gravimetric measurement error of 10 µg, resulting in only a moderate correlation (R=0.51). This lack of sufficient data for a comparison is the result of targeting higher concentrations and a short time period in order to quantify the maximum mineral dust contribution. Nevertheless, on average, the SCC measurements were consistently lower than the VSCC 27%. As noted above, the less-sharp SCC

cutoff can only explain this if ~30% of PM2.5 mass concentration lies directly below the PM2.5 cutoff with very little mass above the PM2.5 cutoff. While this is possible, it is an unusual particle size distribution for mineral dust and should be confirmed with size-resolved composition measurements.

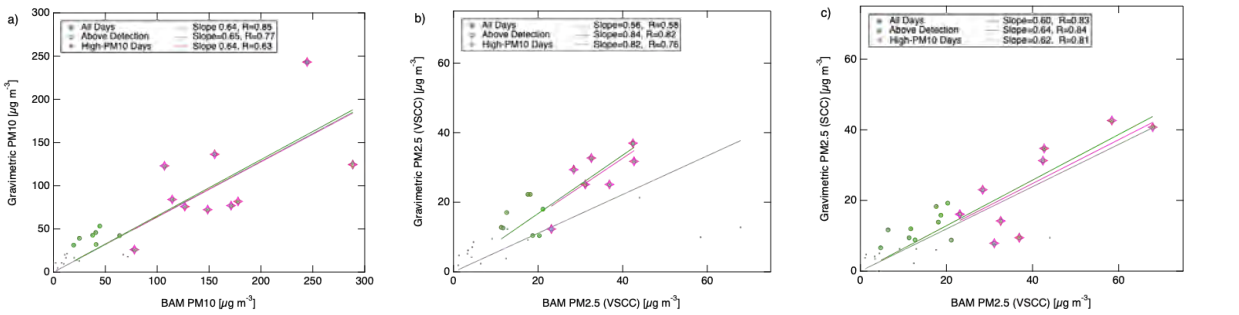

Figure A2. Comparison of gravimetric and BAM PM10 and PM2.5 (VSCC and SCC) at CDF. Legends include slopes and correlation coefficients for linear fits forced to zero.

The SCC method has demonstrated size cut sharpness of 1.25 [Cauda et al., 2014].The VSCC method has a reported sharpness of 1.16 under clean conditions [Kenny and Thorpe, 2000], although that sharpness is expected to increase (i.e. become less sharp) as particles accumulate in the cyclone between cleaning [Kenny et al., 2004]. There is also evidence that performance of similar cyclones degrades at increasing relative humidity due to wall effects [Chen and Huang, 1999]. Desorption or adsorption of semivolatile components can occur during sampling and during storage, tending to increase with higher flow rates, longer sampling times, changing temperatures, and changing ambient conditions [Lipfert, 1994; Appel et al., 1979; Mader et al., 2001].

We can further investigate the PM2.5 differences by comparing the VSCC and the SCC mass concentrations. On the 7 high-PM10 days when both VSCC and SCC sampled, the average gravimetric mass concentration was 27.6 μg m^{-3} for VSCC and 19.5 μg m^{-3} for SCC. Of the difference of 8.1 μg m^{-3}, the concentration that is attributable to salt is 1.2 μg m^{-3} and to mineral dust is 3.6 μg m^{-3} leaving 3.2 μg m^{-3} attributable to differences in semivolatile or unmeasured components. This result indicates that 60% of the difference was due to size cut performance with the VSCC collecting more mass than the SCC, and that up to 40% of the difference may have been due to differences in adsorption and desorption associated with the different flow rates. As expected, this difference is small compared to the 6.3 μg m^{-3} difference between VSCC filters and BAM PM2.5 on high-PM10 days, since both filter methods will have more net desorption of semivolatiles than BAM. The difference in size cut performance of 4.8 μg m^{-3} (18%) between VSCC and SCC is higher than has been reported for other intercomparisons in

the literature [Kenny et al., 2017; Peters et al., 2001]. The low bias of SCC relative to VSCC could only be explained by the larger sharpness value of 1.25 compared to 1.16 if there are higher mass concentrations just below 2.5 µm than above the 2.5 µm, as that would be the condition under which the higher sharpness of VSCC collection exceeds SCC collection [Li et al., 2019]. Further size-resolved chemical measurements could be used to confirm this assertion. This explanation seems unlikely given that SCC penetration curves often show a bias toward larger sizes [Peters et al., 2001]. This result is consistent with previous reports of high PM2.5 relative to PM10 near CDF [Craig, 2011; SLOAPCD, 2007].

There are a number of other reasons that VSCC and SCC differ, including performance degradation caused by changes in loading and humidity that can change VSCC or SCC cutoff performance or sharpness [Chen and Huang, 1999; Lin et al., 2018; Kenny et al., 2004]. For example, changes in VSCC sharpness from 1.16 to 1.19 have been observed after multiple days of high concentrations (150 µg m^{-3}), which resulted in a small positive bias by the VSCC when tested on coarse aerosol [Kenny et al., 2004]. The high bias of VSCC was also present in field tests with high ratios of coarse to fine aerosols, as in Phoenix, Arizona, although observations at high concentrations were not available [Kenny et al., 2004]. SCC differences from the EPA method of record (Well Impactor Ninety-Six, WINS, described in the US Federal Register 40 CFR Part 50, Appendix L, https://www.ecfr.gov/current/title-40/chapter-I/subchapter-C/part-50) for PM2.5 have typically been reported <5% [Lin et al., 2018], with a lower decrease in efficiency from high loading and higher differences for coarse aerosol [Kenny et al. 2000]. It is also possible that the lower flow rate used for the SCC could enhance particle losses in the cyclone [Mader et al., 2001; Appel et al. 1979]. While lower SCC sharpness could account for some of the mass difference between SCC and BAM PM2.5, the remaining difference of 18% for VSCC would still only be explained by evaporation of some components or BAM calibration issues. Moreover, it does not explain the 35% difference between gravimetric and BAM PM10. Records of the BAM internal temperature and relative humidity could show the water content in the BAM, which could have a strong effect on the comparison [Huang and Tai, 2007]. For consistency with the BAM (with VSCC size cut), the VSCC filter results are used for PM2.5 apportionment.

Ambient relative humidity varies during the course of a typical day at CDF, with a minimum of 60-80% at approximately noon (Figure A3). This means the relative humidity in the afternoon is typically increasing to the night time value of 60-80%. When ambient relative humidity is increasing, BAM measurements may tend to be higher than gravimetric even though the 24 hr average may be similar.

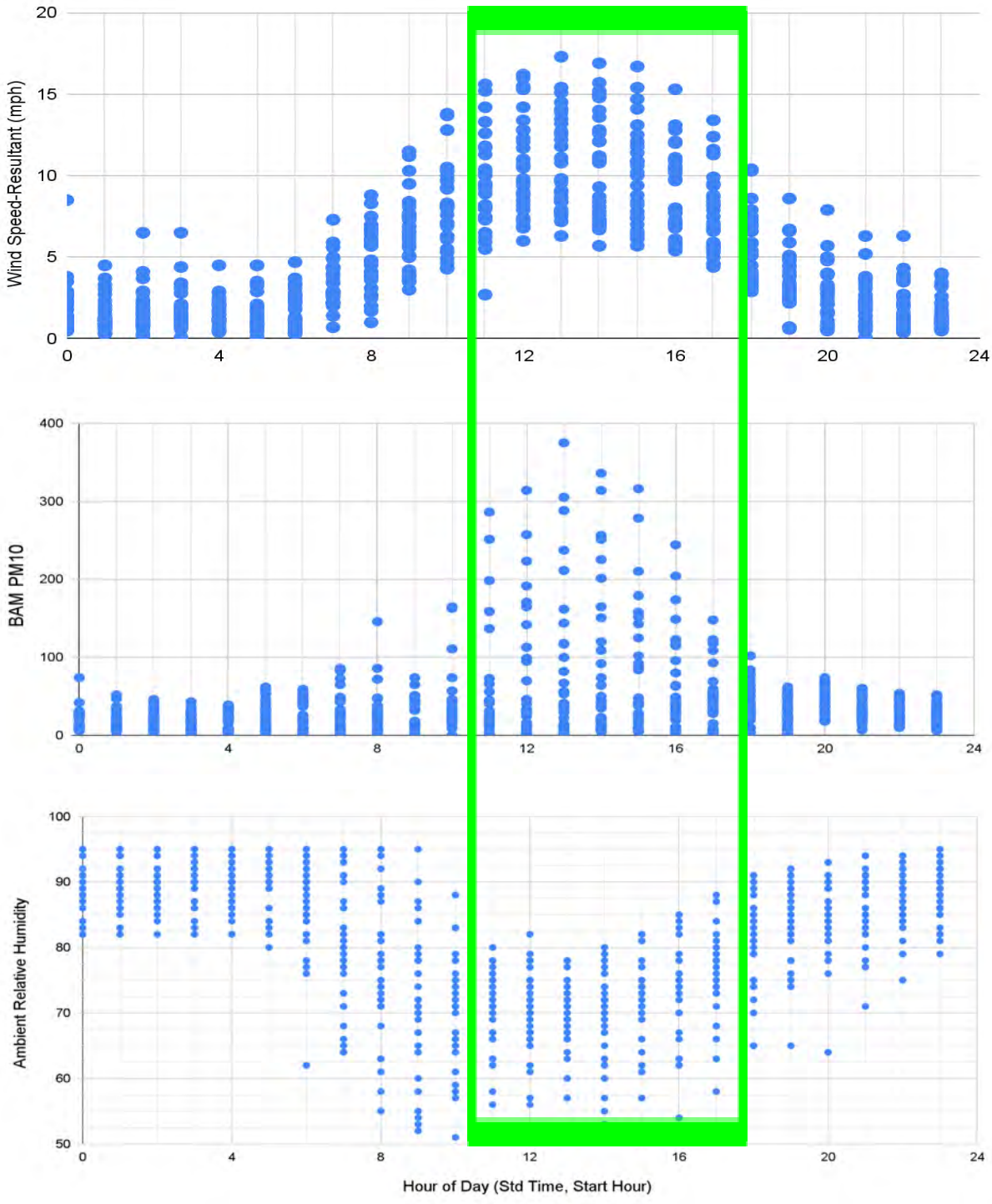

Figure A3. Daily time series of wind speed (top), BAM PM10 (middle), and ambient relative humidity (bottom) from 27 April to 26 May 2021 at CDF. The green box shows the filter sampling time to capture the highest wind speeds with the highest mineral dust contributions. This time period includes increasing ambient relative humidity.

There are several estimates for crustal material from elemental composition that have been introduced. A classic estimate for the western U.S. [Malm et al., 1994; Motallebi et al., 2003] is based on five of the most prevalent elements (Al, Si, Ca, Fe, Ti) and was also used by San Luis Obispo Air Pollution Control District for its Nipomo Mesa Particulate Study (Phase 1) [SLOAPCD, 2007]. A more comprehensive estimate was proposed to account for additional minerals from nine elements (Mg, Al, Si, K, Ca, Ti, Fe, Mn, Ba) [Usher et al., 2003], but needed to be corrected to avoid double counting of sea salt components (Mg, Ca, K) [Gilardoni et al, 2007]. Figure A4 shows that these three estimates are within ±3% of each other.

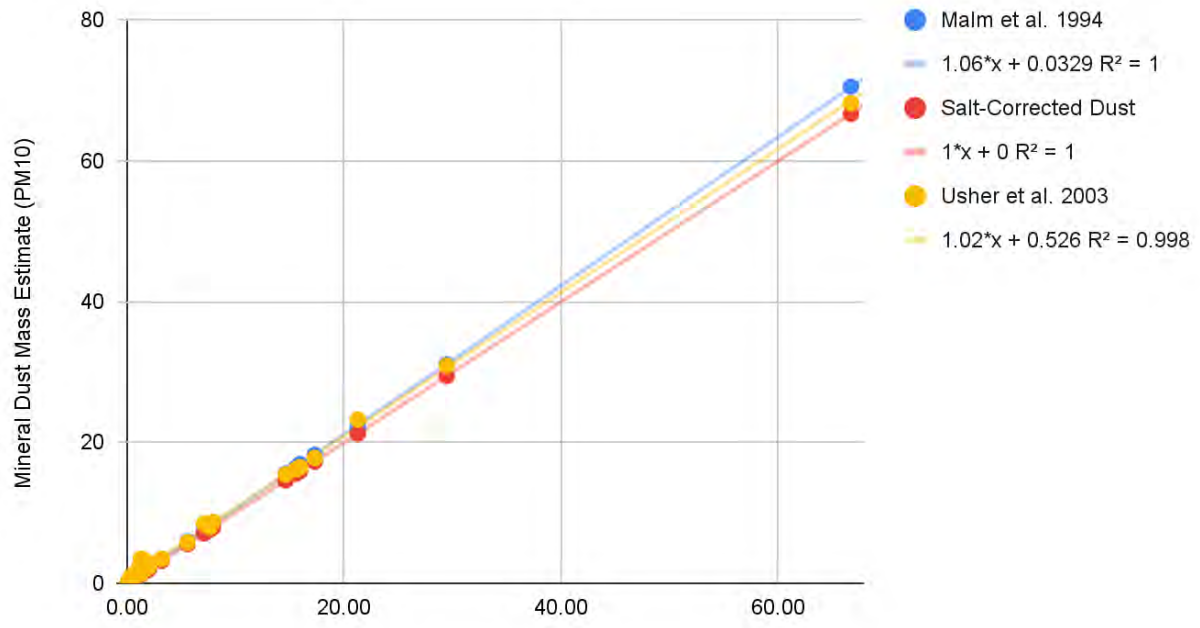

Figure A4. Mineral dust calculation comparison of Usher et al. (2003), after correction to exclude sea salt, and Malm et al. (1994), both without sea salt correction.

To compare these estimates of mineral dust to the specific composition of Oceano Dunes, we also collected samples of sand from Oceano Dunes to be resuspended and measured gravimetrically for PM10 concentration. The resuspension was completed at 35% relative humidity. It shows that at this low relative humidity there is still approximately 27% water present.

Appendix B

B.1 Sampling Flow Configuration Design

The configuration of the sampling flow used by Scripps was designed by calculating the minimum losses using current state-of-the-art calculations. To optimize the sampling for high-wind, high-PM10 conditions, the collection systems used were not based entirely on federal reference methods (FRM), since those methods were not designed for the relevant conditions. Nonetheless, the PM10 sampling inlet and the gravimetric analysis and conditioning were based on FRM.

The PM10 sampling inlet used was the same as that used for BAM. This inlet is designed to be approximately “isokinetic” in many wind conditions, where isokinetic means that the ratio of the wind speed to the velocity in the sampler is equal. In this sense, all sampling for BAM and filters, and by Scripps and SLOAPCD, had the same wind speed to flow conditions, pulling 16.7 lpm through the sampling head.

In order to allow for 7-hr samples with the XRF method that was recommended as most accurate by Chester Labs, the flow after the inlet was split so that only part of the 16.7 lpm was collected on the filters. This plan was discussed with Parks and DRI. The design for a flow splitter varies based on size range and flow ratio, and these factors were considered using a peer-reviewed model of particle losses (Leiden et al., 2009). Scripps calculated the effects of non-isokinetic sampling, non-isoaxial sampling, diffusion losses, sedimentation losses (and gains), turbulent inertial deposition, inertial deposition in a bend, and inertial deposition in a contraction (Figure B1). Because the target of the project was PM10, we optimized the flow sampling to prevent PM10 losses. To do this, for the air flow carrying the sampled PM10, we maintained isoaxial flow in a downward direction, with no bends and laminar conditions. This means that coarse particles are efficiently captured on the filter, and, if anything, the sample provides an upper bound on the coarse particle mass. Specifically we calculated that the supermicron mass could be enhanced 2-40%, with an expected enhancement of 20% for a mean mass diameter of 6 μm. While a custom designed splitter would have allowed fewer losses in the bypass flow removed, it would still have incurred either losses or gains based on the angle of the flow to the filter. For this reason, the potential 20% enhancement was considered acceptable. We note that while a minority of PM10 filter gravimetric samples did exceed BAM concentrations, the majority did not, indicating that the difference between BAM and gravimetric is not from the sampling configuration.

A similar design of flow splitting to the PM10 was used for PM2.5 collection with the VSCC filter, but for fine particles the expected enhancement was only +2%. Since the SCC was used as a backup and comparison to the VSCC, to conserve resources and available equipment, it was collected downstream of two 90-degree sampling bends in the PM10 setup. Such bends cause large losses of coarse particles, but the combined effect of the two bend-splits was -1% for PM2.5. For this reason, the 90-degree bends available with off-the-shelf plumbing was considered sufficient. These -1% to +2% differences are too small to explain the observed differences between PM2.5 VSCC and SCC. They are also too small to explain the differences between PM2.5 gravimetric and BAM concentrations. In addition, the day-to-day differences are most likely due to variability in ambient relative humidity and upwind particle source types that result in differing contributions from semi-volatile particles.

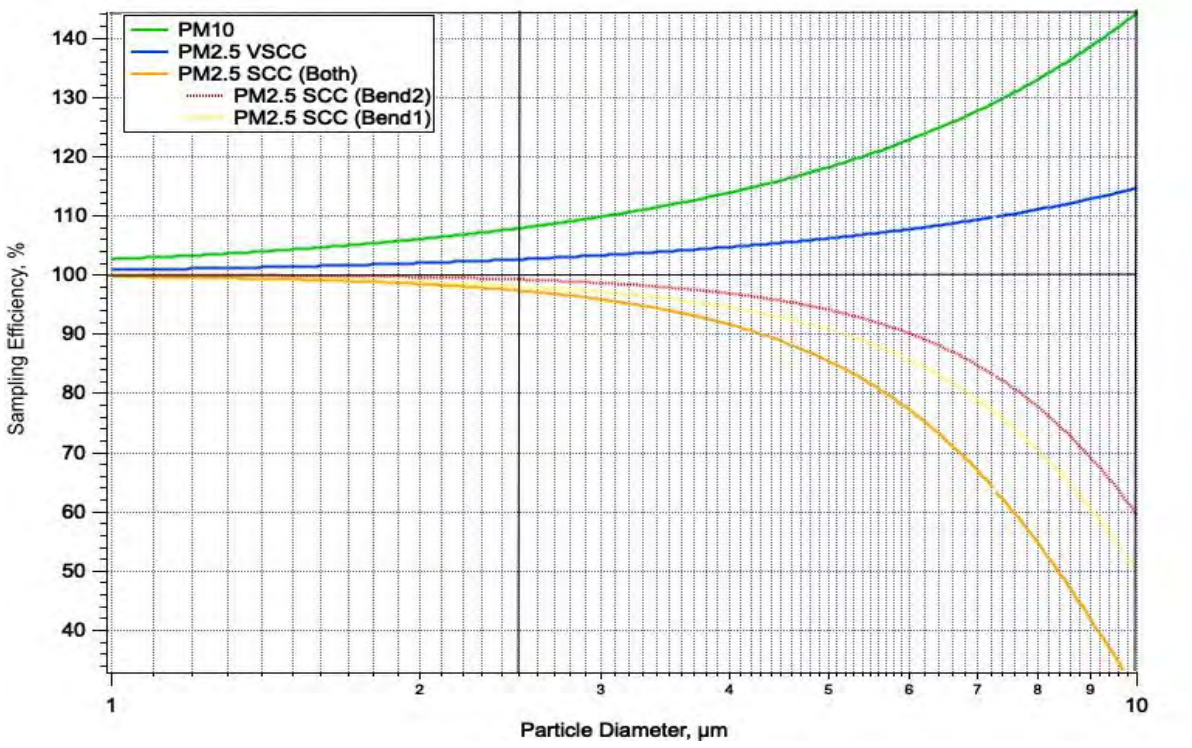

Figure B1. Particle sampling efficiency associated with the flow sampling design for each of the collectors used in the Scripps study. Note that sampling efficiency above 100% indicates increases in concentrations whereas sampling efficiency below 100% indicates decreases in particle concentrations (losses). The PM2.5 SCC flow included two bends with splits, and those are shown separately and as the product of both. The black vertical line indicates the PM2.5 cutoff and the right end shows the PM10 cutoff.

B.2 Evidence of Semivolatile Contribution to Differences between BAM and Gravimetric

Because temperature controls whether particles are in the gas phase or the particle phase for semivolatile components, showing the role of semivolatiles is clear from a consideration of temperature on the differences between the BAM and Gravimetric methods. To do this, we note that the Scripps sampler was suspended on a building and the filters remained on the sampler for only the 7 hr of sampling in the afternoon. In this sense, the sampling and the filters were at ambient temperature. In contrast, the BAM was located inside the APCD shelter at CDF, which is temperature controlled to maintain 20-30^{o}C continuously. This temperature was typically warmer than ambient during May 2021, resulting in a heating of air as it was sampled and then a further heating inside the instrument for the purpose of reducing the relative humidity to below 30%. While the temperature inside the instrument is not recorded, the temperature inside the instrument room is recorded and has been provided by APCD.

If there were no contributions from semivolatile components, then there would be no effect of temperature on either the BAM or Gravimetric results. However, as shown in Figure B2, there is a moderate correlation between the ratio of BAM to Gravimetric and the ambient temperature. This indicates that the warmer the outside temperature, the more BAM exceeded gravimetric. This is consistent with the fact that the saturation pressure of water and other semivolatile components increase with temperature, allowing air to “hold” more in the vapor phase that is then available to condense onto particles (and filter substrates, especially for glass and quartz filters typically used in the BAM). This effect is especially important downwind of the ocean, where air is often near 100% relative humidity.

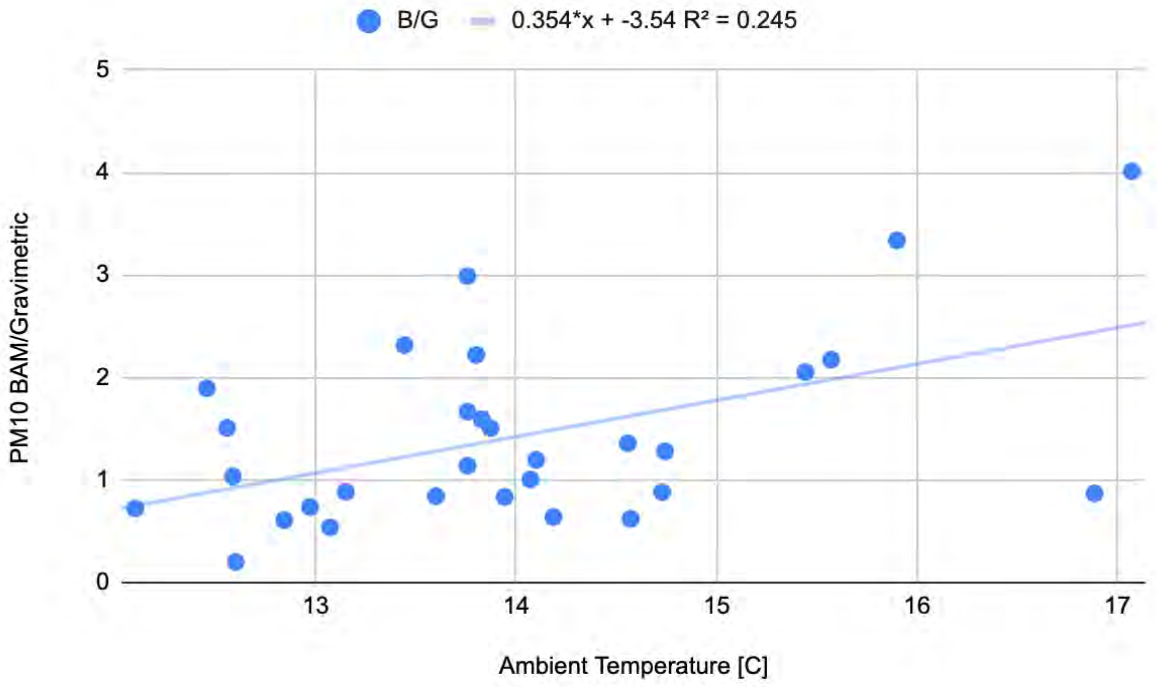

Figure B2. Relationship between the ratio of PM10 APCD BAM to Scripps Gravimetric mass concentrations with the average ambient temperature at CDF during 7-hr afternoon samples in May 2021. The correlation indicates the larger role of gas uptake and evaporation in causing the larger difference between the two PM10 methods at higher temperatures.

To illustrate that there is more water available at higher ambient temperatures for the same relative humidity, it is important to consider how different water amounts represent the same relative humidity for different temperatures. For the May 2021 sampling, the average relative humidity in the afternoon was 71% with a standard deviation of 6%. Figure B3 illustrates the absolute amount of water present for a constant relative humidity of 71% at a series of different ambient temperatures observed during May 2021 (12-17^{o}C). For this temperature range, at the same relative humidity of 71%, the water vapor pressure ranges from 10 to 14 mbar (or equivalently the mass fraction or specific humidity varies from 0.006 to 0.009 g/m^{3}). These data illustrate the water amount changes even more than the temperature even if relative humidity is nearly constant.

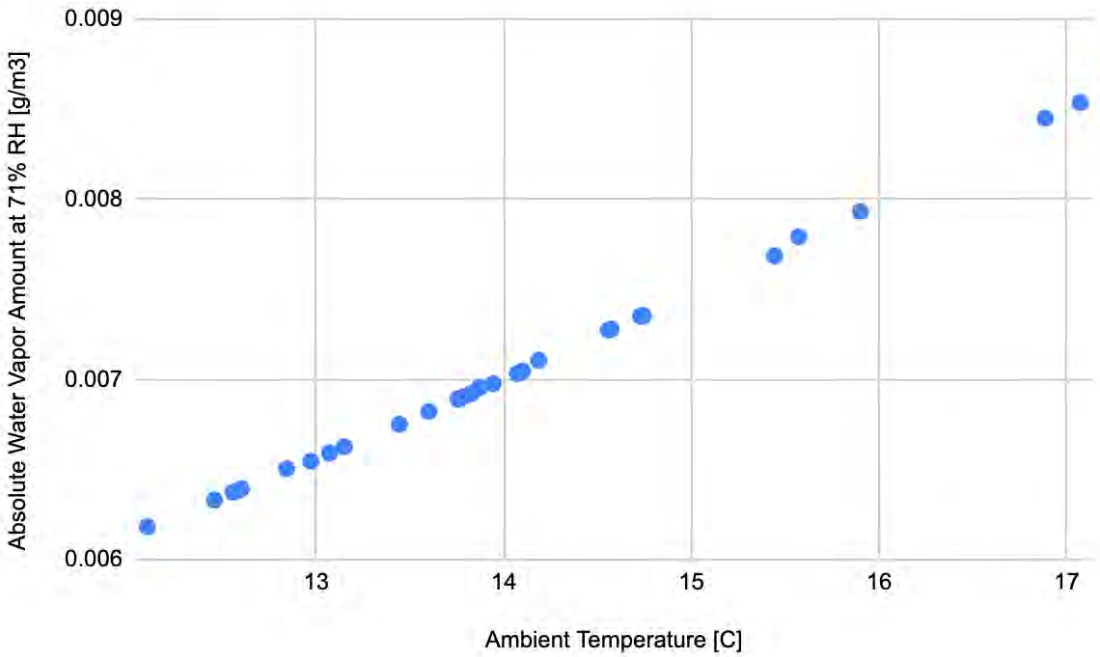

Figure B3. Calculated changes in the absolute water vapor amount (specific humidity) for a constant relative humidity (RH) of 71% as a function of ambient temperature. During May 2021 the average relative humidity for the afternoon sampling period was 71%, but the ambient temperature varied from 12 to 17ºC so that the amount of water vapor also changed as a strong function of temperature.

This result is also similar to the results from another near-coastal site (in suburban Athens) during a 4-year study (Triantafyallou et al., 2016). It is worth noting that this study found that the BAM and gravimetric results were most similar when the same type of filter was used for gravimetric as was present in the BAM, suggesting that if both filters adsorbed the same amount of semivolatile then the results agreed better. However, Scripps used a Teflon filter, which is known to take up fewer semivolatile components from the gas phase (Mader et al., 2001). Generally this means that the Scripps Teflon filters would be expected to be lower in concentration because they had a smaller artifact from the uptake of gases.

There were some Scripps Teflon filters that were higher than BAM, and to understand this effect we consider the difference between the ambient and room temperatures, namely how much the air was heated when entering the room, before it even got to the BAM instrument. This relationship is shown in Figure B4, where the weak correlation indicates a smaller effect, but nonetheless an important relationship. The BAM is lower than the Gravimetric only when the difference between the ambient and room

temperature is highest. Specifically, the trendline for the BAM to Gravimetric ratio falls below the equivalence at 1 when the temperature difference is greater than 11°C.

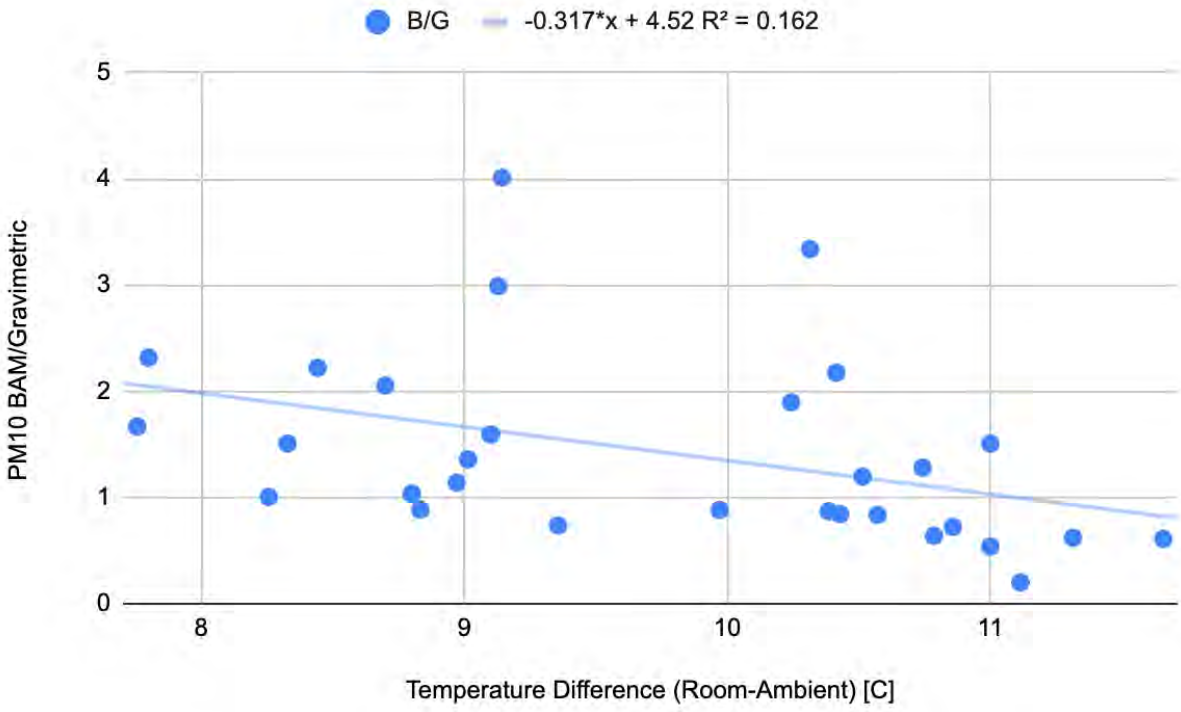

Figure B4. Dependence of the ratio of PM10 APCD BAM to Scripps Gravimetric mass concentrations with the difference between the instrument room temperature and the average ambient temperature at CDF during 7-hr afternoon samples in May 2021. The correlation indicates the role of heating the instrument room relative to the outside temperature in causing the smaller difference between the two PM10 methods.

In addition to temperature, the effect of semivolatile components can be related to the amount of semivolatile components present in the air being sampled. While the relative humidity is a “relative” measure of that amount of water vapor, the absolute humidity (usually called the specific humidity) or the water vapor pressure are metrics used to quantify the amount of water actually present in the air. As suggested by Triantafyallou et al. (2016), this quantity needs to be normalized to the amount of particles in the air, so that the relative effect on the mass concentration will be scaled appropriately. This comparison of the ratio of BAM to Gravimetric mass concentration to the normalized water vapor pressure is shown in Figure B5. Again the correlation is weak though quite evident. The weakness of the correlation is consistent with the expectation that water vapor is not the only semivolatile component contributing to the difference between BAM and Gravimetric, as nitrate and organic components likely also play a role.

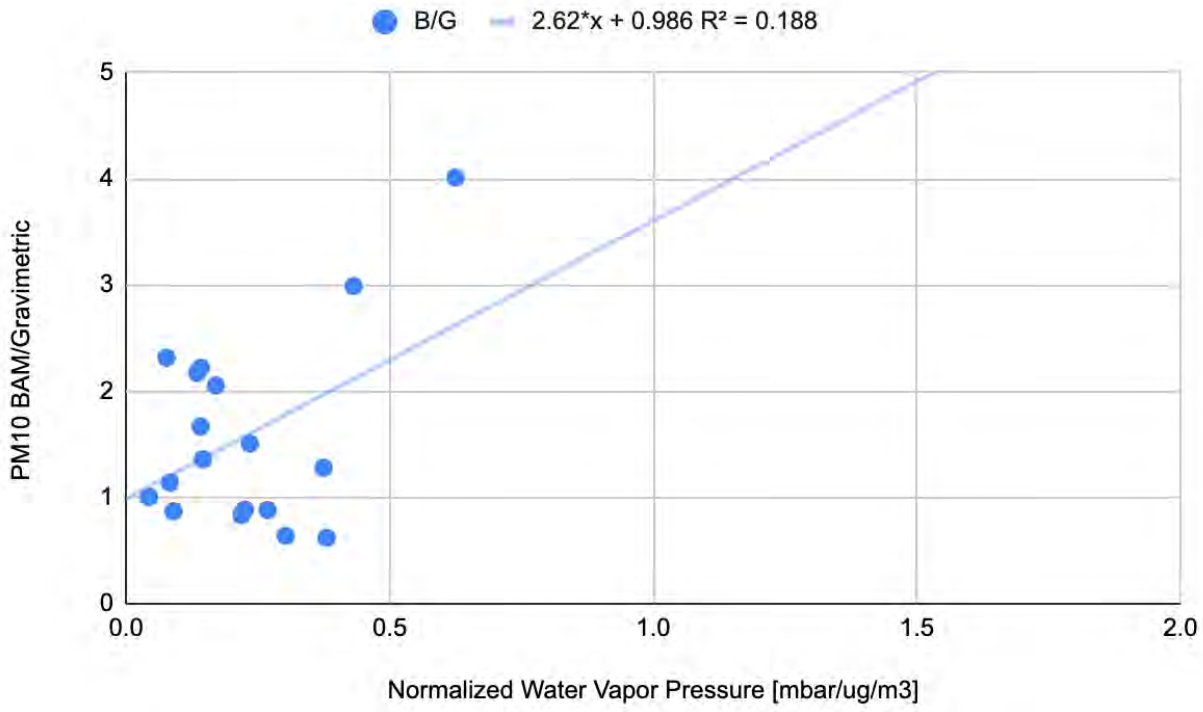

Figure B5. Dependence of the ratio of PM10 APCD BAM to Scripps Gravimetric mass concentrations with the difference between the instrument room temperature and the average ambient temperature at CDF during 7-hr afternoon samples in May 2021. The weak correlation indicates the role of water in causing part of the difference between the two PM10 methods.

B.3 Implications of Evidence for Gas Uptake and Evaporation for Mineral Dust

There is no reason to believe that the Scripps measurements of mineral dust mass concentration would be affected by gas uptake and evaporation. The temperature dependence of the ratio of the BAM and Gravimetric methods shows that gas uptake and evaporation play a major role in the difference between the methods, but the mineral dust does not change with temperature. It is worth noting that this report does not address the question of whether BAM or gravimetric for the 7-hr afternoon sampling is considered “right” -- either atmospherically most accurate or legally most relevant -- as that was not the objective of the Scripps study. However, since BAM has been put forth by APCD as the standard by which exceedances should be determined, the measured mineral dust fraction should be reported on the basis of that same standard. This means that the ratio of mineral dust to BAM mass concentration is completely unaffected by the differences in gas uptake and evaporation between the two methods.

The results of this study do suggest that further consideration of the effects of temperature conditioning on PM10 measurements of the BAM and filter sampling at CDF is merited, even though the mineral dust concentration is not dependent on those results.

November 22, 2021

Memo: SAG Response to Letter from Dr. Lynn M. Russell (Scripps/UCSD) Regarding SAG Review of "Scripps/UCSD Interim Report 2021: Preliminary Results from May 2021 Aerosol Measurements"

From: Scientific Advisory Group (SAG)

To: Jon O'Brien, California Department of Parks and Recreation (CDPR)

Cc: Sarah Miggins, California Department of Parks and Recreation (CDPR)
Liz McGuirk, California Department of Parks and Recreation (CDPR)

To reduce the potential for misinterpretation, the SAG finds it necessary to further clarify their position on the reported findings of the "Scripps/UCSD Interim Report 2021: Preliminary Results from May 2021 Aerosol Measurements" and to respond to the subsequent letter from Dr. Lynn M. Russell (Scripps/UCSD) regarding SAG's initial review ("Memo: SAG Review of Scripps/UCSD 'Interim Report 2021: Preliminary Results from May 2021 Aerosol Measurements'"). The SAG is concerned that the Scripps report and letter have sought to downplay the health effects associated with the mineral components of PM_{10} as a means to challenge the legitimacy of the Stipulated Order of Abatement (SOA). Until the National Ambient Air Quality (NAAQ) Standard for PM_{10}, or the California State Standard, are modified or repealed, there is no legal basis for relaxing the attention that must be given to those Standards and the measures required to achieve those standards through mechanisms like a Stipulated Order of Abatement.

The SAG remains highly critical of the Scripps report conclusion that the mineral dust component of the PM_{10} is a small fraction of the total amount observed at CDF on high wind and particulate matter (PM) days when the wind direction is from the west. The source apportionment presented in the Scripps report suggests that on high PM_{10} days mineral dust contributes approximately 14% to the total observed mass concentration (Scripps report Fig. 3). For the high PM_{10} days in April and May (Scripps report Fig. 1) the wind direction was highly constrained (302°-308°, based on APCD data from CDF) for the daily 7 hour sampling interval. Regarding PM_{10} sources for such high wind days, the SAG refers to the extensive body of dust emission and dispersion modeling, informed by direct PI-SWERL dust emissivity measurements across the Oceano Dunes State Vehicular Recreation Area (ODSVRA), which clearly demonstrate the direct causative relationship between PM_{10} emissions from within the ODSVRA and elevated PM_{10} concentrations at the downwind CDF site (see, for example, 2019 Particulate Matter Reduction Plan Table 4-1 and Fig. 4-1). Model evidence for dune-derived airborne PM_{10} at CDF is further verified by direct measurements of high airborne PM_{10} concentrations at CDF on modeled high PM_{10} days (see, for example, 2020 Annual Report and Work Plan Fig. 2-11). Though the SAG recognizes that efforts to specifically apportion the constituents of this airborne PM_{10} remain ongoing (see 2021 Annual Report and Work Plan Sec. 3.3.1), the existing observational and modeling evidence already provides very strong support for airborne PM_{10} primarily originating from within the ODSVRA on strong westerly wind days.

With winds blowing onshore over the ODSVRA dune surfaces for these high PM_{10} episodes, the Scripps report fails to provide a plausible alternative explanation for the sources of the predominant contributing semi-volatiles and "other" particles in their source apportionment (Scripps report Fig. 3). When the wind blows onshore for multiple hours in conjunction with a frontal system or due to the sea-breeze effect, for example, what are the upwind sources of semi-volatile organic aerosols or "other" that can make such large contributions?

If the PM_{10} was dominated by sources attributed as the Scripps report suggests, then nearby locations should also have concentrations near to those observed at CDF for the same sampling days, minus the contribution associated with mineral dust. For instance, consider the APCD monitoring station at Oso Flaco (Fig. 2) that measures PM_{10} with a BAM, is situated closer to the coastline than CDF, and has much lower upwind areal extent of open sand that could contribute mineral dust particulates during saltation. The PM_{10} measured at Oso Flaco on the same days identified as high-PM in the Scripps report (Fig. 1), is correlated with the PM_{10} at CDF, but is lower by a factor of approximately 0.32 (i.e., Oso Flaco PM_{10}/CDF PM_{10}) when PM_{10} at CDF is >100 µg m^{-3}. If mineral dust was not the primary contributing factor at CDF, why would such lower values (i.e., <<14%) be observed at Oso Flaco, which is less than three miles away (to the south-south-west)?

The Scripps report also suggests that particle-bound water contributes substantially to the observed PM_{10} mass measured by the APCD BAM. Mineral dust particles composed of quartz and feldspar (predominant minerals within the ODSVRA), however, have low adsorption potential for water molecules (i.e., low hygroscopicity) (Engelbrecht et al., 2016;

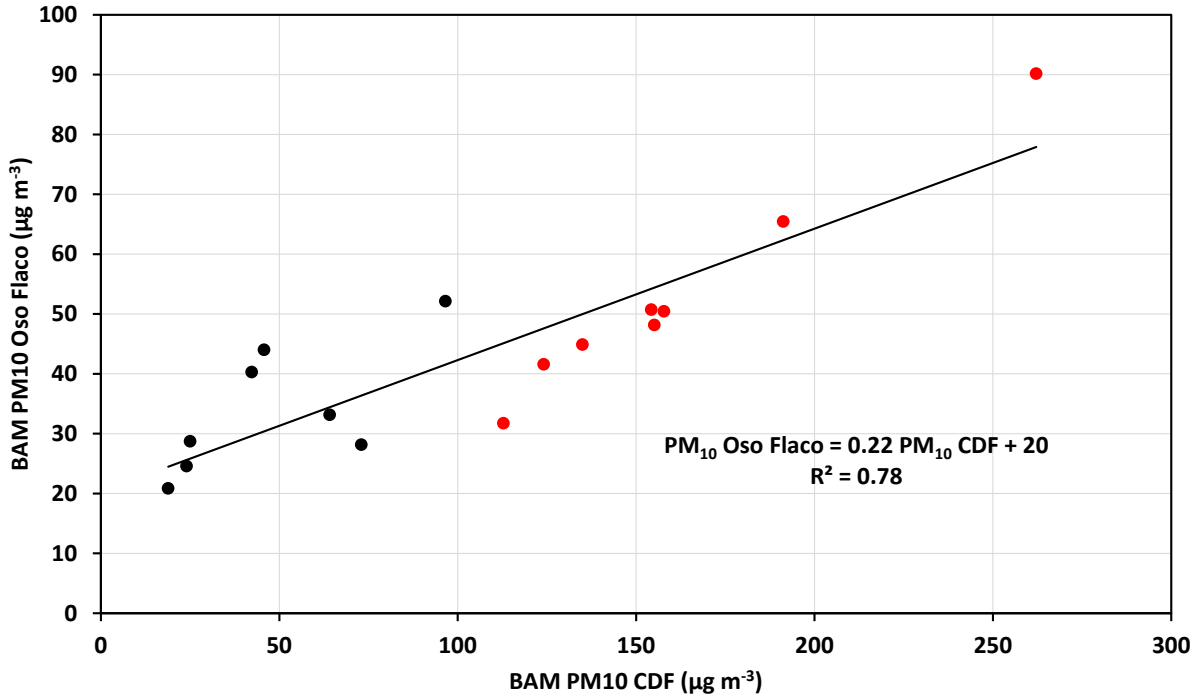

Figure 1. The relation between PM_{10} at Oso Flaco and CDF, for Scripps report sampling days April 27 to May 26, 2021. Red circles highlight high PM_{10} days when the seven hour mean value exceeded 100 µg m^{-3}.

Figure 2. The locations of the APCD monitoring sites CDF, Oso Flaco, and Mesa2.

Formenti et al., 2011; Ito & Wagai, 2017; Journet et al., 2014; Nickovic et al., 2012; Rodriguez-Navarro et al., 2018; Shao et al., 2007). In general, fresh mineral dust particles are usually considered to be rather non-hygroscopic (Herich et al., 2009; Koehler et al., 2009; Ma et al., 2010; Sullivan et al., 2009; Tang et al., 2016). Given this conventional knowledge in mineral dust research, it seems implausible that freshly-emitted mineral dust particles from the ODSVRA would adsorb significant amounts of water even in the high humidity of this coastal setting to contribute to appreciable source attribution in the "other" category. If the particle bound water is predominantly on the hypothesized semi-volatile particles, then it is critically important to identify the off-shore source of those particles to explain the PM_{10} mass concentrations. The Scripps report analyses simply do not convincingly demonstrate that their source apportionment

is correct without a plausible physical explanation for predominant sources other than mineral dust and sea salt.

A second line of evidence on the contribution of mineral dust from ODSVRA to the PM_{10} measured at CDF is provided in the publicly available report commissioned by CDPR and prepared by the Desert Research Institute (DRI):

> Gillies, J.A., E. Furtak-Cole, V. Etyemezian (2020). Increments of Progress Towards Air Quality Objectives – ODSVRA Dust Controls. Report prepared for California State Parks, December 2020.

This report was made publicly available in August 2021, with results presented at the OHV Commission Meeting on August 26, 2021. This report demonstrates, using measurements of PM_{10} and wind speed at CDF, that with the increasing amount of area within the ODSVRA receiving dust control treatments, the concentration of PM_{10} (mean 24 hour) measured at the CDF site has decreased through time for similar wind conditions. If the PM_{10} was dominated by sources other than mineral dust, the demonstrated scaling relation between total area occupied by dust controls and decreasing PM_{10} levels should not be demonstrable as observed.

In summary, the SAG remains concerned about some of the results and questionable interpretations put forth by the Scripps/UCSD report, which confound understanding of the mechanisms and sources of PM_{10} dust emitted from ODSVRA into local monitoring stations. As such, this report understates the contribution of mineral dust to measured PM_{10} air quality exceedance events and, in doing so, risks minimizing the implications for human health in areas downwind of the observed highly emissive sand surfaces within ODSVRA. Given significant efforts implemented by CDPR recently to mitigate dust emissions with corresponding declines in observed PM_{10}, this report also fails to provide constructive insights on how to further improve air quality in local communities downwind of ODSVRA as required by the governing SOA.

Appendix 1 below provides SAG responses to specific comments from the spreadsheet accompanying the Scripps letter. Appendix 2 below provides a list of general references, and Appendix 3 provides selected references regarding dust and human health.

Respectfully,
The Scientific Advisory Group

Dr. Raleigh Martin (Acting chair of SAG); Dr. William Nickling; Dr. Ian Walker; Ms. Carla Scheidlinger; Mr. Earl Withycombe; Mr. Mike Bush, Dr. John A. Gillies

NOTE: The most recent version of the "Scripps/UCSD Interim Report 2021: Preliminary Results from May 2021 Aerosol Measurements" includes an Appendix B on "Sampling Flow Configuration Design" and "Evidence of Semivolatile Contribution to Differences between BAM and Gravimetric." The SAG has not yet had time to review these recent updates, and therefore this current SAG memo does not address these elements of the Scripps/UCSD Interim Report.

Appendix 1. SAG responses to specific comments from the spreadsheet accompanying the Scripps letter

We respond (in Times font) here to the more germane comments provided with the Scripps letter (in Calibri font) in the "Tracking Responses" Excel spreadsheet.

> No citation is provided and the information discussed is not publicly available. The conclusion on weekend/weekday differences is a direct citation from a peer-reviewed publication that is not contradicted by the information provided. The DRI reports I have seen have not shown PM10 impacts at CDF and they provide information on emissive potential not ambient PM10.

The "DRI Emissivity Testing" is in reference to the report that was made publicly available in August 2021 and presented at the OHV Commission Meeting on August 26, 2021. The report referenced is:

Gillies, J.A., E. Furtak-Cole, G. Nikolich, V. Etyemezian (2021). Examining Dust Emissions and OHV Activity at the ODSVRA. Report prepared for California State Parks, April 2021.

The SAG and others have not disputed that the emissions of dust are overwhelmingly attributable to the saltation process, but the effect of OHV to augment the emissivity of the dune sands is demonstrated in the DRI Report through direct measurements of emissivity of riding and non-riding areas and by measurements of PM_{10} in periods when riding was ongoing (2017, 2018, and 2019) and during 2020 when riding was not allowed from March to August due to COVID related restrictions. We also recognize that a weekend/weekday effect on the PM emitted during saltation events is unlikely as the emission system requires months of time, not two days, to adjust to the effects OHV activity has on emissions.

> No citation is provided and the information discussed is not publicly available. The conclusion on the role of coarse dust for health effects is from a peer-reviewed publication that is not contradicted by the unreferenced information provided.

It is not clear what the Scripps letter is referring to regarding information is not publicly available. A large body of peer-reviewed literature is available that documents the effects of coarse dust on human health. In addition, the US EPA still regulates PM_{10}, which confirms that it is a pollutant of concern with respect to adverse health effects for humans. Selected references that show health related impacts due to mineral dust and coarse particulate matter are provided, and the list is by no means exhaustive (see Appendix 3, "Select References on Dust and Human Health").

> No citation is provided and the information discussed is not publicly available. The conclusion on the role of composition for health effects is from a peer-reviewed publication that is not contradicted by the unreferenced information provided.

Citations cataloging the impacts of fine and coarse particulate matter on human health are documented in Appendix 3.

The reviewer is partially correct that the results imply a mode peaking above the PM2.5 cutoff, but not that this implies a higher fraction of mass in PM10 than PM2.5. The explanation is provided that the size distribution is somewhat different than the canonical expectation, but entirely consistent with previous APCD findings about the size distribution of dust, as cited in the report (SLOAPCD memo).

U.S. EPA found that the $PM_{2.5}$ fraction of PM_{10} in fugitive dust was about 10% for most sources with the exceptions of paved road dust, in which the fraction was 15%, and agricultural tilling at 20%.

Background Document for Revisions to Fine Fraction Ratios Used for AP-42 Fugitive Dust Emission Factors, Prepared by Midwest Research Institute for Western Governors' Association, 2006

The report statement is still correct, in that the overlap of analyzed results for both PM10 and PM2.5 are consistent.

While there is some overlap between speciation findings for $PM_{2.5}$ between the 2007 Nipomo Mesa Phase I study and the 2021 Scripps campaign, there is very little overlap between the two studies with respect to PM_{10}. The Phase I study found that while ammonium nitrate, ammonium sulfate, and sea salt contributed an average of ~8 $\mu g/m^3$ to total PM_{10} recorded at the CDF monitoring station, "other" sources contributed ~27 $\mu g/m^3$, or 77% of total PM_{10} (Figure 4, p. 11). Of the quantified contributions, sea salt was responsible for ~4% of PM_{10} mass. Correspondingly, the Scripps 2021 campaign found that sea salt contributed 3.8% to PM_{10} mass on high PM_{10} days. Sea salt is the only overlapping constituent shared by the two studies. As sea salt was responsible for only 4% of PM_{10} mass in each study, the overlap is fairly minimal.

The interpretation given is not consistent with the text. No contradictory peer-reviewed evidence is cited.

The relevant statement in the Scripps report is "The association of high PM_{10} and $PM_{2.5}$ with high wind conditions, even when recreational vehicles were limited at Oceano Dunes compared to prior years, indicates that dune-derived mineral dust is more likely to be primarily caused by natural forces (i.e., wind) rather than human activities." DRI's emissivity testing of ODSVRA riding and non-riding areas demonstrates that riding areas are significantly more emissive than non-riding areas (Gillies et al., 2021 Report to Parks, released Aug. 26, 2021). As a result, human activities augment the emissivity and production of wind/saltation generated PM_{10} from riding areas.

Emissions of dust increase with the size (area) of dunes, as discussed by references cited in the report. As an illustrative example, the amount of emissions from Oceano dunes is smaller than that of the Gobi desert because the area of the dust source at Oceano is smaller than the area of the Gobi desert.

As stated, it suggests that emissions will increase as a function of area similar to wind speed. In the case of wind, emissions increase as a power function of wind speed, but in the case of increasing area, emissivity may well remain constant and the contribution increases due to the increase in source area. The point was these should not, in our opinion, be lumped together as it conflates physical processes with a simple linear scaling factor.

> Comments in prior review did not cite peer-reviewed literature relevant to this issue, so it is not clear what is intended here.

The SAG responses to the 2020 Scripps report provided references that related mineral dust to observed cellular response effects. As mentioned above, references are provided below as a means to demonstrate that there is a significant body of peer-reviewed literature that affirms that mineral dust is associated with health effects in humans.

> The reviewer is partially correct in that the importance of PM2.5, and more so of PM1 (and ultrafine particles), for health effects does not set aside the regulatory restrictions on PM10. However, it does imply that the value to society of regulating PM10 is less than believed at the time the regulations were set in force.

Until those regulations are removed, Parks is required to undertake actions to meet the SOA as stated. The argument that because (as proposed) there is "less harm" associated with PM_{10} doesn't mean safeguards to public health can be lowered. Whether the authors believe mineral dust to be harmful or not is beside the point because it is regulated by the NAAQ PM_{10} standard.

Appendix 2. General references

California State Parks (2019). Oceano Dunes State Vehicular Recreation Area, Draft Particulate Matter Reduction Plan, June 2019.

California State Parks (2020). Oceano Dunes State Vehicular Recreation Area Dust Control Program, 2020 Annual Report and Work Plan, September 30, 2020, Fourth Draft.

California State Parks (2021). Oceano Dunes State Vehicular Recreation Area Dust Control Program, 2021 Annual Report and Work Plan, Conditional Approval Draft, October 1, 2021.

Engelbrecht, J.P., Moosmüller, H., Pincock, S., Jayanty, R. K. M., Lersch, T., & Casuccio, G. (2016). Technical note: Mineralogical, chemical, morphological, and optical interrelationships of mineral dust re-suspensions. *Atmospheric Chemistry and Physics*, 16, 10,809–10,830.

Formenti, P., Schutz, L., Balkanski, Y., Desboeufs, K., Ebert, M., Kandler, K., et al. (2011). Recent progress in understanding physical and chemical properties of African and Asian mineral dust. *Atmospheric Chemistry and Physics*, 11, 8231–8256.

Herich, H., Tritscher, T., Wiacek, A., Gysel, M., Weingartner, E., Lohmann, U., et al. (2009). Water uptake of clay and desert dust aerosol particles at sub- and supersaturated water vapor conditions. *Physical Chemistry Chemical Physics*, 11, 7804–7809.

Ito, A., & Wagai, R. (2017). Global distribution of clay-size minerals on land surface for biogeochemical and climatological studies. *Scientific Data*, 4.

Journet, E., Balkanski, Y., & Harrison, S. P. (2014). A new data set of soil mineralogy for dust-cycle modeling. *Atmospheric Chemistry and Physics*, 14, 3801–3816.

Koehler, K. A., Kreidenweis, S. M., DeMott, P. J., Petters, M. D., Prenni, A. J., & Carrico, C. M. (2009). Hygroscopicity and cloud droplet activation of mineral dust aerosol. Geophysical Research Letters, 36, L08805, doi: 10.01029/02009GL037348.

Ma, Q. X., He, H., & Liu, Y. C. (2010). In situ DRIFTS study of hygroscopic behavior of mineral aerosol. *Journal of Environmental Sciences*, 22, 555–560.

Nickovic, S., Vukovic, A., Vujadinovic, M., Djurdjevic, V., & Pejanovic, G. (2012). Technical note: High-resolution mineralogical database of dust-productive soils for atmospheric dust modeling. *Atmospheric Chemistry and Physics*, 12, 845–855.

Rodriguez-Navarro, C., di Lorenzo, F., & Elert, K. (2018). Mineralogy and physicochemical features of Saharan dust wet deposited in the Iberian Peninsula during an extreme red rain event. *Atmospheric Chemistry and Physics*, 18, 10,089–10,122.

Shao, L. Y., Li, W. J., Yang, S. S., Shi, Z. B., & Lü, S. L. (2007). Mineralogical characteristics of airborne particles collected in Beijing during a severe Asian dust storm period in spring 2002. *Science China Earth Sciences*, 50, 953–959.

Sullivan, R. C., Moore, M. J. K., Petters, M. D., Kreidenweis, S. M., Roberts, G. C., & Prather, K. A. (2009). Effect of chemical mixing state on the hygroscopicity and cloud nucleation properties of calcium mineral dust particles. *Atmospheric Chemistry and Physics*, 9, 3303–3316.

Tang, M. J., Cziczo, D. J., & Grassian, V. H. (2016). Interactions of water with mineral dust aerosol: Water adsorption, hygroscopicity, cloud condensation and ice nucleation. *Chemical Reviews*, 116, 4205–4259.

Appendix 3. Select References on Dust and Human Health

Aragnou, E., Watt, S.F.L., Nguyen Duc, H., Cheeseman, C., Riley, M., Leys, J., White, S., Salter, D., Azzi, M., Tzu-Chi Chang, L., Morgan, G., Hannigan, I., 2021. Dust transport from inland Australia and its impact on air quality and health on the eastern coast of Australia during the February 2019 dust storm. *Atmosphere* 12.

Aust AE, Ball JC, Hu AA, Lighty JS, Smith KR, Straccia AM, Veranth JM, Young WC. (2002) Particle characteristics responsible for effects on human lung epithelial cells. *Res Rep Health Eff Inst*, 110: 1-65.

Beck BD, Feldman HA, Brain JD, Smith TJ, Hallock M, Gerson B. (1987) The pulmonary toxicity of talc and granite dust as estimated from an in vivo hamster bioassay. *Toxicol Appl Pharmacol*, 87(2):222-34.

Becker S, Soukup JM, Sioutas C, Cassee FR. (2003) Response of human alveolar macrophages to ultrafine, fine, and coarse urban air pollution particles. *Exp Lung Res*, 29(1): 29-44.

Bell, M.L.; Ebisu, K.; Peng, R.D.; Walker, J.; Samet, JM; Zeger, S.L.; Dominici, F. (2008). Seasonal and regional short-term effects of fine particles on hospital admissions in 202 US counties, 1999-2005. *Am J Epidemiol*. 168(11):1301-1310.

Bell M.L.; Ebisu K.; Peng R.D.; Samet J.M.; Dominici, F. (2009). Hospital admissions and chemical composition of fine particle air pollution. *Am J Respir Crit Care Med*. 179(12):1115-20.

Cook, A.G., Weinstein, P., Centeno, J.A., 2005. Health effects of natural dust. *Biological Trace Elements Research* 103, 1-15.

Crooks, J.L., Cascio, W.E., Percy, M.S., Reyes, J., Neas, L.M., Hilborn, E.D., 2016. The association between dust storms and daily non-accidental mortality in the United States, 1993-2005. *Environ Health Perspect*. 124, 1735-1743.

Dorman DC, Mokashi V, Wagner DJ, Olabisi AO, Wong BA, Moss OR, Centeno JA, Guandalini G, Jackson DA, Dennis WE, Lewis JA, Thomas RS, Chapman GD. (2012) Biological responses in rats exposed to cigarette smoke and Middle East sand (dust). *Inhal Toxicol*, 24(2):109-24.

Eftim SE, Samet JM, Janes H, McDermott A, Dominici F (2008). Fine Particulate Matter and Mortality: A Comparison of the Six Cities and American Cancer Society Cohorts With a Medicare Cohort. *Epidemiology*, 19: 209- 216.

Franklin, M.; Zeka, A.; Schwartz, J. (2007). Association between PM2.5 and all-cause and specific-cause mortality in 27 US communities. *J Expo Sci Environ Epidemiol*. 17:279-287.

Giannadaki, D., A. Pozzer and J. Lelieveld (2014). Modeled Global Effects of Airborne Desert Dust on Air Quality and Premature Mortality. *Atmospheric Chemistry and Physics* 14: 957-968.

Giltrap, D., Cavanagh, J., Stevenson, B., Ausseil, A.G., 2021. The role of soils in the regulation of air quality. *Philos Trans R Soc Lond B Biol Sci* 376, 20200172.

Grineski, S.E., Staniswalis, J.G., Bulathsinhala, P., Peng, Y., Gill, T.E., 2011. Hospital admissions for asthma and acute bronchitis in El Paso, Texas: do age, sex, and insurance status modify the effects of dust and low wind events? *Environ Res* 111, 1148-1155.

Ito, K.; Thurston, G.; Silverman, R.A. (2007). Characterization of PM2.5 gaseous pollutants and meteorological interactions in the context of time-series health effects models. *J Expo Sci Environ Epidemiol.* 17: 45-60.

Krewski, D.; Burnett, R.T.; Goldberg, M.S.; Hoover, K.; Siemiatycki, J.; Jerrett, M.; Abrahamowicz, M.; White, W.H. (2000). Reanalysis of the Harvard Six Cities study and the American Cancer Society study of particulate air matter pollution and mortality. HEI Research Report, Health Effects Institute, Boston, MA.

Krewski, D.; Jerrett, M.; Burnett, R.T.; Ma, R.; Hughes, E.; Shi, Y.; Turner, M.C.; Pope, C.A. III; Thurston, G.; Calle, E.E.; Thun, M.J. (2009). Extended follow-up and spatial analysis of the American Cancer Society study linking particulate air pollution and mortality. HEI Research Report, 140, Health Effects Institute, Boston, MA.

Krueger, B.J., Grassian, V.H., Cowin, J.P., Laskin, A., 2004. Heterogeneous chemistry of individual mineral dust particles from different dust source regions: the importance of particle mineralogy. *Atmospheric Environment* 38, 6253-6261.

Laden, F., J. Schwartz, F.E. Speizer, and D.W. Dockery. (2006). Reduction in Fine Particulate Air Pollution and Mortality. *American Journal of Respiratory and Critical Care Medicine* 173:667-672

Lipsett MJ, Tsai FC, Roger L, Woo M, & Ostro BD. Coarse Particles and Heart Rate Variability among Older Adults with Coronary Artery Disease in the Coachella Valley, California. *Environmental Health Perspectives*, 114 (8), 1215-1220, Aug. 2006

Medina-Ramón, M.; Zanobetti, A.; Schwartz, J. (2006). The effect of ozone and PM10 on hospital admissions for pneumonia and chronic obstructive pulmonary disease: a national multicity study. *Am J Epidemiol*. 163(6):579-88.

Miousse, I.R., Chalbot, M.-C.G., Pathak, R., Lu, X., Nzabarushimana, E., Krager, K., Aykin-Burns, N., Hauer-Jensen, M., Demokritou, P., Kavouras, I.G., Koturbash, I., 2015. In vitro toxicity and epigenotoxicity of different types of ambient particulate matter. *Toxicological Sciences* 148, 473-487.

Moolgavkar, S. (2000). Air pollution and hospital admissions for chronic obstructive pulmonary disease in three metropolitan areas in the United States. *Inhal Toxicol*. 12(Supplement 4): 75-90.

Moolgavkar, S. (2003). Air pollution and daily deaths and hospital admissions in Los Angeles and Cook counties. pp. 183-198. In: Health Effects Institute Special Report, Revised Analyses of Time-Series Studies of Air Pollution and Health. Health Effects Institute, Cambridge, MA.

Morman, S.A., Plumlee, G.S., 2014. Dust and human health, in: Knippertz, P., Stuut, J.-B.W. (Eds.), *Mineral Dust: A Key Player in the Earth System*. Springer Netherlands, Dordrecht, pp. 385-409.

Ostro, B.; Broadwin, R.; Green, S.; Feng, W.Y.; Lipsett, M. (2006). Fine particulate air pollution and mortality in nine California counties: results from CALFINE. *Environ Health Perspect*. 114(1):29-33.

Perez, L., A. Tobias, X. Querol, N. Kunzli, J. Pey, A. Alastuey, M. Viana, N. Valero, M. Gonzalez-Cabre and J. Sunyer (2008). Coarse particles from Saharan dust and daily mortality. *Epidemiology* 19 (6): 800-807.

Perez, L., A. Tobias, X. Querol, J. Pey, A. Alastuey, J. Diaz and J. Sunyer (2012). Saharan dust, particulate matter and cause-specific mortality: a case-crossover study in Barcelona (Spain). *Environ Int* 48: 150-155.

Pope, C.A. III ; Burnett, R.T. ; Thun, M.J. ; Calle, E.E. ; Krewski, D. ; Ito, K. ; Thurston G.D. (2002). Lung cancer, cardiopulmonary mortality, and long-term exposure to fine particulate air pollution. *JAMA*. 287(9):1132-1141.

Prospero, J.M., Blades, E., Naidu, R., Mathison, G., Thani, H., Lavoie, M.C., 2008. Relationship between African dust carried in the Atlantic trade winds and surges in pediatric asthma attendances in the Caribbean. *International Journal of Biometeorology* 52, 823-835.

Rodopoulo, S., et al. (2014). Air pollution and hospital emergency room and admissions for cardiovascular and respiratory diseases in Doña Ana County, New Mexico. *Environmental Research*, 129, 39-46, doi: 10.1016/j.envres.2013.

Rublee, C.S., Sorensen, C.J., Lemery, J., Wade, T.J., Sams, E.A., Hilborn, E.D., Crooks, J.L., 2020. Associations between dust storms and intensive care unit admissions in the United States, 2000-2015. *Geohealth* 4, e2020GH000260.

Rutherford, S., Clark, E., McTainsh, G., Simpson, R., Mitchell, C., 1999. Characteristics of rural dust events shown to impact on asthma severity in Brisbane, *Australia International Journal of Biometeorology* 42, 217-225.

Sadeghimoghaddam, A., Khankeh, H., Norozi, M., Fateh, S., Farrokhi, M., 2021. Investigating the effects of dust storms on morbidity and mortality due to cardiovascular and respiratory diseases: A systematic review. *J Educ Health Promot* 10, 191.

Smith B. (2009) Newly reported respiratory symptoms and conditions among military personnel deployed to Iraq and Afghanistan: a prospective population-based study. *Am J Epidemiol*, 170:1433–42.

Szema AM, Peters MC, Weissinger KM, Gagliano CA, Chen JJ. (2010) New-onset asthma among soldiers serving in Iraq and Afghanistan. *Allergy Asthma Proc*, 31:67-71.

Taylor K, Foster ML, Law JM, Centeno JA, Fornero E, Henderson MS, Trager SA,Stockelman MG, Dorman DC. (2013) Assessment of geographical variation in the respiratory toxicity of desert dust particles. *Inhal Toxicol*, 25(7):405-16.

Tolbert, P.E.; Klein, M.; Peel, J.L.; Sarnat, S.E.; Sarnat, J.A. (2007). Multipollutant Modeling Issues in a Study of Ambient Air Quality and Emergency Department Visits in Atlanta. *J Expo Sci Environ Epidemiol.* 17: S29-S35.

Uduma, A.U., Jimoh, W.L.O., 2013. High incidence of asthma, bronchitis, pneumonia and sinusitis in Kano State, North West Nigeria during Saharan dust events. *American Journal of Environment, Energy and Power Research* 1, 174-185.

Zanobetti, A.; Schwartz, J. (2009). The effect of fine and coarse particulate air pollution on mortality: A National Analysis. *Environ Health Perspect*. 117(6): 898-903.

Zeger S; Dominici F; McDermott A; Samet J (2008). Mortality in the Medicare population and chronic exposure to fine particulate air pollution in urban centers (2000-2005). *Environ Health Perspect*, 116: 1614.

Zeka, A.; Zanobetti, A.; Schwartz, J. (2005). Short term effects of particulate matter on cause specific mortality: effects of lags and modification by city characteristics. *Occup Environ Med*. 62(10):718-25.

December 1, 2021

Re: "Scripps/UCSD Interim Report 2021: Preliminary Results from May 2021 Aerosol Measurements"

From: Scientific Advisory Group (SAG)

To: California Off-Highway Motor Vehicle Recreation (OHMVR) Commission

Cc: Gary Willey, San Luis Obispo County Air Pollution Control District (SLOAPCD)
Sarah Miggins, California Department of Parks and Recreation (CDPR)
Liz McGuirk, California Department of Parks and Recreation (CDPR)

Chair Ureña and OHMVR Commissioners:

The Scientific Advisory Group (SAG) was established in 2018 through a Stipulated Order of Abatement (SOA), by mutual agreement of SLOAPCD and the OHMVR Division, to address the issue of particulate matter emissions associated with the Oceano Dunes State Vehicular Recreation Area (ODSVRA). The SOA directed the SAG to "evaluate, assess, and provide recommendations on the mitigation of windblown PM10 emissions from ODSVRA," among its responsibilities. (PM10 refers to particulate matter with an aerodynamic diameter of <10 microns, which is subject to California and federal air quality regulations.) The collective expertise on the SAG is unique and highly experienced in terrestrial wind erosion and dust emissions processes and mitigation. As specified by the SOA, the SAG includes experts in the fields of dune geomorphology, wind erosion control, soil ecology, shoreline botany, biophysical sand crust formation, and air quality monitoring and modeling.

Dr. Lynn M. Russell of the Scripps Institution of Oceanography at the University of California, San Diego (UCSD), recently submitted a report to the OHMVR Division, "Scripps/UCSD Interim Report 2021: Preliminary Results from May 2021 Aerosol Measurements." The Scripps report describes analyses of air quality filter samples collected from an independent sampling system at the CDF monitoring site in April-May 2021and compared to PM10 concentrations measured by the co-located SLOAPCD BAM (beta attenuation monitoring) air quality sensor. The BAM sensor is recognized widely as a U.S. EPA-compliant device that is used for regulatory purposes. On the basis of their independent filter sampling, the Scripps report argues, "on average less than one-fifth of the BAM PM10 at CDF can be attributed to dust during the high-PM10 days sampled in April-May 2021."

The SAG is writing to express serious concerns about the accuracy and interpretation of the analyses presented in this recent Scripps report. These concerns are summarized below:

1. Health and legal imperatives. The SAG disagrees with assertions within the Scripps report that minimize the health and legal importance of PM2.5 and PM10 associated with mineral dust. (PM2.5 refers to particulate matter with diameter of <2.5 microns.) From a health perspective, PM2.5 and PM10 are known to cause deleterious health impacts regardless of their chemical

composition. Coarse particulate matter between 2.5 and 10 microns in size is identified by the U.S. EPA in assessments of health effects studies to contribute to increases in thoracic flow resistance and heart rate variability, among other impacts, regardless of elemental or chemical composition. (See Appendix A, "Select References on Dust and Human Health.") It is on the basis of such studies that the U.S. EPA maintains the PM10 ambient air quality standard to protect public health. Statements to the effect that windblown dust particles in the coarser PM10 particulate size range do not contribute to chronic respiratory effects are erroneous. From a legal perspective (and related to the known health impacts), federal and state PM concentration standards do not distinguish between the constituents of particulate matter, nor does the SOA. For these reasons, the SAG argues for the urgent need to continue to reduce ambient PM2.5 and PM10 concentrations at Oceano Dunes regardless of the specific breakdown of PM constituents.

2. Effects of OHV on PM10 emissions. The SAG disagrees with assertions within the Scripps report that minimize the effect of OHV on PM10 emissions at the ODSVRA and PM10 concentrations at receptor sites downwind. By citing a lack of significant difference between weekday and weekend airborne PM10 concentrations as evidence for a lack of OHV impacts on PM10, the report perpetuates the misconception that OHVs produce PM emissions primarily through mechanical action during their operation. Instead, direct measurements and research by the Desert Research Institute (DRI) indicate that the primary effect of OHVs is to degrade dune surfaces and to increase the long-term PM emissivity of the dunes. Eventually, removal of OHVs should reduce PM10 emissions and concentrations, but this adjustment would occur over a matter of many months, not days. The recent DRI report, "Examining Dust Emissions and OHV Activity at the ODSVRA," presents strong evidence, based on years of data collection, for this understanding of the effect of OHVs on PM10 emissions. This DRI report was presented to the OHMVR Commissioners at their meeting on August 26, 2021.

3. Contribution of Mineral Dust to Airborne PM10. The SAG is not convinced by analyses within the Scripps report that lead to their conclusion that only a small percentage of overall ambient PM is composed of mineral dust. The SAG has several specific concerns regarding the methodology for determining the relative mineral dust contribution. (See Appendix B, "Methodological Concerns.") In addition, a large body of evidence, including years of modeling that have guided ODSVRA dust mitigation measures, demonstrates that the ODSVRA is the primary source of airborne PM10 observed at the CDF and Mesa2 receptor sites during typical strong onshore wind days. The recent DRI report, "Increments of Progress Towards Air Quality Objectives – ODSVRA Dust Controls," also presented to the OHMVR Commissioners at their August 26, 2021 meeting, demonstrates a direct causal relationship between ODSVRA dust controls and reductions in airborne PM10. (See Appendix C, "The ODSVRA and PM10 Emissions.")

In summary, the SAG expresses strong concerns about the accuracy of some of the results and questionable interpretations put forth by the Scripps report, which confound understanding of the mechanisms and sources of PM10 dust emitted from ODSVRA and dispersed to local monitoring stations. As such, the Scripps report understates the contribution of mineral dust to measured PM10 air quality exceedance events and, in doing so, risks minimizing the implications for human health in areas downwind of the observed highly emissive sand surfaces within ODSVRA. Given significant recent efforts implemented by California State Parks to

mitigate dust emissions, with corresponding declines in observed PM10, this report also fails to provide constructive insights on how to further improve air quality in local communities downwind of ODSVRA, as required by the governing SOA.

Respectfully,
The Scientific Advisory Group

Dr. Raleigh Martin (Acting chair of SAG); Dr. William Nickling; Dr. Ian Walker; Ms. Carla Scheidlinger; Mr. Earl Withycombe; Mr. Mike Bush, Dr. John A. Gillies

Appendix A. Select References on Dust and Human Health

Aragnou, E., Watt, S.F.L., Nguyen Duc, H., Cheeseman, C., Riley, M., Leys, J., White, S., Salter, D., Azzi, M., Tzu-Chi Chang, L., Morgan, G., Hannigan, I., 2021. Dust transport from inland Australia and its impact on air quality and health on the eastern coast of Australia during the February 2019 dust storm. *Atmosphere* 12.

Aust AE, Ball JC, Hu AA, Lighty JS, Smith KR, Straccia AM, Veranth JM, Young WC. (2002) Particle characteristics responsible for effects on human lung epithelial cells. *Res Rep Health Eff Inst*, 110: 1-65.

Beck BD, Feldman HA, Brain JD, Smith TJ, Hallock M, Gerson B. (1987) The pulmonary toxicity of talc and granite dust as estimated from an in vivo hamster bioassay. *Toxicol Appl Pharmacol*, 87(2):222-34.

Becker S, Soukup JM, Sioutas C, Cassee FR. (2003) Response of human alveolar macrophages to ultrafine, fine, and coarse urban air pollution particles. *Exp Lung Res*, 29(1): 29-44.

Bell, M.L.; Ebisu, K.; Peng, R.D.; Walker, J.; Samet, JM; Zeger, S.L.; Dominici, F. (2008). Seasonal and regional short-term effects of fine particles on hospital admissions in 202 US counties, 1999-2005. *Am J Epidemiol*. 168(11):1301-1310.

Bell M.L.; Ebisu K.; Peng R.D.; Samet J.M.; Dominici, F. (2009). Hospital admissions and chemical composition of fine particle air pollution. *Am J Respir Crit Care Med*. 179(12):1115-20.

Cook, A.G., Weinstein, P., Centeno, J.A., 2005. Health effects of natural dust. *Biological Trace Elements Research* 103, 1-15.

Crooks, J.L., Cascio, W.E., Percy, M.S., Reyes, J., Neas, L.M., Hilborn, E.D., 2016. The association between dust storms and daily non-accidental mortality in the United States, 1993-2005. *Environ Health Perspect*. 124, 1735-1743.

Dorman DC, Mokashi V, Wagner DJ, Olabisi AO, Wong BA, Moss OR, Centeno JA, Guandalini G, Jackson DA, Dennis WE, Lewis JA, Thomas RS, Chapman GD. (2012) Biological responses in rats exposed to cigarette smoke and Middle East sand (dust). *Inhal Toxicol*, 24(2):109-24.

Eftim SE, Samet JM, Janes H, McDermott A, Dominici F (2008). Fine Particulate Matter and Mortality: A Comparison of the Six Cities and American Cancer Society Cohorts With a Medicare Cohort. *Epidemiology*, 19: 209- 216.

Franklin, M.; Zeka, A.; Schwartz, J. (2007). Association between PM2.5 and all-cause and specific-cause mortality in 27 US communities. *J Expo Sci Environ Epidemiol*. 17:279-287.

Giannadaki, D., A. Pozzer and J. Lelieveld (2014). Modeled Global Effects of Airborne Desert Dust on Air Quality and Premature Mortality. *Atmospheric Chemistry and Physics* 14: 957-968.

Giltrap, D., Cavanagh, J., Stevenson, B., Ausseil, A.G., 2021. The role of soils in the regulation of air quality. *Philos Trans R Soc Lond B Biol Sci* 376, 20200172.

Grineski, S.E., Staniswalis, J.G., Bulathsinhala, P., Peng, Y., Gill, T.E., 2011. Hospital admissions for asthma and acute bronchitis in El Paso, Texas: do age, sex, and insurance status modify the effects of dust and low wind events? *Environ Res* 111, 1148-1155.

Ito, K.; Thurston, G.; Silverman, R.A. (2007). Characterization of PM2.5 gaseous pollutants and meteorological interactions in the context of time-series health effects models. *J Expo Sci Environ Epidemiol.* 17: 45-60.

Krewski, D.; Burnett, R.T.; Goldberg, M.S.; Hoover, K.; Siemiatycki, J.; Jerrett, M.; Abrahamowicz, M.; White, W.H. (2000). Reanalysis of the Harvard Six Cities study and the American Cancer Society study of particulate air matter pollution and mortality. HEI Research Report, Health Effects Institute, Boston, MA.

Krewski, D.; Jerrett, M.; Burnett, R.T.; Ma, R.; Hughes, E.; Shi, Y.; Turner, M.C.; Pope, C.A. III; Thurston, G.; Calle, E.E.; Thun, M.J. (2009). Extended follow-up and spatial analysis of the American Cancer Society study linking particulate air pollution and mortality. HEI Research Report, 140, Health Effects Institute, Boston, MA.

Krueger, B.J., Grassian, V.H., Cowin, J.P., Laskin, A., 2004. Heterogeneous chemistry of individual mineral dust particles from different dust source regions: the importance of particle mineralogy. *Atmospheric Environment* 38, 6253-6261.

Laden, F., J. Schwartz, F.E. Speizer, and D.W. Dockery. (2006). Reduction in Fine Particulate Air Pollution and Mortality. *American Journal of Respiratory and Critical Care Medicine* 173:667-672

Lipsett MJ, Tsai FC, Roger L, Woo M, & Ostro BD. Coarse Particles and Heart Rate Variability among Older Adults with Coronary Artery Disease in the Coachella Valley, California. *Environmental Health Perspectives*, 114 (8), 1215-1220, Aug. 2006

Medina-Ramón, M.; Zanobetti, A.; Schwartz, J. (2006). The effect of ozone and PM10 on hospital admissions for pneumonia and chronic obstructive pulmonary disease: a national multicity study. *Am J Epidemiol*. 163(6):579-88.

Miousse, I.R., Chalbot, M.-C.G., Pathak, R., Lu, X., Nzabarushimana, E., Krager, K., Aykin-Burns, N., Hauer-Jensen, M., Demokritou, P., Kavouras, I.G., Koturbash, I., 2015. In vitro toxicity and epigenotoxicity of different types of ambient particulate matter. *Toxicological Sciences* 148, 473-487.

Moolgavkar, S. (2000). Air pollution and hospital admissions for chronic obstructive pulmonary disease in three metropolitan areas in the United States. *Inhal Toxicol*. 12(Supplement 4): 75-90.

Moolgavkar, S. (2003). Air pollution and daily deaths and hospital admissions in Los Angeles and Cook counties. pp. 183-198. In: Health Effects Institute Special Report, Revised Analyses of Time-Series Studies of Air Pollution and Health. Health Effects Institute, Cambridge, MA.

Morman, S.A., Plumlee, G.S., 2014. Dust and human health, in: Knippertz, P., Stuut, J.-B.W. (Eds.), *Mineral Dust: A Key Player in the Earth System*. Springer Netherlands, Dordrecht, pp. 385-409.

Ostro, B.; Broadwin, R.; Green, S.; Feng, W.Y.; Lipsett, M. (2006). Fine particulate air pollution and mortality in nine California counties: results from CALFINE. *Environ Health Perspect*. 114(1):29-33.

Perez, L., A. Tobias, X. Querol, N. Kunzli, J. Pey, A. Alastuey, M. Viana, N. Valero, M. Gonzalez-Cabre and J. Sunyer (2008). Coarse particles from Saharan dust and daily mortality. *Epidemiology* 19 (6): 800-807.

Perez, L., A. Tobias, X. Querol, J. Pey, A. Alastuey, J. Diaz and J. Sunyer (2012). Saharan dust, particulate matter and cause-specific mortality: a case-crossover study in Barcelona (Spain). *Environ Int* 48: 150-155.

Pope, C.A. III ; Burnett, R.T. ; Thun, M.J. ; Calle, E.E. ; Krewski, D. ; Ito, K. ; Thurston G.D. (2002). Lung cancer, cardiopulmonary mortality, and long-term exposure to fine particulate air pollution. *JAMA*. 287(9):1132-1141.

Prospero, J.M., Blades, E., Naidu, R., Mathison, G., Thani, H., Lavoie, M.C., 2008. Relationship between African dust carried in the Atlantic trade winds and surges in pediatric asthma attendances in the Caribbean. *International Journal of Biometeorology* 52, 823-835.

Rodopoulo, S., et al. (2014). Air pollution and hospital emergency room and admissions for cardiovascular and respiratory diseases in Doña Ana County, New Mexico. *Environmental Research*, 129, 39-46, doi: 10.1016/j.envres.2013.

Rublee, C.S., Sorensen, C.J., Lemery, J., Wade, T.J., Sams, E.A., Hilborn, E.D., Crooks, J.L., 2020. Associations between dust storms and intensive care unit admissions in the United States, 2000-2015. *Geohealth* 4, e2020GH000260.

Rutherford, S., Clark, E., McTainsh, G., Simpson, R., Mitchell, C., 1999. Characteristics of rural dust events shown to impact on asthma severity in Brisbane, *Australia International Journal of Biometeorology* 42, 217-225.

Sadeghimoghaddam, A., Khankeh, H., Norozi, M., Fateh, S., Farrokhi, M., 2021. Investigating the effects of dust storms on morbidity and mortality due to cardiovascular and respiratory diseases: A systematic review. *J Educ Health Promot* 10, 191.

Smith B. (2009) Newly reported respiratory symptoms and conditions among military personnel deployed to Iraq and Afghanistan: a prospective population-based study. *Am J Epidemiol*, 170:1433–42.

Szema AM, Peters MC, Weissinger KM, Gagliano CA, Chen JJ. (2010) New-onset asthma among soldiers serving in Iraq and Afghanistan. *Allergy Asthma Proc*, 31:67-71.

Taylor K, Foster ML, Law JM, Centeno JA, Fornero E, Henderson MS, Trager SA,Stockelman MG, Dorman DC. (2013) Assessment of geographical variation in the respiratory toxicity of desert dust particles. *Inhal Toxicol*, 25(7):405-16.

Tolbert, P.E.; Klein, M.; Peel, J.L.; Sarnat, S.E.; Sarnat, J.A. (2007). Multipollutant Modeling Issues in a Study of Ambient Air Quality and Emergency Department Visits in Atlanta. *J Expo Sci Environ Epidemiol.* 17: S29-S35.

Uduma, A.U., Jimoh, W.L.O., 2013. High incidence of asthma, bronchitis, pneumonia and sinusitis in Kano State, North West Nigeria during Saharan dust events. *American Journal of Environment, Energy and Power Research* 1, 174-185.

Zanobetti, A.; Schwartz, J. (2009). The effect of fine and coarse particulate air pollution on mortality: A National Analysis. *Environ Health Perspect*. 117(6): 898-903.

Zeger S; Dominici F; McDermott A; Samet J (2008). Mortality in the Medicare population and chronic exposure to fine particulate air pollution in urban centers (2000-2005). *Environ Health Perspect*, 116: 1614.

Zeka, A.; Zanobetti, A.; Schwartz, J. (2005). Short term effects of particulate matter on cause specific mortality: effects of lags and modification by city characteristics. *Occup Environ Med*. 62(10):718-25.

Appendix B. Methodological Concerns

This section details specific concerns with the methodology presented in the Scripps report.

(p. 9, first paragraph) The mineral dust component of PM2.5 filters collected on high-PM10 days is reported to average 27% by VSCC inlet and 19% by SCC inlet. Typically, the geologic component is predominately higher in PM10 samples than in PM2.5 samples as the mean particle size of windblown dust is about 4 microns. These results suggesting that the geologic component is higher in the PM2.5 fraction than in the PM10 fraction at the CDF monitoring station are unusual and warrant an explanation.

(p. 13, Figure 3) The labeling of the difference between BAM and PM10 filter measurements as "Semivolatile" is speculative in the absence of further testing. The positive identification of only 18% of PM10 mass results in very limited information with respect to the composition of PM10 measured at the CDF monitoring station.

(p. 13, Conclusions, first paragraph, last sentence) The statement that results of this study were consistent with the chemical composition reported by the SLOAPCD in its Nipomo Mesa Particulate Study (Phase 1) is misleading in that the Phase 1 study analyzed only total mass, sulfate, nitrate, and chloride values in PM10 samples collected at the CDF monitoring site. As the Scripps study did not analyze sulfate, nitrate, and chloride contributions at CDF, there is almost no overlap in the constituents measured in the two studies with respect to samples collected at CDF.

(p. 14, second sentence, second paragraph) The statement that a substantial fraction of PM2.5 was not associated with fossil-fuel combustion emissions ignores the failure in the paper to identify the composition and sources of 63.6% of total mass on PM2.5 samples collected on high PM10 days.

Appendix C. The ODSVRA and PM10 Emissions

The SAG is highly critical of the Scripps report conclusion that the mineral dust component of the PM10 is a small fraction of the total amount observed at CDF on high wind and particulate matter (PM) days when the wind direction is from the west. The source apportionment presented in the Scripps report suggests that on high PM10 days mineral dust contributes approximately 14% to the total observed mass concentration (Scripps report Fig. 3). For the high PM10 days in April and May (Scripps report Fig. 1) the wind direction was highly constrained (302°-308°, based on APCD data from CDF) for the daily 7 hour sampling interval. Regarding PM10 sources for such high wind days, the SAG refers to the extensive body of dust emission and dispersion modeling, informed by direct PI-SWERL dust emissivity measurements across the Oceano Dunes State Vehicular Recreation Area (ODSVRA), which clearly demonstrate the direct causative relationship between PM10 emissions from within the ODSVRA and elevated PM10 concentrations at the downwind CDF site (see, for example, 2019 Particulate Matter Reduction Plan Table 4-1 and Fig. 4-1). Model evidence for dune-derived airborne PM10 at CDF is further verified by direct measurements of high airborne PM10 concentrations at CDF on modeled high PM10 days (see, for example, 2020 Annual Report and Work Plan Fig. 2-11). Though the SAG recognizes that efforts to specifically apportion the constituents of this airborne PM10 remain ongoing (see 2021 Annual Report and Work Plan Sec. 3.3.1), the existing observational and modeling evidence already provides very strong support for airborne PM10 primarily originating from within the ODSVRA on strong westerly wind days.

With winds blowing onshore over the ODSVRA dune surfaces for these high PM10 episodes, the Scripps report fails to provide a plausible alternative explanation for the sources of the predominant contributing semi-volatiles and "other" particles in their source apportionment (Scripps report Fig. 3). When the wind blows onshore for multiple hours in conjunction with a frontal system or due to the sea-breeze effect, for example, what are the upwind sources of semi-volatile organic aerosols or "other" that can make such large contributions?

If the PM10 was dominated by sources attributed as the Scripps report suggests, then nearby locations should also have concentrations near to those observed at CDF for the same sampling days, minus the contribution associated with mineral dust. For instance, consider the APCD monitoring station at Oso Flaco (Fig. C1) that measures PM10 with a BAM, is situated closer to the coastline than CDF, and has much lower upwind areal extent of open sand that could contribute mineral dust particulates during saltation. The PM10 measured at Oso Flaco on the same days identified as high-PM in the Scripps report (Fig. C2), is correlated with the PM10 at CDF, but is lower by a factor of approximately 0.32 (i.e., Oso Flaco PM10/CDF PM10) when PM10 at CDF is >100 $\mu g\ m^{-3}$. If mineral dust was not the primary contributing factor at CDF, why would such lower values (i.e., <<14%) be observed at Oso Flaco, which is less than three miles away (to the south-south-west)?

The Scripps report also suggests that particle-bound water contributes substantially to the observed PM10 mass measured by the APCD BAM. Mineral dust particles composed of quartz and feldspar (predominant minerals within the ODSVRA), however, have low adsorption potential for water molecules (i.e., low hygroscopicity) (Engelbrecht et al., 2016; Formenti et al., 2011; Ito & Wagai, 2017; Journet et al., 2014; Nickovic et al., 2012; Rodriguez-Navarro et al.,

2018; Shao et al., 2007). In general, fresh mineral dust particles are usually considered to be rather non-hygroscopic (Herich et al., 2009; Koehler et al., 2009; Ma et al., 2010; Sullivan et al., 2009; Tang et al., 2016). Given this conventional knowledge in mineral dust research, it seems implausible that freshly-emitted mineral dust particles from the ODSVRA would adsorb significant amounts of water even in the high humidity of this coastal setting to contribute to appreciable source attribution in the "other" category. If the particle bound water is predominantly on the hypothesized semi-volatile particles, then it is critically important to identify the off-shore source of those particles to explain the PM10 mass concentrations. The Scripps report analyses simply do not convincingly demonstrate that their source apportionment is correct without a plausible physical explanation for predominant sources other than mineral dust and sea salt.

A second line of evidence on the contribution of mineral dust from ODSVRA to the PM10 measured at CDF is provided in the publicly available report commissioned by California State Parks and prepared by the Desert Research Institute (DRI):

> Gillies, J.A., E. Furtak-Cole, V. Etyemezian (2020). Increments of Progress Towards Air Quality Objectives – ODSVRA Dust Controls. Report prepared for California State Parks, December 2020.

This report was made publicly available in August 2021, with results presented at the OHMVR Commission Meeting on August 26, 2021. This report demonstrates, using measurements of PM10 and wind speed at CDF, that with the increasing amount of area within the ODSVRA receiving dust control treatments, the concentration of PM10 (mean 24 hour) measured at the CDF site has decreased through time for similar wind conditions. If the PM10 was dominated by sources other than mineral dust, the demonstrated scaling relation between total area occupied by dust controls and decreasing PM10 levels should not be demonstrable as observed.

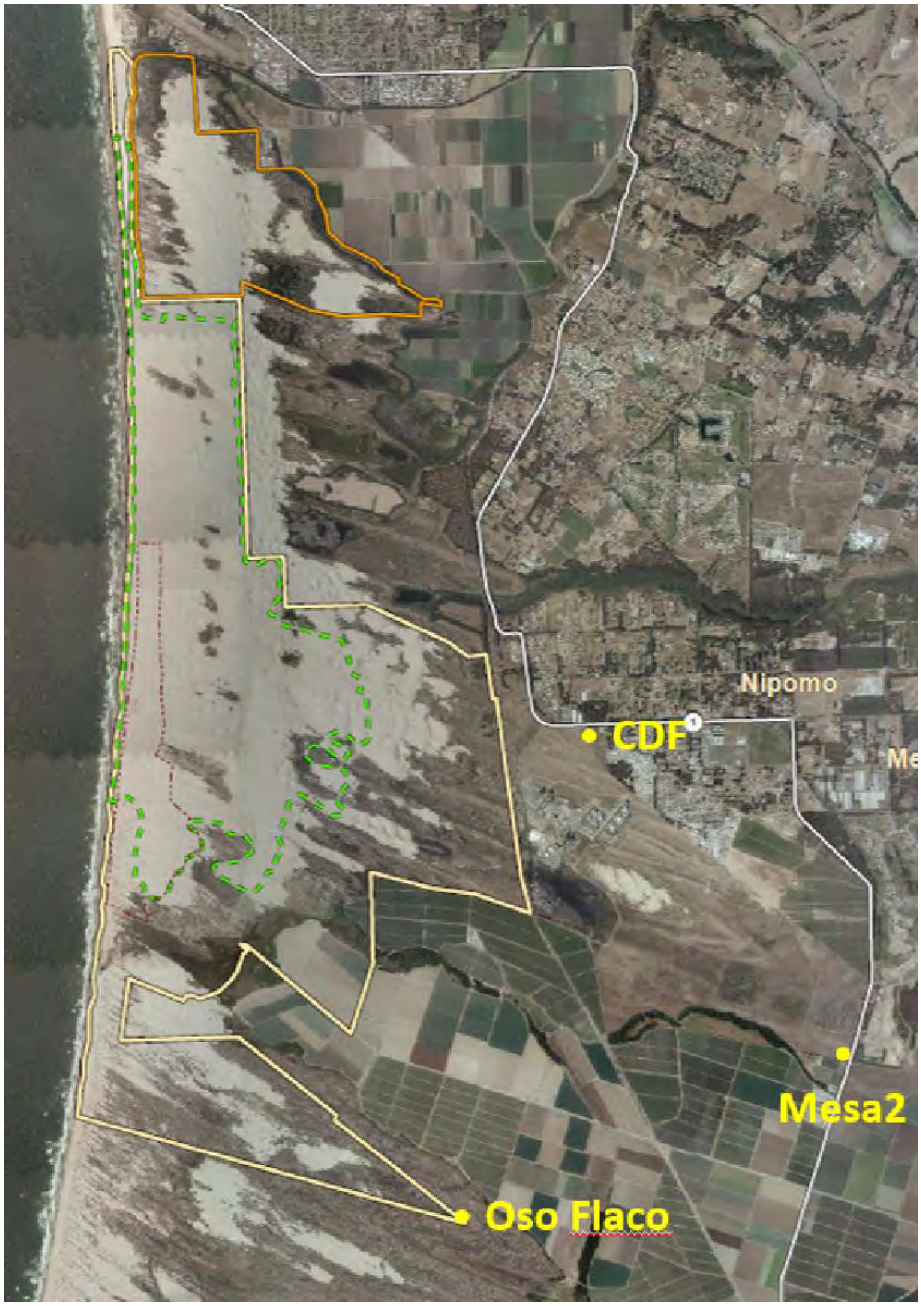

Figure C1. The locations of the APCD monitoring sites CDF, Oso Flaco, and Mesa2.

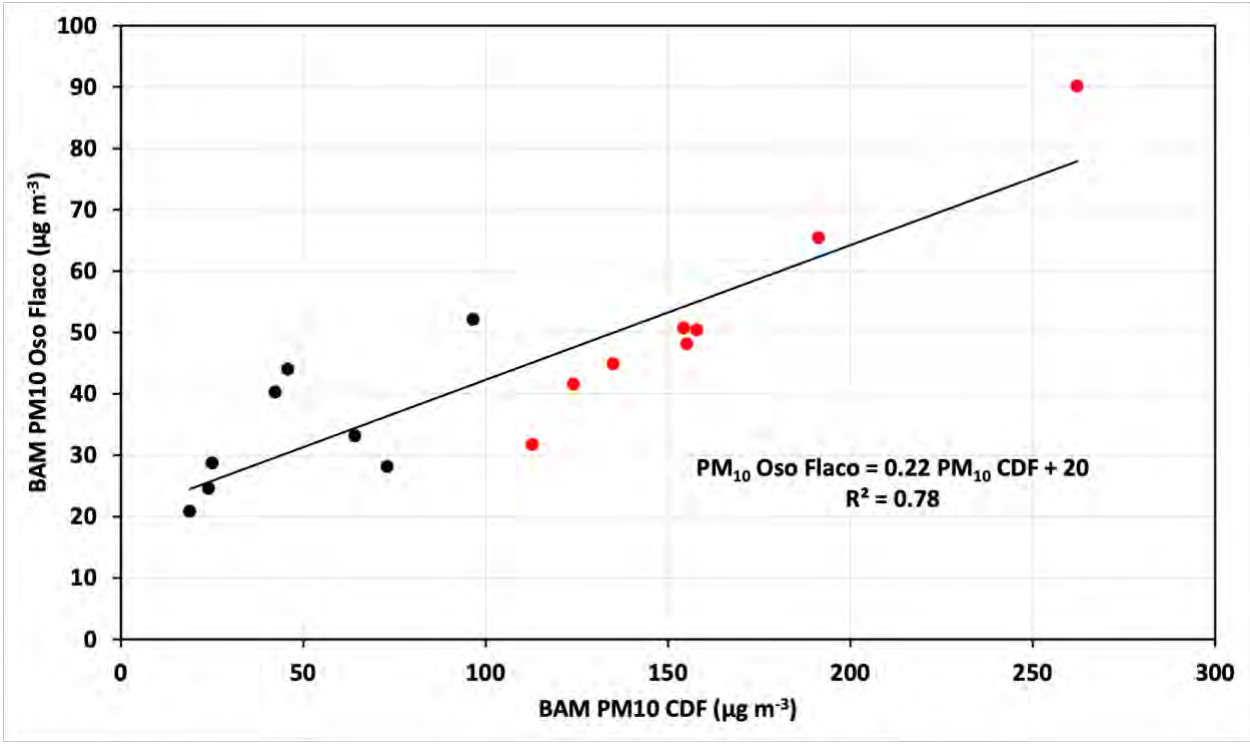

Figure C2. The relation between PM10 at Oso Flaco and CDF, for Scripps report sampling days April 27 to May 26, 2021. Red circles highlight high PM10 days when the seven hour mean value exceeded 100 µg m^{-3}.

References:

California State Parks (2019). Oceano Dunes State Vehicular Recreation Area, Draft Particulate Matter Reduction Plan, June 2019.

California State Parks (2020). Oceano Dunes State Vehicular Recreation Area Dust Control Program, 2020 Annual Report and Work Plan, September 30, 2020, Fourth Draft.

California State Parks (2021). Oceano Dunes State Vehicular Recreation Area Dust Control Program, 2021 Annual Report and Work Plan, Conditional Approval Draft, October 1, 2021.

Engelbrecht, J.P., Moosmüller, H., Pincock, S., Jayanty, R. K. M., Lersch, T., & Casuccio, G. (2016). Technical note: Mineralogical, chemical, morphological, and optical interrelationships of mineral dust re-suspensions. *Atmospheric Chemistry and Physics*, 16, 10,809–10,830.

Formenti, P., Schutz, L., Balkanski, Y., Desboeufs, K., Ebert, M., Kandler, K., et al. (2011). Recent progress in understanding physical and chemical properties of African and Asian mineral dust. *Atmospheric Chemistry and Physics*, 11, 8231–8256.

Herich, H., Tritscher, T., Wiacek, A., Gysel, M., Weingartner, E., Lohmann, U., et al. (2009). Water uptake of clay and desert dust aerosol particles at sub- and supersaturated water vapor conditions. *Physical Chemistry Chemical Physics*, 11, 7804–7809.

Ito, A., & Wagai, R. (2017). Global distribution of clay-size minerals on land surface for biogeochemical and climatological studies. *Scientific Data*, 4.

Journet, E., Balkanski, Y., & Harrison, S. P. (2014). A new data set of soil mineralogy for dust-cycle modeling. *Atmospheric Chemistry and Physics*, 14, 3801–3816.

Koehler, K. A., Kreidenweis, S. M., DeMott, P. J., Petters, M. D., Prenni, A. J., & Carrico, C. M. (2009). Hygroscopicity and cloud droplet activation of mineral dust aerosol. Geophysical Research Letters, 36, L08805, doi: 10.01029/02009GL037348.

Ma, Q. X., He, H., & Liu, Y. C. (2010). In situ DRIFTS study of hygroscopic behavior of mineral aerosol. *Journal of Environmental Sciences*, 22, 555–560.

Nickovic, S., Vukovic, A., Vujadinovic, M., Djurdjevic, V., & Pejanovic, G. (2012). Technical note: High-resolution mineralogical database of dust-productive soils for atmospheric dust modeling. *Atmospheric Chemistry and Physics*, 12, 845–855.

Rodriguez-Navarro, C., di Lorenzo, F., & Elert, K. (2018). Mineralogy and physicochemical features of Saharan dust wet deposited in the Iberian Peninsula during an extreme red rain event. *Atmospheric Chemistry and Physics*, 18, 10,089–10,122.

Shao, L. Y., Li, W. J., Yang, S. S., Shi, Z. B., & Lü, S. L. (2007). Mineralogical characteristics of airborne particles collected in Beijing during a severe Asian dust storm period in spring 2002. *Science China Earth Sciences*, 50, 953–959.

Sullivan, R. C., Moore, M. J. K., Petters, M. D., Kreidenweis, S. M., Roberts, G. C., & Prather, K. A. (2009). Effect of chemical mixing state on the hygroscopicity and cloud nucleation properties of calcium mineral dust particles. *Atmospheric Chemistry and Physics*, 9, 3303–3316.

Tang, M. J., Cziczo, D. J., & Grassian, V. H. (2016). Interactions of water with mineral dust aerosol: Water adsorption, hygroscopicity, cloud condensation and ice nucleation. *Chemical Reviews*, 116, 4205–4259.

Oceano Dunes State Vehicular Recreation Area Dust Control Program

DRAFT 2022 Annual Report and Work Plan

ATTACHMENT 06-03

Quantifying the value of a coastal foredune for wind erosion and dust emissions through numerical simulation

THIS PAGE INTENTIONALLY LEFT BLANK.

Quantifying the value of a coastal foredune for wind erosion and dust emissions through numerical simulation

E. Furtak-Cole, J. Gillies, I. Walker, Z. Hilgendorf

October 28, 2021

Executive Summary

Under the advisement of the Science Advisory Group (SAG), a plan was developed and undertaken by Parks to investigate establishing a foredune system along a portion of the ODSVRA as a method to reduce PM_{10} mass emissions and the mass concentration of PM_{10} downwind of the ODSVRA.

The reason for establishing a foredune system is the expectation that it offers an opportunity to enhance control of dust that originates by wind erosion process within the ODSVRA by reducing sand flux through the area the foredunes occupy and through their modulation of the wind flow within and downwind that results in conditions of lower shear stress than would be present in a flat, sloping beach. Lower shear stress conditions will result in a decrease in dust emissions. Resolving the effect of mature foredunes on the sand transport and dust emissions via experimentation would be a difficult undertaking, prohibitively expensive, and disruptive to Park operations. An effective means to evaluate the effect of foredunes on the system is to use Computational Fluid Dynamic modeling.

The goal of the modeling is to evaluate how the presence of a mature foredune system could alter the dynamics of the saltation and dust emission system in the near shore zone of the ODSVRA. We assume that the Oso Flaco foredune provides a suitable analog for representing a mature foredune system that could be established in the ODSVRA. The CFD model was implemented in the finite volume toolbox openFOAM using a Digital Elevation Model provided by UCSB and ASU to define the topography. Boundary conditions (i.e., the characterization of the incoming flow properties) were derived from wind speed and direction measurements collected upwind and at four locations within the Oso Flaco foredune test area.

The key results of the simulations are:

- Excellent agreement was observed between the measured and simulated ratio, downwind wind speed/upwind (i.e., beach) wind speed providing confidence in the modeling results.
- Very little flow separation is observed for the nebkahs (vegetation-topped mounds) in the foredune indicating a very aerodynamic system. In contrast, the non-vegetated transverse dunes show zones of significant flow separation at the dune crests with zones of re-circulation on the lee-side slip faces.
- Plants exert considerable control of the shear stress distribution within the foredune, sheltering the sand surface underneath and in their lee.
- The integrated shear across the area beginning approximately 300 m from the shoreline through to the end of the sampling domain is lower for the actual geometry than for the geometry with no foredune present (areas are of equivalent size).

- For the boundary condition tested in these simulations, removal of the foredune would result in an 8.2% increase in integrated shear on the test area.
- In the lee of the foredune a zone of shear is created that reaches a minimum at the downwind border of the foredunes and then increases non-linearly with increasing downwind distance. The shear stress at the surfaces reaches approximately 90% of its potential (downwind) value 50 m behind the foredune, returning to its full potential value approximately 250 m behind the foredune.

1 Introduction

Under the advisement of the Science Advisory Group (SAG), a plan was developed and undertaken by Parks to investigate establishing a foredune system along a portion of the ODSVRA as a method to reduce PM_{10} mass emissions and the mass concentration of PM_{10} downwind of the ODSVRA. Six restoration methods are being evaluated to determine which method will result in the most rapid evolution to a foredune system that closely approximates the naturally occurring foredune system along this area of the central California coastline in terms of form and ecological function. The reason for establishing a foredune system is the expectation that it offers an opportunity to enhance control of dust that originates by wind erosion process within the ODSVRA by reducing sand flux through the area the foredunes occupy and through their modulation of the wind flow within and downwind that results in conditions of lower shear stress than would be present in a flat and sloping beach. Lower shear stress conditions will result in a decrease in dust emissions.

The presence of the foredune creates a perturbation in the wind flow coming onshore that affects the wind and sand transport processes due to its complex topography and vegetation on the space it occupies. In addition, the perturbation to the flow is expected to modulate the flow to some distance downwind of the foredune that also reduces sand flux and dust emissions. Collecting sufficient data using measurement techniques to characterize the effects of the foredunes on dust emissions presents a formidable undertaking that would be of considerable expense due to the needed instrumentation, labor, and time required. An alternative approach is to use Computational Fluid Dynamic (CFD) modeling to characterize the flow conditions associated with the movement of wind from the beach, through the foredunes, and to some distance downwind. From this type of simulation, relations can be established to aid in defining how the foredune roughness modulates the flow across space to infer how its presence affects dust emissions as compared to zones of the beach area at the ODSVRA that are currently lacking these types of forms.

CFD models provide complex analysis of fluid flow based on conservation of mass and momentum by resolving the Navier-Stokes equations using finite volume or other methods in three dimensions. The Navier-Stokes equations describe the motion of viscous fluids and arise from Newton's second law (i.e., the acceleration of an object depends directly upon the net force acting upon the object, and inversely upon the mass of the object). The Navier–Stokes equations are used to describe the physics of many phenomena of scientific and engineering interest including the flow of wind over surfaces.

Using CFD to provide realistic simulations requires that careful attention be given to the model boundary conditions (i.e., the correct velocity, pressure, and turbulence properties of the incoming flow) and a reasonable representation of the topography over which the air flows. It is also desirable to have measurements from within the modeling domain to compare with model-derived values to provide confidence that the model has achieved a simulation that is a realistic representation of the real-world conditions. It needs to be noted that all models are a simplification and cannot capture all the complexities of turbulent fluid flow over complex roughness forms.

Here we report on CFD modeling of the air flow and shear stress production for a portion of the mature foredunes in the ODSVRA known as the Oso Flaco Dunes that lie south of the plover exclosure area (Fig. 1). This area is interpreted as having relatively mature foredunes that, to the best of our knowledge, are representative of a foredune complex that would be typical of this part of the Central California coast that developed naturally or developed following the removal of OHV activity. The goal of the modeling is to evaluate how the presence of a mature foredune system could alter the dynamics of the saltation and dust emission system in the near shore zone of the ODSVRA. In this Report we describe the data used in the CFD model (implemented in the finite volume toolbox openFOAM), the measurements made for defining the boundary conditions and model verification, the computational methods defined in openFOAM, and the analysis undertaken to characterize how the presence of a foredune like Oso Flaco could potentially modulate wind erosion and dust emissions if it was present in the beach areas of the ODSVRA where it is currently absent.

Figure 1: The Oso Flaco foredune test site location.

2 Methods

2.1 Digital Elevation Model of the Oso Flaco Foredune

Detailed imagery of the ODSVRA was acquired using an unmanned aerial system (UAS) operated by UCSB and ASU. The acquired images were processed by ASU to produce digital elevation models (DEM) for various regions of the Park including the Oso Flaco foredunes. The constructed DEM has an accuracy level that resolves topographic details to 10 cm of resolution. The dataset from February of 2021 was selected to construct the DEM for the Oso Flaco dunes, as it most closely matches the time period when measurements of wind flow through the dunes were acquired in May 2021 (see Section 2.2).

To be used in a CFD simulation, additional processing was performed on the topographic dataset for the Oso Flaco foredune region of interest. A GeoTIFF of the region was exported to a point cloud, which was made into a 3D surface using 2D Delaunay triangulation. A GeoTIFF is a public domain metadata standard that allows georeferencing information to be embedded within a Tag Image File Format (TIFF). The GeoTIFF was used to create a topographic representation of the surface that is used to create the computational finite volume mesh (see Section 3.2) for the CFD simulation. This surface can be seen in Fig. 2 (top panel).

Two additional topographies were created to simulate surface shear stress patterns on relevant hypothetical surface forms, for comparison with surface shear stresses on the actual surface. In the first, the foredune is effectively flattened to a gently sloping surface. This is accomplished in the DEM by slicing a rectangular region covering the foredune out of the 3D point-cloud (Fig. 2, top panel). An in-house code was written to re-assign elevation values to the rectangular region, based on inverse distance weighting (IDW). The same 2D Delaunay process is then used to create a 3D surface. The result is a smooth gently sloping surface from the shoreline to the area where the large transverse dunes are located. This sloping surface, shown in the middle panel of Fig. 2, is the result of spatially interpolating the edges of the clipped areas together. In the second scenario, a horizontal sloping surface is created behind the foredune (Fig. 2, bottom panel). This is accomplished by clipping the point-cloud and interpolating a transition zone behind the foredune, which smoothly transitions the foredune topography to a flat plane. The height of this plane is 4.2 m above sea level (ASL), which is based on the average height of the beach.

2.2 Atmospheric Measurements

A measurement campaign was carried out to acquire vertically resolved wind speed and turbulence parameter data upwind of the Oso Flaco foredune and at four positions along a roughly west to east transect through the foredunes. Three sonic anemometers were mounted on two 3.05 m (10 ft) towers to collect 3-dimensional wind speed data (*u*-horizontal, *v*-spanwise, *w*-vertical) at 10 Hz. The anemometers were mounted on the towers with their sampling volumes positioned at approximately 0.025 m, 1.56 m and 3.26 m above the surface (Fig. 4). These data were used to set the boundary conditions and for model verification. One tower was installed upwind of the foredunes. The second tower was moved through the foredune but left in position for short periods of time (approximately 30 minutes). The

Figure 2: 3D representation of the topography of the mature Oso Flaco foredune test area (top panel) and two hypothetical geometry scenarios: the land surface with the foredune removed (middle panel), and the surface with a flat region behind the foredune with the transverse dunes removed (bottom panel).

geographic positions of the towers and a summary of time periods for which measurements were taken are shown in Table 1.

Table 1: Locations and durations for velocity profiles measured with the sonic anemometer towers.

Name	Long.	Lat.	Day	Start	End
upwind	-120.6329372	35.0378334	20-05-2021	8:45:00	24:00:00
P1	-120.6319444	35.0380164	20-05-2021	09:40:46	10:51:25
P2	-120.6309242	35.0374855	20-05-2021	11:18:00	11:49:20
P3	-120.6301323	35.0372208	20-05-2021	12:09:29	12:41:16
P4	-120.6296373	35.0367	20-05-2021	13:08:02	13:46:00

Figure 4: Tower configuration for data collected with the sonic anemometers.

Sufficient wind velocity data were collected to build an inlet boundary condition and verification points for numerical simulation. An average velocity profile was constructed over the range of instrument heights by averaging wind speeds for the time period 1:00 PM to 2:00 PM on 05-20-21. The average wind speed for this hour represents a wind speed that is above the threshold for saltation for most of the ODSVRA. A log-law velocity profile was fit to values from the three sonic anemometers, to provide velocity boundary values extending to a height of 100 m above ground level (AGL). A corresponding turbulence intensity, *TI*, profile was created by linearly interpolating calculated values between the three anemometers and extending the value at the 3.23 m anemometer to the top of the computational domain (50 m AGL). A profile of turbulent kinetic energy *k* is calculated from the average velocity *u* and *TI* as,

$$k = \frac{3}{2}(u\,TI^2) \qquad (1)$$

The specific dissipation rate ω can then be calculated as:

$$\omega = C_\mu^{0.75}\ \frac{k^{\,5}}{l} \qquad (2)$$

where the constant C_μ=0.09, and the turbulence length scale is taken to be *TI* = 5. The kinematic energy eddy viscosity can be calculated as:

$$v_t = 0.31\,\frac{k}{\omega} \qquad (3)$$

Values of u, k, ω and v_t are needed as boundary condition inputs for the CFD simulation. Profiles of u and TI are shown in Fig. 5. Zero-gradient pressure was used at the inlet, solid, side, and top walls, while a fixed value of zero was applied at the exit. Slip velocity (no friction) was applied to the top and side walls, a zero velocity condition was applied to the ground, and the outlet was given a zero gradient condition.

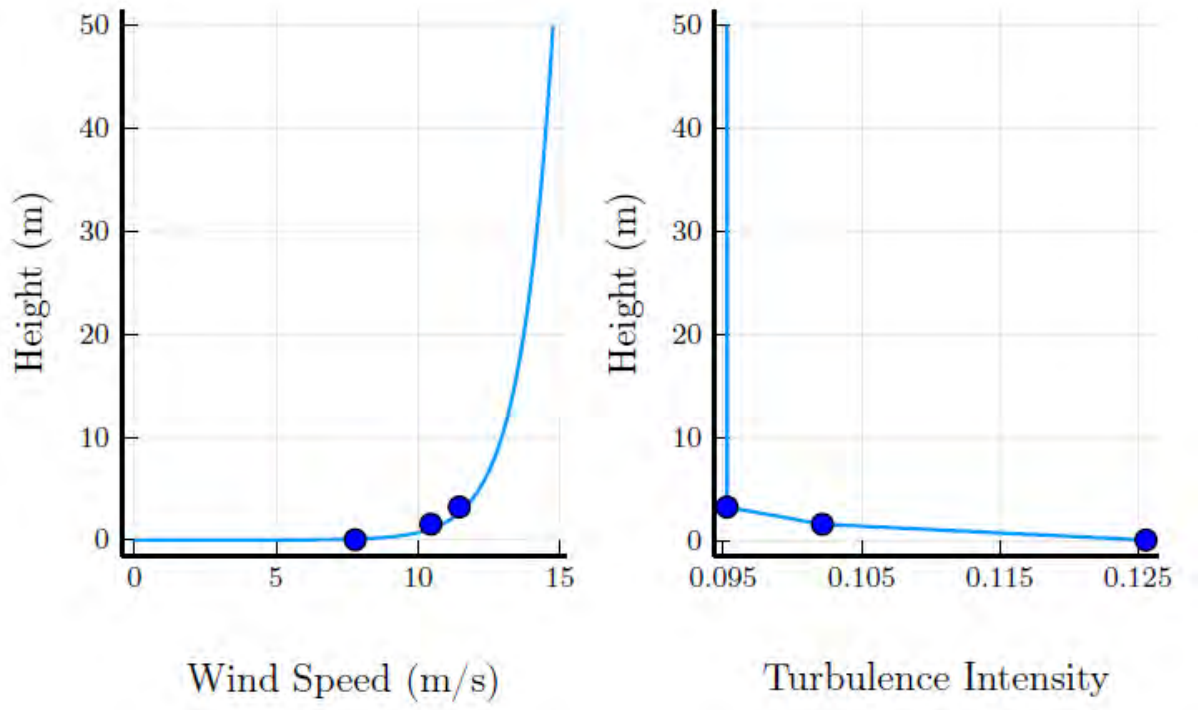

Figure 5: Profiles of u (left) and TI (right) were constructed for the inlet boundary condition. Blue circles represent the near surface measurements from the sonic anemometers.

2.3 Computational Methods

Simulations were performed by numerically solving the steady-state incompressible Navier-Stokes equations:

$$\rho u \nabla u = -\nabla p + \rho g + \mu \Delta u \quad (4)$$

$$\nabla u = 0 \quad (5)$$

where, u is horizontal velocity, p is pressure (Pa), g (9.81 m s^{-2}) is the acceleration due to gravity, and μ is fluid viscosity (Pa s). Turbulence modeling was performed with a Menter's shear stress transport (SST) turbulence model. This model was chosen for its low sensitivity to the vertical dimension above the surface ($y+$), as the large and complex domain of interest presents a difficult meshing problem.

The computational domain is a 900 m $\times$ 200 m $\times$ 100 m prism, rotated to align with the prevailing wind direction along the 900 m fetch. An angled plane was used to cut the inlet boundary, ensuring that the inlet boundary condition is applied across the beach at a

uniform elevation. An illustration of the domain imposed over the topography can be seen in Fig. 6. A domain height of 100 m was chosen to minimize flow acceleration that may occur due to changes in cross-sectional area caused by the topography. The selected height exceeds five heights of the largest topographic feature in the domain.

Meshing was performed with the CFmesh utility. A maximum cell size of 10 m was applied in the upper atmosphere, which is not a region of interest, to conserve computing resources. Cells are progressively refined with decreasing elevation to 0.5 m within 10 m of the ground. Below 10 m seven additional mesh layers were defined with the lowest at ground level (i.e., the bottom of the lowest mesh touches the surface). This lowest mesh layer has the a cell width of 0.02 m. Total cell counts for the simulations performed vary by topography but are on the order of 20 million per simulation.

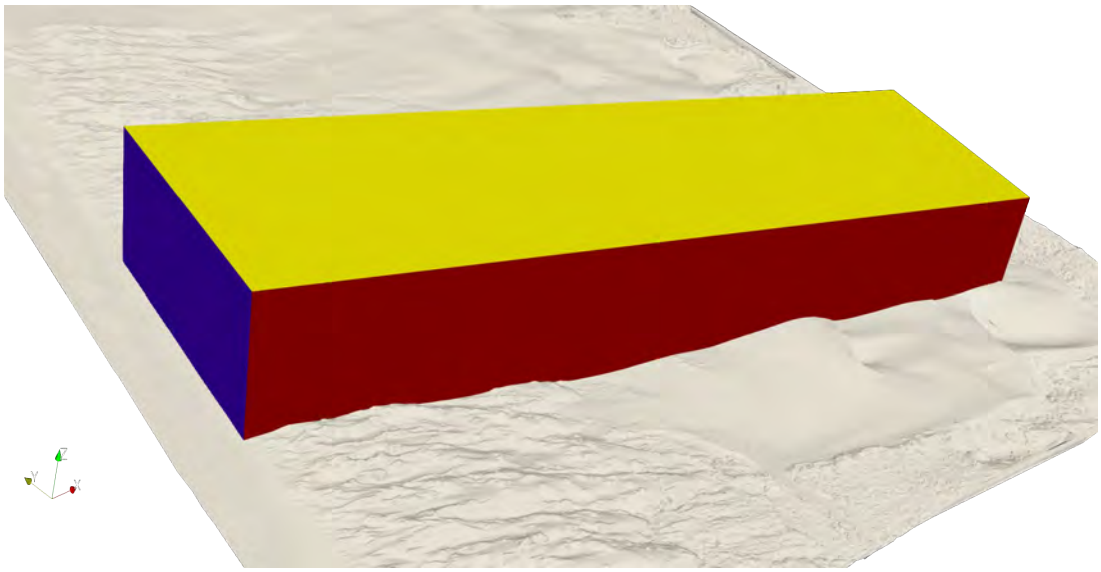

Figure 6: An illustration of the computational domain imposed over the topography. The angled inlet is shown in blue to apply the inlet boundary conditions on the beach across a uniform distance in front of the foredune.

3 Results

3.1 Model Verification

Verification of model results was performed by extracting velocity predictions from the simulation that represent the tower locations and anemometer heights and comparing those values with the sonic anemometer measurements. The dataset measured in the field comes from two towers: one stationary tower positioned at the boundary of the computational domain on the beach, and the second that was moved throughout the day. Consequently, a direct verification (i.e., value predicted to value measured) cannot be carried out at the second tower locations for the time period that was used to construct the boundary condition. Thus, we compare the ratio of upwind velocity to the velocity measured at the mobile tower for the measurements and the simulation. For the highest sonic anemometer,

located 3.26 m above the ground, this ratio for the measured and simulated results is shown in Table 2.

Excellent agreement is observed between the measured and simulated ratio. It is important to note that the measurement data were collected in a natural wind field, which varied in both intensity and direction through time and were made in the lee of dune structures that often exceeded the height of the highest sonic anemometer. In contrast the simulated results are modeled as a steady-state condition. Thus, an average relative error of 11.5% is an exceptional result for work outside of a controlled environment as would be found, for example, in a wind tunnel experiment. Moreover, the simulated results show a decrease in the ratio with distance into the foredune, which matches the measured results and classical boundary-layer theory.

Table 2: Validation results: modeled and measured wind speed ratios: downwind (in dunes)/upwind (beach). P1 is the measurement position in the foredunes closest to the beach and P4 is furthest from the beach.

	P1	P2	P3	P4
Simulated	0.952	0.866	0.835	0.749
Measured	0.964	0.706	0.897	0.886

3.2 Wind Flow and Shear Stress Across the Oso Flaco Test Section

Surface shear stress is created by the fluid, i.e., air, interacting with the surface topography which the CFD calculates using the Navier-Stokes equations and the set boundary conditions. A visualization of the magnitude of this force on the foredune and back dune topography is shown in Fig. 7. As seen in the upper panel of Fig. 7, the foredune has small areas where the highest shear stresses are observed (i.e., the red colored areas). On the western edge of the foredunes these represent the vegetated areas of the nebkahs (vegetation-topped mounds), which are the first major obstacle encountered by the inlet wind profile. The low area behind the complex foredune form is a region of lower shear. Past this area in the lee of the foredune where the bare sand surface begins to rise in elevation, the shear begins to increase again as a function of increasing downwind distance (lower panel of Fig. 7).

To illustrate the pattern of air flow over the foredunes and further downwind, the model can be used to generate near-wall streamlines that represent the movement of neutrally buoyant particles released into the flow at a height of 10 cm above the ground surface. As the simulations are steady-state, these can also be interpreted as being average path-lines for air molecules. Visualizations of the streamlines for the foredune and non-vegetated dune system behind the foredune can be seen in Fig. 8. This visualization provides insight into the different aerodynamics of the two dune systems. The individual nebkahs of the foredune show very little flow separation, indicating for the most part a very aerodynamic system. In contrast, the non-vegetated transverse dunes show zones of significant flow separation at the dune crests with zones of re-circulation on the lee-side slip faces.

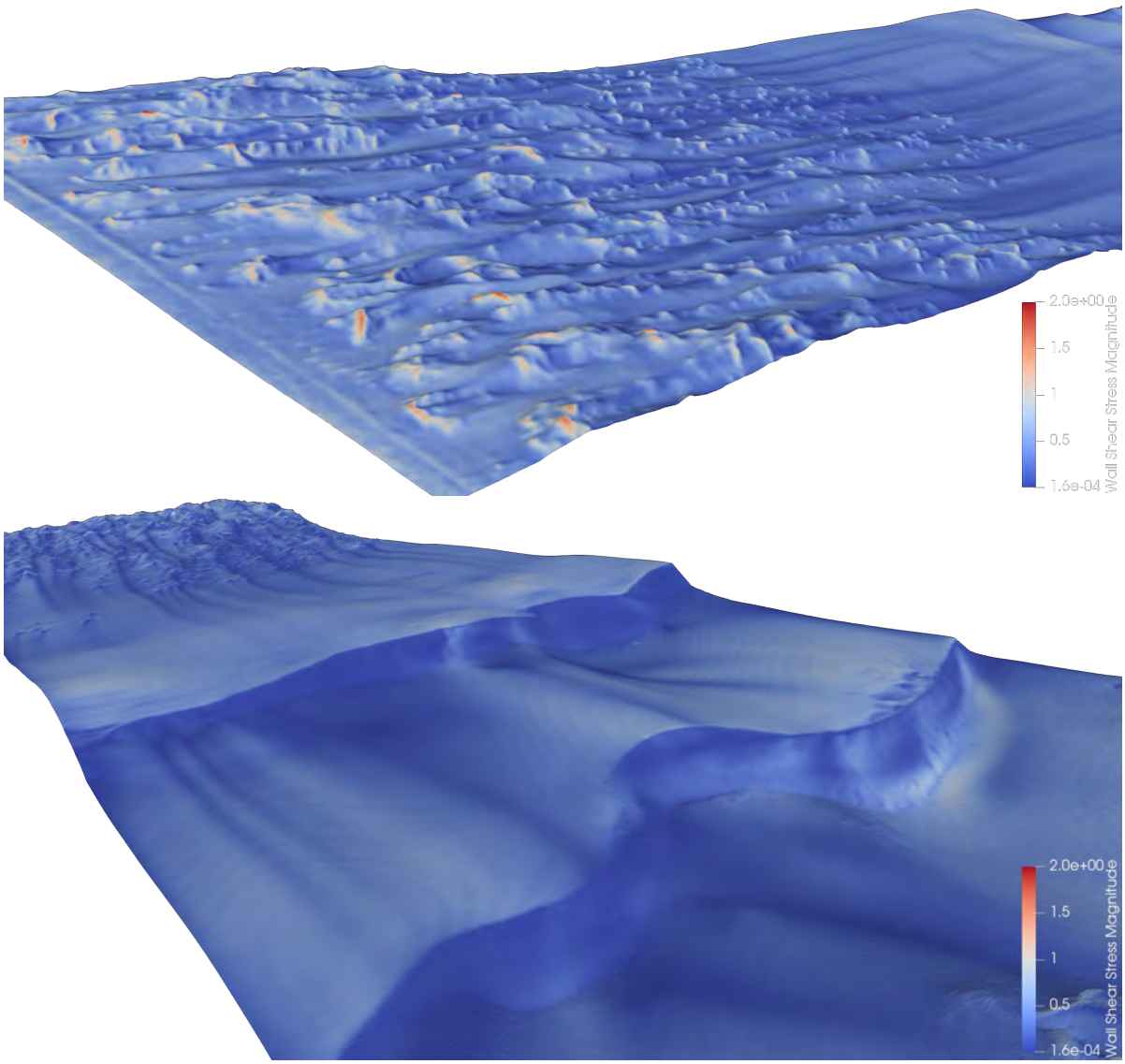

Figure 7: Visualization of the shear stress generated on the topography of the Oso Flaco foredune test area. A view of the foredune looking downwind (left side is west, right side is east) is shown in the upper panel, while a view of the non-vegetated dune system looking upwind (left side of image is west, right side of image is east) is shown in the lower panel.

The aerodynamics of the two dune types motivates an investigation of the role of plants in the shear stress distribution of the foredune. It is obvious from Fig. 7 that the foredune nebkahs receive large amounts of shear, and the low areas between them less so, despite the lack of flow separation. A raster vegetation mask of the foredune was created from spectral data acquired with the ASU/UCSB UAS. A map of this raster is shown superimposed over the magnitude of shear stress in Fig. 9. This image illustrates how plants exert considerable control of the shear stress distribution on the foredune. Areas of high shear are stabilized against entrainment and transport of sand by plants protecting the underlying surface. In the

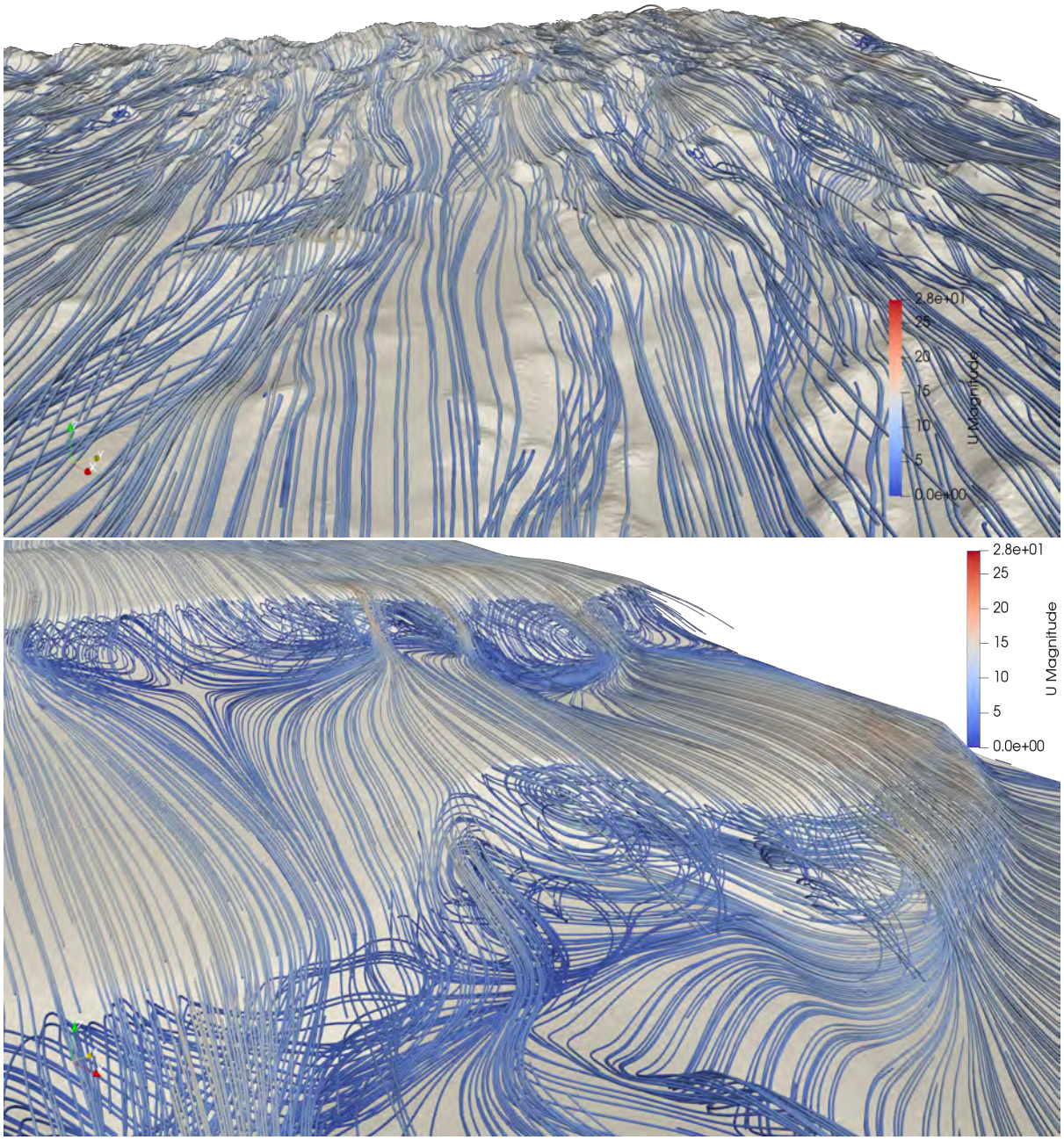

Figure 8: Upper panel: Near-wall streamlines are shown at the foredune, viewed looking upwind (top of image is west [upwind], bottom of image is east [downwind]). Lower panel: Near-wall streamlines are shown for the non-vegetated dune behind the foredune (top of image is west [upwind], bottom of image is east [downwind]).

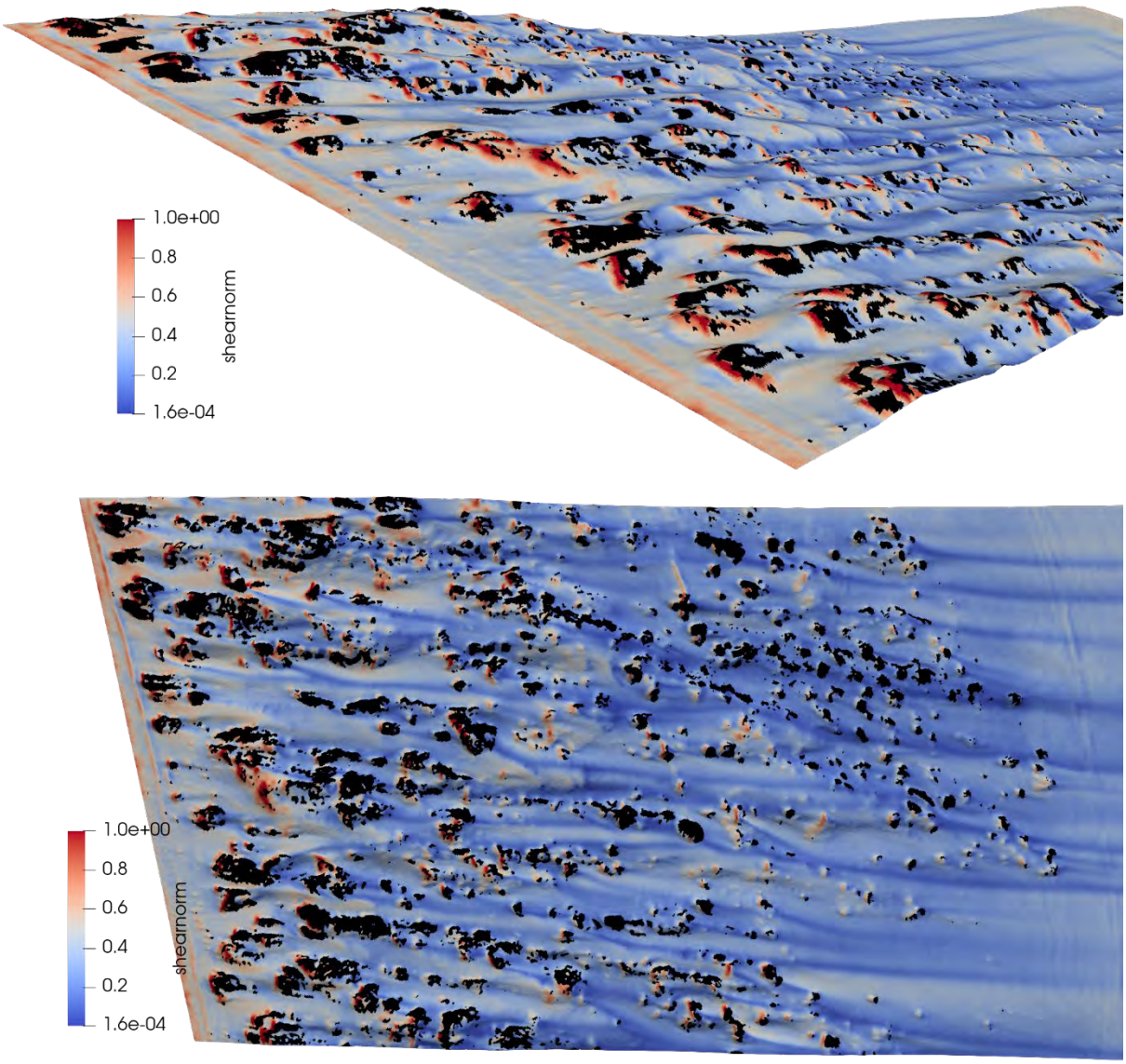

Figure 9: Two views of the Oso Flaco dune test area with a raster vegetation mask of the foredune vegetation superimposed on the foredune shear stress magnitude map. Black denotes locations of vegetation at 10 cm scale. The upwind boundary of the simulation is shown at the left of the image, with flow from left to right.

lee of the vegetation an area of protection, characterized by low shear, is created on the bare ground.

3.3 The Aerodynamic Value of the Foredune

The presence of the foredune inevitably creates aerodynamic effects that affect the shear stress magnitude and distribution within the foredune complex and downwind of the

foredunes. However, these are difficult to quantify in field studies, as the foredune cannot be removed for a paired study. In simulation this can be achieved without high costs or environmental damage. This motivated the creation of the geometry shown in the middle panel of Fig. 2, where the foredune has effectively been removed, and replaced with a smooth sloping surface, similar to what the shoreline of the ODSVRA looked like prior to 2019, when the foredune restoration project was established. Shear created by the simulation of flow over the Oso Flaco test surface is shown in Fig. 7 (the surface shown in Fig. 2, top panel), which we use to compare with the generation of shear stress across the same space for the hypothetical surface.

A comparison is achieved between surface geometries by performing a surface integration of shear (τ [Pa]. Note 1 Pa is equivalent to 1 N m^{-2} and $\tau=\rho u_*^2$ where ρ is air density [kg m^{-3}]) over each surface. In the first comparison the integral is computed over the rear sections of the two geometries (i.e., Fig. 2 top and middle panels) beginning approximately 300 m from the shoreline through to the end of the sampling domain in the east. The resultant integrated shear is 31,326 N for the unmodified geometry (Fig. 2 top panel), and 32,690 N for the geometry with no foredune upwind (Fig. 2 middle panel). The difference in shear can be attributed to changes in the wind field as it passes over the foredune or the absent foredune, with less energy extracted near the ground when the foredune is absent. For the boundary condition tested in these simulations, removal of the foredune resulted in a 4.4% increase in shear on the dune system for distance ≥300 m from the shoreline.

For the entire domain of the simulations, the integrated shear on the flattened geometry (i.e., all of Fig. 2 middle panel) was 56,530 N, which exceeds the integrated shear of the foredune geometry including the shear on the vegetation of 52,238 N (all of Fig. 2 top panel). This is notable, as the Oso Flaco (test area) foredune geometry has a higher surface area due to the complex topography. Moreover, the foredune topography is characterized by zones of high shear on the vegetated nebkahs, as seen in the upper panel of Fig. 7. For the boundary condition tested in these simulations, removal of the foredune would result in an 8.2% increase in shear on the equivalent sized area with no foredune present. In addition to significant shelter effects behind the foredune, the total effect of the foredune topography is a reduction in shear compared to a flattened surface, regardless of the effects of vegetation on the wind field or saltation.

Removing the areas of shear associated with the presence of the vegetation, as it represents areas where sand transport and dust emissions have a low probability of occurrence due to the protection afforded by the vegetation, further decreases the integrated shear on the Oso Flaco test surface (Fig. 2 top panel). The area-integrated shear excluding vegetated areas is 47,570 N. The total integrated shear on the geometry with the foredune removed (Fig. 2 middle panel) is 15.8% higher than on the Oso Flaco test surface (Fig. 2 top panel). There is a significant increase in protection due to the presence of the vegetation. For the entire modeling domain the plant cover is approximately 9%. Within just the foredunes the plant cover is approximately 16%.

3.3 The PM_{10} Emission Reduction Value of the Foredune

The shear stress analysis can be extended to evaluate how the different shear stress conditions on the actual and hypothetical surfaces affect PM_{10} mass emissions. An evaluation

is made for the emissivity conditions represented by the mean riding area and mean non-riding area emissivity relations (DRI, 2021). The average emissions (E, mg m^{-2} s^{-1}) relation for the riding area as a function of shear velocity u_* (m s^{-1}) is:

$$E = 23.65(u_*)^{5.59}, \quad (6)$$

The average emissions relation for the non-riding area as a function of shear velocity u_* is:

$$E = 21.51(u_*)^{6.85}. \quad (7)$$

The model derived shear values (τ) were converted to u_* (remember, $\tau=\rho u_*^2$ where ρ is air density [kg m^{-3}]) and then integrated across the surface areas of the actual and hypothetical geometries. The total integrated emissions are in units of mg s^{-1}. Total emissions and the corresponding total shear force are shown in Table 3. The third scenario of an unmodified topography (i.e., Oso Flaco test surface, Fig. 2 top panel) shows significantly lower emissions than the scenarios that neglect vegetation sheltering or have a flattened foredune. Total emissions calculated with the non-riding emissions curve are an order of magnitude lower than those calculated with the riding area emissions curve in all cases.

Table 3: Shear and total integrated emissions for the surfaces with the foredune removed (Scenario 1), the unmodified surface neglecting the effects of plant cover (Scenario 2), and the unmodified surface with zero emissions from areas that are vegetated (Scenario 3).

	Scenario 1	Scenario 2	Scenario 3
Total Shear Force (N)	56530	52238	47570
Riding Total E (mg s^{-1})	163412	159654	134683
Non-riding Total E (m g s^{-1})	89458	88384	70387

3.4 Foredune Downwind Sheltering Effects

Being able to quantify the sheltering effects of the foredune will be a useful tool for planning remediation projects and evaluating secondary effects on dust emission on the lee side. This is the motivation for the geometry that situates a flat plane behind the foredune, as seen in the bottom panel of Fig. 2. As the actual shear on a given land surface may vary widely depending on the topography behind the foredune, the flat surface offers the best scenario for a generalized result. Shear stress was calculated from a simulation run for this surface using the boundary conditions outlined in Section 2.3. A plot of the average shear stress on the foredune followed by the flat surface (Fig. 2, bottom panel) is shown in Fig. 10. Note that the averaging is across the width of the modeling domain at each length interval along the west to east transect and not just along a narrow corridor through the foredune. The recovery of this relation beginning at zero on the figure (i.e., 0 on the x-axis) illustrates the sheltering behind the foredune. Figure 11 shows the shear stress relation past the foredune (i.e., 0 on the x-axis) in Fig. 10 normalized against the maximum shear stress, which occurs ≈300 m past the end of the foredune. Figure 11 shows that in the lee of the foredune a zone of shear is created that reaches a minimum at the zero point and then increases non-linearly with

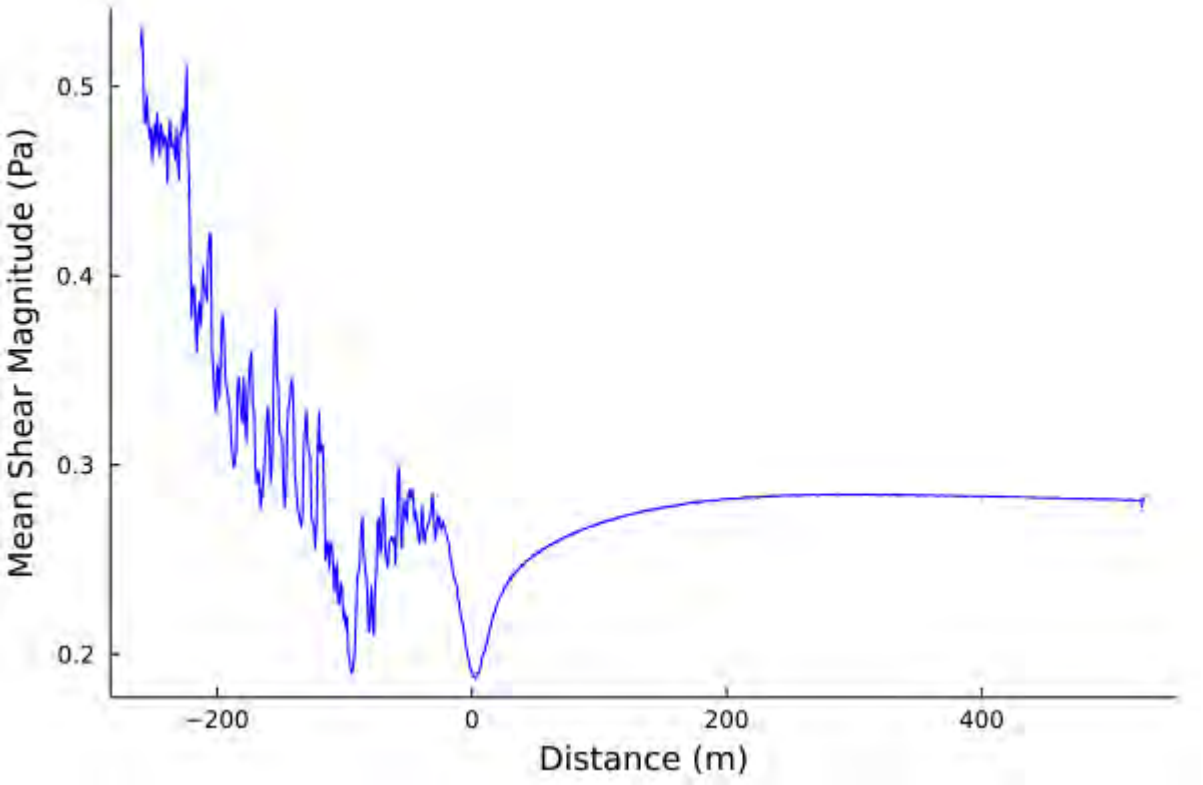

Figure 10: Mean shear magnitude as a function of distance in the freestream direction for the geometry shown in Fig 2., bottom panel. The leeward edge of the foredune is located at x = 0.

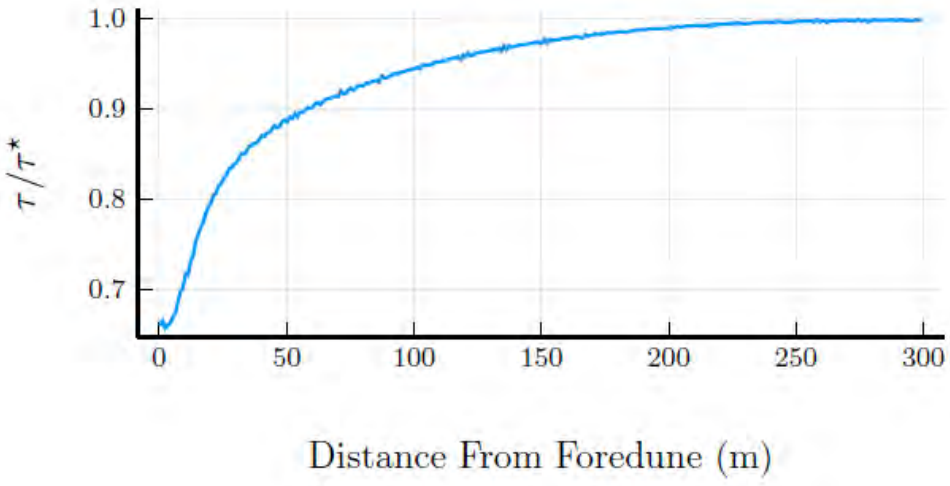

Figure 11: Mean shear τ normalized by maximum shear $\tau^\star$ as a function of distance.

increasing downwind distance. The shear stress at the surfaces reaches approximately 90% of its potential value within a 50 m of fetch behind the foredune.

The shear stress along the west to east length of the domain for the Oso Flaco foredune test area (Fig. 2 top panel) and the geometry with the foredune removed (Fig. 2 middle panel) are compared with Fig. 10 in Fig. 12.

Figure 12 provides a clear indication of the value of a foredune similar to Oso Flaco to modulate surface shear stress that favors a lower production of dust emissions when compared to the condition of an absent foredune. As a first approximation of the potential secondary effect of the foredune on dust emissions specifically in their lee, a recommendation is to apply the relation shown in Fig. 11 to the grid cells in the DRI dispersion model to modulate the CALMET estimated shear velocities from the zero point in Fig. 12 through to a distance equivalent to the start of the large transverse dunes.

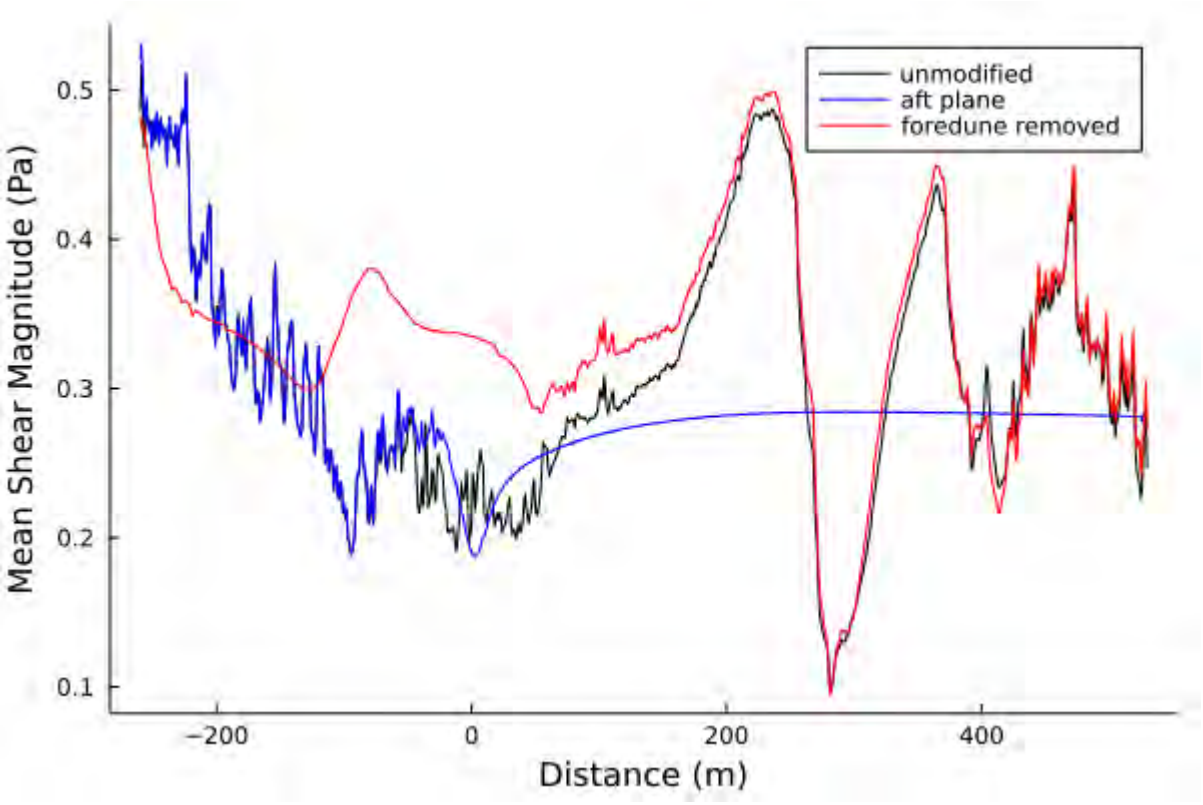

Figure 12: Mean shear magnitude as a function of distance in the freestream direction for the Oso Flaco geometry (Fig. 2, top panel represented by black line), the geometry with the foredune removed (Fig. 2, middle panel represented by red line), and the geometry with the foredune followed by a sloping sand surface (Fig. 2, bottom panel represented by blue line). The downwind edge of the foredune is located at $x = 0$.

Appendix A: CFD Development and Processing

The following summary contextualizes the scope of producing quality CFD results:

- Each simulation takes 4800 core-hours of computing.
- Approximately 15 Julia codes were written to process the input and output of data.
- Over 30 meshes were produced before the final configuration was set.
- Each simulation produces velocity and pressure at >20 million points within the modeling domain.
- Output from each simulation is ≈98 GB of data.

A typical CFD workflow is shown as a flowchart in Fig. A1. The process begins with creation of a surface geometry, which requires creation of a 3D surface from a Digital Elevation Model (DEM). Next a mesh is designed to discretize the domain for the solver. The solver and post processing utilities are run on a computing cluster (University of Utah). The simulation output is checked for integrity. The mesh is then re-designed to increase the quality of the result, and the processes is repeated. When sufficient quality is achieved, based on evaluation of model convergence metrics, additional post processing with custom codes and visualization tasks are performed. A cross section of the computational mesh is shown in Fig. A2, which needed to be carefully designed to resolve turbulent flow features over the topography.

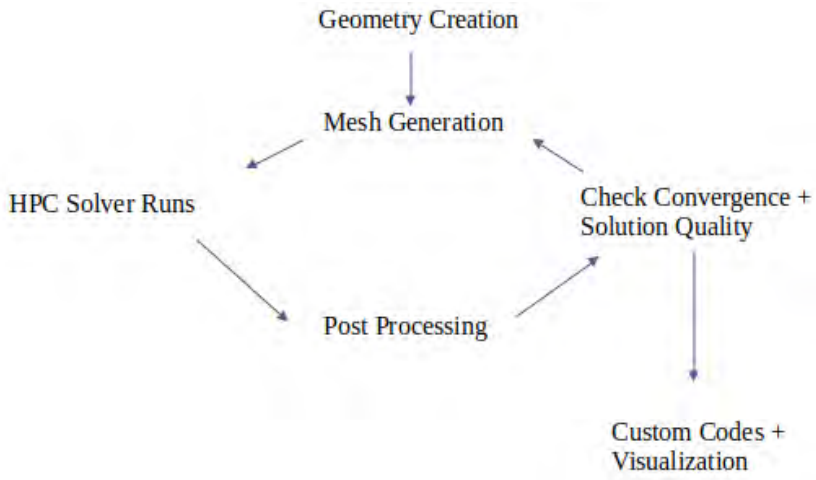

Figure A1. The workflow process for developing and processing the CFD.

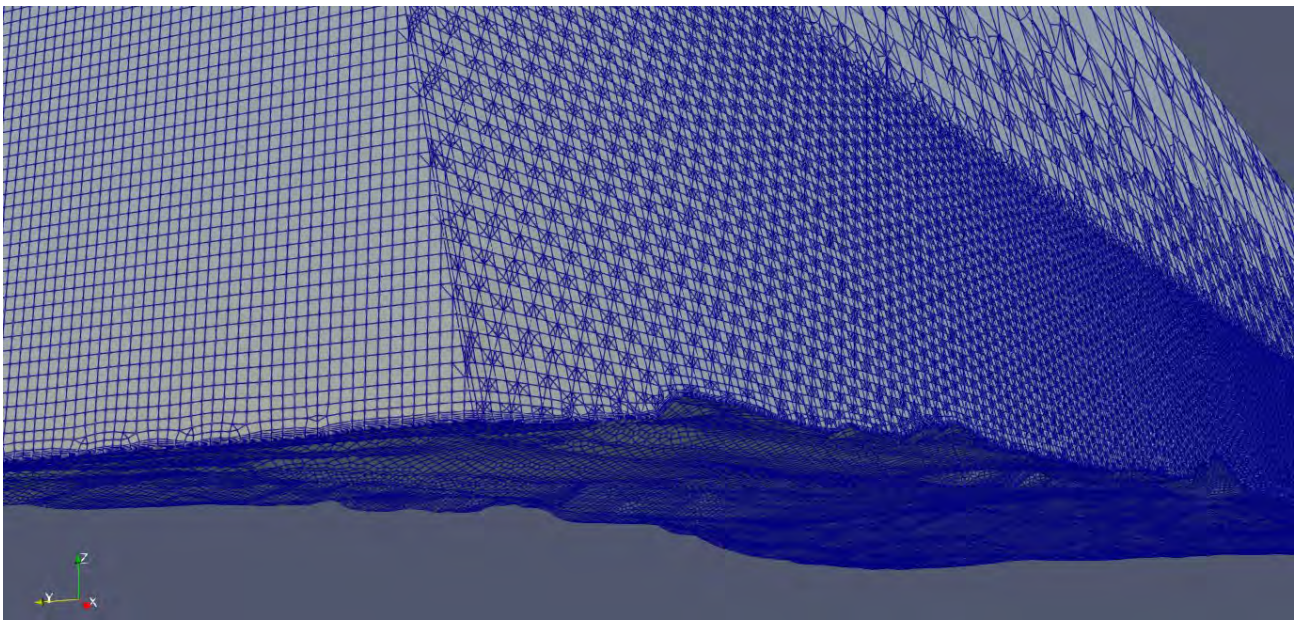

Figure A2. A cross section of the computational mesh developed for the Oso Flaco foredune test area.

November 23, 2021

Memo: SAG Individual Reviews of "Quantifying the value of a coastal foredune for wind erosion and dust emissions through numerical simulation" (E. Furtak-Cole, J. Gillies, I. Walker, Z. Hilgendorf, October 28, 2021)

From: Scientific Advisory Group (SAG)

To: Jon O'Brien, California Department of Parks and Recreation (CDPR)

Cc: Sarah Miggins, California Department of Parks and Recreation (CDPR)
Liz McGuirk, California Department of Parks and Recreation (CDPR)

Below, please find reviews of the report, "Quantifying the value of a coastal foredune for wind erosion and dust emissions through numerical simulation," by 3 individual members of the SAG. The reviews were prepared by Carla Scheidlinger (Reviewer 1), Earl Withycombe (Reviewer 2), and Raleigh Martin (Reviewer 3). The SAG did not prepare a collective review of this report.

Respectfully,
Dr. Raleigh Martin (Acting chair of SAG)

Reviewer 1 (Carla Scheidlinger)

It is a well-presented paper with important findings that fully justify the effort and positioning of the foredune project at Oceano Dunes. I especially appreciated the illustration figures, which were generally well-captioned and helped a lot with envisioning the modeling. The main comment of substance is the one that asserts an "order of magnitude" difference between modeled results for riding and non-riding areas that are shown in Table 3. I saw numbers that were twice another but not an order of magnitude different.

My other comments are in the interests of clarity.

Executive Summary:

Second paragraph, second line: should the word “process” be “processes”?

Second paragraph: Consider 2 sentences: “... area the foredunes occupy. Foredunes also reduce dust through their modulation...”

Regarding this sentence: Resolving the effect of mature foredunes on the sand transport and dust emissions via experimentation would be a difficult undertaking, prohibitively expensive, and disruptive to Park operations. Aren’t we doing exactly that with the foredune experiment?

First bullet: insert comma after second “wind speed”

Introduction:

First paragraph: same change to 2 sentences as shown above

Second paragraph: what this says is that if you were to collect actual emissions data from a foredune system, it would be very expensive. But to collect just wind speed data for the model is much more efficient. Is that correct?

Section 2.2, Figure 2: here in the legend you say that foredune and transverse dunes were "removed"; above you say they were "flattened". Is it the same thing?

Section 3.3. This is the first time you mention riding and non-riding areas. Although you reference your other report, a brief description about what these areas are and how they apply to this model could be helpful.

Table 3: I don't see order of magnitude changes in Table 3. I see emission values that are halved between riding and non-riding in each Scenario but that is all.

Section 3.4, Figure 12. What does “aft plane” mean?

Reviewer 2 (Earl Withycombe)

I am somewhat familiar with CFD modeling, but not sufficiently knowledgeable to offer comments on the details of the modeling setup or input files discussed in the report.

I see no fatal flaws in the modeling setup or input files.

Assuming that the average height of the Oso Flaco foredune is 10 meters, the results – 95% of stress recovery within 100 meters downwind of the lee edge – correspond well with USDA research showing the zone of wind sheltering to be about 10 times the height of a vegetative barrier.

On this basis, I approve of the report.

I have only one comment regarding the CFD report:

- (p. 6, equation 2): The numerator "k 5" is confusing; should it be "5k", "k^5", or something else?

Reviewer 3 (Raleigh Martin)

This report presents a sound approach to using computational fluid dynamics (CFD) simulations to understand how foredune topography affects the spatial distribution of surface shear stress within and downwind of coastal foredunes at the Oceano Dunes State Vehicular Recreation Area (ODSVRA). Three scenarios are presented for CFD modeling (Fig. 2): (a) the actual Oso Flaco foredune / back dune complex; (b) a modified domain with flattened foredune (but actual back dune); and (c) a modified domain with flattened back dune (but actual foredune). The CFD modeling approach is well-grounded in established modeling methodologies, and it is validated through simulation-measurement comparison (Table 2). The modeling results are instructive and relevant for understanding the effect of the foredune on surface shear stress as well as associated saltation and PM10 emissions. Compared to a flat surface, the modeling shows that the foredune produces substantial reductions both in dust emissions within the foredune (Table 3) and surface shear stress downwind of the foredune (Fig. 11). These results will help to improve quantification of the overall effectiveness of the foredune restoration project on reducing dust emissions at the ODSVRA.

My only possible major concern with the CFD modeling methodology is the selection of boundary condition parameters used to construct the model. My confidence in the modeling results would be increased with further justification of the selection of these boundary conditions. Two factors that require clarification (described in further detail in the specific comments below) are: (1) the effects of temporal variability within the transect of wind tower measurements, and (2) possible departures from the assumed neutral profile caused by boundary layer instability and the formation of an internal boundary layer at the marine-land transition.

Otherwise, I think this study offers useful results that will help to inform efforts to quantify the effect of the ongoing ODSVRA foredune restoration project on reductions in PM10 mass emissions. This information is distinctive from but complementary to other metrics of progress for the foredune restoration project (e.g., Hilgendorf, Walker, and Turner, "UCSB-ASU 2020-2021 ODSVRA Foredune Restoration UAS Survey Report," September 2021).

In terms of the specific applicability of these CFD results to quantifying effects of the foredune on PM10 emissions, I wish to raise two additional points. First, it would help to clarify whether or not the shear stress and emissions values presented for the different scenarios (i.e., Table 3 and Fig. 11) account only for differences in topography among the scenarios (Fig. 2) or if they also account for the presence or absence of foredune vegetation (Fig. 9). This is currently unclear. Second, one point for careful consideration going forward is the dynamic nature of the foredune restoration area. The modeling presented here addresses reductions in shear stress for a mature foredune, whereas the 48-acre foredune restoration zone remains immature (with varying levels of maturity among the 6 test parcels). Caution should therefore be exercised when extending these CFD modeling results to inform the dust mitigating effects of the still immature foredune restoration zone.

Further specific comments are provided below.

Specific Comments

(a) pp. 1, 9, 10, 13 - "nebkahs" should be spelled "nebkhas"

(b) Sec. 2.2, first paragraph (p. 4); and Table 1 – The report notes that the second anemometer tower was moved at 30-minute intervals to obtain wind speed and turbulence parameter data along a streamwise transect of the Oso Flaco foredune. Are the authors confident that 30 minutes is adequate to capture the full range of relevant turbulence scales? In addition, based on the variability of wind speed throughout the day, how did the authors ensure comparability of measurements across the transect collected at different times? Based on my experience at the ODSVRA, saltation-generating wind usually picks up around noon, so the fact that some wind measurements are from the late morning (P1 & P2) and others are from the early afternoon (P3 & P4) periods may cause some inconsistency relative to this diurnal variation. To better understand this potential effect, it would help if the report were to include a figure plotting the streamwise wind time series at the upwind tower across the entire day. In addition, it would also be helpful if the report were to provide a map showing the spatial positions of the tower locations across the foredune. Finally, please specify the time zone associated with the values (UTC, Local Standard Time, or Local Daylight Savings Time?).

(c) Sec. 2.2, second paragraph (p. 6) – The log-law velocity profile was extrapolated up to 100m above ground level based on measurements collected at 0.025 m, 1.56 m and 3.26 m above the surface. Use of a log-law velocity profile implicitly assumes a neutral boundary layer profile, but this assumption needs to be further justified. Two concerns are that: (1) the mid-afternoon boundary layer is most likely unstable, causing increasing deviation from the log-law profile with increasing distance above the ground; (2) the transition from a marine to land boundary layer will most likely cause the formation of an internal boundary layer, producing further variation from the assumed log law profile.

(d) Sec. 2.2, second paragraph (p. 6) – Related to comment (b) above, averaged wind values were calculated for the time period of 1-2 PM (time zone unspecified). Would use of a different time period for the boundary condition have significantly affected the results?

(e) Fig. 5 (p. 7) – What is the shear velocity (u*) value associated with this wind profile? Is it possible to also calculate an Obhukov length scale value (L) or vertical profile for the stability parameter (z/L)?

(f) Sec. 3.1, first paragraph (p. 8), and Table 2 – Please explain the reasoning for using the 3.26m anemometer as the basis for simulation-measurement validation comparisons. I assume that the highest height was selected to reduce the effects of noise associated with heterogeneous near-surface topography. In addition, regarding comments (b) and (d) above, please explain how temporal variability in measurement times may have affected these validation comparisons.

(g) Sec. 3.2, second paragraph (p. 9), and Fig. 8 – I am not entirely convinced by the statement that nebkhas show little flow separation. Though this statement makes intuitive sense, it is possible that more flow separation for the non-vegetated dune (bottom panel in Fig. 8) is more apparent simply because of the spatial resolution of the streamline visualization. Would it be possible to produce a higher resolution flow visualization over the foredune to confirm this statement regarding flow separation?

(h) Sec. 3.2, last sentence (p. 10 & 12) – It would help to provide reference(s) here to the peer-reviewed scientific literature supporting this statement about the local protective effects of dune vegetation.

(i) Sec. 3.3 ("The Aerodynamic Value…") and Sec. 3.3 ("The PM10 Emission Reduction Value…") (pp. 12-14) – It is not clear whether or not the values presented in these sections account only for the roughness effects for the different scenarios or whether they also account for the local protective effects of dune vegetation. Please make sure it is crystal clear what exactly is being modeled for each scenario.

(j) Sec. 3.3 ("The Aerodynamic Value…"), 2nd-4th paragraphs (p. 13) and Table 3 – Based on the units presented (N), am I correct to assume that the values presented for integrated shear are calculated over 2-dimensional areas? Two pieces of information that would help to better understand the presented data are: (1) creation of maps showing the spatial coverage of the subdomain areas over which these values are calculated; and (2) calculation of normalized values (i.e., divided by domain area) to obtain mean shear stress (τ) and shear velocity (u^*) values across these domains. Such normalization would be particularly useful given that different subdomains span different areas.

(k) There are two Section 3.3's. Please correct the section numbering.

(l) Sec. 3.3 ("The PM10 Emission Reduction Value…"), 1st full paragraph (p. 14) – Please be sure to include a bibliographic reference for the "(DRI, 2021)" citation.

(m) Sec. 3.3 ("The PM10 Emission Reduction Value…"), 1st full paragraph (p. 14) and Table 3 – It would be useful to also present the emissions values using intuitive units. Two suggested units are: (1) total metric tons, and (2) mg m^{-2} s^{-1}. It would also be helpful to clarify the spatial coverage associated with the scenarios (see also comment (j) above).

Quantifying the value of a coastal foredune for wind erosion and dust emissions through numerical simulation

E. Furtak-Cole, J. Gillies, I. Walker, Z. Hilgendorf

December 2, 2021

Executive Summary

Under the advisement of the Science Advisory Group (SAG), a plan was developed and undertaken by Parks to investigate establishing a foredune system along a portion of the ODSVRA as a method to reduce PM_{10} mass emissions and the mass concentration of PM_{10} downwind of the ODSVRA.

The reason for establishing a foredune system is the expectation that it offers an opportunity to enhance control of dust that originates by wind erosion processes within the ODSVRA by reducing sand flux through the area the foredunes occupy and through their modulation of the wind flow within and downwind that results in conditions of lower shear stress than would be present in a flat, sloping beach. Lower shear stress conditions will result in a decrease in dust emissions. Resolving the effect of mature foredunes on the sand transport and dust emissions via experimentation would be a difficult undertaking, prohibitively expensive, and disruptive to Park operations. An effective means to evaluate the effect of foredunes on the system is to use Computational Fluid Dynamic modeling.

The goal of the modeling is to evaluate how the presence of a mature foredune system could alter the dynamics of the saltation and dust emission system in the near shore zone of the ODSVRA. We assume that the Oso Flaco foredune provides a suitable analog for representing a mature foredune system that could be established in the ODSVRA. The CFD model was implemented in the finite volume toolbox openFOAM using a Digital Elevation Model provided by UCSB and ASU to define the topography. Boundary conditions (i.e., the characterization of the incoming flow properties) were derived from wind speed and direction measurements collected upwind and at four locations within the Oso Flaco foredune test area.

The key results of the simulations are:

- Excellent agreement was observed between the measured and simulated ratio, downwind wind speed/upwind (i.e., beach) wind speed, providing confidence in the modeling results.
- Very little flow separation is observed for the nebkhas (vegetation-topped mounds) in the foredune indicating a very aerodynamic system. In contrast, the nonvegetated transverse dunes show zones of significant flow separation at the dune crests with zones of re-circulation on the lee-side slip faces.
- Plants exert considerable control of the shear stress distribution within the foredune, sheltering the sand surface underneath and in their lee.
- The integrated shear across the area beginning approximately 300 m from the shoreline through to the end of the sampling domain is lower for the actual geometry than for the geometry with no foredune present (areas are of equivalent size).

- For the boundary condition tested in these simulations, removal of the foredune would result in an 8.2% increase in integrated shear on the test area.
- In the lee of the foredune a zone of shear is created that reaches a minimum at the downwind border of the foredunes and then increases non-linearly with increasing downwind distance. The shear stress at the surfaces reaches approximately 90% of its potential (downwind) value 50 m behind the foredune, returning to its full potential value approximately 250 m behind the foredune.

1 Introduction

Under the advisement of the Science Advisory Group (SAG), a plan was developed and undertaken by Parks to investigate establishing a foredune system along a portion of the ODSVRA as a method to reduce PM_{10} mass emissions and the mass concentration of PM_{10} downwind of the ODSVRA. Six restoration methods are being evaluated to determine which method will result in the most rapid evolution to a foredune system that closely approximates the naturally occurring foredune system along this area of the central California coastline in terms of form and ecological function. The reason for establishing a foredune system is the expectation that it offers an opportunity to enhance control of dust that originates by wind erosion process within the ODSVRA by reducing sand flux through the area the foredunes occupy and through their modulation of the wind flow within and downwind that results in conditions of lower shear stress than would be present in a flat and sloping beach. Lower shear stress conditions will result in a decrease in dust emissions.

The presence of the foredune creates a perturbation in the wind flow coming onshore that affects the wind and sand transport processes due to its complex topography and vegetation on the space it occupies. In addition, the perturbation to the flow is expected to modulate the flow to some distance downwind of the foredune that also reduces sand flux and dust emissions. Collecting sufficient data using measurement techniques to characterize the effects of the foredunes on dust emissions presents a formidable undertaking that would be of considerable expense due to the needed instrumentation, labor, and time required. An alternative approach is to use Computational Fluid Dynamic (CFD) modeling to characterize the flow conditions associated with the movement of wind from the beach, through the foredunes, and to some distance downwind. From this type of simulation, relations can be established to aid in defining how the foredune roughness modulates the flow across space to infer how its presence affects dust emissions as compared to zones of the beach area at the ODSVRA that are currently lacking these types of forms.

CFD models provide complex analysis of fluid flow based on conservation of mass and momentum by resolving the Navier-Stokes equations using finite volume or other methods in three dimensions. The Navier-Stokes equations describe the motion of viscous fluids and arise from Newton's second law (i.e., the acceleration of an object depends directly upon the net force acting upon the object, and inversely upon the mass of the object). The Navier–Stokes equations are used to describe the physics of many phenomena of scientific and engineering interest including the flow of wind over surfaces.

Using CFD to provide realistic simulations requires that careful attention be given to the model boundary conditions (i.e., the correct velocity, pressure, and turbulence properties of the incoming flow) and a reasonable representation of the topography over which the air flows. It is also desirable to have measurements from within the modeling domain to compare with model-derived values to provide confidence that the model has achieved a simulation that is a realistic representation of the real-world conditions. It needs to be noted that all models are a simplification and cannot capture all the complexities of turbulent fluid flow over complex roughness forms.

Here we report on CFD modeling of the air flow and shear stress production for a portion of the mature foredunes in the ODSVRA known as the Oso Flaco Dunes that lie south of the plover exclosure area (Fig. 1). This area is interpreted as having relatively mature foredunes that, to the best of our knowledge, are representative of a foredune complex that would be typical of this part of the Central California coast that developed naturally or developed following the removal of OHV activity. The goal of the modeling is to evaluate how the presence of a mature foredune system could alter the dynamics of the saltation and dust emission system in the near shore zone of the ODSVRA. In this Report we describe the data used in the CFD model (implemented in the finite volume toolbox openFOAM), the measurements made for defining the boundary conditions and model verification, the computational methods defined in openFOAM, and the analysis undertaken to characterize how the presence of a foredune like Oso Flaco could potentially modulate wind erosion and dust emissions if it was present in the beach areas of the ODSVRA where it is currently absent.

Figure 1: The Oso Flaco foredune test site location.

2 Methods

2.1 Digital Elevation Model of the Oso Flaco Foredune

Detailed imagery of the ODSVRA was acquired using an unmanned aerial system (UAS) operated by UCSB and ASU. The acquired images were processed by ASU to produce digital elevation models (DEM) for various regions of the Park including the Oso Flaco foredunes. The constructed DEM has an accuracy level that resolves topographic details to 10 cm of resolution. The dataset from February of 2021 was selected to construct the DEM for the Oso Flaco dunes, as it most closely matches the time period when measurements of wind flow through the dunes were acquired in May 2021 (see Section 2.2).

To be used in a CFD simulation, additional processing was performed on the topographic dataset for the Oso Flaco foredune region of interest. A GeoTIFF of the region was exported to a point cloud, which was made into a 3D surface using 2D Delaunay triangulation. A GeoTIFF is a public domain metadata standard that allows georeferencing information to be embedded within a Tag Image File Format (TIFF). The GeoTIFF was used to create a topographic representation of the surface that is used to create the computational finite volume mesh (see Section 3.2) for the CFD simulation. This surface can be seen in Fig. 2 (top panel).

Two additional topographies were created to simulate surface shear stress patterns on relevant hypothetical surface forms, for comparison with surface shear stresses on the actual surface. In the first, the foredune is effectively flattened to a gently sloping surface. This is accomplished in the DEM by slicing a rectangular region covering the foredune out of the 3D point-cloud (Fig. 2, top panel). An in-house code was written to re-assign elevation values to the rectangular region, based on inverse distance weighting (IDW). The same 2D Delaunay process is then used to create a 3D surface. The result is a smooth gently sloping surface from the shoreline to the area where the large transverse dunes are located. This sloping surface, shown in the middle panel of Fig. 2, is the result of spatially interpolating the edges of the clipped areas together. In the second scenario, a horizontal sloping surface is created behind the foredune (Fig. 2, bottom panel). This is accomplished by clipping the point-cloud and interpolating a transition zone behind the foredune, which smoothly transitions the foredune topography to a flat plane. The height of this plane is 4.2 m above sea level (ASL), which is based on the average height of the beach.

2.2 Atmospheric Measurements

A measurement campaign was carried out to acquire vertically resolved wind speed and turbulence parameter data upwind of the Oso Flaco foredune and at four positions along a roughly west to east transect through the foredunes. Three sonic anemometers were mounted on two 3.05 m (10 ft) towers to collect 3-dimensional wind speed data (*u*-horizontal, *v*-spanwise, *w*-vertical) at 10 Hz. The anemometers were mounted on the towers with their sampling volumes positioned at approximately 0.025 m, 1.56 m and 3.26 m above the surface (Fig. 4). These data were used to set the boundary conditions and for model verification. One tower was installed upwind of the foredunes. The second tower was moved through the foredune but left in position for short periods of time (approximately 30 minutes). The

Figure 2: 3D representation of the topography of the mature Oso Flaco foredune test area (top panel) and two hypothetical geometry scenarios: the land surface with the foredune flattened (middle panel), and the surface with a flat region behind the foredune with the transverse dunes flattened (bottom panel).

geographic positions of the towers and a summary of time periods for which measurements were taken are shown in Table 1.

Table 1: Locations and durations for velocity profiles measured with the sonic anemometer towers.

Name	Long.	Lat.	Day	Start	End
upwind	-120.6329372	35.0378334	20-05-2021	8:45:00	24:00:00
P1	-120.6319444	35.0380164	20-05-2021	09:40:46	10:51:25
P2	-120.6309242	35.0374855	20-05-2021	11:18:00	11:49:20
P3	-120.6301323	35.0372208	20-05-2021	12:09:29	12:41:16
P4	-120.6296373	35.0367	20-05-2021	13:08:02	13:46:00

Figure 4: Tower configuration for data collected with the sonic anemometers.

Sufficient wind velocity data were collected to build an inlet boundary condition and verification points for numerical simulation. An average velocity profile was constructed over the range of instrument heights by averaging wind speeds for the time period 1:00 PM to 2:00 PM on 05-20-21. The average wind speed for this hour represents a wind speed that is above the threshold for saltation for most of the ODSVRA. A log-law velocity profile was fit to values from the three sonic anemometers, to provide velocity boundary values extending to a height of 100 m above ground level (AGL). A corresponding turbulence intensity, *TI*, profile was created by linearly interpolating calculated values between the three anemometers and extending the value at the 3.23 m anemometer to the top of the computational domain (50 m AGL). A profile of turbulent kinetic energy *k* is calculated from the average velocity *u* and *TI* as,

$$k = \frac{3}{2}(uTI^2) \qquad (1)$$

The specific dissipation rate ω can then be calculated as:

$$\omega = C_{\mu}^{0.75}\,\frac{k^{0.5}}{l} \qquad (2)$$

where the constant C_{μ}=0.09, and the turbulence length scale is taken to be *TI* = 5. The kinematic energy eddy viscosity can be calculated as:

$$v_t = 0.31 \frac{k}{\omega} \qquad (3)$$

Values of u, k, ω and v_t are needed as boundary condition inputs for the CFD simulation. Profiles of u and TI are shown in Fig. 5. Zero-gradient pressure was used at the inlet, solid, side, and top walls, while a fixed value of zero was applied at the exit. Slip velocity (no friction) was applied to the top and side walls, a zero velocity condition was applied to the ground, and the outlet was given a zero gradient condition.

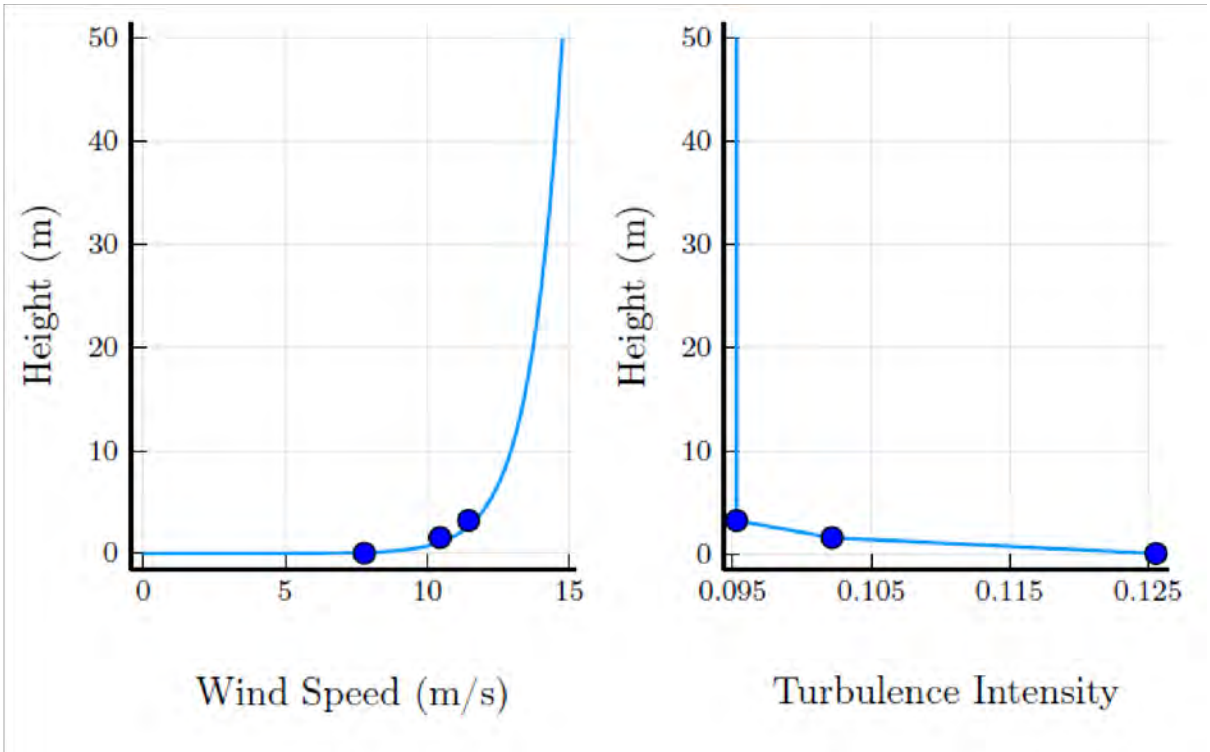

Figure 5: Profiles of u (left) and TI (right) were constructed for the inlet boundary condition. Blue circles represent the near surface measurements from the sonic anemometers.

2.3 Computational Methods

Simulations were performed by numerically solving the steady-state incompressible Navier Stokes equations:

$$\rho u \nabla u = -\nabla p + \rho g + \mu \Delta u \qquad (4)$$

$$\nabla u = 0 \qquad (5)$$

where, u is horizontal velocity, p is pressure (Pa), g (9.81 m s^{-2}) is the acceleration due to gravity, and μ is fluid viscosity (Pa s). Turbulence modeling was performed with a Menter's shear stress transport (SST) turbulence model. This model was chosen for its low sensitivity to the vertical dimension above the surface ($y+$), as the large and complex domain of interest presents a difficult meshing problem.

The computational domain is a 900 m × 200 m × 100 m prism, rotated to align with the prevailing wind direction along the 900 m fetch. An angled plane was used to cut the inlet boundary, ensuring that the inlet boundary condition is applied across the beach at a uniform elevation. An illustration of the domain imposed over the topography can be seen in Fig. 6. A domain height of 100 m was chosen to minimize flow acceleration that may occur due to changes in cross-sectional area caused by the topography. The selected height exceeds five heights of the largest topographic feature in the domain.

Meshing was performed with the CFmesh utility. A maximum cell size of 10 m was applied in the upper atmosphere, which is not a region of interest, to conserve computing resources. Cells are progressively refined with decreasing elevation to 0.5 m within 10 m of the ground. Below 10 m seven additional mesh layers were defined with the lowest at ground level (i.e., the bottom of the lowest mesh touches the surface). This lowest mesh layer has a cell width of 0.02 m. Total cell counts for the simulations performed vary by topography but are on the order of 20 million per simulation.

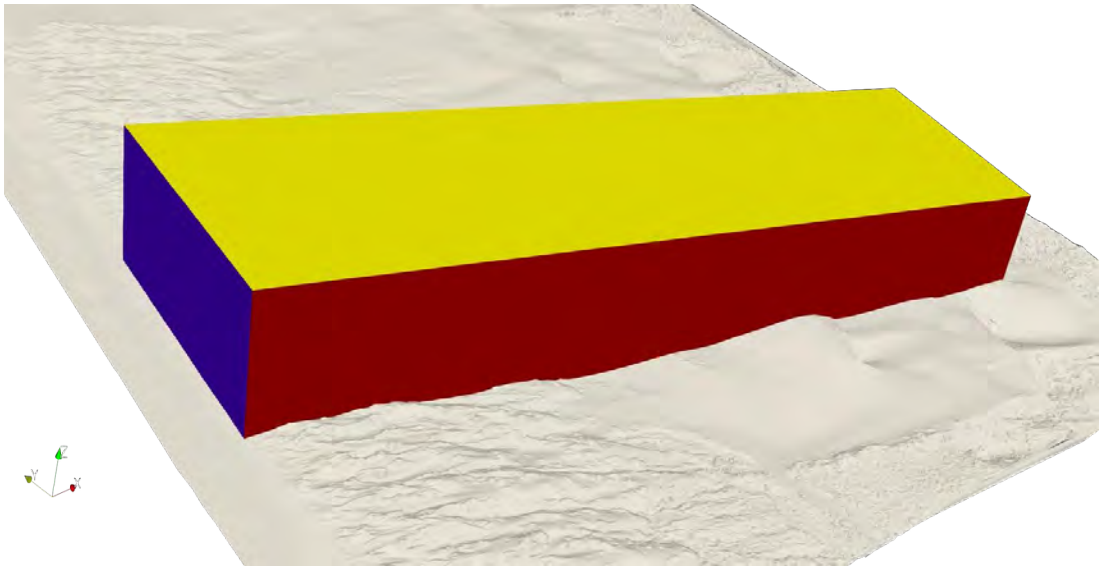

Figure 6: An illustration of the computational domain imposed over the topography. The angled inlet is shown in blue to apply the inlet boundary conditions on the beach across a uniform distance in front of the foredune.

3 Results

3.1 Model Verification

Verification of model results was performed by extracting velocity predictions from the simulation that match the tower locations and anemometer heights and comparing those values with the sonic anemometer measurements. The dataset measured in the field comes from two towers: one stationary tower positioned at the boundary of the computational domain on the beach, and a second that was moved throughout the day. A map of the tower locations can be seen in Figure 7. Consequently, a direct verification (i.e., value predicted to

value measured) cannot be carried out at the second tower locations for the time period that was used to construct the boundary condition. Thus, we compare the ratio of upwind velocity to the velocity measured at the mobile tower for the measurements and the simulation. This is possible, as the upwind tower was in operation for the entire period of time. Thus, validation points are not compared directly against the boundary condition, but additional data collected at the location of the boundary. For the highest sonic anemometer, located 3.26 m above the ground, this ratio for the measured and simulated results is shown in Table 2.

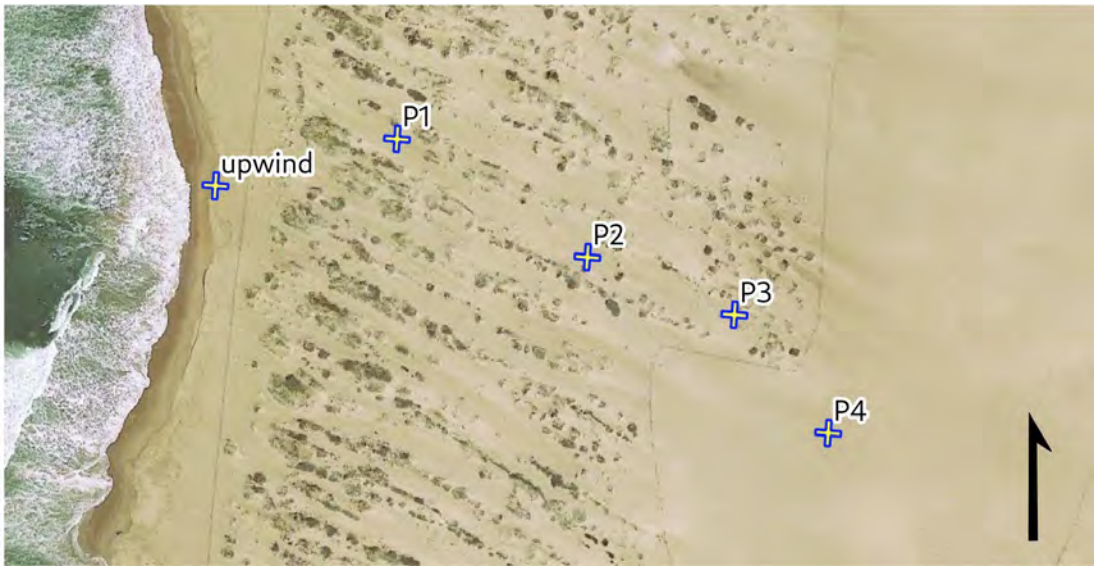

Figure 7: A map of tower locations. The "upwind" tower was fixed, while a second tower was moved to locations P1-P4 throughout the day.

Excellent agreement is observed between the measured and simulated ratio. This ratio serves as a verification that the measured and modeled wind speeds between the two locations in a specified period of time are closely matched even for differing atmospheric conditions. It is important to note that the measurement data were collected in a natural wind field, which varied in both intensity and direction through time and were made in the lee of dune structures that often exceeded the height of the highest sonic anemometer. In contrast the simulated results are modeled as a steady-state condition. Thus, an average relative error of 11.5% is an exceptional result for work outside of a controlled environment as would be found, for example, in a wind tunnel experiment. Moreover, the simulated results show a decrease in the ratio with distance into the foredune, which matches the measured results and classical boundary-layer theory.

Table 2: Validation results: modeled and measured wind speed ratios: downwind (in dunes)/upwind (beach). P1 is the measurement position in the foredunes closest to the beach and P4 is furthest from the beach.

	P1	P2	P3	P4
Simulated	0.952	0.866	0.835	0.749
Measured	0.964	0.706	0.897	0.886

3.2 Wind Flow and Shear Stress Across the Oso Flaco Test Section

Surface shear stress is created by the fluid, i.e., air, interacting with the surface topography which the CFD calculates using the Navier-Stokes equations and the set boundary conditions. A visualization of the magnitude of this force on the foredune and back dune topography is shown in Fig. 8. As seen in the upper panel of Fig. 8, the foredune has small areas where the highest shear stresses are observed (i.e., the red colored areas). On the western edge of the foredunes these represent the vegetated areas of the nebkhas (vegetation-topped mounds), which are the first major obstacle encountered by the inlet wind profile. The low area behind the complex foredune form is a region of lower shear. Past this area in the lee of the foredune where the bare sand surface begins to rise in elevation, the shear begins to increase again as a function of increasing downwind distance (lower panel of Fig. 8).

To illustrate the pattern of air flow over the foredunes and further downwind, the model can be used to generate near-wall streamlines that represent the movement of neutrally buoyant particles released into the flow at a height of 10 cm above the ground surface. As the simulations are steady-state, these can also be interpreted as being average path-lines for air molecules. Visualizations of the streamlines for the foredune and non-vegetated dune system behind the foredune can be seen in Fig. 9. This visualization provides insight into the different aerodynamics of the two dune systems. The individual nebkhas of the foredune show very little flow separation, indicating for the most part a very aerodynamic system. In contrast, the non-vegetated transverse dunes show zones of significant flow separation at the dune crests with zones of re-circulation on the lee-side slip faces.

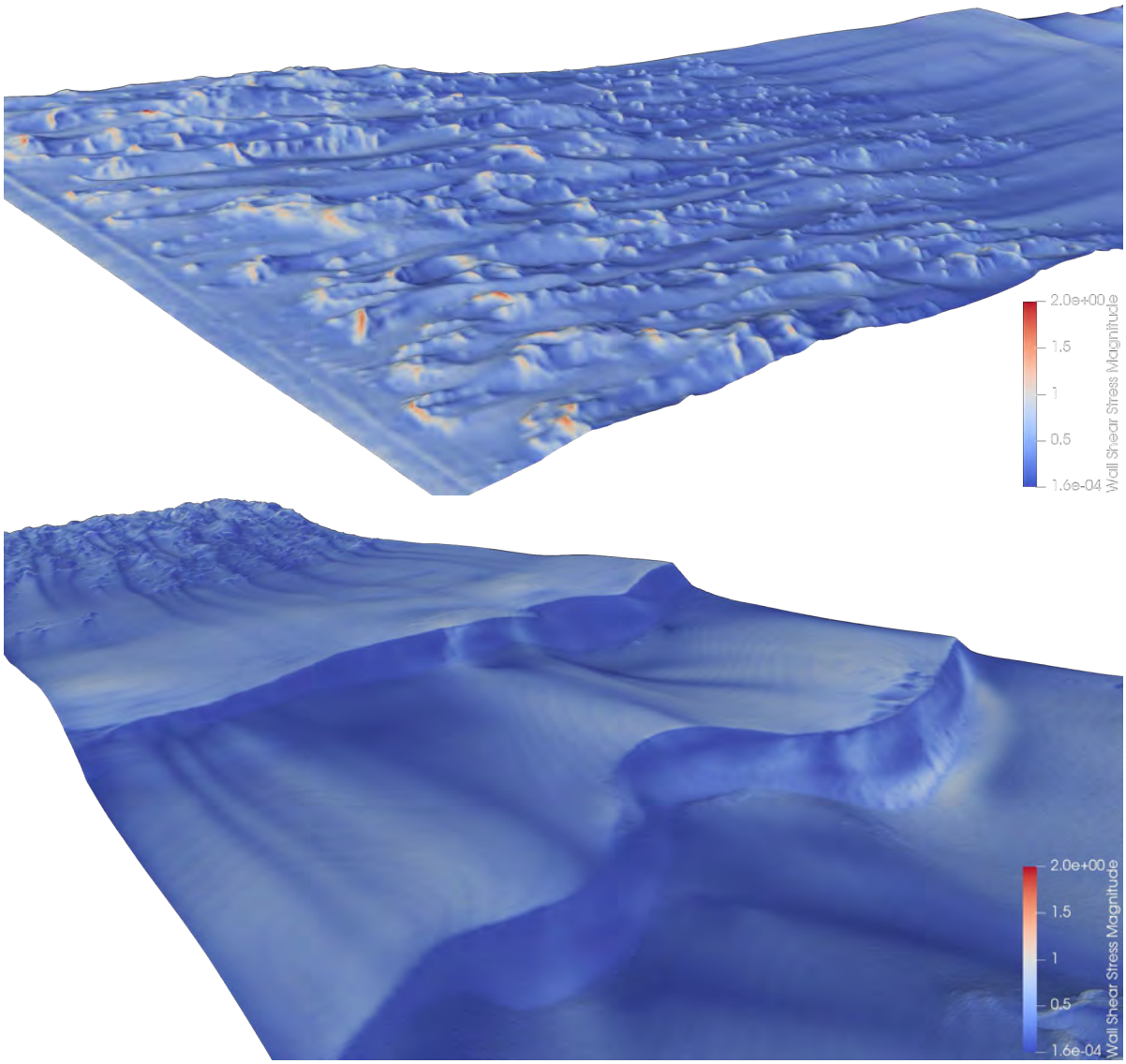

Figure 8: Visualization of the shear stress generated on the topography of the Oso Flaco foredune test area. A view of the foredune looking downwind (left side is west, right side is east) is shown in the upper panel, while a view of the non-vegetated dune system looking upwind (left side of image is west, right side of image is east) is shown in the lower panel.

The aerodynamics of the two dune types motivates an investigation of the role of plants in the shear stress distribution of the foredune. It is obvious from Fig. 8 that the foredune nebkhas receive large amounts of shear, and the low areas between them less so, despite the lack of flow separation. A raster vegetation mask of the foredune was created from spectral data acquired with the ASU/UCSB UAS. A map of this raster is shown superimposed over the magnitude of shear stress in Fig. 9. This image illustrates how plants exert considerable control of the shear stress distribution on the foredune. Areas of high shear are stabilized

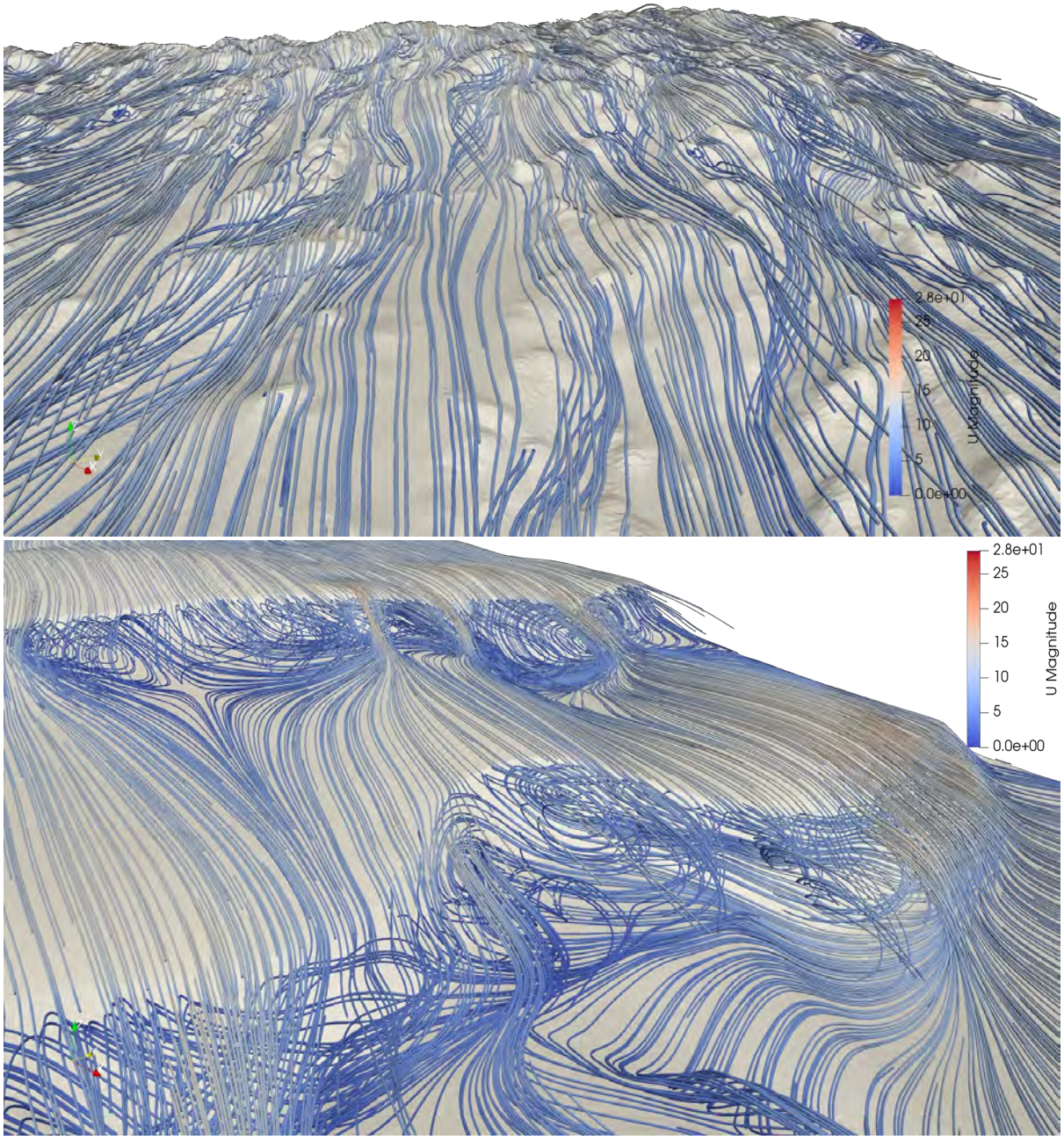

Figure 9: Upper panel: Near-wall streamlines are shown at the foredune, viewed looking upwind (top of image is west [upwind], bottom of image is east [downwind]). Lower panel: Near-wall streamlines are shown for the non-vegetated dune behind the foredune (top of image is west [upwind], bottom of image is east [downwind]).

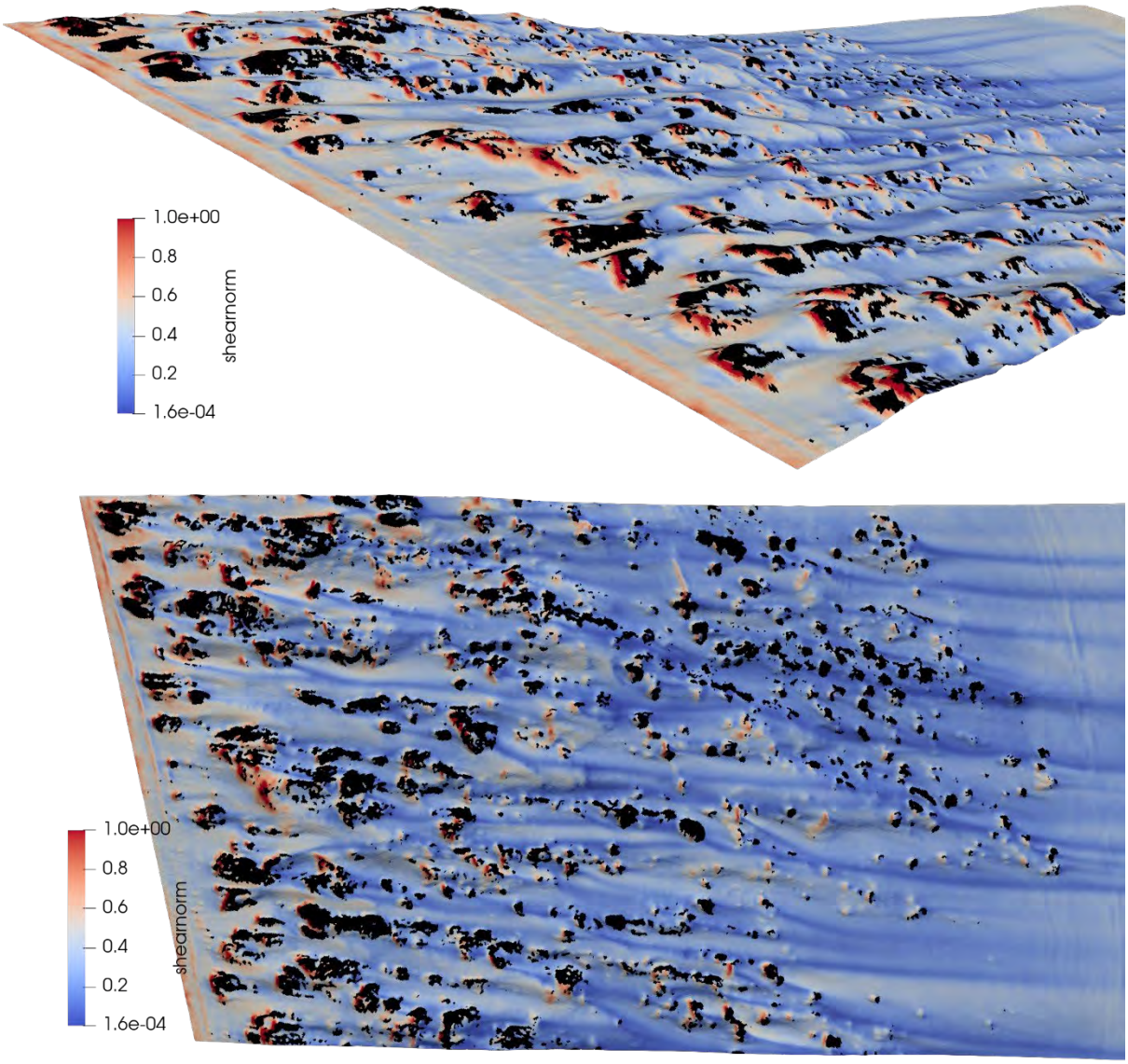

Figure 10: Two views of the Oso Flaco dune test area with a raster vegetation mask of the foredune vegetation superimposed on the foredune shear stress magnitude map. Black denotes locations of vegetation at 10 cm scale. The upwind boundary of the simulation is shown at the left of the image, with flow from left to right.

against entrainment and transport of sand by plants protecting the ng surface (e.g., Wolfe and Nickling, 1983; Gillies et al., 2010, Mayaud and Webb, 2017). In the lee of the vegetation an area of protection, characterized by low shear, is created on the bare ground.

3.3 The Aerodynamic Value of the Foredune

The presence of the foredune inevitably creates aerodynamic effects that affect the shear stress magnitude and distribution within the foredune complex and downwind of the foredunes. However, these are difficult to quantify in field studies, as the foredune cannot be flattened for a paired study. In simulation this can be achieved without high costs or environmental damage. This motivated the creation of the geometry shown in the middle panel of Fig. 2, where the foredune has effectively been flattened, and replaced with a smooth sloping surface, similar to what the shoreline of the ODSVRA looked like prior to 2019, when the foredune restoration project was established. Shear created by the simulation of flow over the Oso Flaco test surface is shown in Fig. 8 (the surface shown in Fig. 2, top panel), which we use to compare with the generation of shear stress across the same space for the hypothetical surface.

A comparison is achieved between surface geometries by performing a surface integration of shear (τ [Pa]. Note 1 Pa is equivalent to 1 N m^{-2} and $\tau=\rho u_*^2$ where ρ is air density [kg m^{-3}]) over each surface. In the first comparison the integral is computed over the rear sections of the two geometries (i.e., Fig. 2 top and middle panels) beginning approximately 300 m from the shoreline through to the end of the sampling domain in the east. The resultant integrated shear is 31,326 N for the unmodified geometry (Fig. 2 top panel), and 32,690 N for the geometry with no foredune upwind (Fig. 2 middle panel). The difference in shear can be attributed to changes in the wind field as it passes over the foredune or the absent foredune, with less energy extracted near the ground when the foredune is absent. For the boundary condition tested in these simulations, removal of the foredune resulted in a 4.4% increase in shear on the dune system for distance ≥300 m from the shoreline.

For the entire domain of the simulations, the integrated shear on the flattened geometry (i.e., all of Fig. 2 middle panel) was 56,530 N, which exceeds the integrated shear of the foredune geometry including the shear on the vegetation of 52,238 N (all of Fig. 2 top panel). This is notable, as the Oso Flaco (test area) foredune geometry has a higher surface area due to the complex topography. Moreover, the foredune topography is characterized by zones of high shear on the vegetated nebkhas, as seen in the upper panel of Fig. 8. For the boundary condition tested in these simulations, removal of the foredune would result in an 8.2% increase in shear on the equivalent sized area with no foredune present. In addition to significant shelter effects behind the foredune, the total effect of the foredune topography is a reduction in shear compared to a flattened surface.

The vegetation on the nebkas produces areas of high shear stress, but critically the area underneath vegetation is protected from this shear. Removing the areas of shear associated with the presence of the vegetation, as it represents areas where sand transport and dust emissions have a low probability of occurrence due to the protection afforded by the vegetation, further decreases the integrated shear on the Oso Flaco test surface (Fig. 2 top panel). The area-integrated shear excluding shear generated on the vegetation is 47,570 N. The total integrated shear on the geometry with the foredune flattened (Fig. 2 middle panel) is 15.8% higher than on the Oso Flaco test surface (Fig. 2 top panel). There is a significant increase in protection due to the presence of the vegetation. For the entire modeling domain

the plant cover is approximately 9%. Within just the foredunes the plant cover is approximately 16%.

3.4 The PM_{10} Emission Reduction Value of the Foredune

The shear stress analysis can be extended to evaluate how the different shear stress conditions on the actual and hypothetical surfaces affect PM_{10} mass emissions. An evaluation is made for the emissivity conditions represented by the mean riding area and mean non-riding area emissivity relations (DRI, 2021). Previous monitoring with the PI SWERL instrument has demonstrated higher emissions in the La Grande Tract as compared to Oso Flaco (Gillies and Etyemezian, 2015; Gillies et al., 2021). The average emissions (E, mg m^{-2} s^{-1}) relation for the riding area as a function of shear velocity u_* (m s^{-1}) is:

$$E = 23.65(u_*)^{5.59}, \quad (6)$$

The average emissions relation for the non-riding area as a function of shear velocity u_* is:

$$E = 21.51(u_*)^{6.85}. \quad (7)$$

The model derived shear values (τ) were converted to u_* (remember, $\tau=\rho u_*^2$ where ρ is air density [kg m^{-3}]) and then integrated across the surface areas of the actual and hypothetical geometries. The total integrated emissions are in units of mg s^{-1}. Total emissions and the corresponding total shear force are shown in Table 3. The third scenario of an unmodified topography (i.e., Oso Flaco test surface, Fig. 2 top panel) shows significantly lower emissions than the scenarios that neglect vegetation sheltering or have a flattened foredune. Total emissions calculated with the non-riding emissions curve are approximately half those calculated with the riding area emissions curve in all cases.

Table 3: Shear and total integrated emissions for the surfaces with the foredune flattened (Scenario 1), the unmodified surface neglecting the effects of plant cover (Scenario 2), and the unmodified surface with zero emissions from areas that are vegetated (Scenario 3).

	Scenario 1	Scenario 2	Scenario 3
Total Shear Force (N)	56530	52238	47570
Riding Total E (mg s^{-1})	163412	159654	134683
Non-riding Total E (m g s^{-1})	89458	88384	70387
Riding Total E (mg m^{-2} s^{-1})	.972	.950	.802
Non-riding Total E (mg m^{-2} s^{-1})	.533	.526	.419

3.5 Foredune Downwind Sheltering Effects

Being able to quantify the sheltering effects of the foredune will be a useful tool for planning remediation projects and evaluating secondary effects on dust emission on the lee side. This is the motivation for the geometry that situates a flat plane behind the foredune, as seen in the bottom panel of Fig. 2. As the actual shear on a given land surface may vary widely depending on the topography behind the foredune, the flat surface offers the best scenario for a generalized result. Shear stress was calculated from a simulation run for this surface using the boundary conditions outlined in Section 2.3. A plot of the average shear stress on the foredune followed by the flat surface (Fig. 2, bottom panel) is shown in Fig. 11. Note that the averaging is across the width of the modeling domain at each length interval along the west to east transect and not just along a narrow corridor through the foredune. The recovery of this relation beginning at zero on the figure (i.e., 0 on the x-axis) illustrates the sheltering behind the foredune. Figure 12 shows the shear stress relation past the foredune (i.e., 0 on the x-axis) in Fig. 11 normalized against the maximum shear stress, which occurs ≈300 m past the end of the foredune. Figure 12 shows that in the lee of the foredune a zone of shear is created that reaches a minimum at the zero point and then increases non-linearly with

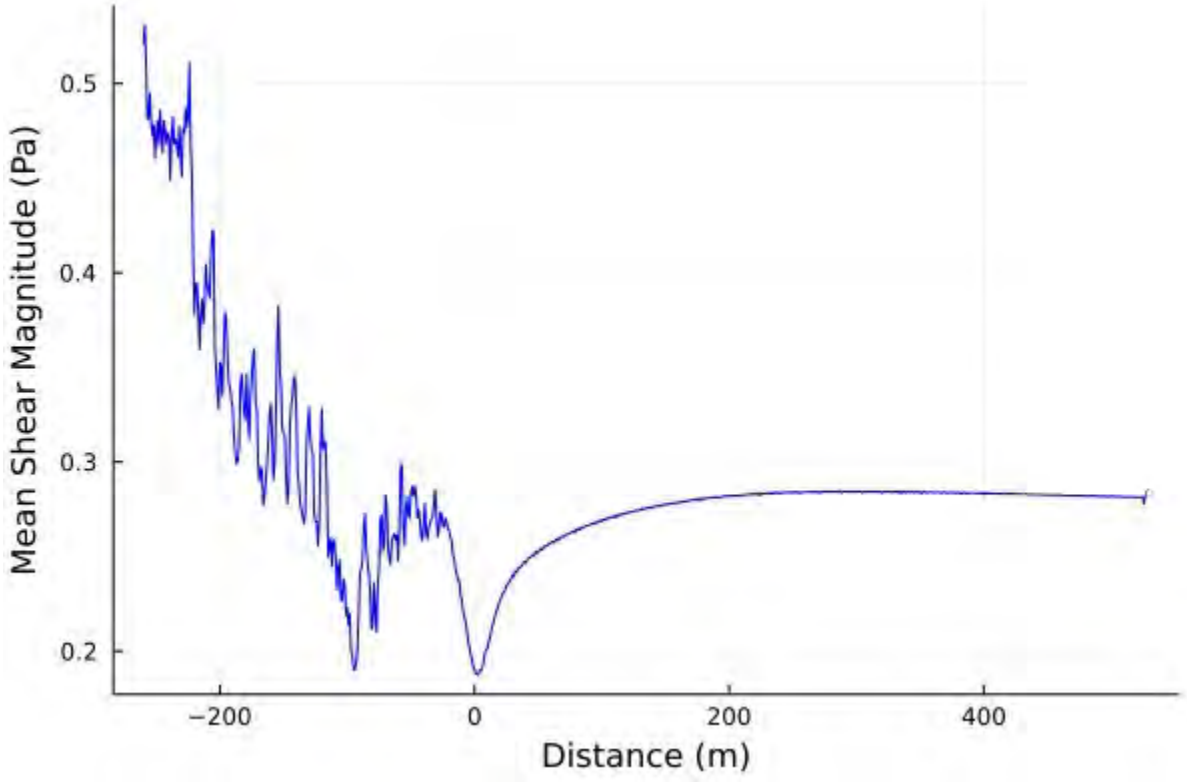

Figure 11: Mean shear magnitude as a function of distance in the freestream direction for the geometry shown in Fig 2., bottom panel. The leeward edge of the foredune is located at x = 0.

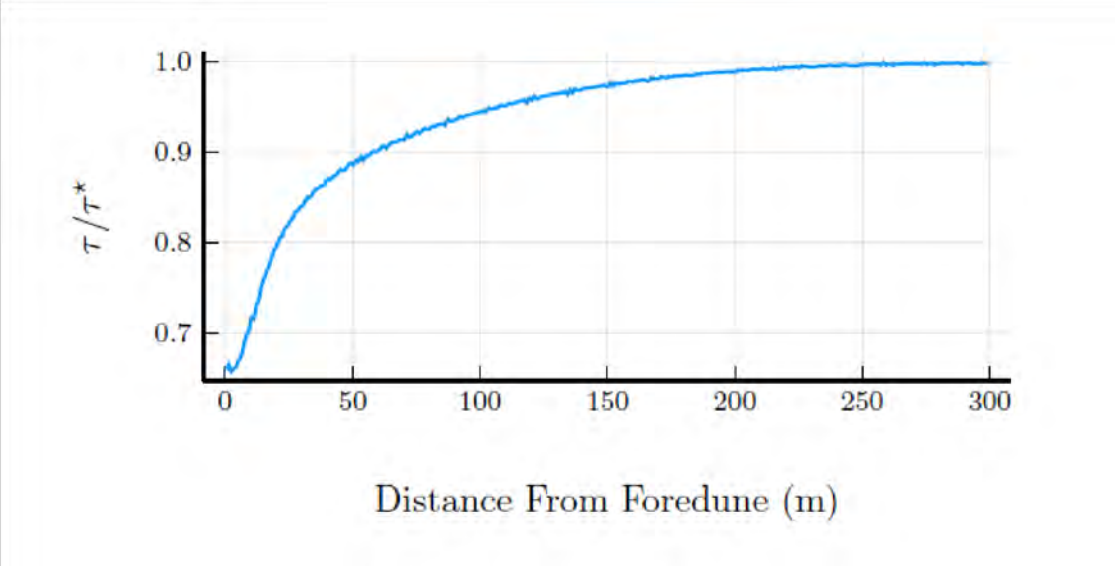

Figure 12: Mean shear τ normalized by maximum shear τ^* as a function of distance.

increasing downwind distance. The shear stress at the surfaces reaches approximately 90% of its potential value within a 50 m of fetch behind the foredune.

The shear stress along the west to east length of the domain for the Oso Flaco foredune test area (Fig. 2 top panel) and the geometry with the foredune flattened (Fig. 2 middle panel) are compared with Fig. 11 in Fig. 13.

Figure 13 provides a clear indication of the value of a foredune similar to Oso Flaco to modulate surface shear stress that favors a lower production of dust emissions when compared to the condition of an absent foredune. As a first approximation of the potential secondary effect of the foredune on dust emissions specifically in their lee, a recommendation is to apply the relation shown in Fig. 12 to the grid cells in the DRI dispersion model to modulate the CALMET estimated shear velocities from the zero point in Fig. 13 through to a distance equivalent to the start of the large transverse dunes.

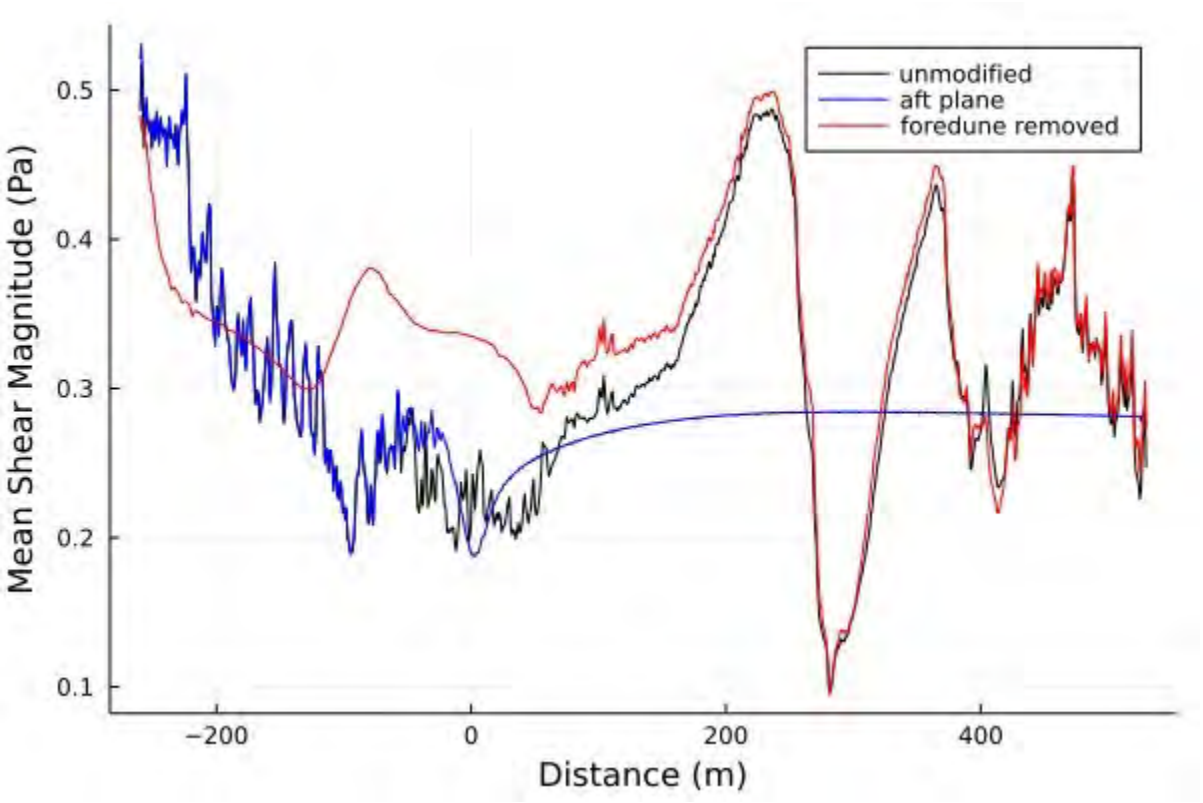

Figure 13: Mean shear magnitude as a function of distance in the freestream direction for the Oso Flaco geometry (Fig. 2, top panel represented by black line), the geometry with the foredune flattened (Fig. 2, middle panel represented by red line), and the geometry with the foredune followed by a sloping sand surface (Fig. 2, bottom panel represented by blue line). The downwind edge of the foredune is located at $x = 0$.

References

Gillies, J.A., Etyemezian, V., 2015. Addendum to the PI-SWERL Report of Etyemezian et al. (2014) Particle Size Distribution Characteristics and PI-SWERL PM_{10} Emission Measurements: Oceano Dunes State Vehicular Recreation Area. Report prepared by the Desert Research Institute for Off-Highway Motor Vehicular Recreation Division, California State Parks, 1725 23rd Street, Suite 200, Sacramento, CA 95816, July 13, 2015 (available upon request).

Gillies, J.A., E. Furtak-Cole, G. Nikolich, V. Etyemezian (2021). The role of off highway vehicle activity in augmenting dust emissions at the Oceano Dunes State Vehicular Recreation Area, Oceano CA. *Atmospheric Environment X* (accepted).

Gillies, J. A., W. G. Nickling, and N. Lancaster (2010), Vegetative roughness controls on wind erosion: a shear stress partitioning approach, paper presented at *Ninth International Conference on Dryland Development: Sustainable Development in the Drylands – Meeting the Challenge of Global Climate Change*, Alexandria, Egypt, 2010.

Mayaud, J. R., and N. P. Webb (2017), Vegetation in drylands: Effects on wind flow and aeolian sediment transport, *Land*, 6(64), doi:10.3390/land6030064.

Wolfe, S. A., and W. G. Nickling (1993), The protective role of sparse vegetation in wind erosion, *Prog. Phys. Geogr*., 17, 50-68.

Appendix A: CFD Development and Processing

The following summary contextualizes the scope of producing quality CFD results:

- Each simulation takes 4800 core-hours of computing.
- Approximately 15 Julia codes were written to process the input and output of data.
- Over 30 meshes were produced before the final configuration was set.
- Each simulation produces velocity and pressure at >20 million points within the modeling domain.
- Output from each simulation is ≈98 GB of data.

A typical CFD workflow is shown as a flowchart in Fig. A1. The process begins with creation of a surface geometry, which requires creation of a 3D surface from a Digital Elevation Model (DEM). Next a mesh is designed to discretize the domain for the solver. The solver and post processing utilities are run on a computing cluster (University of Utah). The simulation output is checked for integrity. The mesh is then re-designed to increase the quality of the result, and the processes is repeated. When sufficient quality is achieved, based on evaluation of model convergence metrics, additional post processing with custom codes and visualization tasks are performed. A cross section of the computational mesh is shown in Fig. A2, which needed to be carefully designed to resolve turbulent flow features over the topography.

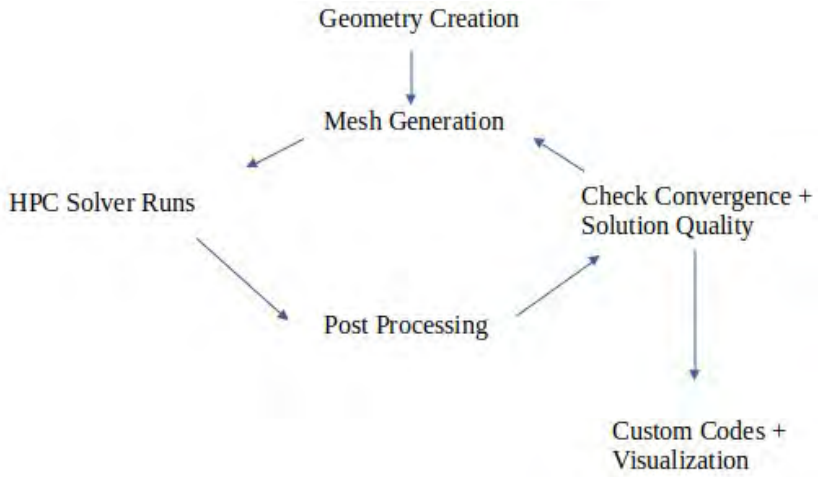

Figure A1. The workflow process for developing and processing the CFD.

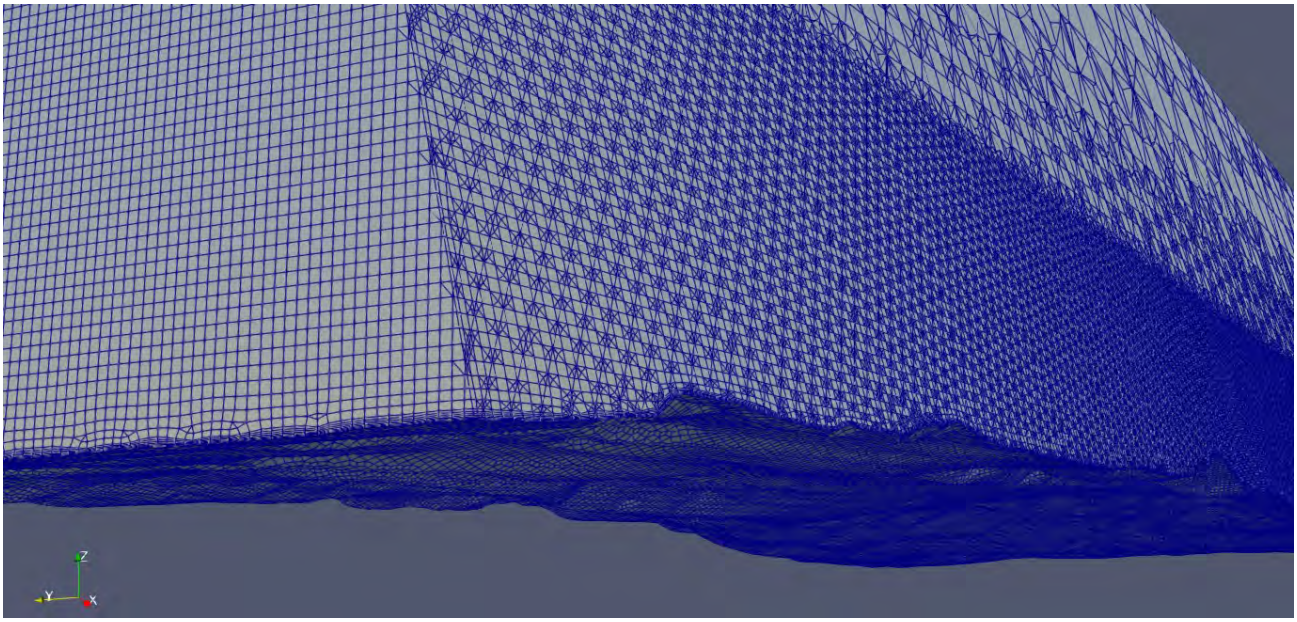

Figure A2. A cross section of the computational mesh developed for the Oso Flaco foredune test area.

THIS PAGE INTENTIONALLY LEFT BLANK.

Oceano Dunes State Vehicular Recreation Area Dust Control Program

DRAFT 2022 Annual Report and Work Plan

ATTACHMENT 06-04

UCSB Historical Vegetation Cover Change Analysis

THIS PAGE INTENTIONALLY LEFT BLANK.

UCSB Historical Vegetation Cover Change Analysis

(1930-2020) within the Oceano Dunes SVRA

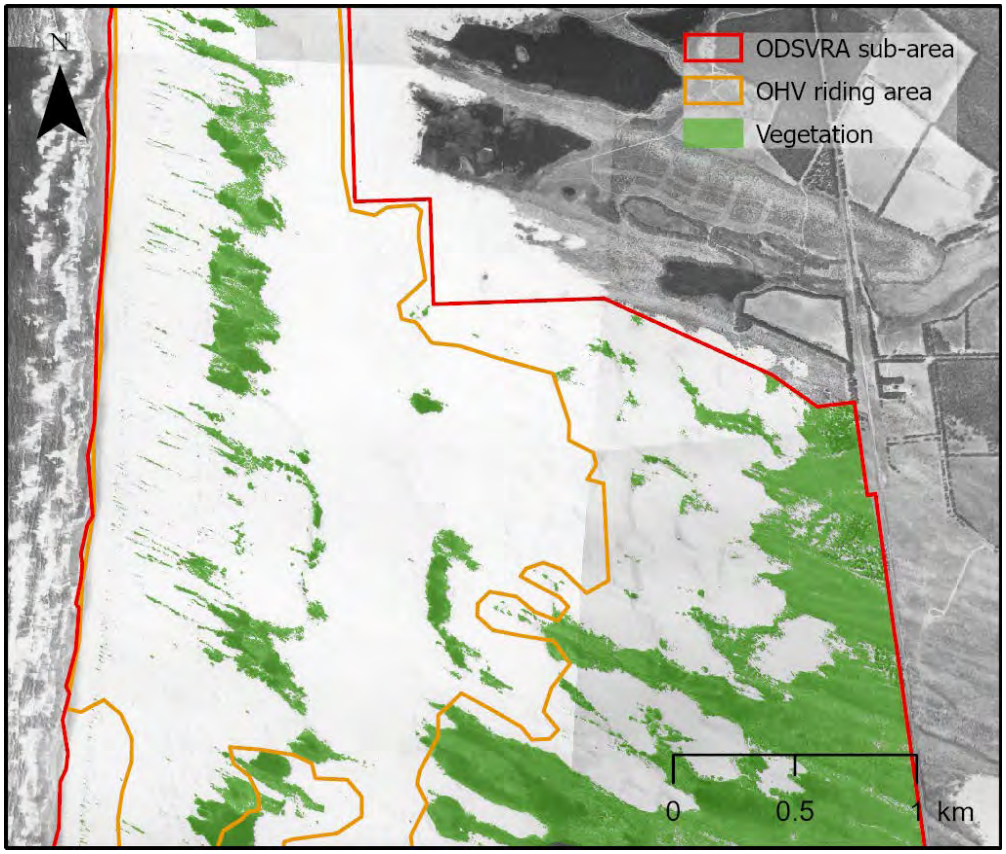

Map of vegetation cover (green) derived from historical 1939 aerial photography of the southern portion of the Oceano Dunes SVRA

Prepared by: Nitzan Swet[1], Zach Hilgendorf[1,2] and Ian Walker[1,3]

[1] Department of Geography, University of California Santa Barbara

[2] School of Geographical Sciences and Urban Planning, Arizona State University

[3] Member of the Oceano Dunes Scientific Advisory Group

December 2021

EXECUTIVE SUMMARY

This report examines 90 years of historical changes in vegetation cover within the ODSVRA as requested by CDPR for the 2020-21 ARWP. Trends in plant cover are mapped and quantified using a Geographic Information System (GIS) and best available aerial photography obtained from CDPR, UCSB Library's Geospatial Collection, and the National Agriculture Imagery Program (NAIP), from 16 years with sufficient coverage of ODSVRA between 1930 and 2020.

To examine and interpret vegetation cover trends and allow comparison between different regions of the ODSVRA, the report focuses on five analytical zones:

- a large sub-area of the ODSVRA located south of Arroyo Grande Creek (~75% of the total area of ODSVRA),
- the OHV riding area within the ODSVRA (c. 2013),
- the foredune zone, or the area in which foredune vegetation would typically exist in the region, that extends ~400 m eastward/inland from the high-water mark,
- the north Oso Flaco foredune complex, closed to OHV activity since 1982,
- the south Oso Flaco dune complex within the ODSVRA boundary, including both foredune and backdune areas, which serves as a reference site for mature foredunes that have not seen OHV activity since 1982,
- the new (2020) foredune restoration sites, located within the foredune zone of the OHV riding area between post markers 4-6.

Plant cover maps and calculations (area and percentage) were obtained for each analytical zone across all image years. Resulting maps were analyzed for locations and extents of change between all years. In addition, changes between 4 specific time periods that relate to different land management intervals were interpreted:

1. 1939-1985: landscape responses preceding the management of ODSVRA by CDPR, which began in 1982,
2. 1985-2012: landscape changes during the management of ODSVRA by CDPR up to adoption of SLO-APCD Rule 1001 (2011) and related particulate matter reduction plans (PMRP),
3. 2012-2020: landscape responses following implementation of PMRP mitigation efforts resulting from Rule 1001 (2011) and the eventual state SOA in 2018, and
4. 1939-2020: total landscape change over the historic aerial photo record that compares a time prior to widespread OHV riding and the current state of vegetation cover.

Plant cover trends within ODSVRA have varied over time and differ notably between the analytical zones. Within the broader ODSVRA sub-area, vegetation change generally increased over time, from approximately 25% in 1939, to a peak of 37% in 2012, to just over 35% in 2020. In the OHV riding area, vegetation cover has been comparatively low across all years and declined appreciably from a peak of 12% in 1966 to 8% in 2020. After 1966, plant cover

decreased to a low of 3.9% in 1985 and remained low (<5%) until the early 2000's when vegetation cover gradually began to increase to 2020 levels. In the southern Oso Flaco area, plant cover changes are similar to those in the broader ODSVRA sub-area, but with generally higher values. Vegetation cover at south Oso Flaco decreased from 26% in 1939 to a historic low of 24% in 1949, then more than doubled to a peak of 66% in 2012. Following this, plant cover declined slightly but remained >60% to 2020.

Similar trends occur within the foredune zone in each analytical area, albeit with generally less plant cover. The foredune zone at south Oso Flaco reference site had very low plant cover (2.3%) in 1939, but increased by an order of magnitude to over 30% in the 2010s. For comparison, foredune vegetation in the OHV riding area also had low cover (2.6%) in 1939, rose to a peak of 5.3% in 1966, but steadily declined to very low values ~1% from 1985 to 1998. Since 2005, plant cover increased slightly in the riding area to 2.4% by 2020, mostly due to new plants on the margins of fenced vegetation islands and in the seasonal bird nesting enclosures. At north Oso flaco, foredune vegetation cover was extremely low (<1%) in the 1930s, less than in the OHV riding area, but after 1985 the values increased to over 24% in 2012.

Broader ecological and climatic conditions aside, observed patterns and differences in vegetation trends across these areas is largely attributable to three main factors: 1) the presence of camping and OHV riding (sanctioned or otherwise) activities in the dunes, 2) widespread and targeted removals of invasive grass species in some areas (e.g., south Oso Flaco), and 3) land management and plant restoration efforts by CDPR since establishment of the park in 1982 and in response to PMRPs associated with Rule 1001 (2011) and the 2018 SOA.

Interpretation of changes over the four reference time periods indicates the following:

- 1939-1985: a general decline in plant cover in the foredune and backdune zones of the OHV riding area (from 11% to 4%) while vegetation in the broader ODSVRA increased notably from 1939-1966, then declined to 1985. In the riding area, overall change is characterized by 10% negative change (plant losses) and only 2% positive gains,
- 1985-2012: mostly increasing plant cover with over 15% gains in the broader ODSVRA sub-area, mainly around existing vegetation and other targeted restoration areas, particularly between 2005 and 2012.
- 2012-2020: a general decline in plant cover across the ODSVRA and south Oso Flaco areas compared to previous intervals with 8% total change in the ODSVRA sub-area. Some of this decline reflects removal of invasive plants by CDPR. Within the OHV riding area, plant cover remained steady at ~8% during this time.

1. Introduction

Vegetation plays a vital role in the development and maintenance of certain dune types and related ecosystems common in the central coast of California (e.g., nebkha and shadow dunes, foredunes, blowouts, parabolic dunes) as well as in the stabilization of sand surfaces to reduce sand drift, wind erosion, and dust emissions. In areas of high recreation activity, natural windblown (aeolian) and related dune ecological processes often become challenged. In turn, this can result in a loss of vital ecosystem services provided by coastal dunes including mitigating sand transport and dust emissions, buffering coastal erosion and flooding, facilitating groundwater recharge, and providing important habitat for a wide range of endemic, migratory, threatened, and endangered plant and animal species.

This report provides a thorough review of historical changes in vegetation cover within the Oceano Dunes State Vehicular Recreation Area (ODSVRA) as requested by the California Department of Parks and Recreation (CDPR) for the 2020-2021 Annual Report and Work Plan (ARWP). Vegetation cover from historical aerial photographs from the 1930s to 2020 was analyzed to interpret changes from the earliest photo records. As such, the analysis documents landscape changes through decades of unsanctioned OHV activity prior to establishment and management of ODSVRA by CDPR in 1982 and through almost another 40 years following. Changes during this later period reflect both OHV activity as well as significant land use management and vegetation restoration initiatives implemented by CDPR to mitigate dust emissions and control invasive species. With more frequent photo coverage in recent years, responses of the landscape following implementation of Particulate Matter Reduction Plans (PMRP) associated with the SLO-APCD Rule 1001 “Coastal Dunes Dust Control Requirements” of 2011 and the State of California Stipulated Order of Abatement (SOA) in 2018 are also quantifiable.

The main objective of the report is to document and analyze historical changes in vegetation cover and related dune landforms within ODSVRA to help inform development of baseline conditions for restoration and dust emissions mitigation strategies in the future 2022-23 ARWP. In particular, it is important to establish what the state of vegetation cover was prior to, and since, the management of ODSVRA by CDPR and related changes in plant cover with sanctioned OHV activity and camping in the dunes. These results can also inform assessment of landscape changes associated with more recent management and restoration activities in response to PMRP activities and act as a tool for identifying future treatment locations and methods.

2. Methods

An extensive dataset of aerial photography for the Oceano Dunes region was obtained from the UCSB Library Geospatial Collection[1], CDPR, and the National Agriculture Imagery Program (NAIP) website[2] consisting of 19 individual years of imagery taken between 1939 to 2020 (Table 1). Due to limitations resulting from limited coverage, image projection, size, and/or shadowing, three image years were omitted from the analysis, leaving a total of 16 image years. The imagery datasets for 1939 to 1985 are composed of a mosaic of individual aerial photos (tiles). The aerial photo tiles for 1930 to 1978 were received as digital scans from the UCSB Library, while the 1985-1998 aerial photo tiles were scanned and processed by CDPR staff. The rest of the imagery used in this report (2005-2020) are in a digital orthophoto mosaic format (one tile) downloaded from different sources. The 1994, 1998, and 2007 images were received from CDPR, however, their sources are uncertain (see Table 1). The 2005 and the 2010 to 2020 images were downloaded from NAIP (Table 1).

For each image year between 1939 and 1985, photo tiles required local alignment to one another, typically completed with a simple shift or 2nd order transformation. Once all tiles were aligned, clipped shapefiles were created for each to remove cataloging data from the edges, interior portions of each tile were extracted, and the resulting images were then loaded into a raster mosaic of the study area as a file geodatabase in ArcGIS Pro. During this step, the tiles were manually assessed and layered so that rasters (digital image grid cells or pixels) with darker, more pronounced, sharper features were on top of those with lighter, or less pronounced features. This also allowed for continual assessment and correction of tile alignment. This alignment and orthorectification step is important as slight misalignments and planar tilt issues can produce appreciable errors in positioning and measurements of ground features. The final mosaic was then exported to a single digital (tiff) file for each photo year.

For all image processing, a 2020 USDA National Agricultural Imagery Program (NAIP) geotiff was used as a reference layer, to which all photo years were compared and aligned. Some photo years (e.g., 1960s-70s) exhibited significant differences in the presence and/or alignment of key anchor features from the 2020 NAIP image (e.g., infrastructure features that were not present in earlier imagery), so these photo years were aligned using orthomosaic images from the early 1990s with high georectification accuracy and common anchor features. The oldest images (e.g., 1930s-1940s) were referenced to the best georectified images from the 1960s. In this way, locational precision for all years was cross-referenced to the position of the high resolution, geolocationally constrained 2020 NAIP imagery by using alignment features from closer years.

[1] University of California Santa Barbara Library geospatial collection of aerial photography is available at: https://www.library.ucsb.edu/geospatial/aerial-photography

[2] National Agriculture Imagery Program (NAIP) is available at: https://www.fsa.usda.gov/programs-and-services/aerial-photography/imagery-programs/naip-imagery/

Table 1 contains metadata of all imagery datasets used in this report, including image resolution (i.e., pixel or raster grid cell size in m), also known as the ground sampling distance (GSD) of the imagery, as well as the number of image tiles used to create the mosaic of the final image file (.tiff). Transformation type refers to the way in which each raster cell was aligned with its real-world location through manual refinement and the selection of static ground control points (GCPs) between images. Of several methods available in ArcGIS Pro, polynomial and spline transformations were found to have the most accurate corrections for the datasets used. This accuracy is reported through the total root mean square (RMS) forward-inverse error, which expresses the projected uncertainty (in pixels), relative to the GCPs and the transformation type for each image set[3]. Pixel depth refers to the range of values that a raster cell type can store. For example, an unsigned 8-bit raster type can store 256 digital values between 0-255. The band number for each raster is a reference to how many layers of data are stacked to produce the raster dataset. Three band types were used in this study, including a single-band (grayscale) dataset for older imagery through 1978, and three- or four-band imagery in the later datasets. Three-band imagery expresses visual color (red-green-blue or RGB) wavelengths. Four-band imagery expresses the visual spectrum in the first three (RGB) bands and an additional near-infrared (NIR) band. The NIR spectrum is particularly useful for mapping, assessing, and extracting vegetation from multispectral imagery[4].

The aligned mosaic image datasets for each year were then classified using the supervised (sampling-based) classification wizard in ArcGIS Pro to identify vegetation and non-vegetation pixels using areas (and spectral signatures of color or grayscale) of known cover identified by the analyst. Classification results were then quality checked by visual inspection to identify wrongly classified pixels, then these cells were manually re-classified using the Pixel Editor tool. For each year, vegetation cover was calculated by area (km^2 and acres) and percentage cover (%) in six different analytical regions (Figure 1):

1. the portion of the ODSVRA located south of Arroyo Grande Creek (known as the ODSVRA sub-area),
2. the OHV riding area, border as in 2013, within the ODSVRA,
3. the foredune zone, defined as the area in which foredune vegetation typically exists in the region, extends about 400m inland from the high water mark. This zone was identified by the average depth of foredunes from Oso Flaco to near Pavillion Hill.
4. the north Oso Flaco foredune complex located north of Oso flaco Creek, which has been closed to OHV riding from the mid 1980s. This location serves as a reference site for foredune development since closure to OHV riding in 1982 (~38 years).

[3] ArcGIS Pro helpdesk-
https://pro.arcgis.com/en/pro-app/latest/help/main/welcome-to-the-arcgis-pro-app-help.htm
[4] Yichun Xie, Zongyao Sha, Mei Yu, Remote sensing imagery in vegetation mapping: a review, Journal of Plant Ecology, Volume 1, Issue 1, March 2008, Pages 9–23, https://doi.org/10.1093/jpe/rtm005

5. the southern Oso Flaco dune complex, which includes both foredune and backdune areas south of Oso Flaco Creek. This area serves as a reference site for mature foredune ecosystems in the region that also have not experienced OHV riding since 1982, and
6. the new foredune restoration sites in the riding area, established in February 2020, located within the riding area between post markers 4-6.

The ODSVRA sub-area was set as the area south of Arroyo Grande Creek due to limited photo coverage across most years north of this area. The northern areas also contribute minimally to dust emissions due to the limited extent of open sand fetch and typically moist beach surfaces. Of note, this sub-area also includes the Pismo Dunes Natural Preserve (light blue area in Figure 1) that is technically not part of the ODSVRA. The preserve area is considered a subunit of Pismo State Beach, which is administered by the Oceano Dunes District of state parks. The broader ODSVRA sub-area is approximately 17 km^2 (4215 acres), or about 74% of the total area managed by the Oceano Dunes District, and 85% of the ODSVRA park unit.

An additional portion of the southernmost area of ODSVRA was also excluded from the analysis (hatched area in Figure 1) due to changes in surface water features and human land use/infrastructure (agriculture, roads, buildings) over the years. These southern excluded areas total approximately 0.9 km^2 (238 acres), which is less than 4% of the total ODSVRA area. Furthermore, three years of imagery had limited photo coverage within the ODSVRA sub-area and, thus, the total area for the calculations differs slightly between years (Table 2).

The OHV riding area used for this report (1584 acres) is per the border of 2013 and includes both the open riding area and the vegetation islands. Since 2013, this area has been changed following implementation of various PMRP.

The South Oso Flaco area (light gray in Figure 1) was analyzed to provide comparison to vegetation dynamics within an area of the ODSVRA that has not seen significant OHV riding for decades (since at least 1982) and, as such, provides insights on a less disturbed and more developed state of vegetation cover and dune geomorphology. The northern border of this area (Figure 1) was chosen due to hydrological changes of the Oso Flaco Creek over the image years.

It is also important to note that invasive plant species are present in ODSVRA and have influenced vegetation cover over time. In the early 1900s, European beach grass (*Ammophila arenaria)* and ice plant (*Carpobrotus edulis*)[5,6] were planted to stabilize sand and dunes around the former La Grande Beach Pavilion. Currently, there are still areas within the ODSVRA and

[5] Guiton-Austin, L. (2011). As cited by Harris, W. California Geological Survey Report, 1 November 2011. "In consideration of Draft Rule 1001 proposed by the San Luis Obispo County Air Pollution Control District: An analysis of wind, soils, and open sand sheet and vegetation acreage in the active dunes of the Callendar Dune Sheet, San Luis Obispo County, California.

[6] Bonk. M. 2010. Mapping Invasive Beachgrass And Veldt Grass In Oceano Dunes Svra Using Multispectral Imagery. CDPR internal report.

Pismo Dunes Natural Preserve that contain these species, as well as invasive South African veldt grass (*Ehrharta calycina*), which is found in backdune areas. Invasive weeds have resulted in increased plant cover and foredune stabilization in ODSVRA. However, since 2009 different removal methods for invasive species have been used (e.g., burning, herbicides, hand-pulling)[7] at various locations.

The classified vegetation raster datasets were used to calculate changes in plant cover over time using the Raster Calculator and Change Detection tools in ArcGIS. From these maps, positive and negative changes were calculated as % values between subsequent image years and over different time periods. For change calculations between years that had limited image coverage, the analysis was conducted only on the area of overlap (union) in both image years. For this report, we focused on three time periods that relate to different land management intervals:

1. 1939-1985: effectively characterizes landscape response during the interval preceding the management of ODSVRA by CDPR, which began in 1982,
2. 1985-2012: captures landscape changes during the management of ODSVRA by CDPR prior to adoption of SLO-APCD Rule 1001 (2011) and related PMRP, and
3. 2012-2020: reflects responses of the ODSVRA landscape following implementation of dust mitigation efforts and PMRP from Rule 1001 and the eventual state SOA (2018).

In addition to these three management intervals, we also characterize changes over the entire 1939 to 2020 period. To the best of our knowledge, the 1939 imagery represents a time prior to OHV activity in the area, and comparison to modern 2020 imagery provides understanding of changes following multiple decades of OHV activity.

Due to the limited image cover of the 1930 image (Table 2), the historical change comparison analysis was done using the 1939 image. To verify the classification of vegetation in this early imagery, the 1939 scene was compared to the 1930 imagery (Figure S1). We found very low differences between the years with less than 7% change (4.1% positive and 2.6% negative) in the total overlapping area of ODSVRA, most of which occurred along the margins of backdune areas (Figures S1 and S2). Some of these changes might also relate to seasonality as the 1930 orthophoto was taken at the end of summer (21 August) while the 1939 imagery was taken in the spring (2 May). All vegetation cover calculations performed for this study are presented in Table S1 in the Supplementary materials at the end of the report.

[7] Glick, R., ODSVRA, Personal communication, October 2021

Table 1. *Imagery available for ODSVRA including metadata and source. Not all available years were used for the analysis due to issues with image projection, size, and/or shadowing that posed limitations for land cover classification (^ grey rows = years not analysed for the report). Asterisk(*) indicates years with limited image coverage (see Table 2).*

Year	Collection date	Resolution (m)	Number of Tiles	Control Points	Transformation Type	Total RMS Forward-Inverse Error (m)	Source	Pixel Depth/Type	Band Number	Mosaic Size (GB)
1930*	Aug-21	0.794	16	12	Spline	0.000	UCSB Library - Geospatial Collection –C-1125A	8 bit unsigned	1	0.299
1939	May-02	0.832	9	27	Spline	0.023	UCSB Library - Geospatial Collection – AXH-1939-ARMY	8 bit unsigned	1	0.136
1949	Mar-31	0.894	NA	24	Spline	<0.001	UCSB Library - Geospatial Collection – AXH-1949	8 bit unsigned	2	0.568
1956	Sep-10	0.937	27	17	3rd Order Polynomial	0.172	UCSB Library - Geospatial Collection –AXH-1956	8 bit unsigned	1	0.617
1960^	Jul-12	0.790	6	13	3rd Order Polynomial	0.125	UCSB Library - Geospatial Collection – HA-GH	8 bit unsigned	1	0.131
1966	Dec-27	1.057	3	NA	NA	NA	UCSB Library - Geospatial Collection – HB-JT	8 bit unsigned	1	0.063
1971*	Jun-13	1.550	2	NA	NA	NA	UCSB Library - Geospatial Collection – HB-SM	8 bit unsigned	1	0.039
1978	Sep-23	1.959	2	19	Spline	0.001	UCSB Library - Geospatial Collection – USDA-40-06079	16 bit unsigned	1	0.068
1985*	May-14	0.149	13	NA	NA	NA	Source unknown – received from CDPR	16 bit unsigned	3	18.980
1994	Feb-28	0.500	1	10	2nd Order Polynomial	0.004	Source unknown – received from CDPR	16 bit unsigned	3	0.879
1998	May-15	0.200	1	12	3rd Order Polynomial	0.036	Source unknown – received from CDPR	8 bit unsigned	4	16.420
2005	Jun-26	1.000	1	11	2nd Order Polynomial	<0.001	NAIP	8 bit unsigned	3	0.524
2007 *^	Jun-01	0.300	1	10	2nd Order Polynomial	0.001	Data obtained from website GlobeXplorer (no longer active).	8 bit unsigned	3	3.320
2010^	Aug-26	1.001	4	11	Spline	0.005	NAIP	8 bit unsigned	4	1.010
2012	May-19	1.000	1	11	2nd Order Polynomial	0.003	NAIP	8 bit unsigned	4	0.697
2014	Sep-24	1.000	1	11	2nd Order Polynomial	NA	NAIP	8 bit unsigned	3	1.640
2016	Aug-07	0.601	1	11	2nd Order Polynomial	0.002	NAIP	8 bit unsigned	4	1.800
2018	Sep-13	0.600	1	0	None	0.000	NAIP	8 bit unsigned	4	0.826
2020	Jun-07	0.600	1	0	Reference	0.000	NAIP	8 bit unsigned	4	1.830

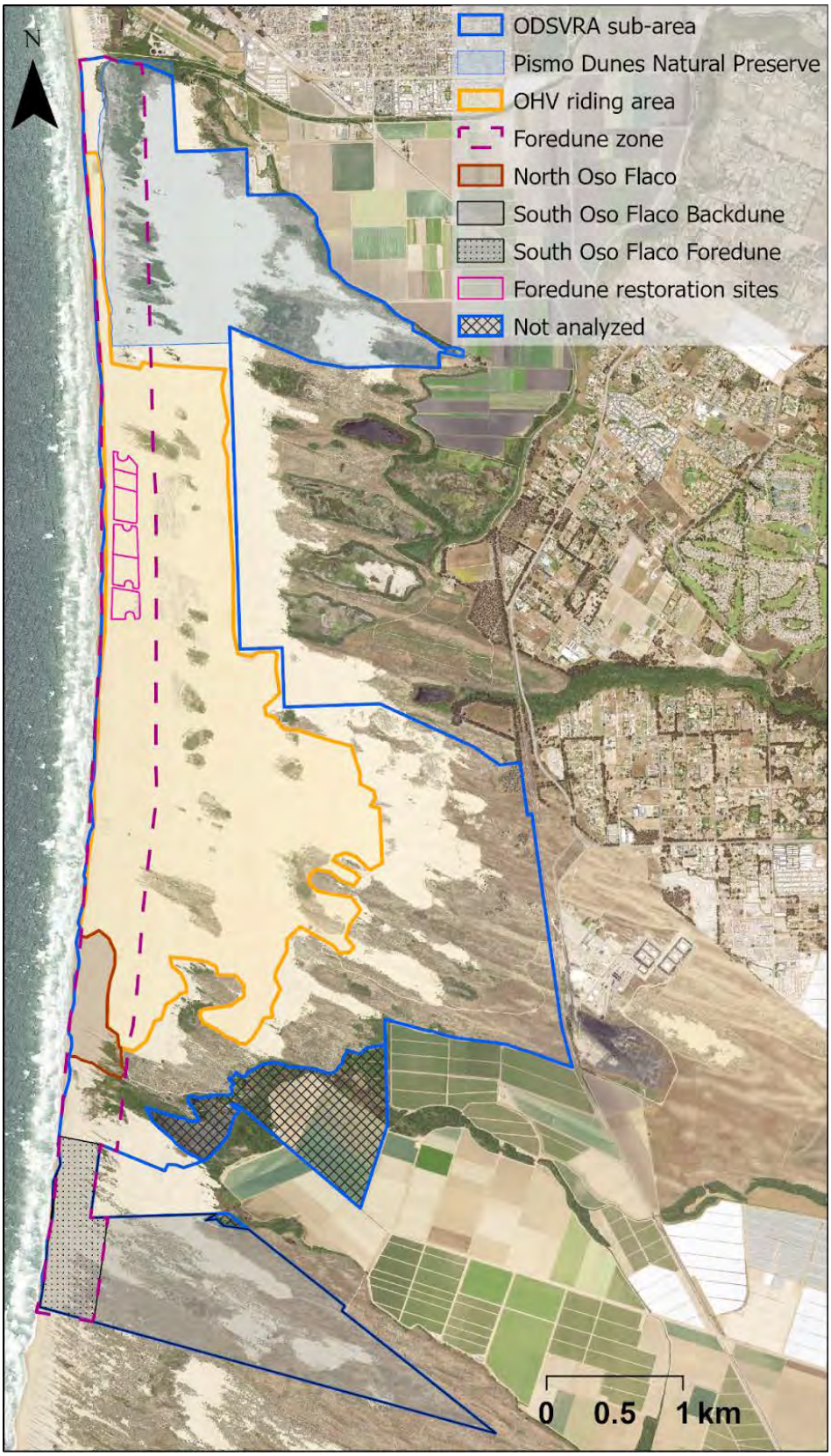

Figure 1. Boundary polygons of the different analytical regions used in the historical vegetation cover change analysis. Orthophoto source from NAIP 2020 (see Table 1).

Table 2. List of image years with limited photo coverage of the ODSVRA sub-area, OHV riding area, and the Oso Flaco area (foredune and backdune) in acres and as a percentage (%). Overall, the sub-area of the ODSVRA is approximately 4215 acres, the OHV riding area is 1584 acres, and the Oso Flaco total area is 577 acres. For specific locations of missing coverage, see Figures S3, S8 and S10 in the supplementary materials.

Area missing						
	ODSVRA sub-area		OHV Riding area		Oso Flaco area	
Year	(acres)	(%)	(acres)	(%)	(acres)	(%)
1930	1108	23.3	338	21.4	0	0.0
1971	348	8.3	0	0.0	243	42.0
1985	9	0.2	0	0.0	9	1.6
Area analyzed						
	ODSVRA sub-area		OHV Riding area		Oso Flaco area	
Year	(acres)	(%)	(acres)	(%)	(acres)	(%)
1930	3107	73.7	1245	78.6	577	100
1971	3866	91.7	1584	100	334	57.3
1985	4206	99.7	1584	100	568	98.4

Our findings (values and maps) were also compared to those derived in previous analyses by CDPR[8,9]. For this comparison, we examined differences within the OHV riding area in four image years (1939, 1978, 2014, 2020) that were also analyzed in the CDPR report. Unfortunately, due to different methods for georeferencing the images, there was no geometric way to compare differences in vegetation patterns for the 1939, 1978, and 2014 maps. We were, however, able to compare the total calculated areas (acres) of vegetation cover between the CDPR reports and our findings. The CDPR reports showed slightly higher values by roughly 3% for 1939 and 2020 images (i.e., 60 and 51 acres, respectively) and by 0.5% (8 acres) for the 1978 images. The 2014 vegetation cover estimates showed essentially negligible differences (<0.1% or 3 acres) between the reports. The greater differences likely result from different methods in the land cover classification process and related quality assurance checks, which can generate uncertainties. Although the magnitude of difference in estimates between these results is relatively small, the location and pattern of differences is notable. For example, in our analysis of the 2020 vegetation cover, the specific locations (pixels) of every shrub, tree, and herbaceous plant were identified systematically by the supervised classification in the GIS, then the pixels were reviewed manually for discrepancies. The CDPR report appears to have taken a different approach by contouring the area around the vegetation as polygons (Figure 2) and, in doing so, included temporary straw cover in the classification in some areas (Figure 3). Our analysis did not include straw cover, only plants, even if they were growing in older straw cover.

[8] Glick, R., ODSVRA,, Personal communication, 2021.
[9] Glick, R., ODSVRA,, 2020, CDF and Oso Flaco Sensors Wind Wedges in Time Series internal report.

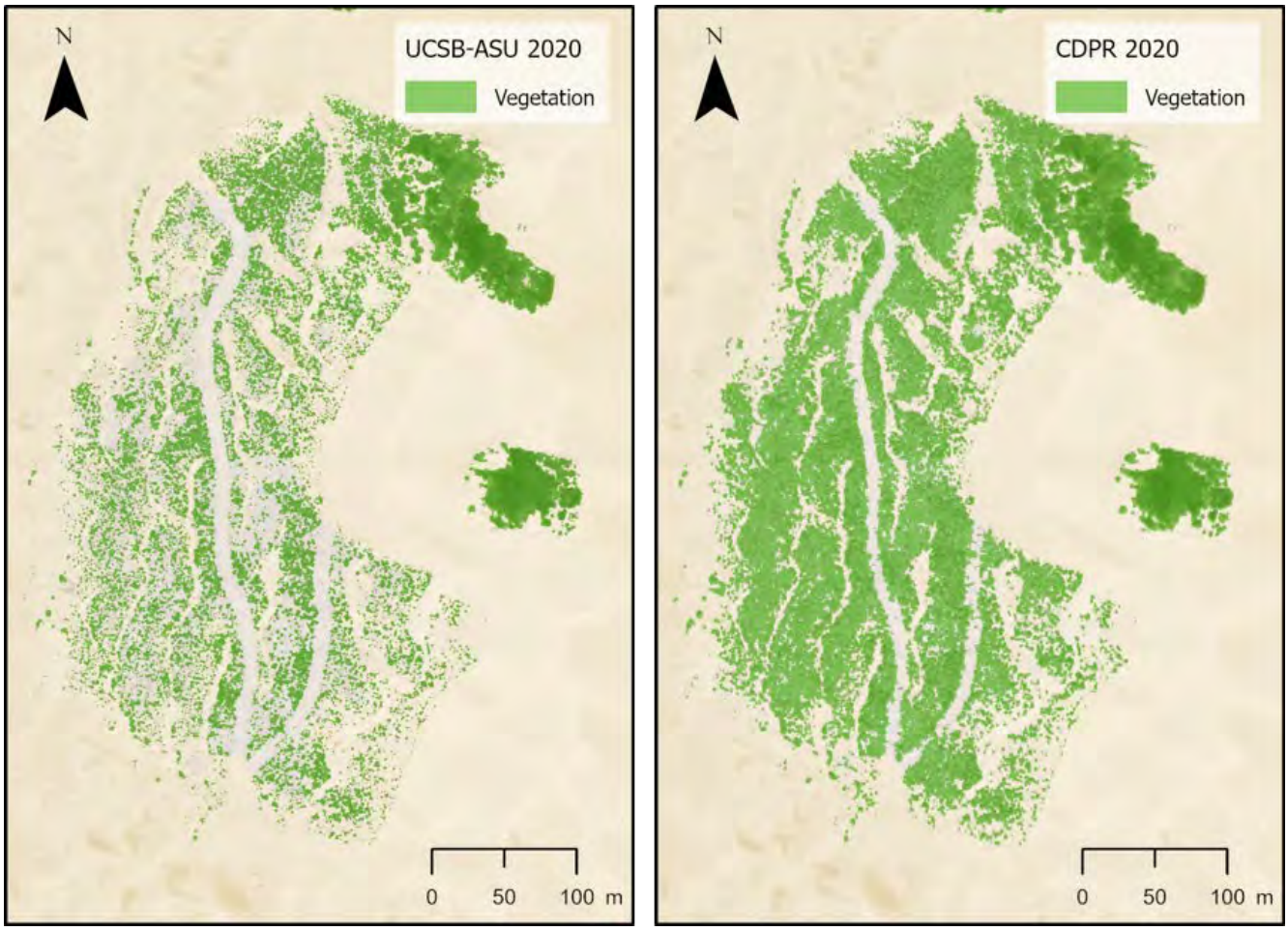

Figure 2. Vegetation cover analysis comparison between the CDPR report (Right) and the current report (Left) for 2020 imagery.

In addition, we tried to compare our findings to those presented in a 2011 report by the California Geological Survey (CGS)[10] that surveyed vegetation cover change between the 1930s and 2010 (Figure S19). In the CGS report, the 1930s dataset used was a combination (mosaic) of image tiles from both 1930 and 1939, while in this report we used tiles only from a single year (1939) that covered the entire sub-area of the ODSVRA. In addition, there were quality issues with the imagery for 2010 that did not allow for proper alignment and classification, so we were unable to conduct a direct comparison of vegetation cover area to the CGS report. A more general comparison of our 1939-2010 results to the CGS change map shows roughly similar plant cover identification (Figures S19 and S20), yet our calculated areas of change are significantly smaller, which could result from different classification methods, multi-year image mosaicing issues, and/or differences in analytical boundaries.

[10] Harris, W.J. 2011. An analysis of wind, soil and open sand sheet and vegetation acreage in the active dunes of the Callender dune sheet, San Luis Obispo County, California. Department of Conservation, California Geological Survey. 10p.

Figure 3. Vegetation cover analysis comparison between the CDPR report (pink) and the current report (green) for 2020 imagery. The arrows indicate areas where there is a straw treatment that was classified by CDPR as vegetation and by UCSB-ASU as non-vegetated area.

3. Results

3.1. Total vegetation cover

Vegetation cover maps for each individual year are presented in the supplemental Figures S3-S18 and the calculated plant coverage by area (km^2 and acres) and percentage values are summarized in Table 3 and Figure 4. The results show that there is a general positive trend of increasing vegetation cover over the years within the analyzed sub-area of the ODSVRA, especially after the mid 1980s (Blue in Figure 4). Between the early years of 1939 and 1949, there was a slight decrease in plant cover

(from 25 to 24%), followed by a gradual increase in vegetation on the dunes up to the mid-1960s (27%). Between the 1960s and 1980s, plant cover declined to values close to that of 1949 (between 1001 and 1033 acres, or around 24%, see values in Table 3 and Table S1). This trend then shifts to a gradual increase in vegetation after 1985 to a peak value of 37% (1569 acres) in 2012.

Within the OHV riding area, vegetation cover is generally much lower than in the broader ODSVRA sub-area and the post-1960s decline in cover is more pronounced with a steady reduction from a peak value of about 196 acres (12%) in 1966 to only 61 acres (4%) in 1985 (orange in Figure 4). After 1985, a slow gradual increase in plant cover was observed in the OHV riding area to 128 acres (8%) by 2020, which remains approximately 67 acres below the peak value in 1966, when the decline in cover began. This does not include the new 48-acre foredune restoration site, however, which did not exist when the 2020 NAIP imagery was captured. As of 2021, plant cover within the foredune restoration area had an average of approximately 2.7%[11], as discussed further in section 3.2 below.

The South and North Oso Flaco areas (light gray and brown in Figure 1, respectively) were also analyzed to provide comparison to vegetation dynamics areas of the ODSVRA that have not seen significant OHV riding for decades (since at least 1982 in S. Oso Flaco). As such, these sites provide insights on a less disturbed and more developed state of vegetation cover and dune geomorphology. At south Oso Flaco, plant cover is substantially higher than other areas of the ODSVRA, showing a general positive trend (Figure 4) from 37 % in 1930 to 66% in 2012 (212 and 373 acres, respectively). Between 1930 and 1949, there was a small decline in plant cover to a historic low of 34% (197 acres). In contrast, plant cover in the OHV riding area has not exceeded 13% over the period of analysis. The area analyzed at south Oso Flaco represents approximately 14% of the total ODSVRA sub-area, yet it contains 14-34% of the vegetation within the park. For comparison, the OHV riding area is just over 37% of the ODSVRA sub-area but contains only 6-18% of the total vegetation, depending on the year.

The north Oso Flaco foredune complex shows a gradual increase in plant cover over time from less than 1% in 1930 to a peak of 24% in 2012, and after that plant cover declined but remained over 19%. The north Oso Flaco site consists only of foredune vegetation, which is generally more exposed to disturbance (natural and anthropogenic), yet plant cover at this site is consistently higher than that in the OHV riding area, which also includes large backdune vegetation.

[11] Hilgendorf, Z., Turner, C., & Walker., I.J. 2021. UCSB-ASU 2020-2021 ODSVRA Foredune Restoration UAS Survey. Report from UCSB and ASU submitted to CDPR.

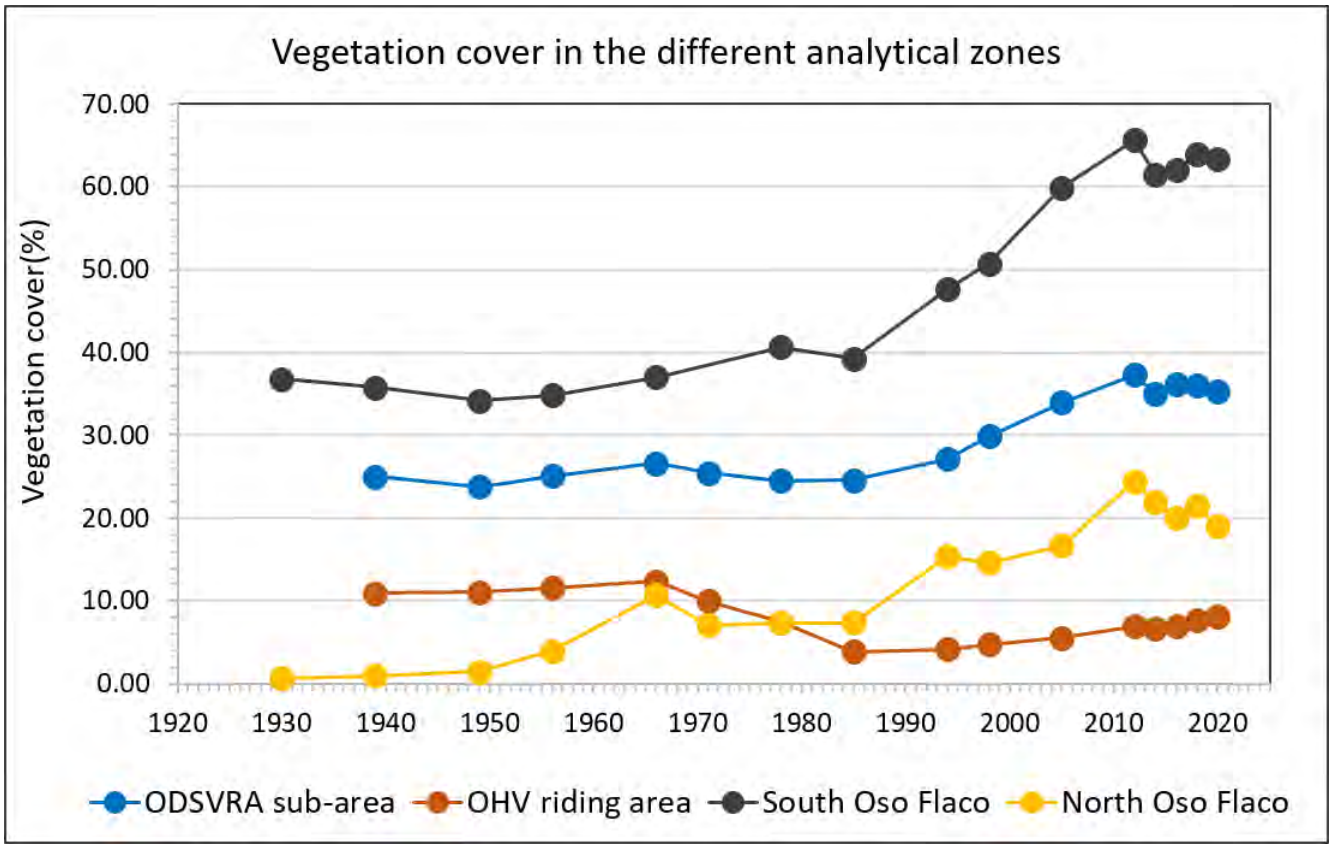

Figure 4. Time series of total vegetation cover (foredune + non-foredune vegetation in Table 3) as a percentage (%) of the ODSVRA sub-area at large (blue), the OHV riding area (orange), South Oso Flaco area (gray), and North Oso Flaco (yellow, foredune vegetation only). Percent cover values are derived as a proportion of the respective areas of each analytical region. Due to limited imagery coverage (Table 2), the 1930 photo year was not included in the ODSVRA sub-area and OHV riding area curves and 1971 was not included for South Oso Flaco (black).

Table 3. Calculated land cover values for vegetation and non-vegetated areas from each image year in the ODSVRA sub-area, OHV riding area, southern Oso Flaco , and the north Oso Flaco area. Values are provided for vegetation in the foredune zone and for other back dune areas (see boundaries in Figure 1). Asterisk (*) represents limited imagery for 1930, 1971, and 1985 (Table 2), resulting values are derived from smaller areas than outlined in Figure 1. All values presented are in relation to the entire area of each analyzed zone (to a total of 100%). Values relative to specific areas within each of these broader areas (e.g., foredune zones) are shown in Figure 5 (Section 3.2) and provided in Table S1 (supplementary materials).

		ODSVRA sub-area			OHV riding area			South Oso Flaco			North Oso Flaco	
		Vegetated		Non vegetated	Vegetated		Non vegetated	Vegetated		Non vegetated	Vegetated	Non vegetated
		Foredune	Backdune		Foredune	Backdune		Foredune	Backdune		Foredune	
1930*	km^2 (acres)	0.07 (16)*	3.37 (832)*	9.14 (2258)*	0.03 (8)*	0.48 (118)*	4.53 (1120)*	0.02 (6)	0.84 (207)	1.48 (365)	0.002 (0.4)	0.28 (68)
	%	0.52*	26.79*	72.69*	0.63*	9.46*	89.91*	0.95	35.83	63.21	0.69	99.31
1939	km^2 (acres)	0.13 (32)	4.14 (1023)	12.78 (3159)	0.05 (12)	0.07 (161)	5.71 (1411)	0.01 (6)	0.83 (204)	1.50 (371)	0.003 (0.7)	0.28 (68)
	%	0.76	24.29	74.95	0.77	10.16	89.08	0.45	35.35	64.2	0.95	99.05
1949	km^2 (acres)	0.23 (57)	3.82 (944)	13.01 (3214)	0.08 (19)	0.63 (157)	5.70 (1408)	0.02 (5)	0.78 (192)	1.54 (380)	0.004 (1)	0.27 (68)
	%	1.34	22.4	76.25	1.18	9.89	88.93	0.84	33.32	65.84	1.49	98.51
1956	km^2 (acres)	0.33 (82)	3.95 (977)	12.78 (3159)	0.07 (16)	0.68 (167)	5.67 (1401)	0.03 (7)	0.78 (194)	1.52 (376)	0.01 (3)	0.26 (66)
	%	1.94	23.17	74.89	1.03	10.56	88.41	1.30	33.52	65.18	3.96	96.04
1966	km^2 (acres)	0.45 (111)	4.09 (1011)	12.52 (3093)	0.10 (24)	0.70 (172)	5.62 (1388)	0.08 (19)	0.79 (195)	1.47 (364)	0.03 (7)	0.25 (61)
	%	2.64	23.99	73.37	1.51	10.85	87.64	3.28	33.71	63.00	10.72	89.28
1971*	km^2 (acres)	0.15 (36)*	3.83 (947)*	11.67 (2883)*	0.03 (9)	0.60 (149)	5.77 (1426)	N/A	0.75 (185)*	1.59 (392)*	0.01 (2)	0.27 (66)
	%	0.93*	24.5*	74.57*	0.54	9.42	90.04	N/A	32.09*	67.91*	3.37	96.63
1978	km^2 (acres)	0.43 (106)	3.75 (927)	12.88 (3182)	0.05 (13)	0.42 (105)	5.93 (1466)	0.09 (23)	0.86 (212)	1.39 (343)	0.02 (5)	0.26 (64)
	%	2.52	21.99	75.49	0.84	6.6	92.56	3.98	36.67	59.36	7.33	92.67
1985*	km^2 (acres)	0.42 (105)*	3.76 (928)*	12.88 (3182)*	0.01 (4)	0.23 (58)	6.16 (1523)	0.07 (18)*	0.83 (205)*	1.40 (345)*	0.02 (5)	0.26 (64)
	%	2.49*	22.02*	75.49*	0.23	3.64	96.13	3.08*	36.15*	60.77*	7.34	92.66
1994	km^2 (acres)	0.50 (125)	4.11 (1016)	12.40 (3065)	0.01 (2)	0.25 (63)	6.15 (1519)	0.11 (26)	0.99 (244)	1.20 (298)	0.02 (5)	0.26 (64)
	%	2.97	24.16	72.87	0.16	3.98	95.87	4.62	42.97	52.41	7.34	92.66
1998	km^2 (acres)	0.54 (133)	4.54 (1122)	11.94 (2950)	0.02 (4)	0.29 (71)	6.11 (1509)	0.11 (28)	1.05 (260)	1.13 (280)	0.04 (10)	0.24 (59)
	%	3.17	26.68	70.15	0.25	4.49	95.26	4.85	45.86	49.29	14.62	85.38
2005	km^2 (acres)	0.70 (173)	5.08 (1254)	11.24 (2778)	0.02 (6)	0.33 (82)	6.05 (1496)	0.15 (38)	1.10 (250)	1.13 (280)	0.05 (11)	0.23 (57)
	%	4.12	29.83	66.05	0.37	5.20	94.43	6.66	44.04	49.29	16.63	83.36
2012	km^2 (acres)	0.81 (200)	5.54 (1369)	10.67 (2637)	0.04 (9)	0.40 (100)	5.97 (1475)	0.16 (40)	1.25 (309)	0.89 (219)	0.07 (18)	0.21 (52)
	%	4.75	32.56	62.69	0.60	6.31	93.09	7.12	54.36	38.52	24.41	75.95
2014	km^2 (acres)	0.69 (170)	5.28 (1304)	11.05 (2732)	0.04 (10)	0.39 (95)	5.98 (1479)	0.15 (36)	1.27 (313)	0.89 (219)	0.06 (15)	0.22 (54)
	%	4.05	31.00	64.95	0.64	6.01	93.35	6.34	55.14	38.52	21.87	78.13
2016	km^2 (acres)	0.70 (173)	5.24 (1296)	11.08 (2737)	0.04 (10)	0.40 (99)	5.97 (1475)	0.14 (34)	1.29 (318)	0.87 (216)	0.06 (14)	0.22 (55)
	%	4.12	30.81	65.08	0.64	6.25	93.11	6.04	55.98	37.98	20.00	80.00
2018	km^2 (acres)	0.68 (168)	5.46 (1348)	10.88 (2689)	0.04 (10)	0.45 (111)	5.92 (1463)	0.14 (36)	1.32 (327)	0.83 (205)	0.06 (15)	0.22 (54)
	%	3.99	32.06	36.95	0.63	7.00	92.37	6.27	57.60	36.12	21.46	78.54
2020	km^2 (acres)	0.64 (157)	5.37 (1328)	11.01 (2720)	0.04 (11)	0.47 (117)	5.89 (1456)	0.12 (30)	1.33 (330)	0.84 (208)	0.05 (13)	0.22 (55)
	%	3.74	31.58	64.68	0.67	7.4	91.93	5.27	58.05	36.68	19.05	80.95

3.2. *Changes in vegetation cover in the foredune zone*

As plant communities, geomorphology, and other ecological processes within foredune ecosystems are distinctly different from those in the larger transgressive dunes, parabolic dunes, and interdune swales in the broader ODSVRA landscape, a separate analysis of vegetation cover was conducted for the foredune zone (see Section 2 and Figure 1). Values presented in this section are specific to the foredune zone within each of the larger analytical regions and are not a proportion of the larger zones themselves (see values in Table S1 in the supplementary materials).

Vegetation cover trends within the foredune zone (Figure 5) are generally similar to those within the broader ODSVRA sub-area and OHV riding areas described above (Figure 4). Peak values (and years) of foredune plant cover within ODSVRA, the OHV riding area, and at the south and north Oso Flaco reference sites are 21% (2012), 5% (1966), 36% (2012) and 24% (2012), respectively. Foredune vegetation cover within the entire ODSVRA sub-area shows a general increase over time, with high positive rates of change from a historic low in 1939 (3.3%) to 1966 (from 32 to 111 acres) and between 1998 and 2012 (133 to 200 acres). From 2012 to 2020, however, there was a net loss of 49 acres of vegetation (from 21% to 16% cover, blue in Figure 5), some of which results from removal of invasive grass species (e.g., *Ammophila breviligulata* or European beach grass) from foredunes in the northern area of the ODSVRA[12].

Within the OHV riding area, foredune vegetation shows an increase in cover from approximately 2.6% (12 acres) in 1939 to 5.3% (24 acres) in 1966 (orange in Figure 5B, Table S1). From 1966 to 1994, plant cover declined sharply to 0.5%, which is well below the historic 1939 value. Since 1998, vegetation cover has risen gradually to about 2.3% by 2020 (Figure 5).

It is important to note that all orthophotos from 2005-2020 were taken during the period of nesting for the Western Snowy Plover (March through September), which results in up to 70% of the foredune zone in the OHV riding area (or roughly 20% of the overall riding area) being closed to OHV traffic and camping for 7 months (see borders in Figure 7). Since 2005, plant cover within the bird nesting enclosure increased from negligible to over 1% by 2012 (Figure S21). From the historic analysis, it seems that the last time vegetation cover was over 1% in this area was in the late 1970s, which is also a big decrease from the early 1930s when this area had over 10% vegetation cover (Figure S21).

At the south Oso Flaco reference site, foredune vegetation cover between 1939 and 1949 (2.4% and 4.3%, respectively) is comparable to that in the foredune zone of the OHV riding area (2.6% and 4.1%, respectively). After this, plant cover remains consistently and appreciably higher at Oso Flaco than in other foredune zones, especially in the OHV riding area (Figure 5). As

[12] Glick, R., ODSVRA, Personal communication, 2021.

in the larger ODSVRA sub-area, foredune vegetation cover at south Oso Flaco shows a positive trend over time to a peak in 2012. Comparatively then, Figure 5 indicates that foredunes at south Oso Flaco that were not subjected to the same amount of OHV activity as that in the nearby riding areas of ODSVRA (at least since 1982) have maintained significantly higher vegetation cover, particularly between 1985 and 2005 (see also Table S1; Figures S3-S18). It is worth noting that the decrease in foredune plant cover following 2012 is partly related to CDPR efforts to remove invasive *Ammophila arenaria* and other weeds, mostly at south Oso Flaco[12].

North Oso Flaco had very low vegetation cover (less than 2%) up to the 1950s, then gradually rose to a peak of 10% in 1966. Following this, plant cover decreased to 7% from 1971 to 1985, then rose to a historic peak of 24% in 2012 (Figure 5). The North Oso Flaco area has been fenced to exclude OHV activity since 1982, which largely explains the rise in vegetation growth since 1985.

Although plant cover within the broader ODSVRA and in both north and south Oso Flaco sites has gradually increased over time, vegetation within the OHV riding area, and its foredune zone in particular, have shown steady declines since 1966 (Figure 5). This corresponds with an era of increasing recreational OHV activity in the region that began in the 1950s[13].

Another area of interest for detecting changes in foredune vegetation cover is within the newly implemented (2020) 48-acre foredune restoration site in the OHV riding area. (Figures 1, 5). Historical plant cover in this area shows a similar trend to that of the foredune zone in the larger OHV riding area with a decline in cover from almost 2% in 1949 to essentially zero cover in 1985. Since then there has been no detectable change in plant cover at the foredune restoration sites until after implementation of the restoration treatments in February 2020. The 2020 NAIP imagery used in this analysis does not reflect these treatments, however.

An independent report by UCSB and ASU[14] explores more recent changes in vegetation cover within the foredune restoration site captured from aerial UAS surveys between October 2019 and February 2021. The report shows that, as of February 2021, plant cover increased to an average of approximately 2% (ranging from 0.04 to 4.91%, depending on treatment type).

[13] Guiton-Austin, L. 2011. As cited by Harris, W. California Geological Survey Report, 1 November 2011. "In consideration of Draft Rule 1001 proposed by the San Luis Obispo County Air Pollution Control District: An analysis of wind, soils, and open sand sheet and vegetation acreage in the active dunes of the Callendar Dune Sheet, San Luis Obispo County, California.

[14] Hilgendorf, Z., Turner, C, Walker, I.J. UCSB-ASU 2020-2021 ODSVRA Foredune Restoration UAS Survey Report. 37p. Produced for CDPR-ODSVRA and published as Attachment 8 in the 2021 ARWP.

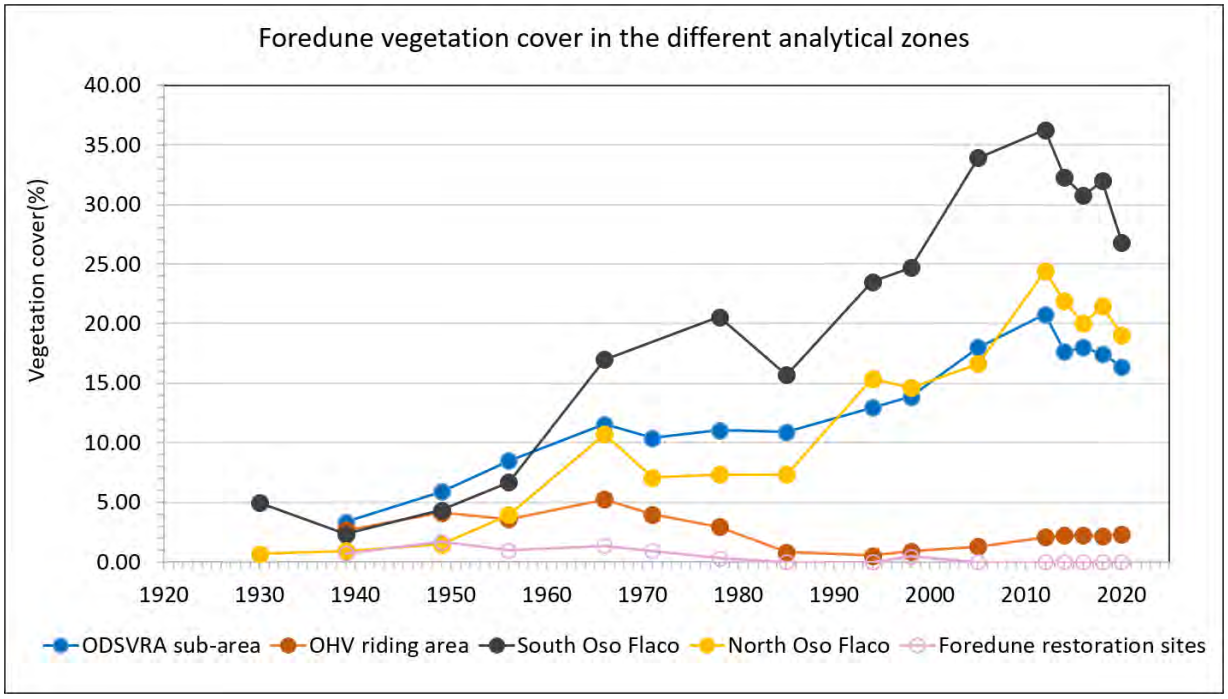

Figure 5. Percent vegetation cover within the foredune zone in the ODSVRA sub-area (Blue), OHV riding area (Orange), southern Oso Flaco area (Gray), and north Oso Flaco (Yellow). Values are relative to areas of the foredune zone within each analytical zone (calculations in Table S1). Plant cover within the foredune restoration zone is shown for comparison (Pink). Due to limited coverage of imagery (Table 2), the 1930 image was not included in the ODSVRA sub-area and OHV riding area curves and 1971 was not included in the ODSVRA sub-area and South Oso Flaco analysis (black).

3.3. Change detection between years

Changes in vegetation coverage between photo years are presented both as change maps (Figures S22-S35) and as plots of rates of positive or negative change over time (% yr^{-1}) (Figure 6), which generally reflect dynamism in plant cover over time. It is noted, however, that change calculations derived by comparing two points over time (i.e. two different image years) inevitably precludes interpretation of changes during the intervening years. This said, there is interpretive value in estimating rates of change between image years particularly given the varying intervals between the photos.

Figure 6 shows negative or positive change rates derived from the number of pixels that either lost or gained vegetation from the earlier image year, respectively, divided by the number of years between the images. Within the broader ODSVRA sub-area, there is an increasing trend in the total amount of change/year between the 1930s to the 1980s, with mainly negative changes (losses) in plant cover from 1966 to 1985, after which more positive changes (gains) occur (Figure 6A). Between 2012 to 2020, there is a large increase in the amount of total change, however, a large portion of this is negative, mostly between 2012-2016 (Figure 6A). Much of the negative change in these years occurs in areas that experienced removal of invasive species (e.g., the Pismo Dunes Natural Preserve and south Oso Flaco areas, see Figures S32, S33) between 2012 and 2015. In addition, some of the detected changes between 2012 and 2014 reflect the time of year when the imagery was taken. The 2012 orthophoto was taken in the middle of May (late spring) when vegetation is in full growth stage (and easier to identify and classify using aerial photo analysis), while the 2014 orthophotos were taken in late September at the end of the growing season, so there is potential for subtle seasonal differences based on time of photo acquisition (Table 1; Figure 6).

In the OHV riding area, there is a similar trend to the larger ODSVRA - before 1985 the majority of changes were negative and after 1985 the changes were largely positive (Figure 6B). Between 1985 and 2005, the change rates are very small (<0.3% yr^{-1}) compared to other analytical zones. Most of the positive changes in the OHV riding area occur after 2005 (Figure 4) largely related to new plants along the margins of fenced vegetation islands, and foredune vegetation establishing in the seasonal bird nesting enclosure area (Figure 7; Figures S31-S35). The reduction of OHV disturbance offered by the seasonal bird nesting enclosures since 2005 corresponds with increases in foredune vegetation cover of about 1% with only 0.1% negative change between 2005 and 2020 (0.07% yr^{-1} and 0.01% yr^{-1}, respectively).

At south Oso Flaco, there is a similar net pattern in the total amount of change as in the other analytical zones (Figure 6C). However, up to 1985 there is generally a more balanced occurrence of positive and negative changes between most years. Following 1985, for the most part, there are more positive changes and between 2012 and 2020, the change rates increase to

over 5% yr^{-1} (Figure 6C). Most of this change occurs around the edges of existing vegetation in both backdune and foredune areas (Figures 8). The backdune zone of south Oso Flaco shows mainly positive rates of change up to 2012 (Figure 8B). The south Oso flaco foredune zone shows a similar trend to the backdune area (Figure 8B), however, the rates of change in the foredune were much higher in all years (Figure 8A and 8B).

In the north Oso Flaco foredune complex, a positive trend of change occurs up to 1966, then shifts to more negative change rates up to 1985 (Figure 6D). Following the closure of the area in the early 1980s, north Oso Flaco showed a strong positive trend of increase. North Oso Flaco shows the highest amount of change between 2012 and 2020 compared to the other analytical zones, peaking at over 7% yr^{-1} of total change between 2012 and 2014 (Figure 6D).

Figures 9-15 provide a focused analysis of vegetation changes during the three broader time periods identified in Section 2. During the 1939-1985 period, roughly prior to the management of ODSVRA by CDPR (in 1982) the total amount of change in the ODSVRA sub-area is relatively high at 18.2%, but this translates to a change rate of only 0.4% yr^{-1} (Figures 9A and 10). The majority of positive change appears mostly between 1966 and 1985 (Figure 6A). Between 1985 and 2012, this area showed increasing positive change rates in plant cover (14.9% or 0.55% yr^{-1}) with only 1.8% loss (0.07% yr^{-1}) (Figure 9A). Many of the areas of negative change between 1939 and 1985 showed subsequent vegetation growth in 2012 (Figures 9A, 10, 11). As above, most of this change occurred in areas subjected to restoration activities implemented by CDPR between 2005 and 2012 (Section 3.3; Figure 6). From 2012 to 2020, a comparatively low amount of total change was observed (8%) with equal amounts of positive and negative change (Figure 9A and 12), yet the rates of change were among the highest (total of 1% yr^{-1}).

Within the OHV riding area (Figure 9B), there is a declining trend in the total amount of change over time. From 1939 to 1985, there was a proportionately large negative change (9.5%) in plant cover in both foredune and backdune zones (Figures 10 and 13). From 1985 to 2012, there was a shift toward proportionately greater positive change (4.4%) with only 1.3% negative change (Figure 10B), mainly around existing vegetation islands in the backdune area (Figures 11 and 14). Between 2012 and 2020, the total amount of change in the riding area is relatively small (3.3%) and mostly positive (2.2%) (Figure 9B), resulting from vegetation growth in backdune restoration areas (straw treatments) implemented by CDPR (Figure 15). Rates of change are moderate (~0.2% yr^{-1}) for both 1939-1985 and 1985-2012 with only 0.2% yr^{-1} and 0.05% yr^{-1} negative change rates, respectively. Between 2012 and 2020 the change rate is slightly higher at 0.4% yr^{-1} with over 0.3% yr^{-1} positive change.

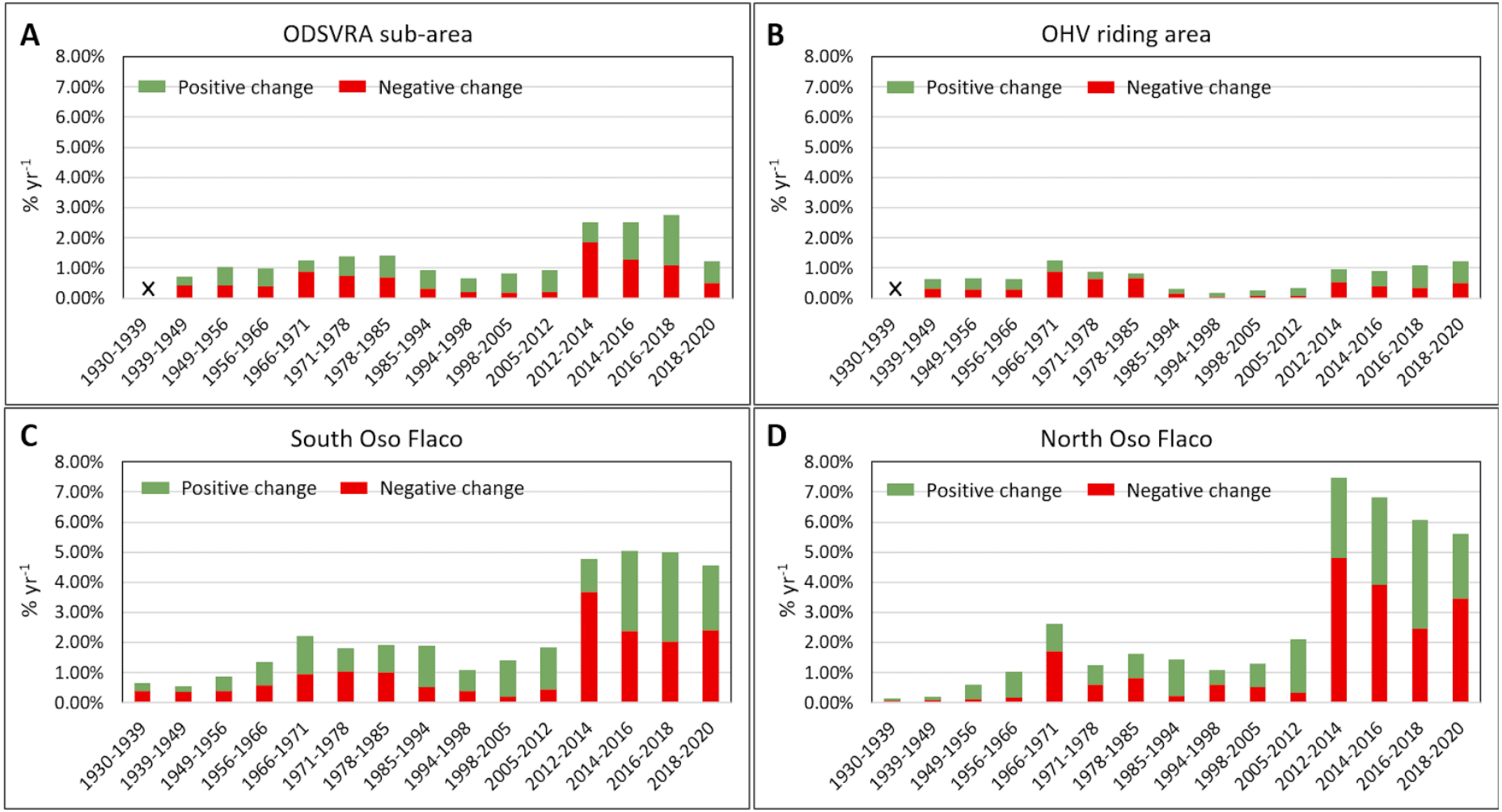

Figure 6. Positive and negative percent change per year (% yr^{-1}) in vegetation between successive imagery years in the entire ODSVRA sub-area (A), OHV riding area (B), southern Oso Flaco area (C), and north Oso Flaco (D) relative to areas of each analytical zone. Areas with no change between years are not shown (hence, values do not total 100%). Due to limited coverage of imagery (Table 2), the 1930 was not included in the ODSVRA sub-area and OHV riding area change analysis (black X sign). In 1971 and 1985, the limited image coverage in the ODSVRA sub-area and south Oso Flaco resulted in some missing data (see Table 2, Figures S8, S10) and possible underestimates of change.

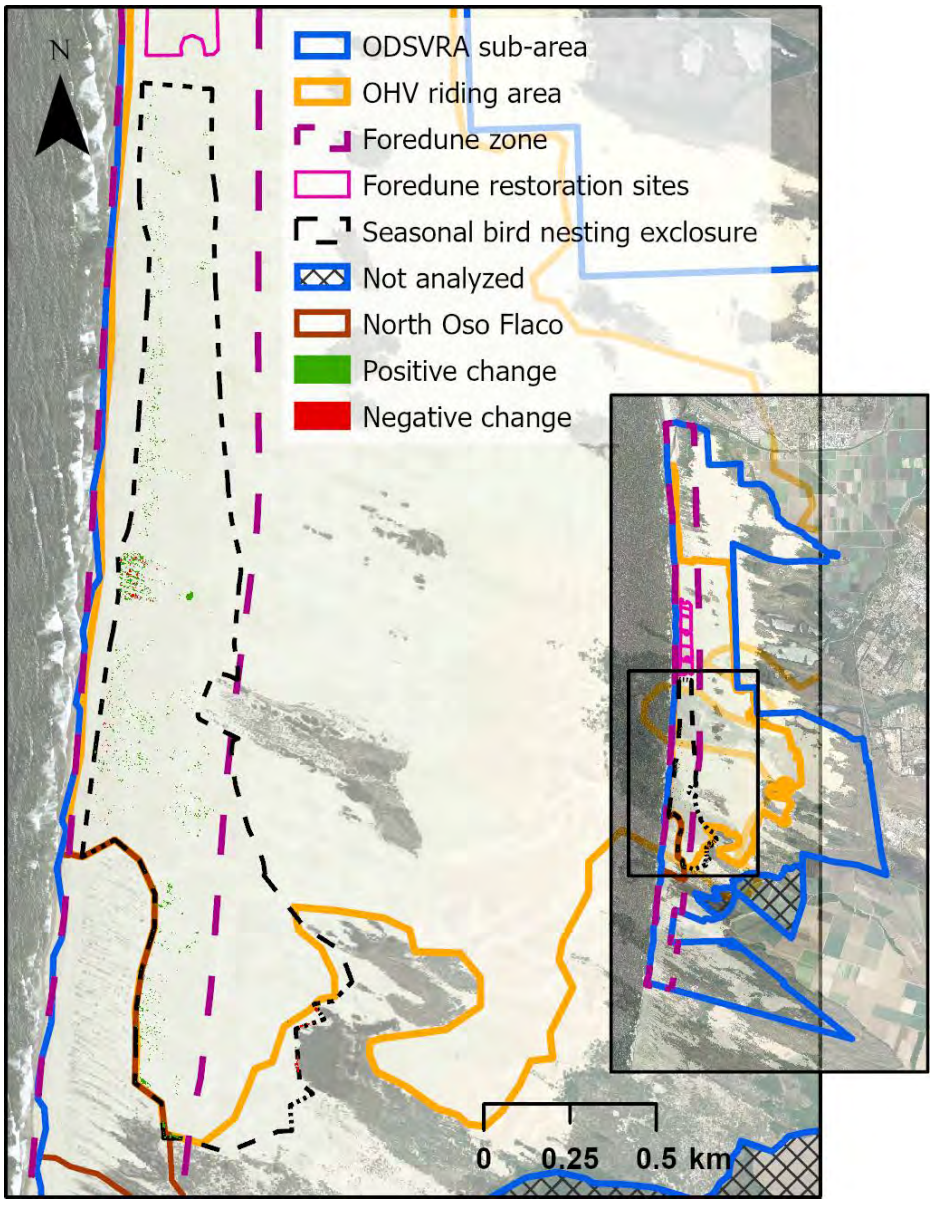

Figure 7. Change map between 2005 and 2020 of the seasonal bird nesting exclosure area (black dashed line) that have been fenced off to OHV activity since 1982[15]. Change map is shown on the 2005 orthophoto.

[15] Glick, R., ODSVRA,, Personal communication, 2021.

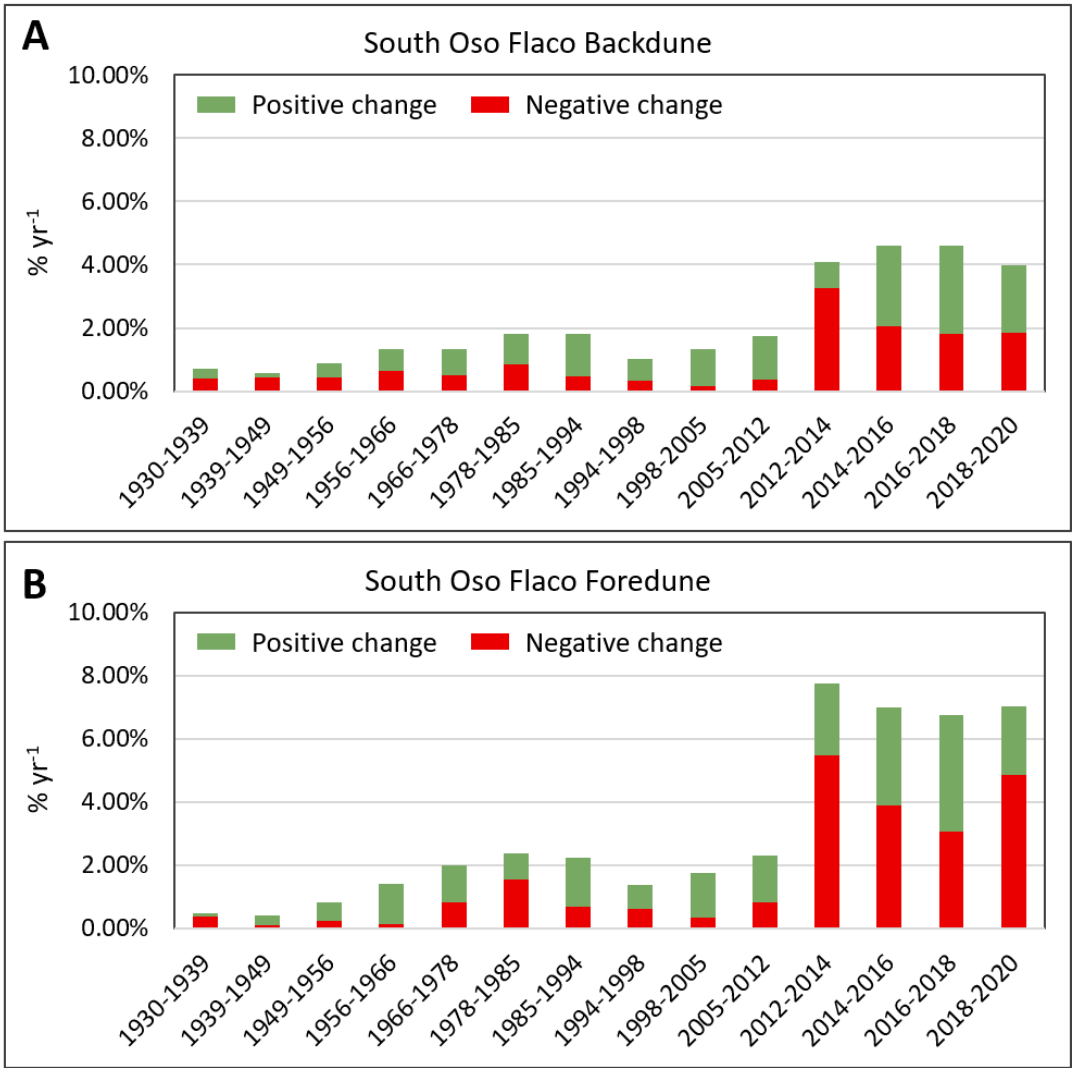

Figure 8. Positive and negative percent change rates (% yr^{-1}) in vegetation between successive imagery years in the southern Oso Flaco backdune (A) and foredune (B) zones relative to areas of each analytical zone. Areas with no change between years are not shown (hence, values do not total 100%). Limited image coverage in 1985 resulted in some missing data (see Table 2, Figure S8) and possible underestimates of change. There was very limited coverage for 1971 and so this year was excluded and an analysis of 1966-1978 was done instead.

At southern Oso Flaco, between 1939 and 1985, the total change in backdune and foredune areas was 22.4% with mostly gains (13.9%) (Figure 9C). Most of the losses occurred in the backdune area between 1966 and 1985 (Figures 6C, 8-10). Between 1985 and 2012, there was a high amount of total change of 32.8% (1.2% yr^{-1}), most of which (30.0%) was positive (Figure 9C) and occurred in the backdune zone and on the landward (eastern) side of the foredune, whereas higher vegetation loss is evident on the shoreward side of the foredune (Figure 11). Between 2012 and 2020, there was 12.1% total change, which is relatively low

compared to previous years, but still high compared to other analytical zones (Figures 9) and at a faster rate of change (1.5% yr^{-1}) than the previous interval. Most of this change was vegetation loss (7.7%) in the Oso Flaco foredune zone and around existing vegetation in the backdune zone (Figures 9C, 12, 15). According to CDPR staff, some of this recent decline in plant cover at south Oso Flaco relates to removal of invasive grasses between 2009 and 2020.

The north Oso Flaco foredune complex shows a comparatively lower total amount of change between 1939 and 1985 (8.4%) with mostly positive changes (7.8%) (Figure 9D). The positive trend continued between 1985 and 2012, with a higher amount of total change (26% or 0.96% yr^{-1}), most of which (23.6%) was positive (Figure 9D). An invasive weed analysis performed by CDPR in 2010[16] suggests that the north Oso Flaco area did not host any invasive species that were found in other foredune and backdune areas in the park. As such, the high positive changes between 1985 and 2012 can be attributed mostly to growth and expansion of native plants in the absence of vehicle activity and other anthropogenic disturbances. Between 2012 to 2020, however, there is mostly negative change in plant cover (11%) with only 3.6% gains.

For this report we used the 1939 orthophoto to represent an era prior to widespread OHV riding in the ODSVRA. Some accounts suggest that intensive riding in the area began in the 1950s[17]. Calculating changes in plant cover between 1939 and 2020 provides a comprehensive look at overall influences and changes that took place in the ODSVRA, including the combined impacts of land management by CDPR and the impact of OHV riding and other human activities over the last 9 decades. The results show that over this period there is a general increase in plant cover in the broader ODSVRA sub-area and in the north and south Oso Flaco reference areas (Figure 16). In the ODSVRA, there is an overall increase of 17.8% plant cover vs. 7% loss. Most of the vegetation gain was in the backdune area and in the Pismo Dunes Natural Preserve, the broader south Oso flaco dune complex, and in backdune areas outside of the riding area (Figure 17). These areas were also found to be affected by growth of invasive weeds. According to a CDPR weed digitizing effort in 2010[16], invasive weeds (beach grass and veldt grass) in 2010 occupied less than 10% of the total vegetation cover within the broader ODSVRA sub-area (134 acres), about 14% of the plant cover in south Oso Flaco (310 acres), and 18% of the vegetation in the Pismo Dunes Nature Preserve (381 acres). It should be noted, however, that since 2010 there has been an increasing effort by the CDPR to remove invasive species in these areas.

[16] Bonk. M. 2010. Mapping Invasive Beachgrass And Veldt Grass In Oceano Dunes Svra Using Multispectral Imagery. CDPR internal report.

[17] Guiton-Austin, L. 2011. As cited by Harris, W. California Geological Survey Report, 1 November 2011. "In consideration of Draft Rule 1001 proposed by the San Luis Obispo County Air Pollution Control District: An analysis of wind, soils, and open sand sheet and vegetation acreage in the active dunes of the Callendar Dune Sheet, San Luis Obispo County, California.

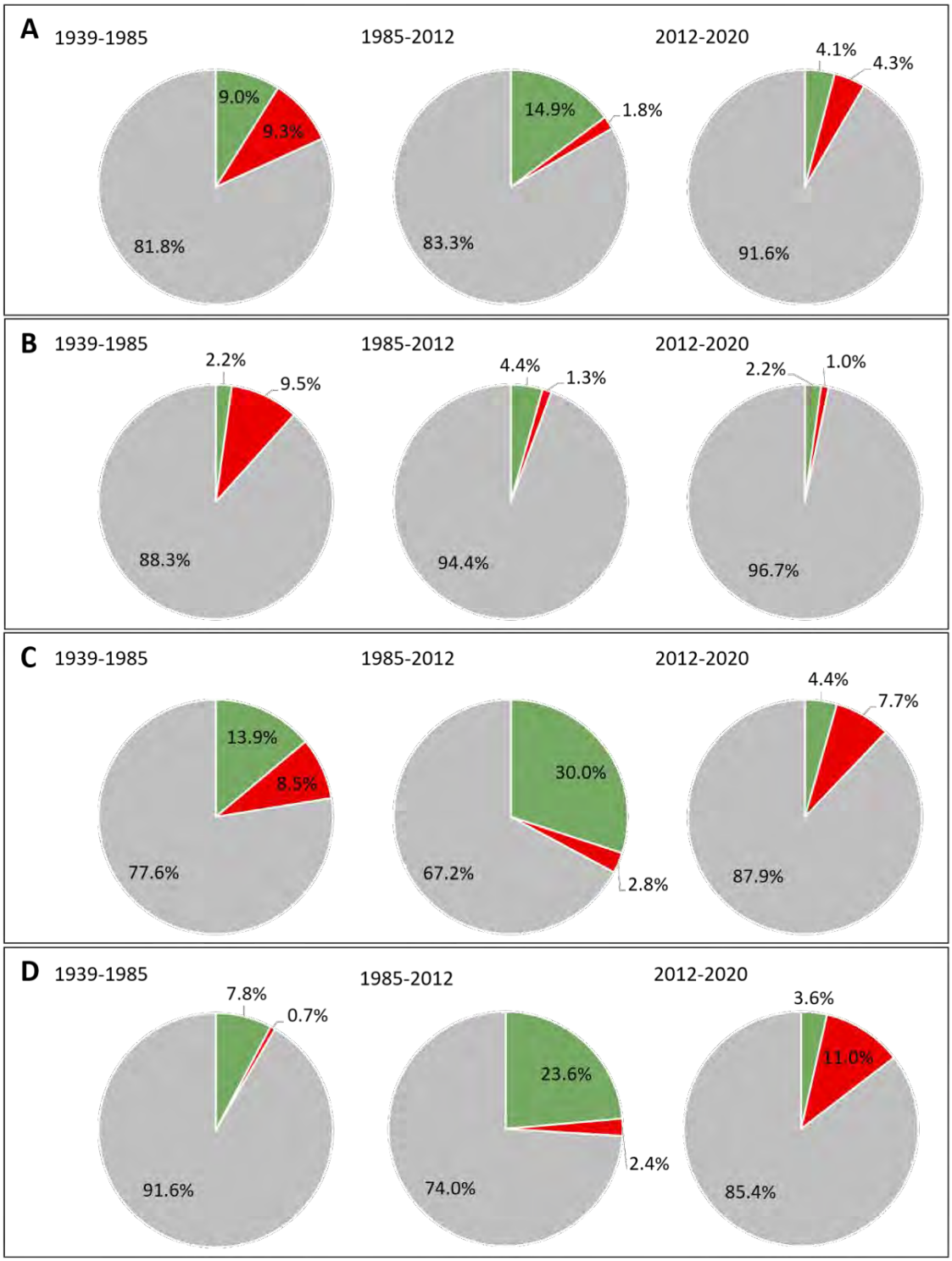

Figure 9. Change analysis (%) of vegetation cover in ODSVRA sub-area (A), OHV riding area (B), south Oso Flaco (C), and area north Oso Flaco (D) during three important management time intervals: i) 1939-1985, ii) 1985-2012, and iii) 2012-2020, as described in Section 2.

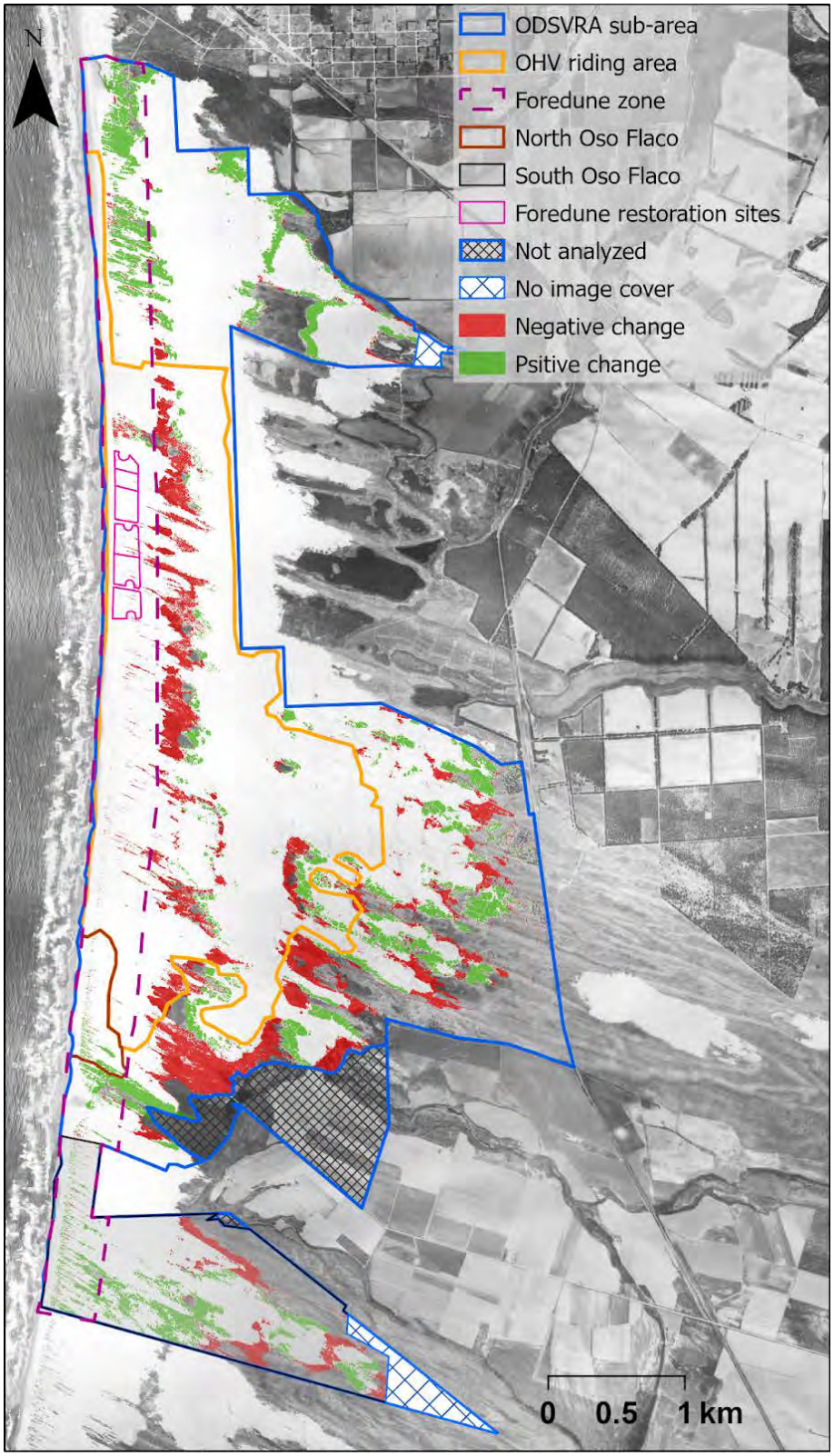

Figure 10. Change in vegetation between 1939 and 1985. Orthophoto from 1939.

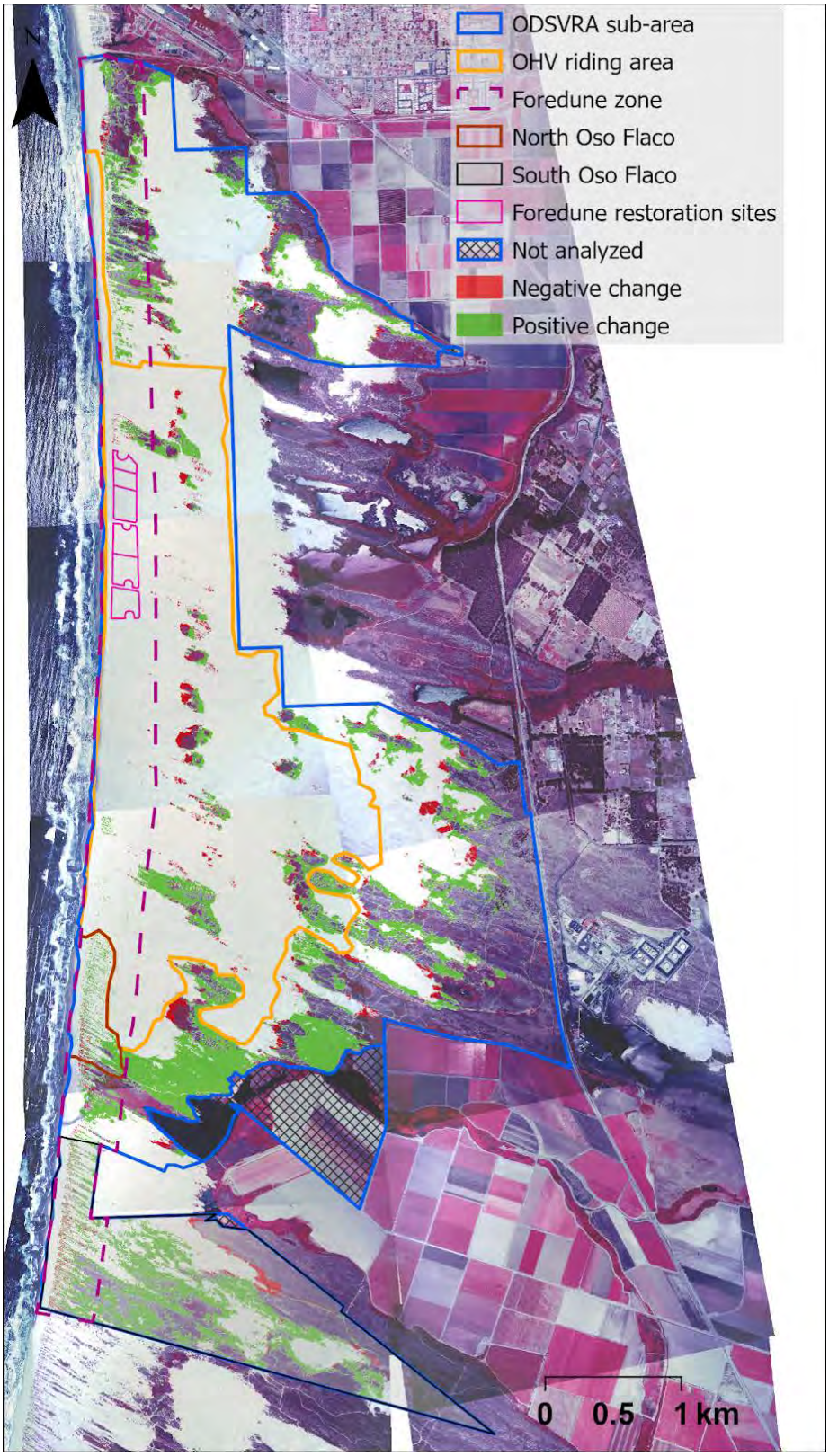

Figure 11. Change in vegetation between 1985 and 2012. Orthophoto from 1985.

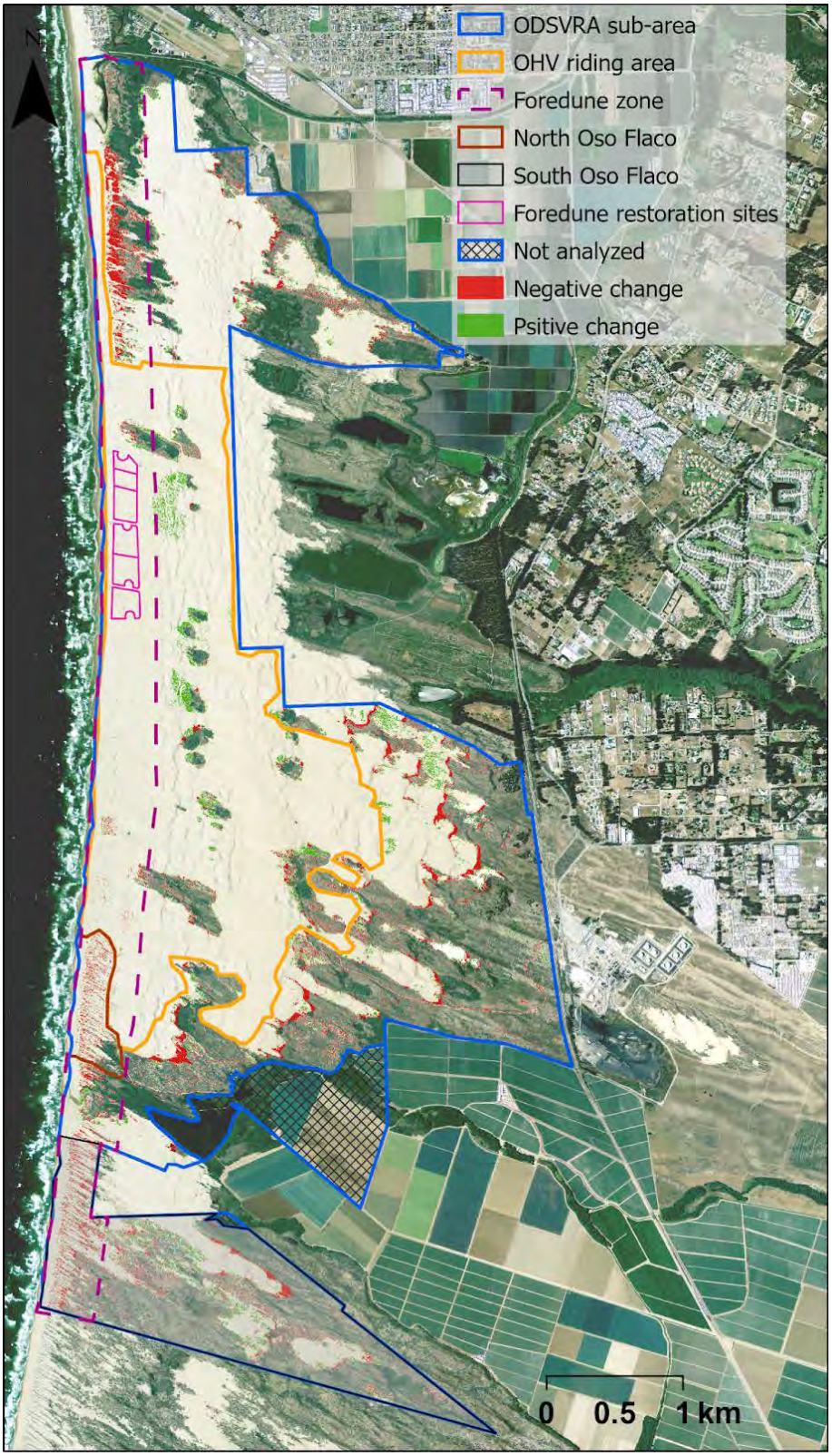

Figure 12. Change in vegetation between 2012 and 2020. Orthophoto of 2012.

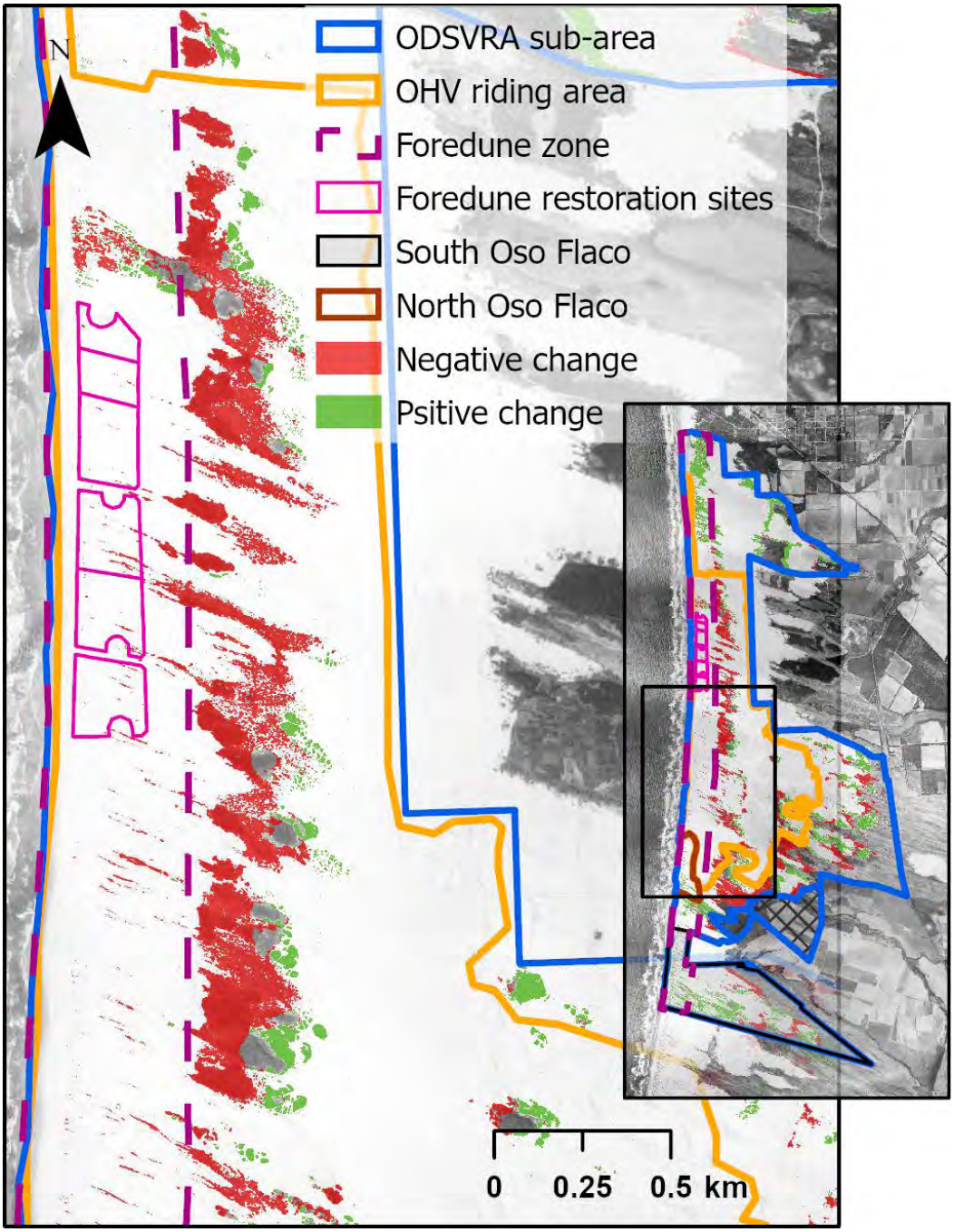

Figure 13. Close-up image of the change in vegetation cover around the foredune restoration sites between 1939 and 1985. Orthophoto from 1939.

Figure 14. Close-up image of the change in vegetation cover around the foredune restoration sites between 1985 and 2012. Orthophoto from 1985.

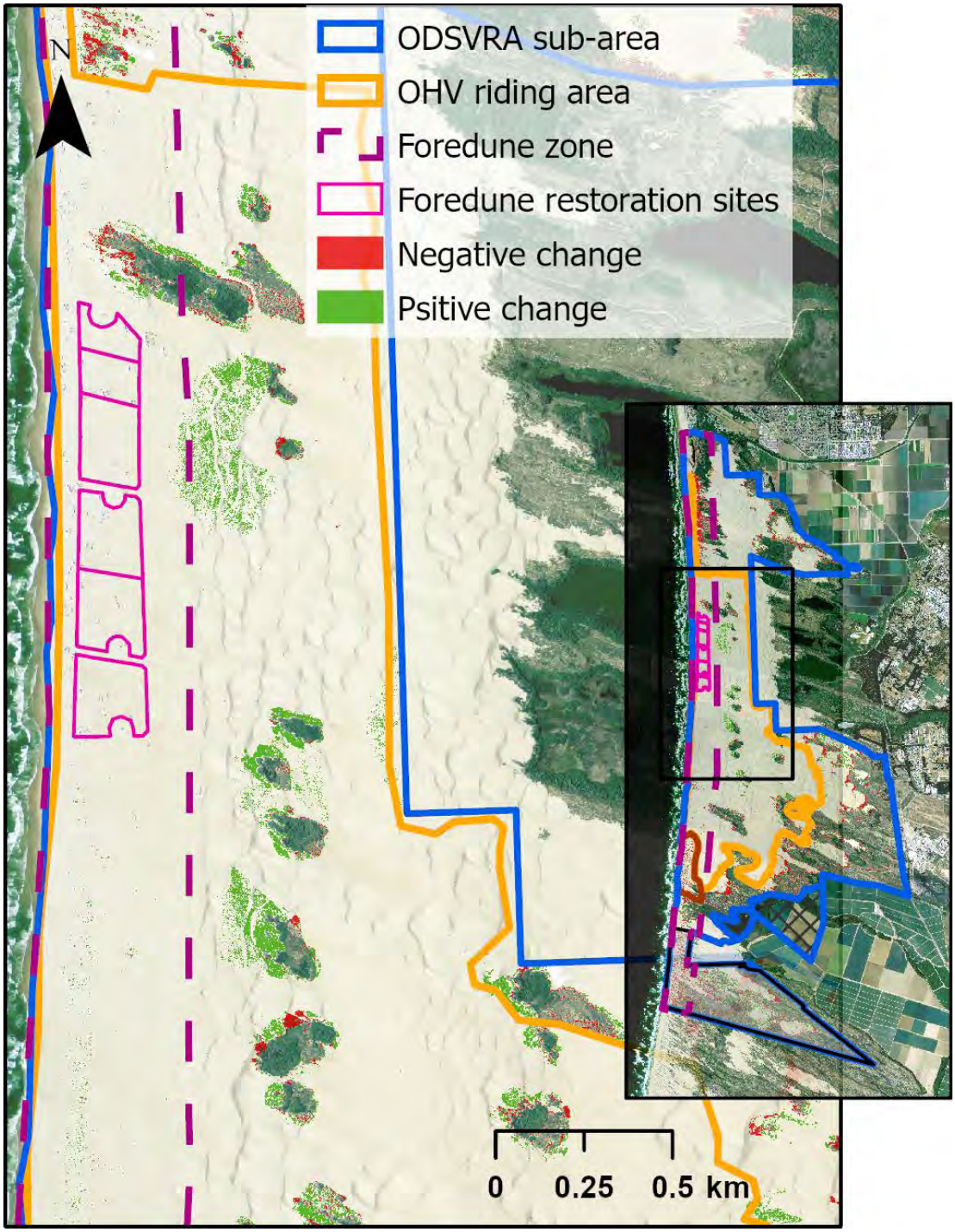

Figure 15. Close-up image of the change in vegetation cover around the foredune restoration sites between 2012 and 2020. Orthophoto from 2012.

Within the OHV riding area over the entire period of analysis, there are lower percentages of total change (13.5%) with mostly negative change (8.2%) in both the foredune and backdune zones (Figures 16-18). Most of the negative changes occurred up to 1985 and were associated

with the loss of hummocky nebkha and foredunes as well as vegetation in foredune swales (Figures 6 and 9B). Positive gains in plant cover in the OHV riding area occurred mostly in the backdune area within fenced vegetation islands (Figure 18).

The south Oso Flaco area showed significantly higher change rates (42%), with over 34% vegetation gain (Figure 16) in both the backdune and the foredune zones. These gains are associated with limited OHV disturbance over at least the last 5 decades, as well as the growth and expansion of invasive weeds.

The more recently fenced north Oso Flaco area experienced significant increases (20%) in plant cover over the total period of analysis with only 0.7% loss (Figure 16). The vast majority of plant growth occurred after the closure of the area for vehicle riding in 1982 (Figures 6 and 9) and is characterized mostly by hummocky nebkhas.

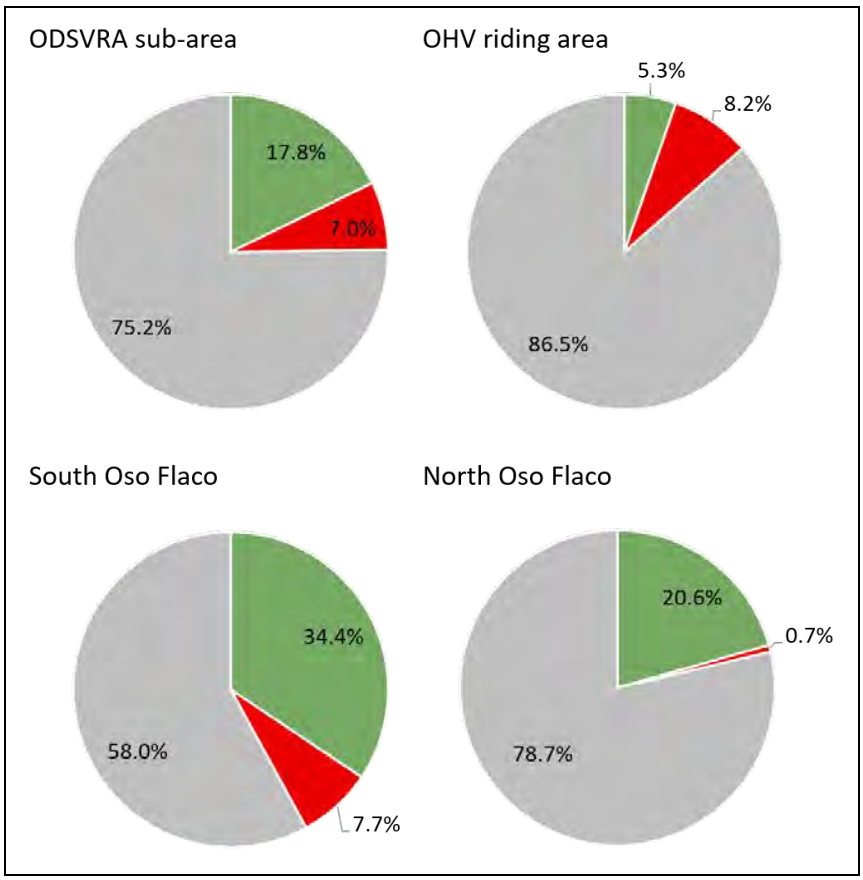

Figure 16. Change analysis (%) of vegetation cover in the ODSVRA sub-area, OHV riding area, and the southern Oso Flaco area between 1939 and 2020.

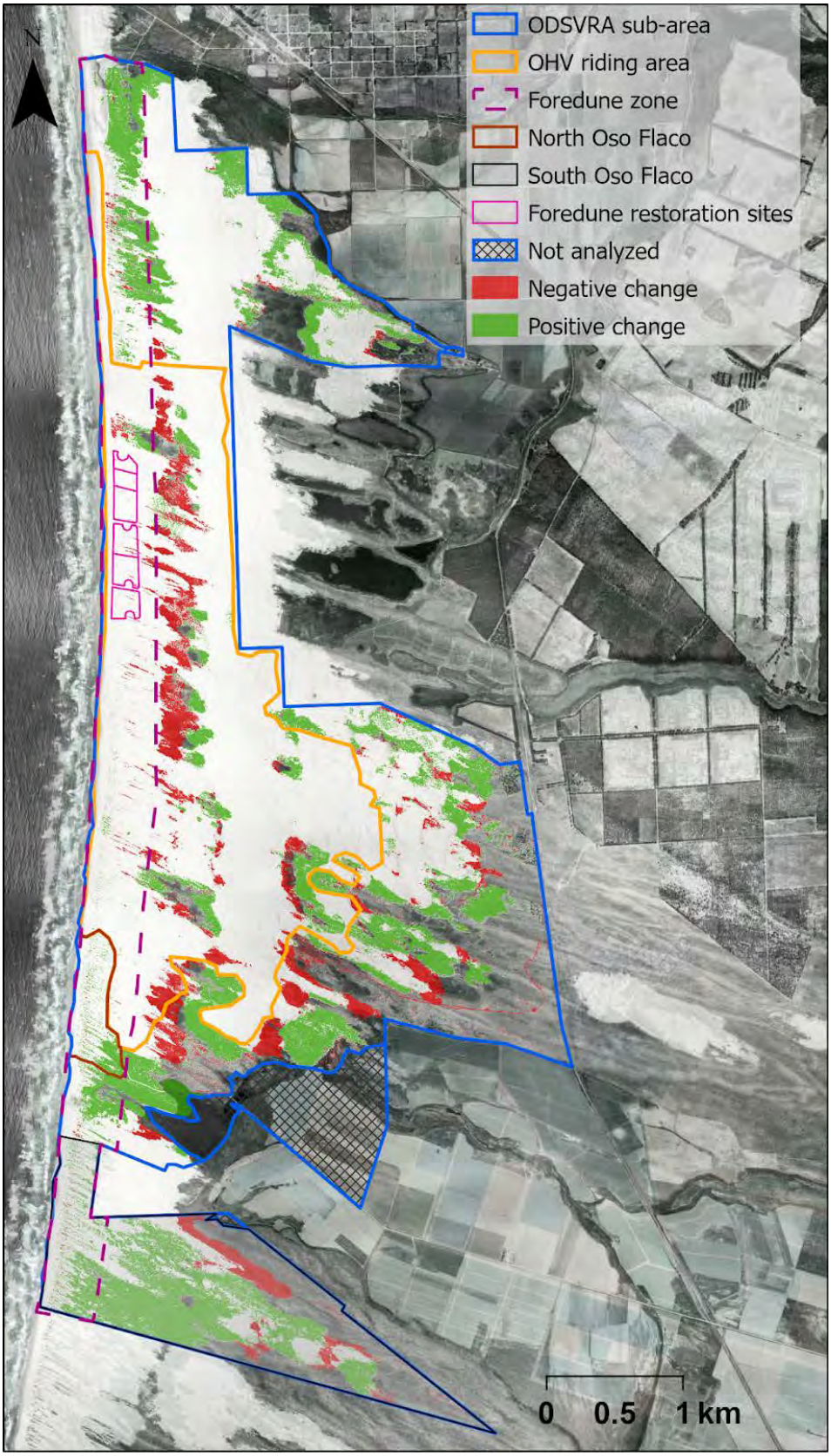

Figure 17. Change in vegetation between 1939 and 2020. Orthophoto from 1939.

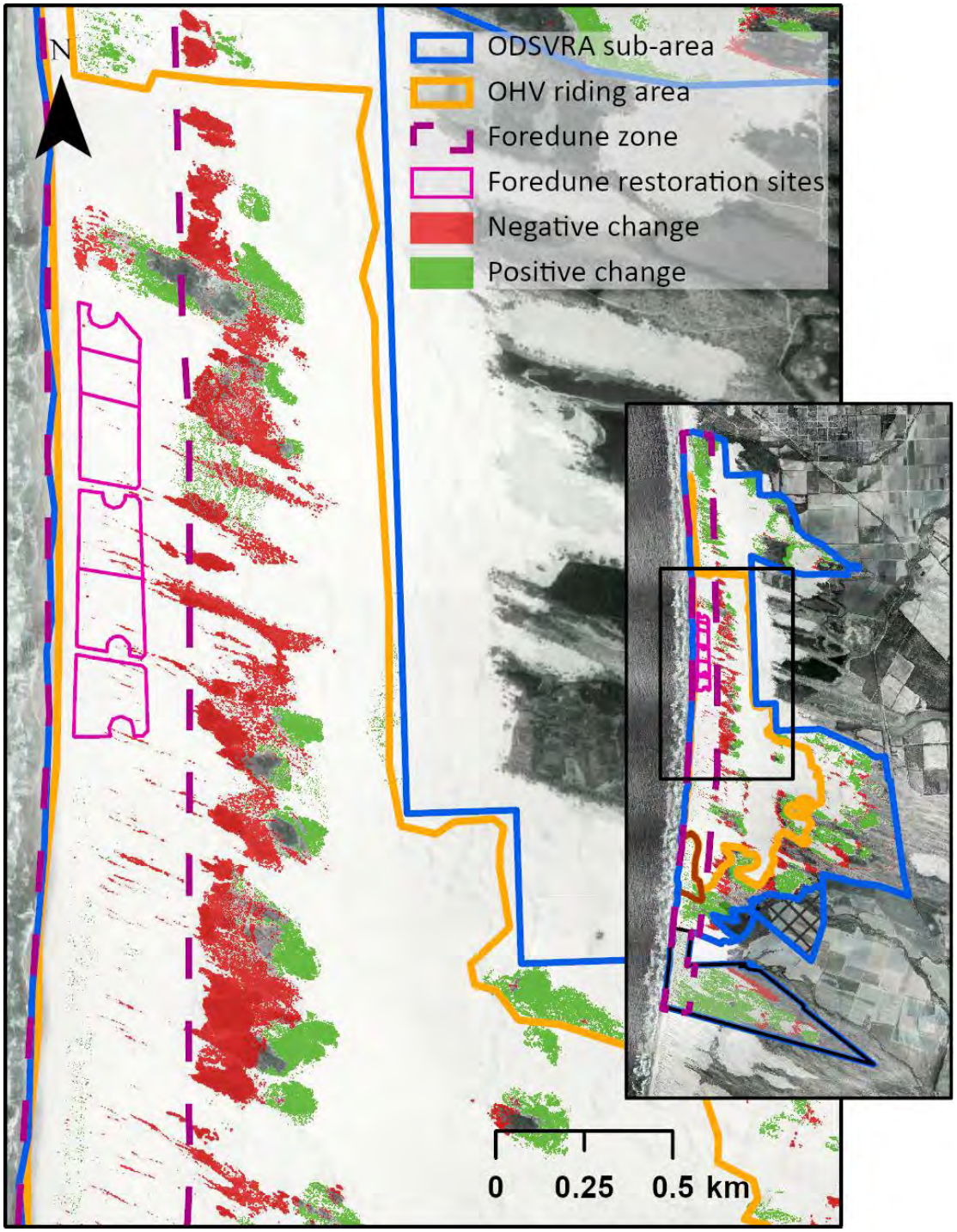

Figure 18. Close-up image of the change in vegetation cover around the foredune restoration sites between 1939 and 2020. Orthophoto from 1939.

4. Summary and Conclusions

As part of the 2020-21 ARWP, the CDPR requested a thorough analysis of historical changes in vegetation cover within the ODSVRA. This report provides a detailed analysis of the best available aerial photography of ODSVRA for 16 image years between 1930 and 2020 obtained from CDPR, the UCSB Library's Geospatial Collection, and the National Agriculture Imagery Program (NAIP). From this, plant cover was carefully and systematically classified and analyzed in a GIS (ArcGIS Pro) to detect, quantify, and interpret changes and trends in vegetation cover.

To allow comparison between different management regions of the ODSVRA, the report focuses on six analytical zones:

- a large sub-area of the ODSVRA located south of Arroyo Grande Creek (~75% of the total area of ODSVRA),
- the OHV riding area within the ODSVRA (c. 2013),
- the foredune zone, or the area in which foredune vegetation would typically exist in the region, that extends ~400 m eastward/inland from the high-water mark,
- the north Oso Flaco foredune complex, closed to OHV activity since 1982,
- the south Oso Flaco dune complex within the ODSVRA boundary, including both foredune and backdune areas, which serves as a reference site for mature foredunes that have not seen OHV activity since 1982,
- the new (2020) foredune restoration sites, located within the foredune zone of the OHV riding area between post markers 4-6.

Plant cover maps and calculations (areas and %) were obtained for each analytical zone in all image years. Results show that vegetation cover trends within ODSVRA have varied over time and differ notably between the analytical regions. Within the broader ODSVRA sub-area, vegetation changes generally increased over time, ranging from 25% in 1939, to a peak of 37% in 2012, to just over 35% in 2020. In the OHV riding area, vegetation cover has been comparatively low across all years and declined appreciably from a peak value of 12% in 1966 to around 8% in 2020. After 1966 plant cover decreased to a low of 3.9% in 1985 and remained low (<5%) until after 1988, when it began to gradually increase to the 2020 levels. The southern Oso Flaco area shows a similar trend as the broader ODSVRA area, although with generally higher percentages. Plant cover at Oso Flaco was 37% in 1939, more than doubled to a peak of 66% by 2012, then remained over 60% up to 2020. The north Oso Flaco foredune area showed almost no plant cover in 1930 (0.7%), but has gradually increased over time, mostly after 1985, up to a peak of 24% in 2012.

Foredunes in the region are typically more sparsely vegetated than back dune environments and are characterized by a hummocky terrain of nebkha and elongated shadow

dunes, blowouts, and narrow parabolic dunes, such as found at the southern Oso Flaco reference site. Accordingly, plant cover in the foredune zone of ODSVRA is generally less than that in the broader analytical zones over time, but shows similar trends. Foredune plant cover at Oso Flaco in 1939 was very low (2.3%), but increased by an order of magnitude to over 30% by the 2010s. For comparison, vegetation in the foredune zone of the OHV riding area had slightly higher cover (2.7%) in 1939, rose to a peak value of 5.4% in 1966, but then steadily declined to very low values around 1% from 1985 to 2005. Since then, vegetation cover has increased slightly in the foredune zone of the OHV area to 2.4% by 2020, mostly due to new plants on the margins of fenced backdune vegetation islands and foredune vegetation establishing in the seasonal bird nesting enclosure.

Both north and south Oso Flaco areas have been fenced off to OHV traffic since roughly 1982 and, therefore, were selected as reference sites for plant cover and dune form in ODSVRA. The positive trend of plant growth over time and high percentages of cover in these areas vs. the OHV riding area attest to natural processes and responses of vegetation growth and dune development that could occur with limited anthropogenic disturbance. It is important to note, however, that some areas within the ODSVRA, including south Oso Flaco, are impacted by invasive species planted in the area during the early 1900s and, as such, plant cover percentages and dune stabilization could be higher than might be expected under natural conditions. Therefore, the specific cover values for south Oso Flaco provide a reference for relatively undisturbed areas in the ODSVRA, but they do not represent ideal natural conditions of this region. Unfortunately, there are no nearby dune systems that are pristine and undisturbed. Over the last decade CDPR have also conducted targeted efforts to remove invasive species in the ODSVRA particularly in backdune areas, south Oso Flaco, the Pismo Dunes Natural Preserve, and on some private land-holdings within and outside of the ODSVRA borders.

Although invasive grass species exist in ODSVRA, studies of sand dunes elsewhere in the world indicate a shift toward 'greening' (i.e., increased vegetation cover) over the last three decades[18,19,20,21] partly in response to climatic changes and enhanced preservation efforts. The results of this report are consistent with this global trend, yet they occur in the presence of intensive recreational use pressures, such as OHV riding and camping (sanctioned or otherwise) in various locations in the dunes. In part, the observed responses within ODSVRA are the result

[18] Ashkenazy, Y., Yizhaq, H., Tsoar, H., 2012. Sand dune mobility under climate change in the Kalahari and Australian deserts. Climatic Change 112, 901–923. https://doi.org/10.1007/s10584-011-0264-9

[19] Gao, J., Kennedy, D.M., Konlechner, T.M., 2020. Coastal dune mobility over the past century: A global review. Progress in Physical Geography: Earth and Environment 44, 814–836. https://doi.org/10.1177/0309133320919612

[20] Jackson, D.W.T., Costas, S., González-Villanueva, R., Cooper, A., 2019. A global 'greening' of coastal dunes: An integrated consequence of climate change? Global and Planetary Change 182, 103026. https://doi.org/10.1016/j.gloplacha.2019.103026

[21] Heathfield, D.K., & Walker, I.J. (2011). Analysis of coastal dune dynamics, shoreline position, and large woody debris at Wickaninnish Bay, Pacific Rim National Park, British Columbia. Canadian Journal of Earth Sciences, 48(7), 1185-1198. https://doi.org/10.1139/e11-043

of land use management and vegetation restoration efforts by CDPR since establishment of the park in 1982.

Detailed examination of change maps of negative (losses) or positive (gains) in plant cover over time show a large amount of change between 1966-1985, with negative change mostly in foredune areas and adjoined inland vegetation islands. Between 1998 and 2012, a large positive change occurred, mostly around existing vegetation islands, which corresponds partly with implementation of protective fencing and restoration projects in different areas outside the OHV riding area. Most positive changes in the OHV riding area were after 2005 and relate to new plants within the margins of fenced vegetation islands and foredune plants and nebkha development in the seasonal bird nesting exclosure between 2005 and 2020. In general, the vast majority of positive changes over the years in all analytical zones were within fenced areas with limited or no OHV activity, such as the seasonal bird nesting exclosures, fenced islands of existing plant cover, restoration project sites, and in the north and south Oso Flaco regions.

In terms of landscape responses during the identified management intervals, the period roughly preceding the establishment of the ODSVRA (1939-1985) saw a general decline in plant cover in the foredune and backdune of the OHV riding area (from 10.9 to 3.9% cover). Although cover increased between 1939-1966, it then declined to 1985 just as the ODSVRA was established. Between 1985 and 2012, there was mostly increasing plant cover with over 14% positive change in the broader ODSVRA sub-area, mainly around existing vegetation and other targeted restoration areas, particularly between 2005 and 2012. In the OHV riding area, plant cover increased mostly in fenced areas in backdune vegetation islands. From 2012 to 2020, there was a general decline in the amount of vegetation cover compared to previous intervals with 8% of total change in the ODSVRA sub-area. Some of this decline relates to invasive plant removal projects at the Pismo Dune Natural Preserve and Oso Flaco and most of the positive changes during this time related to backdune restoration areas implemented by CDPR.

It is clear that vegetation cover within ODSVRA has changed significantly over time and that the effects of OHV traffic, recreational activities, invasive species, and ecosystem restoration projects have collectively influenced the observed patterns and trends in varying ways and extents. Some of these effects are the result of aggregated impacts and, thus, are difficult to disentangle, while others are more clearly related to distinct activities in specific areas. It is important to note that the landscape that was inherited by CDPR when ODSVRA was established in 1982 had already experienced notable changes in vegetation cover related to unsanctioned OHV activity and other land use changes (e.g., agriculture, infrastructure development). Although it is beyond the scope of this report, it is also possible that plant communities at ODSVRA are also influenced by multi-decadal climatic changes similar to other coastal dune systems worldwide. Given the dynamic and compounded nature of forces that have shaped the dunes at ODSVRA, it is essential to recognize that dune ecosystems and their

plant communities are not static features of the landscape and that they will continue to evolve and reflect the changing conditions that shape their form and function. This poses a particular challenge for establishing management targets and restoration strategies in a landscape that has been subject to intensive OHV and recreation activities that destroy vegetation essential for dune development and reduction of dust emissions.

This report is intended to inform further discussions between CDPR, SAG, and SLO-APCD on how historic vegetation cover and change trends can be used to inform future dust mitigation strategies within ODSVRA. For instance, a reference point in time for 'pre-disturbance' or 'pre-CDPR management' conditions within the dunes would be useful for guiding dust emissions simulation modelling and revisiting the SOA target, which currently lacks a baseline condition. In addition, understanding the spatial distribution of plant communities and their changes through time in different disturbance settings is useful for refining decisions on the location and extent of future vegetation restoration dust mitigation strategies. It is anticipated that such discussions and related adaptive management decisions will help define ongoing vegetation for restoration and dust emissions mitigation strategies in the upcoming 2022-23 ARWP.

5. Supplements

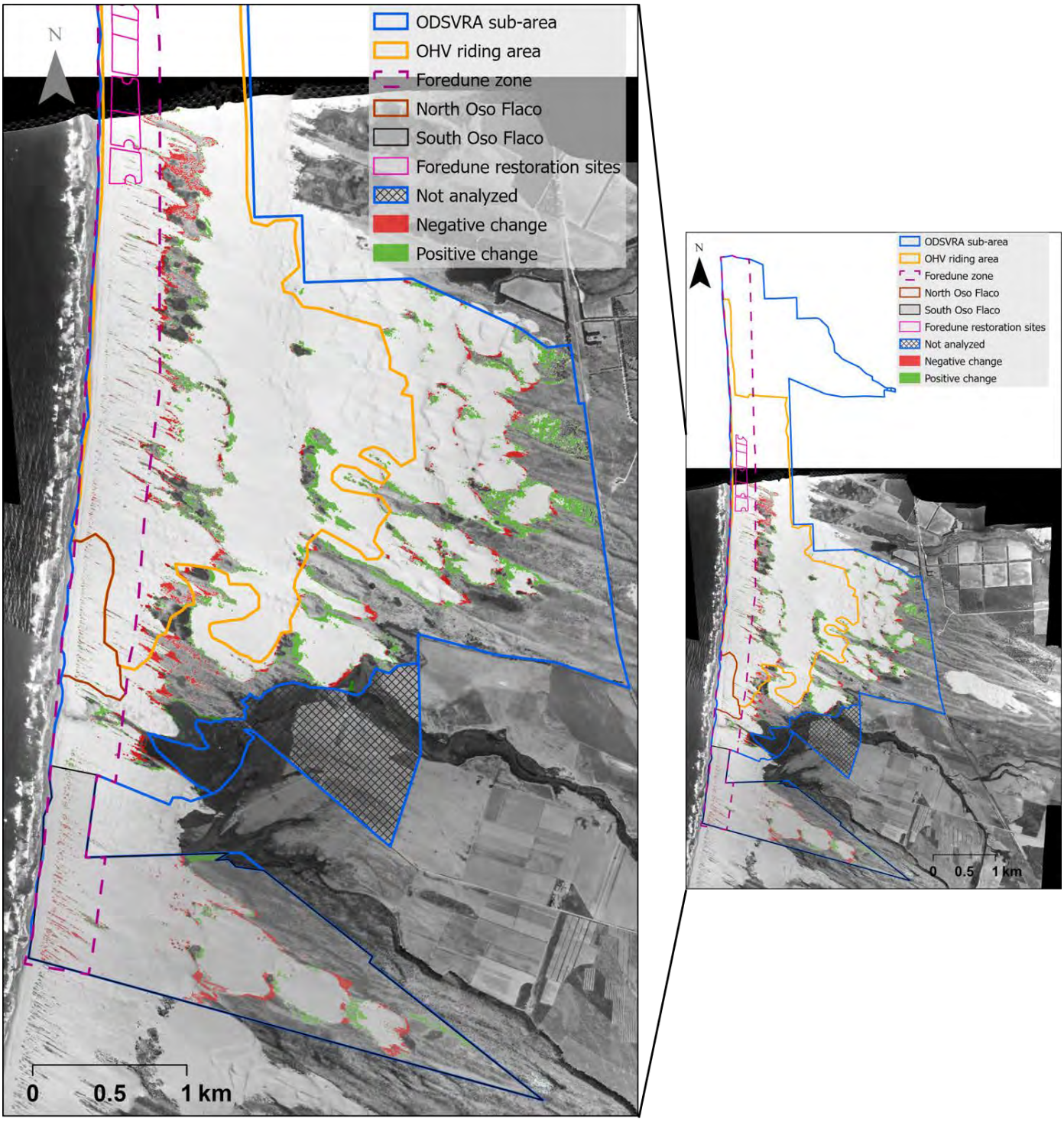

Figure S1. Vegetation change analysis results between 1930 and 1939. Positive change is in green, negative change is in red. Background orthophoto is from 1930.

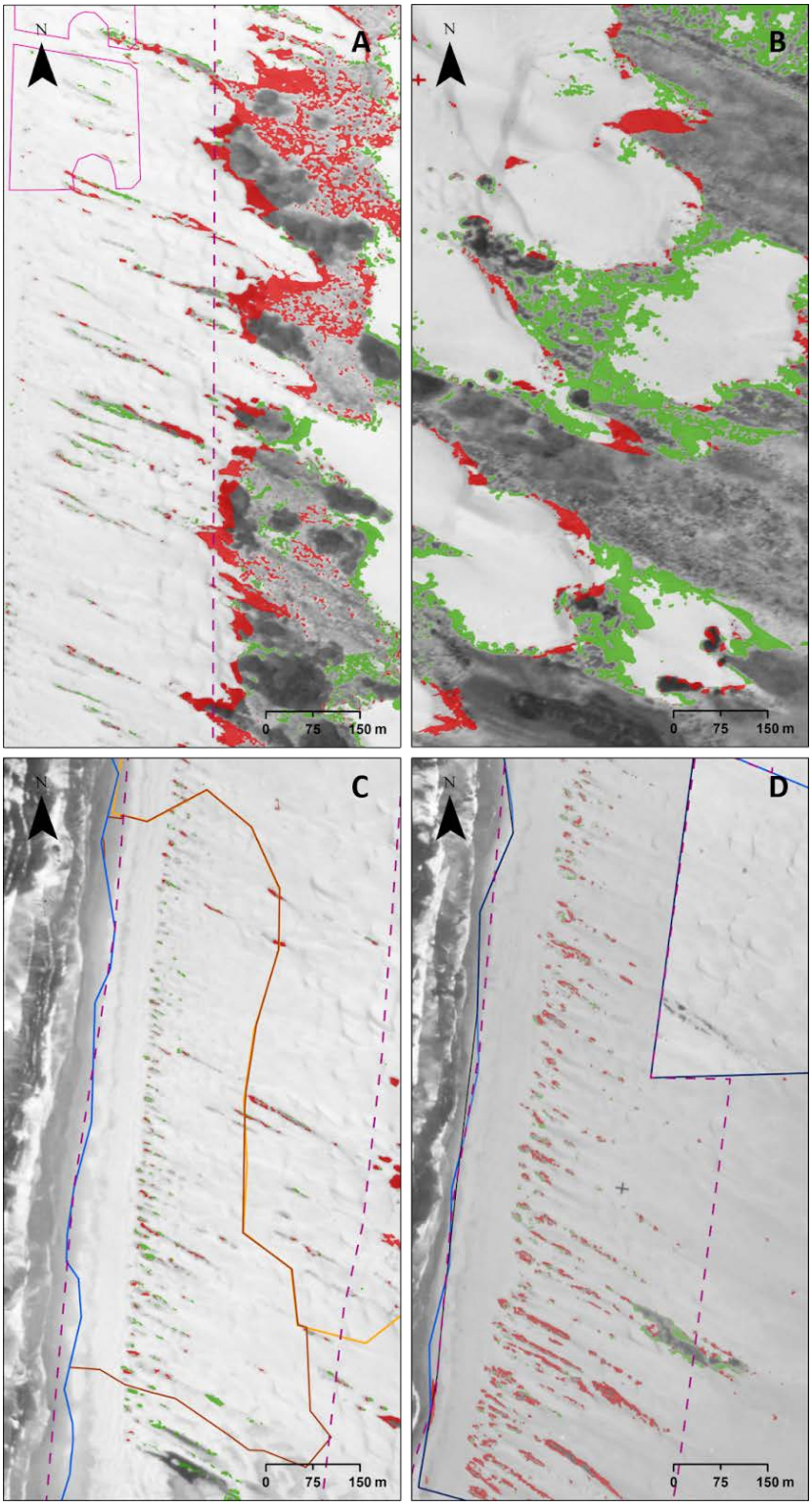

Figure S2. close-ups of vegetation change analysis results between 1930 and 1939 of the OHV riding area (A), backbude of the ODSVRA su-area (B), north Oso Flaco (C), and south Oso Flaco (D). Positive change is in green, negative change is in red. Background orthophoto is from 1930.

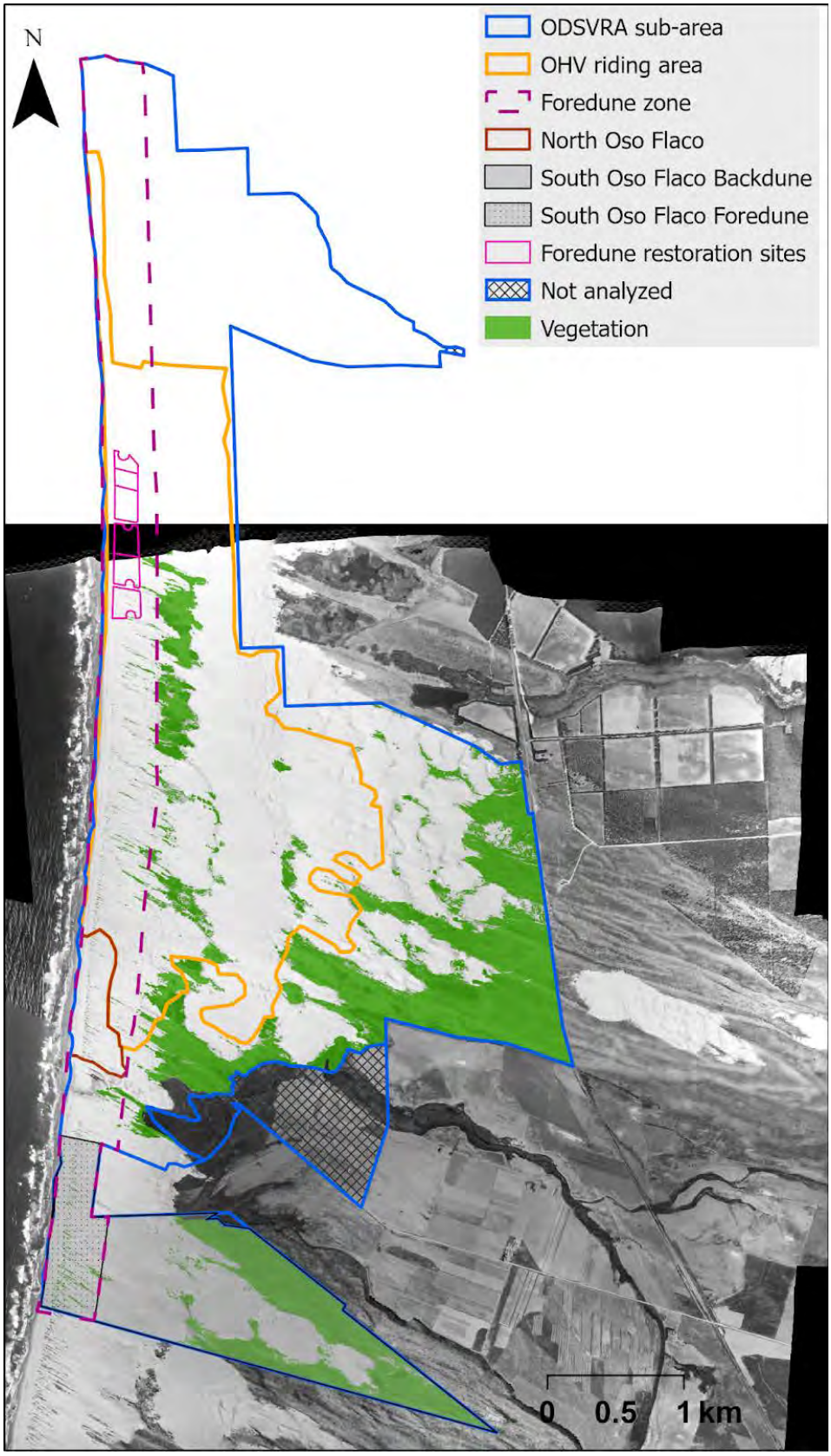

Figure S3. Vegetation cover map of 1930.

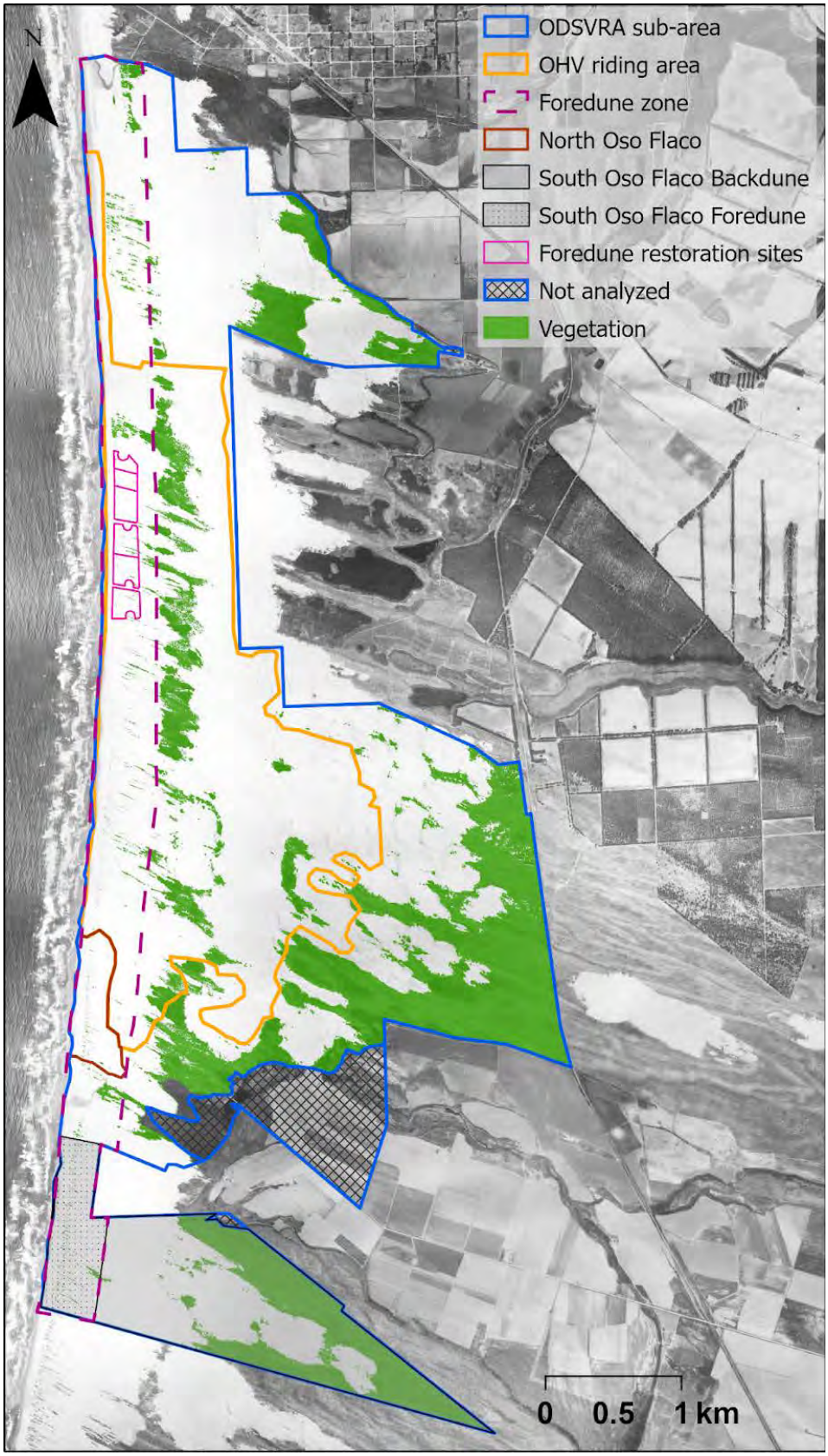

Figure S4. Vegetation cover map of 1939.

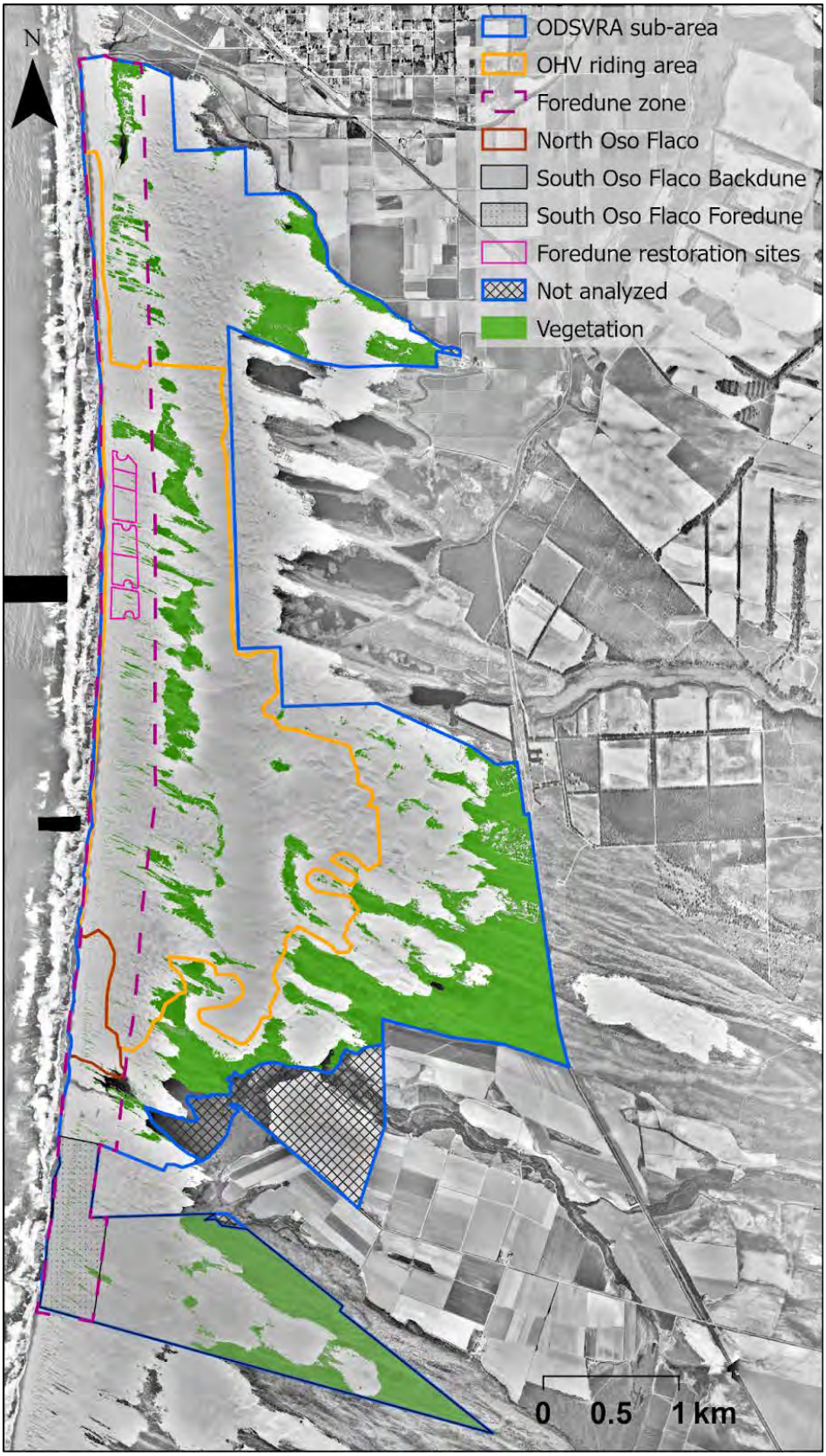

Figure S5. Vegetation cover map of 1949.

Figure S6. Vegetation cover map of 1956.

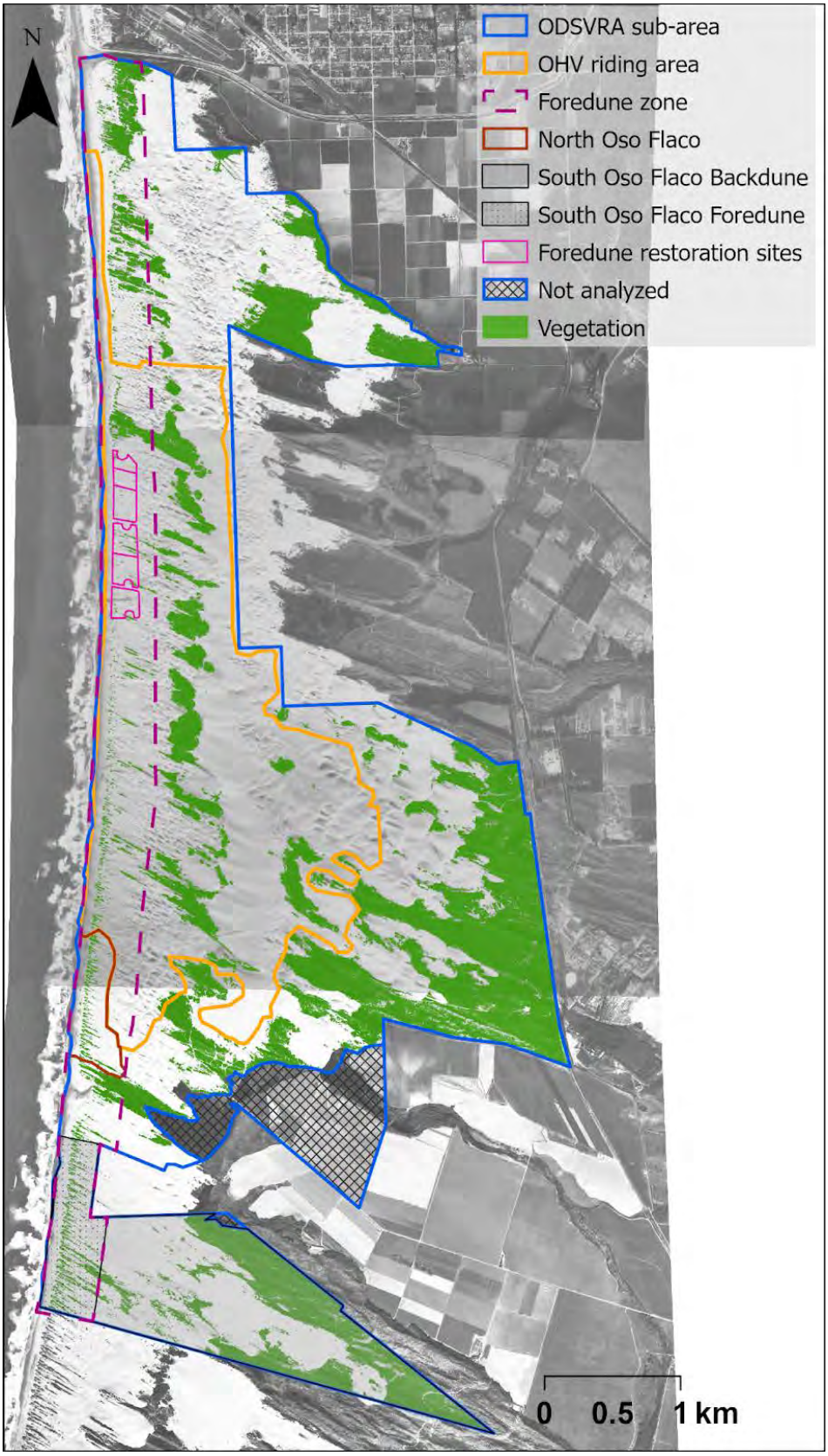

Figure S7. Vegetation cover map of 1966.

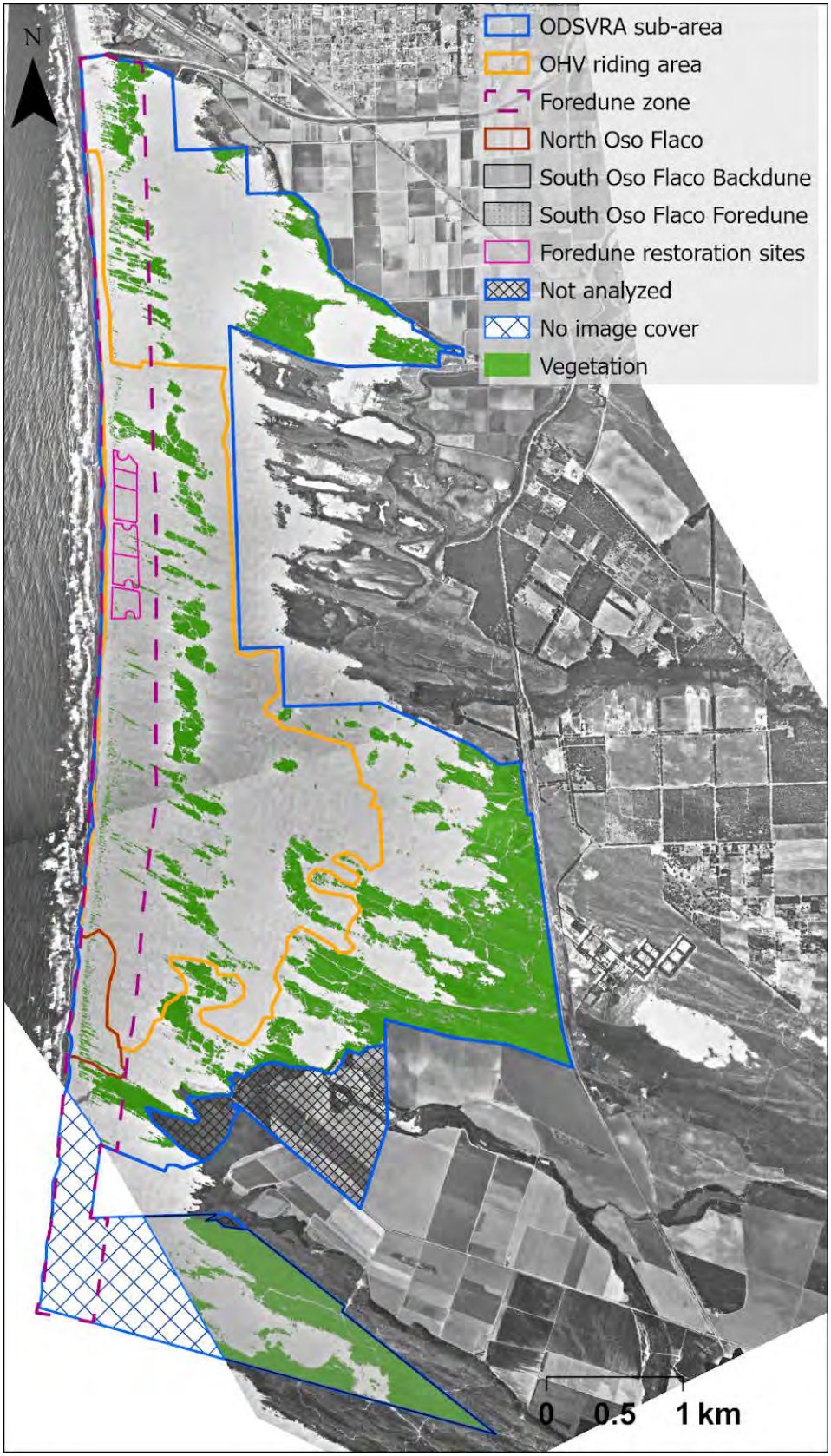

Figure S8. Vegetation cover map of 1971.

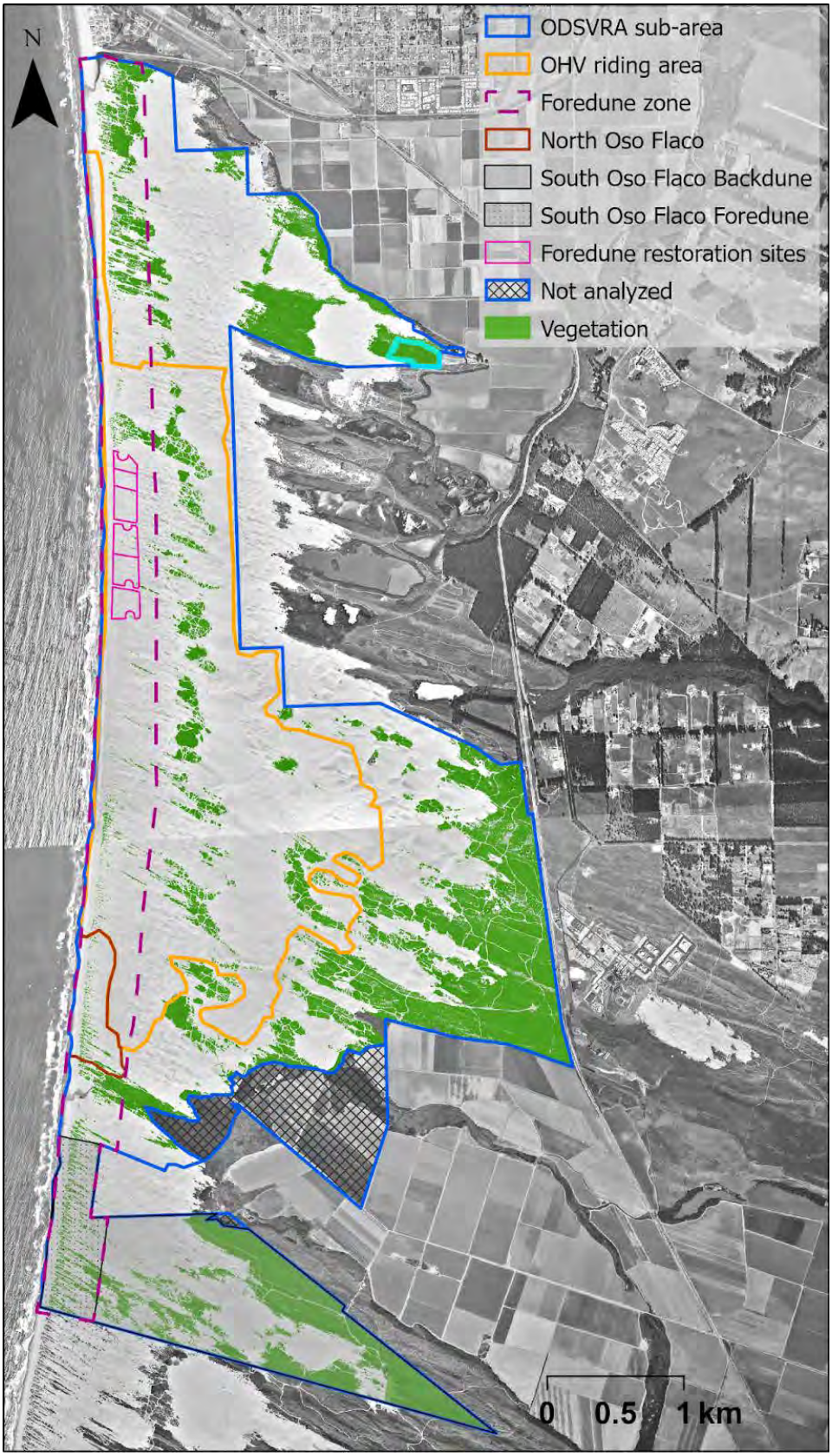

Figure S10. Vegetation cover map of 1978.

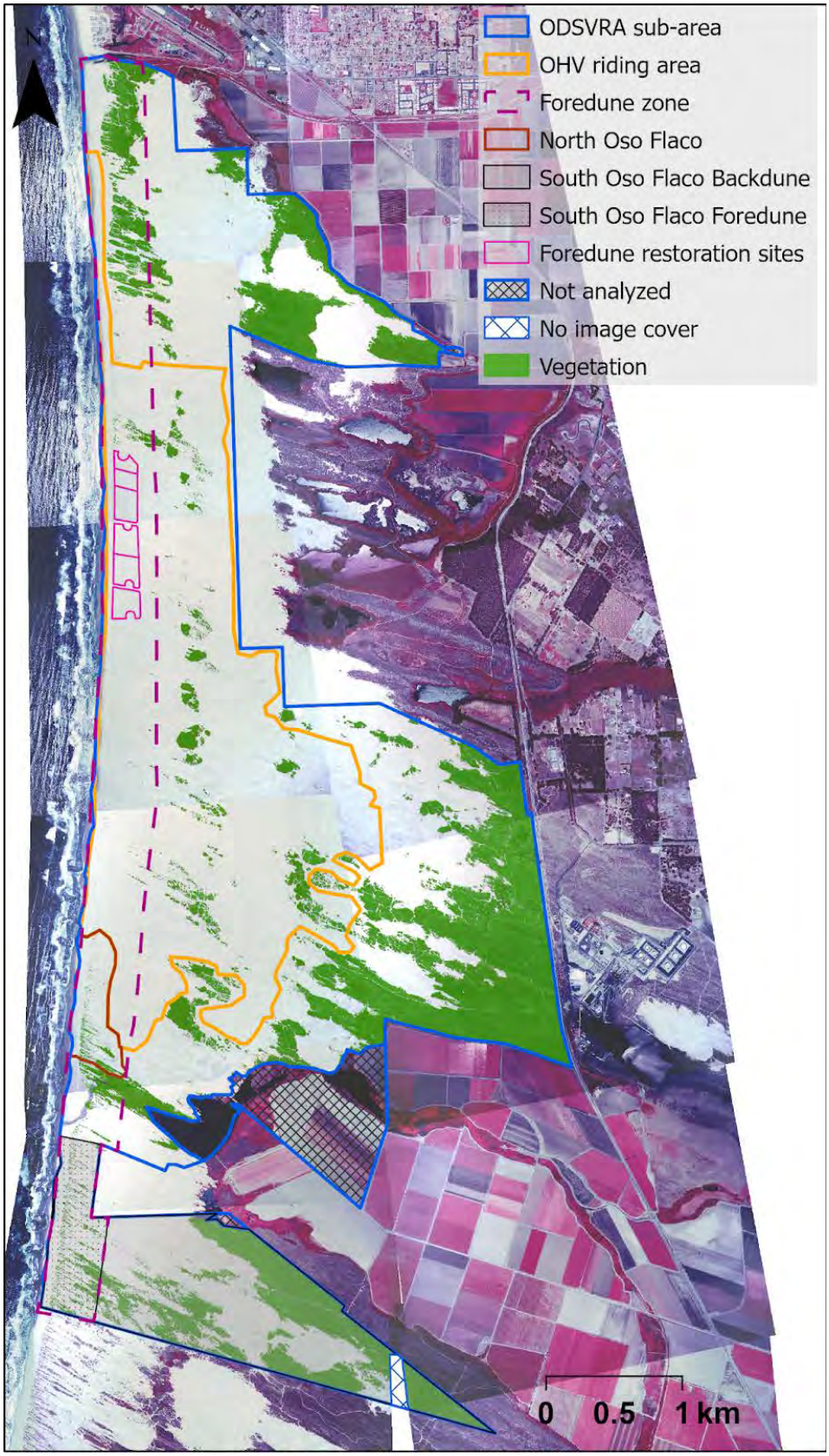

Figure S10. Vegetation cover map of 1985.

Figure S11. Vegetation cover map of 1994.

Figure S12. Vegetation cover map of 1998.

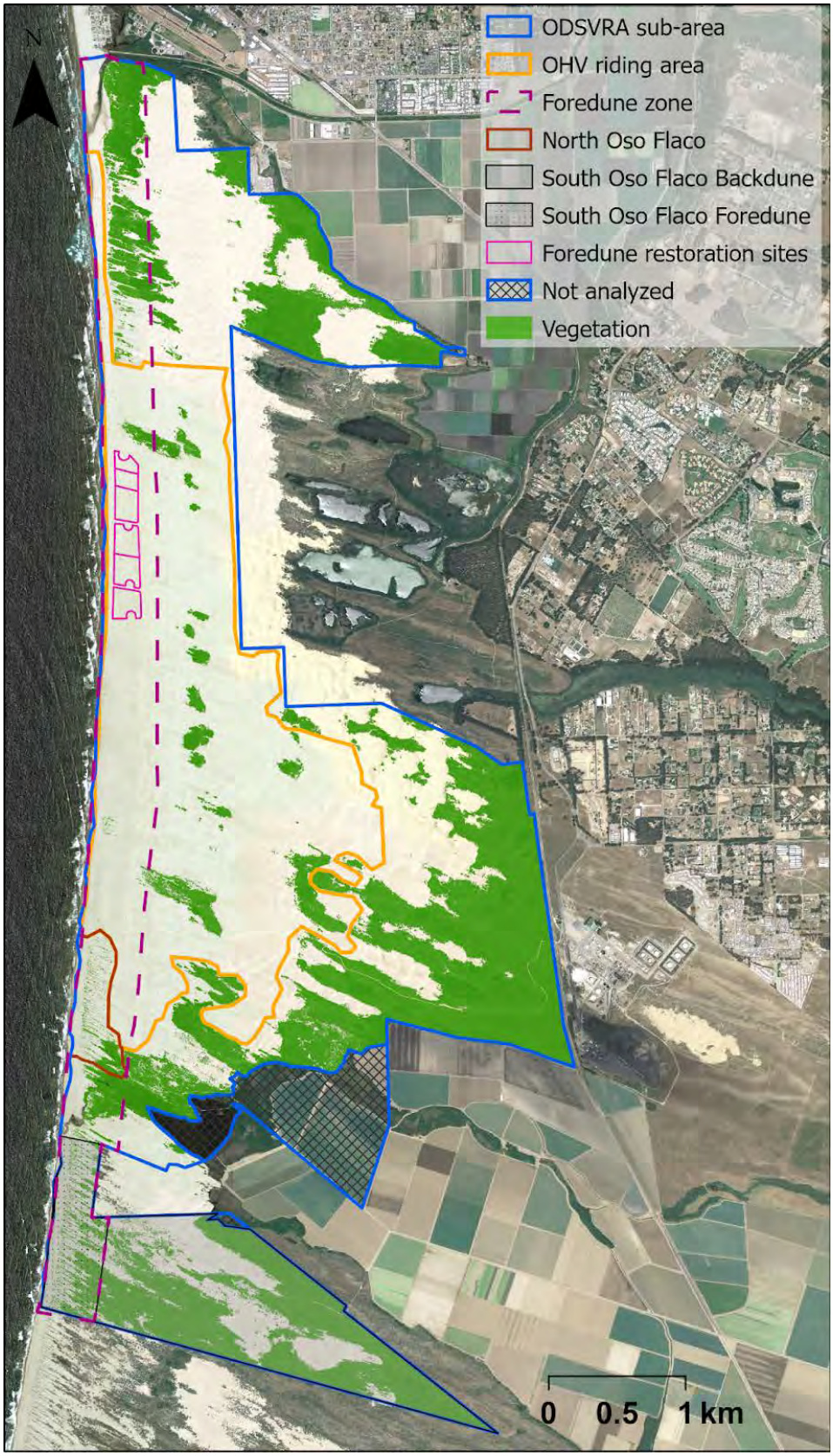

Figure S13. Vegetation cover map of 2005.

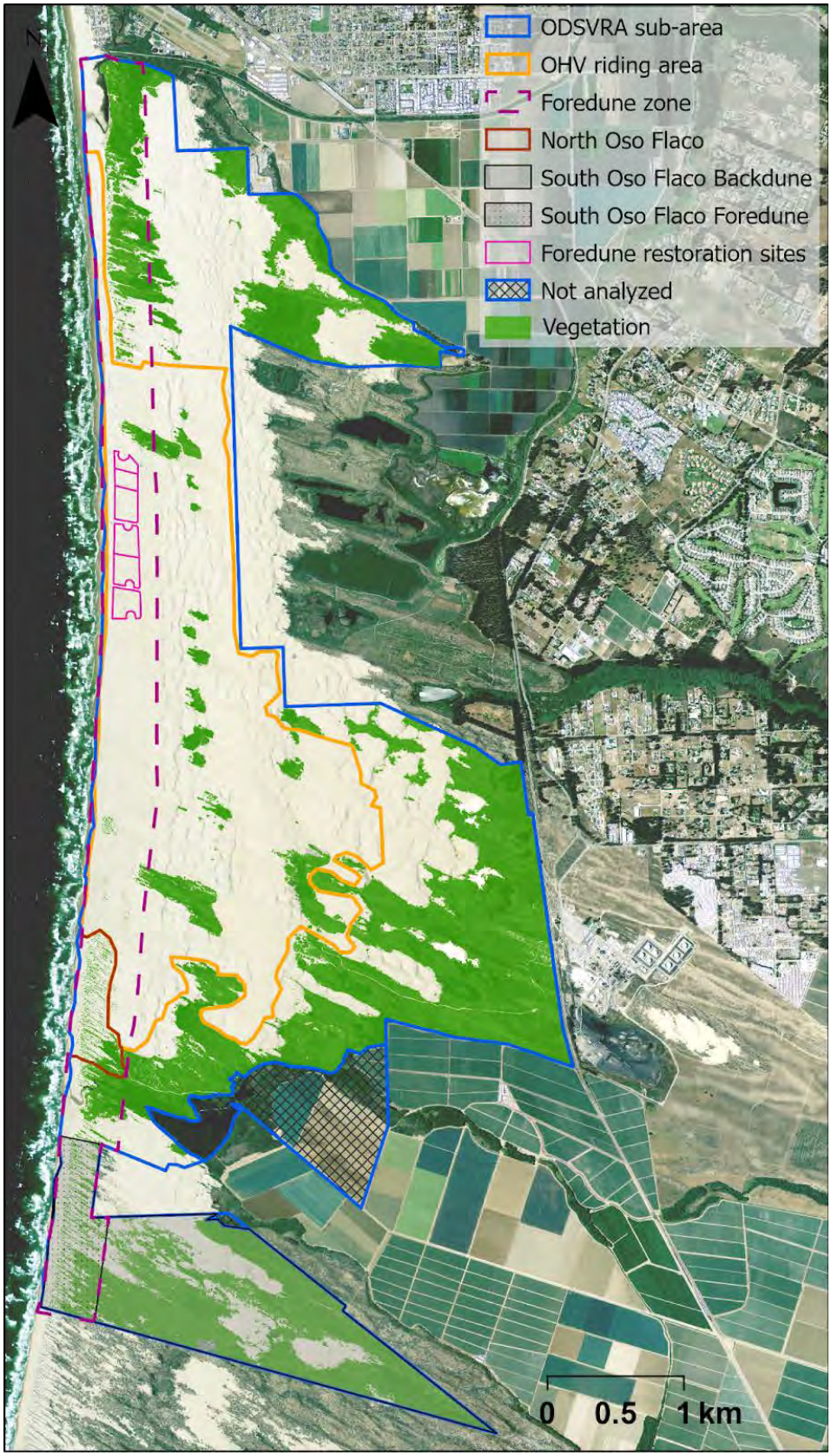

Figure S14. Vegetation cover map of 2012.

Figure S15. Vegetation cover map of 2014.

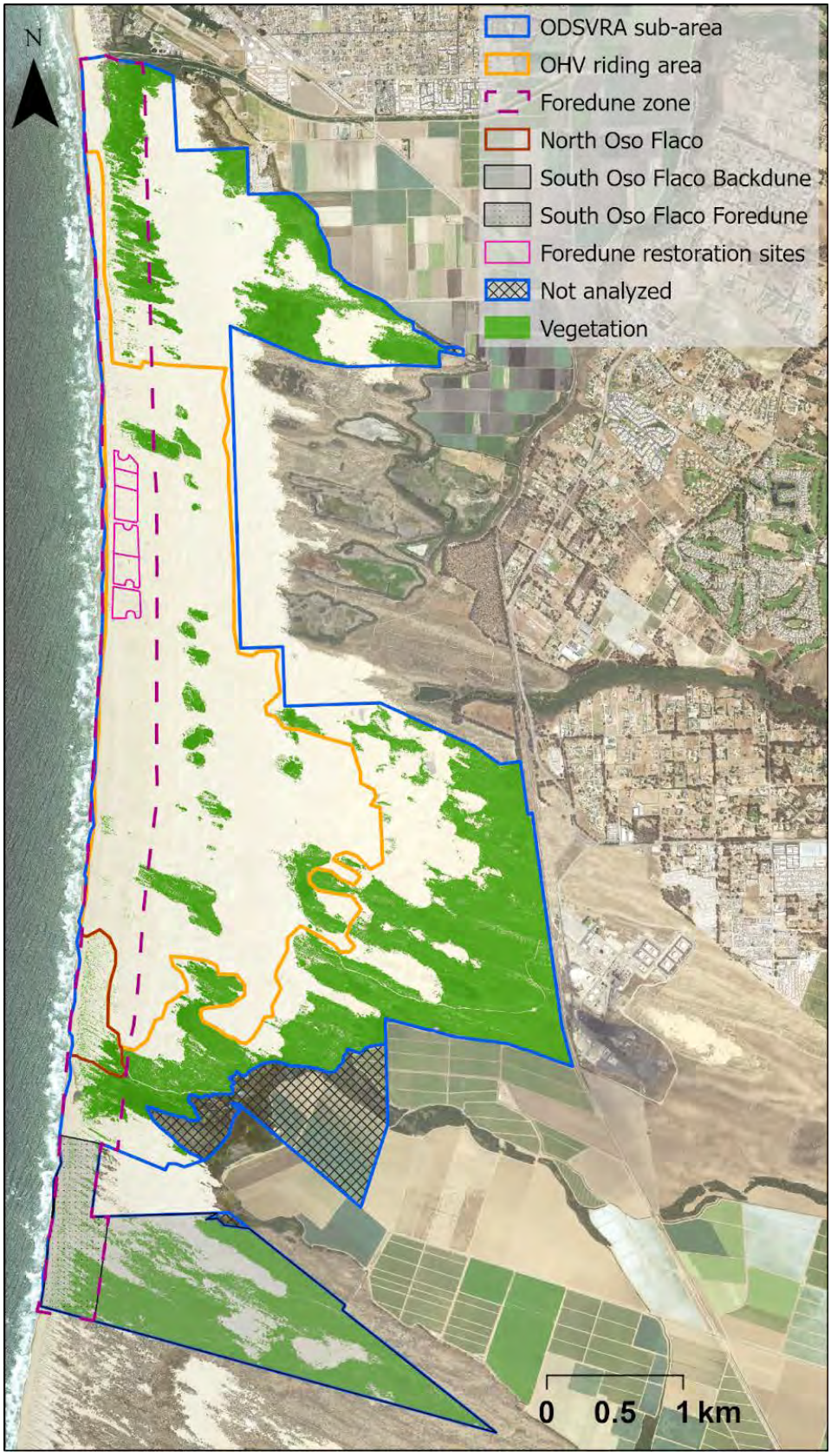

Figure S16. Vegetation cover map of 2016.

Figure S17. Vegetation cover map of 2018.

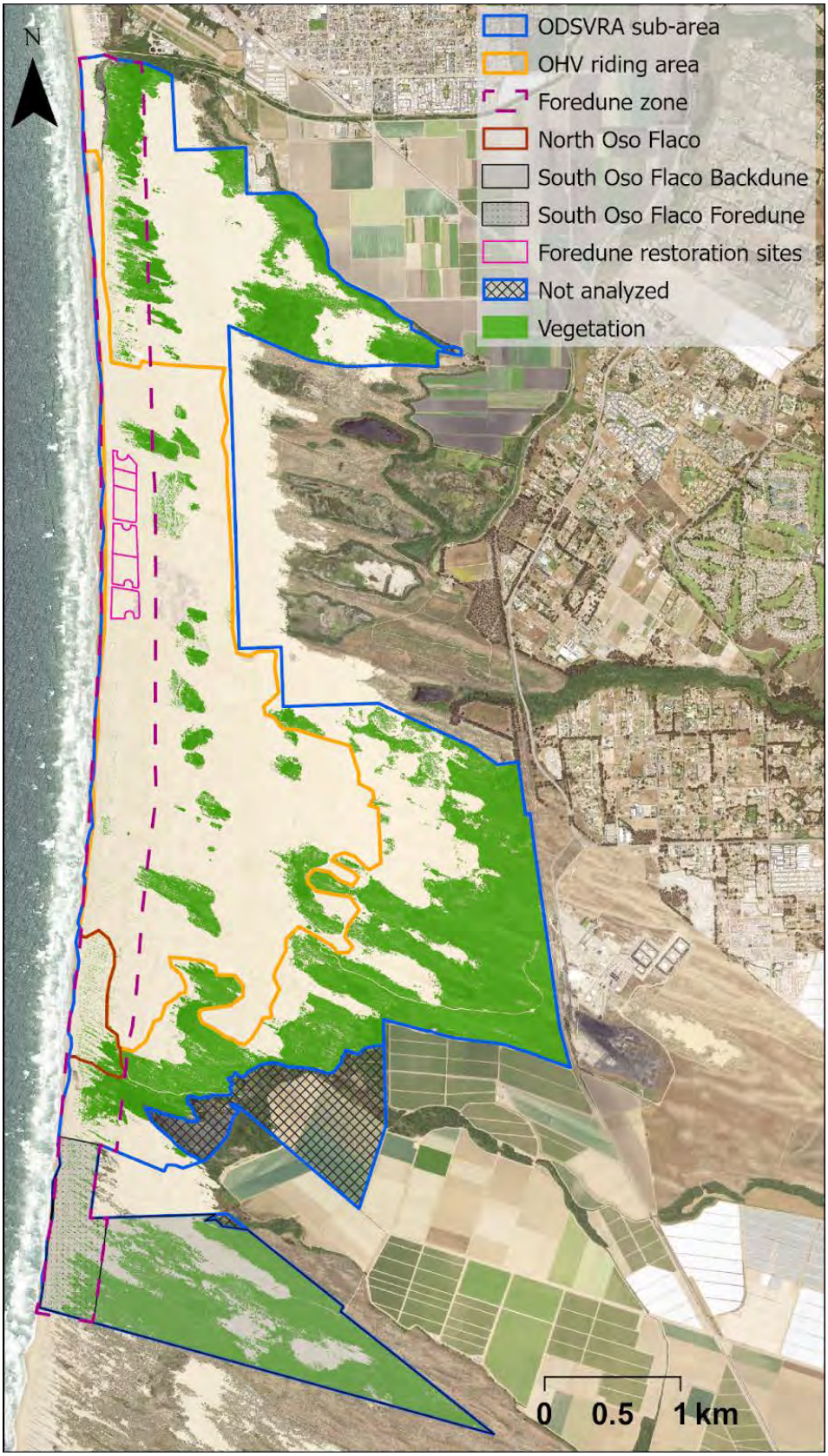

Figure S18. Vegetation cover map of 2020.

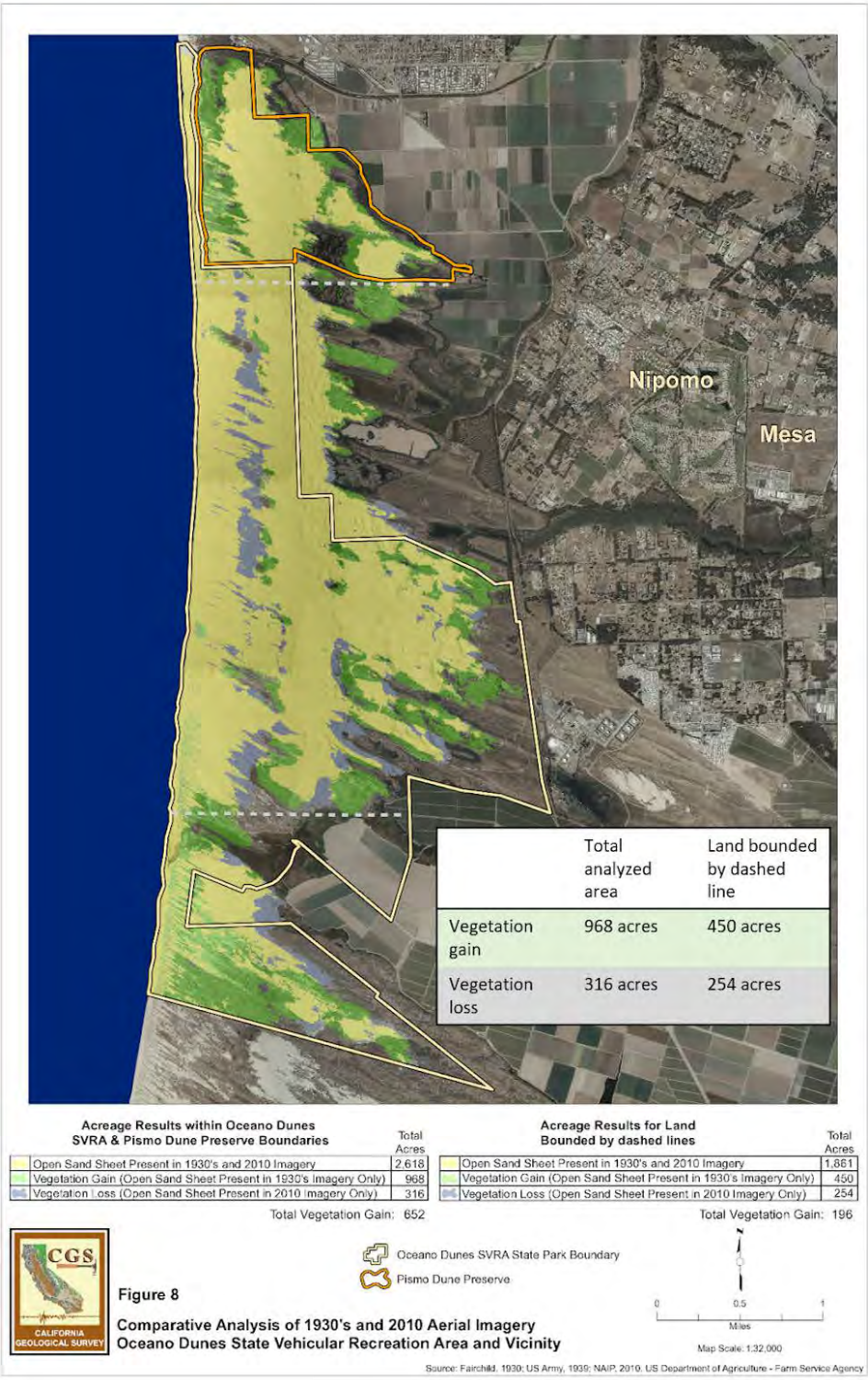

Figure S19. Sand and vegetation acreage results of the comparison between 1930's and 2010 presented in Figure 8 in the CGS report from 2011, positive change is in green, negative change in gray, and no change in yellow (Harris, 2011).

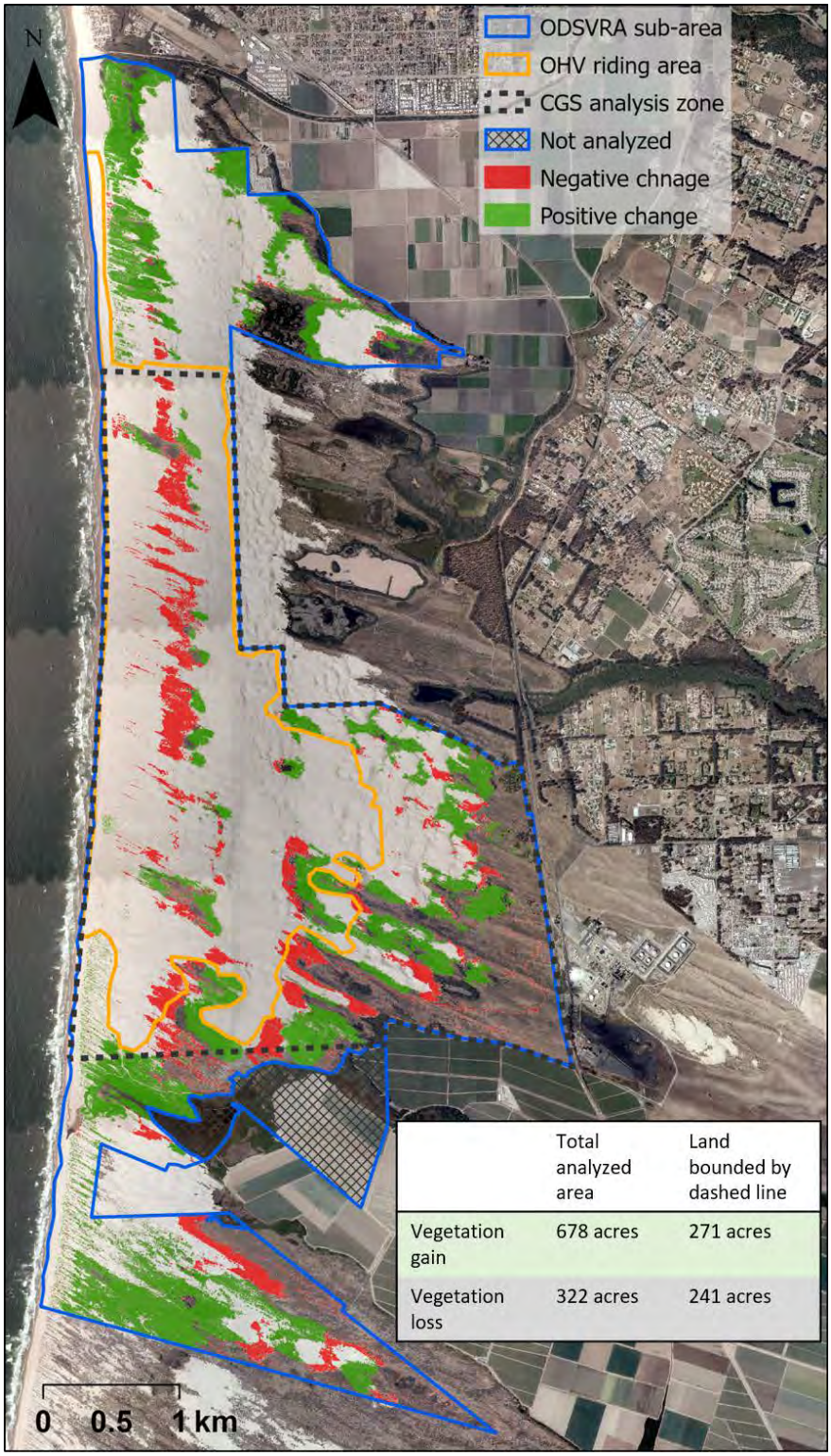

	Total analyzed area	Land bounded by dashed line
Vegetation gain	678 acres	271 acres
Vegetation loss	322 acres	241 acres

Figure S20. Vegetation change analysis results of the 1939 and 2010 UCSB-ASU analysis, positive change is in green, negative change is in red. Orthophoto background is from 2012. The grey dashed line represents the area for comparison with the CGS analysis.

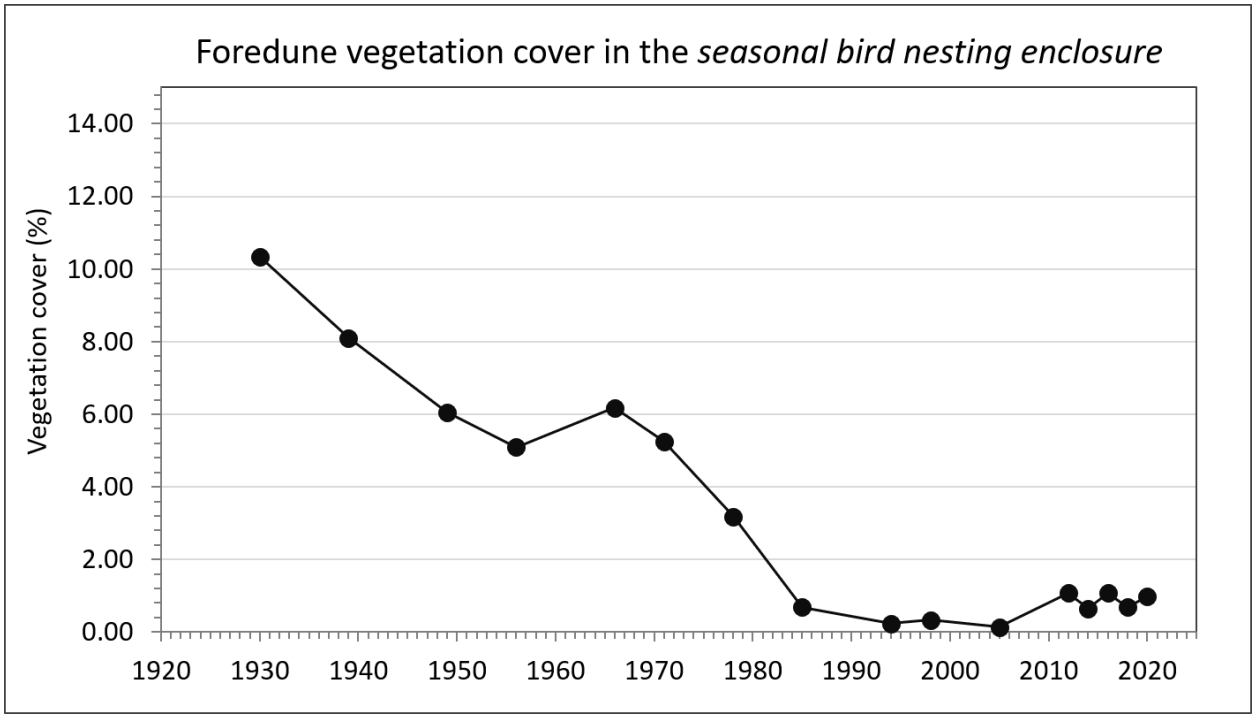

Figure S21. Percent vegetation cover within the seasonal bird nesting enclosure area (see borders in Figure 8). Vegetation cover percentages are related to the area of the analytical region.

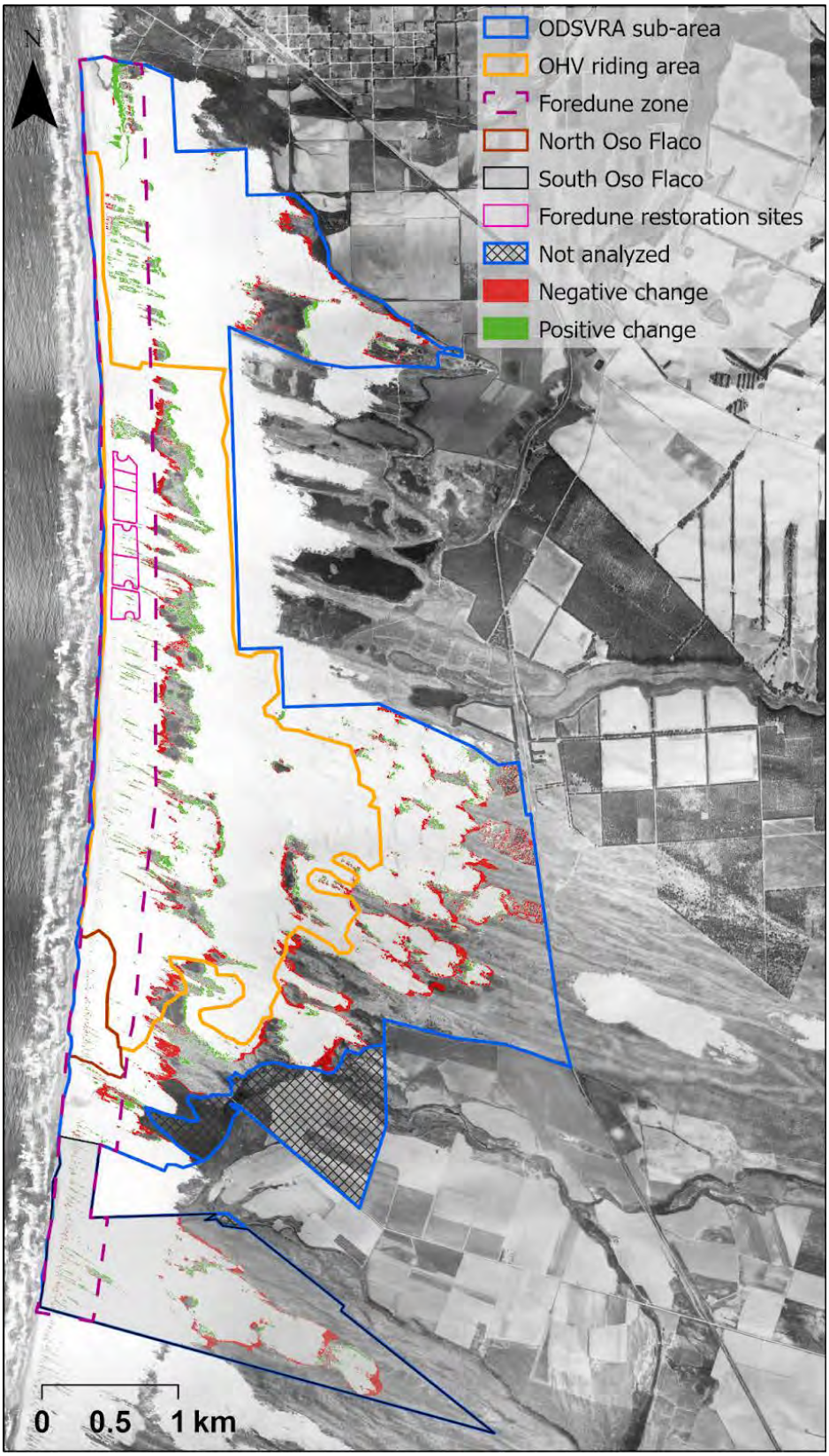

Figure S22. Vegetation change analysis results between 1939 and 1949. Positive change is in green, negative change is in red. Background orthophoto is from 1939.

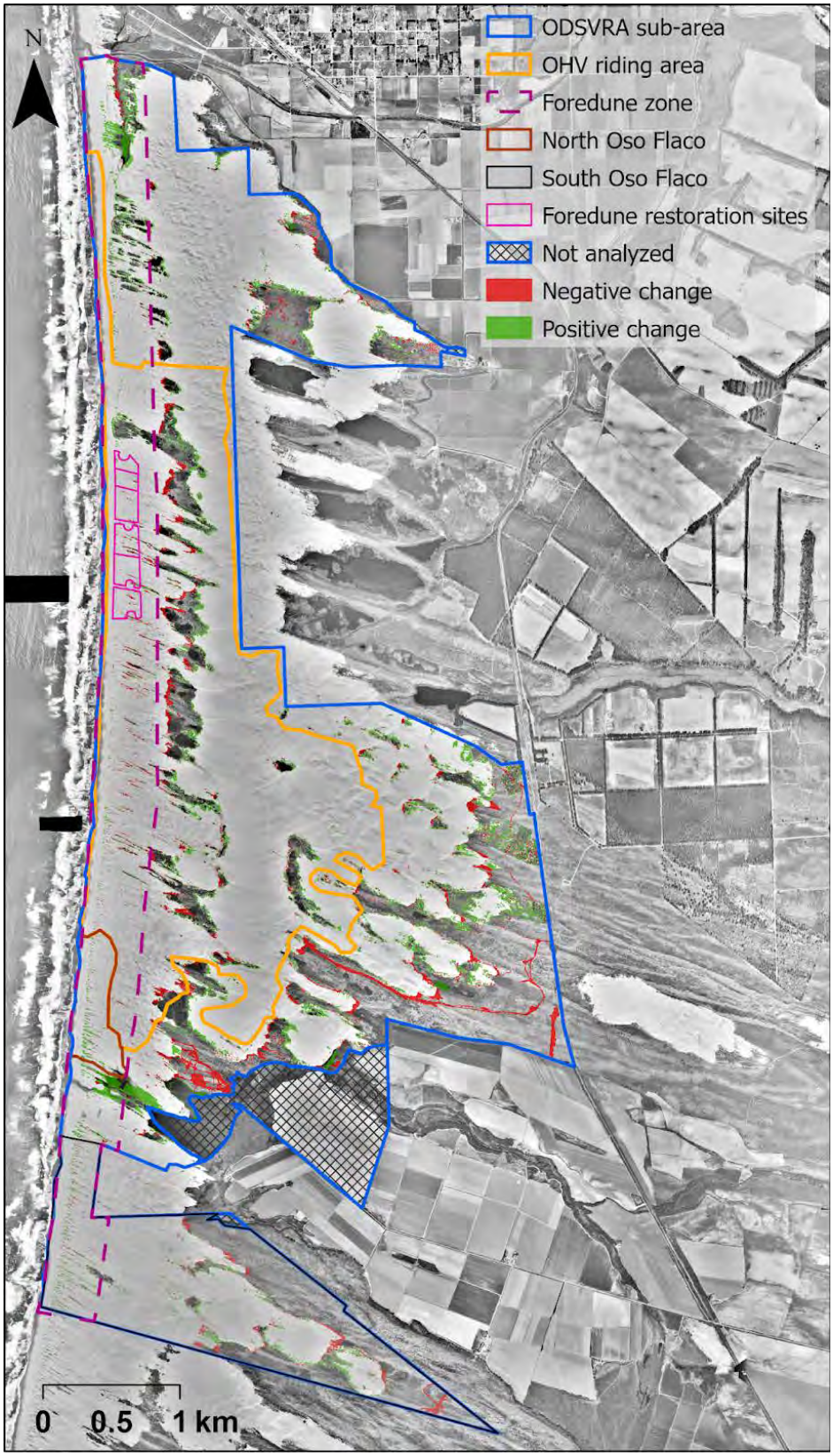

Figure S23. Vegetation change analysis results between 1949 and 1956. Positive change is in green, negative change is in red. Background orthophoto is from 1949.

Figure S24. Vegetation change analysis results between 1956 and 1966. Positive change is in green, negative change is in red. Background orthophoto is from 1956.

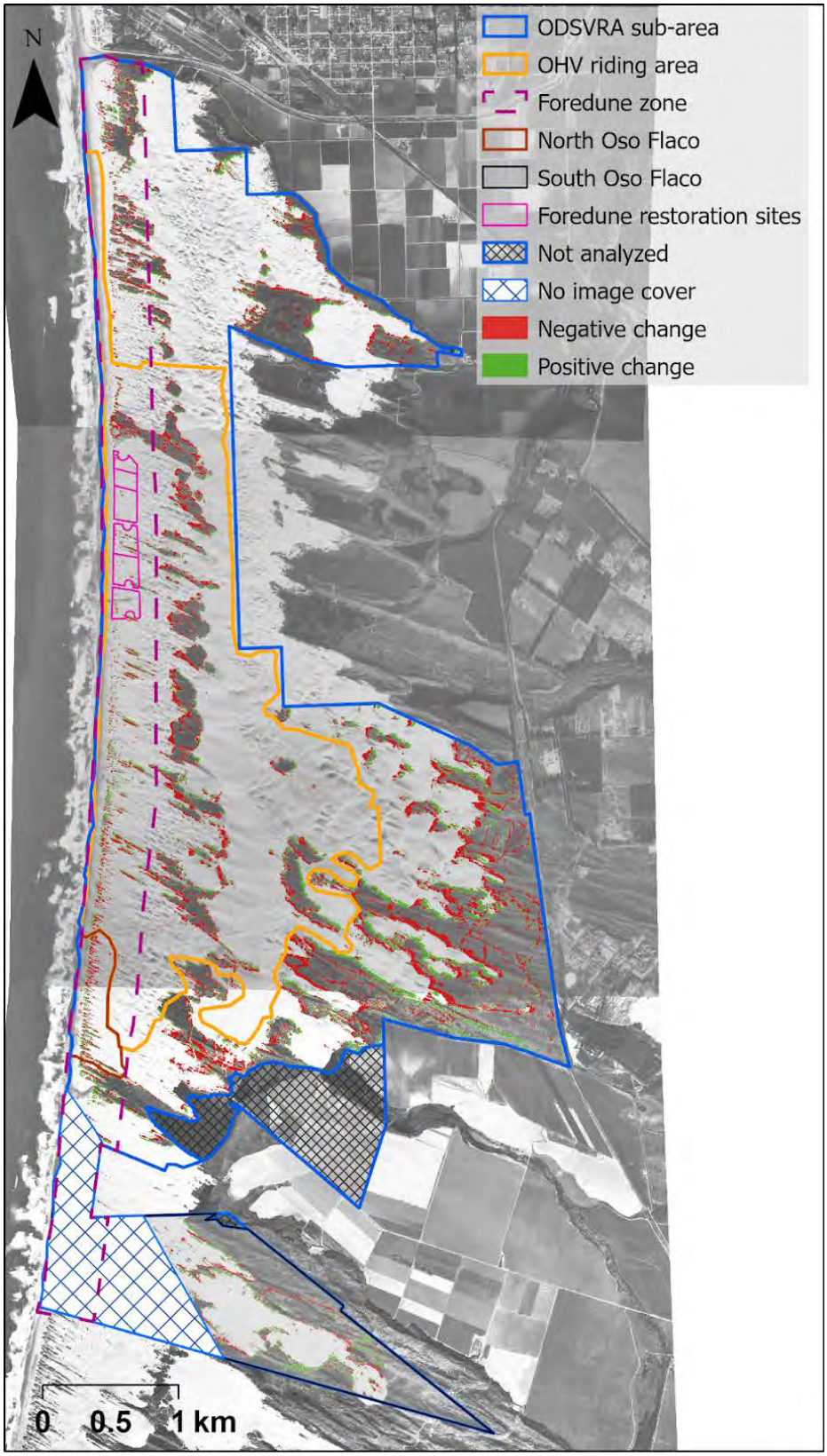

Figure S25. Vegetation change analysis results between 1966 and 1971. Positive change is in green, negative change is in red. Background orthophoto is from 1966.

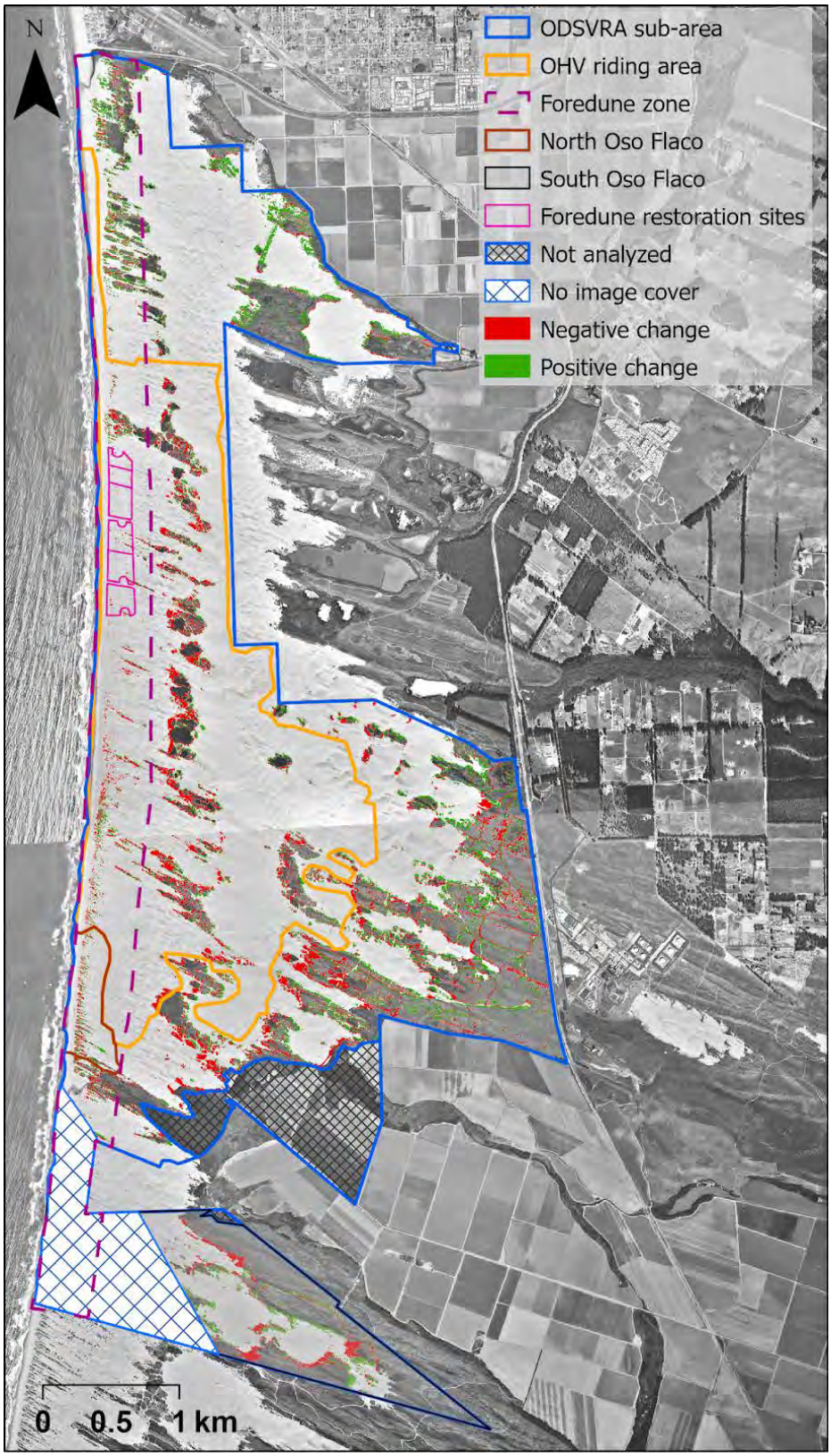

Figure S26. Vegetation change analysis results between 1971 and 1978. Positive change is in green, negative change is in red. Background orthophoto is from 1971.

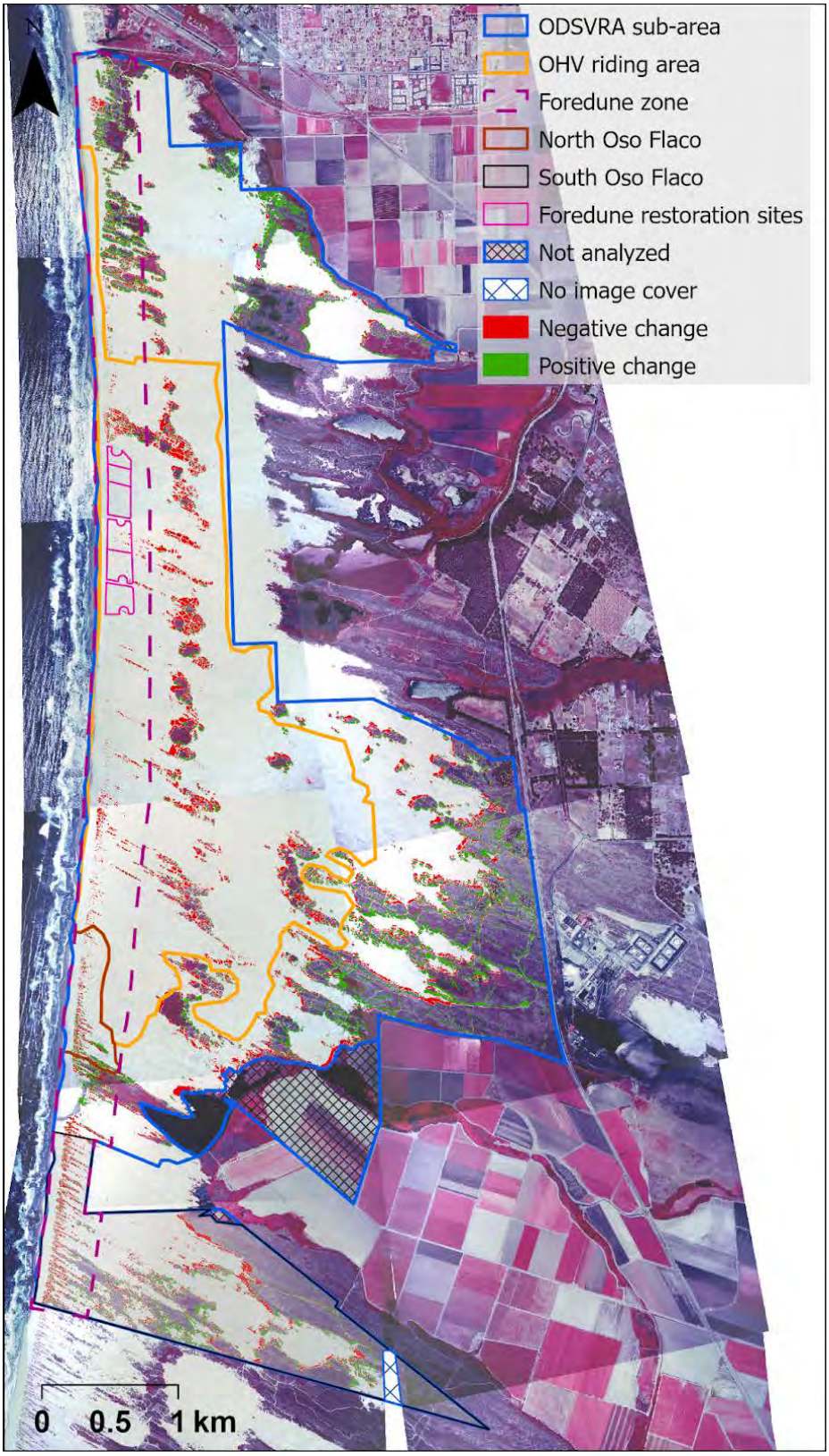

Figure S27. Vegetation change analysis results between 1978 and 1985. Positive change is in green, negative change is in red. Background orthophoto is from 1978.

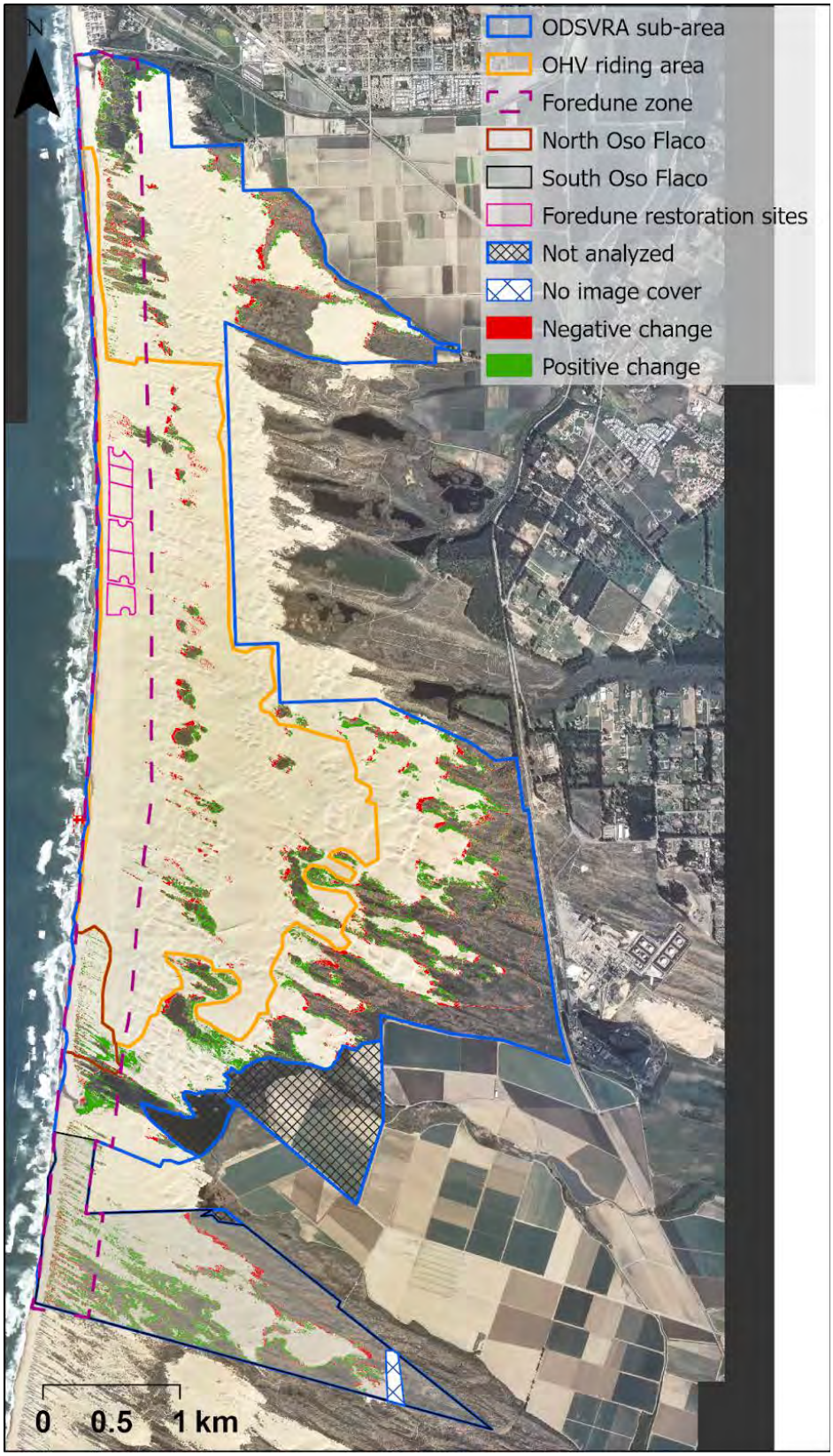

Figure S28. Vegetation change analysis results between 1985 and 1994. Positive change is in green, negative change is in red. Background orthophoto is from 1985.

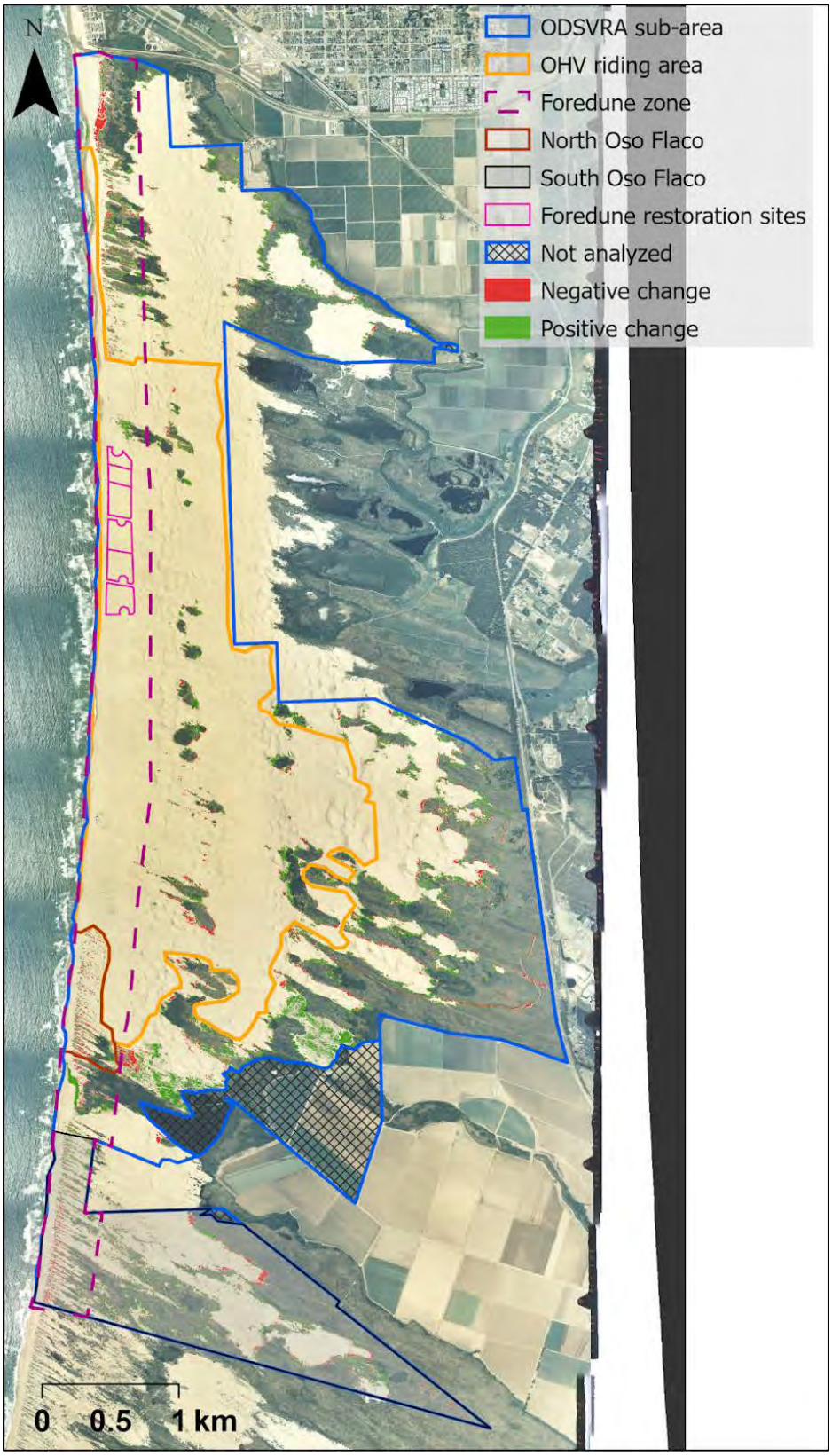

Figure S29. Vegetation change analysis results between 1994 and 1998. Positive change is in green, negative change is in red. Background orthophoto is from 1994.

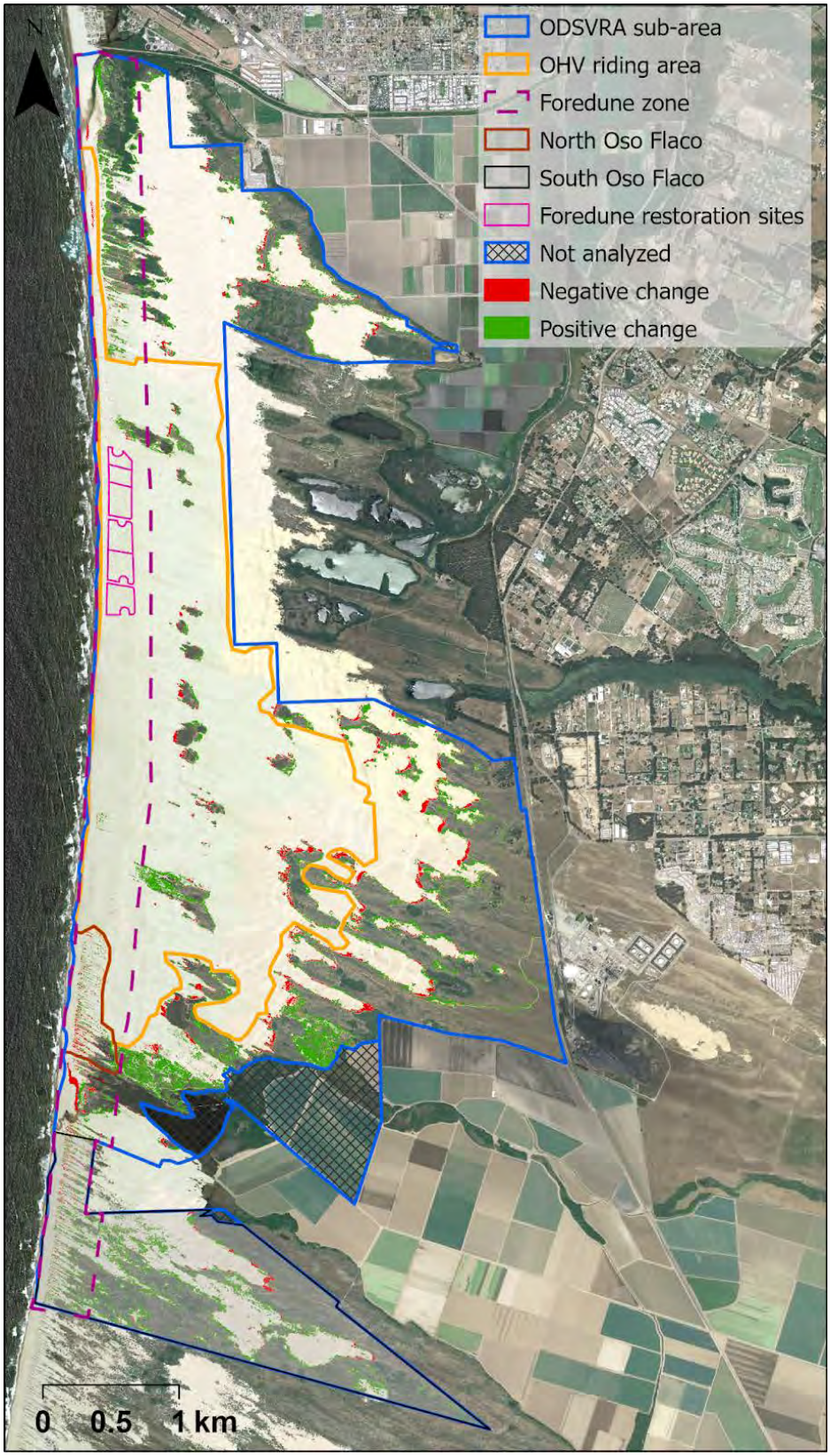

Figure S30. Vegetation change analysis results between 1998 and 2005. Positive change is in green, negative change is in red. Background orthophoto is from 1998.

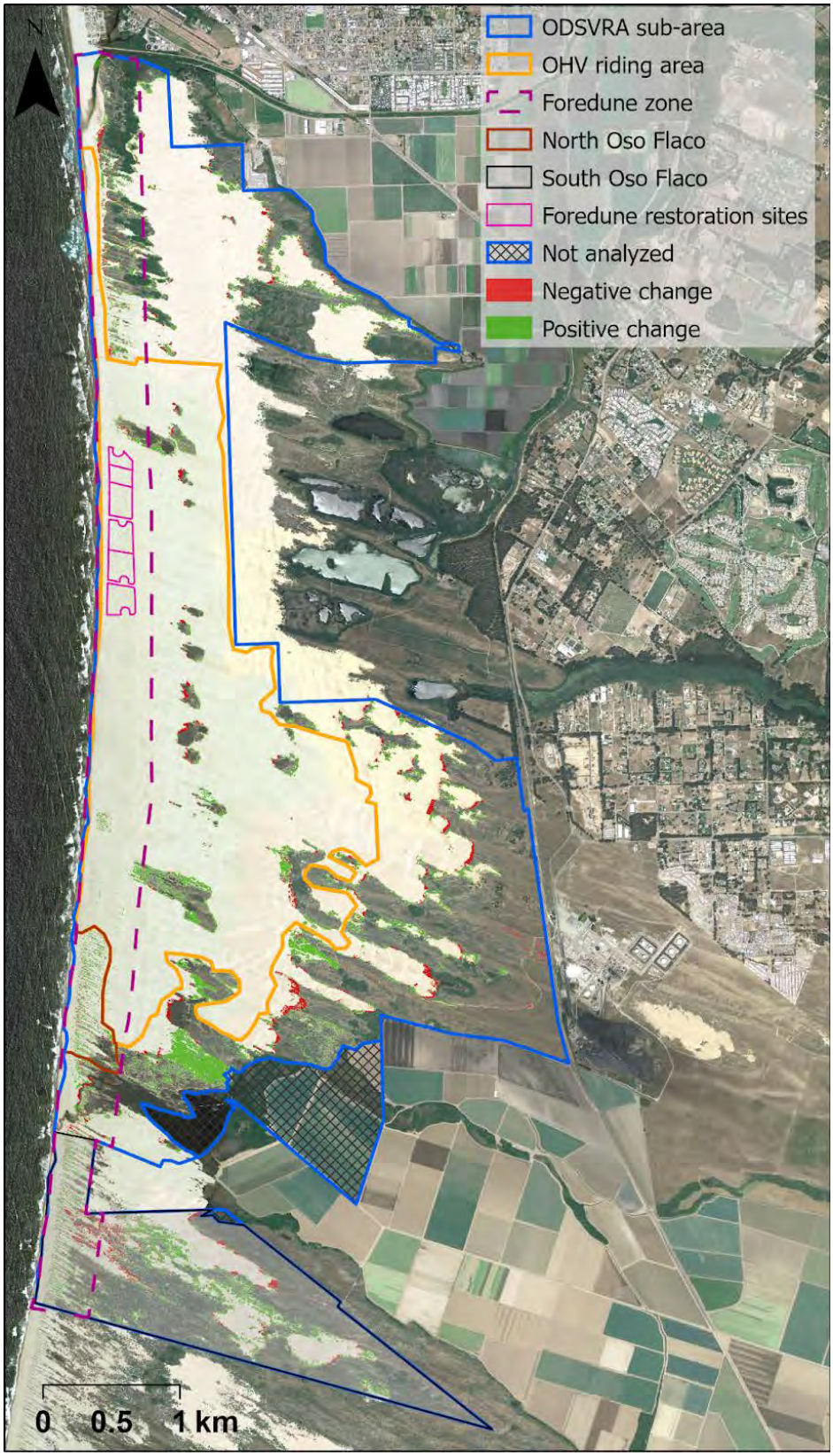

Figure S31. Vegetation change analysis results between 2005 and 2012. Positive change is in green, negative change is in red. Background orthophoto is from 2005.

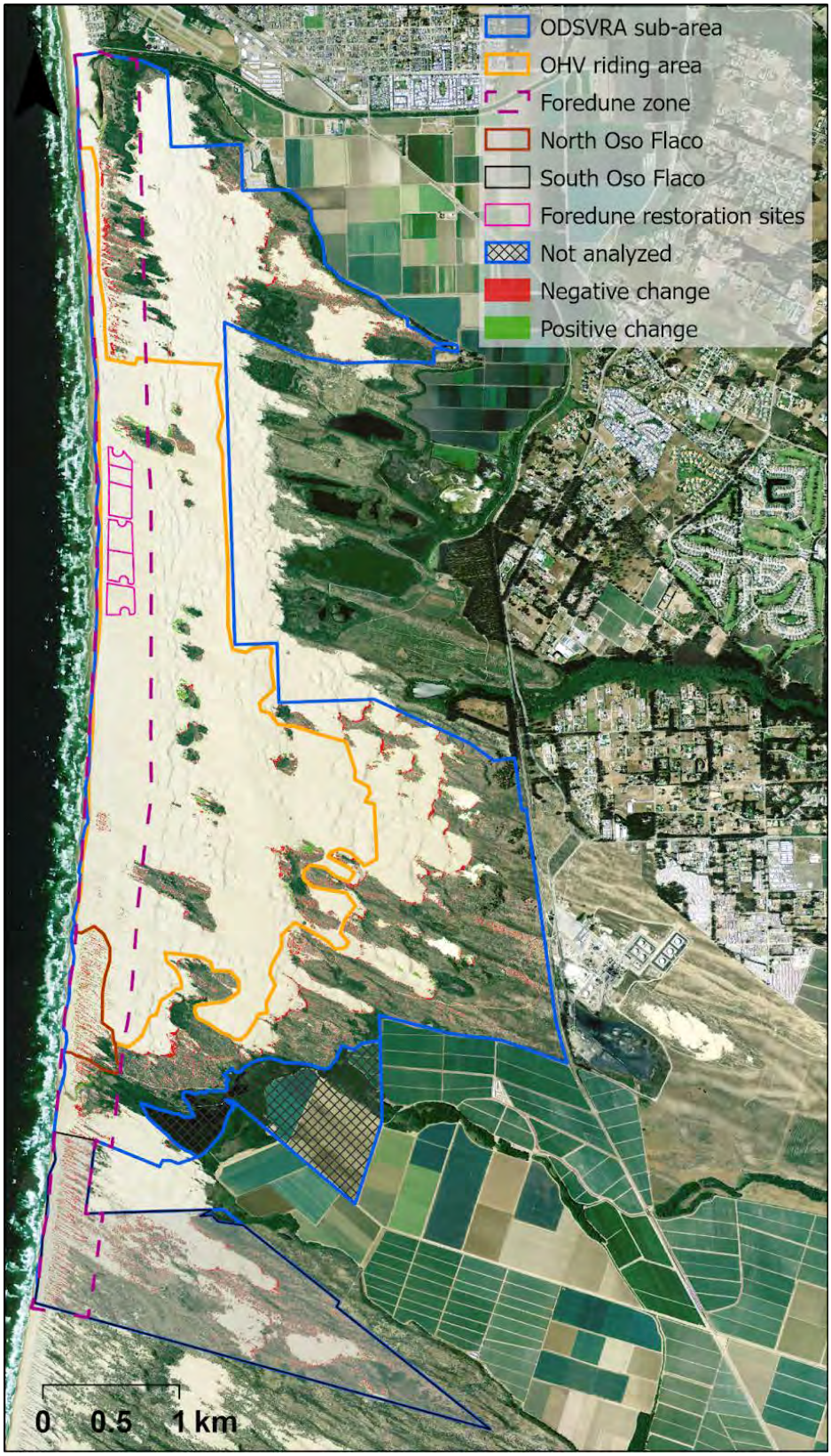

Figure S32. Vegetation change analysis results between 2012 and 2014. Positive change is in green, negative change is in red. Background orthophoto is from 2012.

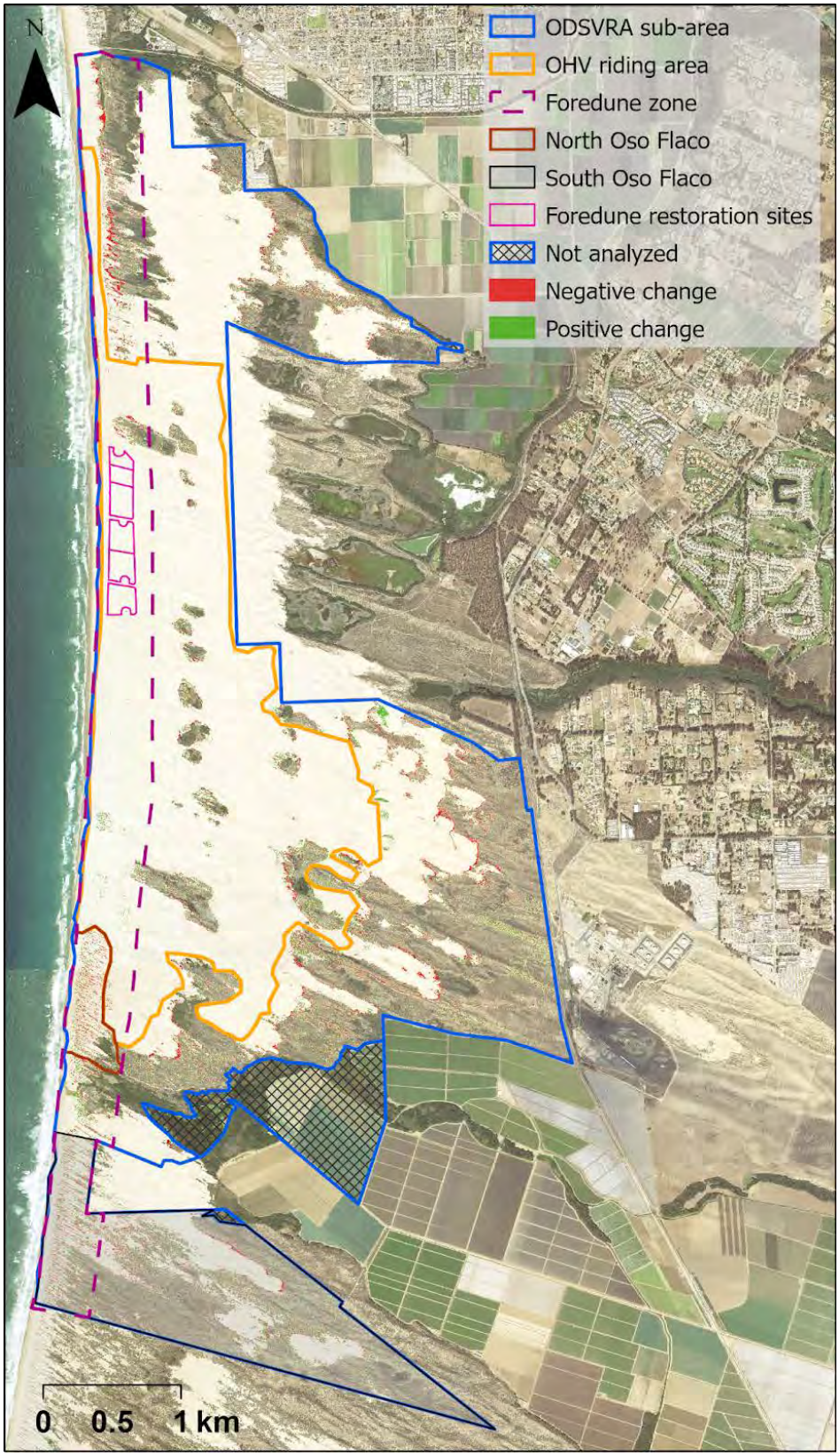

Figure S33. Vegetation change analysis results between 2014 and 2016. Positive change is in green, negative change is in red. Background orthophoto is from 2014.

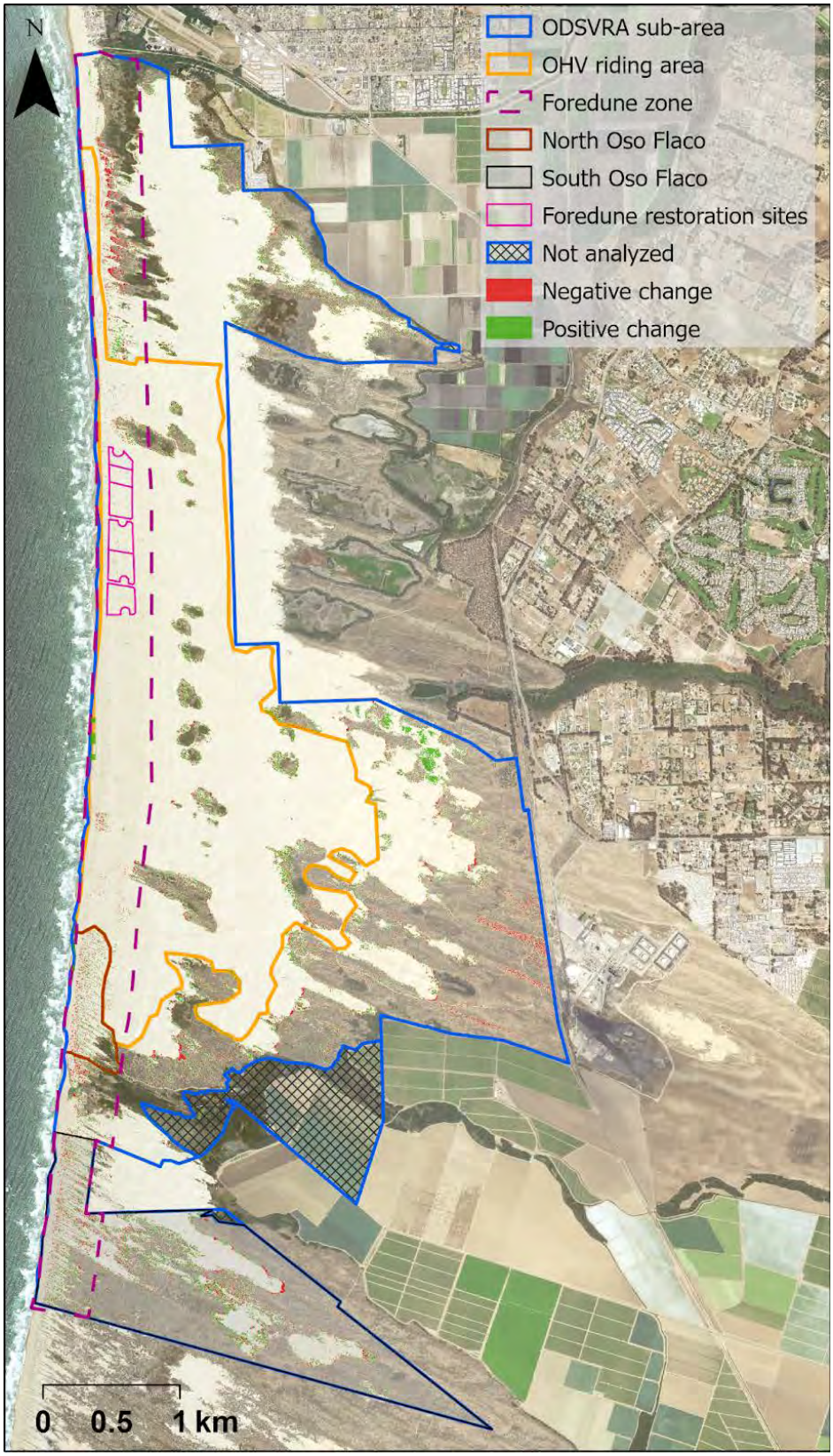

Figure S34. Vegetation change analysis results between 2016 and 2018. Positive change is in green, negative change is in red. Background orthophoto is from 2016.

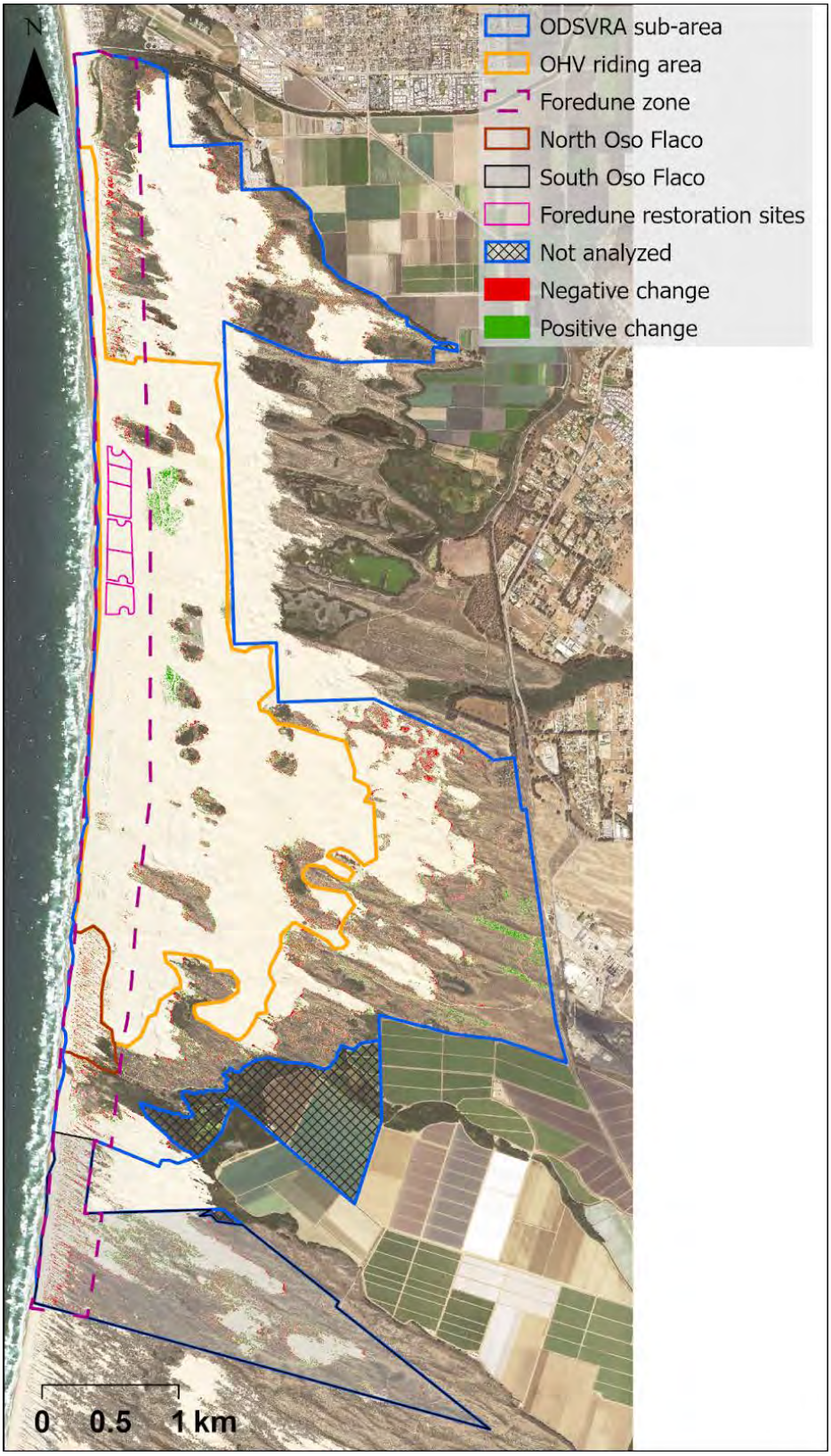

Figure S35. Vegetation change analysis results between 2018 and 2020. Positive change is in green, negative change is in red. Background orthophoto is from 2018.

Table S1. Calculated land cover values for vegetation areas from each image year, in the ODSVRA sub-area, OHV riding area, non riding area (ODSVRA sub-area minus the OHV riding area), and the Oso Flaco area. The vegetation cover (%) was calculated for the total area of each analytical zone and for the vegetation within the foredune zone (400 m from the shoreline) (see boundaries in Figures 1). The area values are presented as km² (acres) and percentage values were calculated in relation to the different analytical zones. Asterisk (*) represents a lack of image cover and thus is calculated for smaller areas (see Table 2 and Figures S3, S8 and S10).

		ODSVRA sub-area	OHV riding area	Non-riding area	South Oso Flaco	Backdune South Oso Flaco	North Oso Flaco	Foredune ODSVRA	Foredune OHV riding area	Foredune South Oso Flaco	Plover nesting enclose	Foredune restoration sites
	Analyzed area km² (acres)	17.05 (4215)	6.4 (1584)	10.64 (2631)	2.34 (577)	1.88 (466)	0.28 (69)	3.89 (932)	1.83 (453)	0.45 (112)	0.98 (243)	0.38 (95)
1930*	Vegetation cover km² (acres)	3.43 (848)*	0.51 (125)*	2.93 (722)*	0.86 (212)	0.84 (207)	0.002 (0.5)	0.07 (16)*	0.03 (8)*	0.02 (6)	0.10 (26)	N/A
	% to analytical zone	N/A	N/A	N/A	36.79	44.41	0.69	N/A	N/A	4.96	10.34	N/A
1939	Vegetation cover km² (acres)	4.27 (1056)	0.70 (173)	3.57 (883)	0.84 (207)	0.83 (204)	0.003 (1)	0.13 (32)	0.05 (12)	0.01 (3)	0.08 (20)	<0.01 (1)
	% to analytical zone	25.05	10.92	33.55	35.80	43.82	0.95	3.33	2.68	2.32	8.10	0.71
1949	Vegetation cover km² (acres)	4.05 (1001)	0.71 (157)	3.34 (826)	0.80 (197)	0.78 (192)	0.004 (1)	0.23 (57)	0.08 (19)	0.02 (5)	0.06 (15)	0.01 (2)
	% to analytical zone	23.75	11.07	31.38	34.16	41.31	1.49	5.88	4.13	4.34	6.06	1.67
1956	Vegetation cover km² (acres)	4.28 (1058)	0.74 (184)	3.54 (875)	0.81 (201)	0.78 (194)	0.01 (3)	0.33(82)	0.07 (16)	0.03 (7)	0.05 (12)	<0.01 (1)
	% to analytical zone	25.11	11.59	33.24	34.82	41.55	3.96	8.49	3.61	6.71	5.09	0.96
1966	Vegetation cover km² (acres)	4.54 (1122)	0.79 (196)	3.75 (927)	0.86 (214)	0.79 (195)	0.03 (7)	0.45 (111)	0.10 (24)	0.08 (19)	0.06 (15)	<0.01 (1)
	% to analytical zone	26.63	12.36	12.36	37.00	41.79	10.72	11.56	5.27	16.99	6.17	1.38
1971*	Vegetation cover km² (acres)	3.98 (983)*	0.64 (158)	3.34 (825)*	0.75 (185)*	0.75 (185)*	0.02 (5)	0.31 (76)	0.07 (18)	N/A	0.05 (13)	<0.01 (1)
	% to analytical zone	23.33	9.96	31.37	32.09	39.78	7.08	N/A	3.99	N/A	5.25	0.93
1978	Vegetation cover km2 (acres)	4.18 (1033)	0.48 (118)	3.70 (915)	0.95 (235)	0.86 (212)	0.02 (5)	0.43 (106)	0.05 (13)	0.09 (23)	0.03 (8)	<0.01 (0.3)
	% to analytical zone	24.51	7.44	34.78	40.64	45.45	7.33	11.03	2.94	20.57	3.18	0.34
1985*	Vegetation cover km² (acres)	4.18 (1033)*	0.25 (61)	3.93 (972)*	0.90 (223)	0.83 (205)*	0.02 (5)	0.42 (105)	0.01 (4)	0.07 (18)	0.01 (2)	<0.01 (<0.01)
	% to analytical zone	24.51	3.87	37.07	38.60	44.08	7.34	10.90	0.81	15.69	0.69	0.00
1994	Vegetation cover km² (acres)	4.62 (1141)	0.26 (65)	4.35 (1076)	1.09 (270)	0.99 (224)	0.04 (11)	0.50 (125)	0.01 (2)	0.11 (26)	0.002 (1)	<0.001 (0.01)
	% to analytical zone	27.13	4.13	41.03	47.59	53.48	15.37	12.97	0.54	23.51	0.24	0.01
1998	Vegetation cover km² (acres)	5.08 (1256)	0.30 (75)	4.78 (1180)	1.17 (288)	1.05 (260)	0.04 (10)	0.54 (133)	0.02 (4)	0.11 (28)	0.003 (1)	0.002 (0.4)
	% to analytical zone	29.85	4.74	45.03	50.71	57.07	14.62	13.86	0.88	24.70	0.33	0.47
2005	Vegetation cover km² (acres)	5.78 (1428)	0.36 (88)	5.42 (1339)	1.38 (340)	1.22 (302)	0.05 (11)	0.70 (173)	0.02 (6)	0.15 (38)	0.001 (0.3)	0.00 (0)
	% to analytical zone	33.95	5.57	51.09	59.90	66.25	16.64	18.01	1.30	33.92	0.13	0.00

		ODSVRA sub-area	OHV riding area	Non-riding area	South Oso Flaco	Backdune South Oso Flaco	North Oso Flaco	Foredune ODSVRA	Foredune OHV riding area	Foredune South Oso Flaco	Plover nesting enclose	Foredune restoration sites
	Analyzed area km² (acres)	17.05 (4215)	6.4 (1584)	10.64 (2631)	2.34 (577)	1.88 (466)	0.28 (69)	3.89 (932)	1.83 (453)	0.45 (112)	0.98 (243)	0.38 (95)
2010^	Vegetation cover km^2 (acres)	5.72 (1413)	0.39 (97)	5.33 (1316)	1.26 (310)	1.14 (283)	0.05 (13)	0.70 (172)	0.04 (9)	0.11 (28)	0.001 (0.3)	<0.01 (0.01)
	% to analytical zone	33.59	6.09	50.20	54.62	61.93	19.07	17.91	2.00	24.70	0.57	0.00
2012	Vegetation cover km^2 (acres)	6.35 (1569)	0.44 (109)	5.91 (1460)	1.51 (373)	1.35 (332)	0.07 (17)	0.81 (200)	0.04 (9)	0.01 (3)	0.01 (3)	0.00 (0)
	% to analytical zone	37.31	6.91	55.68	65.66	72.85	24.41	20.76	2.09	36.24	1.07	0.00
2014	Vegetation cover km^2 (acres)	5.97 (1474)	0.43 (105)	5.45 (1369)	1.41 (346)	1.27 (313)	0.06 (15)	0.69 (170)	0.04 (10)	0.006 (2)	0.07 (17)	<0.01 (0.01)
	% to analytical zone	35.05	6.65	52.21	61.48	68.62	21.87	17.69	2.24	32.27	0.65	0.01
2016	Vegetation cover km^2 (acres)	6.15 (1520)	0.44 (109)	5.71 (1411)	1.43 (352)	1.29 (318)	0.05 (14)	0.70 (173)	0.04 (10)	0.14 (34)	0.01 (3)	0.00 (0)
	% to analytical zone	36.15	6.89	53.83	62.02	69.67	20.00	17.99	2.24	30.76	1.07	0.00
2018	Vegetation cover km2 (acres)	6.14 (1516)	0.49 (121)	5.65 (1395)	1.47 (363)	1.32 (327)	0.06 (15)	0.68 (168)	0.04 (10)	0.14 (36)	0.007 (2)	<0.01 (0.01)
	% to analytical zone	36.05	7.63	53.22	63.88	71.69	21.46	17.46	2.21	31.95	0.68	0.01
2020	Vegetation cover km^2 (acres)	6.01 (1486)	0.52 (128)	5.49 (1358)	1.46 (360)	1.33 (330)	0.05 (13)	0.64 (157)	0.04 (11)	0.12 (30)	0.01 (2)	<0.01 (<0.01)
	% to analytical zone	35.32	8.07	51.79	63.32	72.24	19.05	16.36	2.35	26.83	0.99	0.00

January 7, 2022

Memo: SAG Individual Reviews of "UCSB Historical Vegetation Cover Change Analysis (1930-2020) within the Oceano Dunes SVRA" (N. Swet, Z. Hilgendorf, I. Walker, December 28, 2021)

From: Scientific Advisory Group (SAG)

To: Jon O'Brien, California Department of Parks and Recreation (CDPR)
Ian Walker, University of California, Santa Barbara (UCSB)

Below, please find reviews of the report, "UCSB Historical Vegetation Cover Change Analysis (1930-2020) within the Oceano Dunes SVRA," by 2 individual members of the SAG. The reviews were prepared by Carla Scheidlinger (Reviewer 1) and Raleigh Martin (Reviewer 2). The SAG did not prepare a collective review of this report.

Respectfully,
Dr. Raleigh Martin, on behalf of the SAG

Reviewer 1 (Carla Scheidlinger)

Comments – Carla Scheidlinger
UCSB Historical Vegetation Cover Change Analysis
(1930-2020) within the Oceano Dunes SVRA

This is a very strong report and it has benefitted from the prior discussions we have had about it. Separating the Supplementary materials is a good idea, as those maps are important but not as important as the ones that were included as in-report figures. Nice job!

General comments:

- Standardize how you refer to the North and South Oso Flaco areas. In some places, North and South are capitalized and in others those words begin with lower case letters. Also, sometimes you say "south Oso Flaco" and in other places "southern Oso Flaco". Making references to these locations standardized will avoid confusion.
- The captions for Figures 10, 12, 13, and 15 need to have the word "positive" spelled correctly.
- Make it clear in the Summary and in the Introduction that **both** North and South Oso Flaco are reference areas.
- Close-up figures of foredune areas are very helpful, especially to help sort out the difference between the purples in the 1985 image and the ted of vegetation decreases.

Specific comments:

- Sentence pages 2-3: "After 1966, plant cover decreased to a low of 3.9% in 1985 and remained low (<5%) until the early 2000's when vegetation cover gradually began to increase to 2020 levels." If this is in all probability due to revegetation efforts on the part of Parks, perhaps say so here.
- First bullet Page 3: "…,then declined to 1985". Not clear: declined to 1985 level? Declined until 1985?
- Same bullet: this is the first time you introduce the idea of positive AND negative change. Perhaps clarify that both can be seen in one area, with increases in some places and decreases in others. It will be important for the reader to know when you are referring to a NET gain or loss in a given area or to SEPARATE gains and losses that occur within the same location over the same period of time.
- Page 6, point 4: capitalize Flaco
- Legend and description for Figures 4 and 5: You refer to South Oso Flaco as both gray and black; choose one or the other. Also, the color for OHV riding area really doesn't register to me as "orange"; it looks more like rust or brown. Can it be changed to red?
- Page 17: "It is important to note that all orthophotos from 2005-2020 were taken during the period of nesting for the Western Snowy Plover (March through September)". Perhaps indicate why it is important to note this: that vegetation cover was photographed at a time when it was higher than it would have been had the photo been taken at a different time of year?

- Page 18: “Figure 5 indicates that foredunes at south Oso Flaco that were not subjected to the same amount of OHV activity as that in the nearby riding areas of ODSVRA (at least since 1982) have maintained significantly higher vegetation cover, particularly between 1985 and 2005.” Perhaps say “attained and maintained”.
- Page 36: “From this, plant cover was carefully and systematically classified and analyzed in a GIS (ArcGIS Pro)…” In a GIS what?
- Page 38: “…declined to 1985…” Same issue as above on page 3: the “declined to 1985” is not clear.
- Figure S2: typos: “backbude of the ODSVRA su-area”
- Is there any way you can add the orange OHV Riding Area shown in figure S20 to figure S19? It would help the comparison between the 2 images.
- Can you make a figure that would put the image of S4 (1939) on the same page as S18 (2020)? It would be nice to be able to see them side by side; maybe on a large landscape page. I printed them both out to look at, and it was a useful comparison.

Reviewer 2 (Raleigh Martin)

This report presents a comprehensive study of 90 years of vegetation cover change at the Oceano Dunes State Vehicular Recreation Area (ODSVRA), derived through careful processing and analysis of historic air photos. Analyses address both overall vegetation change across the ODSVRA and vegetation changes within specific subregions, each of which have experienced distinctive management approaches and other drivers of change. In addition, analyses presented in this report address vegetation change within distinctive foredune and back dune morphological settings.

Not surprisingly, the story of vegetation change at the ODSVRA is complicated. The overriding trend is of increasing vegetation cover over time, but there are significant temporal and spatial variations in the direction and rate of change across the park. This report makes it possible to examine some of these variations by breaking out the vegetation change analysis into specific subregions and time periods. The majority of long-term vegetation growth appears to occur in back dunes in the eastern half of the park (i.e., Pismo Dunes Preserve, South Oso Flaco, and areas to the east of the OHV Riding Area), due to a combination of invasive weed growth, management controls, and possibly other driving factors (though this overall trend of increasing vegetation seems to have reversed since about 2010 due to active invasive weed removal campaigns). In contrast, vegetation cover in the OHV Riding Area peaked in 1966, declined rapidly to 1985 with increasing OHV activity, and then has gradually increased as a result of management actions and possibly other factors (e.g., invasive species). Trends within the foredunes are complicated and reflect a combination of management actions, invasive species impacts, and possibly global climate change effects.

One of the motivating factors for this report was to inform ongoing work by the Scientific Advisory Group (SAG) to revisit the initial PM10 mass emissions reduction target for the Stipulated Order of Abatement (SOA). The results of this report regarding vegetation change within the OHV Riding Area subregion could be used to inform this SOA target by specifying vegetation conditions for model simulations of “pre-disturbance” emissions scenarios for the Riding Area. In particular, the results of this study suggest that the period between 1939-1966 (and possibly earlier, though comprehensive photos are lacking), when vegetation cover within the Riding Area subregion was at its peak prior to intensive OHV activity (which seems to have picked up in the 1950s), could serve as the basis for such pre-disturbance scenarios. Also of interest to the SOA target is the fact that negative vegetation change in the OHV Riding Area up to 1985 seems to be concentrated just downwind of the foredune zone (see Fig. 13), an area that recent computational fluid dynamics (CFD) modeling has shown to experience sheltering from strong winds in the presence of a mature foredune. These results could inform attempts to better account for PM10 dust mitigating effects of dune restoration activities in the future.

The results of this report defy easy interpretation, as vegetation change appears to be driven by dynamic and intersecting factors. But it is clear that these new results on vegetation change over time were carefully and rigorously derived. The Methods section describes a thorough, comprehensive, and systematic approach to pre-processing and analyzing historic air photos

(e.g., alignment, orthorectification, classification, pixel correction) to ensure comparability across photo years. In addition, the report helpfully explains differences between these new analyses and previous studies of vegetation cover by the California Department of Parks and Recreation (CDPR) and the California Geological Survey (CGS). The resulting vegetation cover maps for each individual year (shown in supplemental Figures S3-S18), along with calculated plant coverage by area / percentage (summarized in Table 3 and Figure 4), will provide a comprehensive resource to inform future ODSVRA management decisions.

Overall, I think this report is adequate in its present state, and it does not require any significant edits before it is published. That said, I do think some of the results could be more clearly presented, and the framing of certain analyses could be adjusted to more directly inform management questions. Therefore, I offer a few suggestions to increase the clarity and potential value of this report.

1. I appreciate that analyses cover both the full ODSVRA sub-area as well as small subregions contained within the ODSVRA boundaries. However, the way in which these are presented as "6 analytical areas" is confusing, given the distinctive ways in which results are analyzed for these regions. For example, I was confused when I saw that Figure 4 presents results for only 4 (not 6) areas. After spending some time with the report, I finally began to understand the logic of the analytical areas. That said, I think there could be a much clearer way of presenting these results. In my understanding, there is 1 master area (the ODSVRA sub-area) and 3 subregions (OHV Riding, North Oso Flaco, and South Oso Flaco), as depicted in Figure 4. For certain analyses, there is also further subdivision between foredune / back dune and the foredune restoration area, as depicted in Figure 5. I think describing a clearer explanation of how these subregions and sub-analyses are constructed, rather than simply referring to "6 analytical areas," would make the results of this report easier to understand.

2. I appreciate the explicit comparison between 1939 and 2020 (i.e., Fig. 16), which provides an overarching view of historic vegetation changes over the full span of available data. In addition to this and the other existing change analyses (1939-1985, 1985-2012, 2012-2020), I would suggest adding 1939-2012 as a target of change analysis. Such an analysis would provide a helpful perspective on the overall change that occurred at the ODSVRA roughly prior to adoption of Rule 1001 and the associated Particulate Matter Reduction Plan (PMRP).

3. Beyond this particular study, the processed air photos could serve as a very valuable resource for further study of coastal change at the ODSVRA and for comparisons to other coastal dune systems. Therefore, I encourage Parks / UCSB to make the processed photos publicly available within an accessible and long-lived data repository, within a reasonable period of time after publication of this report.

Further specific comments are provided below.

Specific Comments

(a) Executive Summary, p. 2: Instead of "2020-21 ARWP," I suggest simply saying "2020 ARWP." The latter is the terminology used by Parks. This reflects the fact that each ARWP is both a retrospective annual report (i.e., 2019-2020) and prospective work plan (i.e., 2020-21). Please make the same change throughout the document (for example, on p. 39, change "2022-23 ARWP" to "2022 ARWP").

(b) Executive Summary, p. 2: "five" analytical zones => "six" analytical zones

(c) Methods, p. 6: "state parks" => "State Parks"

(d) Methods, p. 8: I'm confused by the following statement: "Due to the limited image cover of the 1930 image (Table 2), the historical change comparison analysis was done using the 1939 image." What I'm inferring is that you wanted to use the oldest possible image as the baseline for the historical change comparison analysis, but that the incompleteness of the 1930 image necessitated using 1939 instead for this baseline.

(e) Methods, p. 11: Please clarify the intended reference for the following statement: "For this comparison, we examined differences within the OHV riding area in four image years (1939, 1978, 2014, 2020) that were also analyzed in the CDPR report." Is the "CDPR report" the 2020 wind wedges report? Please clarify.

(f) Results, p. 20: This finding about overall higher rates of change starting in 2012 (both positive and negative) is very intriguing. I think the reasons given here are plausible, but one other thing that occurs to me from looking at Table 1 is that there was a switchover to consistently using NAIP 4-band imagery starting in 2010. Is it possible that the associated improvement in image quality (and thus the ability to resolve more detailed changes) may also be driving a perception of higher rates of change in recent years?

(g) Results, p. 20-21: Perhaps this is just the convention of change detection studies, but I find myself continually confused by the terminology regarding positive and negative change. I interpret "total change" as absolute positive change PLUS absolute negative change (which I think of "gross change"). Along with these analyses of gross change, it would also be helpful to know more about "net change" (i.e., absolute positive change MINUS absolute negative change). In particular, gross change per year would give a sense of the overall dynamism of the system, whereas net change per year would give a sense of overall trends in vegetation growth and decay. Plots of gross change and net change over time (for each of the analytical areas) would be very instructive. In particular, for existing figures (e.g., Fig. 6), it would help to show an overlay of "net change," as it is hard to tease out such change just from looking at the stacked red and green bars.

(h) Figure 9, p. 26: Please specify the meaning of the colors. I'm assuming gray = unchanged, green = positive change, red = negative change. But it would to confirm this, either via a legend or via description in the caption.

UCSB Historical Vegetation Cover Change Analysis

(1930-2020) within the Oceano Dunes SVRA

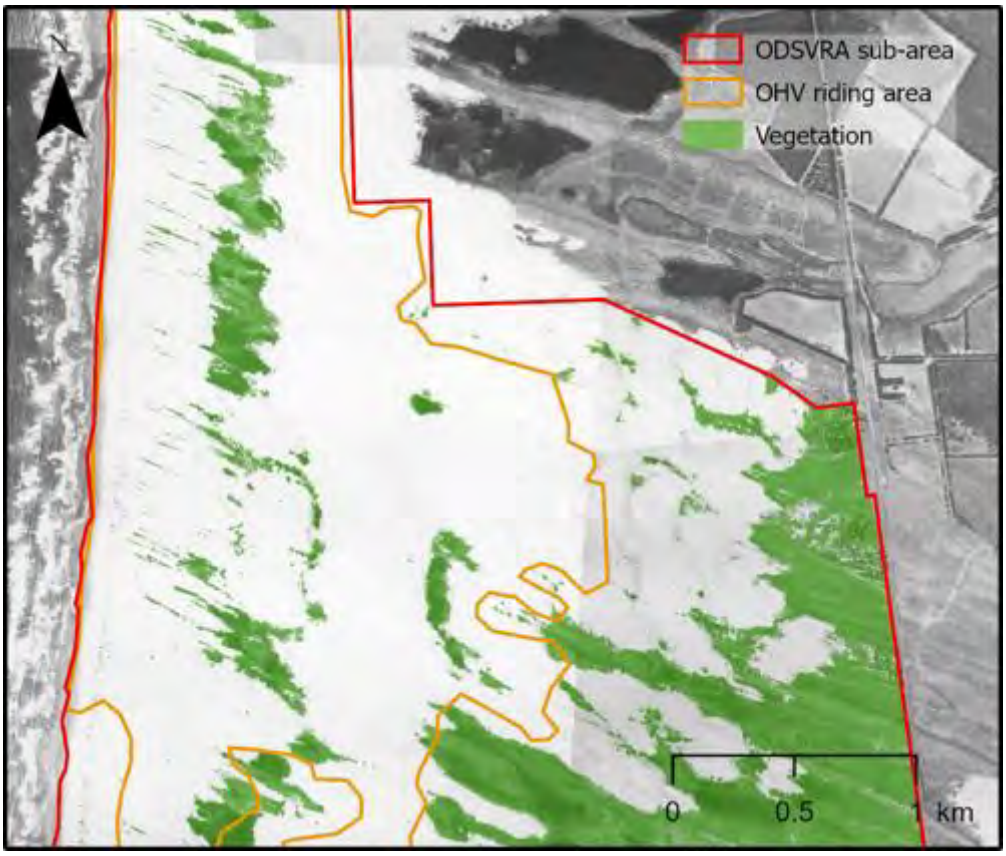

Map of vegetation cover (green) derived from historical 1939 aerial photography of the southern portion of the Oceano Dunes SVRA

Prepared by: Nitzan Swet[1], Zach Hilgendorf[1,2] and Ian Walker[1,3]

[1] Department of Geography, University of California Santa Barbara

[2] School of Geographical Sciences and Urban Planning, Arizona State University

[3] Member of the Oceano Dunes Scientific Advisory Group

February 2022

EXECUTIVE SUMMARY

This report examines 90 years of historical changes in vegetation cover within the ODSVRA as requested by CDPR for the 2020 ARWP. Trends in plant cover are mapped and quantified using a Geographic Information System (GIS) and best available aerial photography obtained from CDPR, UCSB Library's Geospatial Collection, and the National Agriculture Imagery Program (NAIP), from 16 years with sufficient coverage of ODSVRA between 1930 and 2020.

To examine and interpret vegetation cover trends and allow comparison between different regions of the ODSVRA, the report focuses on:

- the overall ODSVRA, located south of Arroyo Grande Creek (~75% of the total area of ODSVRA), presented here as ODSVRA sub-area,
- the OHV riding area (c. 2013),
- the North Oso Flaco foredune complex, which serves as a reference site for foredunes closed to OHV activity since 1982,
- the South Oso Flaco dune complex within the ODSVRA boundary, including both foredune and backdune areas, which serves as a reference site for mature foredunes and backdunes that have not seen OHV activity since 1982,
- the foredune zone of each of the areas above, or the area in which foredune vegetation would typically exist in the region, that extends ~400 m eastward/inland from the high-water mark,
- the new (2020) foredune restoration sites, located within the foredune zone of the OHV riding area between post markers 4-6.

Plant cover maps and calculations (area and percentage) were obtained for each analytical zone across all image years.

Resulting maps were analyzed for locations and extents of change between all years. In addition, changes between 4 specific time periods that relate to different land management intervals were interpreted:

1. 1939-1985: landscape responses preceding the management of ODSVRA by CDPR, which began in 1982,
2. 1985-2012: landscape changes during the management of ODSVRA by CDPR up to adoption of SLO-APCD Rule 1001 (2011) and related particulate matter reduction plans (PMRP),
3. 2012-2020: landscape responses following implementation of PMRP mitigation efforts resulting from Rule 1001 (2011) and the eventual Stipulated Order of Abatement (SOA) in 2018, and
4. 1939-2020: total landscape change over the historic aerial photo record that compares a time prior to widespread OHV riding and the current state of vegetation cover.

Plant cover trends within ODSVRA have varied over time and differ notably between the analytical zones. Within the broader ODSVRA sub-area, vegetation change generally increased over time, from approximately 25% in 1939, to a peak of 37% in 2012, to just over 35% in 2020. In the OHV riding area, vegetation cover has been comparatively low across all years and declined appreciably from a peak of 12% in 1966 to 8% in 2020. After 1966, plant cover decreased to a low of 3.9% in 1985 and remained low (<5%) until the early 2000's when vegetation cover gradually began to increase to 2020 levels following revegetation efforts by CDPR. In the South Oso Flaco area, plant cover changes are similar to those in the broader ODSVRA sub-area, but with generally higher values. Vegetation cover at South Oso Flaco decreased from 26% in 1939 to a historic low of 24% in 1949, then more than doubled to a peak of 66% in 2012. Following this, plant cover declined slightly but remained >60% to 2020.

Similar trends occur within the foredune zone in each analytical area, albeit with generally less plant cover. The foredune zone at the South Oso Flaco reference site had very low plant cover (2.3%) in 1939, but increased by an order of magnitude to over 30% in the 2010s. For comparison, foredune vegetation in the OHV riding area also had low cover (2.6%) in 1939, rose to a peak of 5.3% in 1966, but steadily declined to very low values ~1% from 1985 to 1998. Since 2005, plant cover increased slightly in the riding area to 2.4% by 2020, mostly due to new plants on the margins of fenced vegetation islands and in the seasonal bird nesting enclosures. At North Oso flaco, foredune vegetation cover was extremely low (<1%) in the 1930s, less than in the OHV riding area, but after 1985 the values increased to over 24% in 2012.

Broader ecological and climatic conditions aside, observed patterns and differences in vegetation trends across these areas is largely attributable to three main factors: 1) the presence of camping and OHV riding (sanctioned or otherwise) activities in the dunes, 2) widespread and targeted removals of invasive grass species in some areas (e.g., South Oso Flaco), and 3) land management and plant restoration efforts by CDPR since establishment of the park in 1982 and in response to PMRPs associated with Rule 1001 (2011) and the 2018 SOA.

Interpretation of positive (vegetation gain) and negative (vegetation loss) changes over the four reference time periods indicates the following:

- 1939-1985: a general decline in plant cover in the foredune and backdune zones of the OHV riding area (from 11% to 4%) while vegetation in the broader ODSVRA increased notably from 1939-1966, then declined until 1985. In the riding area, overall change is characterized by 10% negative change (plant losses) and only 2% positive gains,
- 1985-2012: mostly increasing plant cover with over 15% gains in the broader ODSVRA sub-area, mainly around existing vegetation and other targeted restoration areas, particularly between 2005 and 2012.

- 2012-2020: a general decline in plant cover across the ODSVRA and South Oso Flaco areas compared to previous intervals with 8% total change in the ODSVRA sub-area. Some of this decline reflects removal of invasive plants by CDPR. Within the OHV riding area, plant cover remained steady at ~8% during this time.

1. Introduction

Vegetation plays a vital role in the development and maintenance of certain dune types and related ecosystems common in the central coast of California (e.g., nebkha and shadow dunes, foredunes, blowouts, parabolic dunes) as well as in the stabilization of sand surfaces to reduce sand drift, wind erosion, and dust emissions. In areas of high recreation activity, natural windblown (aeolian) and related dune ecological processes often become challenged. In turn, this can result in a loss of vital ecosystem services provided by coastal dunes including mitigating sand transport and dust emissions, buffering coastal erosion and flooding, facilitating groundwater recharge, and providing important habitat for a wide range of endemic, migratory, threatened, and endangered plant and animal species.

This report provides a thorough review of historical changes in vegetation cover within the Oceano Dunes State Vehicular Recreation Area (ODSVRA) as requested by the California Department of Parks and Recreation (CDPR) for the 2020-2021 Annual Report and Work Plan (2020 ARWP). Vegetation cover from historical aerial photographs from the 1930s to 2020 was analyzed to interpret changes from the earliest photo records. As such, the analysis documents landscape changes through decades of unsanctioned OHV activity prior to establishment and management of ODSVRA by CDPR in 1982 and through almost another 40 years following. Changes during this later period reflect both OHV activity as well as significant land use management and vegetation restoration initiatives implemented by CDPR to mitigate dust emissions and control invasive species. With more frequent photo coverage in recent years, responses of the landscape following implementation of Particulate Matter Reduction Plans (PMRP) associated with the SLO-APCD Rule 1001 “Coastal Dunes Dust Control Requirements” of 2011 and the State of California Stipulated Order of Abatement (SOA) in 2018 are also quantifiable.

The main objective of the report is to document and analyze historical changes in vegetation cover and related dune landforms within ODSVRA to help inform development of baseline conditions for restoration and dust emissions mitigation strategies in the future 2022 ARWP. In particular, it is important to establish what the state of vegetation cover was prior to, and since, the management of ODSVRA by CDPR and related changes in plant cover with sanctioned OHV activity and camping in the dunes. These results can also inform assessment of landscape changes

associated with more recent management and restoration activities in response to PMRP activities and act as a tool for identifying future treatment locations and methods.

2. Methods

An extensive dataset of aerial photography for the Oceano Dunes region was obtained from the UCSB Library Geospatial Collection[1], CDPR, and the National Agriculture Imagery Program (NAIP) website[2] consisting of 19 individual years of imagery taken between 1939 to 2020 (Table 1). Due to limitations resulting from limited coverage, image projection, size, and/or shadowing, three image years were omitted from the analysis, leaving a total of 16 image years. The imagery datasets for 1930 to 1985 are composed of a mosaic of individual aerial photos (tiles). The aerial photo tiles for 1930 to 1978 were received as digital scans from the UCSB Library and processed using Agisoft Metashape and standard historic imagery photogrammetric methods[3]. The 1985-1998 aerial photo tiles were scanned and processed by CDPR staff. The rest of the imagery used in this report (2005-2020) are in a digital orthophoto mosaic format (one tile) downloaded from different sources. The 1994, 1998, and 2007 images were received from CDPR, however, their sources are uncertain (see Table 1). The 2005 and the 2010 to 2020 images were downloaded from NAIP (Table 1).

For each image year between 1930 and 1985, photo tiles required local alignment to one another, typically completed with a simple shift or 2nd order transformation. Once all tiles were aligned, clipped shapefiles were created for each to remove cataloging data from the edges, interior portions of each tile were extracted, and the resulting images were then loaded into a raster mosaic of the study area as a file geodatabase in the Geographic Information System (GIS) software ArcGIS Pro. During this step, the tiles were manually assessed and layered so that rasters (digital image grid cells or pixels) with darker, more pronounced, sharper features were on top of those with lighter, or less pronounced features. This also allowed for continual assessment and correction of tile alignment. This alignment and orthorectification step is important as slight misalignments and planar tilt issues can produce appreciable errors in positioning and measurements of ground features. The final mosaic was then exported to a single digital (tiff) file for each photo year.

[1] University of California Santa Barbara Library geospatial collection of aerial photography is available at: https://www.library.ucsb.edu/geospatial/aerial-photography

[2] National Agriculture Imagery Program (NAIP) is available at: https://www.fsa.usda.gov/programs-and-services/aerial-photography/imagery-programs/naip-imagery/

[3] Carvalho, R.C., Kennedy, D.M., Niyazi, Y., Leach, C., Konlechner, T.M., Ierodiaconou, D., 2020. Structure-from-motion photogrammetry analysis of historical aerial photography: Determining beach volumetric change over decadal scales. Earth Surface Processes and Landforms 52, 2540–2555. https://doi.org/10.1002/esp.4911

For all image processing, a 2020 USDA National Agricultural Imagery Program (NAIP) geotiff was used as a reference layer, to which all photo years were compared and aligned. Some photo years (e.g., 1960s-70s) exhibited significant differences in the presence and/or alignment of key anchor features from the 2020 NAIP image (e.g., infrastructure features that were not present in earlier imagery), so these photo years were aligned using orthomosaic images from the early 1990s with high georectification accuracy and common anchor features. The oldest images (e.g., 1930s-1940s) were referenced to the best georectified images from the 1960s. In this way, locational precision for all years was cross-referenced to the position of the high resolution, geolocationally constrained 2020 NAIP imagery by using alignment features from closer years.

Table 1 contains metadata of all imagery datasets used in this report, including image resolution (i.e., pixel or raster grid cell size in m), also known as the ground sampling distance (GSD) of the imagery, as well as the number of image tiles used to create the mosaic of the final image file (.tiff). Transformation type refers to the way in which each raster cell was aligned with its real-world location through manual refinement and the selection of static ground control points (GCPs) between images. Of several methods available in ArcGIS Pro, polynomial and spline transformations were found to have the most accurate corrections for the datasets used. This accuracy is reported through the total root mean square (RMS) forward-inverse error, which expresses the projected uncertainty (in pixels), relative to the GCPs and the transformation type for each image set[4]. Pixel depth refers to the range of values that a raster cell type can store. For example, an unsigned 8-bit raster type can store 256 digital values between 0-255. The band number for each raster is a reference to how many layers of data are stacked to produce the raster dataset. Three band types were used in this study, including a single-band (grayscale) dataset for older imagery through 1978, and three- or four-band imagery in the later datasets. Three-band imagery expresses visual color (red-green-blue or RGB) wavelengths. Four-band imagery expresses the visual spectrum in the first three (RGB) bands and an additional near-infrared (NIR) band. The NIR spectrum is particularly useful for mapping, assessing, and extracting vegetation from multispectral imagery[5].

The aligned mosaic image datasets for each year were then classified using the supervised (sampling-based) classification wizard in ArcGIS Pro to identify vegetation and non-vegetation pixels using areas (and spectral signatures of color or grayscale) of known cover identified by the analyst. Classification results were then quality checked by visual inspection to identify wrongly classified pixels, then these cells were manually re-classified using the Pixel Editor tool. For each year, vegetation cover was calculated by area (km^2 and acres) and percentage cover (%).

[4] ArcGIS Pro helpdesk- https://pro.arcgis.com/en/pro-app/latest/help/main/welcome-to-the-arcgis-pro-app-help.htm

[5] Yichun Xie, Zongyao Sha, Mei Yu, Remote sensing imagery in vegetation mapping: a review, Journal of Plant Ecology, Volume 1, Issue 1, March 2008, Pages 9–23, https://doi.org/10.1093/jpe/rtm005

This report focuses on three analytical zones (regions) within a broader sub-region of the ODSVRA, as presented in Figure 1:

- the OHV riding area, border as in 2013,
- the North Oso Flaco foredune complex located north of Oso Flaco Creek,
- the South Oso Flaco dune complex, which includes both foredune and backdune areas south of Oso Flaco Creek.

The ODSVRA sub-area was set as the area south of Arroyo Grande Creek due to limited photo coverage across most years north of this area. The northern areas also contribute minimally to dust emissions due to the limited extent of open sand fetch and typically moist beach surfaces. Of note, this sub-area also includes the Pismo Dunes Natural Preserve (light blue area in Figure 1) that is technically not part of the ODSVRA. The preserve area is considered a subunit of Pismo State Beach, which is administered by the Oceano Dunes District of State Parks. The broader ODSVRA sub-area is approximately 17 km^2 (4215 acres), or about 74% of the total area managed by the Oceano Dunes District, and 85% of the ODSVRA park unit.

An additional portion of the southernmost area of ODSVRA was also excluded from the analysis (hatched area in Figure 1) due to changes in surface water features and human land use/infrastructure (agriculture, roads, buildings) over the years. These southern excluded areas total approximately 0.9 km^2 (238 acres), which is less than 4% of the total ODSVRA area. Furthermore, two years of imagery had limited photo coverage within the ODSVRA sub-area and, thus, the total area for the calculations differs slightly between years (Table 2).

The OHV riding area used for this report (1584 acres) is per the border of 2013 and includes both the open riding area and the vegetation islands. Since 2013, this area has been changed following implementation of various PMRP.

Both the North and South Oso Flaco areas were analyzed to provide comparison to vegetation dynamics within an area of the ODSVRA that has not seen significant OHV riding for decades (since at least 1982) and, as such, provides insights on a less disturbed and more developed state of vegetation cover and dune geomorphology. The borders of these areas (gray and brown Figure 1) were chosen due to hydrological changes of the Oso Flaco Creek over the image years.

Within each of the analytical zones (ODSVRA sub-area, OHV riding area, South Oso Flaco) a separate calculation was conducted for only the foredune zone, defined as the area in which foredune vegetation typically exists in the region, extends about 400m inland from the high water mark (dashed purple line in Figure 1). This zone was identified by the average depth of foredunes from Oso Flaco to near Pavillion Hill. North Oso Flaco area is entirely within the fordedune zone. In addition, this report also analyzed changes within a focus area of the new foredune restoration

sites, established in February 2020, located within the riding area between post markers 4-6 (pink line in Figure 1).

It is also important to note that invasive plant species are present in ODSVRA and have influenced vegetation cover over time. In the early 1900s, European beach grass (*Ammophila arenaria)* and ice plant (*Carpobrotus edulis*)[6,7] were planted to stabilize sand and dunes around the former La Grande Beach Pavilion. Currently, there are still areas within the ODSVRA and Pismo Dunes Natural Preserve that contain these species, as well as invasive South African Veldt grass (*Ehrharta calycina*), which is found in backdune areas. Invasive weeds have resulted in increased plant cover and foredune stabilization in ODSVRA. However, since 2009 different removal methods for invasive species have been used (e.g., burning, herbicides, hand-pulling)[8] at various locations.

The classified vegetation raster datasets were used to calculate changes in plant cover over time using the Raster Calculator and Change Detection tools in ArcGIS. From these maps, positive and negative changes were calculated as % values between subsequent image years and over different time periods. For change calculations between years that had limited image coverage, the analysis was conducted only on the area of overlap (union) in both image years.

For this report, we focused on three time periods that relate to different land management intervals:

1. 1939-1985: effectively characterizes landscape response during the interval preceding the management of ODSVRA by CDPR, which began in 1982,
2. 1985-2012: captures landscape changes during the management of ODSVRA by CDPR prior to adoption of SLO-APCD Rule 1001 (2011) and related PMRP, and
3. 2012-2020: reflects responses of the ODSVRA landscape following implementation of dust mitigation efforts and PMRP from Rule 1001 and the eventual state SOA (2018).

In addition to these three management intervals, we also characterize changes over the entire 1939 to 2020 period, and between 1939 and 2012. To the best of our knowledge, the 1939 imagery represents a time prior to OHV activity in the area, and comparison to modern 2020 imagery provides understanding of changes following multiple decades of OHV activity. The period between 1939 and 2012 represents these changes in vegetation prior to the SLO-APCD

[6] Guiton-Austin, L. (2011). As cited by Harris, W. California Geological Survey Report, 1 November 2011. "In consideration of Draft Rule 1001 proposed by the San Luis Obispo County Air Pollution Control District: An analysis of wind, soils, and open sand sheet and vegetation acreage in the active dunes of the Callendar Dune Sheet, San Luis Obispo County, California.

[7] Bonk. M. 2010. Mapping Invasive Beachgrass And Veldt Grass In Oceano Dunes Svra Using Multispectral Imagery. CDPR internal report.

[8] Glick, R., ODSVRA, Personal communication, October 2021

Rule 1001 (2011) and related PMRP. All change calculations are presented in Table S2 in the supplementary materials.

We take into consideration that the vegetation cover change rates and percentages presented in this report are influenced by image quality (Table 1). The pixel size (resolution), number of bands, and the overall image condition, generate inaccuracies in vegetation cover classifications and change calculations between the image years. For example, comparing two images with a quality difference can result in some loss of information. In order to address these inaccuracies we conducted thorough manual inspections of the change maps to prevent misclassified pixels.

Due to the limited image cover (Table 2), we were unable to use the oldest imagery available from 1930 in historical change comparison analysis, and thus, this was done using the 1939 image. To verify the classification of vegetation in this early imagery, the 1939 scene was compared to the 1930 imagery (Figure S1). We found very low differences between the years with less than 7% change (4.1% positive and 2.6% negative) in the total overlapping area of ODSVRA, most of which occurred along the margins of backdune areas (Figures S1 and S2). Some of these changes might also relate to seasonality as the 1930 orthophoto was taken at the end of summer (21 August) while the 1939 imagery was taken in the spring (2 May). All vegetation cover calculations performed for this study are presented in Table S1 in the Supplementary materials at the end of the report.

Table 1. *Imagery available for ODSVRA including metadata and source. Not all available years were used for the analysis due to issues with image projection, size, and/or shadowing that posed limitations for land cover classification (^ gray rows = years not analyzed for the report). Asterisk(*) indicates years with limited image coverage (see Table 2).*

Year	Collection date	Resolution (m)	Number of Tiles	Control Points	Transformation Type	Total RMS Forward-Inverse Error (m)	Source	Pixel Depth/Type	Band Number	Mosaic Size (GB)
1930*	Aug-21	0.794	16	12	Spline	0.000	UCSB Library - Geospatial Collection –C-1125A	8 bit unsigned	1	0.299
1939	May-02	0.832	9	27	Spline	0.023	UCSB Library - Geospatial Collection – AXH-1939-ARMY	8 bit unsigned	1	0.136
1949	Mar-31	0.894	NA	24	Spline	<0.001	UCSB Library - Geospatial Collection – AXH-1949	8 bit unsigned	2	0.568
1956	Sep-10	0.937	27	17	3rd Order Polynomial	0.172	UCSB Library - Geospatial Collection –AXH-1956	8 bit unsigned	1	0.617
1960^	Jul-12	0.790	6	13	3rd Order Polynomial	0.125	UCSB Library - Geospatial Collection – HA-GH	8 bit unsigned	1	0.131
1966	Dec-27	1.057	3	NA	NA	NA	UCSB Library - Geospatial Collection – HB-JT	8 bit unsigned	1	0.063
1971*	Jun-13	1.141	14	8	2nd Order Polynomial	NA	UCSB Library - Geospatial Collection – HB-SM	8 bit unsigned	1	0.039
1978	Sep-23	1.856	24	9	2nd Order Polynomial	0.001	UCSB Library - Geospatial Collection – USDA-40-06079	16 bit unsigned	1	0.068
1985	May-14	0.149	13	NA	NA	NA	Source unknown – received from CDPR	16 bit unsigned	3	18.980
1994	Feb-28	0.500	1	10	2nd Order Polynomial	0.004	Source unknown – received from CDPR	16 bit unsigned	3	0.879
1998	May-15	0.200	1	12	3rd Order Polynomial	0.036	Source unknown – received from CDPR	8 bit unsigned	4	16.420
2005	Jun-26	1.000	1	11	2nd Order Polynomial	<0.001	NAIP	8 bit unsigned	3	0.524
2007 *^	Jun-01	0.300	1	10	2nd Order Polynomial	0.001	Source GlobeXplorer – received from CDPR	8 bit unsigned	3	3.320
2010^	Aug-26	1.001	4	11	Spline	0.005	NAIP	8 bit unsigned	4	1.010
2012	May-19	1.000	1	11	2nd Order Polynomial	0.003	NAIP	8 bit unsigned	4	0.697
2014	Sep-24	1.000	1	11	2nd Order Polynomial	NA	NAIP	8 bit unsigned	3	1.640
2016	Aug-07	0.601	1	11	2nd Order Polynomial	0.002	NAIP	8 bit unsigned	4	1.800
2018	Sep-13	0.600	1	0	None	0.000	NAIP	8 bit unsigned	4	0.826
2020	Jun-07	0.600	1	0	Reference	0.000	NAIP	8 bit unsigned	4	1.830

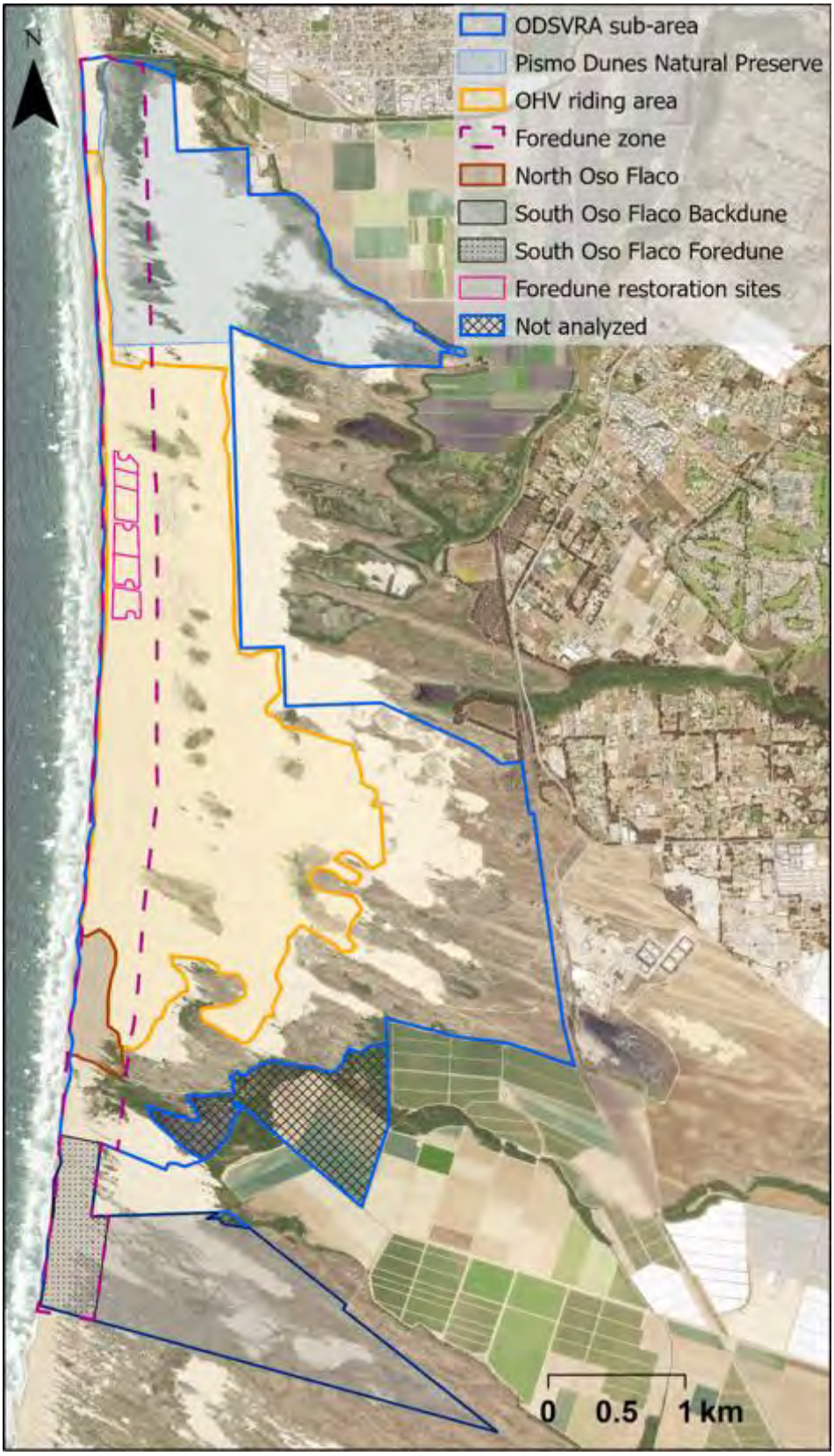

Figure 1. Boundary polygons of the different analytical regions used in the historical vegetation cover change analysis. Orthophoto source from NAIP 2020 (see Table 1).

Table 2. List of image years with limited photo coverage of the ODSVRA sub-area, OHV riding area, and the Oso Flaco area (foredune and backdune) in acres and as a percentage (%). Overall, the sub-area of the ODSVRA is approximately 4215 acres, the OHV riding area is 1584 acres, and the Oso Flaco total area is 577 acres. For specific locations of missing coverage, see Figures S3 and S10 in the supplementary materials.

Area missing						
	ODSVRA sub-area		OHV Riding area		Oso Flaco area	
Year	(acres)	(%)	(acres)	(%)	(acres)	(%)
1930	1108	23.3	338	21.4	0	0.0
1971	135	3.2	0	0.0	129	21.8
Area analyzed						
	ODSVRA sub-area		OHV Riding area		Oso Flaco area	
Year	(acres)	(%)	(acres)	(%)	(acres)	(%)
1930	3107	73.7	1245	78.6	577	100
1971	4080	96.8	1584	100	451	78.1

Our findings (values and maps) were also compared to those derived in previous undocumented analyses by CDPR[9]. For this comparison, we examined differences within the OHV riding area in four image years (1939, 1978, 2014, 2020) that were also analyzed by CDPR for an internal reporting exercise. Unfortunately, due to different methods for georeferencing the images, there was no geometric way to compare differences in vegetation patterns for the 1939, 1978, and 2014 maps. We were, however, able to compare the total calculated areas (acres) of vegetation cover between the CDPR reports and our findings. The CDPR reports showed slightly higher values by roughly 3% for 1939 and 2020 images (i.e., 60 and 51 acres, respectively) and by 0.5% (8 acres) for the 1978 images. The 2014 vegetation cover estimates showed essentially negligible differences (<0.1% or 3 acres) between the reports. The greater differences likely result from different methods in the land cover classification process and related quality assurance checks, which can generate uncertainties. Although the magnitude of difference in estimates between these results is relatively small, the location and pattern of differences is notable. For example, in our analysis of the 2020 vegetation cover, the specific locations (pixels) of every shrub, tree, and herbaceous plant were identified systematically by the supervised classification in the GIS, then the pixels were reviewed manually for discrepancies. The CDPR report appears to have taken a different approach by contouring the area around the vegetation as polygons (Figure 2) and, in doing so, included temporary straw cover in the classification in some areas (Figure 3). Our analysis did not include straw cover, only plants, even if they were growing in older straw cover.

[9] Glick, R., ODSVRA,, Personal communication, 2021.

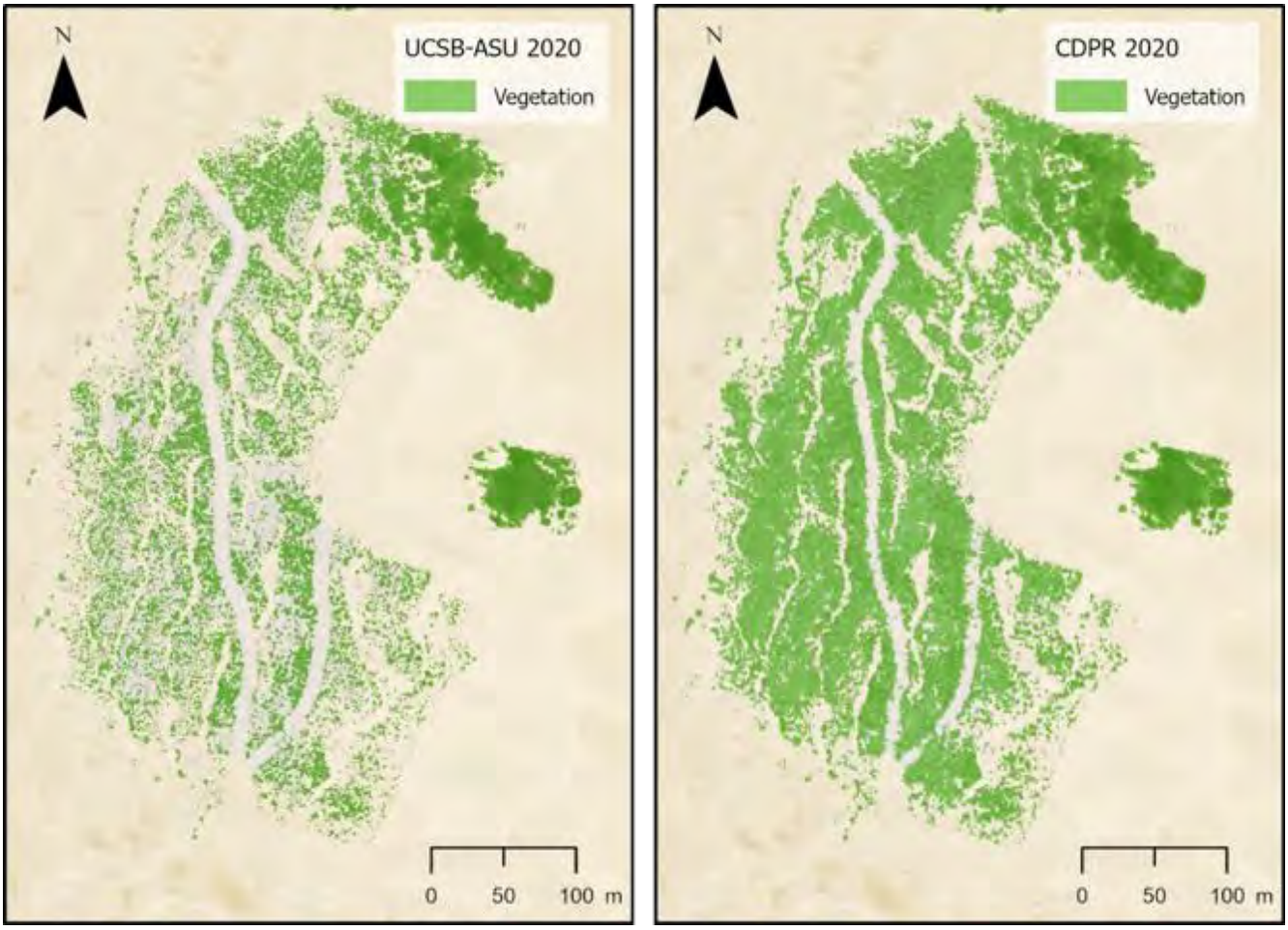

Figure 2. Vegetation cover analysis comparison between the CDPR report (Right) and the current report (Left) for 2020 imagery.

In addition, we tried to compare our findings to those presented in a 2011 report by the California Geological Survey (CGS)[10] that examined vegetation cover change between the 1930s and 2010 (Figure S19). In the CGS report, the 1930s dataset used was a combination (mosaic) of image tiles from both 1930 and 1939, while in this report we used tiles only from a single year (1939) that covered the entire sub-area of the ODSVRA. In addition, there were quality issues with the imagery for 2010 that did not allow for proper alignment and classification, so we were unable to conduct a direct comparison of vegetation cover area to the CGS report. A more general comparison of our 1939-2010 results to the CGS change map shows roughly similar plant cover identification (Figures S19 and S20), yet our calculated areas of change are significantly smaller, which could result from different classification methods, multi-year image mosaicing issues, and/or differences in analytical boundaries.

[10] Harris, W.J. 2011. An analysis of wind, soil and open sand sheet and vegetation acreage in the active dunes of the Callender dune sheet, San Luis Obispo County, California. Department of Conservation, California Geological Survey. 10p.

Figure 3. Vegetation cover analysis comparison between the CDPR report (pink) and the current report (green) for 2020 imagery. The arrows indicate areas where there is a straw treatment that was classified by CDPR as vegetation and by UCSB-ASU as non-vegetated area.

3. Results

3.1. Total vegetation cover

Vegetation cover maps for each individual year are presented in the supplemental Figures S3-S18 and the calculated plant coverage by area (km^2 and acres) and percentage values are summarized in Table 3 and Figure 4. The results show that there is a general positive trend of increasing vegetation cover over the years within the analyzed sub-area of the ODSVRA, especially after the mid 1980s (Blue in Figure 4). Between the early years of 1939 and 1949, there was a slight decrease in plant cover (from

25 to 24%), followed by a gradual increase in vegetation on the dunes up to the mid-1960s (27%). Between the 1960s and 1980s, plant cover declined to values close to that of 1949 (between 1001 and 1033 acres, or around 24%, see values in Table 3 and Table S1). This trend then shifts to a gradual increase in vegetation after 1978 to a peak value of 37% (1569 acres) in 2012.

Within the OHV riding area, vegetation cover is generally much lower than in the broader ODSVRA sub-area and the post-1960s decline in cover is more pronounced with a steady reduction from a peak value of about 196 acres (12%) in 1966 to only 61 acres (4%) in 1985 (orange in Figure 4). After 1985, a slow gradual increase in plant cover was observed in the OHV riding area to 128 acres (8%) by 2020, which remains approximately 67 acres below the peak value in 1966, when the decline in cover began. This does not include the new 48-acre foredune restoration site, however, which did not exist when the 2020 NAIP imagery was captured. As of 2021, plant cover within the foredune restoration area had an average of approximately 2.7%[11], as discussed further in section 3.2 below.

The South and North Oso Flaco areas (light gray and brown in Figure 1, respectively) were also analyzed to provide comparison to vegetation dynamics areas of the ODSVRA that have not seen significant OHV riding for decades (since at least 1982 in S. Oso Flaco). As such, these sites provide insights on a less disturbed and more developed state of vegetation cover and dune geomorphology. At South Oso Flaco, plant cover is substantially higher than other areas of the ODSVRA, showing a general positive trend (Figure 4) from 37 % in 1930 to 66% in 2012 (212 and 373 acres, respectively). Between 1930 and 1949, there was a small decline in plant cover to a historic low of 34% (197 acres). In contrast, plant cover in the OHV riding area has not exceeded 13% over the period of analysis. The area analyzed at South Oso Flaco represents approximately 14% of the total ODSVRA sub-area, yet it contains 14-34% of the vegetation within the park. For comparison, the OHV riding area is just over 37% of the ODSVRA sub-area but contains only 6-18% of the total vegetation, depending on the year.

The North Oso Flaco foredune complex shows a gradual trend similar to the OHV riding area with an increase in vegetation up to the late 1960s, from less than 1% in 1930 to almost 11% in 1966, which then declined to 5% in 1985. Following 1985 plant cover increased to a peak of 24% in 2012, , and after that plant cover declined but remained over 19%. The North Oso Flaco site consists only of foredune vegetation, which is generally more exposed to disturbance (natural and anthropogenic), yet following 1987 the plant cover at this site is consistently higher than that in the OHV riding area, which also includes large backdune vegetation.

[11] Hilgendorf, Z., Turner, C., & Walker., I.J. 2021. UCSB-ASU 2020-2021 ODSVRA Foredune Restoration UAS Survey. Report from UCSB and ASU submitted to CDPR.

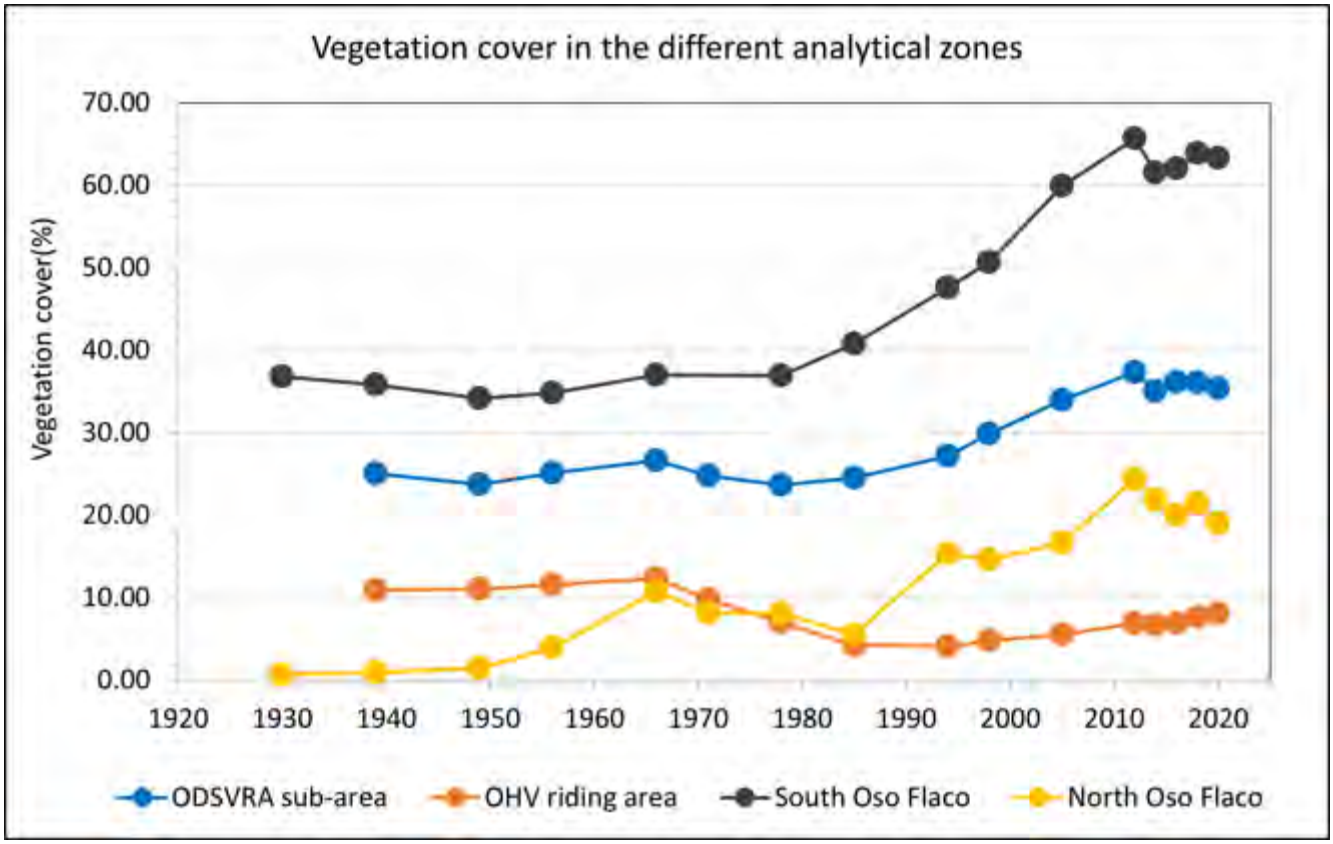

Figure 4. Time series of total vegetation cover (foredune + non-foredune vegetation in Table 3) as a percentage (%) of the ODSVRA sub-area at large (blue), the OHV riding area (orange), South Oso Flaco area (gray), and North Oso Flaco (yellow, foredune vegetation only). Percent cover values are derived as a proportion of the respective areas of each analytical region. Due to limited imagery coverage (Table 2), the 1930 photo year was not included in the ODSVRA sub-area and OHV riding area curves, and 1971 was not included for South Oso Flaco (gray).

Table 3. Calculated land cover values for vegetation and non-vegetated areas from each image year in the ODSVRA sub-area, OHV riding area, South Oso Flaco , and the North Oso Flaco area. Values are provided for vegetation in the foredune zone and for other back dune areas (see boundaries in Figure 1). Asterisk (*) represents limited imagery for 1930, 1971, and 1985 (Table 2), resulting values are derived from smaller areas than outlined in Figure 1. All values presented are in relation to the entire area of each analyzed zone (to a total of 100%). Values relative to specific areas within each of these broader areas (e.g., foredune zones) are shown in Figure 5 (Section 3.2) and provided in Table S1 (supplementary materials).

		ODSVRA sub-area			OHV riding area			South Oso Flaco			North Oso Flaco	
		Vegetated		Non vegetated	Vegetated		Non vegetated	Vegetated		Non vegetated	Vegetated	Non vegetated
		Foredune	Backdune		Foredune	Backdune		Foredune	Backdune		Foredune	
1930*	km² (acres)	0.07 (16)*	3.37 (832)*	9.14 (2258)*	0.03 (8)*	0.48 (118)*	4.53 (1120)*	0.02 (6)	0.84 (207)	1.48 (365)	0.002 (0.4)	0.28 (68)
	%	0.52*	26.79*	72.69*	0.63*	9.46*	89.91*	0.95	35.83	63.21	0.69	99.31
1939	km² (acres)	0.13 (32)	4.14 (1023)	12.78 (3159)	0.05 (12)	0.07 (161)	5.71 (1411)	0.01 (6)	0.83 (204)	1.50 (371)	0.003 (0.7)	0.28 (68)
	%	0.76	24.29	74.95	0.77	10.16	89.08	0.45	35.35	64.2	0.95	99.05
1949	km² (acres)	0.23 (57)	3.82 (944)	13.01 (3214)	0.08 (19)	0.63 (157)	5.70 (1408)	0.02 (5)	0.78 (192)	1.54 (380)	0.004 (1)	0.27 (68)
	%	1.34	22.4	76.25	1.18	9.89	88.93	0.84	33.32	65.84	1.49	98.51
1956	km² (acres)	0.33 (82)	3.95 (977)	12.78 (3159)	0.07 (16)	0.68 (167)	5.67 (1401)	0.03 (7)	0.78 (194)	1.52 (376)	0.01 (3)	0.26 (66)
	%	1.94	23.17	74.89	1.03	10.56	88.41	1.30	33.52	65.18	3.96	96.04
1966	km² (acres)	0.45 (111)	4.09 (1011)	12.52 (3093)	0.10 (24)	0.70 (172)	5.62 (1388)	0.08 (19)	0.79 (195)	1.47 (364)	0.03 (7)	0.25 (61)
	%	2.64	23.99	73.37	1.51	10.85	87.64	3.28	33.71	63.00	10.72	89.28
1971*	km² (acres)	0.37 (90)*	3.86 (955)*	12.26 (3035)*	0.08 (19)	0.55 (1336)	5.79 (1430)	N/A	0.82 (203)*	0.97 (240)*	0.02 (6)	0.25 (63)
	%	2.21*	23.41*	74.38*	1.19	8.56	90.25	N/A	45.82*	54.18*	8.1	91.9
1978	km² (acres)	0.40 (99)	3.64 (899)	13.02 (3218)	0.04 (11)	0.41 (100)	5.96 (1473)	0.07 (17)	0.79 (196)	1.47 (364)	0.02 (6)	0.26 (63)
	%	2.34	21.32	76.34	0.68	6.33	92.98	3.02	33.9	63.08	8.09	91.91
1985	km² (acres)	0.45 (110)	3.73 (922)	12.88 (3183)	0.02 (4)	0.25 (62)	6.14 (1517)	0.10 (24)	0.86 (211)	1.38 (342)	0.02 (4)	0.26 (65)
	%	2.61	21.88	75.51	0.28	3.93	95.79	4.15	36.61	59.24	5.53	94.46
1994	km² (acres)	0.50 (125)	4.11 (1016)	12.40 (3065)	0.01 (2)	0.25 (63)	6.15 (1519)	0.11 (26)	0.99 (244)	1.20 (298)	0.02 (5)	0.26 (64)
	%	2.97	24.16	72.87	0.16	3.98	95.87	4.62	42.97	52.41	7.34	92.66
1998	km² (acres)	0.54 (133)	4.54 (1122)	11.94 (2950)	0.02 (4)	0.29 (71)	6.11 (1509)	0.11 (28)	1.05 (260)	1.13 (280)	0.04 (10)	0.24 (59)
	%	3.17	26.68	70.15	0.25	4.49	95.26	4.85	45.86	49.29	14.62	85.38
2005	km² (acres)	0.70 (173)	5.08 (1254)	11.24 (2778)	0.02 (6)	0.33 (82)	6.05 (1496)	0.15 (38)	1.10 (250)	1.13 (280)	0.05 (11)	0.23 (57)
	%	4.12	29.83	66.05	0.37	5.20	94.43	6.66	44.04	49.29	16.63	83.36
2012	km² (acres)	0.81 (200)	5.54 (1369)	10.67 (2637)	0.04 (9)	0.40 (100)	5.97 (1475)	0.16 (40)	1.25 (309)	0.89 (219)	0.07 (18)	0.21 (52)
	%	4.75	32.56	62.69	0.60	6.31	93.09	7.12	54.36	38.52	24.41	75.95
2014	km² (acres)	0.69 (170)	5.28 (1304)	11.05 (2732)	0.04 (10)	0.39 (95)	5.98 (1479)	0.15 (36)	1.27 (313)	0.89 (219)	0.06 (15)	0.22 (54)
	%	4.05	31.00	64.95	0.64	6.01	93.35	6.34	55.14	38.52	21.87	78.13
2016	km² (acres)	0.70 (173)	5.24 (1296)	11.08 (2737)	0.04 (10)	0.40 (99)	5.97 (1475)	0.14 (34)	1.29 (318)	0.87 (216)	0.06 (14)	0.22 (55)
	%	4.12	30.81	65.08	0.64	6.25	93.11	6.04	55.98	37.98	20.00	80.00
2018	km² (acres)	0.68 (168)	5.46 (1348)	10.88 (2689)	0.04 (10)	0.45 (111)	5.92 (1463)	0.14 (36)	1.32 (327)	0.83 (205)	0.06 (15)	0.22 (54)
	%	3.99	32.06	36.95	0.63	7.00	92.37	6.27	57.60	36.12	21.46	78.54
2020	km² (acres)	0.64 (157)	5.37 (1328)	11.01 (2720)	0.04 (11)	0.47 (117)	5.89 (1456)	0.12 (30)	1.33 (330)	0.84 (208)	0.05 (13)	0.22 (55)
	%	3.74	31.58	64.68	0.67	7.4	91.93	5.27	58.05	36.68	19.05	80.95

3.2. *Changes in vegetation cover in the foredune zone*

As plant communities, geomorphology, and other ecological processes within foredune ecosystems are distinctly different from those in the larger transgressive dunes, parabolic dunes, and interdune areas in the broader ODSVRA landscape, a separate analysis of vegetation cover was conducted for the foredune zone (see Section 2 and Figure 1). Values presented in this section are specific to the foredune within each of the larger analytical regions and are not a proportion of the larger zones themselves (see values in Table S1).

Vegetation cover trends within the foredune zone (Figure 5) are generally similar to those within the broader ODSVRA sub-area and OHV riding areas described above (Figure 4). Peak values (and years) of foredune plant cover within ODSVRA, the OHV riding area, and at the South and North Oso Flaco reference sites are 21% (2012), 5% (1966), 36% (2012) and 24% (2012), respectively. Foredune vegetation cover within the entire ODSVRA sub-area shows a general increase over time, with high positive rates of change from a historic low in 1939 (3.3%) to 1966 (from 32 to 111 acres) and between 1998 and 2012 (133 to 200 acres). From 2012 to 2020, however, there was a net loss of 49 acres of vegetation (from 21% to 16% cover, blue in Figure 5), some of which results from removal of invasive grass species (e.g., *Ammophila breviligulata* or European beach grass) from foredunes in the northern area of the ODSVRA[12].

Within the OHV riding area, foredune vegetation shows an increase in cover from approximately 2.6% (12 acres) in 1939 to 5.3% (24 acres) in 1966 (orange in Figure 5B, Table S1). From 1966 to 1994, plant cover declined sharply to 0.5%, which is well below the historic 1939 value. Since 1998, vegetation cover has risen gradually to about 2.3% by 2020 (Figure 5).

It is important to note that all orthophotos from 2005-2020 were taken during the period of nesting for the Western Snowy Plover (March through September), which results in up to 70% of the foredune zone in the OHV riding area (or roughly 20% of the overall riding area) being closed to OHV traffic and camping for 7 months (see borders in Figure 7). The enclosure reduces the impact of human activity over the foredune area which may allow better conditions for plant establishment in that area. Since 2005, plant cover within the bird nesting enclosure increased from negligible to over 1% by 2012 (Figure S21). From the historic analysis, it seems that the last time vegetation cover was over 1% in this area was in the late 1970s, which is also a big decrease from the early 1930s when this area had over 10% vegetation cover (Figure S21).

At the South Oso Flaco reference site, foredune vegetation cover between 1939 and 1949 (2.4% and 4.3%, respectively) is comparable to that in the foredune zone of the OHV riding area (2.6% and 4.1%, respectively). After this, plant cover remains consistently and appreciably higher

[12] Glick, R., ODSVRA, Personal communication, 2021.

at Oso Flaco than in other foredune zones, especially in the OHV riding area (Figure 5). As in the larger ODSVRA sub-area, foredune vegetation cover at South Oso Flaco shows a positive trend over time to a peak in 2012. Comparatively then, Figure 5 indicates that foredunes at South Oso Flaco that were not subjected to the same amount of OHV activity as that in the nearby riding areas of ODSVRA (at least since 1982) have attained and maintained significantly higher vegetation cover, particularly between 1985 and 2005 (see also Table S1; Figures S3-S18). It is worth noting that the decrease in foredune plant cover following 2012 is partly related to CDPR efforts to remove invasive *Ammophila arenaria* and other weeds, mostly at South Oso Flaco[12].

North Oso Flaco had very low vegetation cover (less than 2%) up to the 1950s, then gradually rose to a peak of 10% in 1966. Following this, plant cover declined to 5% in 1985, then rose to a historic peak of 24% in 2012 (Figure 5). The North Oso Flaco area has been fenced to exclude OHV activity since 1982, which largely explains the rise in vegetation growth since 1985.

Although plant cover within the broader ODSVRA and in both North and South Oso Flaco sites has gradually increased over time, vegetation within the OHV riding area, and its foredune zone in particular, have shown steady declines since 1966 (Figure 5). This corresponds with an era of increasing recreational OHV activity in the region that began in the 1950s[13].

Another area of interest for detecting changes in foredune vegetation cover is within the newly implemented (2020) 48-acre foredune restoration site in the OHV riding area. (Figures 1, 5). Historical plant cover in this area shows a similar trend to that of the foredune zone in the larger OHV riding area with a decline in cover from almost 2% in 1949 to essentially zero cover in 1985. Since then there has been no detectable change in plant cover at the foredune restoration sites until after implementation of the restoration treatments in February 2020. The 2020 NAIP imagery used in this analysis does not reflect these treatments, however.

An independent report by UCSB and ASU[14] explores more recent changes in vegetation cover within the foredune restoration site captured from aerial UAS surveys between October 2019 and February 2021. The report shows that, as of February 2021, plant cover increased to an average of approximately 2% (ranging from 0.04 to 4.91%, depending on treatment type).

[13] Guiton-Austin, L. 2011. As cited by Harris, W. California Geological Survey Report, 1 November 2011. "In consideration of Draft Rule 1001 proposed by the San Luis Obispo County Air Pollution Control District: An analysis of wind, soils, and open sand sheet and vegetation acreage in the active dunes of the Callendar Dune Sheet, San Luis Obispo County, California.

[14] Hilgendorf, Z., Turner, C, Walker, I.J. UCSB-ASU 2020-2021 ODSVRA Foredune Restoration UAS Survey Report. 37p. Produced for CDPR-ODSVRA and published as Attachment 8 in the 2021 ARWP.

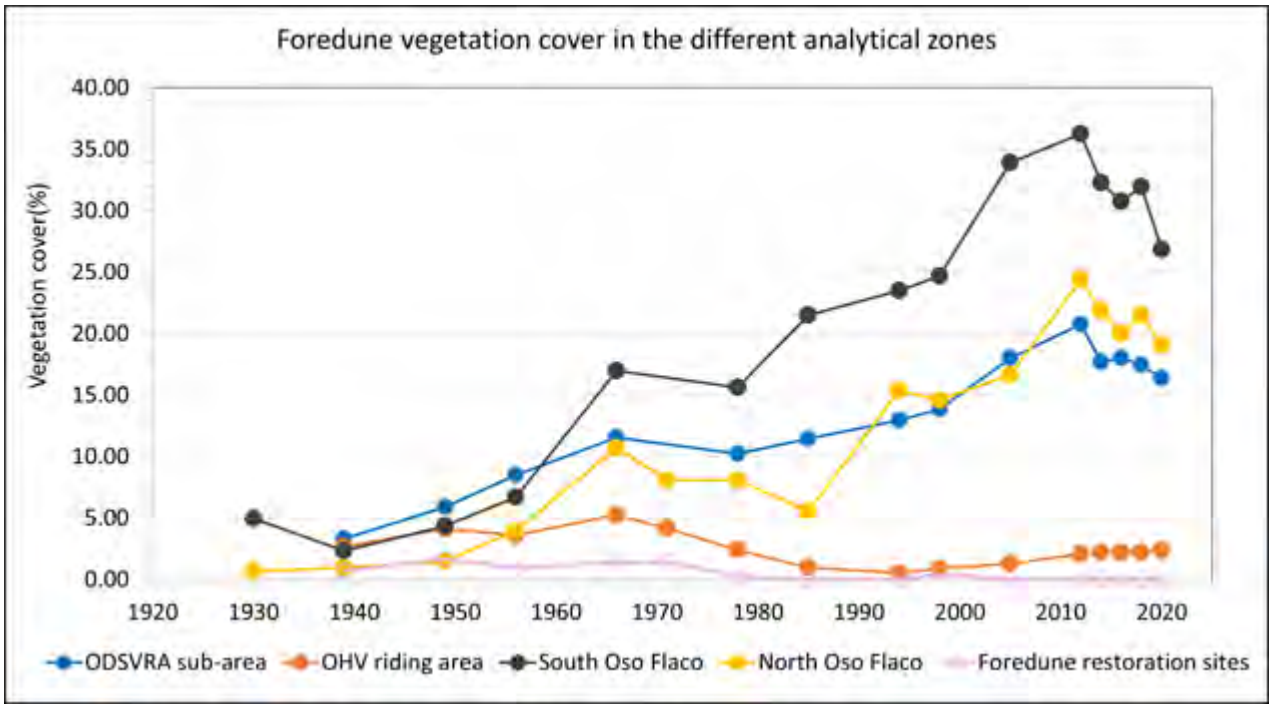

Figure 5. Percent vegetation cover within the foredune zone in the ODSVRA sub-area (blue), OHV riding area (orange), South Oso Flaco area (gray), and North Oso Flaco (yellow). Values are relative to areas of the foredune zone within each analytical zone (calculations in Table S1). Plant cover within the foredune restoration zone is shown for comparison (pink). Due to limited coverage of imagery (Table 2), the 1930 image was not included in the ODSVRA sub-area and OHV riding area curves, and 1971 was not included in the ODSVRA sub-area and South Oso Flaco analysis (gray).

3.3. Change detection between years

Changes in vegetation coverage between photo years are presented both as change maps (Figures S22-S35) and as plots of rates of positive or negative change over time (% yr^{-1}) (Figure 6), which generally reflect dynamism in plant cover over time. It is noted, however, that change calculations derived by comparing two points over time (i.e. two different image years) inevitably precludes interpretation of changes during the intervening years. This said, there is interpretive value in estimating rates of change between image years particularly given the varying intervals between the photos.

Figure 6 shows negative or positive change rates derived from the number of pixels that either lost or gained vegetation from the earlier image year, respectively, divided by the number of years between the images. All change calculations, including total change (sum of all changes, negative + positive) and net change (positive - negative) are presented in Table S2 in the supplementary material. Within the broader ODSVRA sub-area, there is an increasing trend in the total amount of change/year between the 1930s to the 1980s, with mainly negative changes (losses) in plant cover from 1966 to 1985, after which more positive changes (gains) occur (Figure 6A). Between 2012 to 2020, there is a large increase in the amount of total change, however, a large portion of this is negative, mostly between 2012-2016 (Figure 6A). Much of the negative change in these years occurs in areas that experienced removal of invasive species (e.g., the Pismo Dunes Natural Preserve and South Oso Flaco areas, see Figures S32, S33) between 2012 and 2015. In addition, some of the detected changes between 2012 and 2014 reflect the time of year when the imagery was taken. The 2012 orthophoto was taken in the middle of May (late spring) when vegetation is in full growth stage (and easier to identify and classify using aerial photo analysis), while the 2014 orthophotos were taken in late September at the end of the growing season, so there is potential for subtle seasonal differences based on time of photo acquisition (Table 1; Figure 6).

In the OHV riding area, there is a similar trend to the larger ODSVRA - between 1966 to 1985 the majority of changes were negative and after 1985 the changes were largely positive (Figure 6B). Between 1985 and 2005, the change rates are very small (<0.3% yr^{-1}) compared to other analytical zones. Most of the positive changes in the OHV riding area occur after 2005 (Figure 4) largely related to new plants along the margins of fenced vegetation islands, and foredune vegetation establishing in the seasonal bird nesting enclosure area (Figure 7; Figures S31-S35). The reduction of OHV disturbance offered by the seasonal bird nesting enclosures since 2005 corresponds with increases in foredune vegetation cover of about 1% with only 0.1% negative change between 2005 and 2020 (0.07% yr^{-1} and 0.01% yr^{-1}, respectively).

At South Oso Flaco, there is a similar net pattern in the total amount of change as in the other analytical zones (Figure 6C). However, up to 1971 there is generally a more balanced occurrence of positive and negative changes between most years. Following 1971, for the most part, there are more positive changes and between 2012 and 2020, the change rates increased to over 5% yr^{-1} (Figure 6C). Most of this change occurs around the edges of existing vegetation in both backdune and foredune areas (Figures 8). The backdune zone of South Oso Flaco shows mainly positive rates of change up to 2012 (Figure 8B). The South Oso flaco foredune zone shows a similar trend to the backdune area (Figure 8B), however, the rates of change in the foredune were much higher in all years (Figure 8A and 8B).

In the North Oso Flaco foredune complex, a positive trend of change occurs up to 1966, then shifts to more negative change rates up to 1985 (Figure 6D). Following the closure of the area in the early 1980s, North Oso Flaco showed a strong positive trend of increase. North Oso Flaco shows the highest amount of change between 2012 and 2020 compared to the other analytical zones, peaking at over 7% yr^{-1} of total change between 2012 and 2014 with mostly negative change between 2012 and 2016 (Figure 6D).

Figure 6. Positive, negative and net percent change per year (% yr^{-1}) in vegetation between successive imagery years in the entire ODSVRA sub-area (A), OHV riding area (B), South Oso Flaco area (C), and North Oso Flaco (D) relative to areas of each analytical zone. The negative change values were converted to negative numbers (less than zero) to represent the vegetation loss. Areas with no change between years are not shown (hence, values do not total 100%). Due to limited coverage of imagery, the 1930 was not included in the ODSVRA sub-area and OHV riding area change analysis (black X sign). In 1971 the limited image coverage in the ODSVRA sub-area and South Oso Flaco resulted in some missing data (see Table 2, Figure S10) and possible underestimates of change.

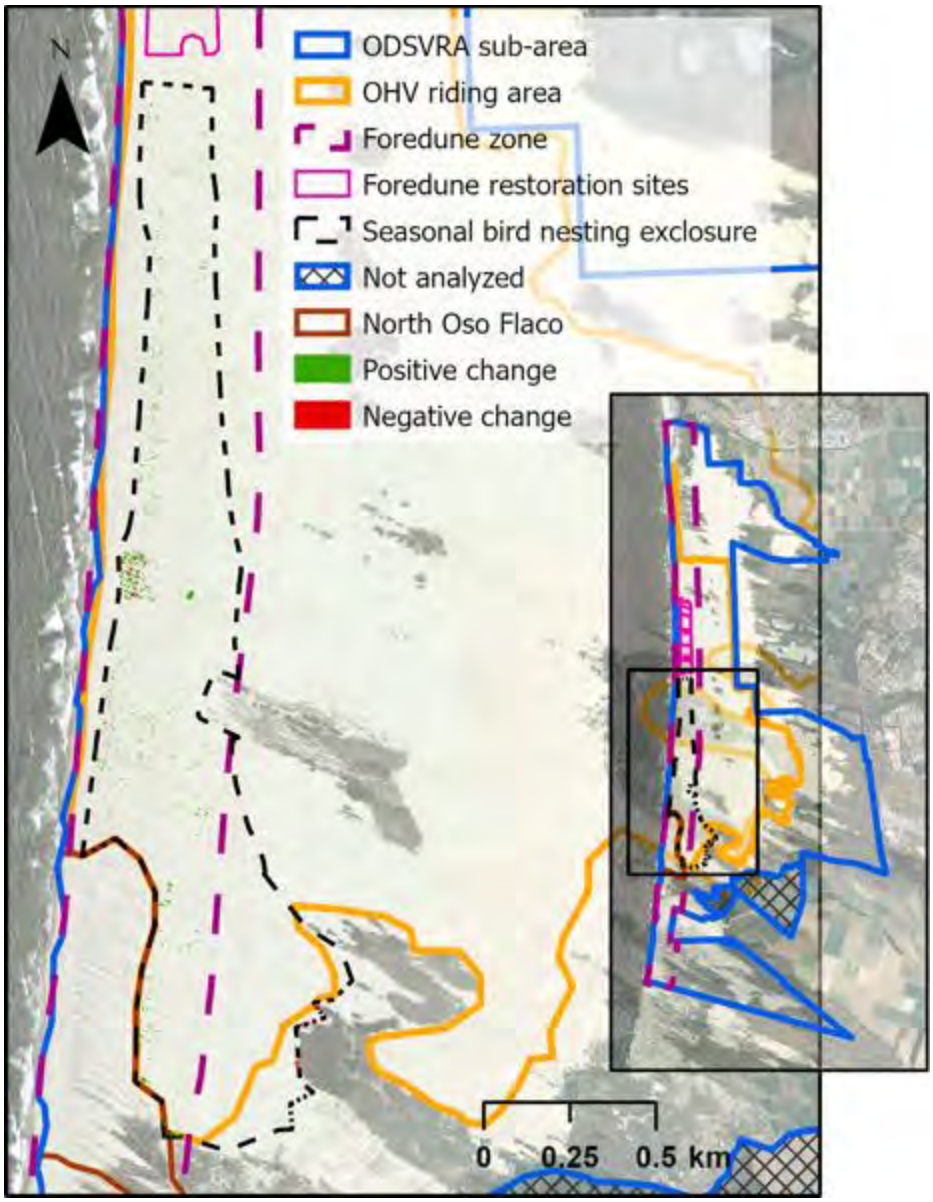

Figure 7. Change map between 2005 and 2020 of the seasonal bird nesting exclosure area (black dashed line) that have been fenced off to OHV activity since 1982[15]. Change map is shown on the 2005 orthophoto.

[15] Glick, R., ODSVRA,, Personal communication, 2021.

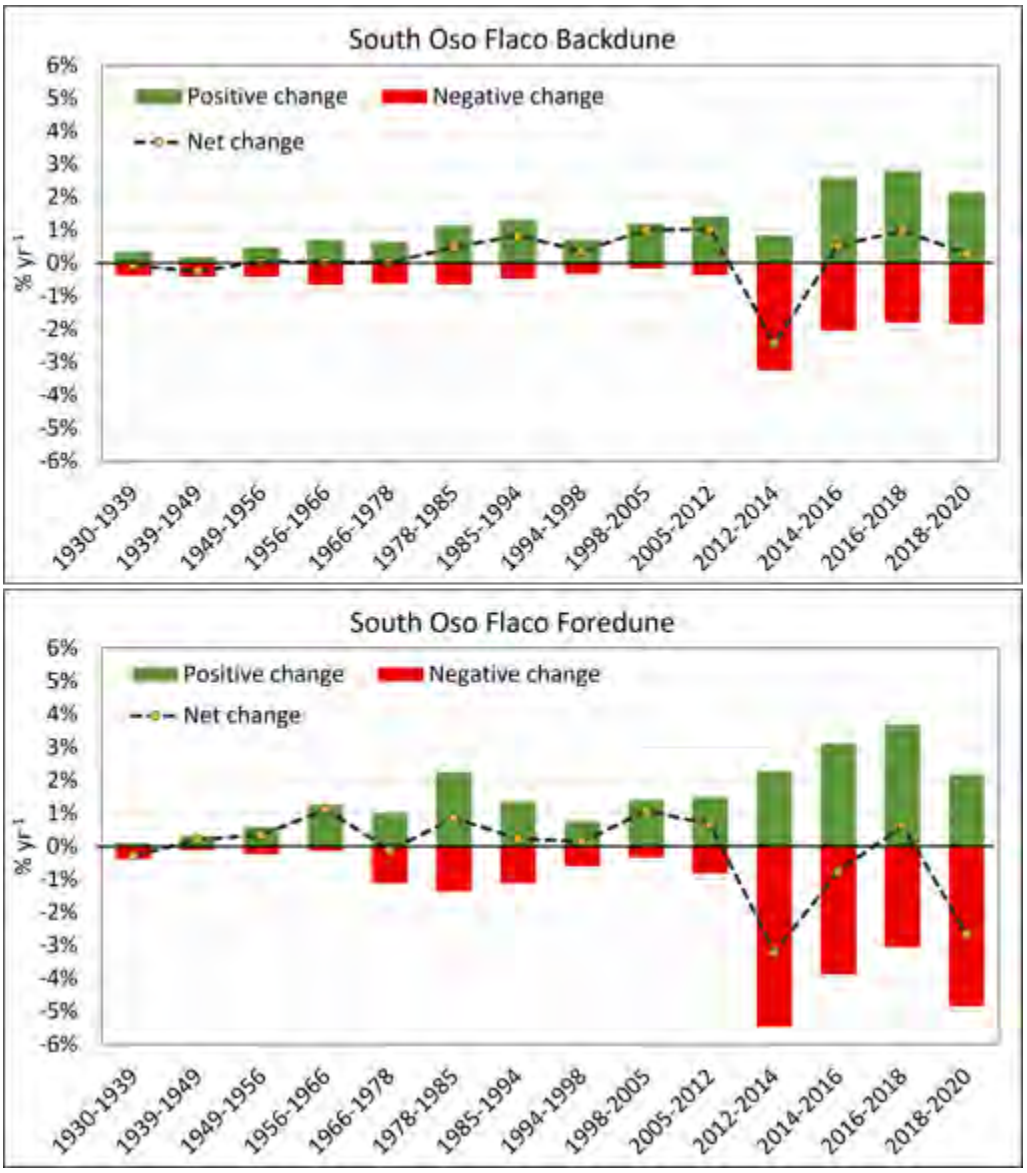

Figure 8. Positive, negative and net percent change rates (% yr^{-1}) in vegetation between successive imagery years in the South Oso Flaco backdune (A) and foredune (B) zones relative to areas of each analytical zone. The negative change values were converted to negative numbers (less than zero) to represent the vegetation loss. Areas with no change between years are not shown (hence, values do not total 100%). Net change (positive change - |negative change|) represent the overall trend of change between the image years. There was very limited coverage for 1971 and so this year was excluded and an analysis of 1966-1978 was done instead.

Figures 9-15 provide a focused analysis of vegetation changes during the three broader time periods identified in Section 2. During the 1939-1985 period, roughly prior to the management of ODSVRA by CDPR (in 1982) the total amount of change in the ODSVRA sub-area is relatively high at 18.72%, but this translates to a change rate of only 0.4% yr^{-1} (Figures 9A and 10, Table

S2). The majority of positive change appears mostly between 1966 and 1985 (Figure 6A). Between 1985 and 2012, this area showed increasing positive change rates in plant cover (1714.9% or 0.6355% yr^{-1}) with only 21.8% loss (0.07% yr^{-1}) (Figure 9A). Many of the areas of negative change between 1939 and 1985 showed subsequent vegetation growth in 2012 (Figures 9A, 10, 11). As above, most of this change occurred in areas subjected to restoration activities implemented by CDPR between 2005 and 2012 (Section 3.3; Figure 6). From 2012 to 2020, a comparatively low amount of total change was observed (8%) with equal amounts of positive and negative change (Figure 9A and 12), yet the rates of change were among the highest (total of 1% yr^{-1}).

Within the OHV riding area (Figure 9B), there is a declining trend in the total amount of change over time. From 1939 to 1985, there was a proportionately large negative change (9.2%) in plant cover in both foredune and backdune zones (Figures 10 and 13). From 1985 to 2012, there was a shift toward proportionately greater positive change (4.2%) with only 1.4% negative change (Figure 10B), mainly around existing vegetation islands in the backdune area (Figures 11 and 14). Between 2012 and 2020, the total amount of change in the riding area is relatively small (3.3%) and mostly positive (2.2%) (Figure 9B), resulting from vegetation growth in backdune restoration areas (straw treatments) implemented by CDPR (Figure 15). Rates of change are moderate (~0.2% yr^{-1}) for both 1939-1985 and 1985-2012 with only 0.2% yr^{-1} and 0.05% yr^{-1} negative change rates, respectively. Between 2012 and 2020 the change rate is slightly higher at 0.4% yr^{-1} with over 0.3% yr^{-1} positive change.

At South Oso Flaco, between 1939 and 1985, the total change in backdune and foredune areas was 22.5% with mostly gains (13.7%) (Figure 9C). Most of the losses occurred in the backdune area between 1966 and 1985 (Figures 6C, 8-10). Between 1985 and 2012, there was a high amount of total change of 31.7% (1.2% yr^{-1}), most of which (28.1%) was positive (Figure 9C) and occurred in the backdune zone and on the landward (eastern) side of the foredune, whereas higher vegetation loss is evident on the shoreward side of the foredune (Figure 11). Between 2012 and 2020, there was 12.1% total change, which is relatively low compared to previous years, but still high compared to other analytical zones (Figures 9) and at a faster rate of change (1.5% yr^{-1}) than the previous interval. Most of this change was vegetation loss (7.7%) in the Oso Flaco foredune zone and around existing vegetation in the backdune zone (Figures 9C, 12, 15). According to CDPR staff, some of this recent decline in plant cover at South Oso Flaco relates to removal of invasive grasses between 2009 and 2020.

The North Oso Flaco foredune complex shows a comparatively lower total amount of change between 1939 and 1985 (6.0%) with mostly positive changes (5.3%) (Figure 9D). The positive trend continued between 1985 and 2012, with a higher amount of total change (26% or 0.96% yr^{-1}), most of which (23.5%) was positive (Figure 9D). An invasive weed analysis performed by

CDPR in 2010[16] suggests that the North Oso Flaco area did not host any invasive species that were found in other foredune and backdune areas in the park. As such, the high positive changes between 1985 and 2012 can be attributed mostly to growth and expansion of native plants in the absence of vehicle activity and other anthropogenic disturbances. Between 2012 to 2020, however, there is mostly negative change in plant cover (11%) with only 3.6% gains.

For this report we used the 1939 orthophoto to represent an era prior to widespread OHV riding in the ODSVRA. Some accounts suggest that intensive riding in the area began in the 1950s[17]. Calculating changes in plant cover between 1939 and 2020 provides a comprehensive look at overall influences and changes that took place in the ODSVRA, including the combined impacts of land management by CDPR and the impact of OHV riding and other human activities over the last 9 decades. The results show that over this period there is a general increase in plant cover in the broader ODSVRA sub-area and in the North and South Oso Flaco reference areas (Figure 16A). In the ODSVRA, there is an overall increase of 17.8% plant cover vs. 7% loss. Most of the vegetation gain was in the backdune area and in the Pismo Dunes Natural Preserve, the broader South Oso flaco dune complex, and in backdune areas outside of the riding area (Figure 17 and S38). These areas were also found to be affected by growth of invasive weeds. According to a CDPR weed digitizing effort in 2010[16], invasive weeds (beach grass and veldt grass) in 2010 occupied less than 10% of the total vegetation cover within the broader ODSVRA sub-area (134 acres), about 14% of the plant cover in South Oso Flaco (310 acres), and 18% of the vegetation in the Pismo Dunes Nature Preserve (381 acres). It should be noted, however, that since 2010 there has been an increasing effort by the CDPR to remove invasive species in these areas.

[16] Bonk. M. 2010. Mapping Invasive Beachgrass And Veldt Grass In Oceano Dunes Svra Using Multispectral Imagery. CDPR internal report.

[17] Guiton-Austin, L. 2011. As cited by Harris, W. California Geological Survey Report, 1 November 2011. "In consideration of Draft Rule 1001 proposed by the San Luis Obispo County Air Pollution Control District: An analysis of wind, soils, and open sand sheet and vegetation acreage in the active dunes of the Callendar Dune Sheet, San Luis Obispo County, California.

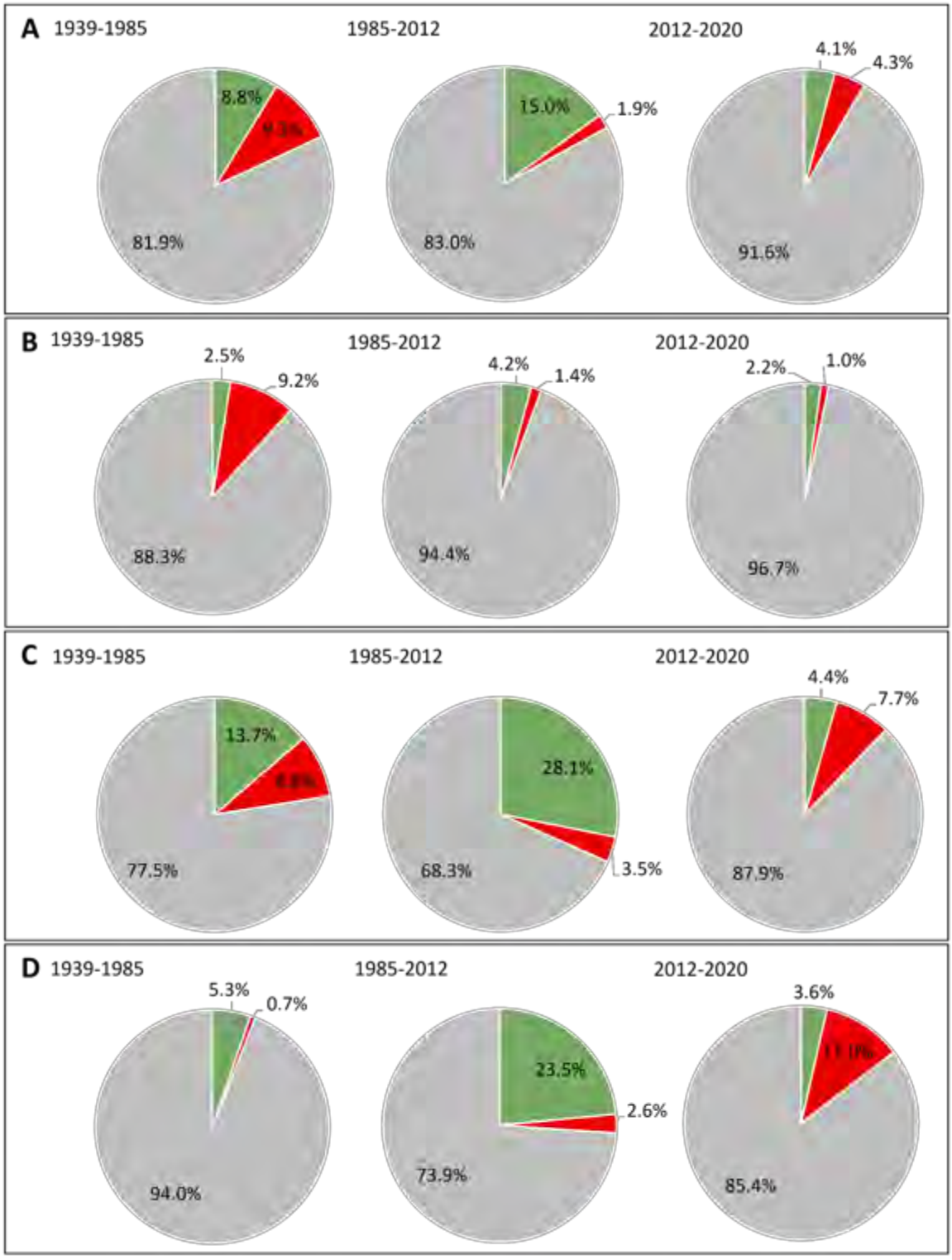

Figure 9. Change analysis (%) of vegetation cover in ODSVRA sub-area (A), OHV riding area (B), South Oso Flaco (C), and North Oso Flaco area (D) during three important management time intervals: i) 1939-1985, ii) 1985-2012, and iii) 2012-2020, as described in Section 2.

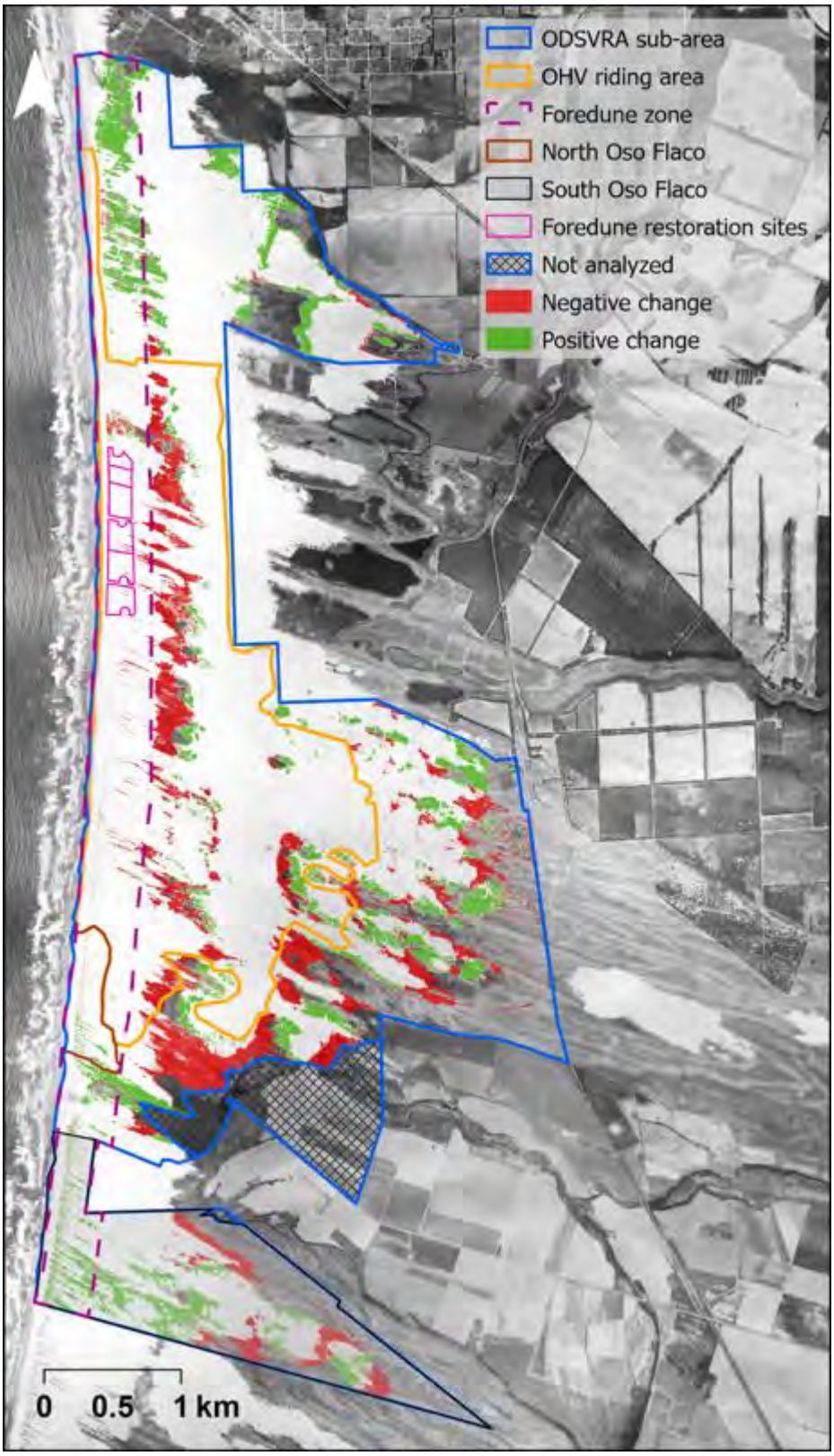

Figure 10. Change in vegetation between 1939 and 1985. Orthophoto from 1939.

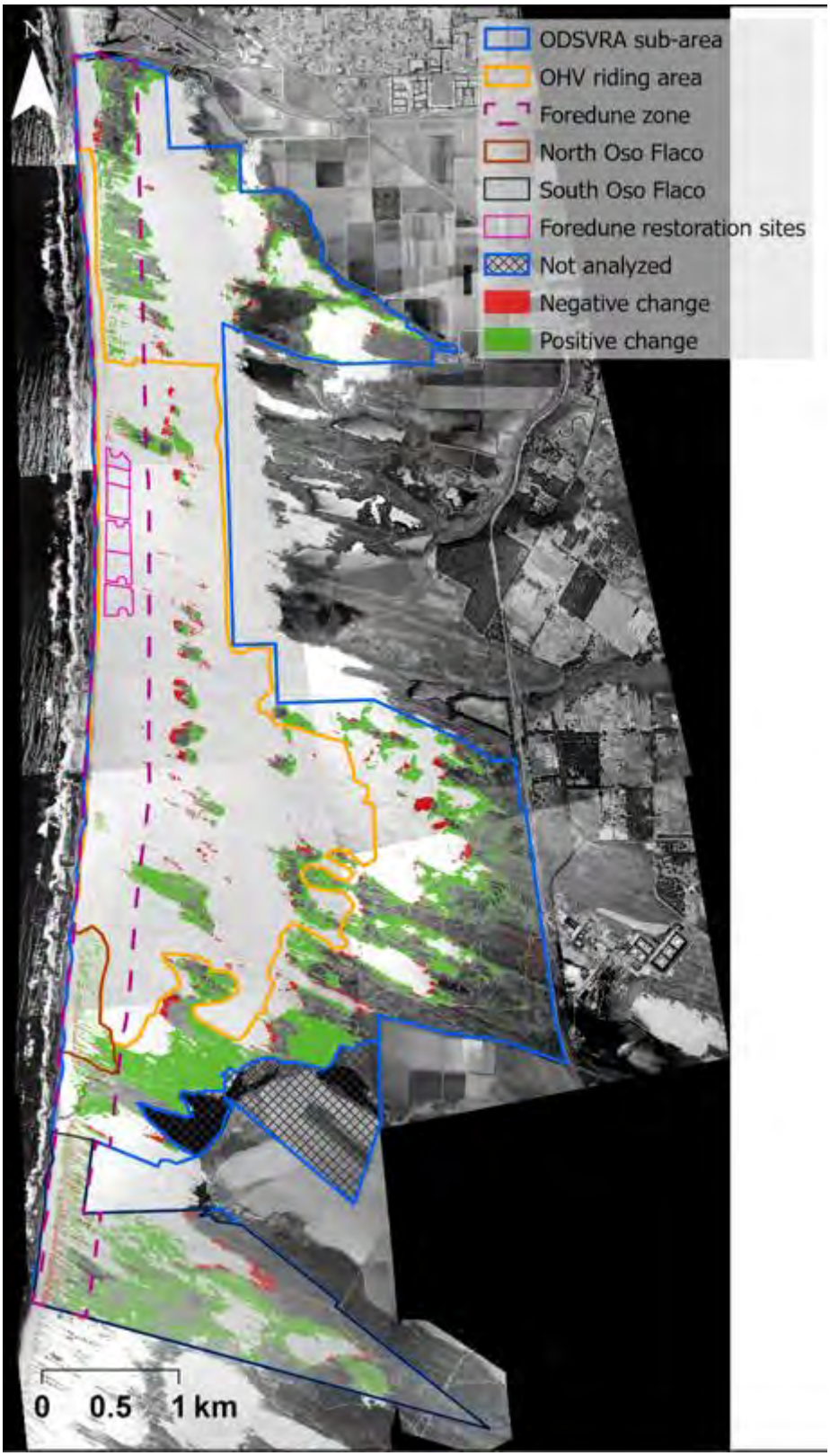

Figure 11. Change in vegetation between 1985 and 2012. Orthophoto from 1985.

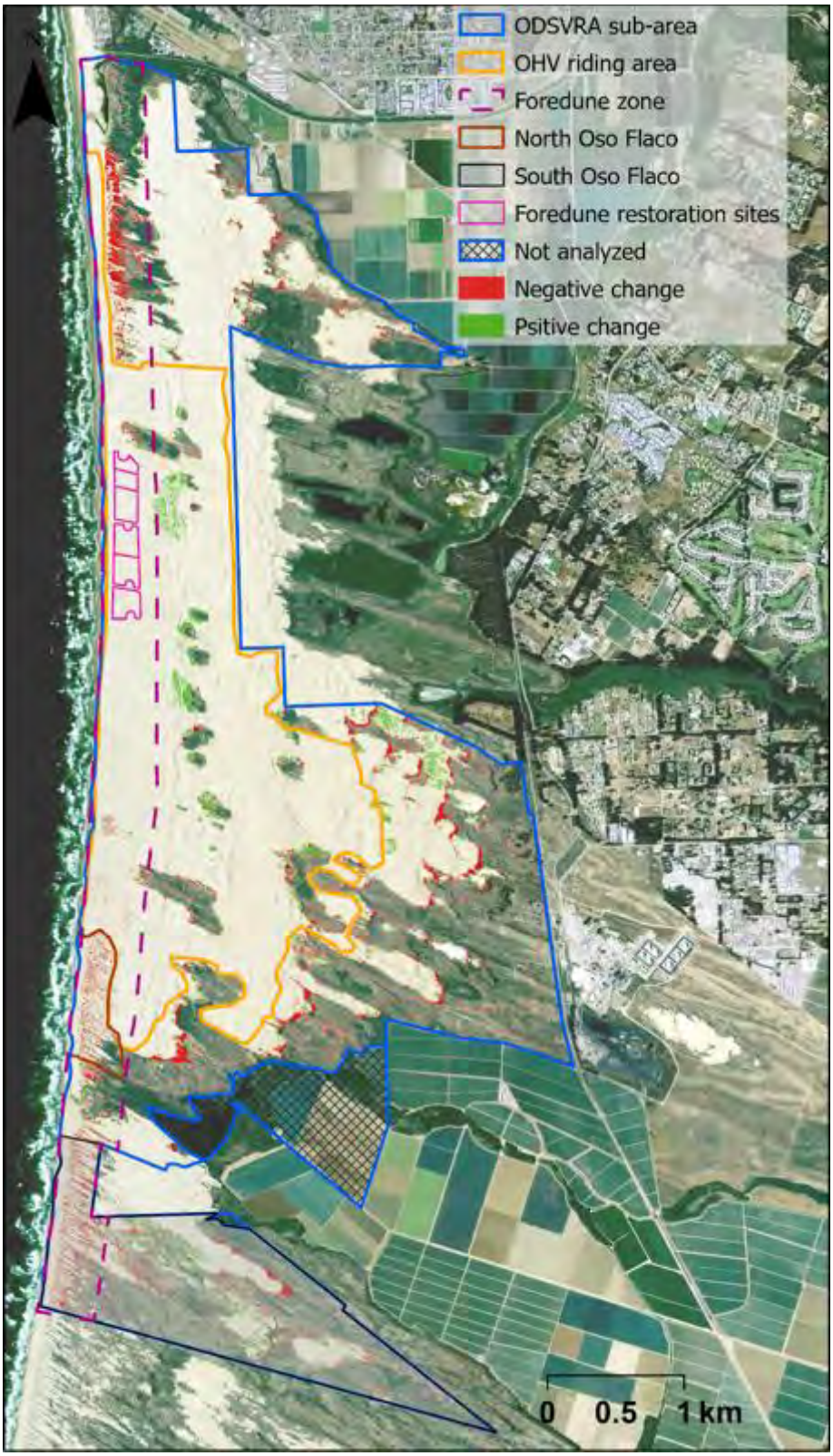

Figure 12. Change in vegetation between 2012 and 2020. Orthophoto of 2012.

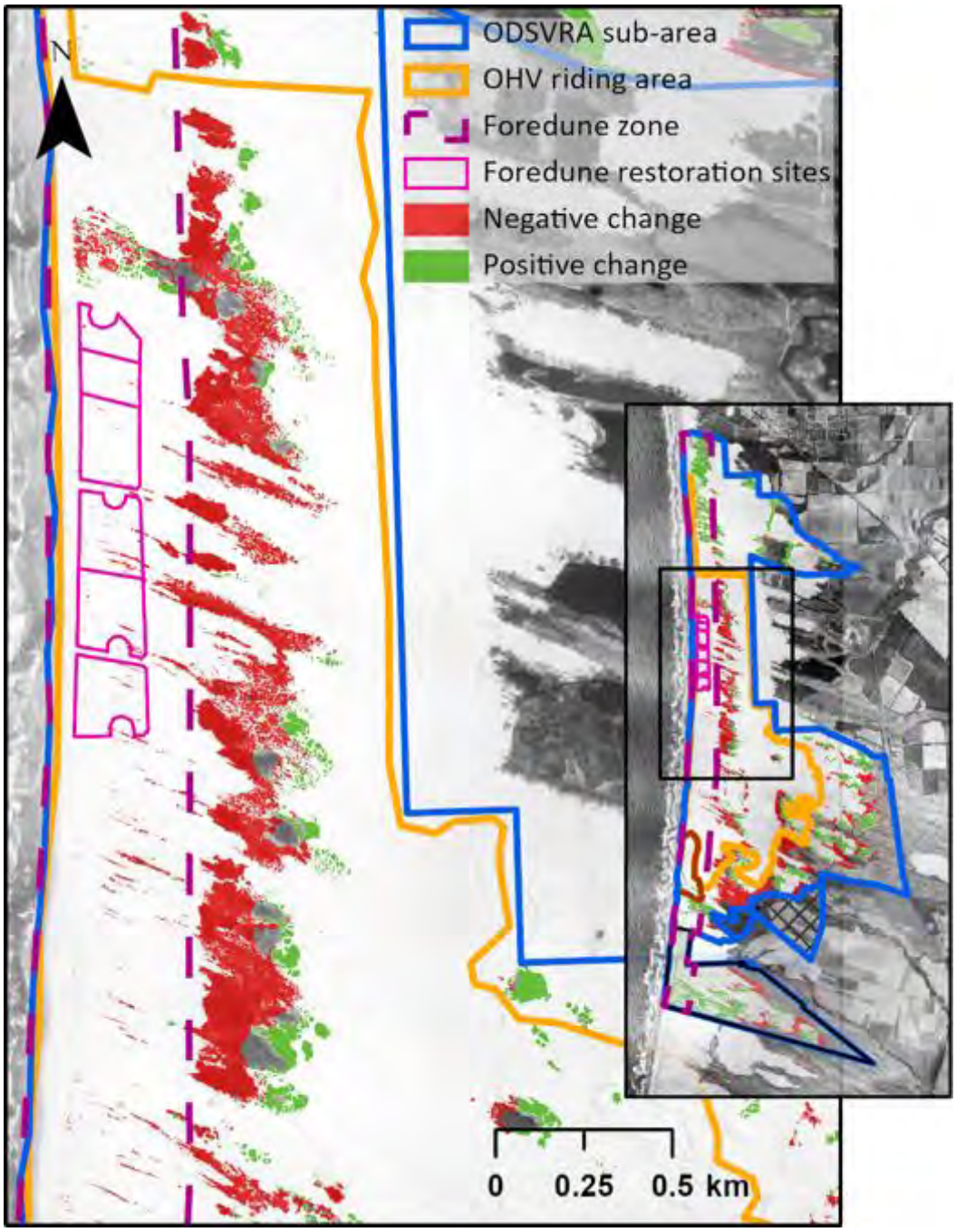

Figure 13. Close-up image of the change in vegetation cover around the foredune restoration sites between 1939 and 1985. Orthophoto from 1939.

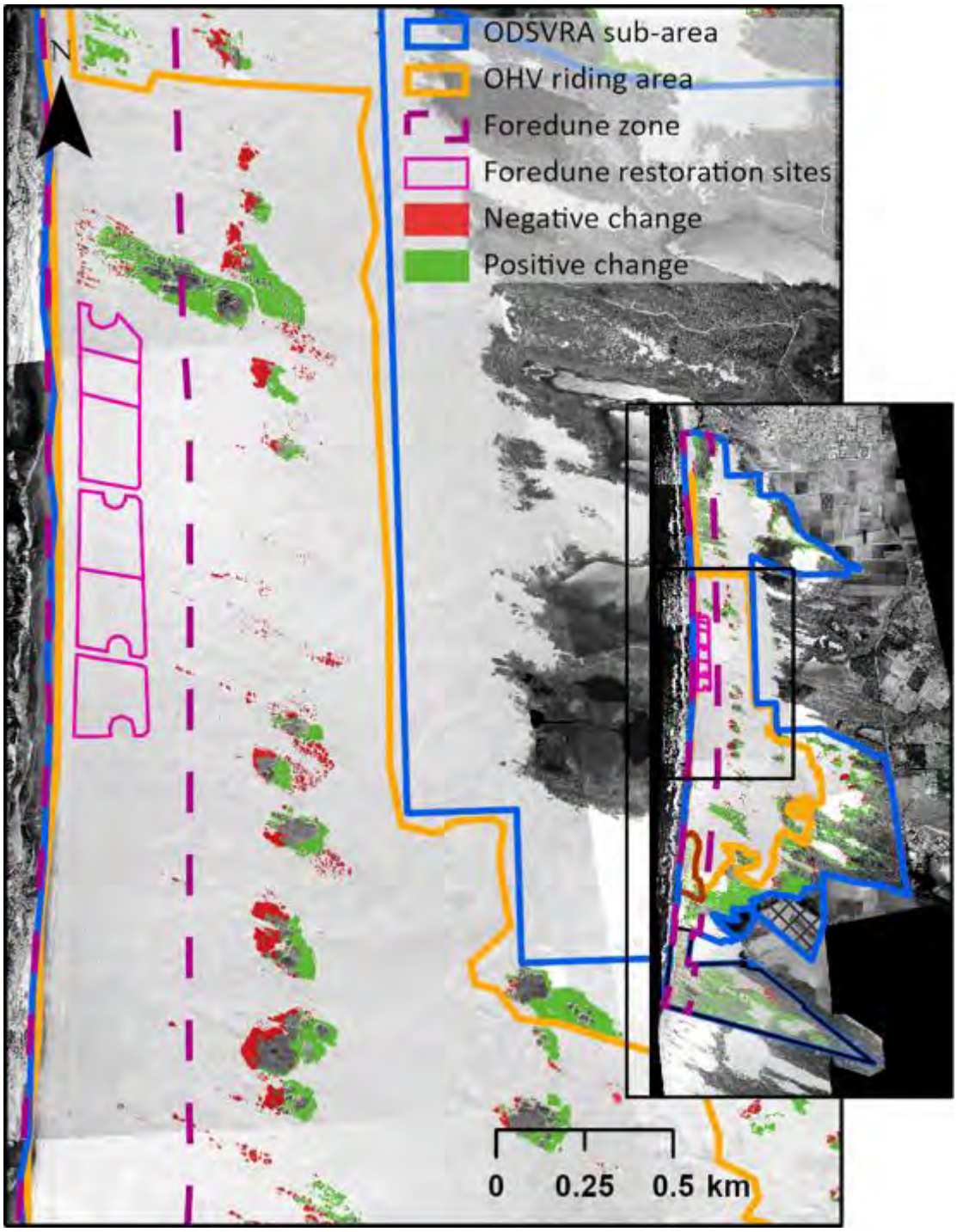

Figure 14. Close-up image of the change in vegetation cover around the foredune restoration sites between 1985 and 2012. Orthophoto from 1985.

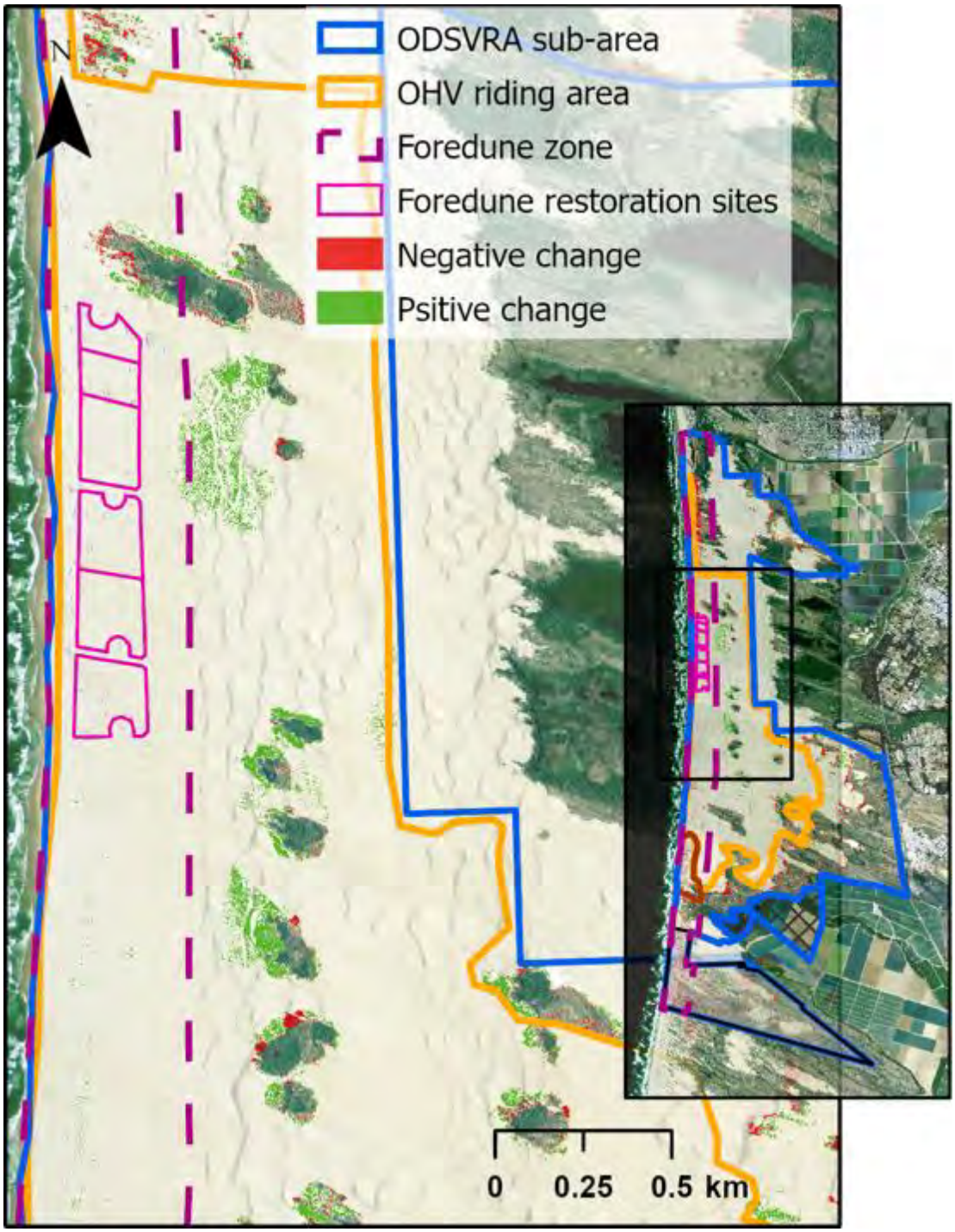

Figure 15. Close-up image of the change in vegetation cover around the foredune restoration sites between 2012 and 2020. Orthophoto from 2012.

Within the OHV riding area over the entire period of analysis, there are lower percentages of total change (13.5%) with mostly negative change (8.2%) in both the foredune and backdune zones (Figures 16A-18). Most of the negative changes occurred up to 1985 and were associated with the loss of hummocky nebkha and foredunes as well as vegetation in foredune swales (Figures 6 and 9B). Positive gains in plant cover in the OHV riding area occurred mostly in the backdune area within fenced vegetation islands (Figure 18).

The South Oso Flaco area showed significantly higher change rates (42%), with over 34% vegetation gain (Figure 16A) in both the backdune and the foredune zones. These gains are associated with limited OHV disturbance over at least the last 5 decades, as well as the growth and expansion of invasive weeds.

The more recently fenced North Oso Flaco area experienced significant increases (20%) in plant cover over the total period of analysis with only 0.7% loss (Figure 16B). The vast majority of plant growth occurred after the closure of the area for vehicle riding in 1982 (Figures 6 and 9) and is characterized mostly by hummocky nebkhas.

The analysis of changes between 1939 to 2012 provides an insight to the changes that occurred prior to the adoption of SLO-APCD Rule 1001 (2011) and related PMRP. The results show a similar trend of change in all analytical zones with slightly higher overall change values compared to the period between 1939 and 2020 (Figures 6B, S35 and S38, Table S2). These results match the trend of vegetation loss in North and South Oso Flaco and vegetation growth in the OHV riding area between 2012 and 2020 (Figures 4 and 9).

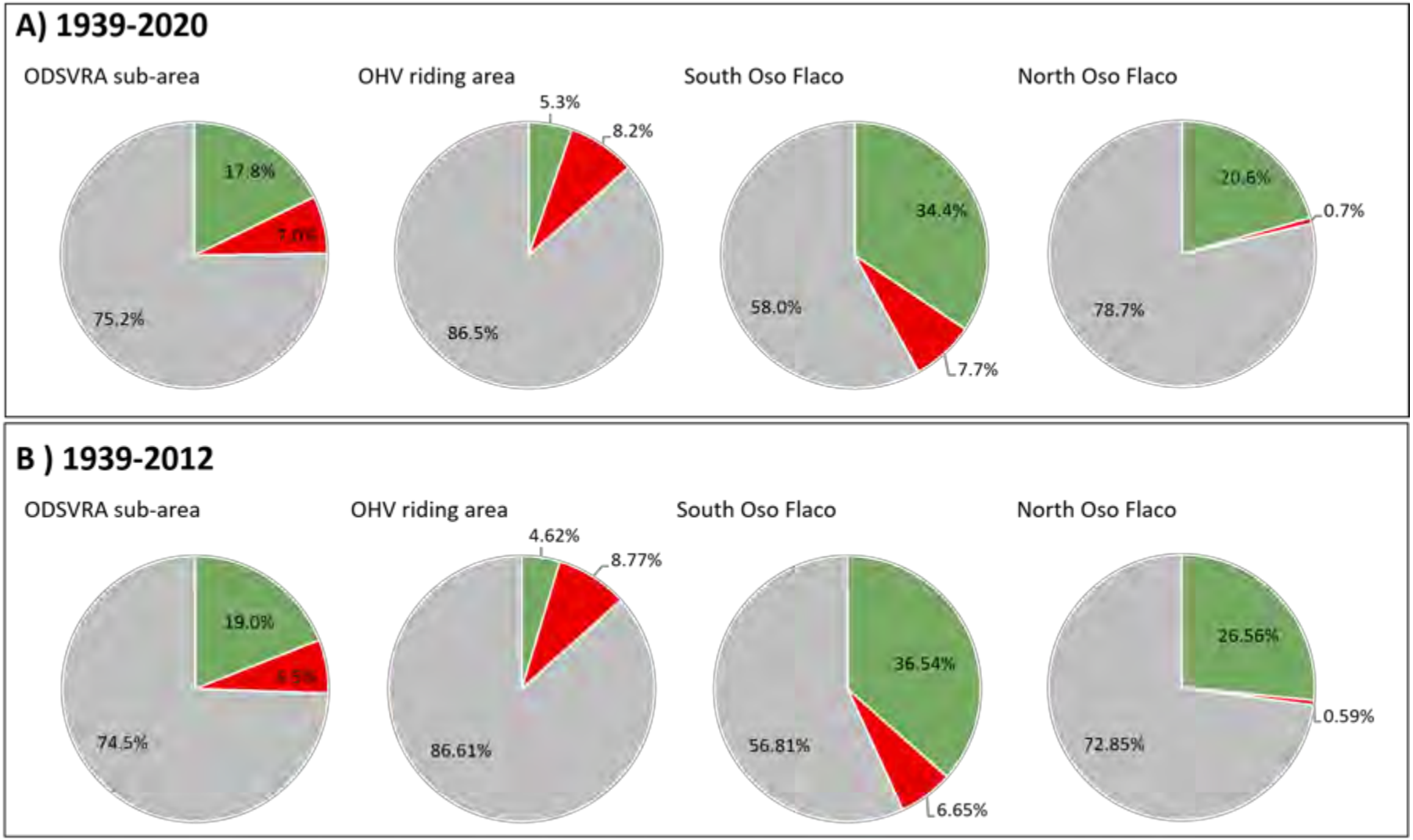

Figure 16. Change analysis (%) of vegetation cover in the ODSVRA sub-area, OHV riding area, and the South Oso Flaco area between A) 1939 and 2020, and B) 1939 and 2012. Positive change is presented in green, negative change in red, and no change in gray. data is in Table S2 in supplements.

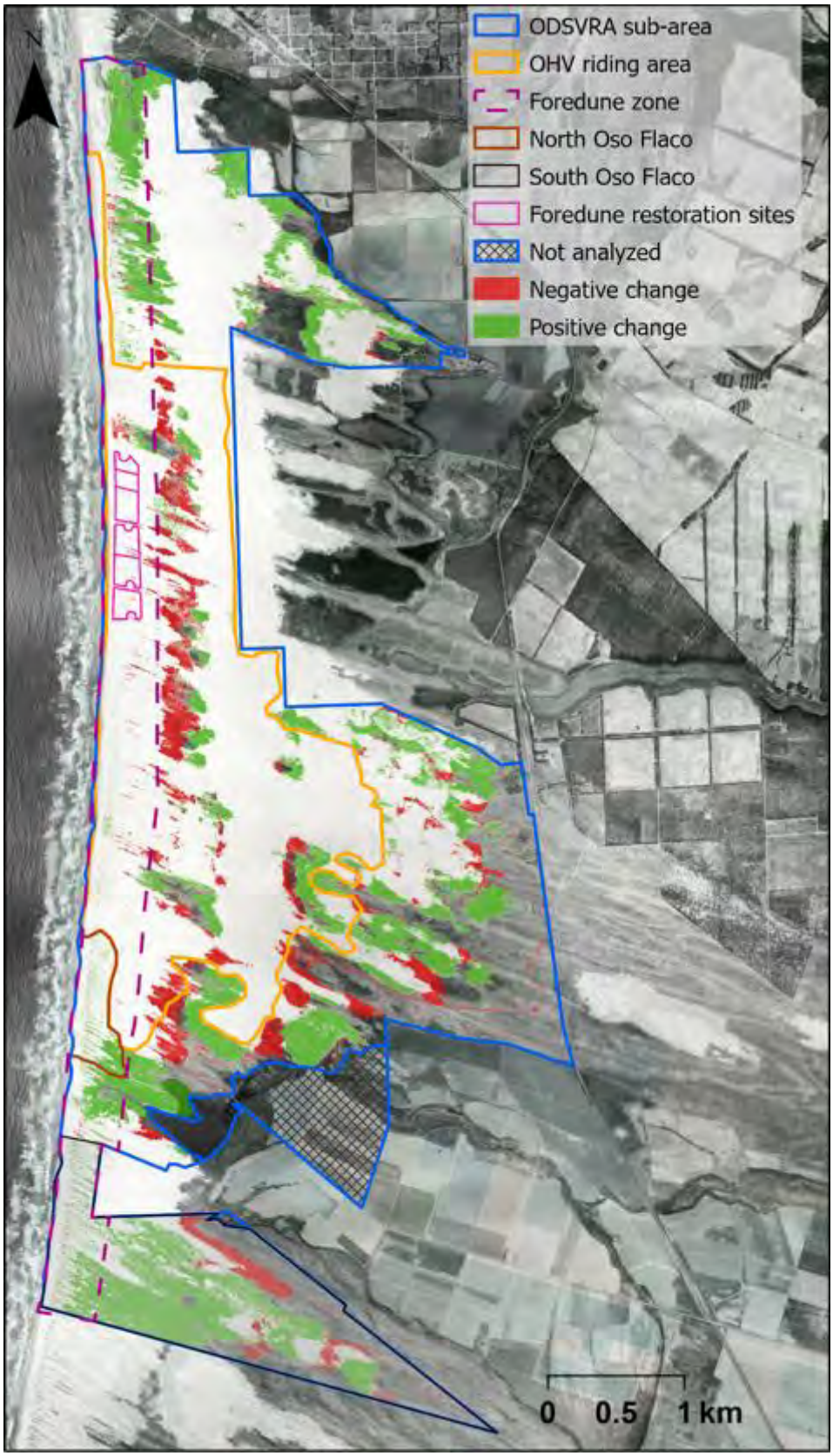

Figure 17. Change in vegetation between 1939 and 2020. Orthophoto from 1939.

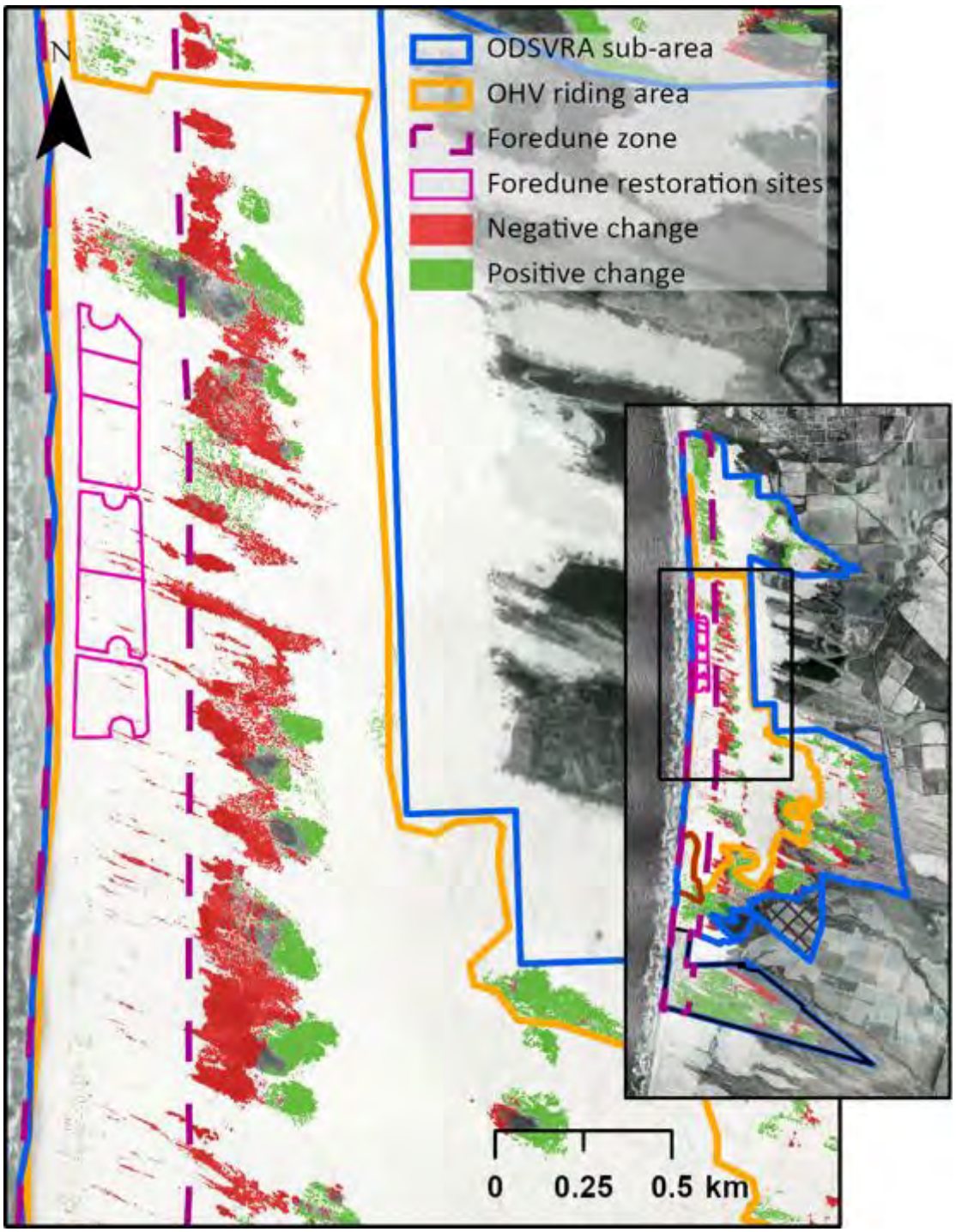

Figure 18. Close-up image of the change in vegetation cover around the foredune restoration sites between 1939 and 2020. Orthophoto from 1939.

4. Summary and Conclusions

As part of the 2020 ARWP, the CDPR requested a thorough analysis of historical changes in vegetation cover within the ODSVRA. This report provides a detailed analysis of the best available aerial photography of ODSVRA for 16 image years between 1930 and 2020 obtained from CDPR, the UCSB Library's Geospatial Collection, and the National Agriculture Imagery Program (NAIP). From this, plant cover was carefully and systematically classified and analyzed in a GIS software (ArcGIS Pro) to detect, quantify, and interpret changes and trends in vegetation cover.

To allow comparison between different management regions, the report focuses on three analytical zones within the sub-area of the ODSVRA south of Arroyo Grande Creek, ~75% of the total area of ODSVRA),

- the OHV riding area within the ODSVRA (c. 2013),
- the North Oso Flaco foredune complex, closed to OHV activity since 1982, serves as a reference site for mature foredunes,
- the South Oso Flaco dune complex within the ODSVRA boundary, including both foredune and backdune areas, which serves as a reference site for mature dunes that have not seen OHV activity since 1982,

In each analytical zone we also focused on the foredune zone, or the area where foredune vegetation would typically exist in the region, which extends ~400 m eastward/inland from the high-water mark. Another area of interest was the new (2020) foredune restoration sites, located within the foredune zone of the OHV riding area between post markers 4-6.

Plant cover maps and calculations (areas and %) were obtained for each analytical zone in all image years. Results show that vegetation cover trends within ODSVRA have varied over time and differ notably between the analytical regions. Within the broader ODSVRA sub-area, vegetation changes generally increased over time, ranging from 25% in 1939, to a peak of 37% in 2012, to just over 35% in 2020. In the OHV riding area, vegetation cover has been comparatively low across all years and declined appreciably from a peak value of 12% in 1966 to around 8% in 2020. After 1966 plant cover decreased to 4% in 1985 and remained low (<5%) until after 1988, when it began to gradually increase to the 2020 levels. The South Oso Flaco area shows a similar trend as the broader ODSVRA area, although with generally higher percentages. Plant cover at Oso Flaco was 37% in 1939, more than doubled to a peak of 66% by 2012, then remained over 60% up to 2020. The North Oso Flaco foredune area showed almost no plant cover in 1930 (0.7%), but has gradually increased over time, mostly after 1985, up to a peak of 24% in 2012.

Foredunes in the region are typically more sparsely vegetated than back dune environments and are characterized by a hummocky terrain of nebkha and elongated shadow dunes, blowouts, and narrow parabolic dunes, such as found at the South Oso Flaco reference site. Accordingly,

plant cover in the foredune zone of ODSVRA is generally less than that in the broader analytical zones over time, but shows similar trends. Foredune plant cover at Oso Flaco in 1939 was very low (2.3%), but increased by an order of magnitude to over 30% by the 2010s. For comparison, vegetation in the foredune zone of the OHV riding area had slightly higher cover (2.7%) in 1939, rose to a peak value of 5.4% in 1966, but then steadily declined to very low values >1% from 1985 to 1998. Since then, vegetation cover has increased slightly in the foredune zone of the OHV area to 2.4% by 2020, mostly due to new plants on the margins of fenced backdune vegetation islands and foredune vegetation establishing in the seasonal bird nesting enclosure.

Both North and South Oso Flaco areas have been fenced off to OHV traffic since roughly 1982 and, therefore, were selected as reference sites for plant cover and dune form in ODSVRA. The positive trend of plant growth over time and high percentages of cover in these areas vs. the OHV riding area attest to natural processes and responses of vegetation growth and dune development that could occur with limited anthropogenic disturbance. It is important to note, however, that some areas within the ODSVRA, including South Oso Flaco, are impacted by invasive species planted in the area during the early 1900s and, as such, plant cover percentages and dune stabilization could be higher than might be expected under natural conditions. Therefore, the specific cover values for South Oso Flaco provide a reference for relatively undisturbed areas in the ODSVRA, but they do not represent ideal natural conditions of this region. Unfortunately, there are no nearby dune systems that are pristine and undisturbed. Over the last decade CDPR have also conducted targeted efforts to remove invasive species in the ODSVRA particularly in backdune areas, South Oso Flaco, the Pismo Dunes Natural Preserve, and on some private land-holdings within and outside of the ODSVRA borders.

Although invasive grass species exist in ODSVRA, studies of sand dunes elsewhere in the world indicate a shift toward 'greening' (i.e., increased vegetation cover) over the last three decades[18,19,20,21] partly in response to climatic changes and enhanced preservation efforts. The results of this report are consistent with this global trend, yet they occur in the presence of intensive recreational use pressures, such as OHV riding and camping (sanctioned or otherwise) in various locations in the dunes. In part, the observed responses within ODSVRA are the result

[18] Ashkenazy, Y., Yizhaq, H., Tsoar, H., 2012. Sand dune mobility under climate change in the Kalahari and Australian deserts. Climatic Change 112, 901–923. https://doi.org/10.1007/s10584-011-0264-9

[19] Gao, J., Kennedy, D.M., Konlechner, T.M., 2020. Coastal dune mobility over the past century: A global review. Progress in Physical Geography: Earth and Environment 44, 814–836. https://doi.org/10.1177/0309133320919612

[20] Jackson, D.W.T., Costas, S., González-Villanueva, R., Cooper, A., 2019. A global 'greening' of coastal dunes: An integrated consequence of climate change? Global and Planetary Change 182, 103026. https://doi.org/10.1016/j.gloplacha.2019.103026

[21] Heathfield, D.K., & Walker, I.J. (2011). Analysis of coastal dune dynamics, shoreline position, and large woody debris at Wickaninnish Bay, Pacific Rim National Park, British Columbia. Canadian Journal of Earth Sciences, 48(7), 1185-1198. https://doi.org/10.1139/e11-043

of land use management and vegetation restoration efforts by CDPR since establishment of the park in 1982.

Detailed examination of change maps of negative (losses) or positive (gains) in plant cover over time show a large amount of change between 1966-1985, with negative change mostly in foredune areas and adjoining inland vegetation islands. Between 1998 and 2012, a large positive change occurred, mostly around existing vegetation islands, which corresponds partly with implementation of protective fencing and restoration projects in different areas outside the OHV riding area. Most positive changes in the OHV riding area were after 2005 and relate to new plants within the margins of fenced vegetation islands and foredune plants and nebkha development in the seasonal bird nesting enclosure between 2005 and 2020. In general, the vast majority of positive changes over the years in all analytical zones were within fenced areas with limited or no OHV activity, such as the seasonal bird nesting exclosures, fenced islands of existing plant cover, restoration project sites, and in the North and South Oso Flaco regions.

In terms of landscape responses during the identified management intervals, the period roughly preceding the establishment of the ODSVRA (1939-1985) saw a general decline in plant cover in the foredune and backdune of the OHV riding area (from 10.9 to 3.9% cover). Although cover increased between 1939-1966, it then declined until 1985 just as the ODSVRA was established. Between 1985 and 2012, there was mostly increasing plant cover with over 14% positive change in the broader ODSVRA sub-area, mainly around existing vegetation and other targeted restoration areas, particularly between 2005 and 2012. In the OHV riding area, plant cover increased mostly in fenced areas in backdune vegetation islands. From 2012 to 2020, there was a general decline in the amount of vegetation cover compared to previous intervals with 8% of total change in the ODSVRA sub-area. Some of this decline relates to invasive plant removal projects at the Pismo Dune Natural Preserve and Oso Flaco and most of the positive changes during this time related to backdune restoration areas implemented by CDPR.

It is clear that vegetation cover within ODSVRA has changed significantly over time and that the effects of OHV traffic, recreational activities, invasive species, and ecosystem restoration projects have collectively influenced the observed patterns and trends in varying ways and extents. Some of these effects are the result of aggregated impacts and, thus, are difficult to disentangle, while others are more clearly related to distinct activities in specific areas. It is important to note that the landscape that was inherited by CDPR when ODSVRA was established in 1982 had already experienced notable changes in vegetation cover related to unsanctioned OHV activity and other land use changes (e.g., agriculture, infrastructure development). Although it is beyond the scope of this report, it is also possible that plant communities at ODSVRA are also influenced by multi-decadal climatic changes similar to other coastal dune systems worldwide. Given the dynamic and compounded nature of forces that have shaped the dunes at ODSVRA, it

is essential to recognize that dune ecosystems and their plant communities are not static features of the landscape and that they will continue to evolve and reflect the changing conditions that shape their form and function. This poses a particular challenge for establishing management targets and restoration strategies in a landscape that has been subject to intensive OHV and recreation activities that destroy vegetation essential for dune development and reduction of dust emissions.

This report is intended to inform further discussions between CDPR, SAG, and SLO-APCD on how historic vegetation cover and change trends can be used to inform future dust mitigation strategies within ODSVRA. For instance, a reference point in time for 'pre-disturbance' or 'pre-CDPR management' conditions within the dunes would be useful for guiding dust emissions simulation modeling and revisiting the SOA target, which currently lacks a baseline condition. In addition, understanding the spatial distribution of plant communities and their changes through time in different disturbance settings is useful for refining decisions on the location and extent of future vegetation restoration dust mitigation strategies. It is anticipated that such discussions and related adaptive management decisions will help define ongoing vegetation for restoration and dust emissions mitigation strategies in the upcoming 2022 ARWP.

5. Supplements

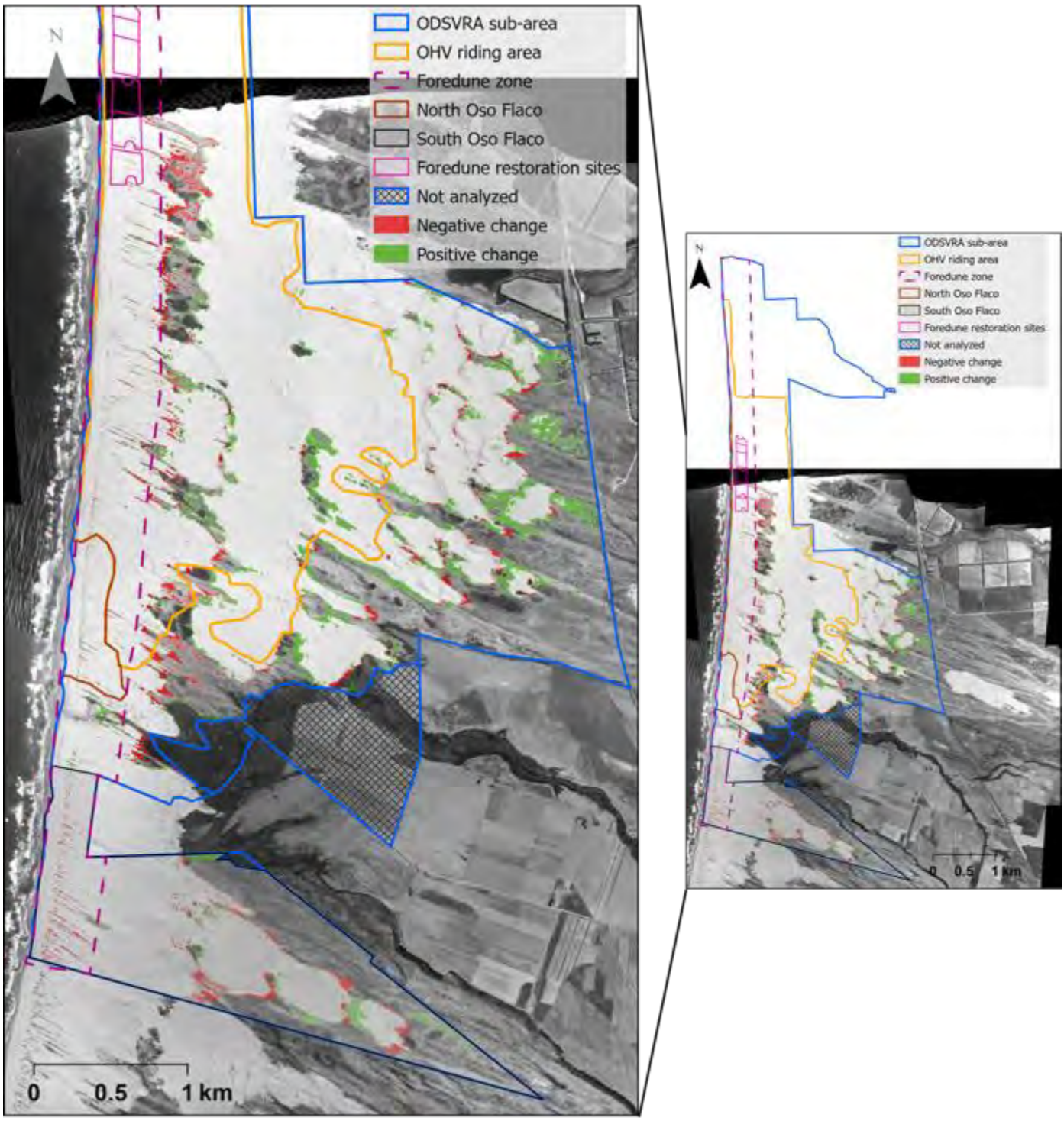

Figure S1. Vegetation change analysis results between 1930 and 1939. Positive change is in green, negative change is in red. Background orthophoto is from 1930.

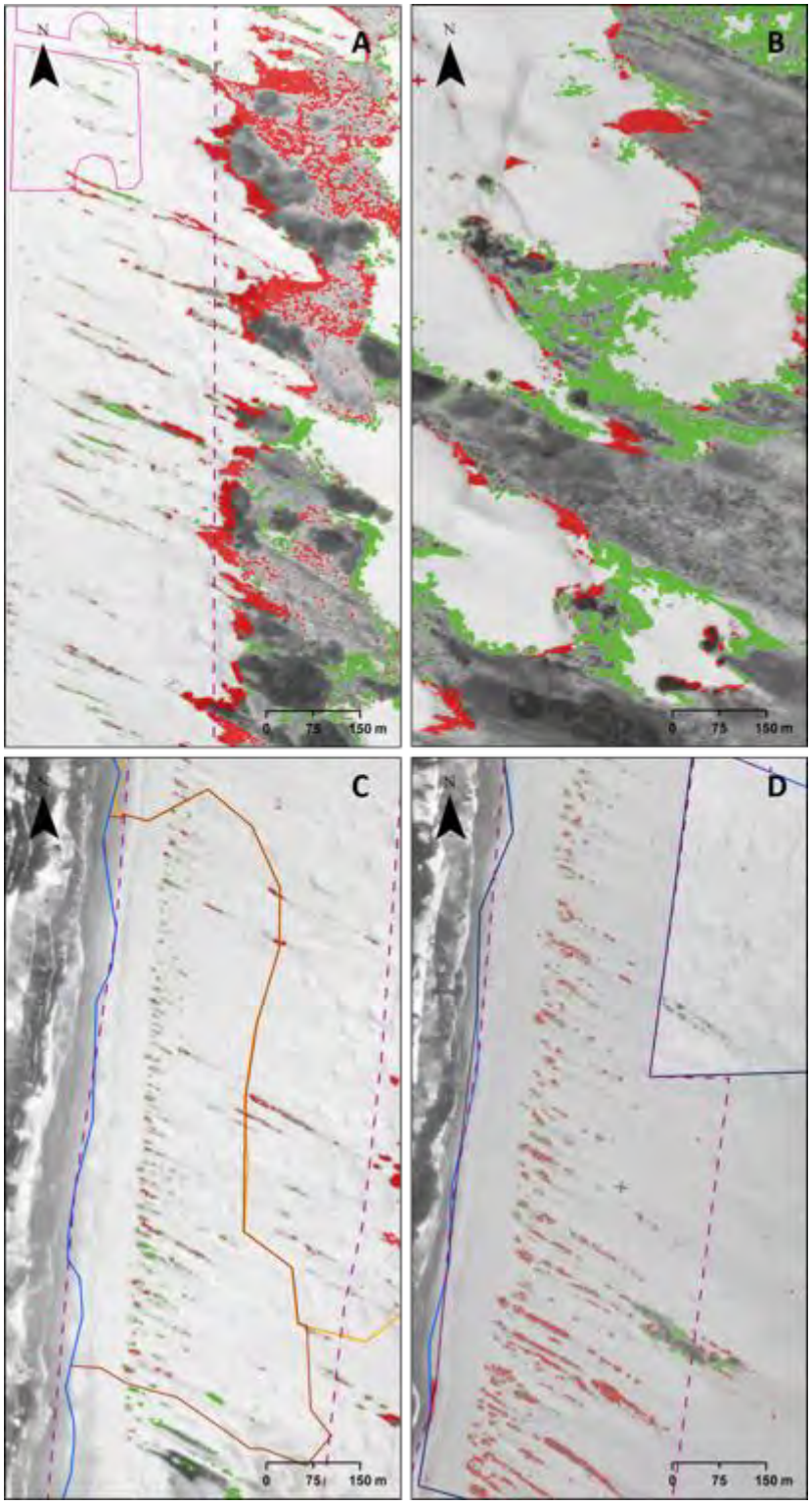

Figure S2. close-ups of vegetation change analysis results between 1930 and 1939 of the OHV riding area (A), backbude of the ODSVRA sub-area (B), North Oso Flaco (C), and South Oso Flaco (D). Positive change is in green, negative change is in red. Background orthophoto is from 1930.

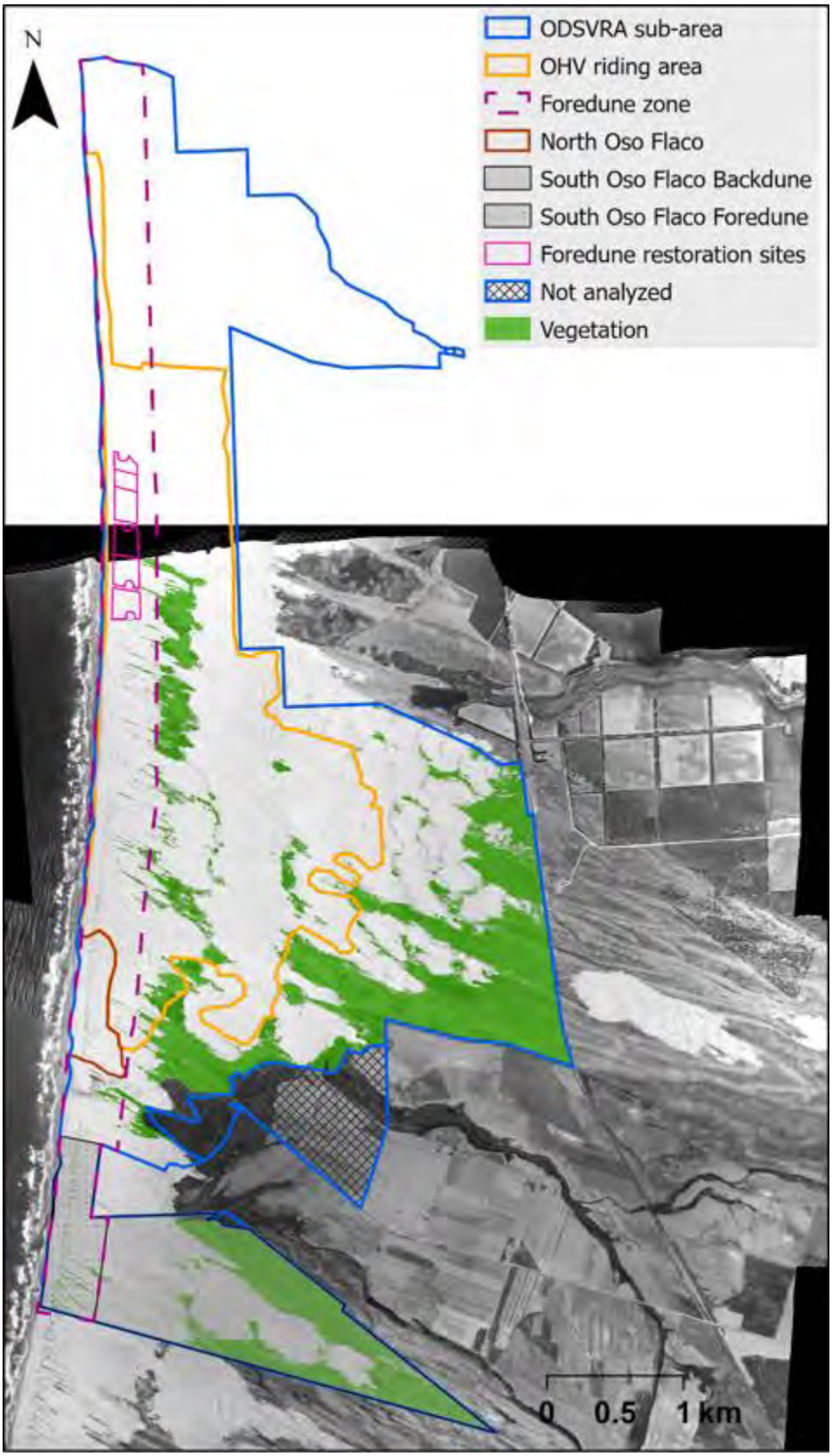

Figure S3. Vegetation cover map of 1930.

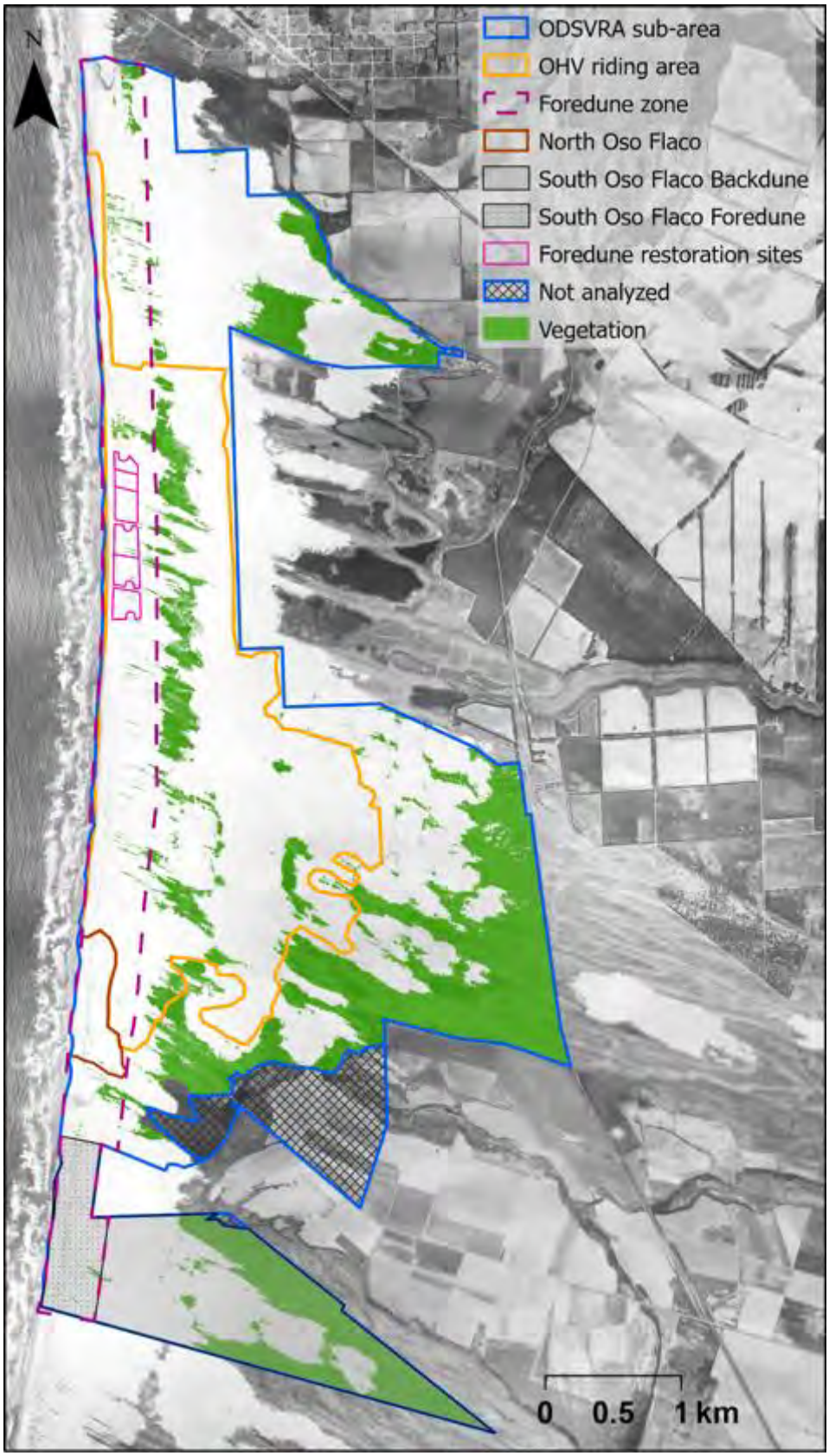

Figure S4. Vegetation cover map of 1939.

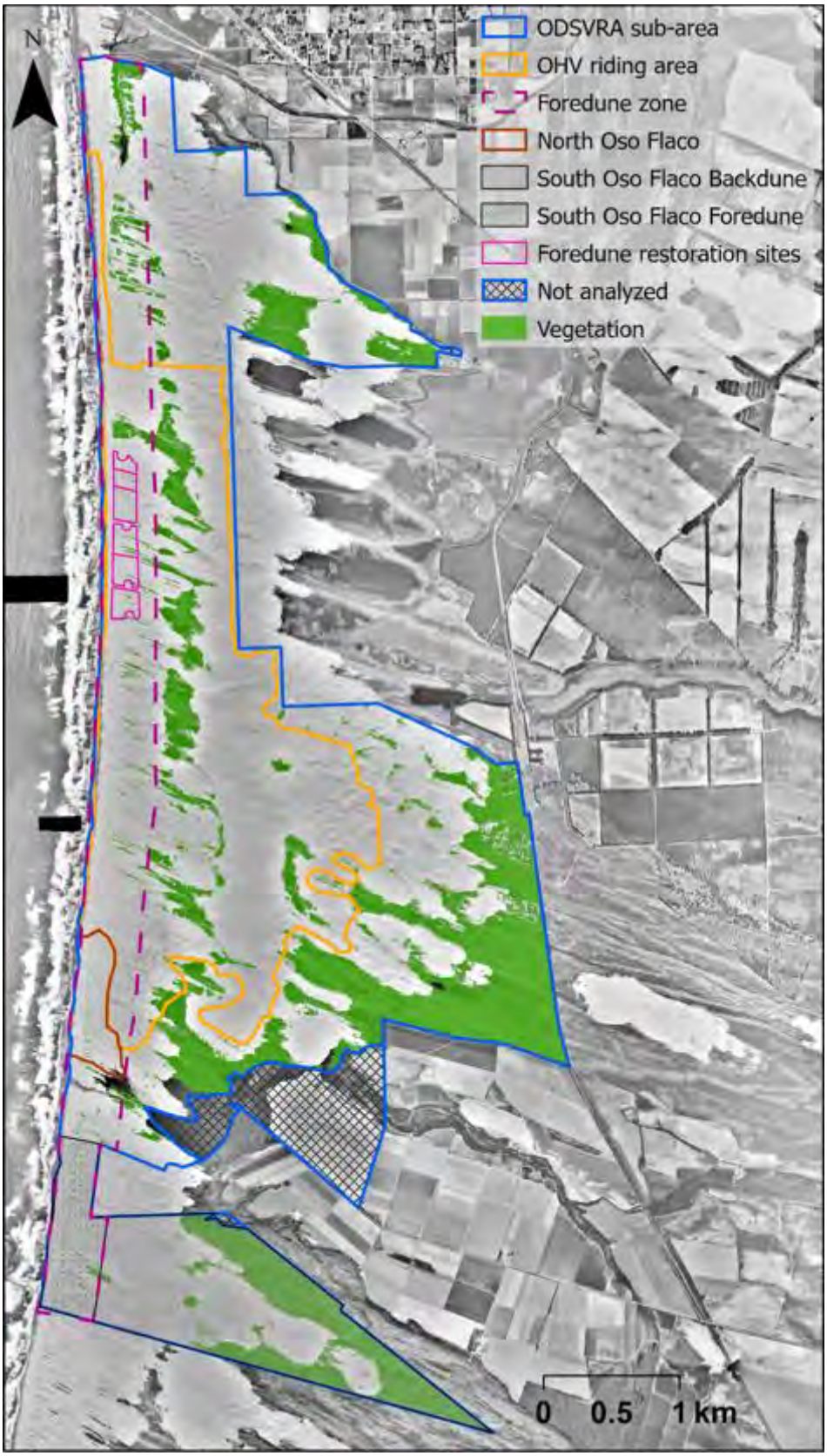

Figure S5. Vegetation cover map of 1949.

Figure S6. Vegetation cover map of 1956.

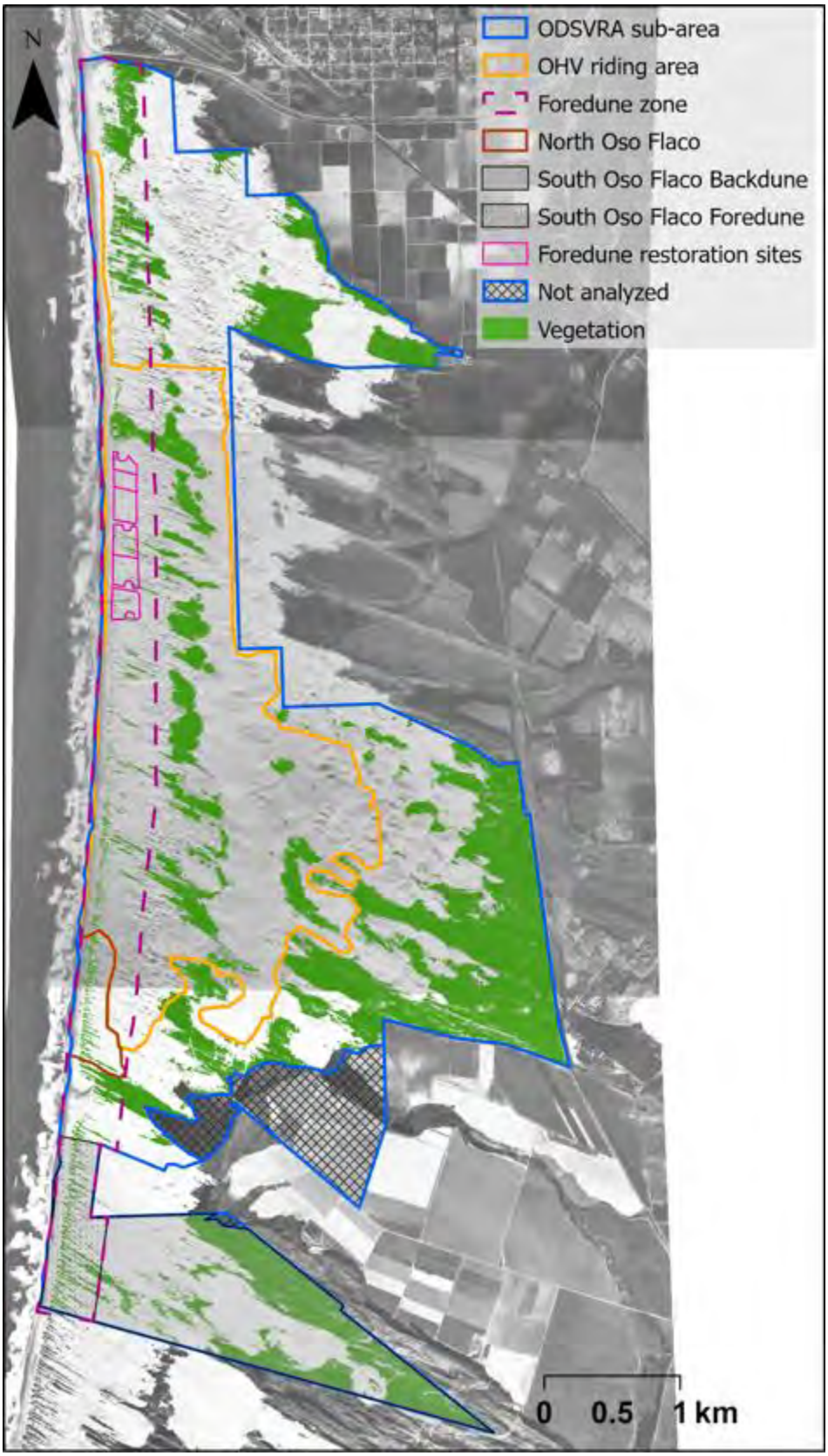

Figure S7. Vegetation cover map of 1966.

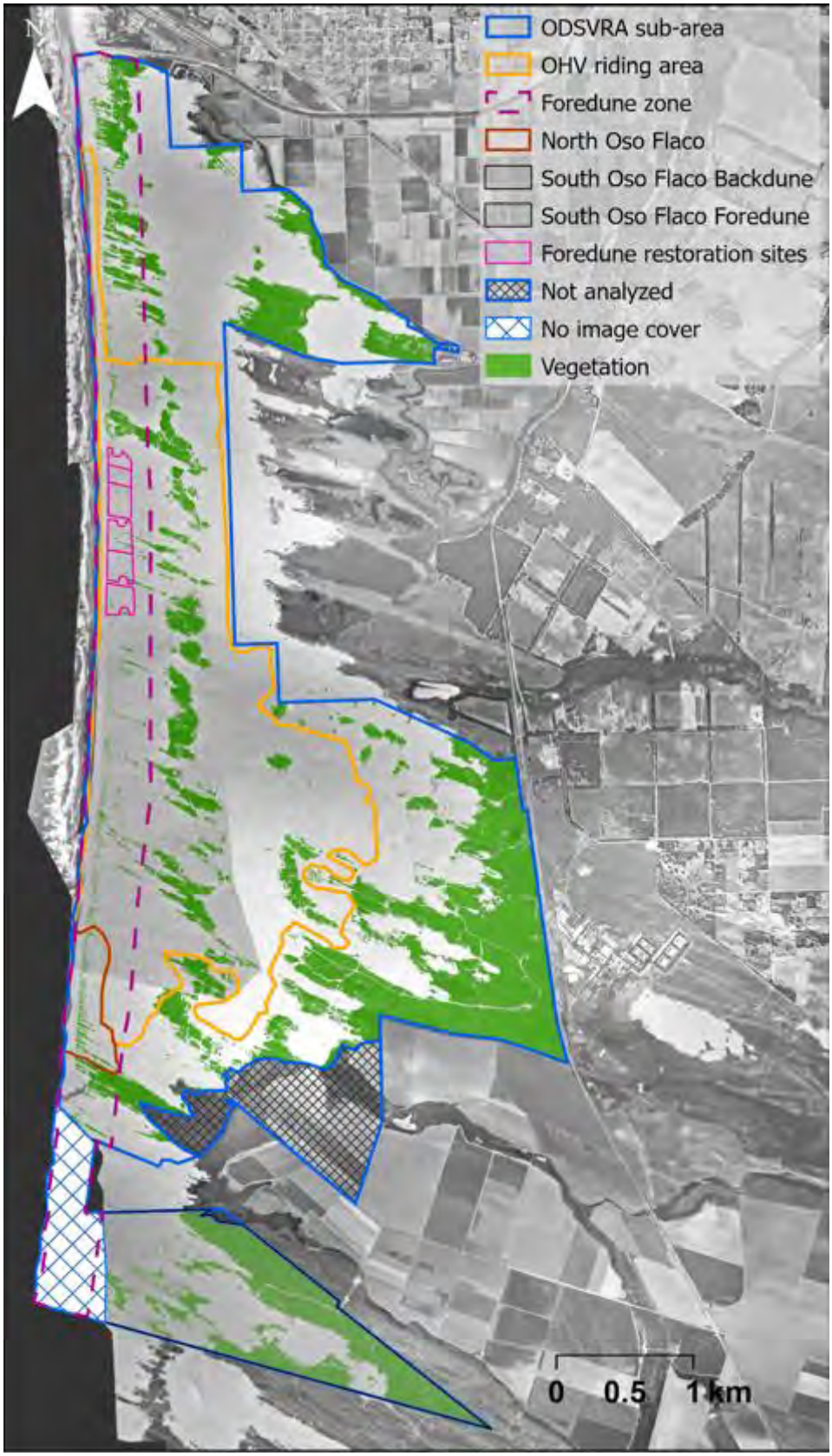

Figure S8. Vegetation cover map of 1971.

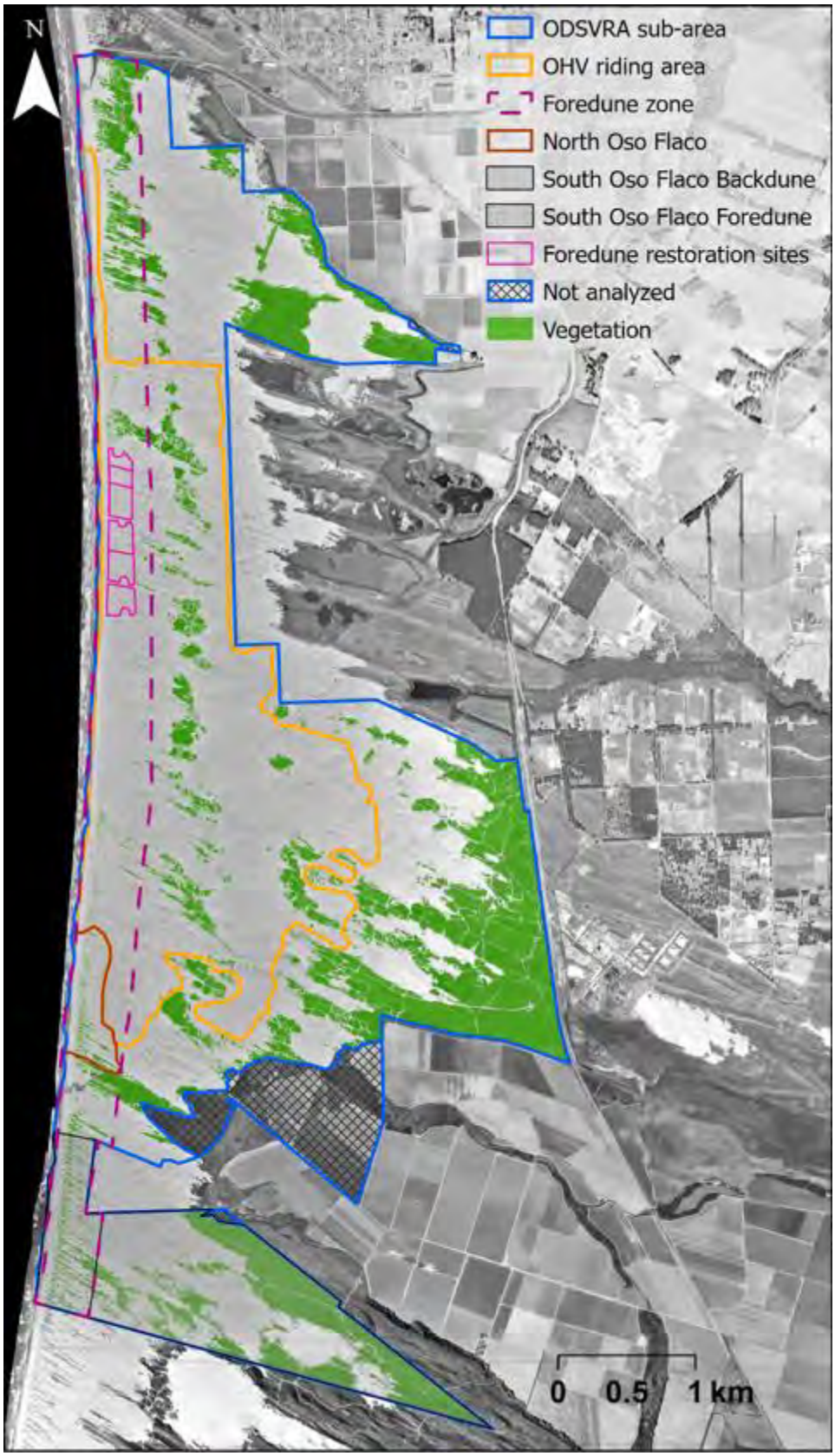

Figure S10. Vegetation cover map of 1978.

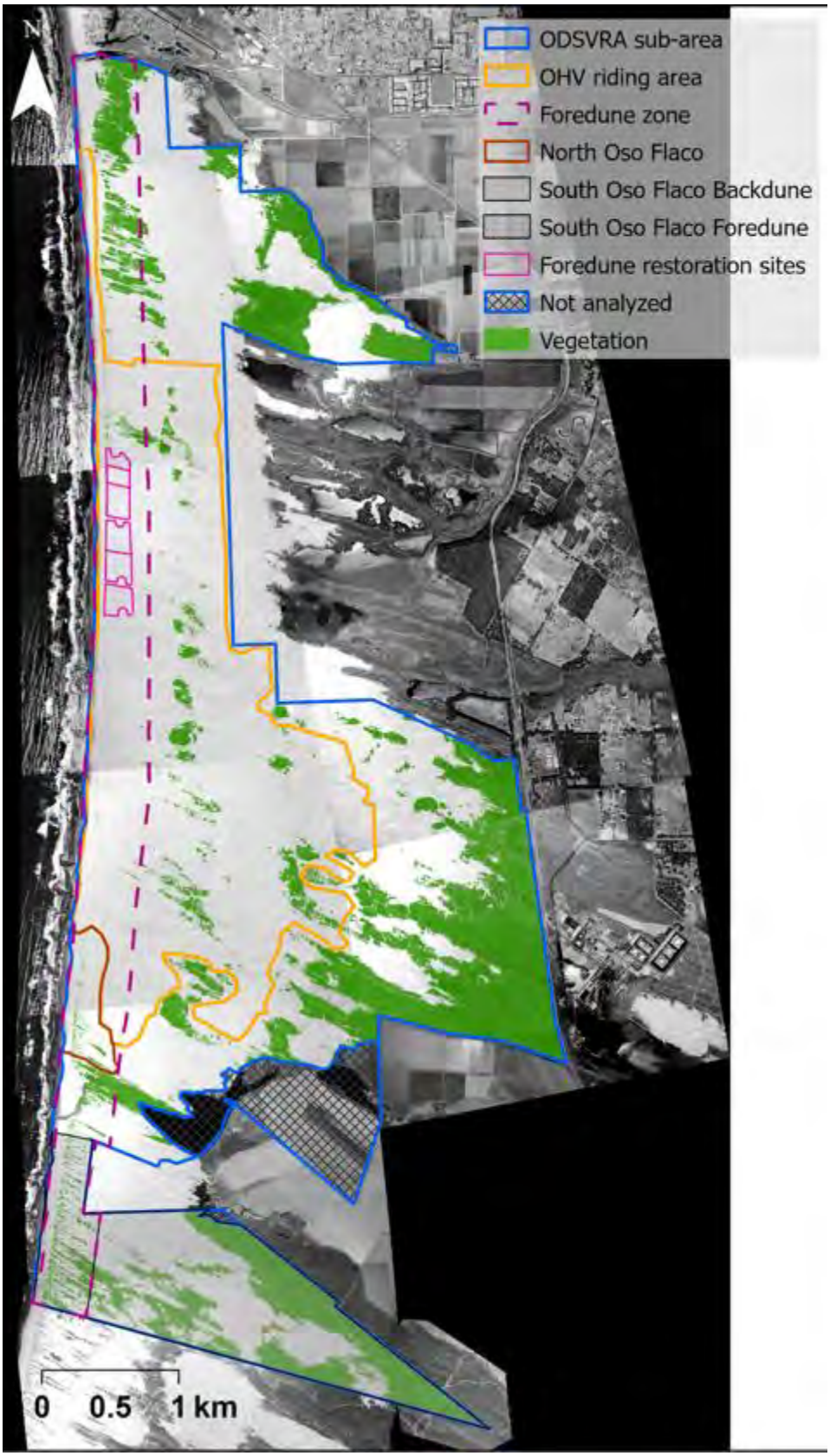

Figure S10. Vegetation cover map of 1985.

Figure S11. Vegetation cover map of 1994.

Figure S12. Vegetation cover map of 1998.

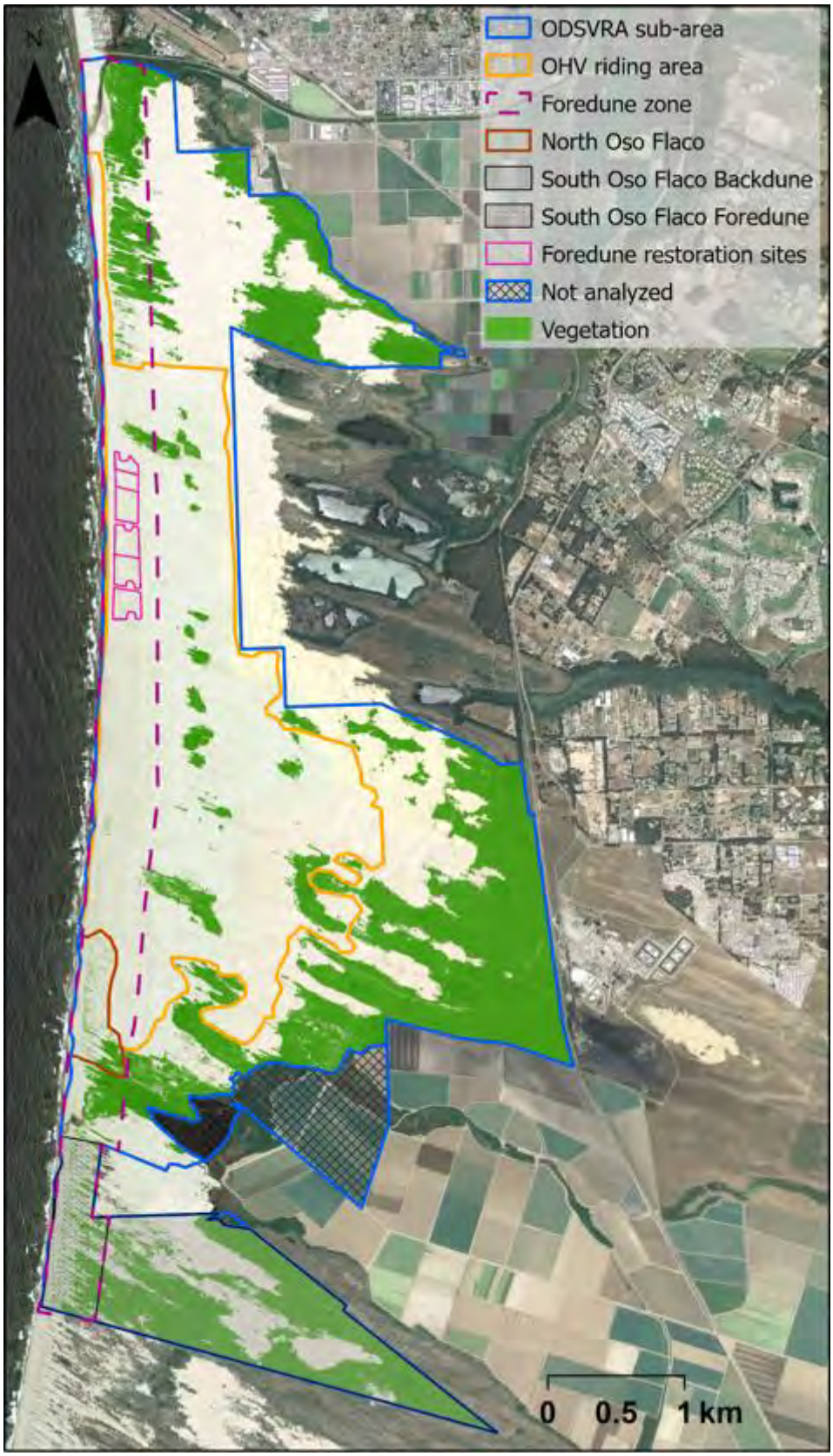

Figure S13. Vegetation cover map of 2005.

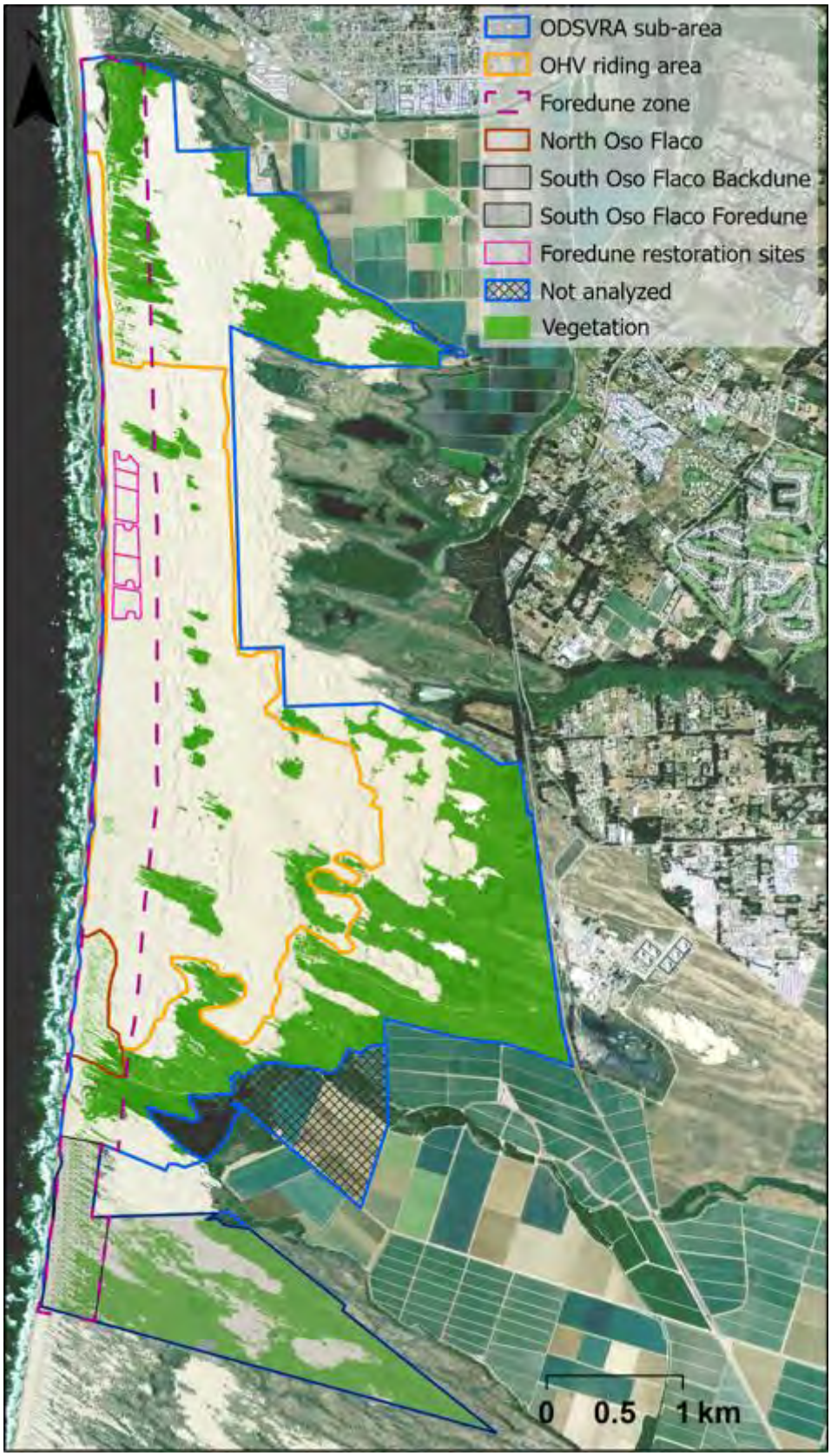

Figure S14. Vegetation cover map of 2012.

Figure S15. Vegetation cover map of 2014.

Figure S16. Vegetation cover map of 2016.

Figure S17. Vegetation cover map of 2018.

Figure S18. Vegetation cover map of 2020.

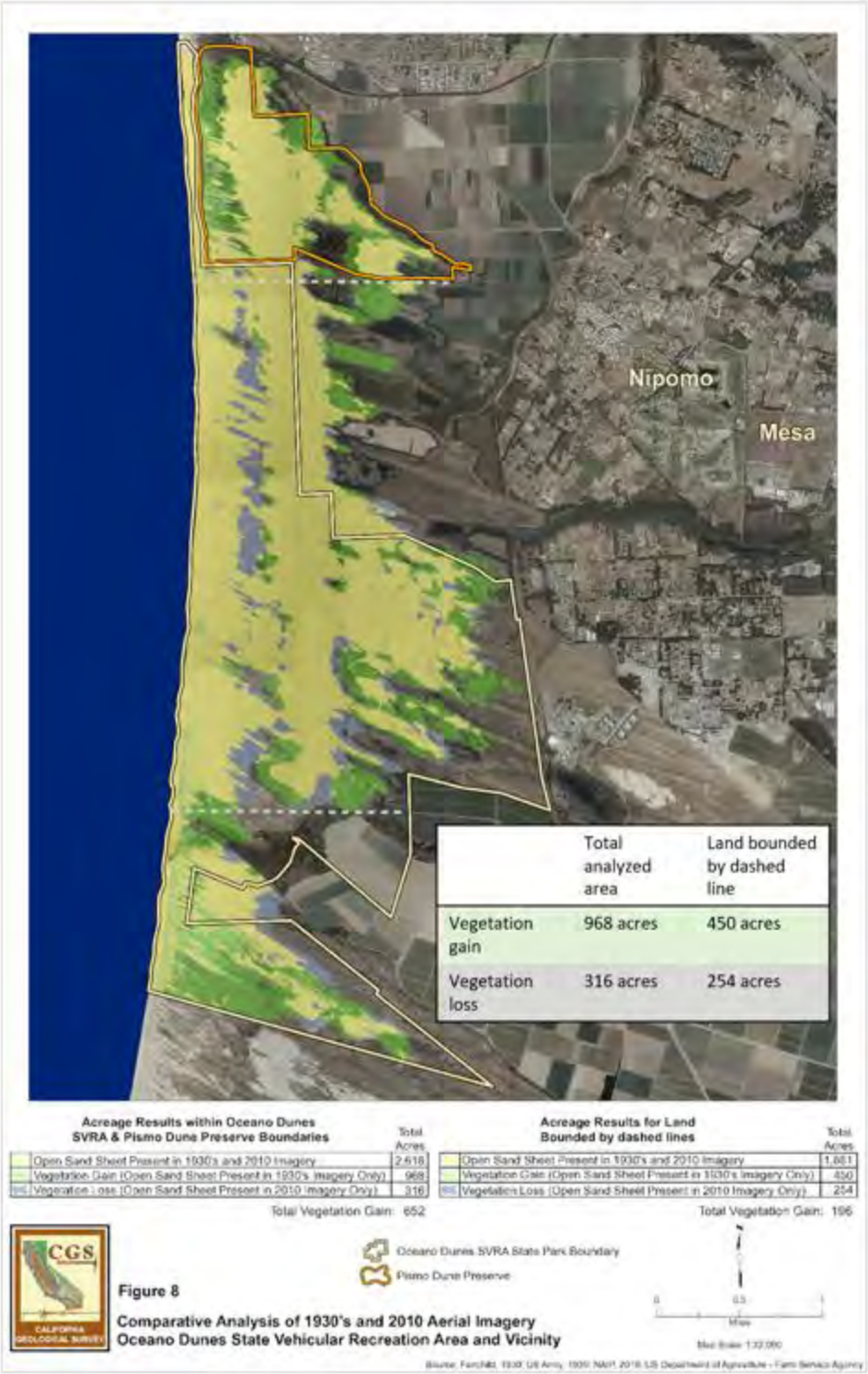

Figure S19. Sand and vegetation acreage results of the comparison between 1930's and 2010 presented in Figure 8 in the CGS report from 2011, positive change is in green, negative change in gray, open sand is in yellow in yellow (Harris, 2011).

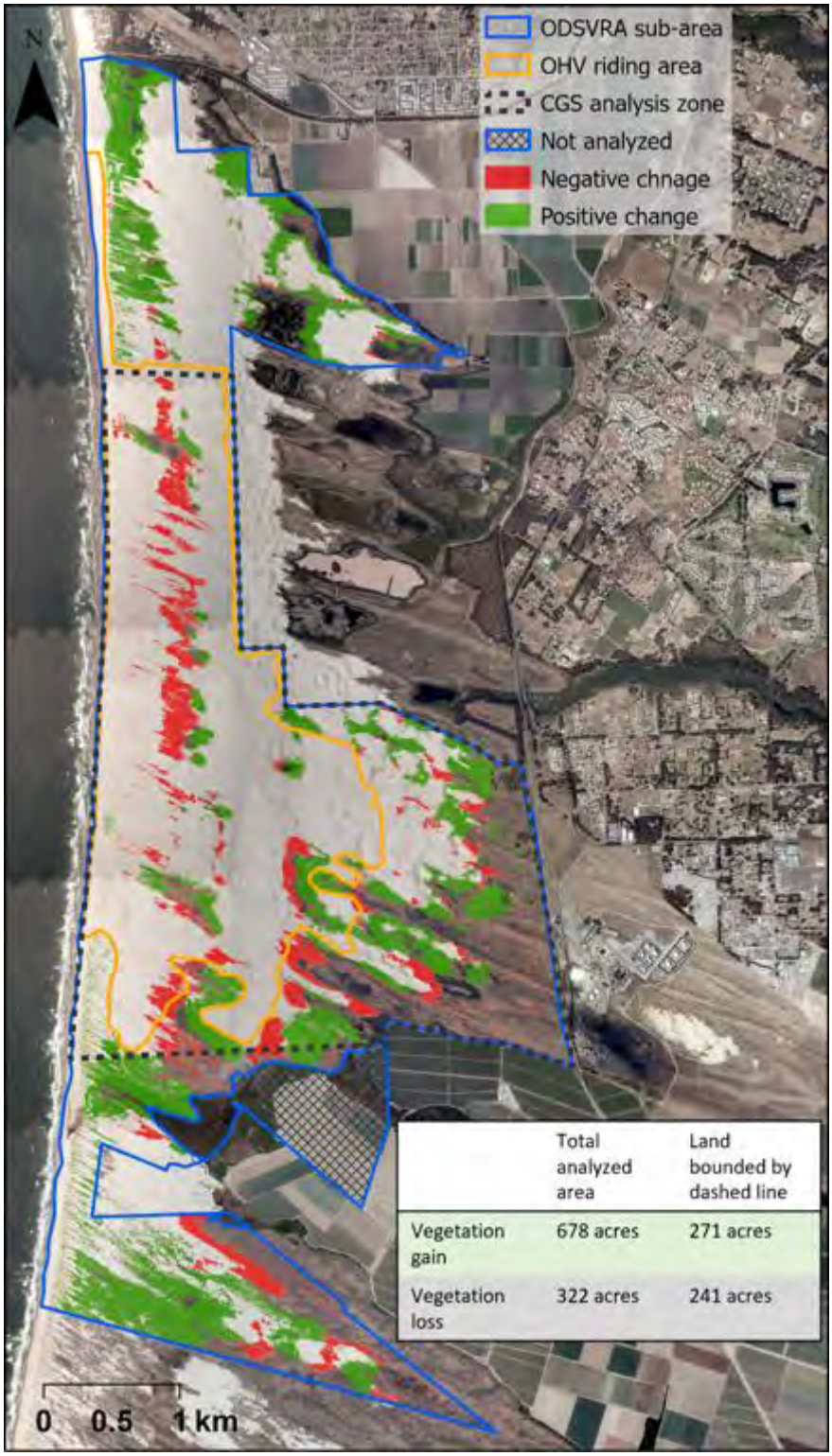

Figure S20. Vegetation change analysis results of the 1939 and 2010 UCSB-ASU analysis, positive change is in green, negative change is in red. Orthophoto background is from 2012. The grey dashed line represents the area for comparison with the CGS analysis.

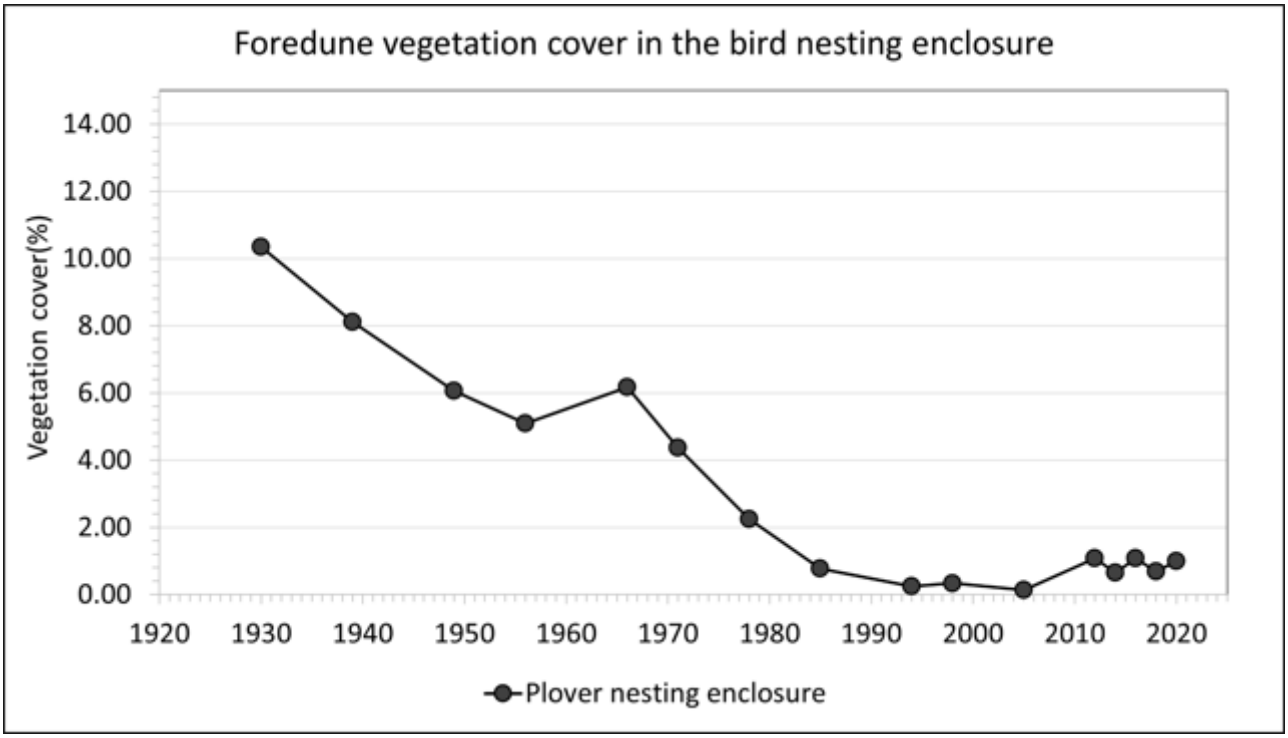

Figure S21. Percent vegetation cover within the seasonal bird nesting enclosure area (see borders in Figure 8). Vegetation cover percentages are related to the area of the analytical region.

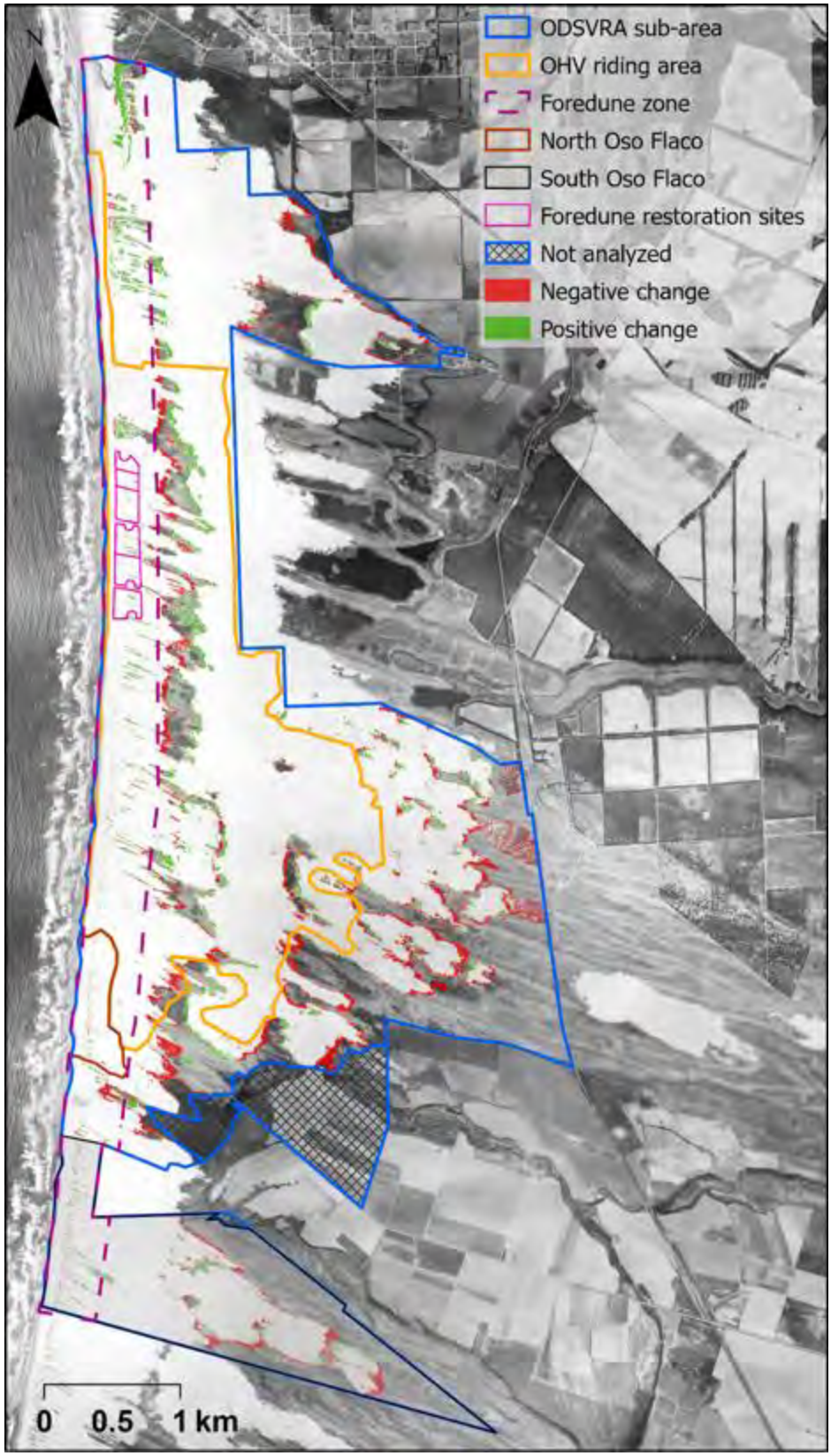

Figure S22. Vegetation change analysis results between 1939 and 1949. Positive change is in green, negative change is in red. Background orthophoto is from 1939.

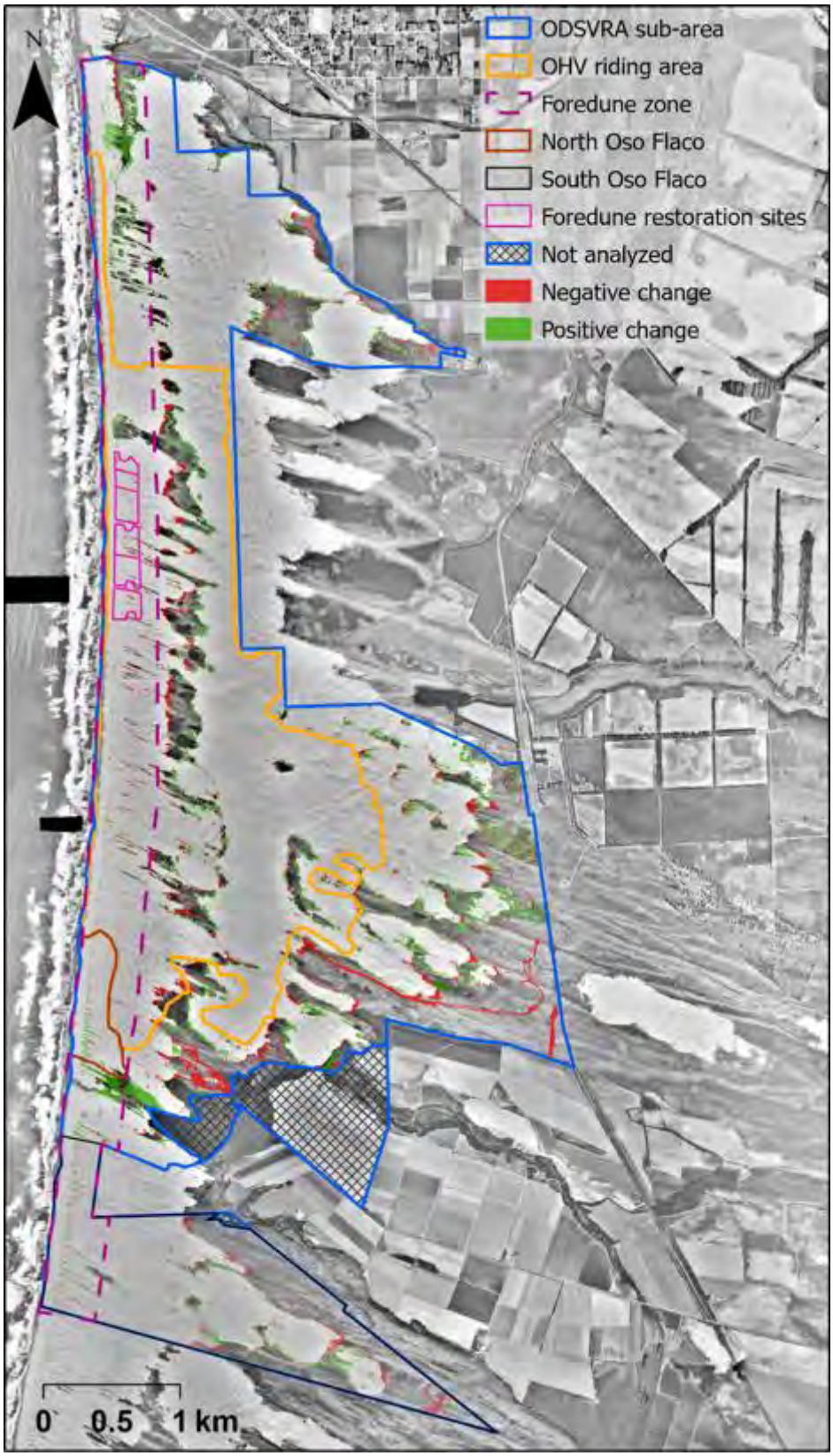

Figure S23. Vegetation change analysis results between 1949 and 1956. Positive change is in green, negative change is in red. Background orthophoto is from 1949.

Figure S24. Vegetation change analysis results between 1956 and 1966. Positive change is in green, negative change is in red. Background orthophoto is from 1956.

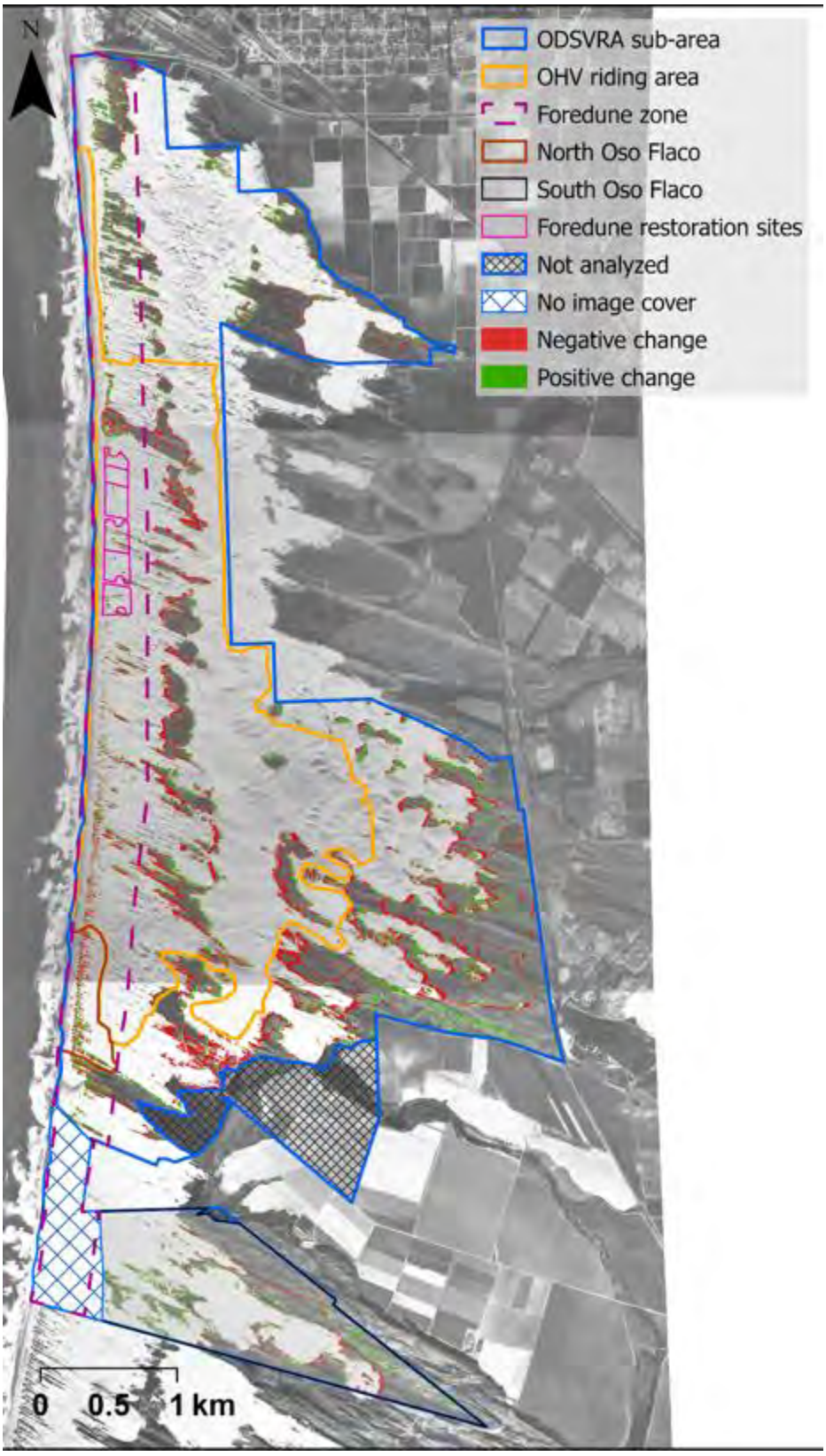

Figure S25. Vegetation change analysis results between 1966 and 1971. Positive change is in green, negative change is in red. Background orthophoto is from 1966.

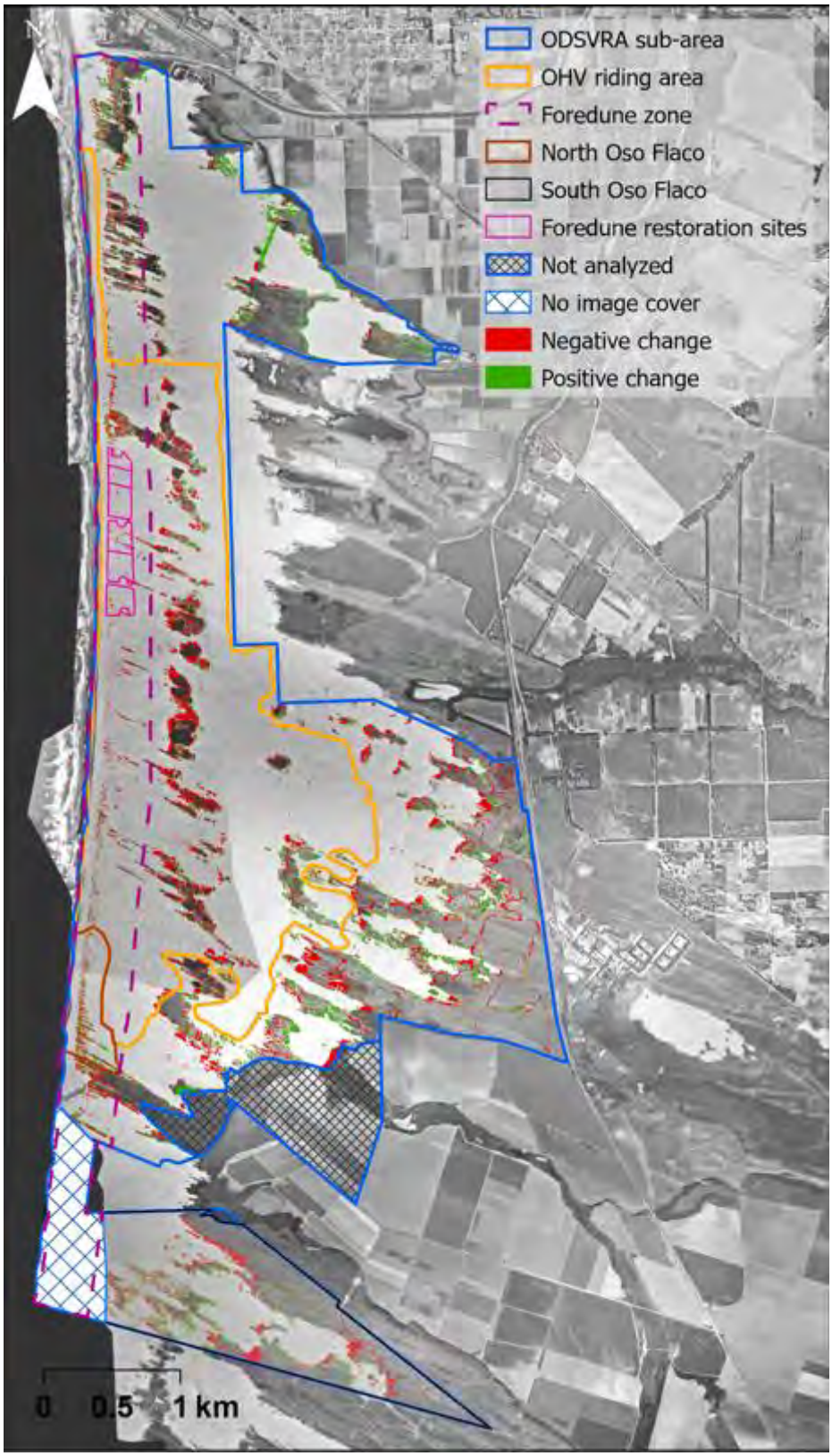

Figure S26. Vegetation change analysis results between 1971 and 1978. Positive change is in green, negative change is in red. Background orthophoto is from 1971.

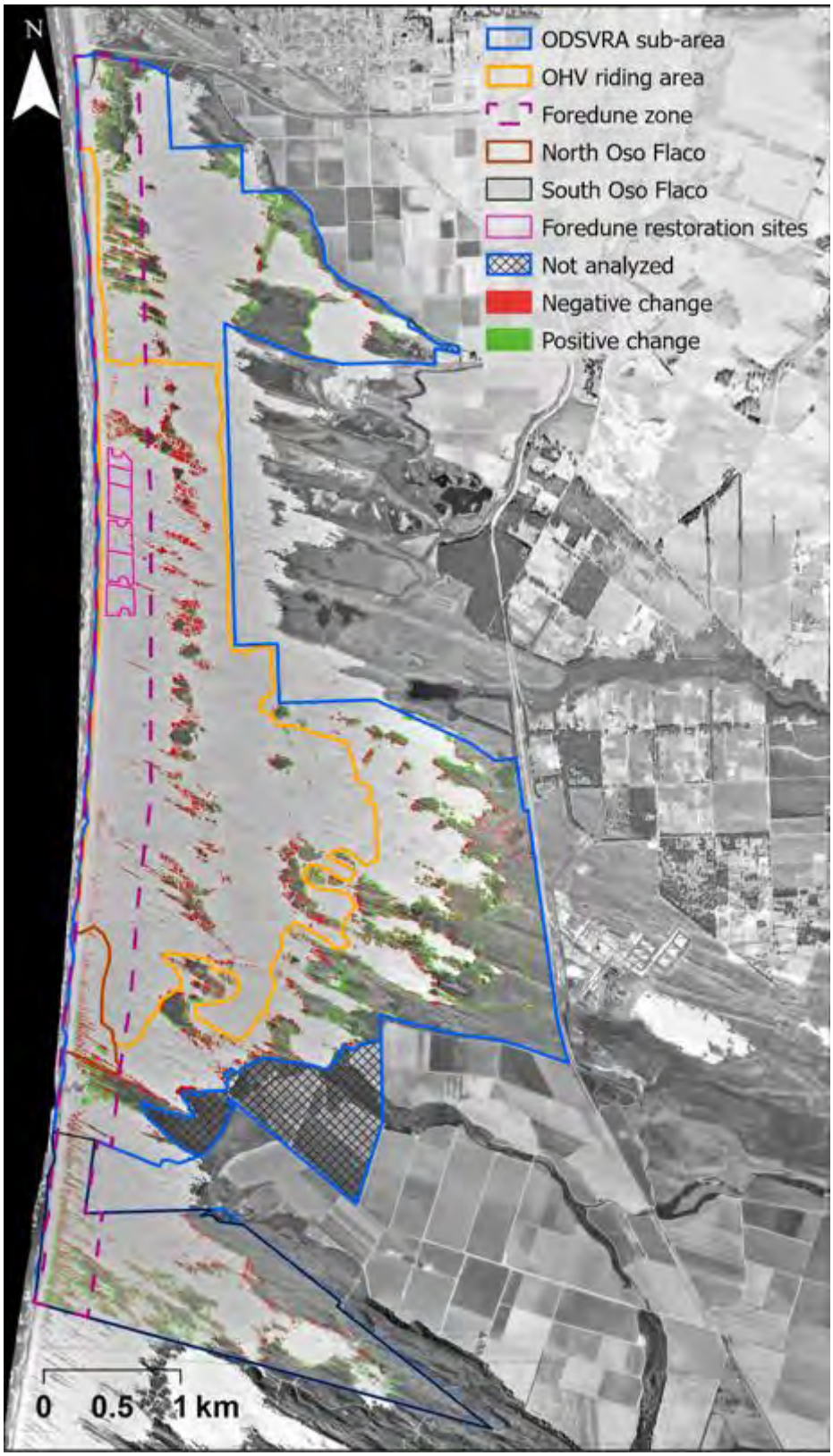

Figure S27. Vegetation change analysis results between 1978 and 1985. Positive change is in green, negative change is in red. Background orthophoto is from 1978.

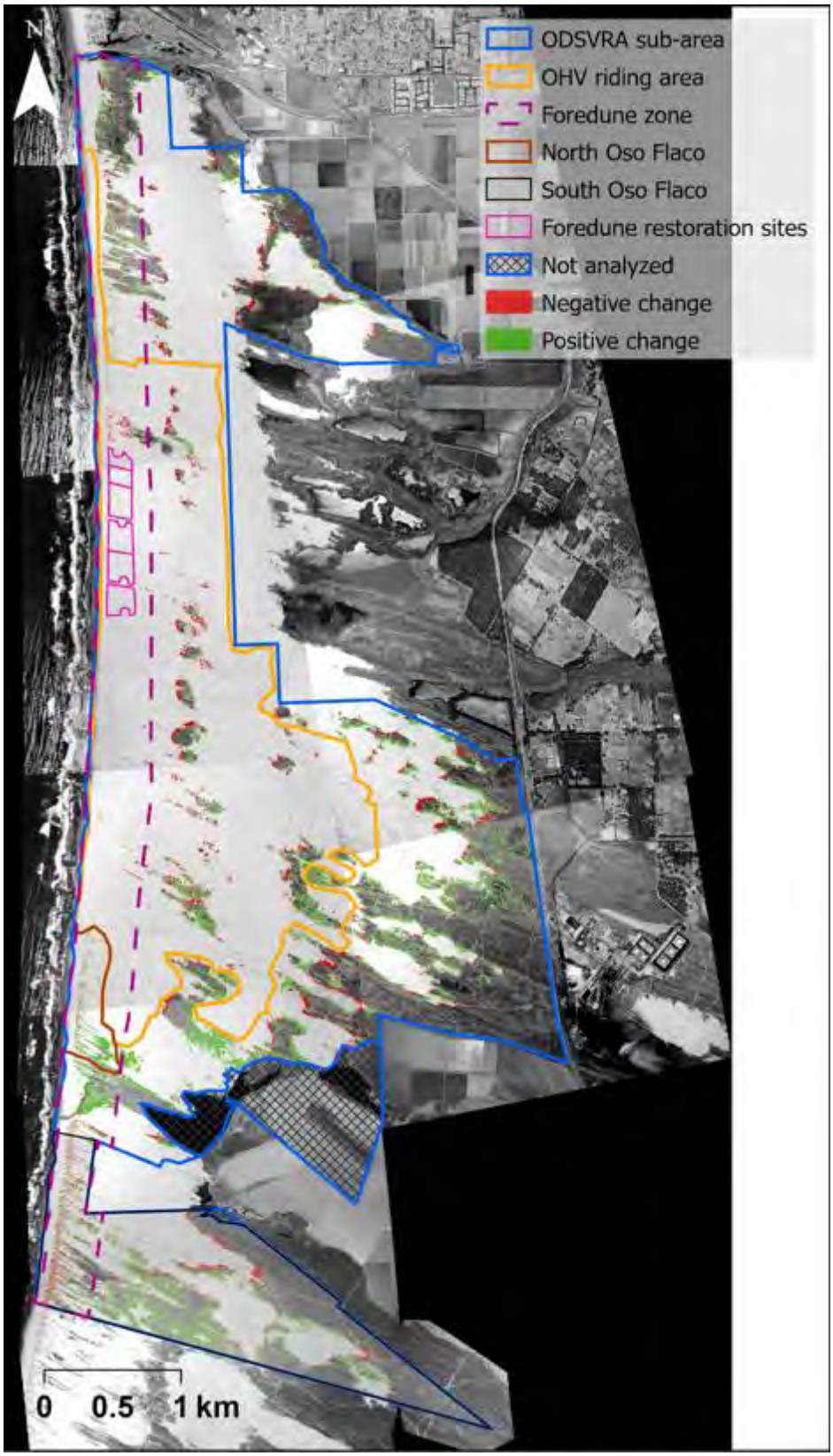

Figure S28. Vegetation change analysis results between 1985 and 1994. Positive change is in green, negative change is in red. Background orthophoto is from 1985.

Figure S29. Vegetation change analysis results between 1994 and 1998. Positive change is in green, negative change is in red. Background orthophoto is from 1994.

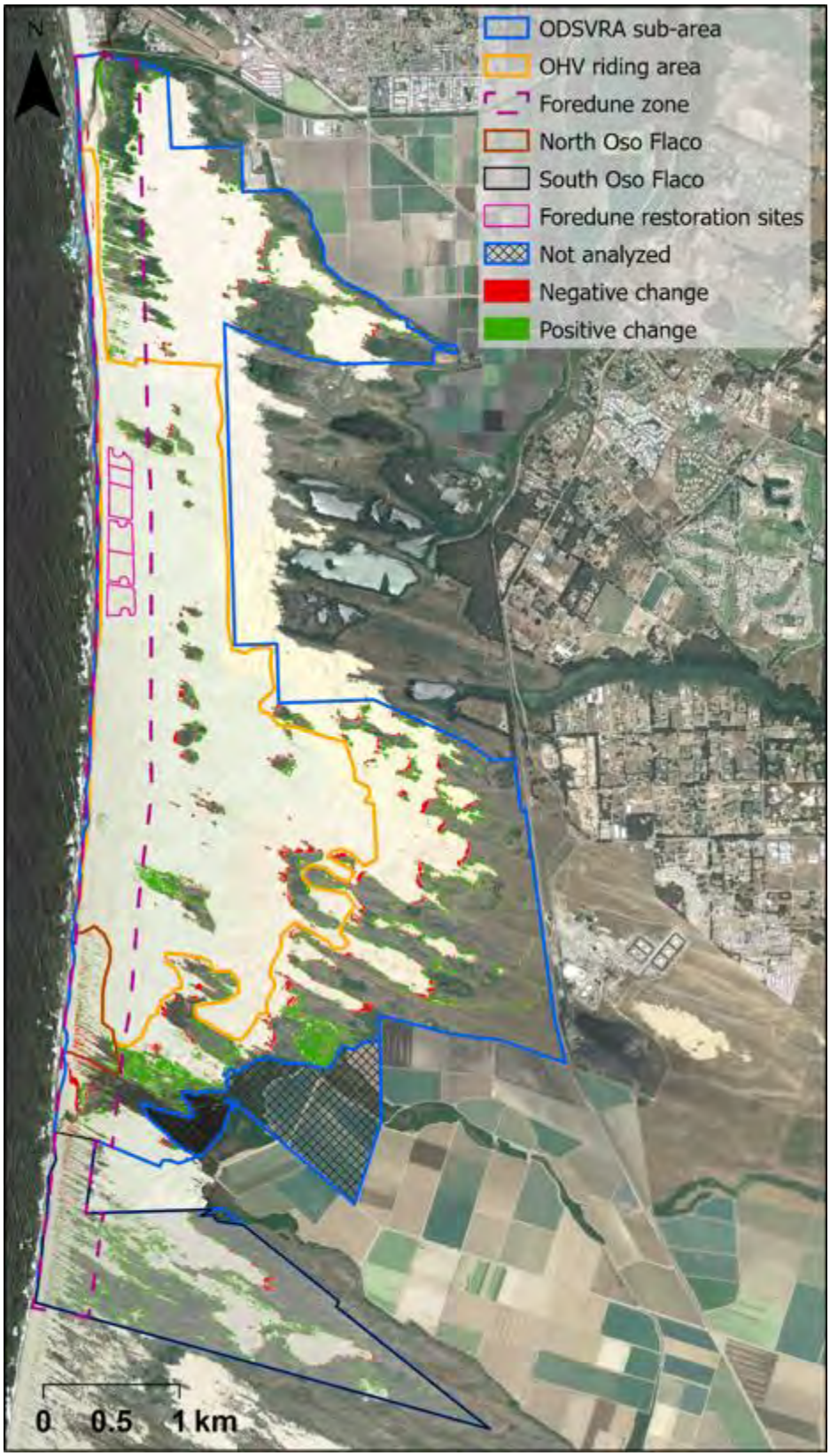

Figure S30. Vegetation change analysis results between 1998 and 2005. Positive change is in green, negative change is in red. Background orthophoto is from 1998.

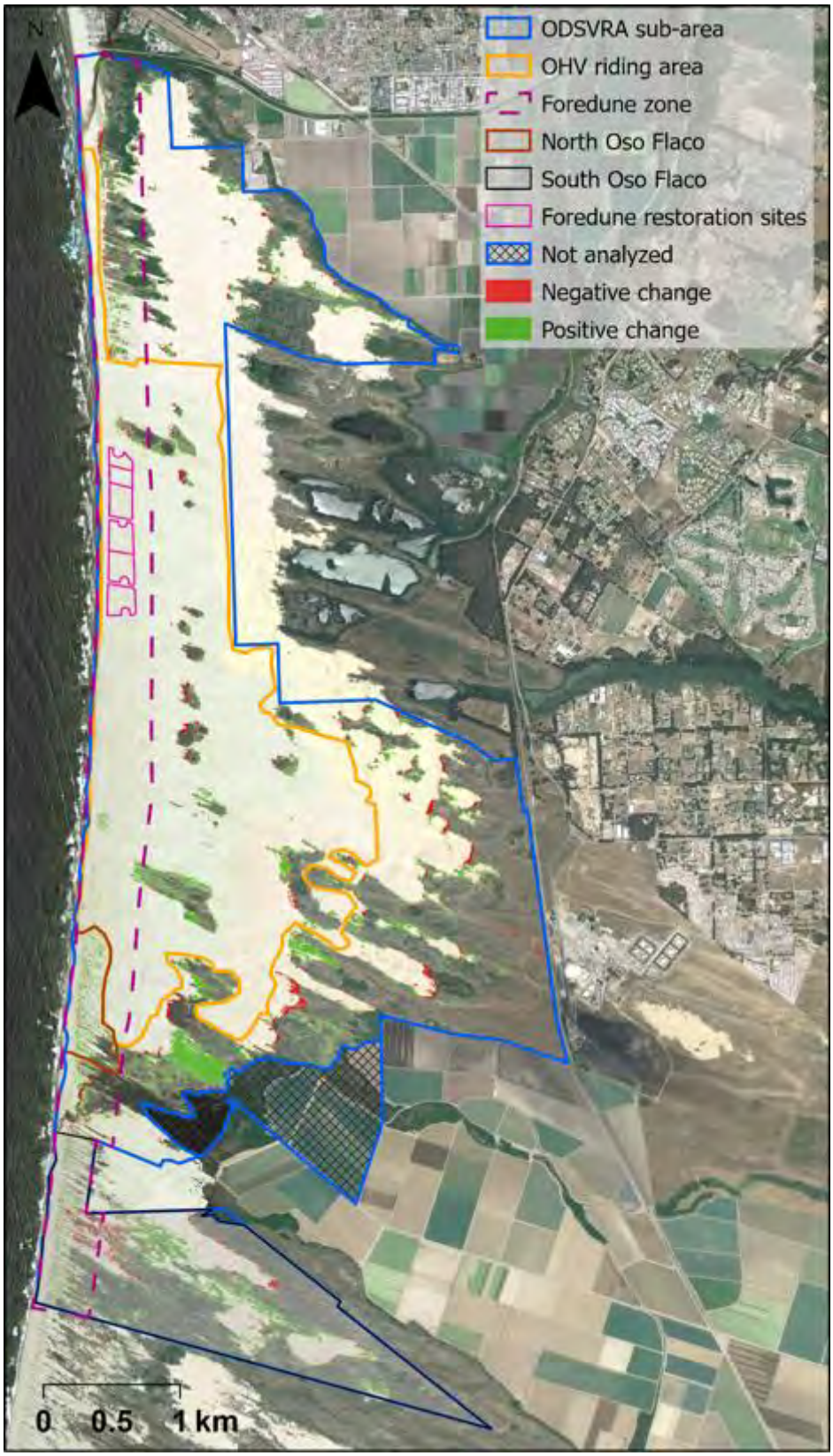

Figure S31. Vegetation change analysis results between 2005 and 2012. Positive change is in green, negative change is in red. Background orthophoto is from 2005.

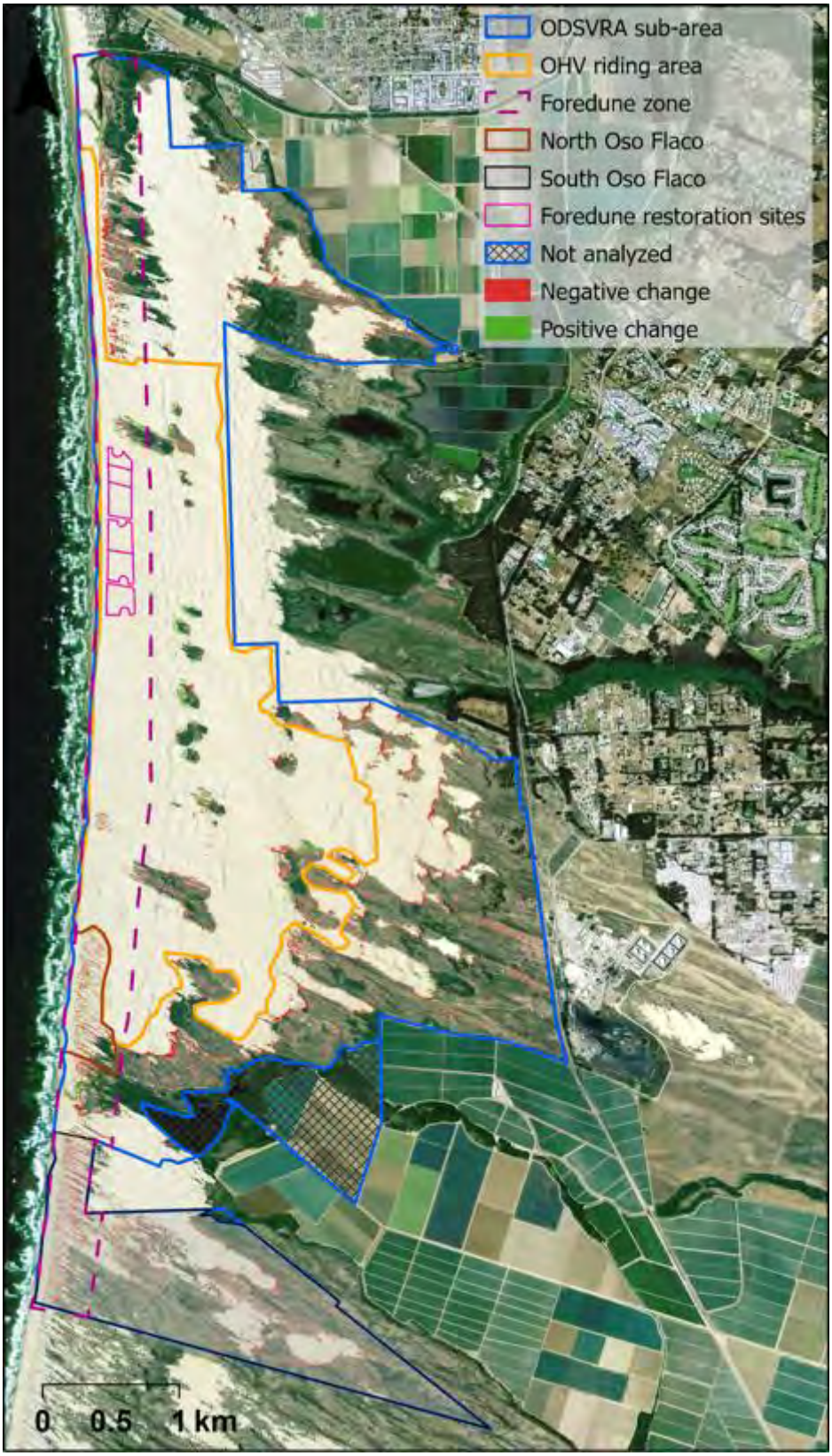

Figure S32. Vegetation change analysis results between 2012 and 2014. Positive change is in green, negative change is in red. Background orthophoto is from 2012.

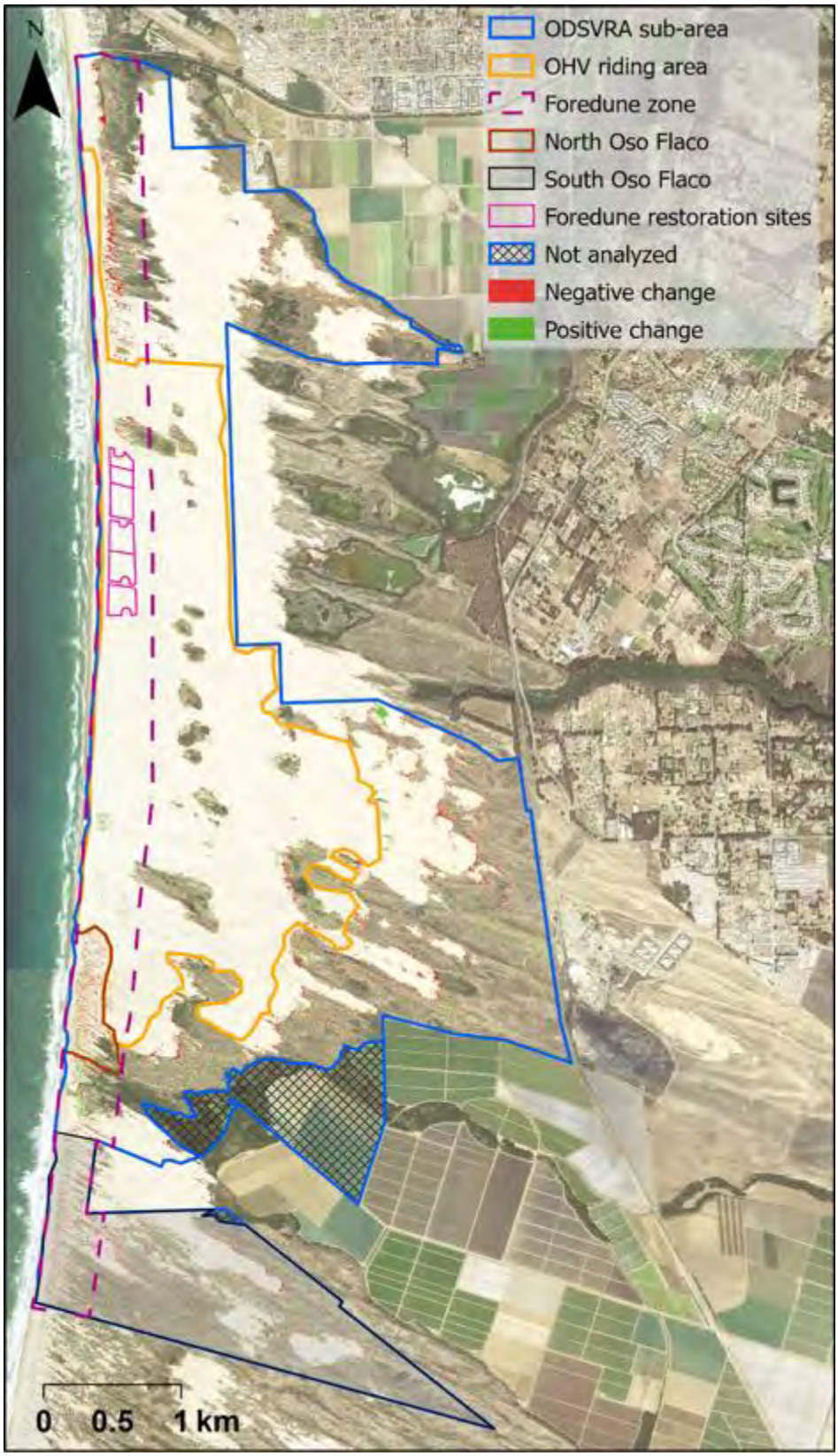

Figure S33. Vegetation change analysis results between 2014 and 2016. Positive change is in green, negative change is in red. Background orthophoto is from 2014.

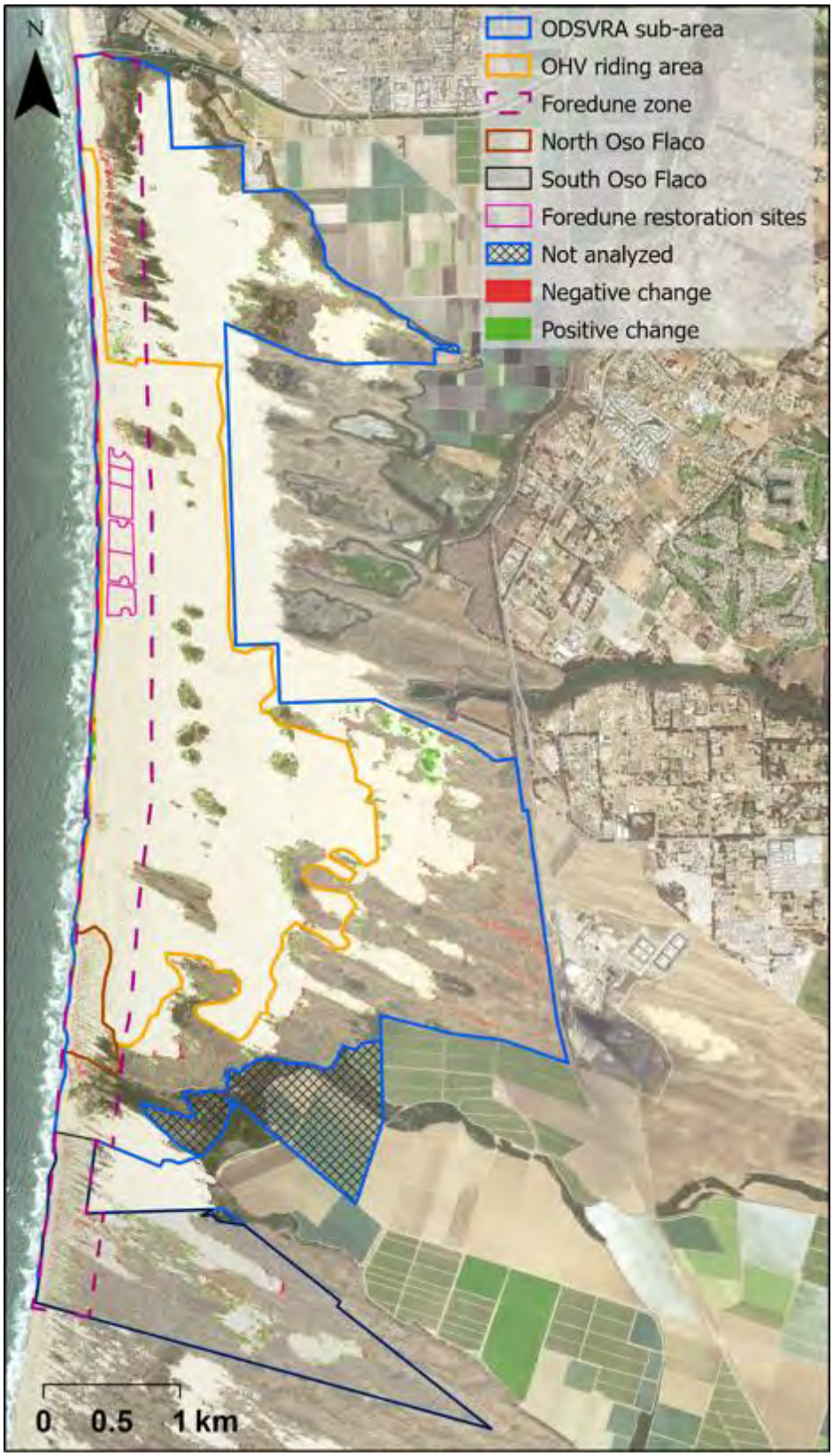

Figure S34. Vegetation change analysis results between 2016 and 2018. Positive change is in green, negative change is in red. Background orthophoto is from 2016.

Figure S35. Vegetation change analysis results between 2018 and 2020. Positive change is in green, negative change is in red. Background orthophoto is from 2018.

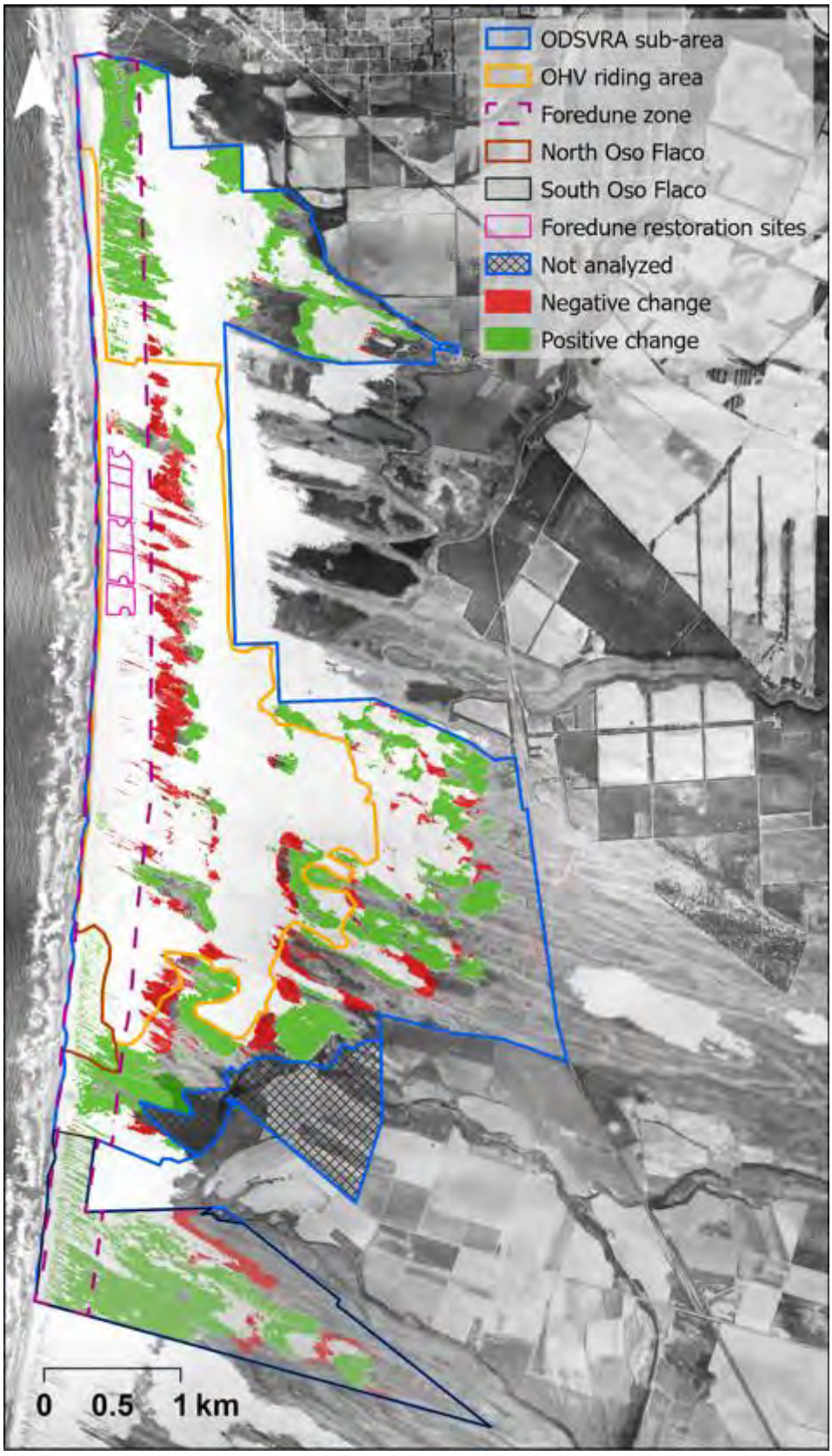

Figure S36. Change in vegetation between 1939 and 2012. Orthophoto from 1939.

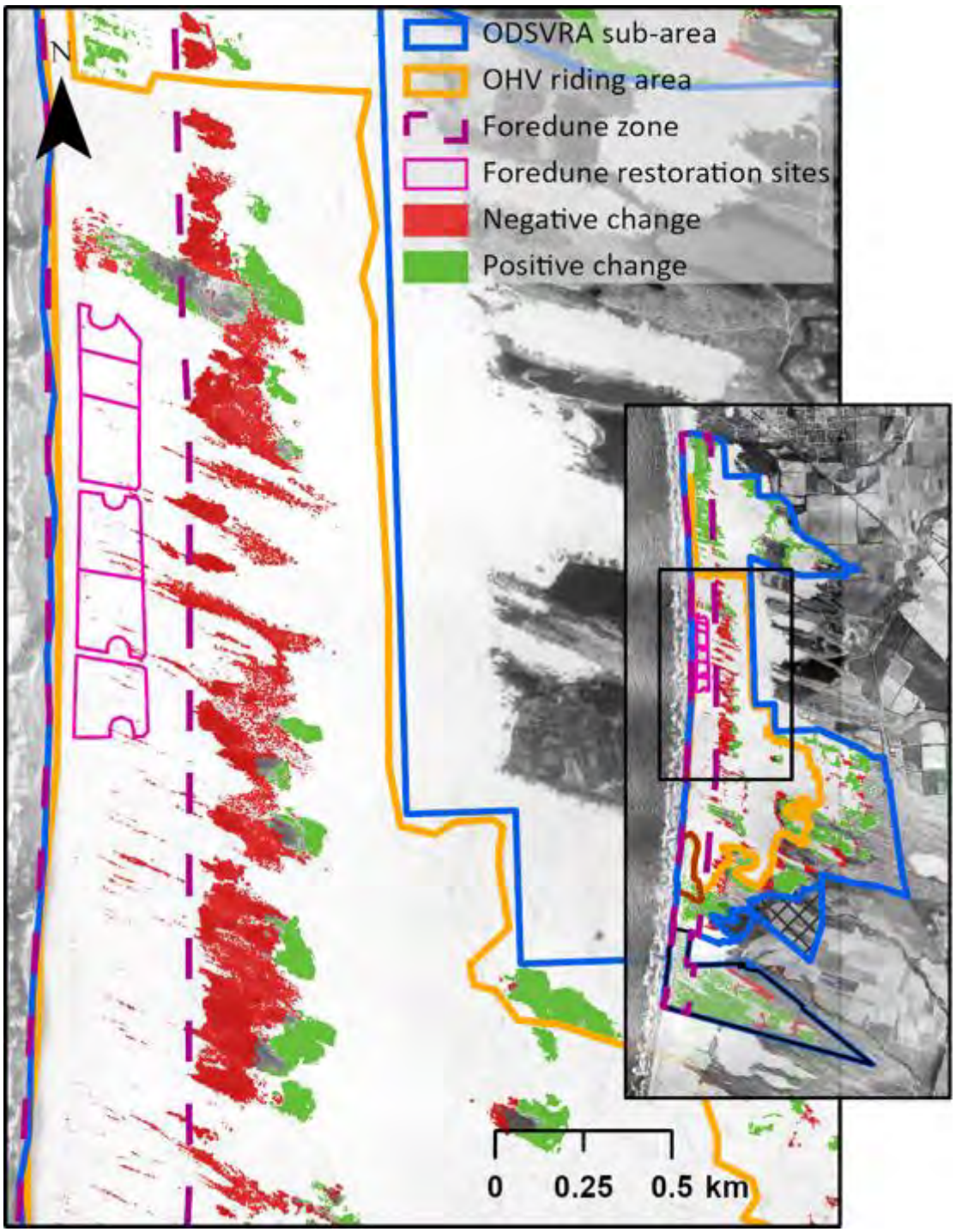

Figure S37. Close-up image of the change in vegetation cover around the foredune restoration sites between 1939 and 2012. Orthophoto from 1939.

Table S1. Calculated land cover values for vegetation areas from each image year, in the ODSVRA sub-area, OHV riding area, non riding area (ODSVRA sub-area minus the OHV riding area), and the Oso Flaco area. The vegetation cover (%) was calculated for the total area of each analytical zone and for the vegetation within the foredune zone (400 m from the shoreline) (see boundaries in Figures 1). The

area values are presented as km^2 (acres) and percentage values were calculated in relation to the different analytical zones. Asterisk (*) represents a lack of image cover and thus is calculated for smaller areas (see Table 2 and Figures S3, S8 and S10).

		ODSVRA sub-area	OHV riding area	Non-riding area	South Oso Flaco	Backdune South Oso Flaco	North Oso Flaco	Foredune ODSVRA	Foredune OHV riding area	Foredune South Oso Flaco	Plover nesting encloser	Foredune restoration sites
	Area analyzed km^2 (acres)	4215.03	1584.07	2630.96	577.29	465.73	68.56	961.90	453.23	111.56	311.42	94.96
1930*	Vegetation cover km^2 (acres)	3.43 (848)*	0.51 (125)*	2.93 (722)*	0.86 (212)	0.84 (207)	0.002 (0.5)	0.07 (16)*	0.03 (8)*	0.02 (6)	0.10 (26)	N/A
	% to analytical zone	N/A	N/A	N/A	36.79	44.41	0.69	N/A	N/A	4.96	10.34	N/A
1939	Vegetation cover km^2 (acres)	4.27 (1056)	0.70 (173)	3.57 (883)	0.84 (207)	0.83 (204)	0.003 (1)	0.13 (32)	0.05 (12)	0.01 (3)	0.08 (20)	0.003 (1)
	% to analytical zone	25.05	10.92	33.55	35.80	43.82	0.95	3.33	2.68	2.32	8.10	0.71
1949	Vegetation cover km^2 (acres)	4.05 (1001)	0.71 (157)	3.34 (826)	0.80 (197)	0.78 (192)	0.004 (1)	0.23 (57)	0.08 (19)	0.02 (5)	0.06 (15)	0.01 (2)
	% to analytical zone	23.75	11.07	31.38	34.16	41.31	1.49	5.88	4.13	4.34	6.06	1.67
1956	Vegetation cover km^2 (acres)	4.28 (1058)	0.74 (184)	3.54 (875)	0.81 (201)	0.78 (194)	0.01 (3)	0.33(82)	0.07 (16)	0.03 (7)	0.05 (12)	0.004 (1)
	% to analytical zone	25.11	11.59	33.24	34.82	41.55	3.96	8.49	3.61	6.71	5.09	0.96
1966	Vegetation cover km^2 (acres)	4.54 (1122)	0.79 (196)	3.75 (927)	0.86 (214)	0.79 (195)	0.03 (7)	0.45 (111)	0.10 (24)	0.08 (19)	0.06 (15)	0.005 (1)
	% to analytical zone	26.63	12.36	12.36	37.00	41.79	10.72	11.56	5.27	16.99	6.17	1.38
1971*	Vegetation cover km2 (acres)	4.23 (1045)*	0.63 (155)	3.60 (891)*	0.82 (203)*	0.82 (203)*	0.02 (6)	0.37 (90)*	0.08 (19)	N/A	0.04 (11)	0.01 (1)
	% to analytical zone	24.80	9.75	33.86	35.11	43.52	8.10	N/A	4.16	N/A	4.36	1.42
1978	Vegetation cover km^2 (acres)	4.04 (997)	0.45 (111)	3.59 (886)	0.86 (213)	0.79 (196)	0.02 (6)	0.40 (99)	0.04 (11)	0.07 (17)	0.02 (5)	0.001 (0.3)
	% to analytical zone	23.66	7.02	33.68	36.92	42.02	8.09	10.24	2.38	15.63	2.24	0.28
1985	Vegetation cover km^2 (acres)	4.18 (1032)	0.27 (67)	3.91 (965)	0.95 (235)	0.86 (211)	0.02 (4)	0.45 (110)	0.02 (4)	0.10 (24)	0.01 (2)	<0.001 (0.01)
	% to analytical zone	24.49	4.21	36.69	40.76	45.37	5.54	11.44	0.97	21.52	0.77	0.01
1994	Vegetation cover km^2 (acres)	4.62 (1141)	0.26 (65)	4.35 (1076)	1.09 (270)	0.99 (224)	0.04 (11)	0.50 (125)	0.01 (2)	0.11 (26)	0.002 (1)	<0.001 (0.01)
	% to analytical zone	27.13	4.13	41.03	47.59	53.48	15.37	12.97	0.54	23.51	0.24	0.01
1998	Vegetation cover km^2 (acres)	5.08 (1256)	0.30 (75)	4.78 (1180)	1.17 (288)	1.05 (260)	0.04 (10)	0.54 (133)	0.02 (4)	0.11 (28)	0.003 (1)	0.002 (0.4)
	% to analytical zone	29.85	4.74	45.03	50.71	57.07	14.62	13.86	0.88	24.70	0.33	0.47
2005	Vegetation cover km^2 (acres)	5.78 (1428)	0.36 (88)	5.42 (1339)	1.38 (340)	1.22 (302)	0.05 (11)	0.70 (173)	0.02 (6)	0.15 (38)	0.001 (0.3)	0.00 (0)
	% to analytical zone	33.95	5.57	51.09	59.90	66.25	16.64	18.01	1.30	33.92	0.13	0.00
2010	Vegetation cover km^2 (acres)	5.72 (1413)	0.39 (97)	5.33 (1316)	1.26 (310)	1.14 (283)	0.05 (13)	0.70 (172)	0.04 (9)	0.11 (28)	0.01 (1.38)	<0.001 (0.01)
	% to analytical zone	33.59	6.09	50.20	54.62	61.93	19.07	17.91	2.00	24.70	0.57	0.01

		ODSVRA sub-area	OHV riding area	Non-riding area	South Oso Flaco	Backdune South Oso Flaco	North Oso Flaco	Foredune ODSVRA	Foredune OHV riding area	Foredune South Oso Flaco	Plover nesting enclosure	Foredune restoration sites
	Area analyzed km^2 (acres)	4215.03	1584.07	2630.96	577.29	465.73	68.56	961.90	453.23	111.56	311.42	94.96
2012	Vegetation cover km2 (acres)	6.35 (1569)	0.44 (109)	5.91 (1460)	1.51 (373)	1.35 (332)	0.07 (17)	0.81 (200)	0.04 (9)	0.01 (3)	0.01 (3)	0.00 (0)
	% to analytical zone	37.31	6.91	55.68	65.66	72.85	24.41	20.76	2.09	36.24	1.07	0.00
2014	Vegetation cover km^2 (acres)	5.97 (1474)	0.43 (105)	5.45 (1369)	1.41 (346)	1.27 (313)	0.06 (15)	0.69 (170)	0.04 (10)	0.006 (2)	0.07 (17)	<0.001 (0.01)
	% to analytical zone	35.05	6.65	52.21	61.48	68.62	21.87	17.69	2.24	32.27	0.65	0.01
2016	Vegetation cover km^2 (acres)	6.15 (1520)	0.44 (109)	5.71 (1411)	1.43 (352)	1.29 (318)	0.05 (14)	0.70 (173)	0.04 (10)	0.14 (34)	0.01 (3)	0.00 (0)
	% to analytical zone	36.15	6.89	53.83	62.02	69.67	20.00	17.99	2.24	30.76	1.07	0.00
2018	Vegetation cover km^2 (acres)	6.14 (1516)	0.49 (121)	5.65 (1395)	1.47 (363)	1.32 (327)	0.06 (15)	0.68 (168)	0.04 (10)	0.14 (36)	0.007 (2)	<0.001 (0.01)
	% to analytical zone	36.05	7.63	53.22	63.88	71.69	21.46	17.46	2.21	31.95	0.68	0.01
2020	Vegetation cover km^2 (acres)	6.01 (1486)	0.52 (128)	5.49 (1358)	1.46 (360)	1.33 (330)	0.05 (13)	0.64 (157)	0.04 (11)	0.12 (30)	0.01 (2)	<0.001 (<0.01)
	% to analytical zone	35.32	8.07	51.79	63.32	72.24	19.05	16.36	2.35	26.83	0.99	0.00

Table S2. Calculated Absolute change (%) and change per year (% yr^{-1}) in vegetation areas between photo years, *in the ODSVRA sub-area, OHV riding area, and the North and South Oso Flaco areas. The positive and* negative change percentages are the percentage of pixels that *gained or lost vegetation from the previous year, respectively,* and were divided by the number of years between the images.

The total change is the cumulative change rate (positive + negative). Net change (positive - negative) represents the trend in change between the image year. *Asterisk (*) represents a lack of image cover and thus is calculated for smaller areas (see Table 2).*

Absolute change (%)																
	ODSVRA sub-area				OHV riding area				South Oso Flaco				North Oso Flaco			
	Positive change	Negative change	Total change	Net change	Positive change	Negative change	Total change	Net change	Positive change	Negative change	Total change	Net change	Positive change	Negative change	Total change	Net change
1930-1939*	N/A	N/A	N/A	N/A	N/A	N/A	N/A	N/A	2.49%	3.49%	5.98%	-1.00%	0.79%	0.53%	1.31%	0.26%
1939-1949	2.95%	4.23%	7.18%	-1.28%	3.31%	3.16%	6.47%	0.15%	1.93%	3.58%	5.51%	-1.65%	1.32%	0.78%	2.10%	0.54%
1949-1956	4.31%	2.94%	7.25%	1.36%	2.58%	2.06%	4.64%	0.51%	3.39%	2.73%	6.12%	0.66%	3.30%	0.84%	4.14%	2.47%
1956-1966	5.88%	3.95%	9.83%	1.93%	3.57%	2.77%	6.34%	0.79%	7.87%	5.63%	13.49%	2.24%	8.71%	1.66%	10.37%	7.04%
1966-1971*	3.77%	5.51%	9.28%	-1.74%	1.95%	4.65%	6.60%	-2.69%	6.30%	4.05%	10.35%	2.25%	6.91%	9.43%	16.34%	-2.52%
1971-1978*	3.30%	5.02%	8.32%	-1.72%	1.27%	4.01%	5.28%	-2.74%	5.30%	7.58%	12.88%	-2.28%	5.43%	5.37%	10.80%	0.06%
1978-1985	5.10%	4.25%	9.35%	0.85%	1.10%	3.90%	5.00%	-2.81%	9.38%	5.52%	14.90%	3.86%	4.31%	6.82%	11.13%	-2.50%
1985-1994	5.86%	2.83%	8.68%	3.03%	1.46%	1.66%	3.13%	-0.20%	11.84%	4.40%	16.24%	7.44%	12.90%	2.01%	14.91%	10.89%
1994-1998	4.21%	1.82%	6.03%	2.39%	1.15%	0.51%	1.66%	0.64%	6.29%	3.46%	9.75%	2.83%	4.53%	5.35%	9.88%	-0.83%
1998-2005	5.69%	1.61%	7.29%	4.08%	1.54%	0.68%	2.22%	0.86%	10.91%	1.81%	12.72%	9.11%	6.99%	4.79%	11.78%	2.20%
2005-2012	5.07%	1.49%	6.55%	3.58%	1.84%	0.46%	2.30%	1.37%	9.83%	3.13%	12.96%	6.70%	12.43%	2.30%	14.72%	10.13%
2012-2014	1.30%	3.71%	5.01%	-2.42%	0.81%	1.08%	1.89%	-0.26%	2.18%	7.34%	9.53%	-5.16%	5.29%	9.62%	14.91%	-4.32%
2014-2016	2.51%	2.54%	5.05%	-0.03%	1.03%	0.79%	1.82%	0.25%	5.34%	4.77%	10.11%	0.56%	5.80%	7.84%	13.64%	-2.04%
2016-2018	5.78%	2.11%	7.90%	3.67%	1.51%	0.68%	2.19%	0.84%	5.91%	4.07%	9.99%	1.84%	7.23%	4.93%	12.15%	2.30%
2018-2020	1.46%	1.01%	2.47%	0.45%	1.46%	1.01%	2.47%	0.45%	4.28%	4.84%	9.12%	-0.56%	4.31%	6.93%	11.23%	-2.62%
1939-1985	8.75%	9.32%	18.07%	-0.57%	2.48%	9.19%	11.67%	-6.72%	13.71%	8.75%	22.46%	4.96%	5.29%	0.70%	5.98%	4.59%
1985-2012	15.04%	1.95%	16.99%	13.09%	4.20%	1.42%	5.63%	2.78%	28.14%	3.53%	31.67%	24.60%	23.47%	2.58%	26.05%	20.89%
2012-2020	4.12%	4.33%	8.45%	-0.22%	2.23%	1.03%	3.26%	1.20%	4.42%	7.72%	12.14%	-3.30%	3.57%	11.03%	14.60%	-7.45%
1939-2012	19.02%	6.51%	25.53%	12.51%	4.62%	8.77%	13.39%	-4.15%	36.54%	6.65%	43.19%	29.89%	26.56%	0.59%	27.15%	25.97%
1939-2020	17.78%	7.00%	24.78%	10.78%	5.30%	8.24%	13.54%	-2.93%	34.39%	7.65%	42.05%	26.74%	20.64%	0.70%	21.34%	19.94%

Change per year (%yr^{-1})																
	ODSVRA sub-area				OHV riding area				South Oso Flaco				North Oso Flaco			
	Positive change	Negative change	Total change	Net change	Positive change	Negative change	Total change	Net change	Positive change	Negative change	Total change	Net change	Positive change	Negative change	Total change	Net change
1930-1939*	N/A	N/A	N/A	N/A	N/A	N/A	N/A	N/A	0.28%	0.39%	0.66%	-0.11%	0.09%	0.06%	0.15%	0.03%
1939-1949	0.29%	0.42%	0.72%	-0.13%	0.33%	0.32%	0.65%	0.01%	0.19%	0.36%	0.55%	-0.16%	0.13%	0.08%	0.21%	0.05%
1949-1956	0.62%	0.42%	1.04%	0.19%	0.37%	0.29%	0.66%	0.07%	0.48%	0.39%	0.87%	0.09%	0.47%	0.12%	0.59%	0.35%
1956-1966	0.59%	0.39%	0.98%	0.19%	0.36%	0.28%	0.63%	0.08%	0.79%	0.56%	1.35%	0.22%	0.87%	0.17%	1.04%	0.70%
1966-1971*	0.75%	1.10%	1.86%	-0.35%	0.39%	0.93%	1.32%	-0.54%	1.26%	0.81%	2.07%	0.45%	1.38%	1.89%	3.27%	-0.50%
1971-1978*	0.47%	0.72%	1.19%	-0.25%	0.18%	0.57%	0.75%	-0.39%	0.76%	1.08%	1.84%	-0.33%	0.78%	0.77%	1.54%	0.01%
1978-1985	0.73%	0.61%	1.34%	0.12%	0.16%	0.56%	0.71%	-0.40%	1.34%	0.79%	2.13%	0.55%	0.62%	0.97%	1.59%	-0.36%
1985-1994	0.65%	0.31%	0.96%	0.34%	0.16%	0.18%	0.35%	-0.02%	1.32%	0.49%	1.80%	0.83%	1.43%	0.22%	1.66%	1.21%
1994-1998	0.47%	0.20%	0.67%	0.27%	0.13%	0.06%	0.18%	0.07%	0.70%	0.38%	1.08%	0.31%	0.50%	0.59%	1.10%	-0.09%
1998-2005	0.63%	0.18%	0.81%	0.45%	0.17%	0.08%	0.25%	0.10%	1.21%	0.20%	1.41%	1.01%	0.78%	0.53%	1.31%	0.24%
2005-2012	0.72%	0.21%	0.94%	0.51%	0.26%	0.07%	0.33%	0.20%	1.40%	0.45%	1.85%	0.96%	1.78%	0.33%	2.10%	1.45%
2012-2014	0.65%	1.86%	2.50%	-1.21%	0.41%	0.54%	0.95%	-0.13%	1.09%	3.67%	4.76%	-2.58%	2.65%	4.81%	7.46%	-2.16%
2014-2016	1.26%	1.27%	2.53%	-0.01%	0.52%	0.39%	0.91%	0.12%	2.67%	2.39%	5.06%	0.28%	2.90%	3.92%	6.82%	-1.02%
2016-2018	2.89%	1.06%	3.95%	1.83%	0.76%	0.34%	1.10%	0.42%	2.96%	2.04%	4.99%	0.92%	3.61%	2.46%	6.08%	1.15%
2018-2020	0.73%	0.50%	1.24%	0.23%	0.73%	0.50%	1.24%	0.23%	2.14%	2.42%	4.56%	-0.28%	2.15%	3.46%	5.62%	-1.31%
1939-1985	0.19%	0.20%	0.39%	-0.01%	0.05%	0.20%	0.25%	-0.15%	0.30%	0.19%	0.49%	0.11%	0.11%	0.02%	0.13%	0.10%
1985-2012	0.56%	0.07%	0.63%	0.48%	0.16%	0.05%	0.21%	0.10%	1.04%	0.13%	1.17%	0.91%	0.87%	0.10%	0.96%	0.77%
2012-2020	0.51%	0.54%	1.06%	-0.03%	0.28%	0.13%	0.41%	0.15%	0.55%	0.96%	1.52%	-0.41%	0.45%	1.38%	1.82%	-0.93%
1939-2012	0.26%	0.09%	0.35%	0.17%	0.06%	0.12%	0.18%	-0.06%	0.50%	0.09%	0.59%	0.41%	0.36%	0.01%	0.37%	0.36%
1939-2020	0.22%	0.09%	0.31%	0.13%	0.07%	0.10%	0.17%	-0.04%	0.42%	0.09%	0.52%	0.33%	0.25%	0.01%	0.26%	0.25%

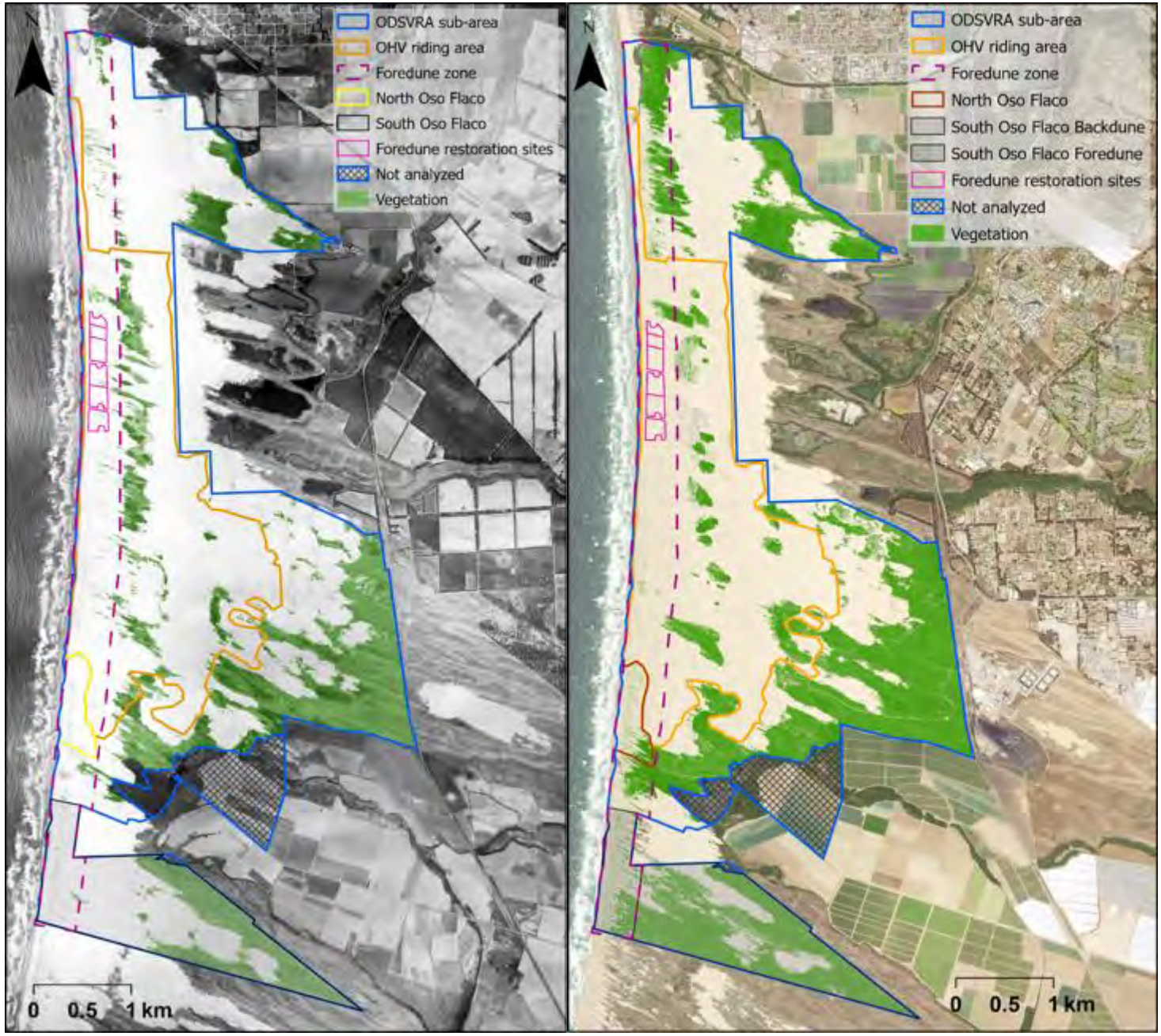

Figure S38. Vegetation cover comparison between 1939 (left) and 2020 (right) as presented in Figures S4 and S18.

Oceano Dunes State Vehicular Recreation Area Dust Control Program

DRAFT 2022 Annual Report and Work Plan

ATTACHMENT 07

ODSVRA Dust Control Program Scientific Review Process

(State Parks and SAG Work Product)

THIS PAGE INTENTIONALLY LEFT BLANK.

ODSVRA Dust Control Program Scientific Review Process

In August 2021, SAG and State Parks agreed to the following process for the review and publication of scientific documents related to dust emissions and dune restoration at ODSVRA.

Background and Goal: There has been, and continues to be, substantial research at Oceano Dunes State Vehicular Recreation Area (ODSVRA) to better understand the science of dust emissions, dust controls, and dune restoration at the park. To date, there has not been a standardized approach for the review and publication or public release of scientific documents regarding dust emissions and/or dune restoration at ODSVRA. The Stipulated Order of Abatement (SOA) establishes a Scientific Advisory Group with the charge to "…evaluate, assess, and provide recommendations on the mitigation of windblown PM10 emissions from ODSVRA…" Furthermore, the California Department of Parks and Recreation (CDPR) periodically commissions and publishes studies by third-party researchers regarding dust emissions, aeolian (windblown) processes, dust controls, and dune geomorphology at ODSVRA.

This section describes the established process by which the SAG, CDPR, and third parties contracted by CDPR, are involved in the preparation, scientific review, publication, and public release of research and scientific reports related to dust/particulate matter, aeolian processes, dust controls, and/or dune restoration at ODSVRA. The process addresses when and how the SAG is asked to provide peer review of a research study, and what steps are needed to release a document to the public.

For clarity, this process only applies to research directly related to dust emissions, aeolian processes, dust controls, or dune geomorphology and restoration at ODSVRA that CDPR has commissioned to be conducted by third parties. (Scientific reports directly produced by the SAG, which is an independent entity established by the SOA, are not subject to this process.) The goal is to streamline and standardize a process to ensure all research related to dust receives the same level of expert review, and to ensure that all research is robust and as defensible as possible before it enters the public sphere.

Process for review of scientific documents:

1. CDPR commissions study by a third-party researcher related to dust emissions and/or aeolian processes, dust controls, or dune geomorphology and restoration at ODSVRA.
2. Third-party researcher submits report/paper to CDPR for review.
3. CDPR informs the San Luis Obispo Air Pollution Control District (SLOAPCD) and SAG that the report exists and that a private (i.e., non-public) review from the SAG will be requested prior to the document going public. Once the document is public at the end of this process, the SAG may choose to prepare an additional public review of, and/or response to, the study.
4. CDPR performs preliminary review of third-party report.
5. Third-party researcher verbally presents report findings to CDPR. This may include a CDPR technical group meeting with the third-party researcher separately to address more technical questions.
6. Once an initial draft is reviewed by CDPR, the draft document is submitted to the SAG for a peer review. The document remains private at this stage of the process.
7. Comments from the SAG and CDPR are submitted privately to the third-party researcher for potential edits.
8. The third-party researcher edits the report in response to SAG and CDPR comments. Though the third-party researcher retains discretion as to how they address the comments, the researcher is expected to ensure that the results of the study are scientifically robust and to work with CDPR toward developing a clear public message regarding the findings of this research.
9. Third-party researcher submits updated version of report/paper to CDPR. CDPR may provide further comments or seek further comments from the SAG, which the third-party researcher would then have the opportunity to address through further edits to their report. Further iteration with CDPR and the SAG may be pursued as needed.
10. Upon completion of the comment-edit process for the third-party research report, CDPR may choose to develop a summary document and/or staff report related to the findings of this report. If so, the third-party researcher assists in developing this CDPR summary document / staff report. If not, CDRP releases the research report publicly in its present form (i.e., skipping steps 11-13 below).
11. CDPR summary document / staff report is submitted to CDPR Executive Team for review.
12. CDPR Exec determines the need for additional Exec review of the CDPR summary document / staff report (Natural Resource Agency, Governor's Office), as appropriate.

13. Once the CDPR summary document / staff report is approved by CDRP Exec and other Executive Offices, as determined above, CDPR concurrently releases the third-party research report and the CDPR summary document / staff report.
14. Concurrent with, or soon after the release of report(s), CDPR may invite the third-party researcher to present findings at an OHV Commission Meeting.
15. Once the document is public, the third-party researcher is free to distribute and publicly comment on the findings of their report.
16. Throughout this process, all terms and conditions of contracts between third parties and CDPR take precedence, including procedures for CDPR comment and public release. Nonetheless, all entities (CDPR, SAG, third-party researchers), will make reasonable efforts to fulfill the process as outlined here.
17. Throughout this process, all parties will aim to provide comments, edits in response to comments, and approvals within 10 business days of receipt of respective reports/comments for consideration. Parties will notify each other of expected significant delays beyond this timeline.

THIS PAGE INTENTIONALLY LEFT BLANK.

Oceano Dunes State Vehicular Recreation Area Dust Control Program

DRAFT 2022 Annual Report and Work Plan

ATTACHMENT 08

2022/2023 ODSVRA Dust Control Program Vegetation Restoration Projects

(State Parks ARWP Work Product)

THIS PAGE INTENTIONALLY LEFT BLANK.

2022-2023 Project List (subject to change)						
Project Name	**Project Acreage**	**Total Plants**	**Plants Per Acre**	**Native Seed (lbs)**	**Native Seed (lbs per Acre)**	**Large Straw Bales (3X4X8 ft)**
New Planting Areas						
East Moy Mell (north) 2020-WF-01	20	55,860	2,793	223	11.2	240
Eucalyptus Tree (west) 2022-ST-02	6.8	19,362	2,847	78	11.5	82
Eucalyptus Tree (center) 2022-VG-09	14.9	41,485	2,784	174	11.7	100
Subtotal	**41.7**	**116,707**	**2,799**	**475**	**11.4**	**422**
Supplemental Areas						
BBQ Flats 2019-VG-01	2.0	4,412	2,206	17.3	8.6	24
North Eucalyptus Tree 2022-VG-04	1.0	2,206	2,206	8.6	8.6	12
Eucalyptus Tree (north) 2022-VG-05	1.0	2,206	2,206	8.6	8.6	12
La Grille Hill 2022-VG-03	1.0	2,157	2,157	13.1	13.1	12
Subtotal	**5.0**	**10,981**	**2,196**	**47.6**	**9.5**	**60**
Total	**46.7**	**127,688**	**2,734**	**522.6**	**11.2**	**482**

THIS PAGE INTENTIONALLY LEFT BLANK.